INSIGHTS IN GENERAL CARDIOVASCULAR MEDICINE: 2021

EDITED BY: Pietro Enea Lazzerini, Junjie Xiao, Maurizio Acampa, Pier Leopoldo Capecchi and Chen Liu

PUBLISHED IN: Frontiers in Cardiovascular Medicine

frontiers Research Topics

frontiers

ISSN 1664-8714
ISBN 978-2-88976-868-4
DOI 10.3389/978-2-88976-868-4

About Frontiers

Frontiers is more than just an open-access publisher of scholarly articles: it is a pioneering approach to the world of academia, radically improving the way scholarly research is managed. The grand vision of Frontiers is a world where all people have an equal opportunity to seek, share and generate knowledge. Frontiers provides immediate and permanent online open access to all its publications, but this alone is not enough to realize our grand goals.

Frontiers Journal Series

The Frontiers Journal Series is a multi-tier and interdisciplinary set of open-access, online journals, promising a paradigm shift from the current review, selection and dissemination processes in academic publishing. All Frontiers journals are driven by researchers for researchers; therefore, they constitute a service to the scholarly community. At the same time, the Frontiers Journal Series operates on a revolutionary invention, the tiered publishing system, initially addressing specific communities of scholars, and gradually climbing up to broader public understanding, thus serving the interests of the lay society, too.

Dedication to Quality

Each Frontiers article is a landmark of the highest quality, thanks to genuinely collaborative interactions between authors and review editors, who include some of the world's best academicians. Research must be certified by peers before entering a stream of knowledge that may eventually reach the public - and shape society; therefore, Frontiers only applies the most rigorous and unbiased reviews.
Frontiers revolutionizes research publishing by freely delivering the most outstanding research, evaluated with no bias from both the academic and social point of view. By applying the most advanced information technologies, Frontiers is catapulting scholarly publishing into a new generation.

What are Frontiers Research Topics?

Frontiers Research Topics are very popular trademarks of the Frontiers Journals Series: they are collections of at least ten articles, all centered on a particular subject. With their unique mix of varied contributions from Original Research to Review Articles, Frontiers Research Topics unify the most influential researchers, the latest key findings and historical advances in a hot research area! Find out more on how to host your own Frontiers Research Topic or contribute to one as an author by contacting the Frontiers Editorial Office: frontiersin.org/about/contact

INSIGHTS IN GENERAL CARDIOVASCULAR MEDICINE: 2021

Topic Editors:
Pietro Enea Lazzerini, University of Siena, Italy
Junjie Xiao, Shanghai University, China
Maurizio Acampa, Siena University Hospital, Italy
Pier Leopoldo Capecchi, University of Siena, Italy
Chen Liu, The First Affiliated Hospital of Sun Yat-sen University, China

Citation: Lazzerini, P. E., Xiao, J., Acampa, M., Capecchi, P. L., Liu, C., eds. (2022). Insights in General Cardiovascular Medicine: 2021. Lausanne: Frontiers Media SA. doi: 10.3389/978-2-88976-868-4

Table of Contents

frontiers | Frontiers in Cardiovascular Medicine

EDITORIAL
published: 26 July 2022
doi: 10.3389/fcvm.2022.957636

Editorial: Insights in General Cardiovascular Medicine: 2021

Lijun Wang[1,2], *Jianyun Liu*[1], *Yi Lu*[1], *Maurizio Acampa*[3]*, *Pier Leopoldo Capecchi*[4]*, *Pietro Enea Lazzerini*[4]* and *Junjie Xiao*[1,2]*

[1] Affiliated Nantong Hospital of Shanghai University (The Sixth People's Hospital of Nantong), School of Medicine, Institute of Geriatrics (Shanghai University), Shanghai University, Nantong, China, [2] Cardiac Regeneration and Ageing Lab, Shanghai Engineering Research Center of Organ Repair, School of Life Science, Institute of Cardiovascular Sciences, Shanghai University, Shanghai, China, [3] Stroke Unit, Department of Emergency-Urgency and Transplants, "Santa Maria alle Scotte" General-Hospital, Azienda Ospedaliera Universitaria Senese, Siena, Italy, [4] Department of Medical Sciences, Surgery and Neurosciences, University of Siena, Siena, Italy

Keywords: General Cardiovascular Medicine Section, Editorial, 2021, cardiovasccular medicine, cardiovascular disease

Editorial on the Research Topic

Insights in General Cardiovascular Medicine: 2021

The goal of this Research Topic collection of articles published in *Frontiers in Cardiovascular Medicine: Insights in General Cardiovascular Medicine: 2021*, is to bring together excellent manuscripts of high-quality and high-citation potential, all of which gave been contributed by our editorial board members. Our criteria for selection include whether the topic addressed is focused on new discoveries and developments, current advances and challenges, as well as future prospects in the field of cardiovascular medicine research. This collection represents the quality and breadth of the papers published in this section, as well as the geographical variety of our scientific community. The rest of this editorial provides an overview of the articles included in the *Insights in General Cardiovascular Medicine: 2021* collection (**Table 1**).

INSIGHTS IN GENERAL CARDIOVASCULAR MEDICINE: 2021

The order of appearance according to the number of views (on May 17, 2022).

– *The Post-thrombotic Syndrome-Prevention and Treatment: VAS-European Independent Foundation in Angiology/Vascular Medicine Position Paper* (Cosmi et al.).

Post-thrombotic syndrome is a common and potentially risky complication of deep vein thrombosis that significantly affects patients' life quality. However, there are still great uncertainties in diagnosis, prevention, and treatment due to limited evidence-based approaches to clinical management. This position paper provided a practical framework and guidance for clinicians in PTS management.

– *Diabetes and Its Cardiovascular Complications: Comprehensive Network and Systematic Analyses* (Wu et al.).

There is currently no cure for diabetes. This review highlights current advances in the study of diabetes mechanisms using multi-omics analytical approaches and recent findings on the relationship between diabetes and other biological processes. This review provides important information for the prediction, diagnosis, and treatment of diabetes that could be useful for both clinicians and researchers.

– *EMbedding and Backscattered Scanning Electron Microscopy: A Detailed Protocol for the Whole-Specimen, High-Resolution Analysis of Cardiovascular Tissues* (Mukhamadiyarov et al.).

Analysis of cardiovascular tissue ultrastructure is complex. The current commonly used study methods have limitations such as low resolution and low signal-to-noise ratio. This protocol

OPEN ACCESS

Edited and reviewed by:
Hendrik Tevaearai Stahel, Bern University Hospital, Switzerland

***Correspondence:**
Junjie Xiao
junjiexiao@live.cn
Pietro Enea Lazzerini
lazzerini7@unisi.it
Pier Leopoldo Capecchi
capecchipl@unisi.it
Maurizio Acampa
M.Acampa@ao-siena.toscana.it

Specialty section:
This article was submitted to General Cardiovascular Medicine, a section of the journal Frontiers in Cardiovascular Medicine

Received: *31 May 2022*
Accepted: *07 June 2022*
Published: *26 July 2022*

Citation:
Wang L, Liu J, Lu Y, Acampa M, Capecchi PL, Lazzerini PE and Xiao J (2022) Editorial: Insights in General Cardiovascular Medicine: 2021. Front. Cardiovasc. Med. 9:957636. doi: 10.3389/fcvm.2022.957636

TABLE 1 | Metrics (on May 17, 2022) of the articles published in Insights in General Cardiovascular Medicine 2021.

Title	First author, Country	Downloads	Views[#]
The Post-thrombotic Syndrome-Prevention and Treatment: VAS-European Independent Foundation in Angiology/Vascular Medicine Position Paper	Benilde Cosmi, Italy	618	1,843
Diabetes and Its Cardiovascular Complications: Comprehensive Network and Systematic Analyses	Hao Wu, United States	273	1,711
EMbedding and Backscattered Scanning Electron Microscopy: A Detailed Protocol for the Whole-Specimen, High-Resolution Analysis of Cardiovascular Tissues	Rinat A. Mukhamadiyarov,Russia	489	1,575
Identification of Novel Single-Nucleotide Variants With Potential of Mediating Malfunction of MicroRNA in Congenital Heart Disease	Wangkai Liu, China	349	1,476
Screening for Asymptomatic Coronary Artery Disease via Exercise Stress Testing in Patients With Type 2 Diabetes Mellitus: A Systematic Review and Meta-Analysis	Yaoshan Dun, China	424	1,436
Relevance of Cor Pulmonale in COPD With and Without Pulmonary Hypertension: A Retrospective Cohort Study	Athiththan Yogeswaran, Germany	305	1,361
Cognitive Impairment in Heart Failure: Landscape, Challenges, and Future Directions	Mengxi Yang, China	269	1,342
Diagnostic and Therapeutic Management of the Thoracic Outlet Syndrome. Review of the Literature and Report of an Italian Experience	Giuseppe Camporese, Italy	194	1,141
Cardiorespiratory Responses During High-Intensity Interval Training Prescribed by Rating of Perceived Exertion in Patients After Myocardial Infarction Enrolled in Early Outpatient Cardiac Rehabilitation	Yaoshan Dun, China	371	1,127
Determination of Agrin and Related Proteins Levels as a Function of Age in Human Hearts	Katie L. Skeffington, United Kingdom	230	1,061
Vascular Stem/Progenitor Cells in Vessel Injury and Repair	Jiaping Tao, China	268	949
Rutaecarpine Inhibits Doxorubicin-Induced Oxidative Stress and Apoptosis by Activating AKT Signaling Pathway	Zi-Qi Liao, China	327	928
Valosin Containing Protein as a Specific Biomarker for Predicting the Development of Acute Coronary Syndrome and Its Complication	Chenchao Xu, China	153	915
NAP1L5 Promotes Nucleolar Hypertrophy and Is Required for Translation Activation During Cardiomyocyte Hypertrophy	Ningning Guo, China	275	857
Computed-Tomography as First-line Diagnostic Procedure in Patients With Out-of-Hospital Cardiac Arrest	John Adel, Germany	250	833
Association of Body Weight Variability With Progression of Coronary Artery Calcification in Patients With Predialysis Chronic Kidney Disease	Sang Heon Suh, South Korea	226	808
Clinical Characteristics for the Improvement of Cushing's Syndrome Complicated With Cardiomyopathy After Treatment With a Literature Review	Sisi Miao, China	250	761
Comparability of Heart Rate Turbulence Methodology: 15 Intervals Suffice to Calculate Turbulence Slope – A Methodological Analysis Using PhysioNet Data of 1,074 Patients	Valeria Blesius, Germany	91	691
Left Ventricular Strains and Myocardial Work in Adolescents With Anorexia Nervosa	Justine Paysal, France	158	686
A Novel Risk Score to Predict In-Hospital Mortality in Patients With Acute Myocardial Infarction: Results From a Prospective Observational Cohort	Lulu Li, China	119	591
Renal Denervation Attenuates Adverse Remodeling and Intramyocardial Inflammation in Acute Myocardial Infarction With Ischemia–Reperfusion Injury	Kun Wang, China	22	353

[#]*The order of appearance according to the number of views (on May 17, 2022).*

developed a new experimental method and provided a novel approach for imaging cardiovascular pathophysiological processes.

– *Identification of Novel Single-Nucleotide Variants With Potential of Mediating Malfunction of MicroRNA in Congenital Heart Disease* (Liu et al.).

Genetic mutation is the major cause of congenital heart defects (CHDs). This study identified miRNAs-mediated regulating on single-nucleotide variants from 3'-UTR of CHD-associated genes. This study suggests that miRNA-related gene regulation may be important but overlooked in the etiology of human congenital heart disease, suggesting that miRNA-related gene regulation should receive more attention in future CHD studies. The observations in this paper have important implications for clinicians.

– *Screening for Asymptomatic Coronary Artery Disease via Exercise Stress Testing in Patients With Type 2 Diabetes Mellitus: A Systematic Review and Meta-Analysis* (Dun, Wu et al.).

This systematic meta-analysis studied the exercise stress testing (ETS) screen program for asymptomatic cardiovascular diseases in type 2 diabetes mellitus, demonstrating its moderate sensitivity and specificity in the initial screening. ETS is a very promising tool due to the advantages of being non-invasive, relatively inexpensive, easily available in most centers, and the fact that it involves no radiation. Further additional studies are warranted to address the detailed flow and timing of ETS.

– *Relevance of Cor Pulmonale in COPD With and Without Pulmonary Hypertension: A Retrospective Cohort Study* (Yogeswaran et al.).

Pulmonary hypertension (PH), a complication of chronic obstructive pulmonary disease, is usually mild to moderate

but can be severe in some patients. This paper suggests that cor pulmonale is associated with disease severity, providing recommendations for clinical researchers that cor pulmonale might be used to predict PH-COPD prognosis.

– *Cognitive Impairment in Heart Failure: Landscape, Challenges, and Future Directions* (Yang et al.).

This review summarizes research advances in the screening, diagnosis, and management of cognitive impairment (CI) in patients with heart failure, as well as the latest preventive therapies. The prevalence of CI in heart failure patients adds a greater burden on the patients' poor prognosis and worsening life quality. This paper provides important directions for clinicians and researchers that future research addresses the knowledge gaps in the field forward CI in heart failure.

– *Diagnostic and Therapeutic Management of the Thoracic Outlet Syndrome. Review of the Literature and Report of an Italian Experience* (Camporese et al.).

This paper reviews the diagnostic, therapy, and management of Thoracic Outlet Syndrome (TOS). A report in Italy was also analyzed. It provides recommendations for clinical researchers in the treatment of TOS.

– *Cardiorespiratory Responses During High-Intensity Interval Training Prescribed by Rating of Perceived Exertion in Patients After Myocardial Infarction Enrolled in Early Outpatient Cardiac Rehabilitation* (Dun, Hammer et al.).

Exercise training is an effective strategy to improve cardiorespiratory and benefits the cardiovascular system (1, 2). This study suggests that high-intensity interval training can be effectively prescribed using perceived exertion in myocardial infarction patients during early outpatient cardiac rehabilitation. This paper also provides information for researchers and clinicians to choose appropriate exercise regimes in cardiovascular medicine.

– *Determination of Agrin and Related Proteins Levels as a Function of Age in Human Hearts* (Skeffington et al.).

A variety of strategies have been studied to promote endogenous proliferation of cardiomyocytes and promote cardiac injury repair (3, 4). This study suggests that agrin was gradually decreased in human right ventricular tissue with aging but not in mice. This study shows the differences between rodents and humans, prompting researchers to pay attention to species differences in future investigations.

– *Vascular Stem/Progenitor Cells in Vessel Injury and Repair* (Tao et al.).

This review summarizes the latest research progress on Vascular Stem/Progenitor Cells in vessel injury and repair. Stem/progenitor cells play an important role in the regeneration and recruitment of damaged vascular cells during vascular repair. This paper discusses potential future research directions for stem cell therapy and provides important ideas for researchers in this field.

– *Rutaecarpine Inhibits Doxorubicin-Induced Oxidative Stress and Apoptosis by Activating AKT Signaling Pathway* (Liao et al.).

Cardiotoxicity is one of the main adverse reactions of doxorubicin in clinical cancer therapy applications (5, 6). This paper studies the protective effects of *Rutaecarpine* in doxorubicin-induced cardiotoxicity. This finding provides a new potential therapeutic option for the treatment of doxorubicin-induced cardiotoxicity.

– *Valosin Containing Protein as a Specific Biomarker for Predicting the Development of Acute Coronary Syndrome and Its Complication* (Xu et al.).

This paper analyzes human serum samples and found that serum valosin containing protein (VCP) levels could act as a biomarker to predict the development of acute coronary syndrome (ACS) and its complication, ventricular dysfunction. Biomarker identification is important for disease diagnosis and treatment. This study could provide important information for clinicians and researchers that VCP should be involved with the diagnosis and treatment of ACS.

– *NAP1L5 Promotes Nucleolar Hypertrophy and Is Required for Translation Activation During Cardiomyocyte Hypertrophy* (Guo et al.).

Cardiac hypertrophy is a compensatory response of the heart to increased hemodynamic stress under various pressures, and if not relieved, it gradually develops into heart failure. This study showed the new role of Nap1l5 in translation control during the progression of cardiac hypertrophy. This paper provides a new potential therapeutic target for the treatment of cardiac hypertrophy and heart failure.

– *Computed-Tomography as First-line Diagnostic Procedure in Patients With Out-of-Hospital Cardiac Arrest* (Adel et al.).

Coronary angiography is critical in patients with suspected causes of coronary arrest. This study reported that computed tomography scans can improve outcomes after out-of-hospital cardiac arrest (OHCA). This observation provides information for clinicians and investigators that CT should be routinely included in the diagnostic workup of OHCA regardless of the presence or absence of an ischemic ECG patterns.

– *Association of Body Weight Variability With Progression of Coronary Artery Calcification in Patients With Predialysis Chronic Kidney Disease* (Suh et al.).

This paper explores the clinical significance of bodyweight variability (BWV) in patients with predialysis chronic kidney disease. It found that high BWV is independently associated with the progression of coronary artery calcification. This study provides important evidence of a high association between BWV and coronary artery calcification, and should be of concern to clinicians.

– *Clinical Characteristics for the Improvement of Cushing's Syndrome Complicated With Cardiomyopathy After Treatment With a Literature Review* (Miao et al.).

Cushing's syndrome (CS) complicated with cardiomyopathy is a rare clinical type with high mortality. This study retrospectively reviewed case reports from literature and demonstrated that cortisol played an important role, and hypercortisolemia can improve significantly after remission. This is an interesting finding, but the detailed mechanism needs further study.

– *Comparability of Heart Rate Turbulence Methodology: 15 Intervals Suffice to Calculate Turbulence Slope – A Methodological Analysis Using PhysioNet Data of 1074 Patients* (Blesius et al.).

This study focused on common variations in the number of intervals after ventricular premature contraction (VPC)

that are used to calculate turbulence slope (TS). Heart rate turbulence (HRT) is a characteristic heart rate pattern triggered by a VPC. This paper provides important information for clinicians that HRT occurred at early intervals after the VPC, whereas TS calculated from a later time interval reflected overall heart rate variability rather than differential responses to VPC.

– *Left Ventricular Strains and Myocardial Work in Adolescents With Anorexia Nervosa* (Paysal et al.).

Cardiovascular disease is a common complication of anorexia nervosa (AN). This study suggests that the cardiac function in AN patients was preserved. The paper outlines that global longitudinal strain was higher in AN patients, while the clinical significance required further investigation.

– *A Novel Risk Score to Predict In-Hospital Mortality in Patients With Acute Myocardial Infarction: Results From a Prospective Observational Cohort* (Li et al.).

This study developed a novel HAMIOT (Heart Failure after Acute Myocardial Infarction with Optimal Treatment) risk score to predict in-hospital mortality of MI patients using 10 highly predictive variables. Using this tool, the risk score is easily calculated and the variables are easily obtained during hospitalization, offering a useful method for clinicians to predict the risk of mortality.

– *Renal Denervation Attenuates Adverse Remodeling and Intramyocardial Inflammation in Acute Myocardial Infarction With Ischemia–Reperfusion Injury* (Wang et al.).

Acute myocardial infarction (AMI) is the most severe symptom of coronary artery disease and the leading cause of morbidity and mortality worldwide. This paper studied the protective effects on renal denervation (RDN) in myocardial ischemia/reperfusion (I/R) pigs. This data provides compelling evidence for the applicability and efficacy of RDN and suggests that this treatment strategy needs further development.

AUTHOR CONTRIBUTIONS

JX, PL, PC, and MA are topic editors of this special issue and contributed to writing and revising of this editorial. LW, JL, and YL drafted the editorial. All authors contributed to the article and approved the submitted version.

FUNDING

This work was supported by the grants from National Key Research and Development Project (2018YFE0113500 to JX), National Natural Science Foundation of China (82020108002 to JX), Innovation Program of Shanghai Municipal Education Commission (2017-01-07-00-09-E00042 to JX), the grant from Science and Technology Commission of Shanghai Municipality (21XD1421300 and 20DZ2255400 to JX), Natural Science Foundation of Shanghai (19ZR1474100 to LW), and the "Dawn" Program of Shanghai Education Commission (19SG34 to JX).

ACKNOWLEDGMENTS

The authors would like to thank the co-editor of this Research Topic, Dr. Chen Liu, for their dedication and involvement in all stages of the editorial process. The contribution of the reviewers of this Research Topic is greatly appreciated.

REFERENCES

1. Wang L, Wang J, Cretoiu D, Li G, Xiao J. Exercise-mediated regulation of autophagy in the cardiovascular system. *J Sport Health Sci.* (2020) 9:203–10. doi: 10.1016/j.jshs.2019.10.001
2. Bernardo BC, Ooi JYY, Weeks KL, Patterson NL, McMullen JR. Understanding key mechanisms of exercise-induced cardiac protection to mitigate disease: current knowledge and emerging concepts. *Physiol Rev.* (2018) 98:419–75. doi: 10.1152/physrev.00043.2016
3. Wu X, Wang L, Wang K, Li J, Chen R, Wu X, et al. ADAR2 increases in exercised heart and protects against myocardial infarction and doxorubicin-induced cardiotoxicity. *Mol Ther.* (2022) 30:400–14. doi: 10.1016/j.ymthe.2021.07.004
4. Vujic A, Lerchenmuller C, Wu TD, Guillermier C, Rabolli CP, Gonzalez E, et al. Exercise induces new cardiomyocyte generation in the adult mammalian heart. *Nat Commun.* (2018) 9:1659. doi: 10.1038/s41467-018-04083-1
5. Bao YW, Hua XW, Zeng J, Wu FG. Bacterial template synthesis of multifunctional nanospindles for glutathione detection and enhanced cancer-specific chemo-chemodynamic therapy. *Research (Wash D C).* (2020) 2020:9301215. doi: 10.34133/2020/9301215
6. Rochette L, Guenancia C, Gudjoncik A, Hachet O, Zeller M, Cottin Y, et al. Anthracyclines/trastuzumab: new aspects of cardiotoxicity and molecular mechanisms. *Trends Pharmacol Sci.* (2015) 36:326–48. doi: 10.1016/j.tips.2015.03.005

Conflict of Interest: The authors declare that the research was conducted in the absence of any commercial or financial relationships that could be construed as a potential conflict of interest.

frontiers in Cardiovascular Medicine

ORIGINAL RESEARCH
published: 10 September 2021
doi: 10.3389/fcvm.2021.739598

Identification of Novel Single-Nucleotide Variants With Potential of Mediating Malfunction of MicroRNA in Congenital Heart Disease

Wangkai Liu[1†], Liangping Cheng[2†], Ken Chen[3†], Jialing Wu[2†], Rui Peng[4], Yan-Lai Tang[1], Jinghai Chen[5], Yuedong Yang[3,6], Peiqiang Li[7*] and Zhan-Peng Huang[2,8,9*]*

[1] Department of Pediatrics, The First Affiliated Hospital, Sun Yat-sen University, Guangzhou, China, [2] Department of Cardiology, Center for Translational Medicine, Institute of Precision Medicine, The First Affiliated Hospital, Sun Yat-sen University, Guangzhou, China, [3] School of Data and Computer Science, Sun Yat-sen University, Guangzhou, China, [4] Obstetrics and Gynecology Hospital, Institute of Reproduction and Development, Fudan University, Shanghai, China, [5] Department of Cardiology, Provincial Key Lab of Cardiovascular Research, Second Affiliated Hospital, Institute of Translational Medicine, Zhejiang University School of Medicine, Hangzhou, China, [6] Key Laboratory of Machine Intelligence and Advanced Computing, Sun Yat-sen University, Ministry of Education, Guangzhou, China, [7] Institute of Genetics, School of Basic Medical Sciences, Lanzhou University, Lanzhou, China, [8] NHC Key Laboratory of Assisted Circulation, Sun Yat-sen University, Guangzhou, China, [9] National-Guangdong Joint Engineering Laboratory for Diagnosis and Treatment of Vascular Diseases, Guangzhou, China

OPEN ACCESS

Edited by:
Yan Zhang,
Peking University, China

Reviewed by:
Pingzhu Zhou,
Boston Children's Hospital and Harvard Medical School, United States
Donghui Zhang,
Hubei University, China

***Correspondence:**
Yuedong Yang
yangyd25@mail.sysu.edu.cn
Peiqiang Li
lipq@lzu.edu.cn
Zhan-Peng Huang
huangzhp27@mail.sysu.edu.cn

[†]These authors have contributed equally to this work

Specialty section:
This article was submitted to General Cardiovascular Medicine, a section of the journal Frontiers in Cardiovascular Medicine

Received: 11 July 2021
Accepted: 09 August 2021
Published: 10 September 2021

Citation:
Liu W, Cheng L, Chen K, Wu J, Peng R, Tang Y-L, Chen J, Yang Y, Li P and Huang Z-P (2021) Identification of Novel Single-Nucleotide Variants With Potential of Mediating Malfunction of MicroRNA in Congenital Heart Disease.
Front. Cardiovasc. Med. 8:739598.
doi: 10.3389/fcvm.2021.739598

Congenital heart defects (CHDs) represent the most common human birth defects. Our previous study indicates that the malfunction of microRNAs (miRNAs) in cardiac neural crest cells (NCCs), which contribute to the development of the heart and the connected great vessels, is likely linked to the pathogenesis of human CHDs. In this study, we attempt to further search for causative single-nucleotide variants (SNVs) from CHD patients that mediate the mis-regulating of miRNAs on their downstream target genes in the pathogenesis of CHDs. As a result, a total of 2,925 3′UTR SNVs were detected from a CHD cohort. In parallel, we profiled the expression of miRNAs in cardiac NCCs and found 201 expressed miRNAs. A combined analysis with these data further identified three 3′UTR SNVs, including NFATC1 c.*654C>T, FGFRL1 c.*414C>T, and CTNNB1 c.*729_*730insT, which result in the malfunction of miRNA-mediated gene regulation. The dysregulations were further validated experimentally. Therefore, our study indicates that miRNA-mediated gene dysregulation in cardiac NCCs could be an important etiology of congenital heart disease, which could lead to a new direction of diagnostic and therapeutic investigation on congenital heart disease.

Keywords: neural crest cells, single nucleotide variant, congenital heart defect, microRNA, post-transcriptional regulation

INTRODUCTION

Congenital heart defects (CHDs) represent the most common human birth defects. Among the spectrum of CHDs, malformations in the aortic arch artery and outflow tract comprise nearly 40% of CHDs, and ventricular septal defect is estimated to account for about 30% of CHDs. Previous studies have demonstrated that cardiac neural crest cells (NCCs), which migrate from the dorsal

neural tube of the embryo, contribute to the development of the ventricular septum and great arteries connected to the heart (1, 2).

Neural crest cells are a transient, migratory population of cells that give rise to myriad derivatives. Neural crest progenitors lie in the neural tube border. After the closure of the neural tube, these cells leave the neural tube and migrate throughout the body along the dorsoventral axis. They can differentiate into many cell types, including cardiac smooth muscle cells, chondrocytes, melanocytes, and neurons (3). Cranial NCCs, which originate from the dorsal neural tube between the middiencephalon and the caudal limit of somite 5, give rise to cranial ganglia, the maxilla, the mandible, and other structures such as muscle and cartilage of the head and neck (4). There is also a subset of NCCs defined as cardiac NCCs, which arise from the dorsal neural tube between the midotic placode and the caudal limit of somite 3. They migrate into pharyngeal arches 3, 4, and 6 (1). Cardiac NCCs populate the aorticpulmonary septum and conotruncal cushion and contribute to the smooth muscle of great vessels. Studies have revealed that several factors, including Wnt (5), Fgf (6), Tgf-β (7), BMP (8) families, and Shh (9), and their signaling pathways are critical to the development of neural crest derivatives. Disruption of these signaling pathways in NCCs in a mouse model leads to multiple developmental defects, which assemble CHDs found in human patients.

MicroRNAs (miRNAs), a large set of small non-coding RNAs, have been discovered in both animals and plants. These small RNAs post-transcriptionally regulate gene expression by destabilization and degradation of mRNA or translational repression (10). Previous studies from our lab and other groups have revealed that miRNAs play important roles in cell proliferation, differentiation, migration, and apoptosis during proper development and diseases (11–13). More importantly, our previous study demonstrated that globe disruption of the expression of miRNAs in NCCs resulted in a spectrum of CHDs in a mouse model (14), which indicates miRNAs could be involved in the pathogenesis of human CHDs. However, how miRNAs connect to CHDs in human patients remains largely unknown.

In this study, we searched for single-nucleotide variants (SNVs) from the 3′UTR region of genes, which could be associated with the CHD through a miRNA regulating mechanism, from a cohort of CHD. Combined with the profiling of miRNA expression in cardiac NCCs, we identified four novel SNVs with potential of interfering with miRNA-mediated gene dysregulation from 2,925 3′UTR SNVs in human patients. Experimental evidences support three out of four predictive miRNA-mediated mis-regulating. Therefore, our data suggest that the malfunction of miRNA is a new direction of mechanistic study and clinical application for congenital heart disease.

MATERIALS AND METHODS

Paired-End Sequencing for Detecting Single-Nucleotide Variants From Patients

Probes were designed to capture open reading frame (ORF), 3′UTR, 5′UTR, and 2KB of upstream promotor of selected genes on Agilent eArray platform against hg19 human genome. Genomic DNA from patients were sonicated into fragments. A DNA library from an individual was barcoded and used for generating the library for paired-end sequencing according to manufacturers' instruction for SureSelect XT Target Enrichment System for Illumina Paired-End Sequencing Library (Agilent). Reads were aligned in the reference genome with Burrows–Wheeler Aligner after filtering low quality reads. Single-nucleotide variants were then identified according to a previous report (15).

Annotating Variants

To obtain the information of SNVs residing in the transcripts, we employed ANNOVAR (version 2018-04-16) to annotate them against the refSeq gene annotation database (hg19_refGene.txt) (16). It should be noted that the deleted/inserted nucleotides in deletions/insertions could not be processed by ANNOVAR directly. We thereby manually converted them into 1-bp insertions or deletions by adding or deleting one more nucleotide after the position of variants to make them compatible with ANNOVAR. In this way, the gene and transcript annotations for all the variants were obtained.

Identifying Single-Nucleotide Variants in miRNA Binding Sites

We first obtained miRNA-transcript pairs predicted by the state-of-the-art MirTarget model (v4.0) from the miRDB database (17) to find which variants reside in the binding sites of miRNAs. Notably, the miRDB database only provides the predicted miRNA-transcript pairs. To solve the problem of lacking the exact location of binding sites of miRNAs, we identified the candidate binding sites based on the rule that canonical binding sites are reverse complementary to the second to eighth nucleotides in miRNA sequences (18, 19). The sequences of miRNAs were obtained from the miRBase database (20), and the sequences of transcripts (mature mRNA sequences) were extracted from the GENCODE GRCh37 reference genome (21).

MicroRNA Profiling With Mouse Embryonic Cardiac NCCs and Non-NCCs

Wnt1-Cre mice were crossed with Rosa-mTmG reporter mice to obtain green fluorescent protein (GFP)-labeled offspring. Green fluorescent protein-labeled embryonic day 10.5 embryos were collected for cardiac NCCs collection. Cardiac NCC-derived third, fourth, and sixth pharyngeal arches and outflow were dissected out and digested with collagenase. Single cells after digestion were subjected to fluorescence-activated cell sorting (FACS) on a MoFlo cell sorter. Some 5–10 $\times$ 10^5 GFP-positive NCCs and non-NCCs were obtained to yield 5–10 μg total RNA for further experiments. Total RNAs were then subjected to detection of global miRNA expression with Affymetrix microRNA microarray (miRNA 1.0) according to the manufacturer's protocol. Signals were obtained with Scanner 3000 Autoloader and analyzed with Expression Console^{TM} software.

Confirmation of SNVs With Singer Sequencing

To confirm the SNVs detected from the paired-end sequencing, primers were designed as follows for polymerase chain reaction (PCR) reaction to amplify the SNV-contained DNA fragments from patients: NFATC1-F: 5′-ACCCTCTGTATG AATGAAGAGA-3′; NFATC1-R: 5′-GCCTAGATATGTA CACACATGC-3′; FGFRL1-F: 5′-ACACAGATAAGCTGCC CAAATG-3′; FGFRL1-R: 5′-AAGGCAGCATTATCTGTGT GTC-3′; CTNNB1-F: 5′-AAGCAGGTGGATCTATTTCATG-3′; CTNNB1-R: 5′-TTACTTACCACCCTCACAAACC-3′; SMAD2-F: 5′-GTTAAAAGTAACATTCTGGGCC-3′; SMAD2-R: 5′-CCA GAAATACCTTAAACGTGTT-3′. Polymerase chain reaction products were then purified for Singer sequencing to confirm the SNV.

Constructs, Cell Culture, and Luciferase Reporter Assays

HEK293T cells were cultured in Dulbecco's modified essential medium (DMEM) supplemented with 10% fetal bovine serum (FBS) in a 5% CO_2 atmosphere at 37°C. For construction of the 3′UTR-luciferase reporter, the multiple cloning site of the pGL3-Control vector (Promega) was removed and placed downstream of the luciferase gene. Short 3′UTR fragments of human NFATC1, FGFRL1, CTNNB1, and SMAD2 genes containing predicted miRNA binding sites were cloned into the modified pGL3-Control vector, resulting in the constructs Luc-NFATC1-WT-UTR, Luc-FGFRL1-WT-UTR, Luc-CTNNB1-WT-UTR, and Luc-SMAD2-WT-UTR. Similarly, mutant 3′UTR fragments harboring SNVs detected in patients were cloned into the modified pGL3-Control vector, resulting in mutant constructs. Luciferase reporter, Renilla control luciferase reporter, and miRNA mimic were transfected into HEK293T cells with Lipofectamine (Invitrogen) reagents according to manufacturers' instruction. Twenty-four hours after transfection, cell extracts were prepared, and luciferase activity was determined with dual luciferase assay kit (Promega). For luciferase assay, normalized Firefly luciferase activity from triplicate samples in 12-well plates relative to Renilla luciferase activity was calculated.

Statistics

Values are reported as means ± SD unless indicated otherwise. The two-tailed Mann–Whitney U-test was used for two-group comparisons. Values of $p < 0.05$ were considered statistically significant.

Data Deposit

Genome-wide raw data in this study were deposited in the Gene Expression Omnibus (GEO) database of the National Center for Biotechnology Information (NCBI) (Series GSE178823).

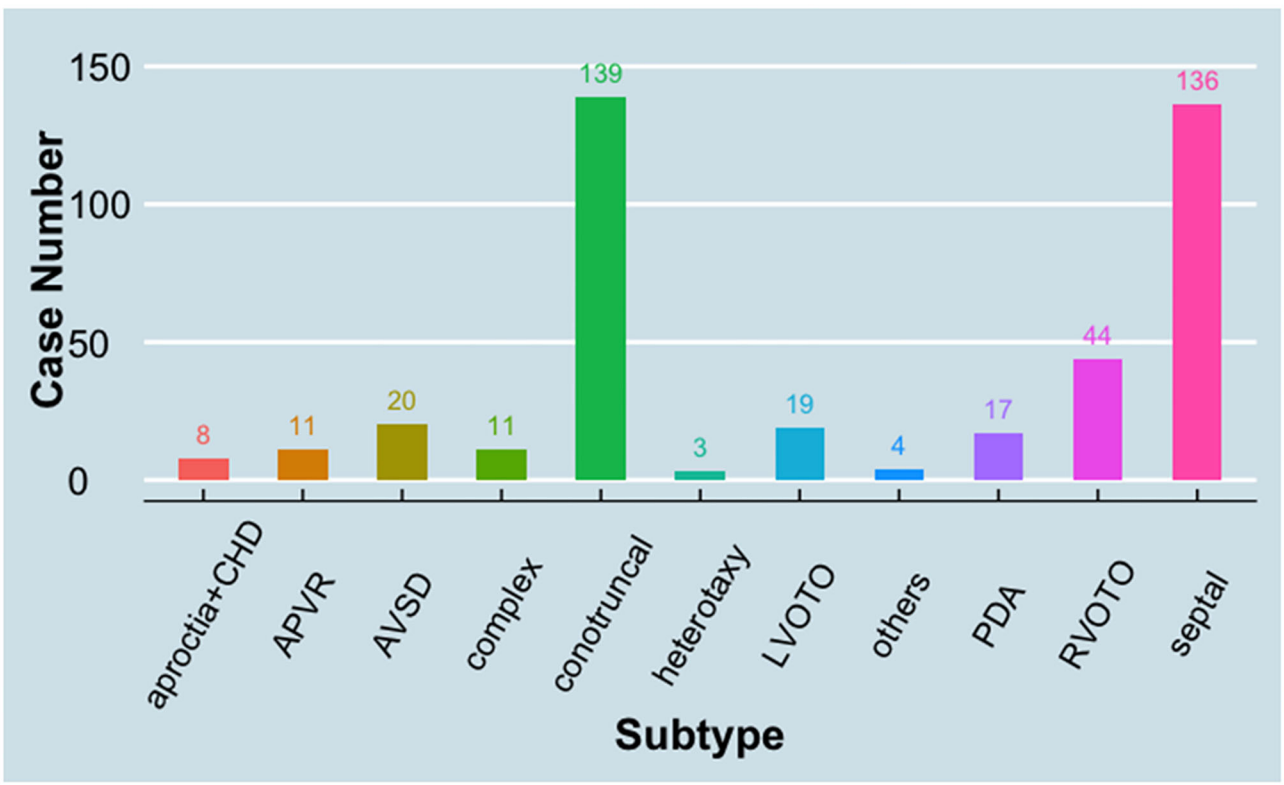

FIGURE 1 | Distribution of case subtypes in the study. APVR, anomalous pulmonary venous return; AVSD, atrioventricular septal defect; CHD, congenital heart defect; LVOTO, left ventricular outflow tract obstruction; PDA, patent ductus arteriosus; RVOTO, right ventricular outflow tract obstruction.

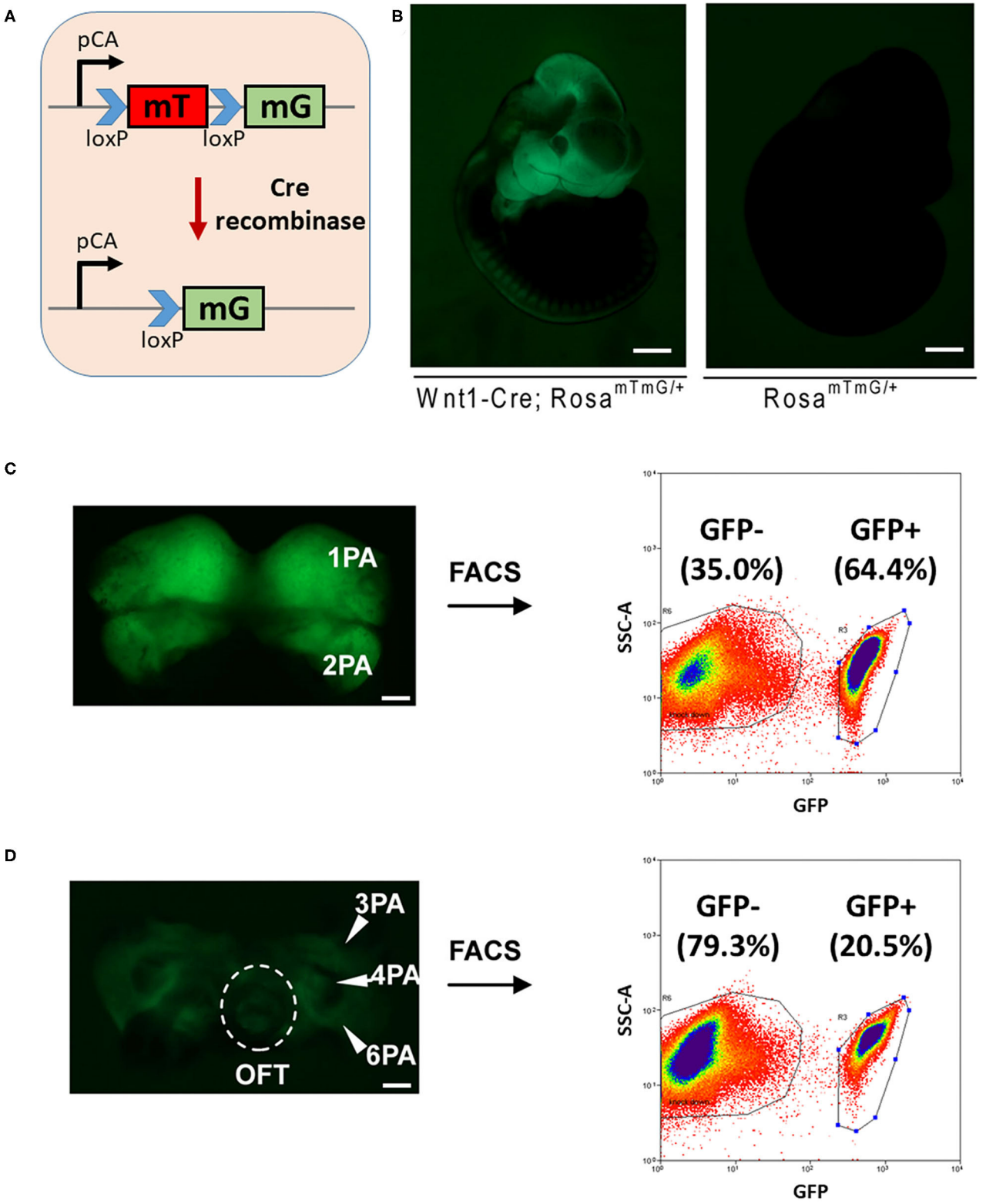

FIGURE 2 | FACS sorting of NCCs from mouse embryos for miRNA profiling. **(A)** A schematic figure shows the *Rosa-mTmG* reporter line. **(B)** *Wnt1-Cre*-mediated tissue-specific expression of GFP in E10.5 embryos. Bar = 500 μm. The cranial-NCCs-derived tissue **(C)** and cardiac-NCCs-derived tissue **(D)** were dissected out, digested, and sorted for both GFP positive NCCs and GFP negative cells. Bar = 100 μm. PA, pharyngeal arch; OFT, outflow tract; FACS, fluorescence-activated cell sorting; NCCs neural crest cells; miRNA, microRNA; GFP, green fluorescent protein.

Ethics Statement

All animal procedures were approved by the medical ethics committee of the First Affiliated Hospital, Sun Yat-sen University. All study protocols related to human patients were reviewed and approved by the local medical Ethics Committee. All individuals involved in the study have signed informed consent.

RESULTS

Detecting 2,925 Single-Nucleotide Variants in 3′UTR of Genes From a CHD Cohort

A cohort of CHDs, including 412 patients (case group) and 213 healthy controls (control group), were enrolled between August 2008 and February 2011 in Shanghai and Shandong, China (22). The average age of the case group vs. control is 2.9 ± 2.7 vs. 7.1 ± 3.7 years. The gender distribution of the case group vs. control group is 231 males and 186 females vs. 106 males and 107 females ($p > 0.05$). The congenital defects were classified into 11 groups according to a previous report (23) (**Figure 1**). Among these groups, conotruncal defect, septal defect, and right ventricular outflow tract obstruction (RVOTO) represent the majority of CHD cases and account for 33.7, 33.0, and 10.7% of the total cases, respectively. There is no family history for CHD in all cases. All patients possess non-comprehensive CHDs, except eight cases of heart defects combined with aproctia.

In order to detect SNVs from CHD patients, a total of 252 genes important for cardiac development were selected for detection of single-nucleotide polymorphisms (SNPs), including 149 genes of signaling transduction (WNT, TGFβ, Notch, ERBB, FGF, and Cilia-Hedgehog), 40 genes of transcriptional factors, 46 genes related to "Folate and one carbon metabolism," and 17 genes of structural proteins. Genomic DNA was chopped, and the regions of ORF, 3′UTR, 5′UTR, and 2KB of upstream promotor were captured by designed probes for paired-end sequencing (22). The sequencing yielded a set of data with average 38.1× coverage of targeted regions (38.7× in the control

TABLE 1 | Top 30 most abundant miRNAs in cardiac NCCs.

microRNAs	Relative expression in cardiac NCCs	Sequence	Cluster
miR-709	13.275	GGAGGCAGAGGCAGGAGGA	Not in cluster
miR-17-5p	12.214	CAAAGUGCUUACAGUGCAGGUAG	miR-17-92 cluster
miR-20a-5p	11.196	UAAAGUGCUUAUAGUGCAGGUAG	miR-17-92 cluster
miR-92a-3p	10.689	UAUUGCACUUGUCCCGGCCUG	miR-17-92 cluster
miR-690	10.651	AAAGGCUAGGCUCACAACCAAA	Not in cluster
miR-106a-5p	10.517	CAAAGUGCUAACAGUGCAGGUAG	miR-106a-363 cluster
miR-93-5p	10.374	CAAAGUGCUGUUCGUGCAGGUAG	miR-106b-25 cluster
miR-103-3p	10.313	AGCAGCAUUGUACAGGGCUAUGA	Not in cluster
miR-214-3p	10.203	ACAGCAGGCACAGACAGGCAGU	miR-199a-214 cluster
miR-18a-5p	10.201	UAAGGUGCAUCUAGUGCAGAUAG	miR-17-92 cluster
miR-99b-5p	10.120	CACCCGUAGAACCGACCUUGCG	miR-99b-125a cluster
miR-16-5p	9.909	UAGCAGCACGUAAAUAUUGGCG	miR-15-16 cluster
miR-20b-5p	9.805	CAAAGUGCUCAUAGUGCAGGUAG	miR-106a-363 cluster
miR-107-3p	9.764	AGCAGCAUUGUACAGGGCUAUCA	Not in cluster
miR-181a-5p	9.763	AACAUUCAACGCUGUCGGUGAGU	miR-181a/b cluster
miR-181b-5p	9.622	AACAUUCAUUGCUGUCGGUGGGU	miR-181a/b cluster
miR-130b-3p	9.573	CAGUGCAAUGAUGAAAGGGCAU	miR-130b-301b cluster
miR-19b-3p	9.526	UGUGCAAAUCCAUGCAAAACUGA	miR-17-92 cluster
miR-26a-5p	9.457	UUCAAGUAAUCCAGGAUAGGCU	Not in cluster
miR-199a-5p	9.437	CCCAGUGUUCAGACUACCUGUUC	miR-199a-214 cluster
miR-125a-5p	9.361	UCCCUGAGACCCUUUAACCUGUGA	miR-99b-125a cluster
miR-199a-3p	9.167	ACAGUAGUCUGCACAUUGGUUA	miR-199a-214 cluster
miR-125b-5p	9.158	UCCCUGAGACCCUAACUUGUGA	miR-99a-125b cluster
miR-199b-3p	9.150	ACAGUAGUCUGCACAUUGGUUA	miR-199b-3154 cluster
miR-130a-3p	9.132	CAGUGCAAUGUUAAAAGGGCAU	Not in cluster
miR-145a-5p	9.010	GUCCAGUUUUCCCAGGAAUCCCU	miR-143-145 cluster
let-7e-5p	8.949	UGAGGUAGGAGGUUGUAUAGUU	miR-99b-125a cluster
miR-106b-5p	8.858	UAAAGUGCUGACAGUGCAGAU	miR-106b-25 cluster
miR-541-5p	8.856	AAGGGAUUCUGAUGUUGGUCACACU	Mirg cluster
miR-1195	8.752	UGAGUUCGAGGCCAGCCUGCUCA	Not in cluster

miRNA, microRNA; NCCs, neural crest cells.

TABLE 2 | Top 30 most abundant miRNAs in non-NCCs.

microRNAs	Relative expression in non-NCCs	Sequence	Cluster
miR-709	13.38065	GGAGGCAGAGGCAGGAGGA	Not in cluster
miR-17-5p	12.06354	CAAAGUGCUUACAGUGCAGGUAG	miR-17-92 cluster
miR-690	11.37133	AAAGGCUAGGCUCACAACCAAA	Not in cluster
miR-99b-5p	10.85722	CACCCGUAGAACCGACCUUGCG	miR-99b-125a cluster
miR-20a-5p	10.73113	UAAAGUGCUUAUAGUGCAGGUAG	miR-17-92 cluster
miR-92a-3p	10.66891	UAUUGCACUUGUCCCGGCCUG	miR-17-92 cluster
miR-93-5p	10.25503	CAAAGUGCUGUUCGUGCAGGUAG	miR-106b-25 cluster
miR-103-3p	10.16812	AGCAGCAUUGUACAGGGCUAUGA	Not in cluster
miR-182-5p	10.07562	UUUGGCAAUGGUAGAACUCACACCG	miR-182-183 cluster
miR-16-5p	10.03377	UAGCAGCACGUAAAUAUUGGCG	miR-15-16 cluster
miR-106a-5p	9.949529	CAAAGUGCUAACAGUGCAGGUAG	miR-106a-363 cluster
miR-125a-5p	9.923689	UCCCUGAGACCCUUUAACCUGUGA	miR-99b-125a cluster
miR-107-3p	9.916354	AGCAGCAUUGUACAGGGCUAUCA	Not in cluster
miR-26a-5p	9.854673	UUCAAGUAAUCCAGGAUAGGCU	Not in cluster
miR-127-3p	9.778021	UCGGAUCCGUCUGAGCUUGGCU	miR-136-431 cluster
miR-145a-5p	9.766548	GUCCAGUUUUCCCAGGAAUCCCU	miR-143-145 cluster
miR-541-5p	9.682595	AAGGGAUUCUGAUGUUGGUCACACU	Mirg cluster
miR-214-3p	9.590926	ACAGCAGGCACAGACAGGCAGU	miR-199a-214 cluster
miR-181b-5p	9.429933	AACAUUCAUUGCUGUCGGUGGGU	miR-181a/b cluster
miR-130b-3p	9.42875	CAGUGCAAUGAUGAAAGGGCAU	miR-130b-301b cluster
miR-23b-3p	9.420783	AUCACAUUGCCAGGGAUUACC	miR-23b-24 cluster
miR-181a-5p	9.411454	AACAUUCAACGCUGUCGGUGAGU	miR-181a/b cluster
miR-125b-5p	9.3161	UCCCUGAGACCCUAACUUGUGA	miR-99a-125b cluster
miR-24-3p	9.314174	UGGCUCAGUUCAGCAGGAACAG	miR-23b-24 cluster
miR-18a-5p	9.269115	UAAGGUGCAUCUAGUGCAGAUAG	miR-17-92 cluster
let-7e-5p	9.152258	UGAGGUAGGAGGUUGUAUAGUU	miR-99b-125a cluster
miR-762	9.083022	GGGGCUGGGGCCGGGACAGAGC	Not in cluster
miR-1195	9.081083	UGAGUUCGAGGCCAGCCUGCUCA	Not in cluster
miR-130a-3p	9.068733	CAGUGCAAUGUUAAAAGGGCAU	Not in cluster
miR-351-5p	9.066365	UCCCUGAGGAGCCCUUUGAGCCUG	miR-322-351 cluster

miRNA, microRNA; NCCs, neural crest cells.

group vs. 38.0× in the case group). Targeted regions, which have an at least 4× coverage, is over 90% average in all samples (91.1% in control group vs. 91.6% in case group). As a result, 13,786 SNVs were identified in the analyses, including 11,486 SNVs in the case group and 5,870 SNVs in the control group. It is worthy to note that CHD patients have more rare SNVs, whose minor allele frequency (MAF) is <1%, than healthy controls. In detail, 66.2% (7,607) SNVs found in CHD patients are rare SNVs, while only 35.3% (2,072) SNVs found in healthy controls are rare ones. These data indicate that DNA mutation is a main contributor of pathogenesis of CHDs in the cohort.

In this study, we aim to explore the potential SNVs in 3′UTR interfering with the regulation between microRNA (miRNA) and mRNA in the pathogenesis of CHD. Therefore, a total of 2,925 SNVs located in 3′UTR of selected genes were obtained from the above identification and subjected to further analyses below.

Profiling MicroRNA Expression in Migrating Neural Crest Cells From Embryo

Cardiac NCCs, which are originated from the third, fourth, and sixth pharyngeal arches, populate the aorticpulmonary septum and conotruncal cushion and contribute to the smooth muscle of great vessels (1). Abnormal development in this group of cells often leads to ventricular septal defect and defects in great vessels connected to the heart (24). In order to study the potential interfering 3′UTR SNVs, which impair the regulation of miRNAs on their target mRNAs in CHD, we investigated the expression of miRNAs in cardiac NCCs. Rosa-mT-mG reporter mice (25), which possess *loxP* sites on either side of a membrane-targeted tdTomato (mT) cassette and express strong red fluorescence in all tissues and cell types, was bred with Wnt1-Cre mice (26). The presence of Cre recombinase will lead to the deletion of the mT cassette and the expression of the membrane-targeted GFP (mG) cassette located just downstream in NCCs (**Figures 2A,B**).

TABLE 3 | A list of differentially distributed miRNAs between cardiac NCCs and non-NCCs.

microRNAs	Relative expression level in cardiac NCCs	Relative expression level in non-NCCs	Log2 fold change
miR-363-3p	5.819	N.D.	N/A
miR-466f-3p	4.940	N.D.	N/A
miR-542-5p	4.983	N.D.	N/A
miR-125b-1-3p	5.203	N.D.	N/A
miR-214-5p	7.908	6.294	1.614
miR-199a-5p	9.437	7.979	1.459
miR-20b-5p	9.805	8.417	1.388
miR-500-3p	6.367	5.160	1.207
miR-199b-3p	9.150	8.032	1.118
miR-23b-3p	8.358	9.421	−1.062
miR-127-3p	8.636	9.778	−1.142
miR-329-3p	4.746	5.950	−1.204
miR-708-5p	5.460	6.693	−1.233
miR-126a-3p	6.073	7.600	−1.526
miR-31-5p	4.626	6.576	−1.951
miR-182-5p	5.056	10.076	−5.020

miRNA, microRNA; NCCs, neural crest cells; N.D., not detected; N/A, not applied.

Embryonic (E) 10.5 Rosa-mT-mG/Wnt1-Cre GFP positive embryos were collected. The first and second pharyngeal arches were dissected out, digested, and sorted for both GFP positive cranial NCCs and GFP negative control cells by FACS sorting, and similarly, the third, fourth, and sixth pharyngeal arches and outflow tract were collected for cardiac NCCs. As a result, around 65 and 20% GFP positive cells were obtained from cranial-NCCs-derived (first and second pharyngeal arches) and cardiac-NCCs-derived (third, fourth, and sixth pharyngeal arches and outflow tract) tissues, respectively (**Figures 2C,D**). RNAs from both GFP positive cardiac NCCs and GFP negative non-NCCs were then subjected to profile the expression of miRNA using the approach of miRNA microarray.

As a result, a total of 201 and 221 miRNAs were detected expressed in GFP positive cardiac NCCs and GFP negative non-NCCs, respectively (**Supplementary Table 1**). miRNA members of several miRNA clusters, such as miR-17-92 cluster, miR-106a-363 cluster, and miR-106b-25 cluster, are highly expressed in GFP positive cardiac NCCs (**Table 1**). To our surprise, a similar list for the 30 most abundant miRNAs is found in GFP negative non-NCCs (**Table 2**). It is worthy to note that members of miR-17-92 clusters, including miR-17, miR-18a, miR-20a, miR-19b, and miR-92a, are highly expressed in both GFP positive and negative cell population. Next, we asked which miRNAs are enriched and which miRNAs have less expression in GFP positive cardiac NCCs when compared with GFP negative non-NCCs. Nine enriched miRNAs and seven less expressed miRNAs were identified with a cutoff in expression fold change (Log2 Fold change >1 or <-1) (**Table 3**).

TABLE 4 | The distribution of four rare SNVs in control and case groups.

SNVs	Number in control group	Number in case group	Defects
NFATC1 c.*654C>T	0	1	Conotruncal (1)
FGFRL1 c.*414C>T	0	1	Conotruncal (1)
CTNNB1 c.*729_*730insT	0	1	Conotruncal (1)
SMAD2 c.*7061G>A	0	2	Conotruncal (1); septal (1)

SNV, single-nucleotide variant.

Prediction of Disease-Related SNVs in 3′UTR That Interfere With miRNA Function

Our previous study demonstrated that disruption of the expression of miRNA in NCCs leads to developmental defects in the heart and great arteries, which resemble defects observed in CHD patients (14). It indicated that miRNAs play critical roles in regulating cardiac NCCs in cardiac development. Therefore, we wonder whether certain SNVs identified above in 3′UTR connect to CHDs by interfering with the regulatory function of miRNA on gene expression. Since the seed sequence (nucleotides 2–8) of miRNA has been demonstrated to be critical to the pairing between miRNA and mRNA 3′UTR (27), we first searched miRDB (28), a miRNA target prediction database, for all predictions of miRNA-3′UTR pairing, in which the SNV is located in the sequence of 3′UTR pairing with seed sequence of miRNA. A total of 802 SNVs were identified being involved in such parings. The expression of miRNA in cardiac NCCs is the prerequisite of their regulatory function on gene expression. Next, we excluded the predictions associated with miRNAs not detected in our miRNA profiling in cardiac NCCs. Fifty-nine predictions remain in the list after selection. In the last step, we asked whether the remaining 59 SNVs were tightly associated with heart defects found in patients. As a result, four SNV candidates, NFATC1 c.*654C>T, FGFRL1 c.*414C>T, CTNNB1 c.*729_*730insT, and SMAD2 c.*7061G>A (**Figure 3A**), were identified in the analyses. miR-143-3p was predicted to mediate the c.*654C>T-induced dysregulation of transcriptional factor, NFATC1; the predictive regulation of fibroblast growth factor receptor like 1 by miR-210-3p is likely interfered by the mutation of c.*414C>T; an insertion of single thymine in the 3′UTR was predicted to lead to the mis-regulating of WNT signaling coactivator, beta-catenin (CTNNB1), by miR-214-3p; and Smad2, a key TGFβ signaling effector, was predicted to be mis-regulated by miR-145-5p because of the c.*7061G>A mutation (**Figure 3B**).

All these four mutations are rare SNVs. Surprisingly, all individuals with these SNVs are associated with conotruncal defect or septal defect based on the classification of CHD defects (**Table 4**), indicating these SNVs are likely causative mutations for congenital cardiac defects. Moreover, cardiac

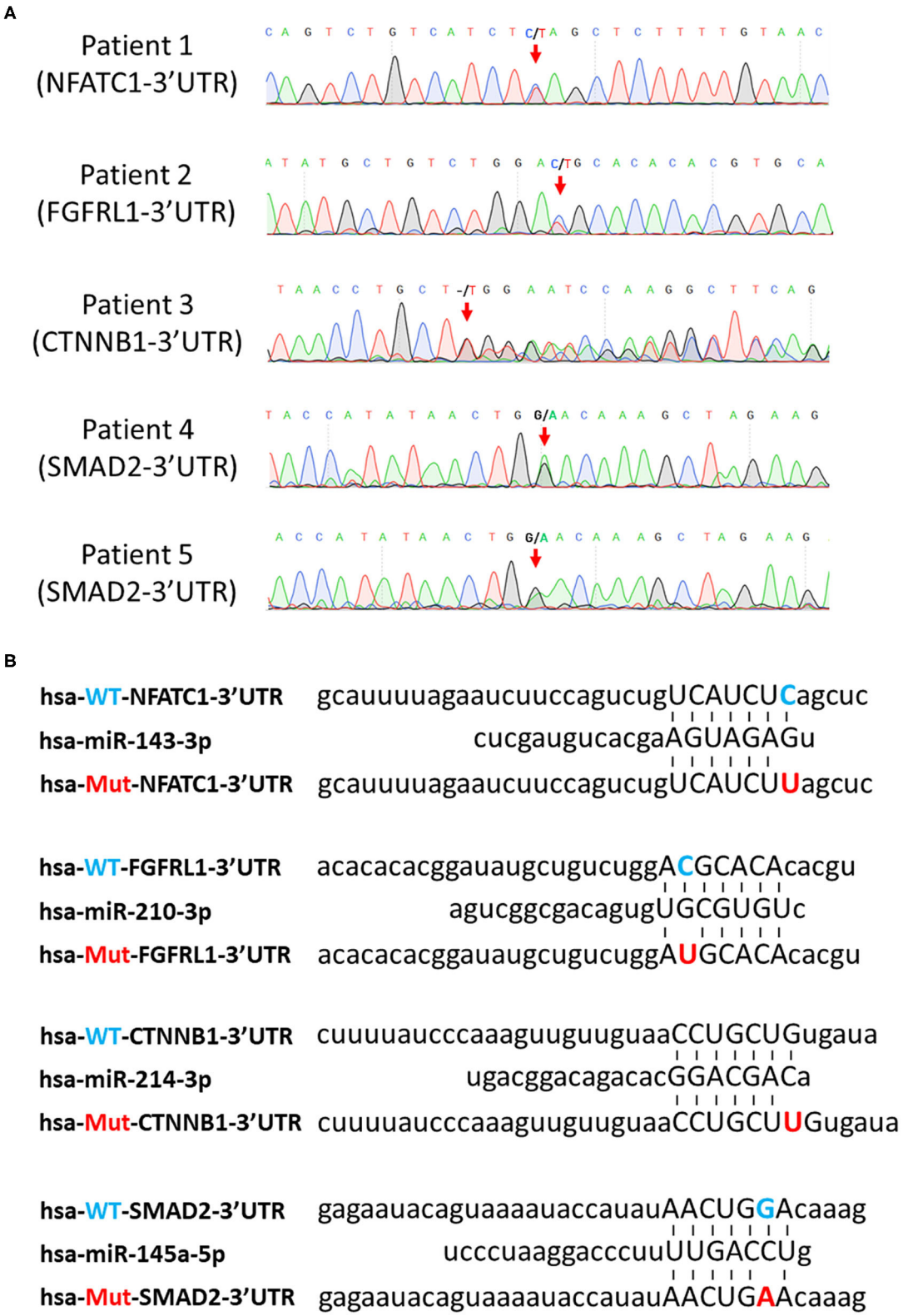

FIGURE 3 | Prediction of SNV-mediated miRNA mis-regulating on their downstream targets. **(A)** Confirmation of selected SNVs by Sanger sequencing. Red arrows indicate the SNVs. **(B)** Prediction of pairing between the seed sequence of miRNAs and the SNV-involved mRNA 3′UTR regions. Blue letters indicate wild-type nucleotides, and red letters indicate mutant nucleotides. SNV, single-nucleotide variant; miRNA, microRNA.

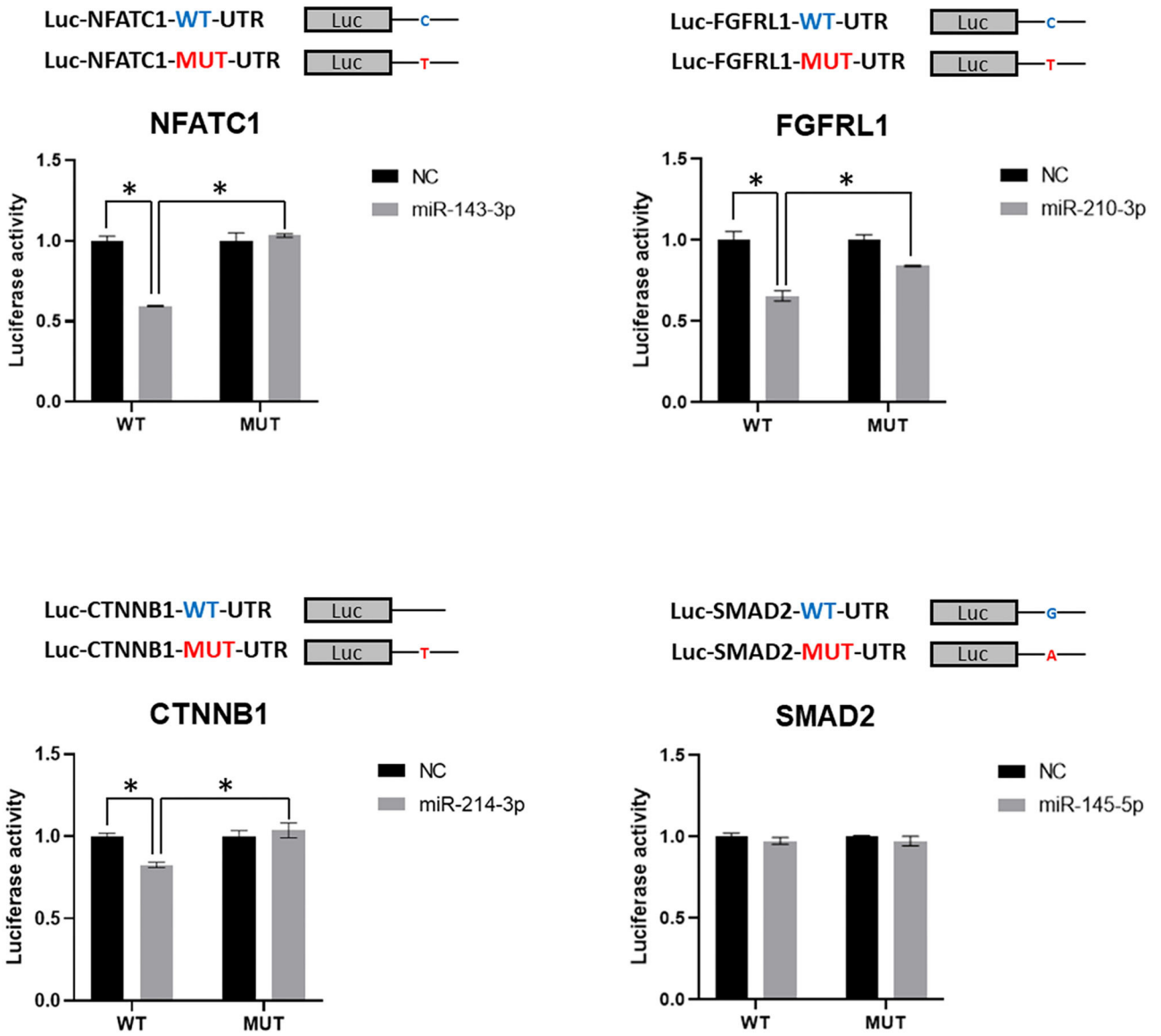

FIGURE 4 | Validation of miRNA-mediated dysregulation induced by SNVs. Luciferase reporter assay was applied in the validation. Luciferase reporters with wild-type or mutant 3′UTR of selected genes were co-transfected with predicted miRNA mimics, which was predicted to target the tested 3′UTR of gene, or negative control (NC), and luciferase activity was determined. Values are presented as relative luciferase activity ± SD relative to the luciferase activity of reporter co-transfected with negative control mimics. Data were obtained from at least three independent experiments. miRNA, microRNA; SNV, single-nucleotide variant. *indicates $p < 0.05$.

NCCs contribute to the development of conotruncus and ventricular septa; the observation of conotruncal or septal defects suggests the developmental defects of cardiac NCCs in these SNV-harbored patients. Since the pairing between mRNA 3′UTR and the seed sequence of miRNA is critical to the regulatory function of miRNA on gene regulation, the pairing between mutant 3′UTRs and miRNAs (**Figure 3B**) indicates that identified SNVs could induce the dys-regulation of NFATC1, FGFRL1, CTNNB1, and SMAD2 and further disturb the normal development of cardiac NCCs, which leads to the cardiac defects in patients.

Experimental Validation of miRNA-Mediated Gene Dysregulation Induced by SNVs

To further confirm the miRNA-mediated gene dysregulation induced by SNVs, wild-type, and mutant 3′UTRs, which harbor the same point mutations as detected SNVs, were cloned into the 3′UTR region of luciferase reporter. The predicted regulatory miRNA was then tested for the repressive effect on luciferase activity of wild-type and mutant reporters in a luciferase assay. As shown in **Figure 4**, miR-143-3p, miR-210-3p, and miR-214-3p inhibited the activities of wild-type Luc-NFATC1-WT-UTR,

Luc-FGFR1-WT-UTR, and Luc-CTNNB1-WT-UTR reporters, respectively, which is consistent with the prediction. However, miR-145-5p, which was predicted to bind to 3′UTR of SMAD2, showed no repression on wild-type Luc-SMAD2-WT-UTR reporter. More importantly, the repressive effects of miR-143-3p, miR-210-3p, and miR-214-3p on NFATC1, FGFR1, and CTNNB1 3′UTR luciferase reporters were diminished when the identified SNV was introduced (**Figure 4**). It is worthy to note that the mutation of NFATC1 c.*654C>T and CTNNB1 c.*729_*730insT, which similarly disrupts the pairing between the second nucleotide of miRNA (the first nucleotide of the miRNA seed sequence) and 3′UTR, totally abolished the regulatory function of miR-143-3p on NFATC1 and miR-214-3p on CTNNB1, respectively. Therefore, our data confirmed that three CHD-associated SNVs identified in this study, NFATC1 c.*654C>T, FGFRL1 c.*414C>T, and CTNNB1 c.*729_*730insT, induce the miRNA-mediated gene dysregulation.

DISCUSSION

The etiology of congenital heart disease is complex. Although environmental factors are involved in the pathogenesis of CHDs, genetic mutation—both inherited mutation and de novo mutation—is the major cause of CHDs. Huge efforts have been spent on investigating the genetic cause responsible for the CHDs we observed, and some mutations have been successfully linked to syndromes associated with CHDs. For example, the deletion of 3 million base pairs on one copy of chromosome 22 results in DiGeorge syndrome in human patients (29). Genetic studies have linked ∼50% of Noonan syndrome to mutations in PTPN11 gene, which encodes SHP-2 protein, an SH2 domain-containing, non-receptor tyrosine phosphatase (PTPase) essential for cellular proliferation, differentiation, and migration (30). However, many CHD cases without apparent linkage to environmental interfering remains idiopathic. miRNAs have been demonstrated to be closely associated with different human diseases, such as cancer, cardiovascular diseases, hepatitis, diabetes, etc. (31). It is not surprising that miRNAs are involved in the pathogenesis of CHDs, which is supported by our previous report (14). In this study, we further showed that three CHD-associated SNVs in 3′UTR could lead to the miRNA-mediated gene dysregulation. More cases should be involved in the future to demonstrate how important this type of mutation is in the cause of human CHDs. Previous studies have shown that precise control of key signaling cascade activity is critical to proper embryonic development (32), including the induction of neural crest (33). Disease-associated SNVs in 3′UTR of these tightly controlled genes could break the balance due to the dysregulation by miRNAs even though the mutation is only present in one allele, which results in the situation that 50% of mRNAs for one gene are mutant in theory and have abnormal miRNA-mediated regulation. The detailed mechanism of this miRNA-mediated gene dysregulation in cardiac developmental defects needs to be further investigated *in vivo*. For example, mutations identified from patients in this study should be introduced in a mouse model to further confirm their CHD-causative effect, and the miRNA-mediated molecular mechanism of CHD should be further validated with these genetically engineered mouse embryo *in vivo* as well.

Several studies indicated that SNVs in human CHD patients could lead to miRNA-mediated gene dysregulation. For example, +1,905G>A in 3′UTR region of methionine synthase (MTR) gene, which is associated with CHDs, was reported to result in dysregulation of MTR by miR-485, miR-608, and miR-1293 (34). Point mutation of TBX5 3′UTR sequence, TBX5 c.*1101C4T, is closely associated with septation defects in human patients and leads to miR-9 and miR-30a-mediated dysregulation of TBX5 expression (35). The expression of these miRNAs during cardiac development is not well-characterized. The majority of conotruncal defect and ventricular septal defect are very likely linked to the defect of cardiac NCCs. The migration and differentiation of cardiac NCCs is transient and happens in the early developmental stage of the embryo. Therefore, it is challenging to obtain cardiac NCCs from the human embryo. Due to the high conservation of mammalian embryo development, we obtained the expression profile of miRNAs from mouse cardiac NCCs and focused on the miRNAs with high expression level in this study. Three rare SNVs were identified with the great potential of disrupting the normal miRNA-mediated gene regulation in our study. More importantly, these SNVs are all associated with cardiac NCCs-involved conotruncal defect and septal defect in human patients. Therefore, our study indicates that miRNA-mediated gene dysregulation in cardiac NCCs could be an important etiology of congenital heart disease.

Due to the limitation of our sequencing strategy, only ∼250 protein-coding genes were studied in this study, although most of them are considered important genes for cardiac development. Since protein-coding genes are widely regulated by miRNAs (27), more genes, if not all, should be investigated with the whole genome sequencing data in the future. Our study provides a cue that miRNA-involved gene regulation might be important but overlooked in the etiological study of human congenital heart disease. Mutations of miRNA coding sequence and sequence regulating the transcription of miRNA primary transcript or the processing of miRNA precursor warrant further investigation in human patients with CHD.

DATA AVAILABILITY STATEMENT

The datasets presented in this study can be found in online repositories. The names of the repository/repositories and accession number(s) can be found below: NCBI (accession: GSE178823).

ETHICS STATEMENT

The studies involving human participants were reviewed and approved by the medical ethics committee of Children's Hospital of Fudan University. Written informed consent to participate in this study was provided by the participants' legal guardian/next of kin. The animal study was reviewed and approved by the

medical ethics committee of the First Affiliated Hospital, Sun Yet-sen University.

AUTHOR CONTRIBUTIONS

WL, LC, KC, JW, and Z-PH prepared the manuscript. WL, LC, RP, and Y-LT analyzed the clinical and sequencing data from the cohort. KC performed related bioinformatic analyses. JW performed cloning experiments and luciferase assay. JC provided sorted NCCs from mouse embryo. YY supervised the process of bioinformatic analyses. PL supervised the analyses of clinical and sequencing data for the cohort. Z-PH drafted the final version of the manuscript. All authors read and approved the final manuscript.

FUNDING

This work was supported by grants from the Guangdong Science and Technology Department (2018A050506026 to Z-PH and 2019B030316024), the Science and Technology Planning Project of Guangzhou, China (202002020064 to WL), the China Postdoctoral Science Foundation (2020M672981 to LC), the National Natural Science Foundation of China (81873463 to Z-PH and 81970227 to JC), the Guangdong Basic and Applied Basic Research Foundation (2019B151502003 to Z-PH), the Fundamental Research Funds for the Central Universities (20ykzd06 to Z-PH), and the donation for scientific research from the Terry Fox Foundation.

ACKNOWLEDGMENTS

We thank members of the Huang laboratory for advice and technical support.

SUPPLEMENTARY MATERIAL

The Supplementary Material for this article can be found online at: https://www.frontiersin.org/articles/10.3389/fcvm.2021.739598/full#supplementary-material

REFERENCES

1. Jiang X, Rowitch DH, Soriano P, McMahon AP, Sucov HM. Fate of the mammalian cardiac neural crest. *Development.* (2000) 127:1607–16. doi: 10.1242/dev.127.8.1607
2. Jiang X, Choudhary B, Merki E, Chien KR, Maxson RE, Sucov HM. Normal fate and altered function of the cardiac neural crest cell lineage in retinoic acid receptor mutant embryos. *Mech Dev.* (2002) 117:115–22. doi: 10.1016/S0925-4773(02)00206-X
3. Knecht AK, Bronner-Fraser M. Induction of the neural crest: a multigene process. *Nat Rev Genet.* (2002) 3:453–61. doi: 10.1038/nrg819
4. Trainor PA, Krumlauf R. Patterning the cranial neural crest: hindbrain segmentation and Hox gene plasticity. *Nat Rev Neurosci.* (2000) 1:116–24. doi: 10.1038/35039056
5. Dorsky RI, Moon RT, Raible DW. Control of neural crest cell fate by the Wnt signalling pathway. *Nature.* (1998) 396:370–3. doi: 10.1038/24620
6. Trainor PA, Ariza-McNaughton L, Krumlauf R. Role of the isthmus and FGFs in resolving the paradox of neural crest plasticity and prepatterning. *Science.* (2002) 295:1288–91. doi: 10.1126/science.1064540
7. Ito Y, Yeo JY, Chytil A, Han J, Bringas PJr, Nakajima A, et al. Conditional inactivation of Tgfbr2 in cranial neural crest causes cleft palate and calvaria defects. *Development.* (2003) 130:5269–80. doi: 10.1242/dev.00708
8. Kanzler B, Foreman RK, Labosky PA, Mallo M. BMP signaling is essential for development of skeletogenic and neurogenic cranial neural crest. *Development.* (2000) 127:1095–104. doi: 10.1242/dev.127.5.1095
9. Passman JN, Dong XR, Wu SP, Maguire CT, Hogan KA, Bautch VL, et al. A sonic hedgehog signaling domain in the arterial adventitia supports resident Sca1+ smooth muscle progenitor cells. *Proc Natl Acad Sci USA.* (2008) 105:9349–54. doi: 10.1073/pnas.0711382105
10. Bartel DP. MicroRNAs: genomics, biogenesis, mechanism, and function. *Cell.* (2004) 116:281–97. doi: 10.1016/S0092-8674(04)00045-5
11. Chen JF, Mandel EM, Thomson JM, Wu Q, Callis TE, Hammond SM, et al. The role of microRNA-1 and microRNA-133 in skeletal muscle proliferation and differentiation. *Nat Genet.* (2006) 38:228–33. doi: 10.1038/ng1725
12. He L, Thomson JM, Hemann MT, Hernando-Monge E, Mu D, Goodson S, et al. A microRNA polycistron as a potential human oncogene. *Nature.* (2005) 435:828–33. doi: 10.1038/nature03552
13. Ma L, Teruya-Feldstein J, Weinberg RA. Tumour invasion and metastasis initiated by microRNA-10b in breast cancer. *Nature.* (2007) 449:682–8. doi: 10.1038/nature06174
14. Huang ZP, Chen JF, Regan JN, Maguire CT, Tang RH, Dong XR, et al. Loss of microRNAs in neural crest leads to cardiovascular syndromes resembling human congenital heart defects. *Arterioscler Thromb Vasc Biol.* (2010) 30:2575–86. doi: 10.1161/ATVBAHA.110.213306
15. Wang Y, Lu J, Yu J, Gibbs RA, Yu F. An integrative variant analysis pipeline for accurate genotype/haplotype inference in population NGS data. *Genome Res.* (2013) 23:833–42. doi: 10.1101/gr.146084.112
16. Wang K, Li M, Hakonarson H. ANNOVAR: functional annotation of genetic variants from high-throughput sequencing data. *Nucleic Acids Res.* (2010) 38:e164. doi: 10.1093/nar/gkq603
17. Liu W, Wang X. Prediction of functional microRNA targets by integrative modeling of microRNA binding and target expression data. *Genome Biol.* (2019) 20:18. doi: 10.1186/s13059-019-1629-z
18. Friedman RC, Farh KK, Burge CB, Bartel DP. Most mammalian mRNAs are conserved targets of microRNAs. *Genome Res.* (2009) 19:92–105. doi: 10.1101/gr.082701.108
19. Nielsen CB, Shomron N, Sandberg R, Hornstein E, Kitzman J, Burge CB. Determinants of targeting by endogenous and exogenous microRNAs and siRNAs. *RNA.* (2007) 13:1894–910. doi: 10.1261/rna.768207
20. Kozomara A, Birgaoanu M, Griffiths-Jones S. miRBase: from microRNA sequences to function. *Nucleic Acids Res.* (2019) 47:D155–62. doi: 10.1093/nar/gky1141
21. Frankish A, Diekhans M, Ferreira AM, Johnson R, Jungreis I, Loveland J, et al. GENCODE reference annotation for the human and mouse genomes. *Nucleic Acids Res.* (2019) 47:D766–73. doi: 10.1093/nar/gky955
22. Zhao JY, Yang XY, Gong XH, Gu ZY, Duan WY, Wang J, et al. Functional variant in methionine synthase reductase intron-1 significantly increases the risk of congenital heart disease in the Han Chinese population. *Circulation.* (2012) 125:482–90. doi: 10.1161/CIRCULATIONAHA.111.050245
23. Botto LD, Lin AE, Riehle-Colarusso T, Malik S, Correa A, National Birth Defects Prevention S. Seeking causes: classifying and evaluating congenital heart defects in etiologic studies. *Birth Defects Res A Clin Mol Teratol.* (2007) 79:714–27. doi: 10.1002/bdra.20403
24. Kirby ML, Waldo KL. Role of neural crest in congenital heart disease. *Circulation.* (1990) 82:332–40. doi: 10.1161/01.CIR.82.2.332
25. Muzumdar MD, Tasic B, Miyamichi K, Li L, Luo L. A global double-fluorescent Cre reporter mouse. *Genesis.* (2007) 45:593–605. doi: 10.1002/dvg.20335
26. Danielian PS, Muccino D, Rowitch DH, Michael SK, McMahon AP. Modification of gene activity in mouse embryos *in utero* by

a tamoxifen-inducible form of Cre recombinase. *Curr Biol.* (1998) 8:1323–6. doi: 10.1016/S0960-9822(07)00562-3
27. Lewis BP, Burge CB, Bartel DP. Conserved seed pairing, often flanked by adenosines, indicates that thousands of human genes are microRNA targets. *Cell.* (2005) 120:15–20. doi: 10.1016/j.cell.2004.12.035
28. Chen Y, Wang X. miRDB: an online database for prediction of functional microRNA targets. *Nucleic Acids Res.* (2020) 48:D127–31. doi: 10.1093/nar/gkz757
29. McDermid HE, Morrow BE. Genomic disorders on 22q11. *Am J Hum Genet.* (2002) 70:1077–88. doi: 10.1086/340363
30. Tartaglia M, Mehler EL, Goldberg R, Zampino G, Brunner HG, Kremer H, et al. Mutations in PTPN11, encoding the protein tyrosine phosphatase SHP-2, cause Noonan syndrome. *Nat Genet.* (2001) 29:465–8. doi: 10.1038/ng772
31. Rupaimoole R, Slack FJ. MicroRNA therapeutics: towards a new era for the management of cancer and other diseases. *Nat Rev Drug Discov.* (2017) 16:203–22. doi: 10.1038/nrd.2016.246
32. Kiecker C, Niehrs C. A morphogen gradient of Wnt/beta-catenin signalling regulates anteroposterior neural patterning in Xenopus. *Development.* (2001) 128:4189–201. doi: 10.1242/dev.128.21.4189
33. Aybar MJ, Mayor R. Early induction of neural crest cells: lessons learned from frog, fish and chick. *Curr Opin Genet Dev.* (2002) 12:452–8. doi: 10.1016/S0959-437X(02)00325-8
34. Zhao JY, Qiao B, Duan WY, Gong XH, Peng QQ, Jiang SS, et al. Genetic variants reducing MTR gene expression increase the risk of congenital heart disease in Han Chinese populations. *Eur Heart J.* (2014) 35:733–42. doi: 10.1093/eurheartj/eht221
35. Wang F, Liu D, Zhang RR, Yu LW, Zhao JY, Yang XY, et al. A TBX5 3'UTR variant increases the risk of congenital heart disease in the Han Chinese population. *Cell Discov.* (2017) 3:17026. doi: 10.1038/celldisc.2017.26

Conflict of Interest: The authors declare that the research was conducted in the absence of any commercial or financial relationships that could be construed as a potential conflict of interest.

Publisher's Note: All claims expressed in this article are solely those of the authors and do not necessarily represent those of their affiliated organizations, or those of the publisher, the editors and the reviewers. Any product that may be evaluated in this article, or claim that may be made by its manufacturer, is not guaranteed or endorsed by the publisher.

frontiers in Cardiovascular Medicine

METHODS
published: 25 October 2021
doi: 10.3389/fcvm.2021.739549

EMbedding and Backscattered Scanning Electron Microscopy: A Detailed Protocol for the Whole-Specimen, High-Resolution Analysis of Cardiovascular Tissues

*Rinat A. Mukhamadiyarov, Leo A. Bogdanov, Tatiana V. Glushkova, Daria K. Shishkova, Alexander E. Kostyunin, Vladislav A. Koshelev, Amin R. Shabaev, Alexey V. Frolov, Alexander N. Stasev, Anton A. Lyapin and Anton G. Kutikhin**

Department of Experimental Medicine, Research Institute for Complex Issues of Cardiovascular Diseases, Kemerovo, Russia

OPEN ACCESS

Edited by:
Manvendra K. Singh, Duke-NUS Medical School, Singapore

Reviewed by:
Maximillian A. Rogers, Brigham and Women's Hospital and Harvard Medical School, United States
Ming-Jie Wang, Fudan University, China

***Correspondence:**
Anton G. Kutikhin
antonkutikhin@gmail.com

Specialty section:
This article was submitted to General Cardiovascular Medicine, a section of the journal Frontiers in Cardiovascular Medicine

Received: *11 July 2021*
Accepted: *21 September 2021*
Published: *25 October 2021*

Citation:
Mukhamadiyarov RA, Bogdanov LA, Glushkova TV, Shishkova DK, Kostyunin AE, Koshelev VA, Shabaev AR, Frolov AV, Stasev AN, Lyapin AA and Kutikhin AG (2021) EMbedding and Backscattered Scanning Electron Microscopy: A Detailed Protocol for the Whole-Specimen, High-Resolution Analysis of Cardiovascular Tissues. Front. Cardiovasc. Med. 8:739549. doi: 10.3389/fcvm.2021.739549

Currently, an ultrastructural analysis of cardiovascular tissues is significantly complicated. Routine histopathological examinations and immunohistochemical staining suffer from a relatively low resolution of light microscopy, whereas the fluorescence imaging of plaques and bioprosthetic heart valves yields considerable background noise from the convoluted extracellular matrix that often results in a low signal-to-noise ratio. Besides, the sectioning of calcified or stent-expanded blood vessels or mineralised heart valves leads to a critical loss of their integrity, demanding other methods to be developed. Here, we designed a conceptually novel approach that combines conventional formalin fixation, sequential incubation in heavy metal solutions (osmium tetroxide, uranyl acetate or lanthanides, and lead citrate), and the embedding of the whole specimen into epoxy resin to retain its integrity while accessing the region of interest by grinding and polishing. Upon carbon sputtering, the sample is visualised by means of backscattered scanning electron microscopy. The technique fully preserves calcified and stent-expanded tissues, permits a detailed analysis of vascular and valvular composition and architecture, enables discrimination between multiple cell types (including endothelial cells, vascular smooth muscle cells, fibroblasts, adipocytes, mast cells, foam cells, foreign-body giant cells, canonical macrophages, neutrophils, and lymphocytes) and microvascular identities (arterioles, venules, and capillaries), and gives a technical possibility for quantitating the number, area, and density of the blood vessels. Hence, we suggest that our approach is capable of providing a pathophysiological insight into cardiovascular disease development. The protocol does not require specific expertise and can be employed in virtually any laboratory that has a scanning electron microscope.

Keywords: cardiovascular research, biocompatibility testing, calcification, mineral deposits, electron microscopy, sample preparation, epoxy resin, grinding and polishing

INTRODUCTION

In spite of the variety of approaches for ultrastructural pathology, which generally include the preparation of formalin-fixed paraffin-embedded, snap-frozen, or fresh tissue specimens further stained with specific dyes or chromogen, fluorescent, or gold-labelled antibodies and visualised by light, epifluorescence, confocal, or electron microscopy (1–3), the processing and imaging of calcified or stent-expanded cardiovascular tissue remain poor (4). The density of mineral deposits and metal implants significantly differs from that of the bulk tissue and, hence, tissue integrity is heavily disrupted through the conventional sectioning procedure. Yet, a proper investigation of atherosclerotic plaques, dysfunctional heart valves, and failed bioprosthetic heart valves all frequently undergoing pathological mineralisation ultimately requires retained tissue architecture and the biocompatibility testing of the metal alloys for stent manufacturing (5, 6).

Another major issue in cardiovascular pathology is that the high-precision and high-throughput analysis of microcirculation demands a magnification exceeding values obtainable by means of light microscopy (LM, 400-fold) and an image acquisition rate superior to confocal microscopy (which is commonly limited to 630-fold magnification, being additionally confounded by antigen expression features and background staining) (7, 8). Transmission electron microscopy provides a perfect magnification range, but the sample preparation is technically challenging, is inevitably associated with a tremendous reduction of the sample amount, and does not permit the representative serial sectioning of the vessels (9). Hence, the existing techniques for the visualisation of microcirculation have considerable shortcomings and also involve sectioning prior to the staining, precluding an analysis of the vascular networks associated with extraskeletal mineral deposits.

An established standard for the evaluation of small-calibre vessels includes immunostaining for endothelial marker CD31 in combination with nuclear counterstaining (10). However, the geometry of microvessels is susceptible to sectioning and staining and often becomes irreversibly altered during these procedures (in particular in calcified or stent-expanded tissues) that complicates the evaluation of microcirculation. Immunostaining for vascular smooth muscle cell markers, such as the smooth muscle myosin heavy chain, alpha smooth muscle actin, or smoothelin, better delineates microvessel contours but does not detect the capillaries, which solely consist of endothelial cells. Therefore, despite excellent specificity and compatibility with recent tools for automated image analysis, immunostaining lacks sensitivity in discriminating microvasculature from surrounding tissue.

Here we developed and validated a conceptually novel histological approach that couples whole-specimen formalin fixation with heavy metal staining (i.e., incubation in osmium tetroxide, uranyl acetate, and lead citrate solutions), epoxy resin embedding, grinding, and polishing of epoxy resin blocks, and backscattered scanning electron microscopy (BSEM). As this technique fully retains the integrity of calcified or stent-expanded tissues and combines high-magnification visualisation, rapid image acquisition, and the possibility to perform elemental analysis, we suggest it as an optimal solution for cardiovascular research, especially for studies on calcification and microcirculation.

Development of the Protocol

To design this protocol, we combined a classical tissue fixation in neutral phosphate buffered formalin—which, in this setting, is not restricted to 24 h as in the case with immunohistochemistry—with post-fixation and long-term staining with ascending concentrations of osmium tetroxide. After washing and dehydration, samples are counterstained in alcoholic uranyl acetate (or its substitutes such as lanthanides if desired), impregnated and embedded into epoxy resin, and then grinded and polished to retrieve the sample and flatten its surface for electron microscopy. Visualisation is performed utilising BSEM upon counterstaining with lead citrate and carbon sputtering. The protocol provides an opportunity to investigate the entire and intact tissue sample, conduct layer-by-layer examination by serial grinding, and acquire high-quality images of tissue architecture, extracellular matrix, and cells at a magnification from 40- to 5,000-fold. For the investigation of mineral deposits or metal implants, visual inspection can be reinforced by an elemental analysis. Employing a proposed technique, we carried out an ultrastructural analysis of atherosclerotic plaques as compared with failing native and bioprosthetic heart valves, posing the integrity of the extracellular matrix as a pivotal factor for the prevention of structural valve deterioration (11).

Applications of the Method

The histological interrogation of blood vessels and heart valves and their polymer and bioprosthetic substitutes is frequently complicated by an extensive calcification, which leads to the loss of tissue integrity during the sectioning. Our approach avoids this drawback as it implies processing of the entire tissue explant through all sample preparation stages. Moreover, it adds the ability to analyse the chemical composition of the minerals or implants. Furthermore, the magnification of BSEM is optimal for the analysis of vascular architecture, allowing the clear visualisation of the endothelium, tunica intima, vascular smooth muscle cell layers, elastic fibres, collagen meshwork, *vasa vasorum*, plaque neovessels, immune cell clusters, peripheral nerves, and perivascular adipose tissue. Alterations detectable by our approach include but are not limited to extraskeletal calcification, lipid retention and foam cell formation, intraplaque or intravalvular haemorrhages, elastic lamina degradation, and neutrophil adhesion/migration. By optimising the staining and dehydration protocol, BSEM distinguishes endothelial cells, vascular smooth muscle cells, fibroblasts, mast cells, neutrophils, macrophages (including foam cells and foreign-body giant cells), lymphocytes, and perivascular adipocytes. The applicability of our technique for vascular pathology tasks has been confirmed on a sample of coronary artery bypass graft surgery conduits (saphenous veins and internal mammary arteries), demonstrating an association of increased *vasa vasorum* density with pre-implantation stenosis (12). An independent validation

sample included balloon-injured rat aortas, which indicated the correlation of *vasa vasorum*, a surrogate vascular inflammation marker, with immune cell clusters also associated with neointima formation (13). Finally, we have been able to show the relation of plaque neovessels with calcium deposition, further reporting the positive role of the microvessels around the mineral deposits and the negative role of total plaque vascularisation (14).

Experimental Design

This protocol provides a step-by-step guide to prepare the blood vessels, heart valves, and their polymer and bioprosthetic substitutes for the analysis of their gross and microscopic anatomy by BSEM. It can be divided into the following stages: (i) fixation, staining, and preparation for epoxy resin embedding; (ii) embedding into epoxy resin and preparation of the sample for BSEM; (iii) BSEM visualisation and analysis. The protocol, although being developed for studying cardiovascular pathology, is not restricted to this field and can be modified at any stage to optimise the results with respect to specific organs and tissues. The procedure described in the study has been optimised for atherosclerotic plaques, native and bioprosthetic heart valves, coronary artery bypass graft surgery conduits (autologous internal mammary arteries and saphenous veins), ovine carotid arteries (including those with implanted tissue-engineered vascular grafts), and rat aortas. We expect the performance of the method would be similar if applied to any other human or animal organ or tissue.

Fixation, Staining, and Preparation for Epoxy Resin Embedding (Steps 1–18)

This part of the protocol includes the standard fixation of the tissue in neutral phosphate buffered formalin immediately upon its collection, postfixation, and staining in ascending concentrations of osmium tetroxide, dehydration steps combined with the counterstaining in alcoholic uranyl acetate or lanthanides, and impregnation into epoxy resin. Although the modification and even substitution of some steps here are possible without affecting the result, we recommend adhering to the protocol in this part as it employs the basic principles of histology.

Embedding into Epoxy Resin and Preparation of the Sample for BSEM (Steps 19–24)

Here, we describe a critical step (sample orientation and epoxy resin embedding) of further sample retrieval by grinding and polishing and the final preparations that ensure high-quality BSEM (lead citrate counterstaining and carbon sputter coating). Serial grinding can be employed for the sequential scanning of the sample at ascending tissue depth. Various types of epoxy resin may be used here depending on the desired penetration into the tissue and subsequent modes of analysis. We recommend using Araldite 502 (in preference to Araldite-EMbed 812, Embed-812, and Spurr low-viscosity resin), a widely utilised embedding resin for embedding, which provides advantages that include rapid penetration, good contrasting properties, easy grinding, and stability under the electron beam. Different variants of lead citrate for counterstaining are available, yet we refer to Reynolds' formulation. Monostaining with lanthanides facilitates the further elemental analysis of mineral deposits, if applicable, in comparison with uranyl acetate/lead citrate treatment.

Backscattered Scanning Electron Microscopy Visualisation (Step 25)

Upon sample preparation, an ultrastructural analysis can be conducted by means of BSEM, which provides a high-resolution image from $\times 40$ to $\times 5{,}000$ magnification. This imaging modality is similar to transmission electron microscopy (TEM) in terms of visualisation patterns, facilitating the integration of EM-BSEM into the existing electron microscopy techniques applied in histopathology. Furthermore, BSEM is fully compatible with elemental analysis (e.g., energy-dispersive x-ray spectroscopy) and automated machine learning algorithms for post-acquisition image analysis.

Expertise Needed to Implement the Protocol

The implementation of the protocol does not require any specific expertise, and all steps can be performed by a competent graduate student or postdoctoral researcher without the need to involve a core facility or the use of a specific protective equipment. Yet, a grinding and polishing machine, a vacuum sputter coater, and a scanning electron microscope equipped with a backscattered electron detector are mandatory for the experiments utilising this protocol. The workflow is reminiscent of a routine histological sample preparation and includes the sequential incubation of the sample(s) in various chemical solutions, the orientation of the specimen in the embedding mould, grinding and polishing upon epoxy resin polymerisation, counterstaining followed by a sputter coating, and BSEM. The acquisition of relevant and high-quality images and their interpretation and semi-quantitative analysis require expertise and, ideally, experience in cardiovascular pathology (or a respective pathology field if studying other tissues). The development of neural networks for the automated analysis of acquired images would demand skills in data science.

MATERIALS AND EQUIPMENT

Biological Materials

1. Although the approach has been optimised for cardiovascular tissues, it can be applied to virtually any tissue. **CAUTION:** For all materials collected from live vertebrates or higher invertebrates, all experiments must be performed in accordance with relevant guidelines and regulations (e.g., European Convention for the Protection of Vertebrate Animals used for Experimental and Other Scientific Purposes, Strasbourg, 1986). For all materials obtained from human subjects, their collection must conform to the latest revision of Declaration of Helsinki (2013), and written informed consent to participate in the study must be obtained from all subjects.

Reagents

1. Ice-cold 1X phosphate-buffered saline (e.g., P4417, Sigma-Aldrich; St. Louis, MO, USA, dissolve five tablets in 1,000 ml of double-distilled water) or a physiological saline solution

[0.9% (wt/vol) NaCl, can be prepared by dissolving 9 g of NaCl (e.g., 31434, Sigma-Aldrich) in 1,000 ml of double-distilled or deionised water] as a transportation medium for the tissue samples. Can be stored at 4°C for 3 months.

CRITICAL: All reagents mentioned below must not be of a grade less than the ACS grade (≥99% purity) to obtain high-quality images.

2. Ice-cold 10% (vol/vol) neutral phosphate-buffered formalin (e.g., HT501128, Sigma-Aldrich) for the sample fixation by: (1) protein–protein and protein–nucleic acid cross-linking *via* amino or imino groups including those of adenine and cytosine (15–18); (2) reacting with the ethylenic double bonds of unsaturated lipids (19, 20). Can be prepared by dissolving 4 g of anhydrous monobasic sodium phosphate (NaH_2PO_4, e.g., S0751, Sigma-Aldrich) and 6.5 g of anhydrous dibasic sodium phosphate (Na_2HPO_4, e.g., S0876, Sigma-Aldrich) in 900 ml of double-distilled or deionised water and adding 100 ml of 37% (wt/vol) formaldehyde (e.g., 15680, Electron Microscopy Sciences; Hatfield, PA, USA or 252549, Sigma-Aldrich). Can be stored at 4°C for 1 year.

CAUTION: Fatal if swallowed, causes severe skin and eye irritation, may cause respiratory irritation, allergy or asthma symptoms, or breathing difficulties if inhaled. Wear protective clothing (gloves and face protection), do not breathe dust/fume/gas/mist/vapours/spray, wash gloves and hands thoroughly after handling, use only in a well-ventilated area such as a fume hood.

3. One percent (wt/vol) phosphate-buffered osmium tetroxide (OsO_4, e.g., 19100, Electron Microscopy Sciences) for the sample post-fixation by: (1) the polymerisation of unsaturated lipids through the cross-linking of ethylenic double bonds (21, 22); (2) protein–protein cross-linking *via* amino/imino groups (22, 23); (3) protein–lipid cross-linking by an unrecognised mechanism (23). Prepare by dissolving 1 g of osmium tetroxide in 100 ml of 0.1 M phosphate buffer [pH 7.4, can be prepared by: (1) dissolving 14.2 g of anhydrous Na_2HPO_4 in 1 L of double-distilled or deionised water; (2) dissolving 12 g of anhydrous NaH_2PO_4 in 1 L of double-distilled or deionised water; (3) mixing 405 ml of a Na_2HPO_4 solution with 95 ml of a NaH_2PO_4 solution, can be stored at 4°C for 1 year]. Can be stored tightly wrapped into a sealing film (e.g., Parafilm M, P7793, Sigma-Aldrich) at 4°C for 3 months. Protect from light.

CAUTION: Fatal if swallowed, in contact with skin, or inhaled and causes severe skin burns and eye damage. Wear protective clothing (gloves and face protection), do not breathe dust or mists, wash gloves and hands thoroughly after handling, use only in a well-ventilated area such as a fume hood, and strictly use glass vials (e.g., 23188, Supelco) for incubating the specimens, as glass is a chemically inert material that does not react with osmium tetroxide, in contrast to plastic.

4. Two percent (wt/vol) aqueous osmium tetroxide (OsO_4, e.g., 19100, Electron Microscopy Sciences) to better stain proteins and lipids. Prepare by dissolving 1 g of osmium tetroxide in 50 mL double-distilled or deionised water. Can be stored tightly wrapped into a sealing film at 4°C for 3 months. Protect from light.

CAUTION: Fatal if swallowed, in contact with skin, or inhaled and causes severe skin burns and eye damage. Wear protective clothing (gloves and face protection), do not breathe dust or mists, wash gloves and hands thoroughly after handling, use only in a well-ventilated area such as a fume hood, and strictly use glass vials for incubating the specimens, as glass is a chemically inert material that does not react with osmium tetroxide, in contrast to plastic.

5. Absolute ethanol (CH_3CH_2OH, 200 proof, e.g., 15058, Electron Microscopy Sciences) further diluted to 95 (vol/vol), 80 (vol/vol), 70 (vol/vol), 60 (vol/vol), and 50% (vol/vol) ethanol in double-distilled or deionised water. Such graded ethanol series is used for tissue dehydration and mild delipidation. Store at room temperature (RT).

CAUTION: Highly flammable liquid and vapour, harmful if swallowed or in contact with skin, and causes skin and eye irritation. Keep away from heat/sparks/open flames/hot surfaces, do not smoke around reagent, use explosion-proof electrical/ventilating/lighting/equipment, use only non-sparking tools, take precautionary measures against static discharge, wear protective clothing (gloves and face protection), and wash gloves and hands thoroughly after handling.

6. Uranyl acetate ($C_4H_6O_6U$, e.g., 22400, Electron Microscopy Sciences) further diluted to 2% (wt/vol) in 95% (vol/vol) ethanol (e.g., add 25 ml of 95% ethanol to 0.5 g of uranyl acetate). Uranyl acetate binds to sialic acid carboxyl groups of glycoproteins and gangliosides abundant in cell membranes, to amino groups of proteins, and to phosphate groups of nucleic acids (24), thereby contrasting nuclei and ribosomes. Must be prepared *ex tempore* and left for 4 h to settle. Protect from air and light.

CAUTION: Highly flammable liquid and vapour, toxic if swallowed, inhaled or in contact with skin, causes serious skin and eye irritation, and suspected of causing genetic defects and damaging fertility or the unborn child. Keep away from heat/sparks/open flames/hot surfaces, do not smoke around reagent, use explosion-proof electrical/ventilating/lighting/equipment, use only non-sparking tools, take precautionary measures against static discharge, do not breathe dust/fume/gas/mist/vapours/spray, wear protective clothing (gloves and face protection), and wash gloves and hands thoroughly after handling.

ALTERNATIVE: Use undiluted UranyLess, a proprietary mix of lanthanides (e.g., 22409, Electron Microscopy Sciences; Hatfield, PA, USA) binding to calcium, phosphates, and phospholipids and to amino groups of proteins and therefore staining cell membranes, organelles, and nuclei (25–30). Compared with uranyl acetate, UranyLess is a harmless reagent and generally shows similar efficiency to a contrasting agent. Store at RT for 1 year. Protect from light.

7. 2-propanol {[$(CH_3)_2CHOH$], e.g., 190764, Sigma-Aldrich}, a degreasing and dehydrating agent. More potent degreasing agent than ethanol. Store at RT.

CAUTION: Highly flammable liquid and vapour, harmful if swallowed or in contact with skin, causes skin and eye irritation, a d may cause drowsiness or dizziness. Keep away from heat/sparks/open flames/hot surfaces, do not smoke around the reagent, use explosion-proof electrical/ventilating/lighting/equipment, use only non-sparking tools, take precautionary measures against static discharge, wear protective clothing (gloves and face protection), and wash gloves and hands thoroughly after handling.

8. Acetone [$(CH_3)_2CO$], e.g., 179124, Sigma-Aldrich, a more potent dehydrating and degreasing agent as compared with ethanol and 2-propanol. Miscible with epoxy resin and less toxic as compared with propylene oxide. Store at RT.

CAUTION: Highly flammable liquid and vapour, toxic if swallowed or inhaled, causes skin and eye irritation, and may cause drowsiness or dizziness. Keep away from heat/sparks/open flames/hot surfaces, do not smoke around reagent, use explosion-proof electrical/ventilating/lighting/equipment, use only non-sparking tools, take precautionary measures against static discharge, wear protective clothing (gloves and face protection), wash gloves and hands thoroughly after handling, and use only in a well-ventilated area such as a fume hood.

9. Epoxy resin: Araldite 502 (e.g., 13900, Electron Microscopy Sciences), Araldite-EMbed 812 (e.g., 13940, Electron Microscopy Sciences), EMbed-812 (e.g., 14120 or 14121, Electron Microscopy Sciences), or Spurr low-viscosity resin (e.g., 14300, Electron Microscopy Sciences). We recommend using Araldite 502 as an option of choice, while EMbed-812 or Spurr low-viscosity resin may show better results when applied to bone tissues or samples with a high proportion of calcified tissue. Must be prepared *ex tempore*. To prepare Araldite 502, mix 20 ml of Araldite 502, 22 ml of dodecenyl succinic anhydride (a hardener), and 0.8 ml of DMP-30 (an accelerator). To prepare Araldite-EMbed 812, mix 25 ml of EMbed-812, 15 ml of Araldite 502, 55 ml of dodecenyl succinic anhydride, and 1.9 ml of DMP-30. To prepare EMbed-812, mix 20 ml of EMbed-812, 22/16/9 ml of dodecenyl succinic anhydride (for soft/medium/hard blocks, respectively), 5/8/12 ml of nadic methyl anhydride (another hardener, for soft/medium/hard blocks, respectively), and 0.9, 0.85, and 0.80 ml of DMP-30 (an accelerator, for soft/medium/hard blocks, respectively). To prepare the Spurr low-viscosity resin, mix 18 ml of ERL 4221, 14 ml of DER 736, 48 ml of non-enyl succinic anhydride (a hardener), and 0.6 ml of dimethylaminoethanol (an accelerator). Retain the abovementioned proportions when preparing larger epoxy resin amounts.

CAUTION: Harmful if swallowed, in contact with skin, or inhaled, causes serious skin and eye irritation, and may cause respiratory irritation and allergic skin reaction. Do not breathe dust/fume/gas/mist/vapours/spray, wear protective clothing (gloves and face protection), wash gloves and hands thoroughly after handling, and use only in a well-ventilated area such as a fume hood. Additionally, dimethylaminoethanol (an accelerator for Spurr low-viscosity resin) is a flammable liquid and vapour and causes severe skin burns and eye damage. When working with this reagent, keep away from heat/sparks/open flames/hot surfaces, do not smoke around reagent, use explosion-proof electrical/ventilating/lighting/equipment, use only non-sparking tools, and take precautionary measures against static discharge.

10. Silicone oil (e.g., 40300076, Struers; Sarasota, FL, USA) to facilitate the removing of epoxy resin blocks from the moulds upon the embedding.
11. Graded (9, 6, and 3 μm in diameter) diamond spray series for the polishing of epoxy resin blocks (e.g., DP-Spray M, 40600154, 40600153, and 40600152, Struers).
12. Water-based cooling and lubricating liquid for the diamond polishing of epoxy resin blocks (e.g., DP-Lubricant Green, 40700024, Struers).
13. Lead citrate trihydrate [$Pb(C_6H_5O_7)_2 \cdot 3H_2O$, e.g., 17800, Electron Microscopy Sciences] to further contrast lipids and proteins as it interacts with both osmium tetroxide and uranyl acetate and also binds to cysteine, ortho- and pyrophosphate groups, and glycogen (31). Alternatively, it can be prepared by adding 1.33 g of lead nitrate (e.g., 17900, Electron Microscopy Sciences), 1.76 g of sodium citrate (e.g., 21140, Electron Microscopy Sciences), and 30 ml of fresh double-distilled or deionised water into a 50 ml conical tube (e.g., 91050, Techno Plastic Products; Trasadingen, Switzerland). Shake vigorously for 1 min and intermittently for 30 min. Then, add 8 ml of 1 N NaOH to the mixture and swirl. Again, add fresh double-distilled or deionised water to reach a 50-ml final volume. Shake vigorously for 1 min and cheque the pH (must be 11.9–12.1). Adjust the pH with 1 N NaOH if needed while stirring the solution. Pass the solution through a 0.2-μm pore size regenerated cellulose syringe philtre (e.g., 431222, Corning; Corning, NY, USA). It can be stored tightly wrapped into a sealing film at 4°C for 6 months. Protect from air and light.

CAUTION: Toxic if swallowed or inhaled and may damage fertility or the unborn child. Do not breathe dust/fume/gas/mist/vapours/spray, wear protective clothing (gloves and face protection), wash gloves and hands thoroughly after handling, and use only in a well-ventilated area such as a fume hood.

Consumables

1. Polypropylene mounting cups (e.g., FixiForm, 40300085, Struers) acting as a mould for epoxy resin embedding.
2. Silicon carbide foil (200 mm in diameter) with poly-(ethylene terephthalate) foil backing for the wet grinding of materials (HV 30–800); grit 800 (e.g., 40400206, Struers), 1,000 (e.g., 40400207, Struers), and 1,200 (e.g., 40400208, Struers) for reaching the sample surface. These must be attached to an adapter for magnetic fixation on an

aluminium disc of the grinding and polishing machine (e.g., MD-Gekko, 200 mm in diameter, 49900047, Struers) or used with a self-adhesive foil (e.g., Gekko PSA, 200 mm in diameter, e.g., 49900053, Struers), which is to be glued on an aluminium disc.
3. Wool woven polishing cloth discs to use with 6- or 3-μm diameter monocrystalline diamonds for flattening the surface of the epoxy resin block (e.g., M300, NX-MET; Échirolles, France).
4. Carbon thread for sputter coating (e.g., 16771511116, Leica Microsystems; Wetzlar, Germany).
5. Glass Petri dish with lid for lead citrate counterstaining (e.g., 100 mm in diameter and 20 mm in height, BR455743, Sigma-Aldrich).
6. Laboratory glass bottles, 100–1,000 ml (e.g., Duran graduated laboratory bottles, Z232076, Z232084, Z232092, and Z232106), and their respective caps (GL 32 and GL 45 neck thread, Z232351 and Z153958) for preparing the phosphate-buffered and physiological saline, neutral phosphate-buffered formalin, osmium tetroxide, uranyl acetate, and ethanol dilutions.
7. Laboratory glass measuring cylinders, 10, 50, and 1,000 ml (e.g., BR31708, BR31728, and BR31762, Sigma-Aldrich), for measuring chemical solutions.
8. Laboratory glass beakers, 10 ml (e.g., Z231797, Sigma-Aldrich), for washing the specimens.
9. Laboratory glass vials (with caps), 40 ml (e.g., 23188, Supelco), for incubating the specimens. Ensure that the diameter of your vial fits the sample size and vice versa. Wide-mouth vials are preferable as they expand the maximum size of the specimens.
10. Polypropylene conical 50-ml tubes (with caps) for preparing the epoxy resin and lead citrate (e.g., 91050, Techno Plastic Products).
11. Long stainless-steel forceps to transfer the tissue and epoxy resin blocks between the solutions and short stainless-steel forceps (fine tip, curved) for specimen embedding (e.g., 12 and 4.5 inches, Z225622 and Z168785, Sigma-Aldrich).
12. Flexible stainless-steel wire ≈1–2 mm in diameter for removing the samples from the glass vials.
13. Single-channel, variable volume (20–200 μl and 100–1,000 μl) pipettes (e.g., 3123000055 and 3123000063, Eppendorf; Hamburg, Germany).
14. Disposable, clear 200–300- and 1,000-μl pipette philtre tips (e.g., TF-350 and TF-1000, Corning). May be non-sterile.
15. Gauze sponges for humidifying glass Petri dishes during lead citrate counterstaining (e.g., 8065-2, Covidien; Dublin, Ireland). May be non-sterile.

Equipment

1. Double-distilled water system (e.g., A4000, Antylia Scientific) or deionised water system (e.g., Milli-DI Water Purification System for Deionized Water, Merck; Kenilworth, NJ, USA).
2. pH metre (e.g., pH 211, Hanna Instruments; Woonsocket, RI, USA).
3. Thermostat capable of heating to 60°C (70°C if Spurr low-viscosity resin is applied).
4. Vacuum impregnation unit (e.g., CitoVac, Struers).
5. Grinding and polishing machine (e.g., TegraPol-11, Struers).
6. Vacuum sputter coater (e.g., EM ACE200, Leica).
7. Scanning electron microscope equipped with a backscattered electron detector (e.g., Hitachi S-3400N, Hitachi; Tokyo, Japan) and, optionally, with an energy-dispersive x-ray detector (e.g., XFlash 4010, Bruker; Billerica, MA, USA).

METHODS

All steps of the procedure should be performed at RT unless otherwise stated.

1. **DAY 1:** Carefully excise the tissue specimen and place it immediately into the transportation medium (ice-cold 1X phosphate-buffered saline or physiological saline). Ensure that the specimen is fully submerged into the transportation medium to prevent dehydration. Transfer the specimen into the tissue processing laboratory as soon as possible to prevent autolysis.

CRITICAL STEP: The transportation medium (1X phosphate-buffered saline or physiological saline) and fixative (10% neutral phosphate-buffered formalin) must be ice-cold (4°C) to restrict autolysis as much as possible. Do not ever allow the tissue to dry out. At any step of the protocol, ensure that the specimen is fully submerged into the liquid.

2. Dissect the tissue specimen to ∼5- × 5- × 5- (not more than 20- × 20- × 13-, L × W × H) mm segments if working with parenchymal organs. The advantage of cardiovascular tissue is that hollow organs such as blood vessels and thin heart valves are highly permeable for the formaldehyde molecules. Blood vessels and atherosclerotic plaques should be cut into ≈1-cm (not more than 1.3 cm) length segments for the convenience of embedding. The indicated dimensions ensure the proper and convenient orientation for epoxy resin embedding. The calcium deposits are typically well distinguishable from the surrounding tissue. To minimise the volume of the reagents used, calcified segments should be withdrawn just before formalin fixation. Wash the specimen in two or three changes of ice-cold 1X phosphate-buffered saline or physiological saline. Alternatively, intensively irrigate the specimen using a syringe if the tissue does not require a delicate treatment, as this technique is superior to dipping with regards to removing excessive blood.
3. Transfer the specimen into ice-cold 10% (vol/vol) neutral phosphate-buffered formalin as soon as possible to prevent autolysis. Despite the slower fixation rate, 10% neutral phosphate-buffered formalin is preferential to 4% paraformaldehyde and glutaraldehyde because of the smaller size and molecular weight of the molecules and, therefore, its better capability to penetrate the unprocessed tissue (32). Leave the sample overnight at 4°C.

PAUSE POINT: The specimen can be safely stored at 4°C for up to a week without any quality loss.

4. **DAY 2:** Change the formalin in the morning and leave it until the end of a 24-h incubation period.

PAUSE POINT: The specimen can be safely stored at 4°C for up to a week without any quality loss.

5. Wash the specimen by incubating it in 0.1 M phosphate buffer (pH 7.4, three changes, 10 min per each).
6. Transfer the specimen directly into a 1% phosphate-buffered osmium tetroxide solution. Hereinafter, strictly use glass and not plastic vials when working with osmium tetroxide to avoid any undesirable chemical interactions. Tightly wrap the container into a sealing film and leave the sample overnight at RT.
7. **DAY 3:** Transfer the specimen directly into a 2% aqueous osmium tetroxide solution. Tightly wrap the container into a sealing film and leave the sample for 40 h at RT.

PAUSE POINT: The specimen can be safely stored at RT for a weekend (72 h) without any quality loss.

8. **DAY 5:** Wash the specimen by incubating it in 0.1 M phosphate buffer (pH 7.4, four changes, 15 min per each). Select the counterstain (UranyLess or uranyl acetate). If choosing UranyLess, proceed to a step 9, exclude steps 11 and 12, and continue the protocol from a step 13. If choosing uranyl acetate, skip step 9 and continue the protocol from step 10 (in this variant of the protocol, steps 10 and 11 would be performed at day 5 and day 6 would start at a step 12).
9. If using UranyLess for counterstaining, transfer the specimen directly into undiluted UranyLess and leave the sample overnight at RT.

CRITICAL STEP: If planning an elemental analysis, UranyLess is strongly preferable to uranyl acetate, as lanthanides are typically not detected by energy-dispersive x-ray detector and, therefore, UranyLess staining does not result in an artefact peak, in contrast to uranyl acetate.

10. **DAY 6:** Transfer the specimen sequentially into 50, 60, 70, 80, and 95% ethanol (two changes per concentration, 15 min per change) without any washing steps.
11. If using uranyl acetate for counterstaining, transfer the specimen directly into freshly prepared 2% alcoholic uranyl acetate. Tightly wrap the container into a sealing film (if using uranyl acetate) and leave the sample overnight at RT. Protect from light.
12. Wash the specimen by incubating it in 95% ethanol (two changes, 15 min each).
13. Transfer the specimen directly into 2-propanol and incubate for 2 h. If the sample contains a high amount of fat, repeat the incubation in another change of 2-propanol.
14. Transfer the specimen directly into acetone and incubate for 2 h. If the sample contains a high amount of fat, repeat the incubation in another two changes of acetone (1 h per each).
15. Prepare the epoxy resin of desired formulation by (1) gentle mixing epoxy resin with a hardener/s until a homogeneous blend is obtained and (2) adding an accelerator and gently stirring until the mixture is uniform in colour.

CRITICAL STEP: After the preparation, place an epoxy resin under vacuum to remove air bubbles as they might impede the embedding.

16. Transfer the specimen directly into a freshly prepared epoxy resin:acetone mixture (1:1) and leave overnight at RT.
17. **DAY 7:** Repeat step 15. Transfer the specimen directly into freshly prepared epoxy resin and leave overnight at RT.
18. **DAY 8:** Repeat the step 15.

CRITICAL STEP: Upon preparation, it is mandatory to place the epoxy resin under vacuum to remove air bubbles as they might disrupt sample integrity during epoxy resin polymerisation.

19. Lubricate the polypropylene mounting cup from inside with silicone oil. Transfer the specimen directly into the polypropylene mounting cup and slowly fill the mould to a quarter with freshly prepared epoxy resin. Orientate the sample (e.g., blood vessels) if needed and continue filling the mould with epoxy resin until reaching the top of the cup. Place the mould into a thermostat and leave it for 24 h at 60°C.

CRITICAL STEP: Ensure the proper orientation of samples at all times until placing the mounting cups into the thermostat. The orientation of the sample is unalterable upon the epoxy resin polymerisation, and improper orientation (e.g., falling of blood vessels) often leads to a loss of the sample.

CRITICAL STEP: If working with hollow organs such as blood vessels, place the mould with the sample under vacuum to remove air bubbles before putting it into a thermostat.

20. **DAY 9:** Retrieve the epoxy resin blocks from the moulds. Sequentially grind the blocks until the sample surface is reached using the silicon carbide foil for the wet grinding of materials.
21. Polish the sample utilising wool-woven cloth discs and three monocrystalline diamond sprays (9-, 6-, and 3-μm diamond size, 20 min each) to flatten the surface of the epoxy resin block. The last stage of the polishing must be carried out without a diamond spray, i.e., using only a cloth disc for 20 min. **Figure 1** illustrates the appearance of grinded and polished epoxy resin blocks containing various tissue samples.

CRITICAL STEP: The use of a cooling and lubricating liquid is mandatory for high-quality diamond polishing.

22. Place the epoxy resin block onto wet gauze in a glass Petri dish. Counterstain the specimen by pipetting a lead citrate solution onto the surface of the epoxy resin block for 7 min. Ensure that the lead citrate fully covers the specimen surface.

CRITICAL STEP: Prepare lead citrate solution at least 3 days before this step (i.e., not later than on day 6) to achieve better staining results.

CRITICAL STEP: Close the Petri dish as soon as possible to prevent the contact of the lead citrate with air, which induces its precipitation.

CRITICAL STEP: Do not counterstain the specimen with lead citrate if planning an elemental analysis as it will result in an artefact peak.

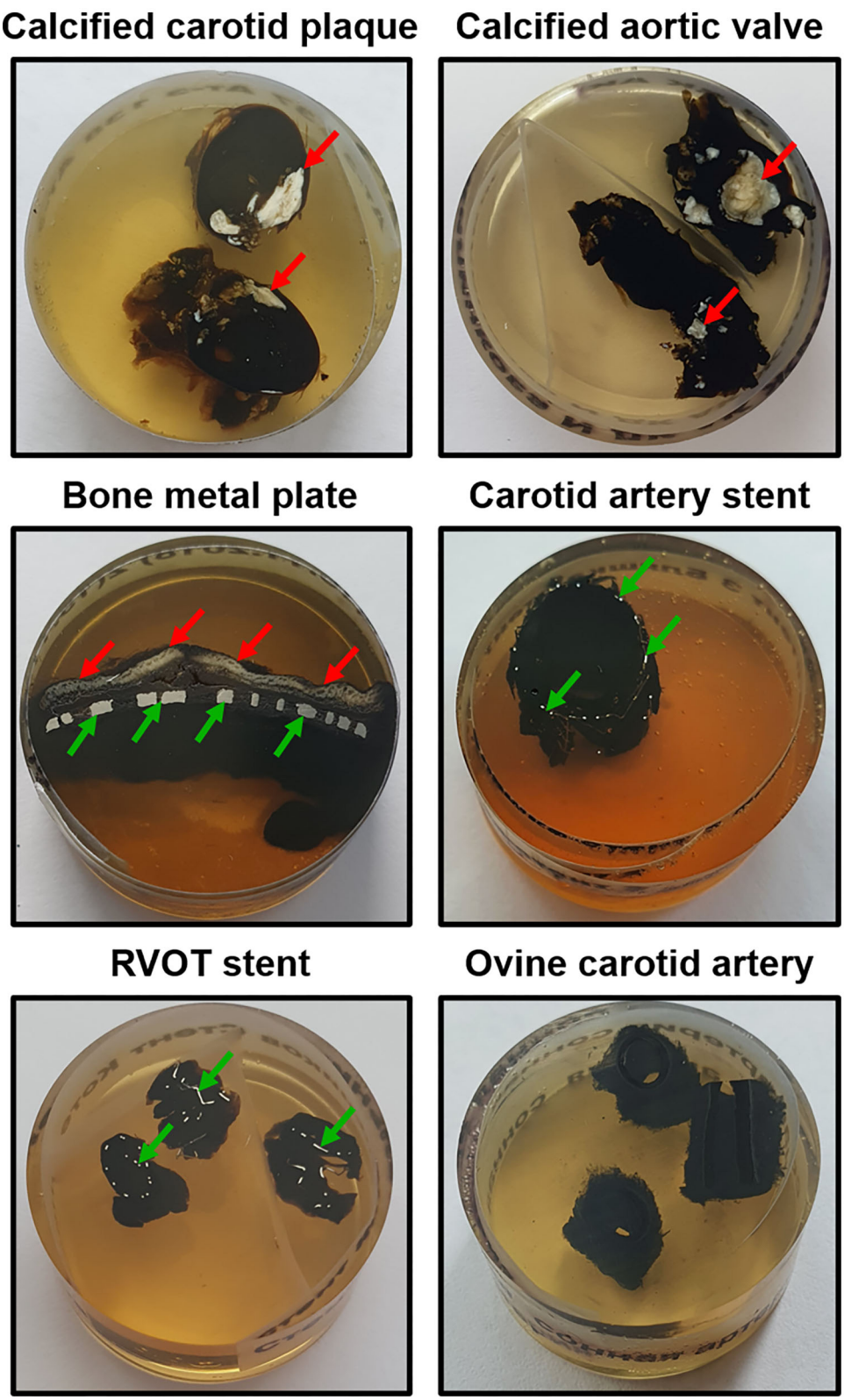

FIGURE 1 | Appearance of grinded and polished epoxy resin blocks containing various tissue samples (mineralised carotid plaque, calcified aortic valve, bone metal plate, stented carotid artery and right ventricular outflow tract, and intact non-calcified ovine carotid artery). Calcified and metal inclusions are indicated by red and green arrows, respectively. RVOT, right ventricular outflow tract.

23. Wash the specimen by incubating the epoxy resin block in double-distilled or deionised water (three changes, 5 min each).
24. Sputter coat the epoxy resin block with carbon utilising a vacuum coater. An optimal sputtered coating thickness is 10–12 nm. If the sputter coating thickness exceeds 15 nm, repeat steps 21–24.

CRITICAL STEP: At this step, do not touch an epoxy resin block without gloves as it may leave the fingerprints on the specimen. If this occasionally occurred, repeat steps 21–24.

CRITICAL STEP: Set a carbon correction if planning an elemental analysis to exclude the contribution of carbon sputter coating to the elemental profile.

25. Visualise the specimen by means of BSEM at a 10- or 15-kV accelerating voltage. If using a Hitachi S-3400N electron microscope, set a BSECOMP mode. Perform the elemental analysis if desired employing an energy-dispersive x-ray detector.

Timing

1. Fixation (10% neutral phosphate-buffered formalin): 24 h
2. Washing (0.1 M phosphate buffer): 30 min
3. Post-fixation (1% phosphate-buffered osmium tetroxide): 16 h
4. Staining (2% aqueous osmium tetroxide): 40 h
5. Washing (0.1 M phosphate buffer): 1 h
6. Counterstaining with UranyLess or 2% uranyl acetate: 16 h
7. Mild dehydration: 2.5 h
8. Degreasing/dehydration: 4 h (8 h if working with samples containing high amounts of fat)
9. Epoxy resin impregnation/degreasing/dehydration: 16 h
10. Epoxy resin impregnation: 24 h
11. Epoxy resin embedding (polymerisation): 24 h
12. Grinding and polishing: 2.5 h
13. Counterstaining with lead citrate: 7 min
14. Washing: 15 min
15. Sputter coating: 15 min
16. Visualisation and analysis: purpose-dependent

Total time: 171 h (**Table 1**, **Figures 2**, **3**).

TABLE 1 | Sequence and timing of the sample incubation in chemical reagents.

Solution	Temperature	Time
10% neutral phosphate buffered formalin	+4°C	2 × 12 h
0.1 M phosphate buffer (pH 7.4, mix of Na_2HPO_4-Na_2HPO_4)	RT	3 × 10 min
1% phosphate-buffered osmium tetroxide (OsO_4)	RT	Overnight
2% aqueous osmium tetroxide (OsO_4)	RT	40 h
0.1 M phosphate buffer (pH 7.4, mix of Na_2HPO_4-Na_2HPO_4)	RT	4 × 15 min
UranyLess (*if choosing lanthanide counterstaining*)	RT	Overnight
50% ethanol (CH_3CH_2OH)	RT	2 × 15 min
60% ethanol (CH_3CH_2OH)	RT	2 × 15 min
70% ethanol (CH_3CH_2OH)	RT	2 × 15 min
80% ethanol (CH_3CH_2OH)	RT	2 × 15 min
95% ethanol (CH_3CH_2OH)	RT	2 × 15 min
2% alcoholic uranyl acetate ($C_4H_6O_6U$) (*if choosing uranyl acetate counterstaining*)	RT	Overnight
95% ethanol (*if choosing uranyl acetate counterstaining*)	RT	2 × 15 min
2-propanol [$(CH_3)_2CHOH$]	RT	2 h or 2 × 2 h
Acetone	RT	2 h or 2 + 2 × 1 h
Epoxy resin: acetone mixture (1:1)	RT	Overnight
Epoxy resin	RT	Overnight
Epoxy resin	+60°C	24 h
Lead citrate trihydrate [$Pb(C_6H_5O_7)_2 \cdot 3H_2O$]	RT	7 min
Double distilled or deionised water	RT	3 × 5 min

Troubleshooting

1. If one adheres to the protocol, steps 1–18 generally do not cause any troubles. Regularly cheque the pH of the formalin solution. Allow the uranyl acetate to settle at least for 3 h upon its preparation. Always protect the uranyl acetate from air and light to avoid any precipitation. Gently mix the epoxy resin and a hardener, this blend and an accelerator, and ready-to-use epoxy resin and acetone until the mixtures become uniform in colour. Avoid any bubbles within the epoxy resin by a brief vacuuming to ensure proper impregnation and safe embedding. Control the storage temperature of all reagents and incubation temperature at all steps of the protocol.
2. At step 19 (embedding), if the sample lost its proper orientation (e.g., a blood vessel fell on its side), it can be liberated by employing a mini circular saw and embedded again.
3. Steps 20 and 21 are typically trouble-free if there is a sufficient amount of tap water and lubricating liquid during grinding and polishing, respectively.
4. Before conducting the step 22, cheque the pH and turbidity of the lead citrate solution. If the pH is below 11.9 or above 12.1, or if any precipitate is visible, prepare a fresh lead citrate solution. The precipitation of the lead citrate significantly contaminates the sample. If this occurs, prepare a fresh lead citrate solution and repeat steps 21–25. Always use freshly prepared double-distilled or deionised water while preparing the lead citrate to avoid its precipitation as it is highly reactive with carbon dioxide. In general, minimise the contact of the lead citrate with air.
5. Always cheque the thickness of the sputter coating as it must be from 10 to 15 nm to obtain a high-quality image.
6. If any scratches are observed during the visualisation, replace the polishing cloth disc and repeat steps 21–25.
7. If uranium and lead peaks are observed during the elemental analysis, replace uranyl acetate with UranyLess and do not perform lead citrate counterstaining. This will require repeating the procedure with the tissue backup.

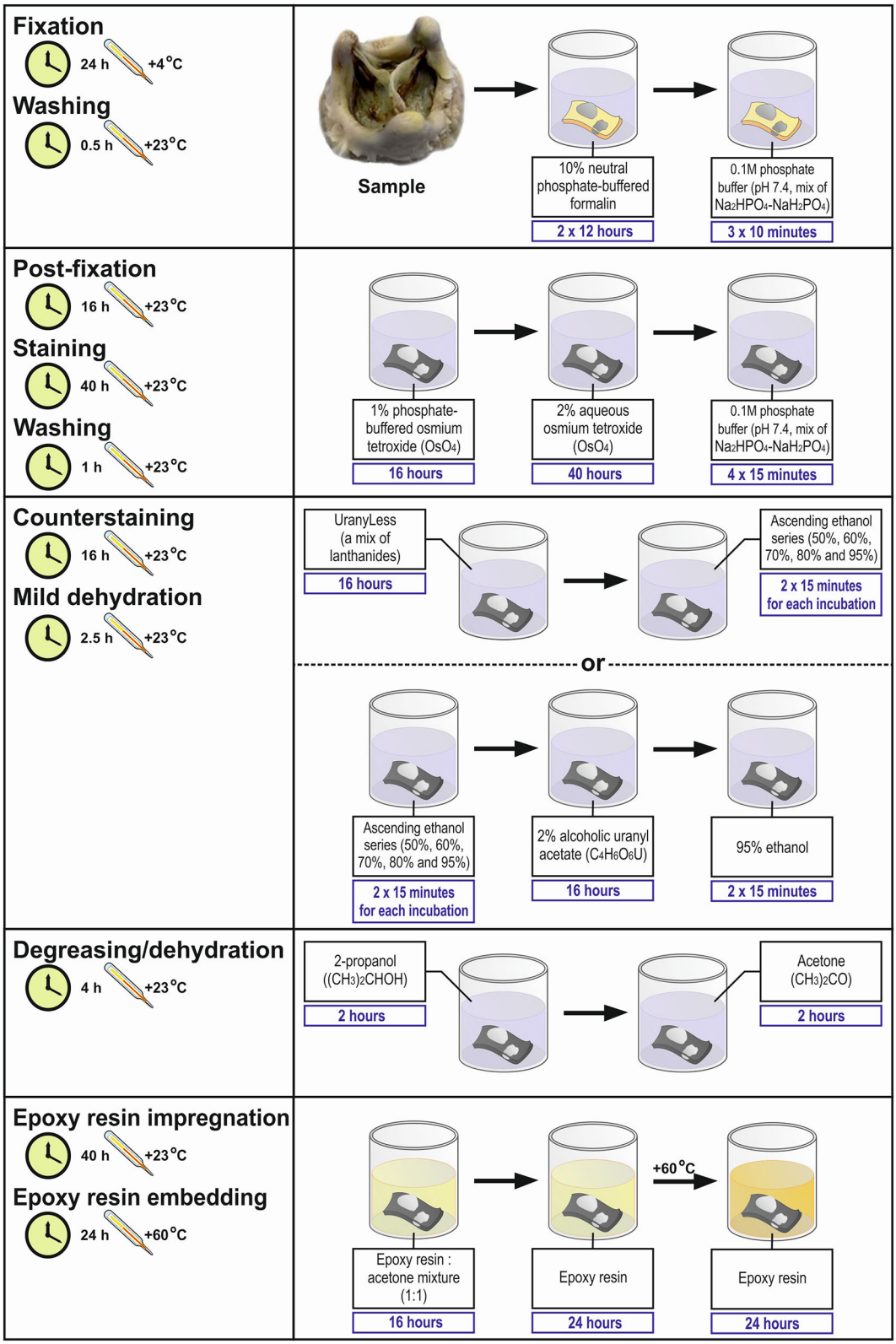

FIGURE 2 | Workflow diagram for Embedding and Backscattered Scanning Electron Microscopy (EM-BSEM) from fixation to epoxy resin embedding.

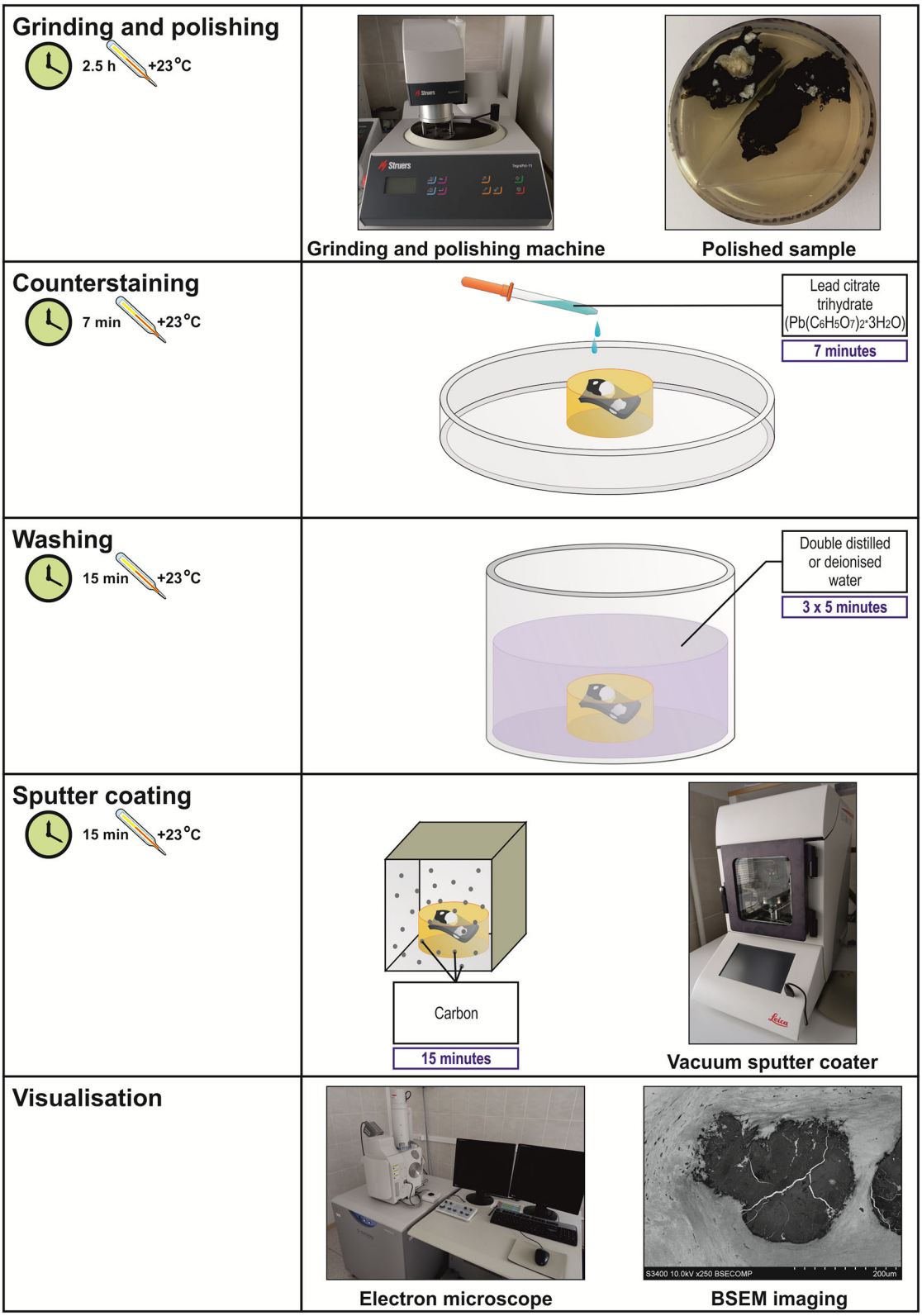

FIGURE 3 | Workflow diagram for EM-BSEM from grinding and polishing to visualisation.

ANTICIPATED RESULTS

Ethics Statement

All animal specimens (**Table 2**) have been collected in accordance with the European Convention for the Protection of Vertebrate Animals used for Experimental and Other Scientific Purposes (Strasbourg, 1986). The collection of human specimens (**Table 3**) conformed to the latest revision of the Declaration of Helsinki (2013). Written informed consent has been obtained from all individuals and medical care has been provided in accordance with the principles of Good Clinical Practise. The collection of all animal and human specimens has been approved by the Local Ethical Committee of the Research Institute for Complex Issues of Cardiovascular Diseases (Kemerovo, Russian Federation, protocol numbers AK_2019_02-10 and AK_2020_01-17 for the collection of animal and human specimens, respectively).

TABLE 2 | Animal samples collected to suggest the usefulness of EM-BSEM in general and cardiovascular pathology.

Animal	Excised tissue	Initial surgical intervention	Figures
Male Wistar rat 6-months-old 500 g body weight	Descending aorta Heart Liver Spleen Kidney	None	**Figures 4**, **6**
Male New Zealand White rabbit			
8-months-old	Skull	Cranioplasty	**Figure 1**
4.5 kg weight			
Female Edilbay sheep	Tissue-engineered carotid artery	Carotid artery interposition	
3-years-old 45 kg body weight	interposition graft	graft implantation for 1.5 years	**Figures 1**, **5**

Applications of the Method

Figure 4 illustrates the pairwise comparison of H&E staining, the most frequently applied pathological technique, and EM-BSEM at the highest magnification employed for scanning images for digital pathology needs (×400). When applied to blood vessels (e.g., rat descending aorta), EM-BSEM is preferable for annotating microvasculature in tunica adventitia and perivascular adipose tissue, as it clearly delineates blood vessel geometry and highlights red blood cells (**Figure 4**). Furthermore, it contrasts elastic fibres stained as black curves, which are easily distinguishable from the background, while that is not always the case for H&E staining (**Figure 4**). Another advantage of EM-BSEM is that it better preserves tissue integrity, excluding sectioning artefacts (**Figure 4**) and simplifying the preparation of specimens with a heterogeneous density, even those without calcium deposits. Although EM-BSEM has been initially designed for cardiovascular tissue, in particular calcified blood vessels, heart valves, and their bioprostheses, we suggest it can be applied for virtually all biological samples and for different research purposes (**Figure 4**).

TABLE 3 | Clinical samples collected to exhibit the applicability of EM-BSEM in cardiovascular pathology.

Clinical sample	Patient	Cardiovascular pathology	Surgical intervention	Figures
Atherosclerotic plaques	Female 58 years	Carotid atherosclerosis	Carotid endarterectomy	**Figures 1**, **5**, **6**, **8**, **10**
	Male 67 years	In-stent restenosis		**Figures 1**, **5**
Calcified aortic valve	Male 66 years	Calcific aortic valve disease	Surgical aortic valve replacement	**Figures 1**, **5**
Bioprosthetic xenopericardial bovine aortic valves	Female 72 years	Structural valve deterioration	Repeated surgical aortic valve replacement	**Figures 5**, **8**
	Male 70 years			
	Female 72 years			**Figure 8**
Stented right ventricular outflow tract	Male 6 months	Tetralogy of Fallot	Total surgical repair	**Figures 1**, **5**
Left internal mammary artery	Male 53 years	Chronic coronary syndrome	Pedicled internal mammary artery harvesting for coronary artery bypass graft surgery	**Figures 6**, **8**, **9**
Saphenous vein	Male 65 years	Chronic coronary syndrome	Open saphenous vein harvesting for coronary artery bypass graft surgery	**Figure 7**

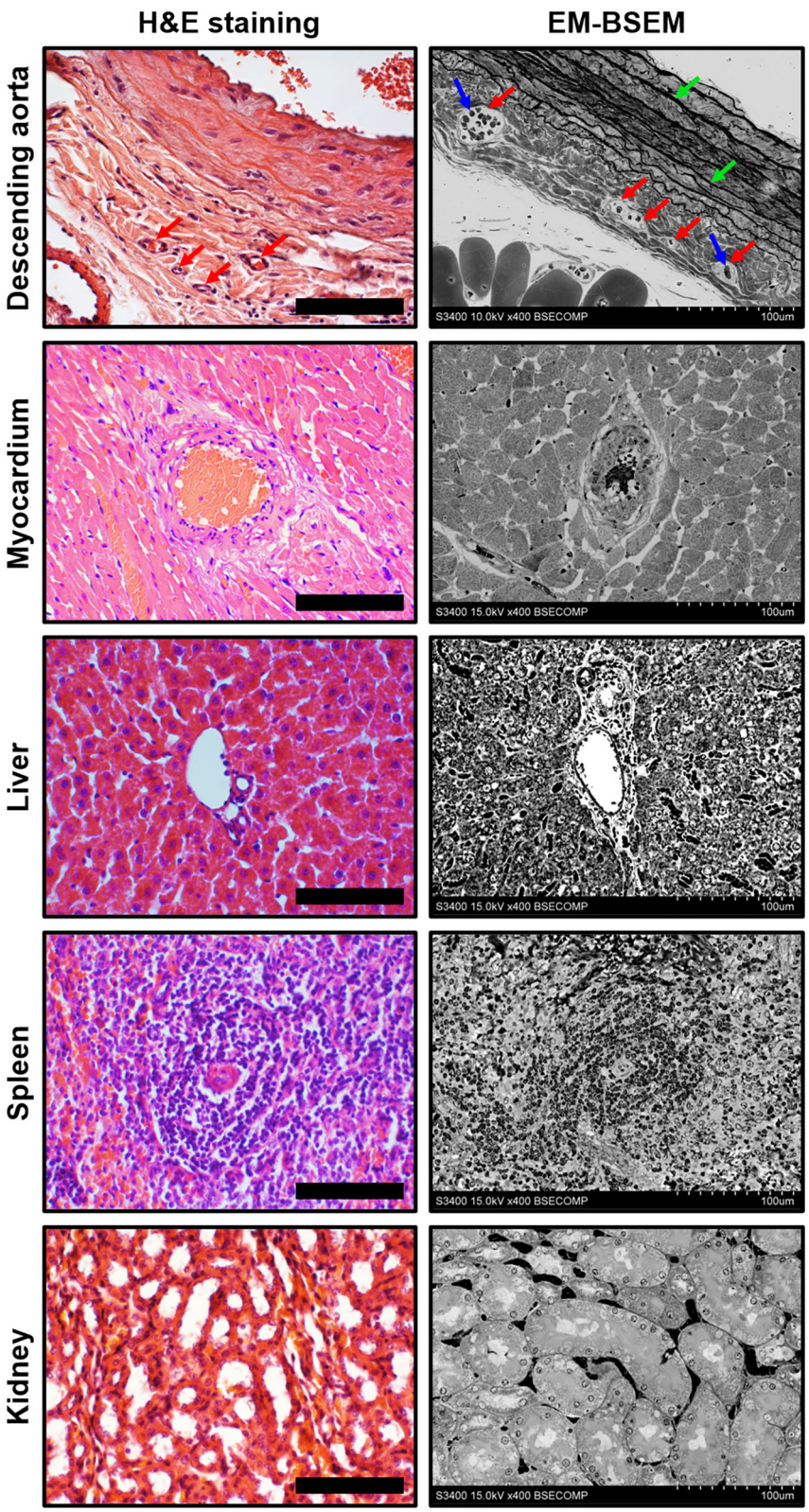

FIGURE 4 | Side-by-side comparison of H&E staining and EM-BSEM of rat descending aorta, myocardium, liver, spleen, and kidney. Scale bar (100 μm) and magnification (×400) for H&E staining (left side) are equal to those on the BSEM images (right side). Accelerating voltage was 15 kV for all BSEM images, except that of the descending aorta (10 kV). The *vasa vasorum* in the tunica adventitia of the descending aorta are indicated by red arrows, while the red blood cells inside their lumen and elastic fibres are indicated by blue and green arrows, respectively.

We further demonstrate EM-BSEM applications in relation to the clinical samples of cardiovascular tissue (**Table 3**).

The assessment of calcifications and stents in different parts of the circulatory system revealed the fully retained integrity of the surrounding tissue regardless of location or pathological condition (**Figure 5**). Atherosclerotic calcifications were frequently demarcated by a connective tissue capsule (**Figure 5A**) in contradistinction to valvular mineral deposits, which developed during calcific aortic stenosis (**Figure 5B**) or the structural deterioration of bioprostheses within the disorganised extracellular matrix (**Figure 5C**). Calcifications on the border between the tunica media and tunica adventitia within the tissue-engineered vascular grafts (**Figure 5D**) resembled medial arterial calcification, which is a common finding in patients with advanced chronic kidney disease and end-stage renal disease (33, 34). The connective tissue enveloping metal stents upon carotid angioplasty (**Figure 5E**) or right ventricular outflow tract stenting (**Figure 5F**) was also intact, permitting an analysis of biocompatibility of these devices.

An important benefit of EM-BSEM is that it allows the detailed evaluation of blood vessels and heart valves, as most of cardiovascular pathology phenomena can be investigated at $\leq \times$5,000 magnification. As portrayed in **Figure 6**, EM-BSEM can be applied to study neointimal calcification (**Figure 6A**), which is often accompanied by the alterations of cellular phenotype such as the transformation of macrophages or vascular smooth muscle cells into foam cells because of the massive lipid deposition near the vessel lumen or around *vasa plaquorum* (**Figure 6B**) (35–38). The progression of atherosclerosis is also enhanced by intraplaque haemorrhages occurring through leaky plaque neovessels (36, 39–41) and is notable for the large amount of red blood cells in their vicinity (**Figure 6C**). A mandatory condition of neointimal hyperplasia, however, is breach of the internal elastic lamina (42, 43), which is well detectable by EM-BSEM and can even be quantified (**Figure 6D**). The development of neointima is associated with increased quantities of immune cell clusters within the adventitia and perivascular adipose tissue (**Figure 6E**), in agreement with an outside–in route of atherosclerosis progression (44–47). Furthermore, EM-BSEM affords both the high-quality visualisation of these structures and their distinction from the sympathetic trunk (**Figure 6F**).

A compulsory requirement for any histological approach applicable in vascular biology is its ability to differentiate the arterioles nourishing the blood vessels, venules removing metabolic wastes, and capillaries responsible for the exchange of gases, nutrients, and waste products. As shown in **Figure 7**, EM-BSEM discriminates concentric arterioles consisting of endothelium and several smooth muscle cell layers, distended collecting venules, and tiny capillaries whose diameters are similar to that of a red blood cell. This indicates its potential usefulness to analysing the evolution of the microvascular networks in growing blood vessels, tissue-engineered constructs, and for other developmental biology applications.

All mentioned applications, however, generally do not demand high ($> \times$1,000) magnifications, although a possibility to operate within the $\times$400–1,000 magnification range and to acquire high-resolution images is beneficial for the analysis of tissue architecture. Yet, higher magnifications are needed to investigate ultrastructural cardiovascular pathology and to identify the characteristic features of cell populations. Employing EM-BSEM, we were able to image foam cells with clear-cut lipid droplets in the cytosol (**Figure 8A**), multinucleated giant cells containing processed components of the extracellular matrix (**Figure 8B**), and canonical macrophages having round or oval nuclei (**Figure 8C**). For this reason, EM-BSEM can be particularly advantageous for the analysis of atherosclerotic plaques that contain major amounts of foam cells (i.e., macrophages and vascular smooth muscle cells engulfing lipid molecules) and bioprosthetic heart valves, which are notable for multiple foreign-body giant cells (11). In addition, EM-BSEM also discerns neutrophils, which have segmented nuclei and small granules (**Figure 8D**), mast cells with a round nucleus and large electron-dense granules (**Figure 8E**), and lymphocytes differing from other immune cells by a high nuclear-cytoplasmic ratio (**Figure 8F**).

Besides the descriptive findings, EM-BSEM might be harnessed to investigate pathophysiological events. For instance, we noticed the adhesion of neutrophils to endothelial cells (**Figure 9A**) and their migration through the vascular wall (**Figure 9B**) in the *vasa vasorum* locating at the perivascular adipose tissue of human internal mammary arteries, which are frequently used as conduits for coronary artery bypass graft surgery. The applicability of EM-BSEM to vascular pathophysiology is underscored by the opportunity to clearly distinguish endothelial cells, vascular smooth muscle cells (**Figure 9**), adventitial cell populations (macrophages, mast cells, and fibroblasts), and perivascular adipocytes (**Supplementary Figure 1**).

In addition to conventional cardiovascular biology applications, EM-BSEM can be coupled with an elemental analysis to interrogate the chemical composition and heterogeneity of calcifications (**Figure 10**).

DISCUSSION

To our knowledge, all currently available histological techniques include sectioning, which inflicts irreversible damage to calcified and stent-expanded tissues and are, therefore, unsuitable for the subsequent analysis of such specimens. Furthermore, none of the existing techniques allows the detailed and high-throughput analysis of cardiovascular microanatomy. Vascular and valvular cell types are often barely distinguishable even at the highest conventional LM magnification (400-fold) if routine stains are applied. In addition, a significant proportion of small-calibre *vasa vasorum* and adventitial or perivascular immune cell clusters cannot be well-discriminated from the surrounding connective tissue and quantified by means of LM.

Confocal and multiphoton microscopy permits 3D image acquisition with the subsequent visualisation, qualitative assessment, and quantification of cell populations, cellular structures, and cell–cell interactions (48–50). In contrast to

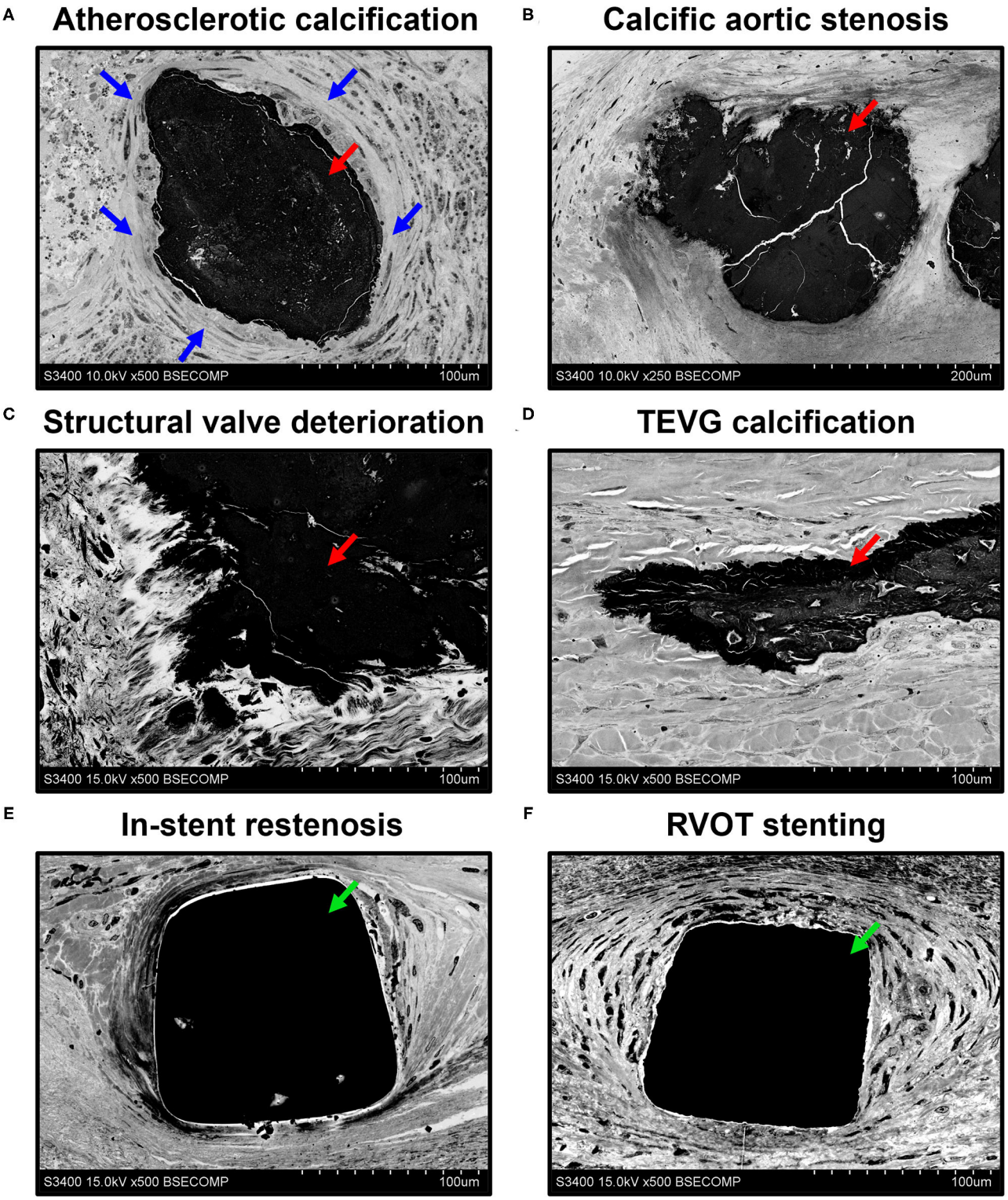

FIGURE 5 | Visualisation of mineral deposits (indicated by red arrows) and metal implants (indicated by green arrows) in cardiovascular tissue by EM-BSEM shows the retained integrity of calcified [carotid plaque **(A)**, native **(B)**, and bioprosthetic **(C)** aortic valves, and tissue-engineered vascular grafts implanted into the ovine carotid artery **(D)**] and metal-incorporating tissues [human carotid artery **(E)** and right ventricular outflow tract **(F)**]. Note the clear-cut connective tissue capsule (indicated by blue arrows) around the atherosclerotic but not the valvular or vascular graft calcifications. A magnification of ×500 (scale bar: 100 μm) for all images, except that of the calcified native aortic valve (×250 magnification, scale bar: 200 μm). The accelerating voltage was 15 kV for all images, except those of the atherosclerotic plaque and calcified native aortic valve (10 kV).

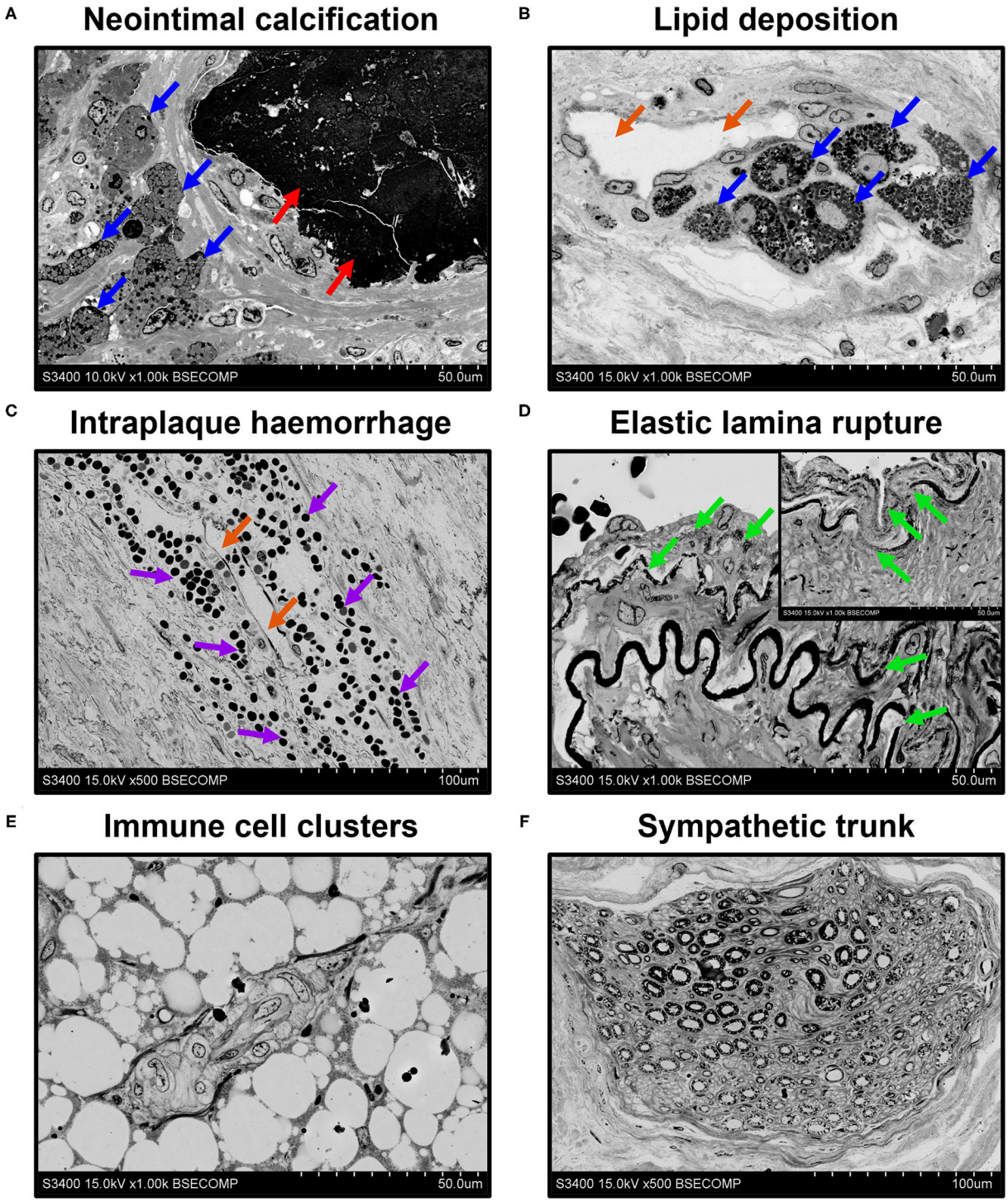

FIGURE 6 | EM-BSEM imaging of cardiovascular pathology. Note the abundance of **(A,B)** foam cells (indicated by blue arrows) and **(C)** red blood cells (indicated by violet arrows) near the calcium deposit (indicated by red arrows) and neovessels (indicated by orange arrows) within the carotid plaque. **(D)** Also note the age-dependent degradation of the elastic laminae (indicated by green arrows) of the left internal mammary artery excised for coronary artery bypass graft surgery purposes. Note the vascular smooth muscle cells between the elastic laminae and the traceable contours of the internal elastic lamina repeating that of the following elastic laminae. The insert in the upper-right corner indicates the visible decomposition of two sequential elastic laminae. **(E)** Immune cell clusters frequent in the adventitia and perivascular adipose tissue of rat descending aorta undergo hyperplasia at inflammation and might represent a valuable marker of immune response but should be clearly distinguished from **(F)** a sympathetic trunk. A magnification $\times$1,000 (scale bar: 50 μm) for all images, except, that of intraplaque haemorrhage and sympathetic trunk (x500 magnification, scale bar: 100 μm). The accelerating voltage was 15 kV for all images excepting that of neointimal calcification (10 kV).

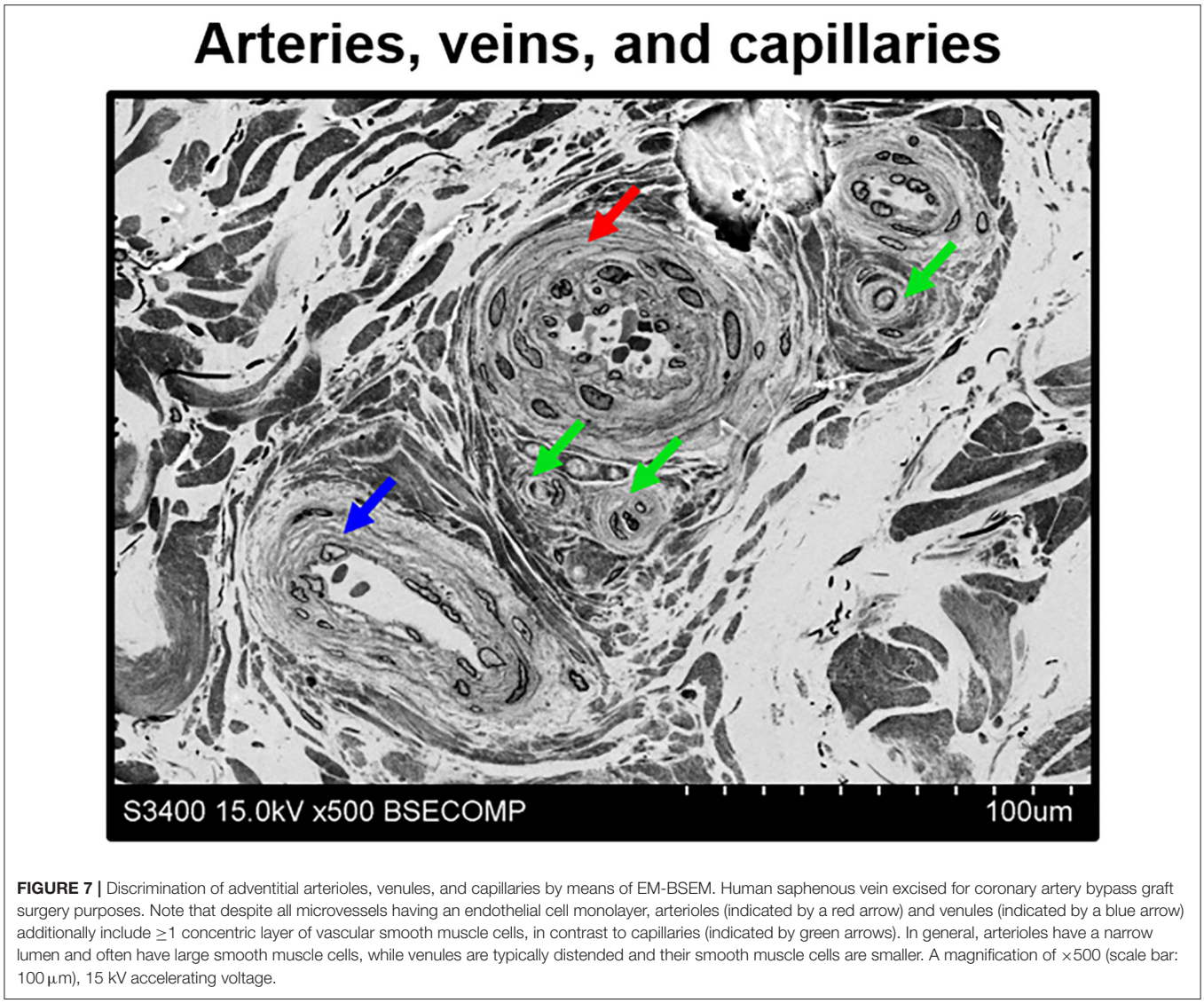

FIGURE 7 | Discrimination of adventitial arterioles, venules, and capillaries by means of EM-BSEM. Human saphenous vein excised for coronary artery bypass graft surgery purposes. Note that despite all microvessels having an endothelial cell monolayer, arterioles (indicated by a red arrow) and venules (indicated by a blue arrow) additionally include ≥1 concentric layer of vascular smooth muscle cells, in contrast to capillaries (indicated by green arrows). In general, arterioles have a narrow lumen and often have large smooth muscle cells, while venules are typically distended and their smooth muscle cells are smaller. A magnification of ×500 (scale bar: 100 μm), 15 kV accelerating voltage.

single-photon confocal microscopy, multiphoton (e.g., two-photon) microscopy uses longer-wavelength photons that penetrate deeper into the tissue (500 μm−1 mm) and inflict less damage on the sample (48). The main advantage of two-photon microscopy is its better focus, allowing the obtainment of clearer images as compared to single-photon confocal microscopy (48). The combination of a high penetration capability and low phototoxicity provides an opportunity to visualise the undissected tissues of living animals (48, 50). However, two-photon microscopy requires expensive and highly specific equipment that significantly confines its use to specialised laboratories having certified specialists employed. Furthermore, immunostaining demarcates specific cell types or extracellular matrix components but is not informative of tissue architecture.

The mentioned drawbacks can be resolved by TEM, which is incompatible with large samples (e.g., most of the blood vessels) due to a critically reduced amount of analysable tissue, needs difficult sample preparation, and the final sample represents a single tissue snapshot rather than serial sections evenly distributed along or across the specimen. Notably, the visualisation of calcified tissues is often performed by means of density-dependent scanning electron microscopy (SEM), which implies the superimposing of images acquired by secondary and backscattered electron detectors and further assigning them to the distinct colour channels (e.g., green and red), thereby permitting the coloured mapping of calcific nodules and distinguishing them from soft tissues (51–53). The main advantage of this technique is that it allows the simultaneous visualisation of both topography and density in a single image (51). Although it is perfect for the visualisation and morphometrics of calcifications, density-dependent SEM generally does not furnish the ultrastructural details of their biological microenvironments and, therefore, the phenotyping of the neighbouring cell populations is complicated.

In biomedicine, BSEM is broadly used for the imaging of unstained, freeze-dried cell cultures (54), wet calcified

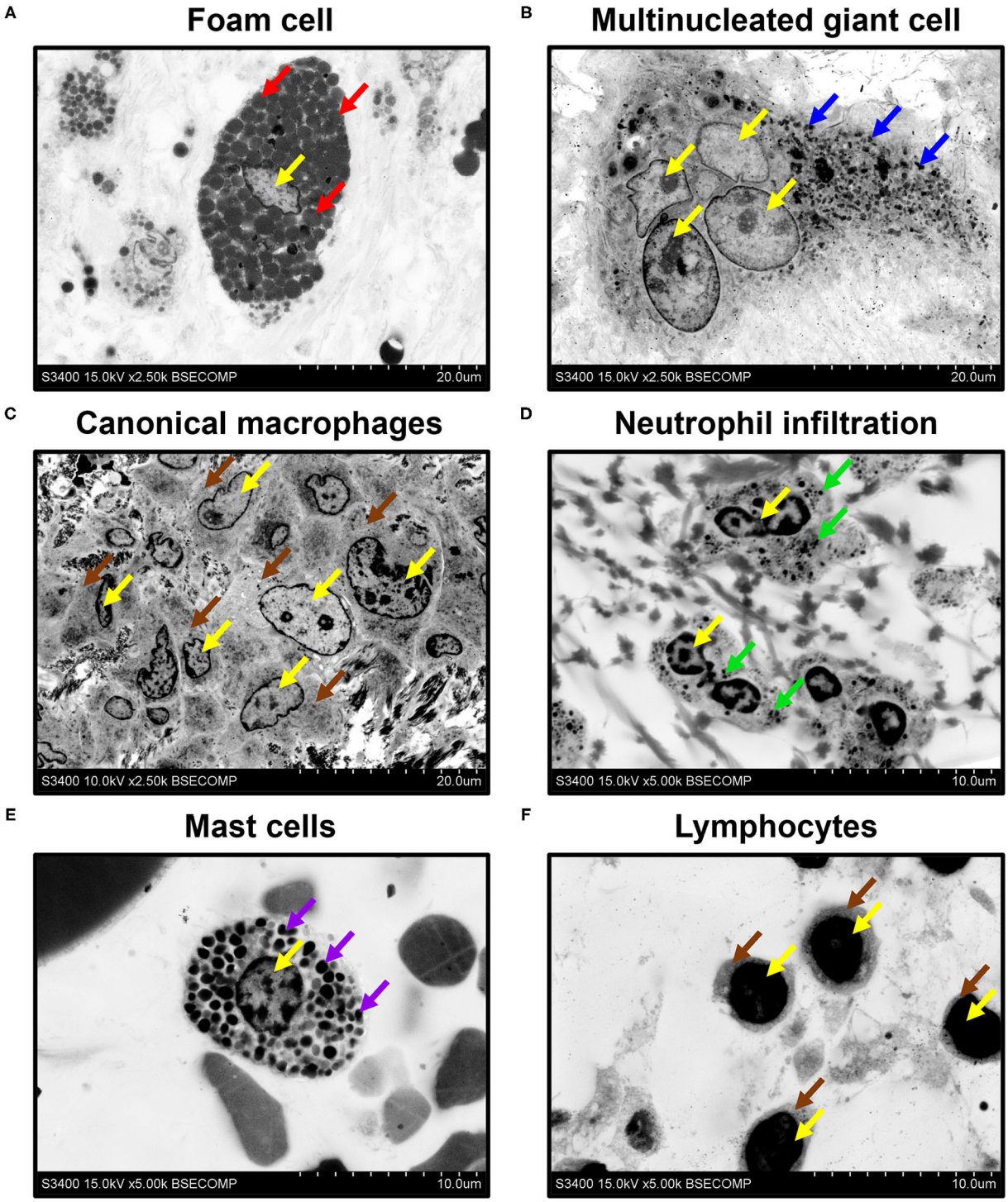

FIGURE 8 | Phenotyping of immune cells and mast cells by EM-BSEM. Nuclei are indicated by yellow arrows. Note **(A)** the large spherical lipid granules within the foam cells of carotid plaque (indicated by red arrows) and **(B)** multiple small granules within the multinucleated (foreign body) giant cells of the bioprosthetic aortic valve (indicated by blue arrows). **(C)** Canonical macrophages of the same valve lack granules within the cytoplasm (indicated by brown arrows). **(D)** The neutrophils of rapid-failing bioprosthetic aortic valve were characterised by numerous small granules within the cytosol (indicated by green arrows) and polymorphic nuclei. **(E)** In contrast, mast cells from the perivascular (human coronary artery) adipose tissue have large spherical inclusions in the cytosol (indicated by violet arrows) and round nuclei. **(F)** Lymphocytes from the same adipose tissue sample were distinct from other cells because of a high nuclear-cytoplasmic ratio (cytoplasm is indicated by brown arrows): ×2,500 magnification (scale bar: 20 μm) for images of foam cells, multinucleated giant cells, and canonical macrophages; ×5,000 magnification (scale bar: 10 μm) for images of neutrophils, mast cells, and lymphocytes. The accelerating voltage was 15 kV for all images, except that of canonical macrophages (10 kV).

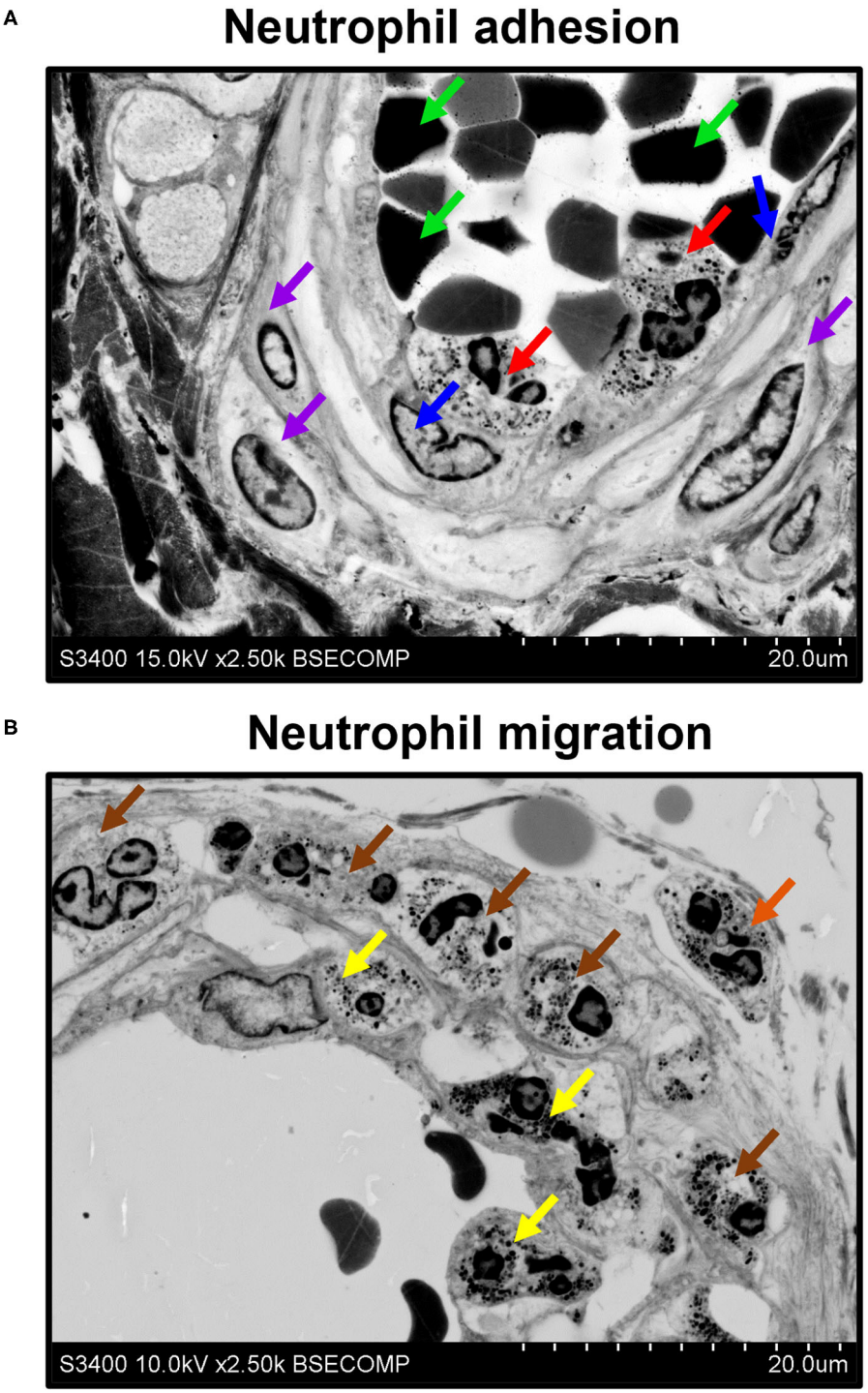

FIGURE 9 | EM-BSEM visualisation of neutrophil adhesion and migration. Left internal mammary artery excised for coronary artery bypass graft surgery purposes. **(A)** Note the neutrophils (indicated by red arrows) adhering to endothelial cells (indicated by blue arrows). Red blood cells and vascular smooth muscle cells are indicated by green and violet arrows, respectively. **(B)** Note adhering neutrophils (indicated by yellow arrows), invading neutrophils (indicated by brown arrows), and migrating neutrophils (indicated by an orange arrow). A magnification of ×2,500 (scale bar: 20 μm) and accelerating voltage of 15 kV (upper image) and 10 kV (lower image).

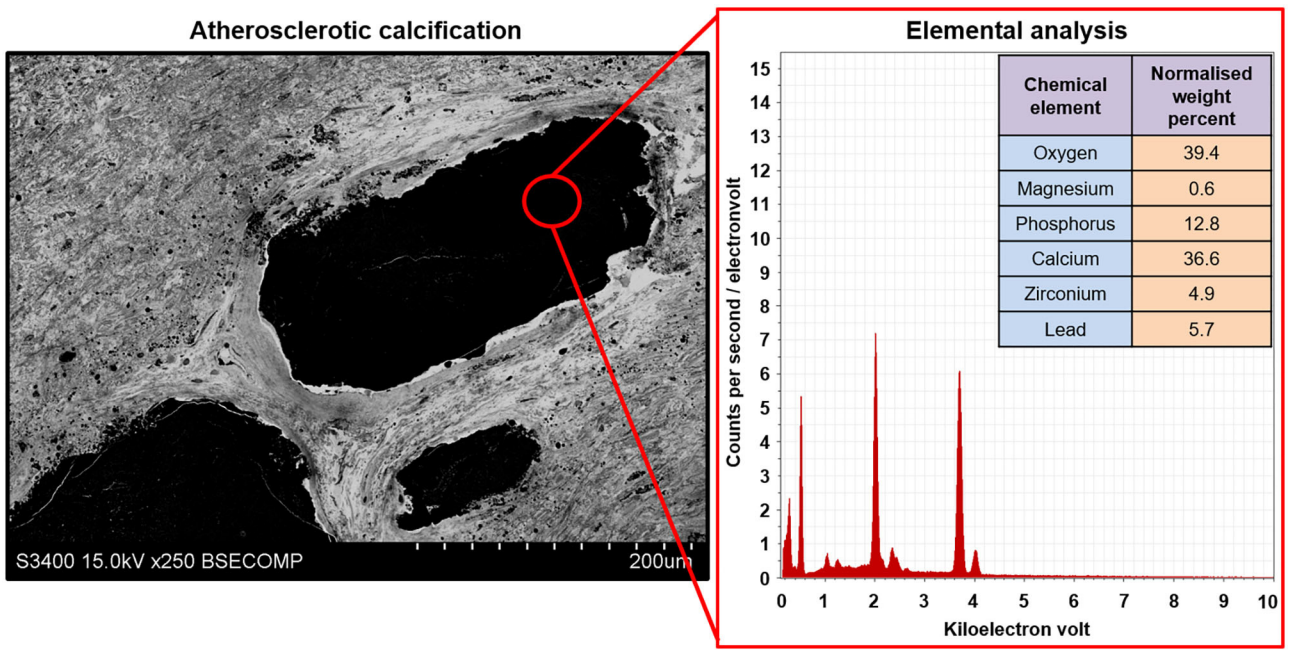

FIGURE 10 | Elemental analysis of the atherosclerotic calcium deposit within the carotid plaque visualised employing EM-BSEM. Note the high calcium, phosphorus, and oxygen content suggestive of a hydroxyapatite. For a more precise elemental analysis, uranyl acetate should be replaced by UranyLess, and lead citrate should be avoided. Yet, this results in a worse detailing of cells and the extracellular matrix. A magnification of ×250 (scale bar: 200 μm) and accelerating voltage of 15 kV.

TABLE 4 | Comparison of light microscopy (LM), EM-BSEM, and transmission electron microscopy (TEM).

Feature	LM	Confocal/multiphoton microscopy	TEM	Density-dependent SEM	EM-BSEfM
Resolution	Low	Low	High	High	Average
Representativeness	High	High	Low	High	High
Informativeness	Average	Average	Average	Average	High
Versatility	Average	Average	Average	Low	High
Technical complexity	Average	High	High	Low	Low
Labour intensity	Average	Average	High	Average	Average
Hands-on time	Average	Average	High	Average	Average
Time to complete	Average	Average	High	Average	High

LM, light microscopy; TEM, transmission electron microscopy; SEM, scanning electron microscopy; EM-BSEM, EMbedding and Backscattered Scanning Electron Microscopy.

atherosclerotic lesions (55), implant-bone interface (56), cartilage and bone tissue (57), and a diversity of other tissues (58). Despite high-resolution BSEM and field emission SEM having been earlier employed for the multiscale visualisation of semi-thin and ultra-thin sections, respectively (58, 59), these sample preparation approaches are inconvenient when working with mineralised tissues or specimens with incorporated solid implants. The techniques of correlative histology [i.e., a time-resolved combination of imaging modalities from lower to higher magnifications (1, 60)], such as the three-sectioning method, where epoxy resin-embedded tissue is sequentially cut into thick (≈300 μm), semi-thin (1–3 μm), and ultra-thin (60–90 nm) sections to specify regions of interest, have been proposed for working with hard tissues (61). However, correlative microscopy is typically time consuming, labour intensive, and is designed to focus on a few tissue segments rather than for screening purposes and semi-quantitative image analysis. Another correlative histology approach includes cryosectioning and combination of immunogold labelling with subsequent confocal laser scanning microscopy (62). Then, stained sections on the glass slides are fixed in glutaraldehyde, incubated in a gold-enhancing solution to enlarge nanogold particles, stained with osmium tetroxide, uranyl acetate, and lead citrate, and dehydrated and embedded into epoxy resin with the following ultramicrotome sectioning, with repeated adhering to a glass slide, carbon coating, and BSEM (62). Alternatively, specific acrylic resins (e.g., LR White) enable the post-embedding immunofluorescence staining and confocal laser scanning microscopy of semi-thin sections, which

can then be stained with heavy metals and prepared for BSEM (63–65). This correlative microscopy approach has the advantage of combining the immunophenotyping and ultrastructural examination of the same field of view, though to the detriment of the area available for the analysis and being incompatible with calcified tissues. A recent protocol suggested by Goggin et al. (66) implies glutaraldehyde fixation, 1-week decalcification with ethylenediaminetetraacetic acid, and combined staining with 2% osmium tetroxide and 1.5% potassium ferrocyanide, with a subsequent incubation in thiocarbohydrazide [to cross-link the osmium layers and enhance further osmium binding by bridging two osmium molecules (67–69)], pure osmium tetroxide, uranyl acetate, and Walton's lead aspartate solutions followed by dehydration and resin embedding (66). Albeit it provides good results with regards to hard tissues (e.g., bone), prolonged exposure to ethylenediaminetetraacetic acid deteriorates tissue integrity and reduces image quality when visualising soft tissues, e.g., cardiovascular tissue surrounding calcium deposits. In addition to working with tissues, ultra-thin epoxy resin embedding has also been applied to the preparation of cell cultures for scanning electron microscopy to image individual cells and cell–cell interactions on planar and three-dimensional substrates in preference to critical point drying, but this technique was not optimised for BSEM to visualise intracellular compartments (70).

Importantly, high-resolution images have been obtained only in studies examining semi-thin and ultra-thin sections (58, 59), where staining with uranyl acetate and lead citrate enabled the reaching of a BSEM resolution comparable to that of transmission electron microscopy because such samples can be fully penetrated by an electron beam. However, this method demands tissue sectioning, which rarely allows one to keep the integrity of the samples including mineral deposits or metal implants. Our technique (EM-BSEM) entirely retains the integrity of calcified or metal-containing samples, affords the analysis of their chemical composition, and combines the advantages of LM and TEM, providing both gross and high-resolution images and detailed histological characteristics of all vascular and valvular tissue structures and cell types. The sequential grinding of the sample permits consecutive, layer-by-layer scanning that is principally similar to serial sectioning but does not cause any damage to mineralised tissues. The sample preparation is relatively straightforward and has only one extremely critical step (sample orientation during epoxy resin embedding) with a high risk of losing the sample. During visualisation, the penetration depth of an electron beam depends on accelerating voltage, beam current, and the concentration of heavy metals at or beneath the surface of the sample. The first two parameters are tuned while visualising the sample while the latter is optimised when designing an experimental pipeline. Here, we presented a detailed protocol that enables (1) the retaining of the integrity of calcified and stent-expanded cardiovascular tissues; (2) the obtainment of high-resolution images, thus allowing the visualisation of mineral deposits and their microenvironment, annotation of different microvessel types (i.e., arterioles, venules, and capillaries), and identification of various cardiovascular pathologies and cell populations; (3) the elemental analysis of calcifications. The protocol has been optimised for working with cardiovascular tissues but can be applied for virtually any tissue. A comparison of the features attributed to LM, confocal or multiphoton microscopy, TEM, density-dependent SEM, and EM-BSEM are represented in **Table 4**.

The possible limitation of our protocol is that it is hardly compatible with immunoelectron microscopy because of its insufficient resolution [even the largest gold particles labelling the secondary antibodies (25 nm in diameter) are barely detectable even at ×10,000 magnification], although some acrylic resins (e.g., LR White) allow the penetration of primary and secondary antibodies into the embedded tissue.

We suggest that EM-BSEM is superior to both H&E staining and TEM for studying cardiovascular pathology. The benefits of EM-BSEM include: (1) an image resolution sufficient for both the gross and detailed examination of elastic lamina degradation, (neo)intimal hyperplasia, (neo)vascularisation, intraplaque or intravalvular haemorrhages, lipid retention and foam cell formation, and disintegration of the extracellular matrix (including those mediated by the specialised macrophages); (2) a reliable identification of vascular cell populations (endothelial cells, vascular smooth muscle cells, macrophages, fibroblasts, mast cells, and adipocytes) and the recognition of immune cell lineages (macrophages, foam cells, foreign-body giant cells, neutrophils, and lymphocytes); (3) an opportunity to perform a chemical analysis of mineral deposits and metal implants in combination with obtaining a holistic overview of their tissue environment; (4) a technical possibility to quantify any distinguishable feature across the entire sample surface (e.g., blood vessel area) and at variable depth through the serial grinding; (5) a compatibility with modern machine learning algorithms for the automated annotation of histological and cellular patterns; (6) low technical complexity together with moderate labour intensity and hands-on time. Although the sample preparation in EM-BSEM is possibly too long for the broad implementation of this approach to clinical medicine, we assume it can be widely established in basic and translational research and would probably find its applications in other branches of biomedical science beyond the cardiovascular field.

DATA AVAILABILITY STATEMENT

The original contributions presented in the study are included in the article/**Supplementary Material**, further inquiries can be directed to the corresponding author.

ETHICS STATEMENT

The animal study was reviewed and approved by Local Ethical Committee of the Research Institute for Complex Issues of Cardiovascular Diseases. Studies involving human subjects were reviewed and approved by Local Ethical Committee of the Research Institute for Complex Issues of Cardiovascular Diseases. The patients/participants provided their written informed consent to participate in this study.

AUTHOR CONTRIBUTIONS

RM conceived and designed the EM-BSEM approach and prepared **Tables 1**, **4**, **Figures 5**, **6**, **8**. LB, TG, and DS prepared **Figures 4**, **6**, **7**, **9**, **10**. AEK prepared **Figures 2**, **3**. VK prepared **Figure 1**. ARS provided the clinical specimens for the preparation of **Figures 1**, **5**, **6**, **8**, **10**. AF provided the clinical specimens for the preparation of **Figures 6–9**. ANS provided the clinical specimens for the preparation of **Figures 1**, **5**, **8**. AL provided the clinical specimens for the preparation of **Figures 1**, **5**. AGK prepared **Tables 2**, **3** and wrote the manuscript. All authors contributed to the article and approved the submitted version.

FUNDING

This study was supported by the Complex Program of Basic Research under the Siberian Branch of the Russian Academy of Sciences within the Basic Research Topic of Research Institute for Complex Issues of Cardiovascular Diseases No. 0546-2019-0002. Pathogenetic basis for the development of cardiovascular implants from biocompatible materials using a patient-oriented approach, mathematical modelling, tissue engineering, and genomic predictors.

ACKNOWLEDGMENTS

The authors sincerely thank Emiliya Vellingtone for her assistance in the copyediting and proofreading of the manuscript. AGK thanks Emiliya Vellingtone for her unflagging patience and support, which propelled the team to conduct and finish this research, eventually leading to the development of EM-BSEM approach.

SUPPLEMENTARY MATERIAL

The Supplementary Material for this article can be found online at: https://www.frontiersin.org/articles/10.3389/fcvm.2021.739549/full#supplementary-material

REFERENCES

1. de Boer P, Hoogenboom JP, Giepmans BN. Correlated light and electron microscopy: ultrastructure lights up! *Nat Methods.* (2015) 12:503–13. doi: 10.1038/nmeth.3400
2. Ryan J, Gerhold AR, Boudreau V, Smith L, Maddox PS. Introduction to modern methods in light microscopy. *Methods Mol Biol.* (2017) 1563:1–15. doi: 10.1007/978-1-4939-6810-7_1
3. Combs CA, Shroff H. Fluorescence microscopy: a concise guide to current imaging methods. *Curr Protoc Neurosci.* (2017) 79:2.1.1–25. doi: 10.1002/cpns.29
4. Mukhamadiyarov RA, Sevostyanova VV, Shishkova DK, Nokhrin AV, Sidorova OD, Kutikhin AG. Grinding and polishing instead of sectioning for the tissue samples with a graft: implications for light and electron microscopy. *Micron.* (2016) 85:1–7. doi: 10.1016/j.micron.2016.03.005
5. Fu J, Su Y, Qin YX, Zheng Y, Wang Y, Zhu D. Evolution of metallic cardiovascular stent materials: a comparative study among stainless steel, magnesium and zinc. *Biomaterials.* (2020) 230:119641. doi: 10.1016/j.biomaterials.2019.119641
6. Oliver AA, Sikora-Jasinska M, Demir AG, Guillory RJ 2nd. Recent advances and directions in the development of bioresorbable metallic cardiovascular stents: insights from recent human and *in vivo* studies. *Acta Biomater.* (2021) 127:1–23. doi: 10.1016/j.actbio.2021.03.058
7. Pereira T, Betriu A, Alves R. Non-invasive imaging techniques and assessment of carotid vasa vasorum neovascularization: promises and pitfalls. *Trends Cardiovasc Med.* (2019) 29:71–80. doi: 10.1016/j.tcm.2018.06.007
8. Jensen E. Technical review: colocalization of antibodies using confocal microscopy. *Anat Rec.* (2014) 297:183–7. doi: 10.1002/ar.22835
9. Tizro P, Choi C, Khanlou N. Sample preparation for transmission electron microscopy. *Methods Mol Biol.* (2019) 1897:417–24. doi: 10.1007/978-1-4939-8935-5_33
10. Ribatti D, Tamma R, Ruggieri S, Annese T, Crivellato E. Surface markers: an identity card of endothelial cells. *Microcirculation.* (2020) 27:e12587. doi: 10.1111/micc.12587
11. Kostyunin A, Mukhamadiyarov R, Glushkova T, Bogdanov L, Shishkova D, Osyaev N, et al. Ultrastructural pathology of atherosclerosis, calcific aortic valve disease, and bioprosthetic heart valve degeneration: commonalities and differences. *Int J Mol Sci.* (2020) 21:7434. doi: 10.3390/ijms21207434
12. Frolov AV, Zagorodnikov NI, Bogdanov LA, Mukhamadiyarov RA, Terekhov AA, Kutikhin AG. Anatomy of adventitial and perivascular vasa vasorum as a key factor of a long-term coronary artery bypass graft surgery success. *Clin Exp Surg.* (2020) 8:65–73. doi: 10.33029/2308-1198-2020-8-4-65-73
13. Shishkova DK, Velikanova EA, Krivkina EO, Mironov AV, Kudryavtseva YA, Kutikhin AG. Calcium-phosphate bions do specifically induce hypertrophy of damaged intima in rats. *Russ J Cardiol.* (2018) 23:33–8. doi: 10.15829/1560-4071-2018-9-33-38
14. Osyaev NYu, Bogdanov L, Mukhamadiyarov RA, Shabaev AR, Shishkova DK, Markova VE, et al. Regularities of plaque stabilization in various scenarios of neointimal calcification and vascularization. *Russ J Cardiol.* (2021) 26:4051. doi: 10.15829/1560-4071-2021-4051
15. Orlando V, Strutt H, Paro R. Analysis of chromatin structure by *in vivo* formaldehyde cross-linking. *Methods.* (1997) 11:205–14. doi: 10.1006/meth.1996.0407
16. Orlando V. Mapping chromosomal proteins *in vivo* by formaldehyde-crosslinked-chromatin immunoprecipitation. *Trends Biochem Sci.* (2000) 25:99–104. doi: 10.1016/S0968-0004(99)01535-2
17. Hoffman EA, Frey BL, Smith LM, Auble DT. Formaldehyde crosslinking: a tool for the study of chromatin complexes. *J Biol Chem.* (2015) 290:26404–11. doi: 10.1074/jbc.R115.651679
18. Tayri-Wilk T, Slavin M, Zamel J, Blass A, Cohen S, Motzik A, et al. Mass spectrometry reveals the chemistry of formaldehyde cross-linking in structured proteins. *Nat Commun.* (2020) 11:3128. doi: 10.1038/s41467-020-16935-w
19. Jones D, Gresham GA. Reaction of formaldehyde with unsaturated fatty acids during histological fixation. *Nature.* (1966) 210:1386–8. doi: 10.1038/2101386b0
20. Jones D. The reaction of formaldehyde with unsaturated fatty acids during histological fixation. *Histochem J.* (1969) 1:459–91. doi: 10.1007/BF01086985
21. Wigglesworth VB. The use of osmium in the fixation and staining of tissues. *Proc R Soc Lond B Biol Sci.* (1957) 147:185–99. doi: 10.1098/rspb.1957.0043
22. Wigglesworth VB. The union of protein and nucleic acid in the living cell and its demonstration by osmium staining. *J Cell Sci.* (1964) s3-105:113–22. doi: 10.1242/jcs.s3-105.69.113
23. Nielson AJ, Griffith WP. Tissue fixation by osmium tetroxide. *A possible role for proteins. J Histochem Cytochem.* (1979) 27:997–9. doi: 10.1177/27.5.479559
24. Lombardi L, Prenna G, Okolicsanyi L, Gautier A. Electron staining with uranyl acetate. Possible role of free amino groups. *J Histochem Cytochem.* (1971) 19:161–8. doi: 10.1177/19.3.161
25. Doggenweiler CF, Frenk S. Staining properties of lanthanum on cell membranes. *Proc Natl Acad Sci USA.* (1965) 53:425–30. doi: 10.1073/pnas.53.2.425

26. Weihe E, Hartschuh W, Metz J, Brühl U. The use of ionic lanthanum as a diffusion tracer and as a marker of calcium binding sites. *Cell Tissue Res.* (1977) 178:285–302. doi: 10.1007/BF00218693
27. Rosoff B, Spencer H. Binding of rare earths to serum proteins and DNA. *Clin Chim Acta.* (1979) 93:311–9. doi: 10.1016/0009-8981(79)90280-8
28. Shaklai M, Tavassoli M. Lanthanum as an electron microscopic stain. *J Histochem Cytochem.* (1982) 30:1325–30. doi: 10.1177/30.12.6185564
29. Shaklai M, Tavassoli M. Preferential localization of lanthanum to nuclear-pore complexes. *J Ultrastruct Res.* (1982) 81:139–44. doi: 10.1016/S0022-5320(82)90069-7
30. Leeson TS, Higgs GW. Lanthanum as an intracellular stain for electron microscopy. *Histochem J.* (1982) 14:553–60. doi: 10.1007/BF01011888
31. Reynolds ES. The use of lead citrate at high pH as an electron-opaque stain in electron microscopy. *J Cell Biol.* (1963) 17:208–12. doi: 10.1083/jcb.17.1.208
32. Kiernan JA. Formaldehyde, formalin, paraformaldehyde and glutaraldehyde: what they are and what they do. *Microsc Today.* (2018) 8:8–13. doi: 10.1017/S1551929500057060
33. Hassan NA, D'Orsi ET, D'Orsi CJ, O'Neill WC. The risk for medial arterial calcification in CKD. *Clin J Am Soc Nephrol.* (2012) 7:275–9. doi: 10.2215/CJN.06490711
34. Manzoor S, Ahmed S, Ali A, Han KH, Sechopoulos I, O'Neill A, et al. Progression of medial arterial calcification in CKD. *Kidney Int Rep.* (2018) 3:1328–35. doi: 10.1016/j.ekir.2018.07.011
35. Zhang Y, Cliff WJ, Schoefl GI, Higgins G. Immunohistochemical study of intimal microvessels in coronary atherosclerosis. *Am J Pathol.* (1993) 143:164–72.
36. Parma L, Baganha F, Quax PHA, de Vries MR. Plaque angiogenesis and intraplaque hemorrhage in atherosclerosis. *Eur J Pharmacol.* (2017) 816:107–15. doi: 10.1016/j.ejphar.2017.04.028
37. Guerrini V, Gennaro ML. Foam cells: one size doesn't fit all. *Trends Immunol.* (2019) 40:1163–79. doi: 10.1016/j.it.2019.10.002
38. Bäck M, Yurdagul A Jr, Tabas I, Öörni K, Kovanen PT. Inflammation and its resolution in atherosclerosis: mediators and therapeutic opportunities. *Nat Rev Cardiol.* (2019) 16:389–406. doi: 10.1038/s41569-019-0169-2
39. Kolodgie FD, Gold HK, Burke AP, Fowler DR, Kruth HS, Weber DK, et al. Intraplaque hemorrhage and progression of coronary atheroma. *N Engl J Med.* (2003) 349:2316–25. doi: 10.1056/NEJMoa035655
40. Takaya N, Yuan C, Chu B, Saam T, Polissar NL, Jarvik GP, et al. Presence of intraplaque hemorrhage stimulates progression of carotid atherosclerotic plaques: a high-resolution magnetic resonance imaging study. *Circulation.* (2005) 111:2768–75. doi: 10.1161/CIRCULATIONAHA.104.504167
41. de Vries MR, Parma L, Peters HAB, Schepers A, Hamming JF, Jukema JW, et al. Blockade of vascular endothelial growth factor receptor 2 inhibits intraplaque haemorrhage by normalization of plaque neovessels. *J Intern Med.* (2019) 285:59–74. doi: 10.1111/joim.12821
42. Chang CJ, Chen CC, Hsu LA, Chang GJ, Ko YH, Chen CF, et al. Degradation of the internal elastic laminae in vein grafts of rats with aortocaval fistulae: potential impact on graft vasculopathy. *Am J Pathol.* (2009) 174:1837–46. doi: 10.2353/ajpath.2009.080795
43. Libby P, Buring JE, Badimon L, Hansson GK, Deanfield J, Bittencourt MS, et al. Atherosclerosis. *Nat Rev Dis Primers.* (2019) 5:56. doi: 10.1038/s41572-019-0106-z
44. Henrichot E, Juge-Aubry CE, Pernin A, Pache JC, Velebit V, Dayer JM, et al. Production of chemokines by perivascular adipose tissue: a role in the pathogenesis of atherosclerosis? *Arterioscler Thromb Vasc Biol.* (2005) 25:2594–9. doi: 10.1161/01.ATV.0000188508.40052.35
45. Moos MP, John N, Gräbner R, Nossmann S, Günther B, Vollandt R, et al. The lamina adventitia is the major site of immune cell accumulation in standard chow-fed apolipoprotein E-deficient mice. *Arterioscler Thromb Vasc Biol.* (2005) 25:2386–91. doi: 10.1161/01.ATV.0000187470.31662.fe
46. Kim HW, Shi H, Winkler MA, Lee R, Weintraub NL. Perivascular adipose tissue and vascular perturbation/atherosclerosis. *Arterioscler Thromb Vasc Biol.* (2020) 40:2569–76. doi: 10.1161/ATVBAHA.120.312470
47. Tinajero MG, Gotlieb AI. Recent developments in vascular adventitial pathobiology: the dynamic adventitia as a complex regulator of vascular disease. *Am J Pathol.* (2020) 190:520–34. doi: 10.1016/j.ajpath.2019.10.021
48. Helmchen F, Denk W. Deep tissue two-photon microscopy. *Nat Methods.* (2005) 2:932–40. doi: 10.1038/nmeth818
49. Egawa G, Ono S, Kabashima K. Intravital imaging of vascular permeability by two-photon microscopy. *Methods Mol Biol.* (2021) 2223:151–7. doi: 10.1007/978-1-0716-1001-5_11
50. Zong W, Wu R, Chen S, Wu J, Wang H, Zhao Z, et al. Miniature two-photon microscopy for enlarged field-of-view, multi-plane and long-term brain imaging. *Nat Methods.* (2021) 18:46–9. doi: 10.1038/s41592-020-01024-z
51. Bertazzo S, Gentleman E, Cloyd KL, Chester AH, Yacoub MH, Stevens MM. Nano-analytical electron microscopy reveals fundamental insights into human cardiovascular tissue calcification. *Nat Mater.* (2013) 12:576–83. doi: 10.1038/nmat3627
52. Tan ACS, Pilgrim MG, Fearn S, Bertazzo S, Tsolaki E, Morrell AP, et al. Calcified nodules in retinal drusen are associated with disease progression in age-related macular degeneration. *Sci Transl Med.* (2018) 10:eaat4544. doi: 10.1126/scitranslmed.aat4544
53. Ruiz JL, Hutcheson JD, Cardoso L, Bakhshian Nik A, Condado de Abreu A, Pham T, et al. Nanoanalytical analysis of bisphosphonate-driven alterations of microcalcifications using a 3D hydrogel system and in vivo mouse model. *Proc Natl Acad Sci U S A.* (2021) 118:e1811725118. doi: 10.1073/pnas.1811725118
54. Fernández-Segura E, Cañizares FJ, Cubero MA, Revelles F, Campos A. Backscattered electron imaging of cultured cells: application to electron probe X-ray microanalysis using a scanning electron microscope. *J Microsc.* (1997) 188(Pt 1):72–78. doi: 10.1046/j.1365-2818.1997.2329792.x
55. Kamari Y, Cohen H, Shaish A, Bitzur R, Afek A, Shen S, et al. Characterisation of atherosclerotic lesions with scanning electron microscopy (SEM) of wet tissue. *Diab Vasc Dis Res.* (2008) 5:44–7. doi: 10.3132/dvdr.2008.008
56. Wierzchos J, Falcioni T, Kiciak A, Woliński J, Koczorowski R, Chomicki P, et al. Advances in the ultrastructural study of the implant-bone interface by backscattered electron imaging. *Micron.* (2008) 39:1363–70. doi: 10.1016/j.micron.2008.01.022
57. Lafuente P, Franch J, Durall I, Manzanares C. Experimental study of bone lengthening in dogs by means of backscattered scanning electron microscopy. *Vet Surg.* (2009) 38:388–97. doi: 10.1111/j.1532-950X.2009.00505.x
58. Reichelt M, Sagolla M, Katakam AK, Webster JD. Unobstructed multiscale imaging of tissue sections for ultrastructural pathology analysis by backscattered electron scanning microscopy. *J Histochem Cytochem.* (2020) 68:9–23. doi: 10.1369/0022155419868992
59. Cohen Hyams T, Mam K, Killingsworth MC. Scanning electron microscopy as a new tool for diagnostic pathology and cell biology. *Micron.* (2020) 130:102797. doi: 10.1016/j.micron.2019.102797
60. Timmermans FJ, Otto C. Contributed review: review of integrated correlative light and electron microscopy. *Rev Sci Instrum.* (2015) 86:011501. doi: 10.1063/1.4905434
61. Gayoso J, Garrosa M, Gayoso S, Rodríguez-Arias CA, Martin-Ferrero MÁ, Gayoso MJ. Three-sectioning method: a procedure for studying hard tissues and large pieces under light and electron microscopy. *Micron.* (2020) 132:102841. doi: 10.1016/j.micron.2020.102841
62. Kusumi S, Koga D, Watanabe T, Shibata M. Combination of a cryosectioning method and section scanning electron microscopy for immuno-scanning electron microscopy. *Biomed Res.* (2018) 39:21–25. doi: 10.2220/biomedres.39.21
63. Koga D, Kusumi S, Shodo R, Dan Y, Ushiki T. High-resolution imaging by scanning electron microscopy of semithin sections in correlation with light microscopy. *Microscopy (Oxf).* (2015) 64:387–94. doi: 10.1093/jmicro/dfv042
64. Rizzo NW, Duncan KE, Bourett TM, Howard RJ. Backscattered electron SEM imaging of resin sections from plant specimens: observation of histological to subcellular structure and CLEM. *J Microsc.* (2016) 263:142–7. doi: 10.1111/jmi.12373
65. Koga D, Kusumi S, Watanabe T. Backscattered electron imaging of resin-embedded sections. *Microscopy.* (2018) 67:196–206. doi: 10.1093/jmicro/dfy028
66. Goggin P, Ho EML, Gnaegi H, Searle S, Oreffo ROC, Schneider P. Development of protocols for the first serial block-face scanning electron microscopy (SBF SEM) studies of bone tissue. *Bone.* (2020) 131:115107. doi: 10.1016/j.bone.2019.115107
67. Seligman AM, Wasserkrug HL, Hanker JS. A new staining method (OTO) for enhancing contrast of lipid–containing membranes and droplets in osmium tetroxide–fixed tissue with osmiophilic thiocarbohydrazide(TCH). *J Cell Biol.* (1966) 30:424–32. doi: 10.1083/jcb.30.2.424

68. Malick LE, Wilson RB. Modified thiocarbohydrazide procedure for scanning electron microscopy: routine use for normal, pathological, or experimental tissues. *Stain Technol.* (1975) 50:265–9. doi: 10.3109/10520297509117069
69. Willingham MC, Rutherford AV. The use of osmium-thiocarbohydrazide-osmium (OTO) and ferrocyanide-reduced osmium methods to enhance membrane contrast and preservation in cultured cells. *J Histochem Cytochem.* (1984) 32:455–60. doi: 10.1177/32.4.6323574
70. Belu A, Schnitker J, Bertazzo S, Neumann E, Mayer D, Offenhäusser A, et al. Ultra-thin resin embedding method for scanning electron microscopy of individual cells on high and low aspect ratio 3D nanostructures. *J Microsc.* (2016) 263:78–86. doi: 10.1111/jmi.12378

Conflict of Interest: The authors declare that the research was conducted in the absence of any commercial or financial relationships that could be construed as a potential conflict of interest.

frontiers in Cardiovascular Medicine

SYSTEMATIC REVIEW
published: 01 November 2021
doi: 10.3389/fcvm.2021.770648

Screening for Asymptomatic Coronary Artery Disease *via* Exercise Stress Testing in Patients With Type 2 Diabetes Mellitus: A Systematic Review and Meta-Analysis

Yaoshan Dun[1,2,3], *Shaoping Wu*[1], *Ni Cui*[1], *Randal J. Thomas*[3], *Thomas P. Olson*[3], *Nanjiang Zhou*[1], *Qiuxia Li*[1] *and Suixin Liu*[1,2*]

[1] *Division of Cardiac Rehabilitation, Department of Physical Medicine & Rehabilitation, Xiangya Hospital of Central South University, Changsha, China,* [2] *National Clinical Research Centre for Geriatric Disorders, Xiangya Hospital of Central South University, Changsha, China,* [3] *Division of Preventive Cardiology, Department of Cardiovascular Medicine, Mayo Clinic, Rochester, MN, United States*

OPEN ACCESS

Edited by:
Yihua Bei,
Shanghai University, China

Reviewed by:
Richard Yang Cao,
Shanghai Xuhui Central Hospital, China
Jing Shi,
Nanjing Medical University, China

***Correspondence:**
Suixin Liu
liusuixin@csu.edu.cn

Specialty section:
This article was submitted to General Cardiovascular Medicine, a section of the journal Frontiers in Cardiovascular Medicine

Received: *04 September 2021*
Accepted: *08 October 2021*
Published: *01 November 2021*

Citation:
Dun Y, Wu S, Cui N, Thomas RJ, Olson TP, Zhou N, Li Q and Liu S (2021) Screening for Asymptomatic Coronary Artery Disease via Exercise Stress Testing in Patients With Type 2 Diabetes Mellitus: A Systematic Review and Meta-Analysis. Front. Cardiovasc. Med. 8:770648. doi: 10.3389/fcvm.2021.770648

Objectives: This meta-analysis aims to investigate the diagnostic value of exercise stress testing (EST) for asymptomatic coronary artery disease (CAD) among patients with type 2 diabetes mellitus (T2DM) and to ascertain the influence of different variables on the sensitivity and specificity of EST.

Background: Asymptomatic CAD occurs in >1 in five diabetes mellitus patients, and it is associated with an increased risk of complications. Methods for screening asymptomatic CAD in T2DM patients are still not unified.

Methods: MEDLINE (*via* Ovid), Embase (*via* Ovid), Cochrane Library, SCOPUS, PubMed, Ovid, EBSCO ASP, and Web of Science were systematically searched on June 8 and 9, 2021, for diagnostic cohort and case-control studies. We included studies that used EST to screen for CAD in asymptomatic patients with T2DM, and that used coronary angiography to diagnose CAD and had reported the basic diagnostic indicators. The Quality Assessment of Diagnostic Accuracy Studies 2 tool was used to assess study quality. The combined effect sizes were calculated by overall analysis and multiple variable effects were explored by regression analysis and subgroup analysis.

Results: Nine groups of data from eight diagnostic cohort studies, totaling 515 participants, were included. Included studies showed a low risk of bias in most items, except for flow and timing. The combined sensitivity and specificity of EST for asymptomatic CAD in patients with T2DM were 55 (48 to 61%) and 66 (61 to 70%), respectively. When non-diagnostic tests were excluded, sensitivity increased to 73 (56 to 88%). The proportion receiving angiography also significantly affected sensitivity. No significant difference was found in the duration of diabetes or other additional risk factors.

Conclusions: EST is a tool of moderate sensitivity and specificity to be used for the initial screening of asymptomatic CAD in T2DM. It has the advantage of being non-invasive, relatively inexpensive, easily available in most settings, and has no radiation associated

with its use. Additional research with higher quality studies in which tests that are non-diagnostic are included and flow and timing is described clearly, will be important to further our understanding of EST for asymptomatic CAD detection in patients with T2DM.

Systematic review registration: PROSPERO CRD42021259555.

Keywords: exercise stress testing (EST), coronary artery disease (CAD), type 2 diabetes mellitus(T2DM), diagnostic test, meta-analysis

INTRODUCTION

By modern estimates, approximately 425 million (6%) people have diabetes worldwide, with type 2 diabetes mellitus (T2DM) accounting for the majority (>85%) (1). The incidence of asymptomatic coronary artery disease (CAD) in diabetics is between two and seven times higher than in non-diabetic patients (2). Studies (2) have demonstrated that asymptomatic CAD occurs in >1 in five (22%) diabetics, which is associated with autonomic neuropathy involving afferent sympathetic fibers (3, 4). Asymptomatic myocardial ischemia is associated with an increased risk of complications such as myocardial infarction due to delayed diagnosis and treatment (5). Moreover, patients with T2DM present a higher incidence of cardiovascular events and death after a first myocardial infarction (4, 6, 7).

A recent meta-analysis (8) concluded that compared with standard care, non-invasive CAD screening reduced cardiac events by 27% in asymptomatic diabetic patients. In practice, Wackers et al. (2) found that selecting only patients who met the American Diabetes Association guidelines would have failed to identify 41% of patients with silent ischemia. Current recommendations (9) advocate CAD screening in asymptomatic diabetics with high risk. Further research into screening strategies for asymptomatic diabetic patients is warranted.

The methods for screening asymptomatic CAD in diabetics may vary and are not unified. While coronary angiography is the gold standard for identifying CAD, this invasive technique is reserved for patients with evidence of ischemia on a stress test or for those with continuous cardiac symptoms (10). Therefore several non-invasive tools have been recommended for primary screening of asymptomatic CAD in diabetics, including exercise stress testing (EST), single-photon emission computed tomography (SPECT), multidetector computed tomography (MDCT), coronary computed tomography angiogram (CCTA), and stress echocardiography (11).

Among those approaches, EST is the most common tool applied to individuals with suspected CAD (12). Compared with alternative methods, EST is non-invasive, cost-effective, free from radiation, and widely available, affirming its appropriateness as an initial screening tool. In addition, it also has prognostic value by providing information on exercise capacity, dysrhythmia evaluation, heart rate response and hemodynamic response (13).

Gianrossi et al. (14) observed high sensitivity and specificity of EST for CAD in the general population, but with wide variability (mean sensitivity, 68%; range, 23–100%; and mean specificity, 77%; range, 17–100%). While the diagnostic values of exercise electrocardiograph (ECG) testing in diabetics was first explored in a review (15), no combined diagnostic values of EST were calculated based on the small size and higher verification bias of included studies. To date, there is no higher-level clinical evidence to probe into the diagnostic value of EST in asymptomatic patients with T2DM. Moreover, due to the wide variability of diagnostic values across different studies, we lack a systematic understanding of how various factors contribute to the sensitivity and specificity of EST detecting asymptomatic CAD for diabetics.

Therefore, the purpose of this meta-analysis is to investigate the diagnostic value of EST for detecting asymptomatic CAD patients with T2DM; and to ascertain the influence of different variables (population, technical and methodologic factors) on the sensitivity and specificity of EST for asymptomatic CAD detection of T2DM patients.

METHODS

The methods and results of this meta-analysis are presented according to the Preferred Reporting Items for Systematic reviews and Meta-Analysis statement (PRISMA) (**Supplementary PRISMA DTA Checklist**). The meta-analysis was registered at PROSPERO (CRD42021259555).

Criteria for Screening Studies

Inclusion Criteria

Articles were included if they fulfilled the following criteria; (a) cohort or case-control studies; (b) participants diagnosed with T2DM but without any coronary disease (e.g., stable angina, unstable angina, myocardial infarction) confirmed prior to participation; (c) EST must be used to screen CAD in T2DM patients on a bicycle ergometer or treadmill with a 12-lead ECG recorded during testing, with invasive coronary angiography as the gold standard; (d) the outcome data can be derived, including true positive (TP), false positive (FP), false negative (FN), and true negative (TN).

Exclusion Criteria

Studies were excluded if the full-text was unavailable, participants were only type 1 diabetes mellitus, the EST detection criteria was not ST depression, such as exercise capacity, heart rate response, or a 2 × 2 diagnostic table could not be reconstructed.

Search Methods

MEDLINE, Embase, SCOPUS, PubMed, Ovid, EBSCO ASP, and Web of Science were searched by using a strategy combining selected Medical Subject Headings (MeSH) terms (Exercise test;

Diabetes Mellitus, Type 2; Coronary Artery Disease, Myocardial Ischemia, Heart disease) and free-text terms. Additionally, we searched ClinicalTrial.gov to determine whether there were related clinical trials being carried out. The search term regarding diagnostic study design (sensitiv* OR [sensitivity and specificity] OR [predictive AND value*] OR predictive value of tests OR accuracy*), was obtained through the website of McMaster university health information. We imposed no language or other limitations. The detailed search strategies are listed in **Supplementary Methods**. The last search was performed on June 9, 2021.

Information regarding the inclusion/exclusion of studies is summarized in **Figure 1**.

Data Collection

Two authors (NC and SW) independently screened each record retrieved from the search after deduplication. The full-text reports of all potentially relevant diagnostic studies were obtained and independently assessed for eligibility based on the defined inclusion criteria. Thereafter, participant characteristics, outcomes, technical and methodologic factors of the included studies were extracted using a standardized data collection form which had been piloted on two records included in the meta-analysis.

Any disagreement during the process was resolved through discussion, and where uncertainty remained, two additional authors (YD and SL) were consulted for consensus.

Assessment of Methodologic Quality

We used the Quality Assessment of Diagnostic Accuracy Studies 2 (QUADAS-2) tool to assess the quality of included studies (17). Two authors independently evaluated the risk of bias and the applicability concerns, and if there were discrepancies, these were resolved *via* discussion or reviewed by other authors.

Overall Analysis

Heterogeneity amongst included studies was explored from both diagnostic and non-diagnostic thresholds in Meta-DiSc 1.4 (18) and STATA 15.1 (StataCorp LLC, US). Where appropriate, the results from included studies were combined for each outcome to give an overall estimate of diagnostic effect. A fixed-effect meta-analysis would be used if $I^2 \leq 50\%$, if not, a random-effects model would be used.

The Spike plot was used for sensitivity analysis to check for particularly influential observations using Cook's distance. The Deek's funnel plot asymmetry test was used to examine publication bias for outcomes.

Univariate Regression Analysis

To explore the origin of heterogeneity, we carried out regression analysis in JMP Pro 14 (SAS, NC, USA). Given the relatively small ratio of trials to covariates, multivariable meta-regression was not appropriate, and instead, limited to a univariate analysis. Subsequently, we carried out subgroup analysis for further exploration of statistically significant items. Regarding missing data, we made a chart to present the detailed percentage we collected, and we would discard those missing more than 60% of the data. All collected information is displayed in **Table 1**.

Subgroup Analysis

Subgroup analysis was performed in STATA 15.1 to examine potential diagnostic effect modifiers. We tested the following a priori hypotheses that there may be differences in the diagnostic effect of EST on sensitivity and specificity:

- Type of diabetes (mixed: type 1 and 2; or only type 2);
- Exercise protocol (treadmill or bicycle ergometer);
- The proportion of included participants (all-included or proportion-included);
- Angiographic criteria of CAD (50% or others).

RESULTS

Description of Studies

Results of the Search

We traced 1,909 results from multiple electronic sources. After removal of duplicates, title and abstract screening, 55 records remained. Then, 47 records were excluded after the full-text screening. Finally, eight (16, 19–25) studies were included in our meta-analysis and systematic review. This selection process is summarized in **Figure 1**.

Included Studies

All of the eight studies (nine datasets) were diagnostic cohort studies and included 515 asymptomatic diabetics. The sample size of most studies was relatively small (median 64 participants, range: 28–104). Among 515 patients, 177 diabetics (34%) were diagnosed with CAD by angiography (range 27–51% in a single study). The average age of participants in the trials ranged from 48 to 60 years, and the mean duration of diabetes ranged from 6.0 to 12.9 years. Moreover, many participants had co-existing cardiovascular risk factors apart from diabetes, 67% had hypertension (range: 28–100%), 34% with smoking history (range: 17–65%), 67% with lipid abnormalities (rang: 45–89%) and 35% with a family history of CAD (range: 5–63%). One study (16) only included women. Men accounted for 51% of the total included participants. Two studies (19, 22) included a mixed population with type 1 and type 2 diabetes and the remaining six studies included only type 2 diabetics.

In two studies (20, 21), the angiographic definition of CAD was a narrowing of 70% or greater in the cross-sectional area of one coronary artery. One study (22) defined CAD as a $\geq$70% narrowing of the coronary artery, or $\geq$50% diameter narrowing of the left main coronary artery, while the remaining studies defined CAD as a 50% narrowing. In five studies (19–22, 25), participants were screened by two or more non-invasive screenings, including EST and other tools such as SPECT or MDCT or stress echocardiography. When at least one of these non-invasive tests was positive, angiography would be conducted and only patients who received both EST and angiography were included in our meta-analysis. While this may contribute to ascertainment bias, those studies were included due to the small number of relevant studies available. We had performed

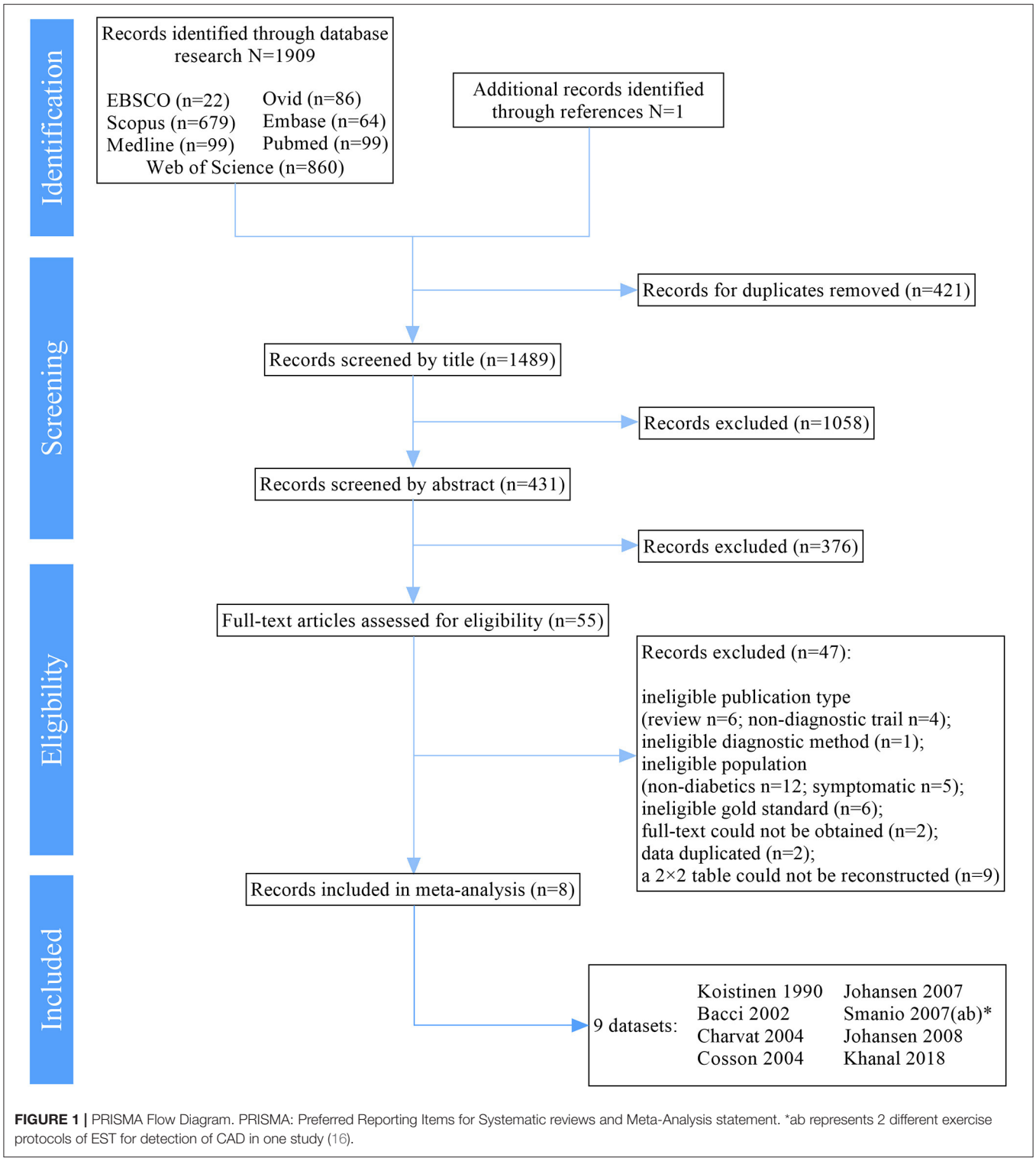

FIGURE 1 | PRISMA Flow Diagram. PRISMA: Preferred Reporting Items for Systematic reviews and Meta-Analysis statement. *ab represents 2 different exercise protocols of EST for detection of CAD in one study (16).

subgroup analysis (the proportion of included participants) to assess the impact of bias. EST indication in four studies (19, 20, 23, 24) was an ST depression ≥1 mm persisting for at least 0.08s after the J point, and in two studies (21, 22) was an ST depression >1 mm and in one study was an ST depression ≥1.5 mm (16). Five studies (19, 21–24) used cycle ergometry and the others used treadmill ergometry. Only one study (19) reported no adverse events during EST.

All studies reported diagnostic values available for a 2 × 2 table reconstruction. Details of included studies are listed in **Table 2**.

TABLE 1 | Variables abstracted from exercise stress testing literature.

Population characteristics (15 variables)	Technical factors (12 variables)	Methodologic factors (5 variables)
Mean age	Publication year	Was the exercise ECG being compared with a better test? (yes/no)
Percent men	Continent of study center	
Mean duration of diabetes (years)	Exercise protocol (treadmill, bicycle)	Whether all participants were included? (yes/no)
Were patients with these conditions excluded from the study? (yes/no)	Smallest amount of ST depression deemed abnormal (1, > 1, 1.5 mm)	Did the authors comply with these standards? (yes/no)
Left ventricular hypertrophy	Point in time when measurement was made ST depressions adjusted for heart rate? (yes/no)	
Right bundle branch block		Blind reading of angiogram
Left bundle branch block		Blind reading of ECG
Mitral valve prolapse	Computer algorithm used to analyze ST	Treatment of equivocal or non-diagnostic test were
Resting repolarization abnormalities?	Segment? (yes/no)	
	Percent patients achieving "adequate heart rate"	Excluded from analysis
Whether all patients were T2DM?		Included and considered as normal tests
Percent of the study group with	Mean workload achieved (W)	Not mention about these patients
Hypertension	Mean heart rate achieved (bpm)	
Smoking	Mean double product achieved	
Lipid abnormalities	Time interval between exercise test and coronary angiogram	
Family history of CAD		
Were patients taking these medications excluded from the study? (yes/no)	Angiographic definition of disease (50% vs. others)	
P-receptor-blocking agents		
Long-acting nitrates		

CAD, Coronary heart disease; ECG, Electrocardiograp; T2DM, Type 2 diabetes mellitus.

Risk of Bias in Included Studies

Details on the methodologic quality of included studies are available in **Supplementary Figures 1**, **2**. Only one study (23) showed a low risk of bias in all items, and five studies (19–22, 25) reported a high risk in flow and timing.

While two studies reported low risk in patient selection, five studies showed unclear risk. Two studies (20, 23) included consecutive or randomized patients, while one (16) recruited patients *via* phone-call or e-mail. All included studies avoided inappropriate exclusions except for one study (24) which did not report exclusion criteria of participants.

Most studies reported low risk in the index test, except one study (16) reported unclear risk. Reference test was performed before index test in one study (16), without description blinding assessment of index test.

The details that the reference standard results interpreted without knowledge of the index test results were only described in four studies. In general, four studies (20–22, 25) were judged as unclear risks of standard reference bias.

A high risk of bias was observed in the flow and timing. Information about the interval between index tests and the reference standard was not described in four included studies (21, 22, 24, 25). Five studies (19–22, 25) were judged as high risk of bias without appropriate analysis of all included patients.

Diagnostic Performance of EST

Overall Analysis

The data of the overall meta-analysis are provided in **Supplementary Table 1**: 2 × 2 table.

The Spearman correlation coefficient was 0.21 ($p = 0.59 > 0.05$), showing no significant threshold effect in this study. Furthermore, the symmetric SROC curve (**Supplementary Figure 3**) was drawn without "shoulder and arm shape," which further demonstrates no threshold effect.

The result of the Cochran-Q test for DOR indicated heterogeneity caused by the non-threshold effect exists in included studies (Cochran-Q = 25.98, $p < 0.01$). Furthermore, I^2 of sensitivity, specificity, positive likelihood ratio (LR^+), negative likelihood ratio (LR^-), and DOR were all significantly high. A random-effect model was used to estimate the five effect sizes above, which might only serve as a reference on account of its high heterogeneity.

Based on the nine datasets, the combined sensitivity and specificity of EST were 55 (48 to 61%) and 66 (61 to 70%), respectively (**Supplementary Figure 4**). Combined LR^+ of EST was 1.52 (1.08 to 2.13), combined LR^- was 0.74 (0.55 to 0.99), the combined area under the curve (AUC) was 0.66, combined Q index was 0.62, and combined DOR was 2.33 (1.17 to 4.65). Besides, the combined positive predictive value was 47 (34 to 59%), and the

TABLE 2 | Characteristics of included studies.

References	Study design	Sample size (*n*)	Population constitution	Clinical presentation	Exercise protocol	EST indication of CAD	Reference standard used	Angiographic criteria of CAD
Koistinen et al. (19)	Cohort	33	Type 1 and type 2 diabetics	Asymptomatic	Bicycle	ST depression ≥1 mm and persisted for at least 0.08 s after the J point	Coronary angiogram	≥50% narrowing
Bacci et al. (20)	Cohort	71	Type 2 diabetics	Asymptomatic	Treadmill	ST depression ≥1 mm and persisted for at least 0.08 s after the J point	Coronary angiogram	≥70% narrowing
Charvat et al. (21)	Cohort	30	Type 2 diabetics	Asymptomatic	Bicycle	ST depression >1 mm and persisted for at least 0.08 s after the J point	Coronary angiogram	≥70% narrowing
Cosson et al. (22)	Cohort	76	Type 1 and type 2 diabetics	Asymptomatic	Bicycle	ST depression >1 mm and persisted for at least 0.08 s after the J point	Coronary angiogram	≥50% or ≥70% narrowing*
Johansen et al. (23)	Cohort	82	Type 2 diabetics	Asymptomatic	Bicycle	ST depression ≥1 mm	Coronary angiogram	≥50% narrowing
Smanio et al. (16)†	Cohort	104	Type 2 diabetics	Asymptomatic	Treadmill	ST depression ≥1.5 mm in relation to baseline or exercise-induced ischemia	Coronary angiogram	≥50% narrowing
Smanio et al. (16)†	Cohort	104	Type 2 diabetics	Asymptomatic	Bicycle	ST depression ≥1.5 mm in relation to baseline or exercise-induced ischemia	Coronary angiogram	≥50% narrowing
Johansen et al. (24)	Cohort	91	Type 2 diabetics	Asymptomatic	Bicycle	ST depression ≥1 mm	Coronary angiogram	≥50% narrowing
Khanal et al. (25)	Cohort	28	Type 2 diabetics	Asymptomatic	Treadmill	Exercise ECG	Coronary angiogram	≥50% narrowing

CAD, Coronary heart disease; ECG, Electrocardiograph. EST, Exercise stress testing.

**≥50% for the left main coronary artery and ≥70% for others coronary artery.*

† Different exercise protocols of EST for detection of CAD in one study (16).

TABLE 3 | Variables associated with sensitivity and specificity by univariate regression analysis.

Variables	Sensitivity coefficient [95%CI]	*p*	Specificity coefficient [95%CI]	*p*
Mean age	−0.02 [−0.08 to 0.03]	0.33	−0.01 [−0.06 to 0.04]	0.75
Percent men	0.107 [−0.56 to 0.78]	0.72	−0.003 [−0.50 to 0.49]	0.99
Mean duration of diabetes (years)	0.05 [−0.03 to 0.13]	0.17	−0.02 [−0.10 to 0.05]	0.42
Left ventricular hypertrophy	−0.08 [−0.36 to 0.20]	0.5	0.16 [−0.004 to 0.32]	0.06
Right bundle branch block	−0.08 [−0.36 to 0.20]	0.5	0.16 [−0.004 to 0.32]	0.06
Left bundle branch block	−0.09 [−0.29 to 0.12]	0.34	0.02 [−0.14 to 0.18]	0.76
Mitral valve prolapse	−0.08 [−0.36 to 0.20]	0.5	0.16 [−0.004 to 0.32]	0.06
Resting repolarization abnormalities?	−0.03 [−0.24 to 0.19]	0.79	0.01 [−0.16 to 0.17]	0.94
only type 2 or mixed type 1/2	−0.07 [−0.28 to 0.14]	0.46	0.05 [−0.10 to 0.20]	0.47
Hypertension	0.16 [−0.67 to 1.00]	0.64	−0.05 [−0.84 to 0.73]	0.87
smoking	−0.43 [−1.80 to 0.95]	0.46	0.26 [−1.05 to 1.57]	0.63
Lipid abnormalities	−0.46 [−4.11 to 3.18]	0.64	0.76 [−1.11 to 2.63]	0.22
Family history of CAD	−0.48 [−1.25 to 0.30]	0.17	0.48 [−0.20 to 1.16]	0.13
p-receptor-blocking agents	0.09 [−0.11 to 0.30]	0.33	−0.03 [−0.19 to 0.13]	0.7
long-acting nitrates	0.09 [−0.11 to 0.30]	0.33	−0.03 [−0.19 to 0.13]	0.7
Publication year	−0.01 [−0.04 to 0.01]	0.37	−0.01 [−0.03 to 0.01]	0.17
Continent of study center*		0.57		0.18
Exercise protocol (treadmill, bicycle)	0.001 [−0.18 to 0.18]	0.99	−0.004 [−0.14 to 0.13]	0.94
Smallest amount of ST depression deemed abnormal (1, >1, 1.5 mm)*		0.57		0.11
ST depressions adjusted for heart rate (yes/no)	0.16 [−0.10 to 0.41]	0.18	−0.03 [−0.24 to 0.18]	0.75
Computer algorithm used to analyze ST segment	0.16 [−0.1 to 0.41]	0.18	−0.03 [−0.24 to 0.18]	0.75
Percent patients achieving "adequate heart rate"	1.33 [−8.00 to 10.65]	0.6	2.33 [−6.98 to 11.64]	0.39
Mean heart rate achieved (bpm)	0.02 [−0.01 to 0.06]	0.09	0.001 [−0.04 to 0.04]	0.94
Time interval between exercise test and coronary angiogram	−0.05 [−0.24 to 0.15]	0.42	−0.002 [−0.14 to 0.14]	0.96
Angiographic definition of disease (50% vs. others)	−0.09 [−0.27 to 0.08]	0.24	0.01 [−0.14 to 0.15]	0.93
Was the exercise ECG being compared with a "better" test (yes/no)	−0.04 [−0.22 to 0.14]	0.64	0.05 [−0.08 to 0.17]	0.43
Whether all participants were included? (yes/no)	0.18 [0.09 to 0.27]	0.002	−0.05 [−0.18 to 0.07]	0.37
Blind reading of angiogram	0.12 [−0.03 to 0.27]	0.1	−0.07 [−0.19 to 0.05]	0.22
Blind reading of ECG	−0.04 [−0.26 to 0.17]	0.66	−0.07 [−0.22 to 0.07]	0.28
Treatment of equivocal or non-diagnostic test were	0.15 [0.02 to 0.28]	0.03	0.01 [−0.12 to 0.15]	0.85

**p-value among the two factors in this item was calculated.*

combined negative predictive value was 74 (68 to 80%) (**Supplementary Figure 5**).

Supplementary Figure 6 demonstrates the result of sensitivity analysis. The sensitivity of all the original studies is low suggesting the results of this study are relatively stable.

We found no publication bias in the regression test for funnel plot asymmetry (Deek's test $p = 0.25 > 0.05$; **Supplementary Figure 7**).

Univariate Regression Analysis

Supplementary Figure 8 shows the percentage of missing data for those items in **Table 1**. Two variables (mean double product achieved and mean workload achieved) were excluded in univariate regressions analysis because more than 60% of the data were missing for these variables. One variable (point in time when the measurement was made) was excluded as it was the same in all studies.

Table 3 displays the results of the univariate regressions analysis. Studies that included patients who had partially received angiography calculated significantly higher sensitivity than those all received ($p < 0.001$). Also, studies that excluded non-diagnostic tests from analysis reported significantly higher sensitivity than studies that did not mention these patients ($p = 0.03$). Other variables showed no significant relationship with both sensitivity and specificity in the analysis.

Subgroup Analysis

Forest Plots of Sensitivity and Specificity of EST for CAD detection in different subgroups are presented in **Figures 2**, **3**. **Figure 2** shows the sensitivity and specificity of different types of diabetes (**Figures 2A,B**), different exercise protocol (**Figures 2C,D**), and different proportions of patients included from studies (**Figures 2E,F**). **Figure 3** shows the sensitivity and specificity of different angiographic criteria of CAD (**Figures 3A,B**) and different treatment equivocal or non-diagnostic tests (**Figures 3C,D**).

Type of Diabetes

No significant heterogeneity was observed in sensitivity between two subgroups ($p = 0.50$) (**Figure 2A**), while it existed in

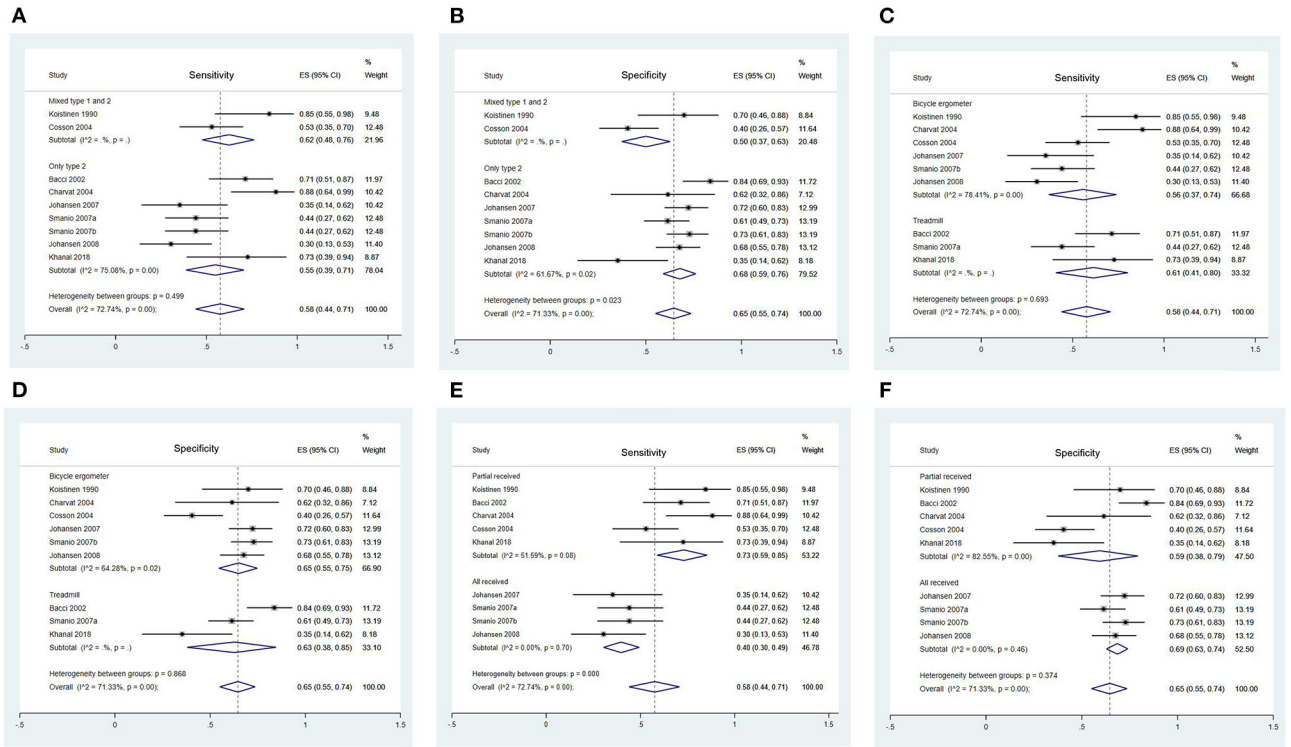

FIGURE 2 | Forest Plots of Sensitivity and Specificity of EST in Different Subgroups. **(A)** Forest plot of sensitivity of EST in different type of diabetes; **(B)** Forest plot of specificity of EST in different type of diabetes; **(C)** Forest plot of sensitivity of EST in different exercise protocol; **(D)** Forest plot of specificity of EST in different exercise protocol; **(E)** Forest plot of sensitivity of EST in different proportion of included participants; **(F)** Forest plot of specificity of EST in different proportion of included participants.

specificity ($p = 0.02$) (**Figure 2B**). It might indicate that the specificity of EST in mixed type 1 and 2 diabetics [50 (37 to 63%)] was significantly lower than only type 2 diabetics population [68 (59 to 76%)].

Exercise Protocol

No significant heterogeneity was observed in sensitivity and specificity between two subgroups (sensitivity: $p = 0.69$; specificity: $p = 0.87$) (**Figures 2C,D**).

The Proportion of Included Participants

Significant heterogeneity was observed in sensitivity between two groups ($p < 0.001$) (**Figure 2E**). Studies where only a proportion of participants were included presented a higher sensitivity [73 (59 to 85%)] than those in which all participants included [40 (30 to 49)]. No significant heterogeneity was observed in specificity between two subgroups ($p = 0.37$) (**Figure 2F**).

Angiographic Criteria of CAD

No significant heterogeneity was observed in both sensitivity ($p = 0.11$) and specificity ($p = 0.84$) between two subgroups (**Figures 3A,B**).

Treatment of Equivocal or Non-diagnostic Test

Significant heterogeneity was shown in sensitivity between two groups ($p = 0.004$) (**Figure 3C**). Sensitivity in studies that excluded these patients [73 (56 to 88%)] from the analysis was significantly higher than those without mention [43 (32 to 54%)]. No significant heterogeneity was observed in specificity ($p = 0.84$) between two subgroups (**Figure 3D**).

The sensitivity and specificity of EST for CAD according to total population and subgroups are listed in **Table 4**.

DISCUSSION

To our knowledge, this is the first systematic meta-analysis to investigate the EST screening programme for asymptomatic CAD in T2DM. The results of which suggest that EST is a tool with moderate sensitivity and specificity in the initial screening of asymptomatic CAD in T2DM. It is particularly appealing compared to other screening tool options, since it is non-invasive, relatively inexpensive, easily available in most centers, and involves no radiation.

The present study suggested that studies with proportional participants included had significantly higher sensitivity than those in which all participants were included, suggesting an influence of ascertainment bias in those results. Still, the use of angiography in patients with an abnormal EST may be a cost-effective and clinically feasible approach. We also found that the specificity of EST in the group of mixed type 1 and

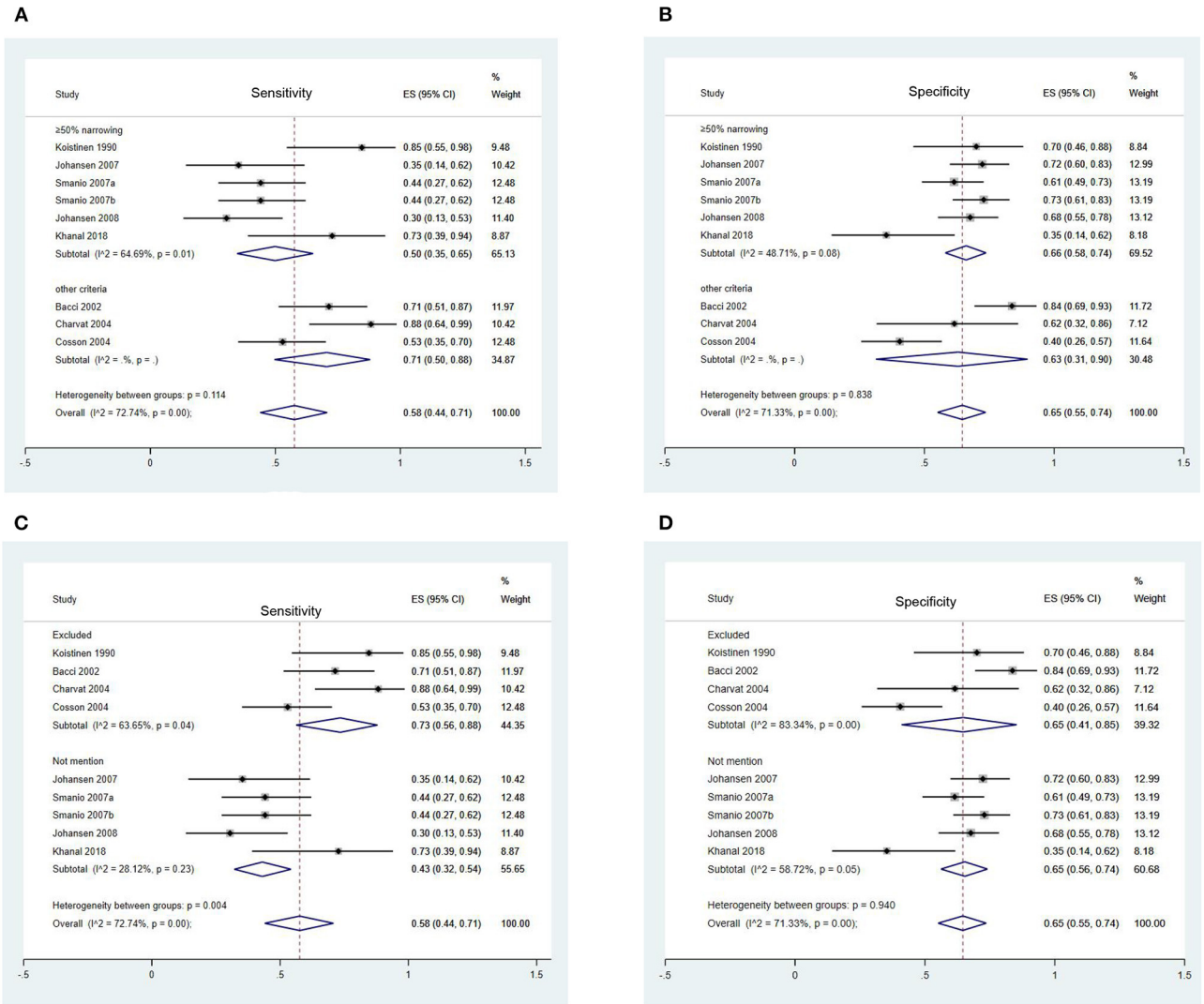

FIGURE 3 | Forest Plots of Sensitivity and Specificity of EST in Different Subgroups. **(A)** Forest plot of sensitivity of EST in different angiographic criteria of CAD; **(B)** Forest plot of specificity of EST in different angiographic criteria of CAD; **(C)** Forest plot of sensitivity of EST in different treatment equivocal or non-diagnostic test; **(D)** Forest plot of specificity of EST in different treatment equivocal or non-diagnostic test.

2 diabetics were significantly lower than that of only type 2 diabetics in subgroup analysis. This suggests that EST is relatively accurate in identifying T2DM patients without asymptomatic CAD possibly due to patients with T1DM generally developing the disease at a younger age than those with T2DM, as EST has been demonstrated a relatively lower specificity in the youth population (26). Additionally, if the non-diagnostic tests were excluded, the sensitivity of EST would increase substantially from 55 to 73%. Non-diagnostic was defined as "the patient interrupted the test before they reached a heart rate corresponding to 85% of the maximal aerobic capacity without ischemic changes in ECG." As for the "not mentioned" group, where they did not clarify how non-diagnostic tests were identified, it is not clear whether non-diagnostic tests were included and considered as normal EST screening tests. This may have contributed to why the sensitivity in studies that excluded the non-diagnostic patients (73%) from the analysis was significantly higher than that in studies that did not mention the disposition of non-diagnostic tests (43%). These findings highlight the critical importance of closely following standardized methodology when conducting and interpreting EST in clinical practice. Standardized guidelines (27, 28) have been published detailing specific absolute and relative EST termination and interpretation criteria. In the event that an EST is terminated prior to meeting predefined standardized criteria, that test should be defined as non-diagnostic and data should be interpreted with caution.

Contrary to our expectations, the univariate regression analysis did not find a significant difference regarding the mean duration of diabetes and left bundle branch block. This may

TABLE 4 | Sensitivity and specificity of EST for coronary artery disease according to total population and subgroups.

	Diagnostic performance estimate			
	Sensitivity		Specificity	
	Estimate	95% CI	Estimate	95% CI
Total	0.58	0.44–0.71	0.65	0.55–0.74
Type of diabetes				
Mixed type 1 and 2	0.62	0.48–0.76	0.50*	0.37–0.63
Only type 2	0.55	0.39–0.71	0.68*	0.69–0.76
Exercise protocol				
Bicycle ergometer	0.56	0.37–0.74	0.65	0.55–0.75
Treadmill	0.61	0.41–0.80	0.63	0.38–0.85
The proportion of included participants†				
All included	0.40*	0.30–0.49	0.69	0.63–0.74
Proportional included	0.73*	0.59–0.85	0.59	0.38–0.79
Angiographic criteria of CAD				
Other criteria	0.71	0.50–0.88	0.63	0.31–0.90
≥50% narrowing	0.5	0.35–0.65	0.66	0.58–0.74
Treatment of equivocal or non-diagnostic test				
Excluded	0.73*	0.56–0.88	0.65	0.41–0.85
Not mention	0.43*	0.32–0.54	0.65	0.56–0.74

*$p \leq 0.05$ in heterogeneity test between groups.
†Only participants who received both EST and angiography were included into our analysis. This is the proportion of participants we include in the original studies.

be due to the small heterogeneity in diabetes duration of the nine datasets (five articles' mean duration of diabetes = 6 years), or the big difference in article numbers between two subgroups (left bundle branch block: exclude to include = 1 to 8). However, this also indicates that the screening effects of EST are stable, and it would not be interfered with by the above factors.Furthermore, EST in the clinical setting may be achieved with relative safety, a 18-year cross-sectional study from our team, which included 50,142 consecutive tests, suggested that EST is safe with a low rate of adverse events at 0.6 per 10,000 tests (0.2–1.8) (29).

In clinical practice, there are several methods used to assess CAD in asymptomatic diabetic patients. A cost-effectiveness study (30) previously recommended that applying a low-cost test to a large-scale population with selective use of more expensive testing at a later stage for patients with a higher probability of suffering disease is more cost-effective than applying the more expensive test as the initial step. The major advantage of EST is its lower cost compared with most of other methods. Besides, it is readily available and free from radiation, which supports its use as an initial test. Especially when combining clinical information with EST data, they could yielded a 94% sensitivity and 92% specificity (31). Meanwhile, it should be acknowledged that physical disability and vascular and neuropathic changes would make it difficult to reach the target heart rate in EST, which may limit the ability of some patients to complete an EST. Generally, more higher quality studies are needed, in which non-diagnostic tests are excluded and the flow and timing is described clearly.

Limitations

It is important to recognize potential limitations regarding this meta-analysis. First, over half of the selected articles included only proportional participants from the original studies. Only participants with positive EST or other non-invasive exams would be lead to further gold standard examination, which might increase bias as these included participants might not well-represent this population. To investigate the effect of this bias on the results, we performed a subgroup analysis and offered a detailed explanation. Second, missing data in our subgroup analysis resulted in decreased power of the outcome. Third, these diagnostic studies are often based on preselected populations. The need for exercise ability may limit some patients, which may result in selection bias. Last, most websites we searched have only English reports even though we did not set any limitations in languages and consequently, we may have missed data from essential studies published in other languages.

CONCLUSIONS

EST is a tool with moderate sensitivity and specificity in the initial screening of asymptomatic CAD in T2DM. It is appealing, compared to other screening tools, because it is non-invasive, relatively inexpensive, easily available in most centers, and does not involve radiation. Additional higher-quality studies, where non-diagnostic tests are excluded and the flow and timing are described clearly, are needed to study the use of EST for screening for CAD in T2DM patients.

DATA AVAILABILITY STATEMENT

The raw data supporting the conclusions of this article will be made available by the authors, without undue reservation.

ETHICS STATEMENT

The studies involving human participants were reviewed and approved by the Ethics Committee of Xiangya Hospital of Central South University.

AUTHOR CONTRIBUTIONS

YD contributed to the design, acquisition of data, analysis, funding acquisition and writing (review and editing). SW contributed to the acquisition of data, analysis and writing (original draft). NC contributed to the acquisition of data, analysis and writing (original draft). RT and TO contributed to conceptualization, writing (review and editing). NZ and QL contributed to conceptualization and writing (review). SL contributed to conceptualization, supervision, and funding acquisition. All authors contributed to the article and approved the submitted version, and accept full responsibility for the work and conduct of this study.

FUNDING

Grants support were received from the National Natural Science Foundation of China (82002403), Hunan Provincial Natural Science Foundation of China (2021JJ40981), and the Youth Science Foundation of Xiangya Hospital (2019Q03) to YD.

ACKNOWLEDGMENTS

We are grateful to the authors who provided valued data and information in eligible studies.

SUPPLEMENTARY MATERIAL

The Supplementary Material for this article can be found online at: https://www.frontiersin.org/articles/10.3389/fcvm.2021.770648/full#supplementary-material

REFERENCES

1. Forouhi NG, Wareham NJ. Epidemiology of diabetes. *Medicine.* (2019) 47:22–7. doi: 10.1016/j.mpmed.2018.10.004
2. Wackers FJ, Young LH, Inzucchi SE, Chyun DA, Davey JA, Barrett EJ, et al. Detection of silent myocardial ischemia in asymptomatic diabetic subjects: the DIAD study. *Diabetes Care.* (2004) 27:1954–61. doi: 10.2337/diacare.27.8.1954
3. Di Carli MF, Hachamovitch R. Should we screen for occult coronary artery disease among asymptomatic patients with diabetes? *J Am Coll Cardiol.* (2005) 45:50–3. doi: 10.1016/j.jacc.2004.09.055
4. Nesto RW, Phillips RT. Asymptomatic myocardial ischemia in diabetic patients. *Am J Med.* (1986) 80:40–7. doi: 10.1016/0002-9343(86)90451-1
5. Pikto-Pietkiewicz W, Przewlocka M, Chybowska B, Cyciwa A, Pasierski T. Simple exercise test score versus cardiac stress test for the prediction of coronary artery disease in patients with type 2 diabetes. *Pol Arch Med Wewn.* (2014) 124:157–64. doi: 10.20452/pamw.2182
6. Abbott RD, Donahue RP, Kannel WB, Wilson PW. The impact of diabetes on survival following myocardial infarction in men vs women. *JAMA.* (1988) 260:3456–60. doi: 10.1001/jama.1988.03410230074031
7. Manson JE, Colditz GA, Stampfer MJ, Willett WC, Krolewski AS, Rosner B, et al. A prospective study of maturity-onset diabetes mellitus and risk of coronary heart disease and stroke in women. *Arch Intern Med.* (1991) 151:1141–7. doi: 10.1001/archinte.1991.00400060077013
8. Clerc OF, Fuchs TA, Stehli J, Benz DC, Grani C, Messerli M, et al. Non-invasive screening for coronary artery disease in asymptomatic diabetic patients: a systematic review and meta-analysis of randomised controlled trials. *Eur Heart J Cardiovasc Imaging.* (2018) 19:838–46. doi: 10.1093/ehjci/jey014
9. Cosentino F, Grant PJ, Aboyans V, Bailey CJ, Ceriello A, Delgado V, et al. 2019 ESC Guidelines on diabetes, pre-diabetes, and cardiovascular diseases developed in collaboration with the EASD. *Eur Heart J.* (2020) 41:255–323. doi: 10.1093/eurheartj/ehz486
10. Roelker E. Screening for coronary artery disease in patients with diabetes. *Diabetes Spectrum.* (2008) 21:166. doi: 10.2337/diaspect.21.3.166
11. Budoff MJ, Raggi P, Beller GA, Berman DS, Druz RS, Malik S, et al. Noninvasive cardiovascular risk assessment of the asymptomatic diabetic patient: the imaging council of the American college of cardiology. *JACC Cardiovascular imaging.* (2016) 9:176–92. doi: 10.1016/j.jcmg.2015.11.011
12. Gibbons RJ, Balady GJ, Bricker JT, Chaitman BR, Fletcher GF, Froelicher VF, et al. ACC/AHA 2002 guideline update for exercise testing: summary article. A report of the American college of cardiology/American heart association task force on practice guidelines (committee to update the 1997 exercise testing guidelines). *J Am Coll Cardiol.* (2002) 40:1531–40. doi: 10.1016/S0735-1097(02)02164-2
13. Roger VL, Jacobsen SJ, Pellikka PA, Miller TD, Bailey KR, Gersh BJ. Prognostic value of treadmill exercise testing: a population-based study in Olmsted County, Minnesota. *Circulation.* (1998) 98:2836–41. doi: 10.1161/01.CIR.98.25.2836
14. Gianrossi R, Detrano R, Mulvihill D, Lehmann K, Dubach P, Colombo A, et al. Exercise-induced ST depression in the diagnosis of coronary artery disease. A meta-analysis. *Circulation.* (1989) 80:87–98. doi: 10.1161/01.CIR.80.1.87
15. Albers AR, Krichavsky MZ, Balady GJ. Stress testing in patients with diabetes mellitus: diagnostic and prognostic value. *Circulation.* (2006) 113:583–92. doi: 10.1161/CIRCULATIONAHA.105.584524
16. Smanio PEP, Carvalho AC, Tebexreni AS, Thom A, Rodrigues F, Meneghelo R, et al. Coronary artery disease in asymptomatic type-2 diabetic women. A comparative study between exercise test, cardiopulmonary exercise test, and dipyridamole myocardial perfusion scintigraphy in the identification of ischemia. *Arq Bras Cardiol.* (2007) 89:290–7.
17. Whiting PF, Rutjes AW, Westwood ME, Mallett S, Deeks JJ, Reitsma JB, et al. QUADAS-2: a revised tool for the quality assessment of diagnostic accuracy studies. *Ann Intern Med.* (2011) 155:529–36. doi: 10.7326/0003-4819-155-8-201110180-00009
18. Zamora J, Abraira V, Muriel A, Khan K, Coomarasamy A. Meta-DiSc: a software for meta-analysis of test accuracy data. *BMC Med Res Methodol.* (2006) 6:31. doi: 10.1186/1471-2288-6-31
19. Koistinen MJ, Huikuri HV, Pirttiaho H, Linnaluoto MK, Takkunen JT. Evaluation of exercise electrocardiography and thallium tomographic imaging in detecting asymptomatic coronary artery disease in diabetic patients. *Br Heart J.* (1990) 63:7–11. doi: 10.1136/hrt.63.1.7
20. Bacci S, Villella M, Villella A, Langialonga T, Grilli M, Rauseo A, et al. Screening for silent myocardial ischaemia in type 2 diabetic patients with additional atherogenic risk factors: applicability and accuracy of the exercise stress test. *Eur J Endocrinol.* (2002) 147:649–54. doi: 10.1530/eje.0.1470649
21. Charvat J, Michalova K, Taborska K, Chlumsky J, Kvapil M. Comparison of the exercise ECG and stress myocardial SPECT in detection of the significant coronary artery disease in the asymptomatic patients with diabetes mellitus type 2. *Bratisl Lek Listy.* (2004) 105:56–61.

22. Cosson E, Paycha F, Paries J, Cattan S, Ramadan A, Meddah D, et al. Detecting silent coronary stenoses and stratifying cardiac risk in patients with diabetes: ECG stress test or exercise myocardial scintigraphy? *Diabetic Medicine.* (2004) 21:342–8. doi: 10.1111/j.1464-5491.2004.01157.x
23. Johansen OE, Birkeland KI, Orvik E, Flesland Ø, Wergeland R, Ueland T, et al. Inflammation and coronary angiography in asymptomatic type 2 diabetic subjects. *Scand J Clin Lab Invest.* (2007) 67:306–16. doi: 10.1080/00365510601045088
24. Johansen OE, Birkeland KI, Endresen K, Blaasaas KG, Bjurö T, Aakhus S, et al. Heart rate adjustments and analysis of recovery patterns improves detection of coronary artery disease in patients with type 2 diabetes. *Diabetes.* (2008) 56:A168–9. doi: 10.1016/j.ijcard.2007.04.022
25. Khanal S, Rao G R, Sood A, Dutta P. Effective early screening modalities for asymptomatic coronary artery disease in patients with type 2 diabetes mellitus. *J Cardiovasc Dis Res*. (2018) 9:63–7. doi: 10.5530/jcdr.2018.2.16
26. Hermann LK, Weingart SD, Duvall WL, Henzlova MJ. The limited utility of routine cardiac stress testing in emergency department chest pain patients younger than 40 years. *Ann Emerg Med.* (2009) 54:12–6. doi: 10.1016/j.annemergmed.2009.01.006
27. Balady GJ, Arena R, Sietsema K, Myers J, Coke L, Fletcher GF, et al. Clinician's Guide to cardiopulmonary exercise testing in adults: a scientific statement from the American Heart Association. *Circulation.* (2010) 122:191–225. doi: 10.1161/CIR.0b013e3181e52e69
28. Guazzi M, Adams V, Conraads V, Halle M, Mezzani A, Vanhees L, et al. EACPR/AHA Scientific Statement. Clinical recommendations for cardiopulmonary exercise testing data assessment in specific patient populations. *Circulation.* (2012) 126:2261–74. doi: 10.1161/CIR.0b013e31826fb946
29. Dun Y, Olson TP, Ripley-Gonzalez JW, Xie K, Zhang W, Cai Y, et al. Safety of exercise testing in the clinical chinese population. *Front Cardiovasc Med.* (2021) 8:638682. doi: 10.3389/fcvm.2021.638682
30. Miller TD, Askew JW, Anavekar NS. Noninvasive stress testing for coronary artery disease. *Cardiol Clin.* (2014) 32:387–404. doi: 10.1016/j.ccl.2014.04.008
31. Harris GD, White RD. Exercise stress testing in patients with type 2 diabetes: when are asymptomatic patients screened? *Clinical Diabetes.* (2007) 25:126–30. doi: 10.2337/diaclin.25.4.126

Conflict of Interest: The authors declare that the research was conducted in the absence of any commercial or financial relationships that could be construed as a potential conflict of interest.

Publisher's Note: All claims expressed in this article are solely those of the authors and do not necessarily represent those of their affiliated organizations, or those of the publisher, the editors and the reviewers. Any product that may be evaluated in this article, or claim that may be made by its manufacturer, is not guaranteed or endorsed by the publisher.

frontiers in Cardiovascular Medicine

ORIGINAL RESEARCH
published: 01 December 2021
doi: 10.3389/fcvm.2021.777964

Clinical Characteristics for the Improvement of Cushing's Syndrome Complicated With Cardiomyopathy After Treatment With a Literature Review

Sisi Miao[1,2], Lin Lu[1], Ling Li[3], Yining Wang[4], Zhaolin Lu[1], Huijuan Zhu[1], Linjie Wang[1], Lian Duan[1], Xiaoping Xing[1], Yong Yao[5], Ming Feng[5] and Renzhi Wang[5]*

[1] Key Laboratory of Endocrinology of National Health Commission, Department of Endocrinology, Peking Union Medical College Hospital, Chinese Academy of Medical Science and Peking Union Medical College, Beijing, China, [2] School of Clinical Medicine, Guizhou Medical University, Guiyang, China, [3] Department of Cardiology, Peking Union Medical College Hospital, Chinese Academy of Medical Science and Peking Union Medical College, Beijing, China, [4] Department of Radiology, Peking Union Medical College Hospital, Chinese Academy of Medical Science and Peking Union Medical College, Beijing, China, [5] Department of Neurosurgery, Peking Union Medical College Hospital, Chinese Academy of Medical Science and Peking Union Medical College, Beijing, China

OPEN ACCESS

Edited by:
Yan Zhang,
Peking University, China

Reviewed by:
Zhe Bao Wu,
Shanghai Jiao Tong University, China
Hongying Ye,
Fudan University, China

***Correspondence:**
Lin Lu
lulin88@sina.com

Specialty section:
This article was submitted to General Cardiovascular Medicine, a section of the journal Frontiers in Cardiovascular Medicine

Received: *16 September 2021*
Accepted: *10 November 2021*
Published: *01 December 2021*

Citation:
Miao S, Lu L, Li L, Wang Y, Lu Z, Zhu H, Wang L, Duan L, Xing X, Yao Y, Feng M and Wang R (2021) Clinical Characteristics for the Improvement of Cushing's Syndrome Complicated With Cardiomyopathy After Treatment With a Literature Review. Front. Cardiovasc. Med. 8:777964. doi: 10.3389/fcvm.2021.777964

Background: Endogenous Cushing's syndrome (CS), also called hypercortisolism, leads to a significant increase in mortality due to excessive cortisol production, which is mainly due to cardiovascular disease. CS complicated with cardiomyopathies, which is a rare and severe condition, has rarely been reported in the literature.

Objective: To investigate the clinical characteristics of CS complicated with cardiomyopathies, we retrospectively reviewed the clinical manifestations, laboratory results, cardiac imaging results and prognosis to further understand the diagnosis, treatment, and management of these cases.

Methods: The clinical data of patients diagnosed with CS complicated with cardiomyopathies obtained from discharge sheets from Peking Union Medical College Hospital from January 1986 to August 2021 were collected. Case reports of CS complicated with cardiomyopathies were retrieved from PubMed. In addition, Cushing's disease (CD) patients without cardiomyopathies were collected as controls to compare the clinical features.

Results: A total of 19 cases of CS complicated with cardiomyopathies and cases of CD without cardiomyopathies (n = 242) were collected. The causes of CS included pituitary adenoma (n = 8, 42.11%), adrenal adenoma (n = 7, 36.84%), ectopic adrenocorticotropic hormone (ACTH) tumor (n = 2, 10.53%) and unclear causes (n = 2, 10.53%) in the CS complicated with cardiomyopathies group. The types of cardiomyopathies were dilated cardiomyopathies (n = 15, 78.94%) and hypertrophic cardiomyopathies (n = 4, 21.05%). The serum sodium concentration was significantly higher [145.50 (140.50–148.00) mmol/L vs. 141.00 (140.00–143.00) mmol/L], while the serum potassium concentration was significantly lower [2.70 (2.40–3.60) mmol/L] vs.

3.90 (3.50–4.20 mmol/L)] in the CS complicated with cardiomyopathies group compared to the CD patients without cardiomyopathies. There were no significant differences between the CS complicated with cardiomyopathies group and the CD patients without cardiomyopathies in the serum cortisol concentration and 24-h urine free cortisol, but a significant difference in the adrenocorticotropic hormone level [109.00 (91.78–170.30) pg/ml vs. 68.60 (47.85–110.00) pg/ml]. Twelve/16 (75.0%) patients showed significant improvement or even a complete healing of the heart structure and function after remission of hypercortisolemia after treatment with CS.

Conclusions: CS complicated with cardiomyopathies is a very rare clinical entity, in which cortisol plays an important role and it can be greatly improved after remission of hypercortisolemia.

Keywords: Cushing's syndrome, cardiomyopathies, hypercortisolism, cardiac structure, cardiac function

INTRODUCTION

Cushing's syndrome (CS) is a rare disease, which caused by a variety of etiologies and is characterized by excessive cortisol production by the adrenal glands due to a pituitary adenoma, ectopic adrenocorticotropin syndrome secondarily or by adrenal tumor, or autonomous hyperplasia. CS can be complicated by several metabolic abnormalities, such as hypertension, impaired glucose tolerance, and hyperlipidemia, and patients with CS have a high risk of opportunistic infection and coagulation problems due to hypercortisolemia. The mortality in CS is increased significantly with a standard mortality rate (SMR) of 3.68 (2.34–5.33) (1). A study of adrenal incidentaloma with a mean follow-up of 7.5 years showed that, compared with patients with non-secretory adrenal incidentaloma, patients with subclinical hypercortisolism had a nearly four-fold increase in all-cause mortality (8.8 vs. 43%), a 10% higher incidence of cardiovascular events (6.7 vs. 16.7%) and a 7.6 times higher incidence of cardiovascular mortality (2.5 vs. 21.6%) (2). In addition, compared with the patients with a cortisol level <1.8 μg/dL after the dexamethasone suppression test, the patients with a cortisol level between 1.85 and 5 μg/dL had a higher mortality hazard ratio of 12.0 (1.6–92.6), and patients with a cortisol level >5 μg/dL had the highest mortality hazard ratio of 22.0 (2.6–188.3). Notably, 50% of deaths were due to cardiovascular disease (3). Because CS is often diagnosed months or years after the onset of symptoms, an increased risk of cardiovascular disease could be present even before the diagnosis (4).

Given the significantly increased risk of death and cardiovascular disease, several studies have assessed the changes in the cardiac structure and function in CS. Patients with CS often have an increased left ventricular mass and relative wall thickness (5), a higher proportion of impaired diastolic function (6), and a lower left ventricular ejection fraction (LVEF) (7). Several studies investigated whether the cardiac structure and function could improve after remission of hypercortisolism. Toja et al. (5) found that cardiac mass abnormalities (such as an increased left ventricular mass and an increased relative wall thickness) were improved but not completely recovered after curative treatment in CS. Moreover, although the LVEF was within the normal range after remission of CS, the value was still slightly lower than that of the control group. Peter Kamenický et al. (7) found that the subclinical cardiac systolic dysfunction was recovered and the LVEF increased by 15% after remission of CS.

Cardiomyopathies are a group of heterogeneous myocardial diseases characterized by cardiomyocyte disorders, which lead to myocardial mechanical and/or electrical dysfunction. Based on the anatomy and physiology, cardiomyopathies consist of the following types (each with a variety of different causes): dilated cardiomyopathies (DCM), hypertrophic cardiomyopathies (HCM), restrictive cardiomyopathies (RCM), arrhythmic right ventricular cardiomyopathies/dysplasia (ARVC/D) and undefined cardiomyopathies. Since CS is a rare disease with an incidence of 2–5/10^6/year, CS complicated with cardiomyopathy is rarely seen among the known causes. A search of the literature found that there were only a few case reports about CS complicated with cardiomyopathies, in which the major type was DCM (8–19). If CS induces cardiomyopathies, it is speculated that the mortality risk of CS patients will be further aggravated. To investigate the clinical characteristics of CS complicated with cardiomyopathies, this study described the diagnosis, treatment, management and prognosis of patients with CS complicated with cardiomyopathies in Peking Union Medical College Hospital and a literature review is also discussed.

SUBJECTS AND METHODS

Subjects

CS Complicated With Cardiomyopathies in Peking Union Medical College Hospital

The data from the CS cases complicated with cardiomyopathies were obtained through a search of the discharge sheet from the hospital information system at Peking Union Medical College Hospital from January 1986 to August 2021. Written informed consent was obtained from the patients or their family

members for the publication of the images and data. The Ethics Committee of Peking Union Medical College Hospital approved this retrospective study.

The inclusion criteria were as follows: (1) a diagnosis of CS, including the typical clinical manifestations of CS, increased midnight cortisol or 24-h urine free cortisol (UFC), and no suppression of cortisol after the low-dose dexamethasone suppression test; and (2) evidence of a cardiomyopathy: an echocardiography or a cardiac magnetic resonance imaging (MRI) showing ventricular dilation and decreased myocardial contractility or left ventricular wall thickening (interventricular septum dimension or left ventricular posterior wall dimension $\geq$15 mm).

The exclusion criteria were as follows: (1) an enlarged left ventricle and decreased myocardial systolic function resulting from other identified causes, such as long-term poorly controlled hypertension, diabetes, valvular heart disease, congenital or ischemic heart disease; (2) left ventricular wall thickening caused by other identified causes, such as hypertension, aortic stenosis, or congenital subaortic septum; (3) infectious disease; (4) cardiomyopathies diagnosed prior to the onset of CS symptoms; (5) familial cardiomyopathies; (6) systemic autoimmune disease; (7) evidence of amyloidosis; (8) thyroid disorders without treatment; and (9) lack of clinical information.

Altogether, 7 patients who met the enumerated inclusion/exclusion criteria were enrolled. We collected information about these cases, including (1) the demographic features such as age and sex; (2) the time of onset of CS; (3) the clinical symptoms of cardiomyopathies such as dyspnea, fatigue, edema; (4) the physical examination data, such as height, weight, body mass index (BMI), and blood pressure; (5) the laboratory examinations, including routine blood tests, blood glucose, serum potassium, serum sodium, blood lipids, and hypersensitive C-reactive protein; (6) the pituitary and adrenal hormone tests, including adrenocorticotrophic hormone (ACTH), serum cortisol, 24-hour urine free cortisol (24-h UFC), high- and low-dose dexamethasone suppression tests; (7) the electrocardiogram and echocardiography findings; (8) the treatment of hypercortisolemia; and (9) the outcomes after the diagnosis and treatment.

Literature Review of CS Complicated With Cardiomyopathies

The literature search of the PubMed online database was conducted up to August 1, 2021; we searched for keywords including [Cushing syndrome], [Hypercortisolism], and [cardiomyopathy]. The inclusion and exclusion criteria were the same as those mentioned above.

Twenty patients from 13 studies had CS complicated with cardiomyopathies, of which 8 patients from 1 study (20) were excluded due a lack of detailed clinical data. Finally, 12 patients met the inclusion and exclusion criteria, and relevant medical information was collected.

Cases of Cushing Disease Without Cardiomyopathies

Since most cases of CS complicated with cardiomyopathies were ACTH-dependent CS in our medical center, 242 CD cases without cardiomyopathies who had detailed clinical evaluation of cardiac structure and function were collected from the hospital information system of Peking Union Medical College Hospital for comparison. All the 242 cases were admitted to the inpatient department and had through cardiac evaluation including echocardiography, showing no evidence of cardiomyopathy.

Statistical Methods

Qualitative data are presented as frequencies and percentages. Quantitative data are presented as the mean $\pm$ standard deviation if conforming to a normal distribution or medians (25th, 75th percentile). Independent two-sample *t*-tests, chi-square tests, or Mann-Whitney *U*-tests were used to evaluate the statistical significance. Statistical analysis was performed using GraphPad Prism 8 (GraphPad Software, La Jolla, California, USA). $P < 0.05$ indicated significance.

RESULTS

A total of 19 patients who had a diagnosis of CS complicated with cardiomyopathies were identified in our center [Case 1 to Case 7 ($n = 7$)] and in the literature [Case 8 to Case 19 ($n = 12$)]. A total of 242 patients diagnosed with CD without cardiomyopathies were identified as controls.

The Demographic of CS Complicated With Cardiomyopathies

The 19 patients with CS complicated with cardiomyopathies included 10 males (52.63%) and 9 females (47.37%), and there was a males to females ratio of 1.11:1. The mean age at diagnosis of CS with cardiomyopathies was 35.33 $\pm$ 19.75 years old. The average BMI was 28.78 $\pm$ 5.178 kg/m^2 ($n = 11$) (**Table 1**).

The causes of CS with cardiomyopathies were pituitary adenoma ($n = 8$, 42.11%), adrenal adenoma ($n = 7$, 36.84%), ectopic ACTH syndrome ($n = 2$, 10.53%), and unclear causes ($n = 2$, 10.53%). The types of cardiomyopathies were DCM ($n = 15$, 78.95%) and HCM (n=4, 21.05%). At the same time, 11/18 (61.11%) patients also had hypertension, 5/12 (41.67%), diabetes, 8/11 (72.72%), hyperlipemia, and hypokalemia 6/12 (50.00%) (**Table 1**).

The cardiac symptoms of these patients were mainly dyspnea (10/19), and 5 patients had no relevant symptoms when the cardiomyopathies were detected by ultrasonography. Based on the cardiac function standard of the New York Heart Association, 3/10 patients were grade I, 3/10 were grade II, and 4/10 were grade III (**Table 1**).

The Manifestation of Electrocardiography and Echocardiogram or Cardiac MRI

In the available electrocardiograph (ECG) examination, 7/13 patients presented with sinus tachycardia, 1/13 patients presented with atrial premature beat, 1/13 patients presented with ventricular premature beat, 1/13 patients presented paroxysmal atrial fibrillation, and 3/13 patients had no arrhythmia. A total of 2/8 patients had prolonged QTc intervals (469 and 471 ms). ECG ST-T changes were observed in 6/9 patients.

TABLE 1 | Clinical characteristics of CS complicated with cardiomyopathies.

	Case 1	Case 2	Case 3	Case 4	Case 5	Case 6	Case 7	Case 8	Case 9	Case 10	Case 11	Case 12	Case 13	Case 14	Case 15	Case 16	Case 17	Case 18	Case 19
Sex	F	M	F	M	M	M	M	F	F	F	F	F	M	M	F	M	M	F	M
Age (year)	30	59	26	31	25	28	20	48	43	28	50	67	20	43	63	64	26	7 (weeks)	4 (months)
BMI (kg/m^2)	29.6	31.3	28.58	27.9	38.3	25.9	22.5	NA	35.5	26.5	NA	NA	30.12	NA	NA	NA	NA	NA	20.43
Cause of cushing syndrome	Pituitary adenoma	Pituitary adenoma	Pituitary adenoma	Pituitary adenoma	NA	Lung carcinoid	NA	Adrenal adenoma	Adrenal adenoma	Adrenal adenoma	Pituitary adenoma	Adrenal adenoma	Pituitary adenoma	Pituitary adenoma	Adrenal adenoma	SCLC	Pituitary adenoma	Adrenal adenoma	Adrenal adenoma
Type of cardiomyopathies	DCM	HCM	HCM	DCM	DCM	DCM	DCM	DCM	DCM	DCM	DCM	DCM	DCM	DCM	DCM	DCM	DCM	HCM	HCM (Obstructive)
Symptoms of cardiomyopathies	Dyspnea cough	No	Edema of lower extremities	Dyspnea, edema	Cough, fatigue and edema	Fatigue and edema	Dyspnea, cough and edama	Dyspnea	Dyspnea	Dyspnea and cough	No	No	Dyspnea	Dyspnea	No	Dyspnea	Dyspnea exhaustion	Edema	No
Time between the onset of CS and presence of cardiac symptoms (months)	96	NA	24	27	16	8	9	NA	30	17	NA	NA	NA	NA	NA	NA	NA	NA	NA
Complications																			
Hypertension	No	Yes	Yes	Yes	No	Yes	Yes	No	Yes	No	No	Yes	No	Yes	NA	Yes	No	Yes	Yes
Diabetes	No	No	No	No	No	No	Yes	NA	NA	No	Yes	Yes	NA	NA	NA	Yes	No	Yes	NA
Hyperlipidemia	Yes	Yes	Yes	Yes	Yes	Yes	Yes	NA	NA	No	No	Yes	NA	NA	NA	NA	No	NA	NA
Hypokalemia	No	No	Yes	No	No	Yes	Yes	NA	NA	No	NA	Yes	NA	Yes	NA	Yes	No	NA	NA
Systolic blood pressure (mmHg)	140	160	181	160	140	190	160	130	150	140	NA	173	120	NA	NA	189	NA	120	110
Diastolic blood pressure (mmHg)	100	100	121	100	90	120	120	85	80	80	NA	116	90	NA	NA	101	NA	80	65
NYHA	II	I	I	II	III	III	II	NA	NA	III	NA	III	NA	NA	NA	NA	NA	NA	I
Treatments to relieve hypercortisolemia	Pituitary surgery	Repeated Pituitary surgerys	Repeated Pituitary surgerys	Pituitary surgery	No surgery due to severe heart failure	Failure pituitary surgery and radiotherapy, then pulmonary carcinoid resection	Pituitary surgery and bilateral adrenalectomy	Drug plus adrenal adenoma resection	Adrenal resection (left)	Drug plus adrenal resection (right)	Drug plus radiotherapy	Adrenal resection	Pituitary surgery	Drug	Adrenal resection	Drug plus chemotherapy	Pituitary surgery	Drug plus adrenal surgery	Adrenal surgery
Number of treatment methods	1	2	2	1	0	3	2	2	1	2	2	1	1	1	1	2	1	2	1
Outcome of cardiomyopathies in the followup	NA	No significant change	NA	NA	No significant change	Improvement	Death	Improvement	Improvement	Improvement	Improvement	Improvement	Improvement	No significant change	Improvement	Improvement	Improvement	Improvement	Improvement

F, Female; M, Male; DCM, dilated cardiomyopathies; HCM, hypertrophic cardiomyopathies; SCLC, small-cell lung cancer; NYHA, New York Heart Association classification for congestive heart failure.

TABLE 2 | Echocardiography or cardiac magnetic resonance imaging of cases with CS complicated with cardiomyopathies.

	Case 1	Case 2	Case 3	Case 4	Case 5	Case 6	Case 7	Case 8	Case 9	Case 10	Case 11	Case 12	Case 13	Case 14	Case 15	Case 16	Case 17	Case 18	Case 19
LA (mm)	44	41	28	44	66 × 49	47	57 × 52 × 48	NA	NA	NA	NA	NA	NA	NA	NA	NA	NA	NA	NA
LVDd (mm)	61	53	50	56	79	70	68	NA	NA	65.7	NA	56	NA	64	61	57	NA	NA	NA
IVSd (mm)	9	22	16	12	10	7	11	NA	NA	8.6	NA	13	NA	NA	12	11	NA	NA	18
LVPWd (mm)	9	10	11	10	8	7	11	NA	NA	9.8	NA	NA	NA	NA	NA	11	NA	NA	NA
LVEF (%)	33	73	77.1	50	31	28	26	27	45	34	NA	36	20	28–30	24	31	10	NA	NA
FS (%)	16	NA	NA	27	15	14	9.5	NA	NA	NA	NA	NA	NA	NA	NA	NA	NA	NA	NA

LA, left atrium dimension; LVDd, left ventricular end diastolic dimension; IVSd, interventricular septum dimension; LVPWd, left ventricular posterior wall dimension; LVEF, left ventricular ejection fraction; FS, (Left ventricular) fractional shortening.

In patients with DCM, the left ventricular end diastolic dimension (LVDd) ranged from 56 to 79 mm, with an average of 63.77 mm ($n = 10$); the interventricular septum dimension (IVSd) ranged from 7 to 13 mm, with an average of 10.40 mm ($n = 9$), among which 3 patients had thickened IVSd; the left ventricular posterior wall dimension (LVPWd) ranged from 7 to 11 mm with an average of 9.4 mm ($n = 7$); and the LVEF ranged from 10 to 50% with an average of 30.39% ($n = 14$). In the HCM patients, the IVSd ranged from 16 to 22 mm with an average of 18.67 mm ($n = 3$); the LVPWd was 10 and 11 mm; the LVDd was 53 mm and 50 mm; and the LVEF was 70% and 69%, which was within the normal range, respectively, in Case 2 and Case 3 (**Table 2**).

The Outcomes After Treatment

Among the patients with CS complicated with cardiomyopathies, 8 patients underwent pituitary surgery, and among them, in Case 2 and Case 3, a repeated pituitary operation was performed due to the failure of the first pituitary operation. In Case 6, pulmonary carcinoid leading to excessive ectopic ACTH secretion was diagnosed by further examination after the failure of the first pituitary operation and pituitary radiotherapy, and a resection was performed. In Case 7, a bilateral adrenalectomy was performed due not achieving remission after the pituitary operation and the continued severe hypercortisolism. Seven patients underwent adrenal surgery, and among them, hypercortisolemia drugs were administered prior to surgery in Case 8, Case10, and Case 18. One patient (Case 14) was given medications for hypercortisolemia; 2 patients were administered radiotherapy (Case 11) or chemotherapy (Case 16) after drug therapy; and 1 patient (Case 5) was not treated and was given the recommendation to continue follow up due to the unclear cause of CS and the presence of cyclic hypercortisolism (**Table 3**).

In 12/16 (75.0%) patients who had a follow-up examination, the cardiac structure and function were significantly improved or even completely reversed after remission of hypercortisolemia. Three patients (Case 2, Case 5, and Case 14) showed no significant improvement. Case 2 was a 59-year-old man diagnosed with CD and HCM, who developed cortisol remission after repeated pituitary surgery. Case 5 was a 25-year-old male with CS due to an unknown cause, which was complicated with DCM, who did not undergo surgery due to severe heart failure. Case 14 was a 43-year-old male diagnosed with CD complicated with DCM who did not undergo surgical treatment due to severe heart failure. He was treated with two drugs (metyrapone and ketoconazole) to normalize his cortisol, but myocardial infarction occurred during the follow-up, which led to a rupture of the mitral papillary muscle and mitral regurgitation. A 20-year-old male patient (Case 7) with DCM with an unclear etiology of CS underwent unsuccessful pituitary surgery. Then, a bilateral adrenalectomy was performed to treat the hypercortisolemia. He suffered from sudden cardiac arrest and died 22 days after the adrenal surgery (**Table 3**).

Ten of 13(76.9%) patients with DCM improved significantly and even completely recovered in regard to their cardiac structure and function after cortisol remission. Their LVEF

TABLE 3 | Outcomes of cases with CS complicated with cardiomyopathies.

	Case 1	Case 2	Case 3	Case 4	Case 5	Case 6	Case 7	Case 8	Case 9	Case 10	Case 11	Case 12	Case 13	Case 14	Case 15	Case 16	Case 17	Case 18	Case 19
ACTH post treatment (pg/ml)	NA	5.3	42.7	12.1	NA	<5	768	NA	NA	NA	NA	NA	8.3	NA	NA	NA	NA	NA	NA
Cortisol post treatment (μg/dl)	0.96	0.7	25.35	7.7	NA	0.62	13.58	NA	NA	NA	NA	NA	0.238	Normal	NA	NA	NA	NA	NA
Improvement time post treatment	–	–	–	–	–	33	–	12	12	6	216	6	18	–	12	2	3	1	10
Change of LVDd	NA	53–48	NA	NA	79–77	70–58	68–71	Normal	NA	65.7–49	NA	56–57	NA	NA	61–51	Normal	NA	NA	NA
Change of IVSd	NA	22–20	NA	NA	10–7	7–7	11–8	Normal	NA	8.6–8.9	NA	NA	NA	NA	12–8	NA	NA	NA	18–6
Change of LVPWd	NA	10–12	NA	NA	8–8	7–8	11–11	Normal	NA	9.8–8.7	NA	NA	NA	NA	NA	NA	NA	NA	NA
Change of LVEF	NA	73–69	NA	NA	31–30	28–57	26–26	27–69	45–60	34–67	?–58	36–51	20–53	29–31	24–50	31–50	10–30	NA	NA

The symbol ? indicates that pre-treatment data for hypercortisolemia are not available.

increased by 25.78 ± 9.28% on average (15–42%), and the median improvement time was 12 months (5.25–21.75 months). One patient (Case 19) with HCM achieved reduction of 12 mm in the IVSd and had cardiac structure normalization within 10 months, while another patient (Case 18) recovered completely with regard to the symptoms of CD, including improvement in HCM just 1 month after surgery.

Comparison Between CS Patients With and Without Cardiomyopathies

To investigate whether there were some clinical features related to cardiomyopathies due to CS, a comparison was made between ACTH-dependent CS patients with and without cardiomyopathies in our center. The ACTH-dependent CS complicated with cardiomyopathy included 8 patients with CD (Case 1, Case 2, Case 3, Case 4, Case 11, Case 13, Case 14, Case 17) and 2 patients with ectopic ACTH syndrome (Case 6 and Case 16). Compared with CS patients without cardiomyopathies, the proportion of males and the proportion of hyperlipidemia were significantly increased in the CS with cardiomyopathies group ($p = 0.005$ and $p = 0.0119$, respectively). There were no significant differences between the two groups in age ($p = 0.4708$), BMI ($p = 0.0864$), the proportion of patients with hypertension ($p = 0.2735$), or the proportion of patients with diabetes ($p = 0.6430$). The median time from CS symptoms to symptoms/diagnosis of cardiomyopathies was 25.50 (12.00–78.75) months in 4 patients (**Table 4**).

The median level of morning serum cortisol in CS complicated with cardiomyopathies was 35.48 (28.26–47.10) μg/dl ($n = 6$), and in CS patients without cardiomyopathies, it was 28.19 (22.78–34.96) μg/dl. There was no significant difference ($p = 0.0896$). The median ACTH was 109.0 (91.78–170.30) pg/ml in the CS complicated with cardiomyopathies group ($n = 7$), which was significantly higher than that in CS patients without cardiomyopathies, which was 68.60 (47.85–110.00) pg/ml ($p = 0.0199$; **Table 4**).

The 24 h UFC level, and high-dose dexamethasone suppression test rate were 729.40 (234.30–821.20) μg ($n = 7$), and 92.37% (87.03–96.45%) ($n = 3$), respectively, in the CS complicated with cardiomyopathies group, while those in CS patients without cardiomyopathies were 456.8 (230.1–782.9) μg, and 87.00 (71.97–95.5) %, respectively. There were no statistically significant differences in the 24-h UFC or high-dose dexamethasone suppression rates between the two groups ($p = 0.3420$ and $p = 0.3999$, respectively) (**Table 4**).

In addition, there were no significant differences in the white blood cell count ($p = 0.2100$), hemoglobin concentration ($p = 0.2448$) or hematocrit ($p = 0.2524$) between the two groups. The platelet levels in CS patients complicated with cardiomyopathies were significantly lower than those in CD patients without cardiomyopathies [150.00 (110.50–253.50) $\times 10^9$/L vs. 254.5 (214.5–295.3) $\times 10^9$/L] ($p = 0.0249$; **Table 4**).

The serum sodium concentration was higher in the CS complicated with cardiomyopathies group [145.50 (140.50–148.00) mmol/L vs. 141.00 (140.00–143.00) mmol/L] ($p = 0.0316$), while the serum potassium concentration was

TABLE 4 | Comparison between patients with CS complicated with cardiomyopathies and CD patients without cardiomyopathies.

	CS complicated with cardiomyopathies (n=10)	CD without cardiomyopathies (n = 242)	*P*-value
Sex, M (%)	7 (70.00)	42 (17.36)	0.0005*
Age, year	30.50 (26.00–52.25)	32.00 (24.75–40.25)	0.4708
BMI, kg/m^2	29.09 (27.40–30.42)	26.90 (24.55–28.82)	0.0864
Course of disease (months)	25.50 (12.00–78.75)	36.00 (12.00–72.00)	0.7010
Hypertension, *n* (%)	6/10 (60.00)	183/242 (75.62)	0.2735
Diabetes, *n* (%)	2/8 (25.00)	44/241 (18.26)	0.6430
Hyperlipidemia, *n* (%)	5/7 (71.43)	57/240 (23.75)	0.0119*
Cortisol (μg/dl)	35.48 (28.26–47.10)	28.19 (22.78–34.96)	0.0896
ACTH (pg/ml)	109.00 (91.78–170.30)	68.60 (47.85–110.00)	0.0199*
24-hUFC (μg)	729.40 (234.30–821.20)	456.80 (230.10–782.90)	0.3420
Inhibition rate of high dose dexamethasone suppression test (%)	92.37 (87.03–96.45)	87.00 (71.97–95.5)	0.3999
White blood cells ($\times 10^9$/L)	9.58 (8.64–12.38)	8.42 (6.98–10.20)	0.2100
Platelets ($\times 10^9$/L)	150.00 (110.50–253.50)	254.50 (214.50–295.30)	0.0249*
Hemoglobin (g/L)	134.50 (116.50–153.00)	144.00 (134.00–154.00)	0.2448
Hematocrit (%)	46.20 (40.70–48.10)	42.40 (40.00–45.70)	0.2524
Serum sodium (mmol/L)	145.50 (140.50–148.00)	141.00 (140.00–143.00)	0.0316*
Serum potassium (mmol/L)	2.70 (2.40–3.60)	3.90 (3.50–4.20)	0.0014*
Triglycerides (mmol/L)	2.42 (1.52–3.39)	1.53 (1.09–2.37)	0.1442
Total cholesterol (mmol/L)	8.22 (5.26–8.49)	5.79 (4.86–6.52)	0.1234
Low density lipoprotein cholesterol (mmol/L)	5.98 (3.18–6.28)	3.62 (2.96–4.25)	0.1009
Fasting plasma glucose (mmol/L)	4.56 (4.05–6.40)	4.80 (4.50–5.40)	0.5889
Hypersensitive C-reactive protein (ng/L)	0.47 (0.16–1.30)	0.31 (0.0013–3.30)	0.8344

*M, Male; *P < 0.05 indicated significant difference.*

significantly lower than CD patients without cardiomyopathies [2.70 (2.40–3.60) mmol/L vs. 3.90 (3.50–4.2) mmol/L] (p = 0.0014; **Table 4**).

There were no significant differences in triglycerides (p = 0.1442), total cholesterol (p = 0.1234), low-density lipoprotein cholesterol (p = 0.1009), fasting blood glucose (p = 0.5889) or hypersensitive C-reactive protein (p = 0.8344) between the two groups (**Table 4**).

DISCUSSION

Generally, CS is more common in females and has a males to females ratio of ∼1:3–4. However, in the 19 CS cases complicated with cardiomyopathies collected in this paper, the ratio of males to females was 1.11:1, which showed no sex difference. Based on the existing data and research, it is difficult to explain the gender difference in this rare phenomenon at present time. The highest incidence of CS was in patients aged between 20 and 40 years old. In this case series, the mean age of patients was 35.33 ± 19.75 years old, which was consistent with that of patients with common CS.

It is well-known that the most common cause of CS is pituitary corticotropin adenoma, namely, Cushing's disease, followed by ectopic ACTH syndrome and ACTH-independent Cushing's syndrome caused by adrenal lesions. In this study, the most common cause of CS was pituitary corticotropin adenoma, followed by adrenal adenoma, and ectopic ACTH syndrome, which was similar to common CS. However, among the cases in the literature, there were more adrenal lesions, with a prevalence of 58.33% and there was an additional 8 CS patients with cardiomyopathy who were not included in this study due to lack of clinical data. But in our case series, both of the Cushing's disease and adrenal adenoma were included to investigate whether they complicated with the cardiomyopathy. And it was found the Cushing's disease was the major etiology type in our center, which means that CS with cardiomyopathy may be due to the different etiologies of CS. There were still requirements for larger studies to determine whether patients with Cushing's syndrome with adrenal lesions are more likely to develop cardiomyopathies.

The prevalence of DCM and HCM differs greatly in various studies. Data have shown that the prevalence of DCM is 1/2,500 (21, 22), and that the HCM prevalence is 1/500 in general population (23, 24). In addition, the prevalence of DCM in Europe and North America was 36/100,000 (22, 25), which was significantly higher than that in East Asia (for example, 14/100,000 in Japan) (26), and the prevalence of HCM in Eurasia and North America was 200–500/100,000 (27–29). In addition, the prevalence of DCM and HCM in China was 19/100,000 and 80/100,000, respectively (30). These data showed that the prevalence of HCM was higher than that of DCM. There are no epidemiological data on the prevalence of CS complicated with cardiomyopathy since it is a rare type of disease. In this study, CS complicated with DCM was more common than with HCM, with

a ratio of 3.75:1, which was in contrast to most epidemiological data for common cardiomyopathies regarding the prevalence of HCM and DCM.

Among the CS complicated with DCM, Case 4, Case 6, and Case 7 had only a year hypertension history and had no other conditions that could lead to an enlarged left ventricle and decreased myocardial systolic function, such as valvular heart disease or congenital or ischemic heart disease. In addition, although the LVDd and LVEF in Case 4 were critical, a further review of the data revealed that the patient's LVPd was 63 mm 2 months prior to this, which was treated with anti-heart failure treatments. The echocardiogram showed moderate mitral regurgitation without abnormal valve structure and no opening/closing abnormalities in Case 1, which indicated relative mitral insufficiency due to an enlarged left ventricle. Case 5 and other patients in the literature did not have concomitant risk factors for ventricular dilation, decreased cardiac function, and/or cardiomyopathy confirmed by echocardiography, cardiac MRI, etc. Therefore, these patients were diagnosed with CS complicated with DCM.

DCM mainly occurs in young people and is more common in males, is asymptomatic in the early stage and gradually progresses to heart failure. In this study the ratio of males to females with CS complicated with DCM was 1.14:1, which was not a significant sex difference. In a cohort study of 3,078 hospitalized heart failure patients in Denmark and Sweden, patients with DCM were 10 years younger (median age: 64 years) and had more severe conditions than patients with heart failure due to other causes (31). In this study, the mean age of CS patients complicated with DCM was 39.07 years old, which was younger than that of patients with common DCM. The prognosis of DCM is quite poor. Prazak et al. (32) reported that 52 patients with idiopathic DCM had 1-year, 5-year and 10-year survival rates of 89, 48, and 30%, respectively. Due to pharmacological and non-pharmacological therapeutic strategies, earlier diagnosis, and individualized long-term follow-up and continuous risk refinement, the prognosis of patients with DCM has improved significantly over the past few decades with survival free from heart transplantation rising to more than 80% at 8-year follow-up (33). However, a complete recovery of the cardiac structure and function is unusual, which only occurs in patients in which the acute injury does not cause significant myocardial damage (34). However, among the patients with CS combined with DCM, 10/13 (76.9%) patients showed a significant improvement or even a complete reversal of the heart structure and function after remission of hypercortisolemia after treatment with CS. The average LVEF of CS patients complicated with cardiomyopathies increased by 25.78% at a median time of 12 months after recovery from hypercortisolism. The prognosis of CS with DCM was much better than that of common DCM. It is suggested that the cause of CS complicated with DCM is acquired, and the patient may have a recovery, which could be related to the treatment of the hypercortisolemia.

In this study, 4 CS patients with HCM were included. HCM is characterized by asymmetrical but sometimes symmetrical ventricular hypertrophy, and the systolic function is mostly but not all maintained, while the diastolic function is decreased to varying degrees. Other conditions causing ventricular hypertrophy should be ruled out before the diagnosis of HCM. Most of HCM are hereditary cardiomyopathies. Genetic studies have shown that HCM is caused by dominant mutations in 11 or more genes encoding the contractile myofilament protein components of the sarcomere or the adjacent Z-disc. Approximately 70% of people have mutations in two genes, the β-myosin heavy chain (MYH7) and myosin binding protein C (MYBPC3) (35–38). HCM also usually occurs in adolescents and young adults, but a growing number of children with HCM are being identified at a young age (<10 years, including in infancy), and adults survive to advanced ages (>80 years) (39, 40). The ages of 2 patients in our center were 59 years (Case 2) and 26 years old (Case 3). Although they had a past history of hypertension, their blood pressure was maintained with the normal range with oral antihypertensive medicine. This means that the HCM was unlikely to be affected by hypertension. Neither of them had diabetes, hyperlipemia, or coronary artery disease. Above all, there was a large difference between the IVSd and LVPWd of Case 2 and Case 3, indicating uneven ventricular wall hypertrophy, and cardiac MRIs suggested the presence of hypertrophic cardiomyopathy (**Figure 1**). The other 2 patients with HCM (Case 18 and Case 19) in the literature were newborns, and they did not mention other risk factors for HCM for a long enough time.

HCM is one of the leading causes of sudden death in adolescents and during exercise. A study suggested that the annual mortality rate was ∼1% for HCM (39, 41). In the present study, Case 18 and Case 19 recovered completely immediately after remission of hypercortisolemia, while Case 2 had no improvements in cardiac structure after 2 years of remission of hypercortisolism. Case 2 was a 59-year-old male who achieved the remission of hypercortisolemia after the repeated pituitary surgery, that was 6 years after the first pituitary surgery. And he also had hypertension for 10 years, which may affect the improvement of cardiomyopathy. He had no family history of HCM and developed HCM after the occurrence of CS. The gene panel test for HCM was also completed with negative result. So it should be considered that his cardiomyopathy was closely related to hypercortisolemia. In addition, a report showed that a male newborn was diagnosed with hypertrophic obstructive cardiomyopathy. His cortisol level was 4.34 μg/dL, and his mother had CD during pregnancy (42).This special case suggested that CS with HCM was related to the hypercortisolemia, which improved after treatment.

Patients with CS may develop a range of metabolic syndrome conditions, including central obesity, hypertension, insulin resistance, impaired glucose tolerance, hyperglycemia and hyperlipidemia. These factors all have a negative impact on the heart and may promote ventricular hypertrophy, fibrosis and fat deposition, leading to cardiac insufficiency.

However, these metabolic factors do not fully explain the changes in the hearts of patients with CS. Avenatti et al. (43) enrolled 25 patients with CS and 25 controls (9 normotensive and 16 hypertensive patients in each group), and the analysis confirmed that the left ventricular mass and relative wall thickness were increased in CS patients compared with matched

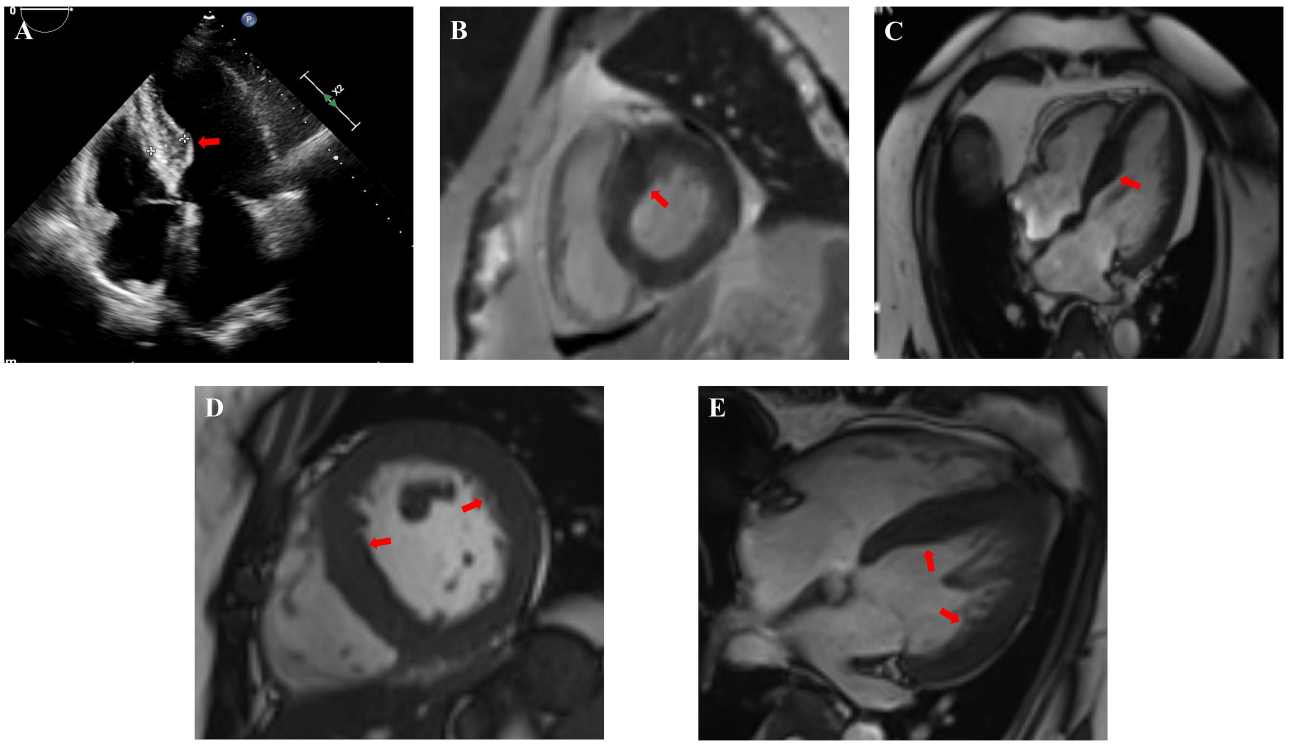

FIGURE 1 | Cardiac images indicated non-uniformly thickened ventricular walls and hypertrophic cardiomyopathy of Case 2 **(A–C)** and Case 3 **(D,E)**. **(A)** Echocardiogram in Case 2 showed significant thickening of the base of the interventricular septum. **(B,C)** Cardiac MRI in Case 2 showed the lateral wall of the left ventricle was about 8–10 mm and the thickening of the basal and intermediate segments of the interventricular septum was uneven with the thickest part about 20–22 mm (red arrow). **(D,E)** Cardiac MRI in Case 3 showed the lateral wall of the left ventricle was about 9–11 mm and the interventricular septum thickened, about 14–16 mm. The red arrows indicate non-uniformly thickened ventricular wall.

controls, but this was not directly related to blood pressure. In the cases of CS complicated with cardiomyopathies in this paper, cardiac function recovered in a short time after hypercortisolemia remission, showing a close relationship with the effect of overproduction of cortisol. Hypertension is not invariably present in CS, LV hypertrophy has also been described in CS patients without hypertension (5).

Therefore, apart from the effects of metabolic changes caused by hypercortisolism, the direct effect of cortisol on the myocardium should be considered. Mineralocorticoid receptors are widely expressed in cardiomyocytes, cardiac fibroblasts, vascular smooth muscle cells, endothelial cells and other cardiovascular system cells and lead to oxidative stress, inflammation, myocardial interstitial fibrosis and so on after activation (44, 45). Cortisol-mediated myocardial fibrosis mediated by activating mineralocorticoid receptors may be an important factor leading to cardiomyopathies.

The study of Frustaci et al. (15) further explained the pathogenesis of CS cardiomyopathies. At the time of diagnosis, cell swelling, myocardial fibrinolysis and partial sarcomere disorder were obvious. One year after adrenal surgery, the cell volume, cytoplasmic density and body tissue showed improvements. Meanwhile, atrogin-1 mRNA was 30 times higher in patients at baseline than in normal controls and returned to normal after adrenal resection. Shortly thereafter, Frustaci et al. (20) observed cardiomyopathy features in 8 patients (4 males and 4 females, mean age 61 $\pm$ 4.9 years) with CS caused by adrenal adenoma complicated with DCM. The common features of CS cardiomyopathies were cardiac hyperplasia, myofibrinolysis, and myocardial fibrosis. Atrogin-1 levels were 28 times higher in patients with CS cardiomyopathies than in normal controls and 3.5 times higher than in patients with idiopathic DCM. The atrogin-1 levels returned to normal after adrenal resection and were negatively correlated with LVEF. Elevated plasma cortisol levels could activate the FOXO transcription factor, leading to a significant increase in atrogin-1 and ubiquitin levels (46). However, it was reported that the reduction in the myofiber content of cardiomyocytes was a reversible event, and the atrogin-1 level returned to physiological levels 1 year after adrenal resection and after the normalization of plasma cortisol levels. There was also a concurrent reduction in fibrinolytic cell area from 61 to 22%, paralleling the recovery of cardiac structure and function (20).

Compared with CD patients without cardiomyopathies, there were no significant differences in the course of disease, sex, and age, but CS patients complicated with

cardiomyopathies had higher serum sodium levels, lower serum potassium levels, and higher ACTH levels. In addition, although no significant difference was observed, patients with CS complicated with cardiomyopathies had a shorter course of disease and higher serum cortisol levels than CD patients without cardiomyopathies. Although no significant difference was observed, this suggests that patients with CS complicated with cardiomyopathies tend to be more severe and have a greater tendency to be affected by hypercortisolemia.

In conclusion, CS complicated with cardiomyopathies is a very rare clinical type, and the most common cardiomyopathy is DCM, followed by HCM. Cortisol plays an important role in the development of cardiomyopathies in CS, and the cardiomyopathies can be greatly improved with remission of hypercortisolemia.

The number of cases in this study is limited, and a larger study is needed to explain the clinical features and prognosis of CS complicated with cardiomyopathies.

DATA AVAILABILITY STATEMENT

The raw data supporting the conclusions of this article will be made available by the authors, without undue reservation.

ETHICS STATEMENT

The studies involving human participants were reviewed and approved by the Ethics Committee of Peking Union Medical College Hospital. Written informed consent from the participants' legal guardian/next of kin was not required to participate in this study in accordance with the national legislation and the institutional requirements. Written informed consent was obtained from the individual(s) for the publication of any potentially identifiable images or data included in this article.

AUTHOR CONTRIBUTIONS

LLu was responsible for the study concept and design. SM did the statistical analysis and wrote the manuscript. LLi, YW, ZL, HZ, LW, LD, XX, YY, MF, and RW collected clinical specimens. All authors critically revised the paper and approved the final version.

ACKNOWLEDGMENTS

Thanks to all participators in this study and thanks to all clinicians for their tremendous work in this study.

REFERENCES

1. Lindholm J, Juul S, Jorgensen JO, Astrup J, Bjerre P, Feldt-Rasmussen U, et al. Incidence and late prognosis of cushing's syndrome: a population-based study. *J Clin Endocrinol Metab.* (2001) 86:117–23. doi: 10.1210/jcem.86.1.7093
2. Di Dalmazi G, Vicennati V, Garelli S, Casadio E, Rinaldi E, Giampalma E, et al. Cardiovascular events and mortality in patients with adrenal incidentalomas that are either non-secreting or associated with intermediate phenotype or subclinical Cu.shing's syndrome: a 15-year retrospective study. *Lancet Diabetes Endocrinol.* (2014) 2:396–405. doi: 10.1016/S2213-8587(13)70211-0
3. Debono M, Bradburn M, Bull M, Harrison B, Ross RJ, Newell-Price J. Cortisol as a marker for increased mortality in patients with incidental adrenocortical adenomas. *J Clin Endocrinol Metab.* (2014) 99:4462–70. doi: 10.1210/jc.2014-3007
4. Dekkers OM, Horvath-Puho E, Jorgensen JO, Cannegieter SC, Ehrenstein V, Vandenbroucke JP, et al. Multisystem morbidity and mortality in Cushing's syndrome: a cohort study. *J Clin Endocrinol Metab.* (2013) 98:2277–84. doi: 10.1210/jc.2012-3582
5. Toja PM, Branzi G, Ciambellotti F, Radaelli P, De Martin M, Lonati LM, et al. Clinical relevance of cardiac structure and function abnormalities in patients with Cushing's syndrome before and after cure. *Clin Endocrinol.* (2012) 76:332–8. doi: 10.1111/j.1365-2265.2011.04206.x
6. Maurice F, Gaborit B, Vincentelli C, Abdesselam I, Bernard M, Graillon T, et al. Cushing syndrome is associated with subclinical lv dysfunction and increased epicardial adipose tissue. *J Am Coll Cardiol.* (2018) 72:2276–7. doi: 10.1016/j.jacc.2018.07.096
7. Kamenicky P, Redheuil A, Roux C, Salenave S, Kachenoura N, Raissouni Z, et al. Cardiac structure and function in Cushing's syndrome: a cardiac magnetic resonance imaging study. *J Clin Endocrinol Metab.* (2014) 99:E2144–53. doi: 10.1210/jc.2014-1783
8. Marazuela M. Dilated cardiomyopathy as a presenting feature of Cushing's syndrome. *Int J Cardiol.* (2003) 88:331–3. doi: 10.1016/S0167-5273(02)00403-5
9. Peppa M, Ikonomidis I, Hadjidakis D, Pikounis V, Paraskevaidis I, Economopoulos T, et al. Dilated cardiomyopathy as the predominant feature of Cushing's syndrome. *Am J Med Sci.* (2009) 338:252–3. doi: 10.1097/MAJ.0b013e3181a927e0
10. Yong TY, Li JY. Reversible dilated cardiomyopathy in a patient with Cushing's syndrome. *Congest Heart Fail.* (2010) 16:77–9. doi: 10.1111/j.1751-7133.2009.00123.x
11. Ma RC, So WY, Tong PC, Chan JC, Cockram CS, Chow CC. Adiposity of the heart revisited: reversal of dilated cardiomyopathy in a patient with Cushing's syndrome. *Int J Cardiol.* (2011) 151:e22–3. doi: 10.1016/j.ijcard.2010.04.041
12. Shibusawa N, Yamada M, Hashida T, Hashimoto K, Satoh T, Horiguchi J, et al. Dilated cardiomyopathy as a presenting feature of Cushing's syndrome. *Intern Med.* (2013) 52:1067–71. doi: 10.2169/internalmedicine.52.9051
13. Kim JH, Kim SY, Park JH. Dilated cardiomyopathy with left ventricular thrombi as a presenting feature of Cushing disease. *Can J Cardiol.* (2014) 30:1462 e11–3. doi: 10.1016/j.cjca.2014.06.018
14. Marchand L, Segrestin B, Lapoirie M, Favrel V, Dementhon J, Jouanneau E, et al. Dilated cardiomyopathy revealing cushing disease: a case report and literature review. *Medicine.* (2015) 94:e2011. doi: 10.1097/MD.0000000000002011
15. Frustaci A, Letizia C, Verardo R, Grande C, Petramala L, Russo MA, et al. Cushing syndrome cardiomyopathy: clinicopathologic impact of cortisol normalization. *Circ Cardiovasc Imaging.* (2016) 9:e004569. doi: 10.1161/CIRCIMAGING.116.004569
16. Pingle SR, Shah T, Mosleh W, Kim AS. Cushing syndrome cardiomyopathy: an unusual manifestation of small-cell lung cancer. *ESC Heart Fail.* (2020) 7:3189–92. doi: 10.1002/ehf2.12860
17. Sheikh T, Shuja H, Zaidi SR, Haque A. Glucocorticoid-induced cardiomyopathy: unexpected conclusion. *BMJ Case Rep.* (2020) 13:e237173. doi: 10.1136/bcr-2020-237173
18. Gessler P, Ranke MB, Wollmann H, Aicher KP, Feine U, Kaiserling E, et al. [Adrenocortical nodular hyperplasia as a cause of Cushing syndrome in the neonatal period]. *Klin Padiatr.* (1991) 203:462–6. doi: 10.1055/s-2007-1025475
19. Hauser J, Riedl S, Michel-Behnke I, Minkov M, Perneczky E, Horcher E. Hypertrophic obstructive cardiomyopathy in an infant with an adrenocortical tumor. *Pediatrics.* (2013) 132:e535–9. doi: 10.1542/peds.2012-2692
20. Frustaci A, Letizia C, Verardo R, Grande C, Calvieri C, Russo MA, et al. Atrogin-1 pathway activation in cushing syndrome cardiomyopathy. *J Am Coll Cardiol.* (2016) 67:116–7. doi: 10.1016/j.jacc.2015.10.040

21. Manolio TA, Baughman KL, Rodeheffer R, Pearson TA, Bristow JD, Michels VV, et al. Prevalence and etiology of idiopathic dilated cardiomyopathy (summary of a national heart, lung, and blood institute workshop. *Am J Cardiol.* (1992) 69:1458–66. doi: 10.1016/0002-9149(92)90901-A
22. Codd MB, Sugrue DD, Gersh BJ, Melton LJ III. Epidemiology of idiopathic dilated and hypertrophic cardiomyopathy. A population-based study in Olmsted County, Minnesota, 1975-1984. *Circulation*. (1989) 80:564-72. doi: 10.1161/01.CIR.80.3.564
23. Maron BJ, Gardin JM, Flack JM, Gidding SS, Kurosaki TT, Bild DE. Prevalence of hypertrophic cardiomyopathy in a general population of young adults. Echocardiographic analysis of 4111 subjects in the CARDIA Study. Coronary artery risk development in (young) adults. *Circulation.* (1995) 92:785–9. doi: 10.1161/01.CIR.92.4.785
24. Maron BJ, Spirito P, Roman MJ, Paranicas M, Okin PM, Best LG, et al. Prevalence of hypertrophic cardiomyopathy in a population-based sample of American Indians aged 51 to 77 years (the strong heart study). *Am J Cardiol.* (2004) 93:1510–4. doi: 10.1016/j.amjcard.2004.03.007
25. Torp A. Incidence of congestive cardiomyopathy. *Postgrad Med J.* (1978) 54:435–9. doi: 10.1136/pgmj.54.633.435
26. Miura K, Matsumori A, Nasermoaddeli A, Soyama Y, Morikawa Y, Sakurai M, et al. Prognosis and prognostic factors in patients with idiopathic dilated cardiomyopathy in Japan. *Circ J.* (2008) 72:343–8. doi: 10.1253/circj.72.343
27. Hada Y, Sakamoto T, Amano K, Yamaguchi T, Takenaka K, Takahashi H, et al. Prevalence of hypertrophic cardiomyopathy in a population of adult Japanese workers as detected by echocardiographic screening. *Am J Cardiol.* (1987) 59:183–4. doi: 10.1016/S0002-9149(87)80107-8
28. Corrado D, Basso C, Schiavon M, Thiene G. Screening for hypertrophic cardiomyopathy in young athletes. *N Engl J Med.* (1998) 339:364–9. doi: 10.1056/NEJM199808063390602
29. Nistri S, Thiene G, Basso C, Corrado D, Vitolo A, Maron BJ. Screening for hypertrophic cardiomyopathy in a young male military population. *Am J Cardiol.* (2003) 91:1021–3, A8. doi: 10.1016/S0002-9149(03)00132-2
30. Zou Y, Song L, Wang Z, Ma A, Liu T, Gu H, et al. Prevalence of idiopathic hypertrophic cardiomyopathy in China: a population-based echocardiographic analysis of 8080 adults. *Am J Med.* (2004) 116:14–8. doi: 10.1016/j.amjmed.2003.05.009
31. Pecini R, Moller DV, Torp-Pedersen C, Hassager C, Kober L. Heart failure etiology impacts survival of patients with heart failure. *Int J Cardiol.* (2011) 149:211–5. doi: 10.1016/j.ijcard.2010.01.011
32. Prazak P, Pfisterer M, Osswald S, Buser P, Burkart F. Differences of disease progression in congestive heart failure due to alcoholic as compared to idiopathic dilated cardiomyopathy. *Eur Heart J.* (1996) 17:251–7. doi: 10.1093/oxfordjournals.eurheartj.a014842
33. Merlo M, Pivetta A, Pinamonti B, Stolfo D, Zecchin M, Barbati G, et al. Long-term prognostic impact of therapeutic strategies in patients with idiopathic dilated cardiomyopathy: changing mortality over the last 30 years. *Eur J Heart Fail.* (2014) 16:317–24. doi: 10.1002/ejhf.16
34. Wittstein IS, Thiemann DR, Lima JA, Baughman KL, Schulman SP, Gerstenblith G, et al. Neurohumoral features of myocardial stunning due to sudden emotional stress. *N Engl J Med.* (2005) 352:539–48. doi: 10.1056/NEJMoa043046
35. Alcalai R, Seidman JG, Seidman CE. Genetic basis of hypertrophic cardiomyopathy: from bench to the clinics. *J Cardiovasc Electrophysiol.* (2008) 19:104–10. doi: 10.1111/j.1540-8167.2007.00965.x
36. Ackerman MJ, VanDriest SL, Ommen SR, Will ML, Nishimura RA, Tajik AJ, et al. Prevalence and age-dependence of malignant mutations in the beta-myosin heavy chain and troponin T genes in hypertrophic cardiomyopathy: a comprehensive outpatient perspective. *J Am Coll Cardiol.* (2002) 39:2042–8. doi: 10.1016/S0735-1097(02)01900-9
37. Niimura H, Bachinski LL, Sangwatanaroj S, Watkins H, Chudley AE, McKenna W, et al. Mutations in the gene for cardiac myosin-binding protein C and late-onset familial hypertrophic cardiomyopathy. *N Engl J Med.* (1998) 338:1248–57. doi: 10.1056/NEJM199804303381802
38. Bos JM, Towbin JA, Ackerman MJ. Diagnostic, prognostic, and therapeutic implications of genetic testing for hypertrophic cardiomyopathy. *J Am Coll Cardiol.* (2009) 54:201–11. doi: 10.1016/j.jacc.2009.02.075
39. Maron BJ, Casey SA, Hauser RG, Aeppli DM. Clinical course of hypertrophic cardiomyopathy with survival to advanced age. *J Am Coll Cardiol.* (2003) 42:882–8. doi: 10.1016/S0735-1097(03)00855-6
40. Maron BJ, Casey SA, Haas TS, Kitner CL, Garberich RF, Lesser JR. Hypertrophic cardiomyopathy with longevity to 90 years or older. *Am J Cardiol.* (2012) 109:1341–7. doi: 10.1016/j.amjcard.2011.12.027
41. Olivotto I, Maron MS, Adabag AS, Casey SA, Vargiu D, Link MS, et al. Gender-related differences in the clinical presentation and outcome of hypertrophic cardiomyopathy. *J Am Coll Cardiol.* (2005) 46:480–7. doi: 10.1016/j.jacc.2005.04.043
42. Fayol L, Masson P, Millet V, Simeoni U. Cushing's syndrome in pregnancy and neonatal hypertrophic obstructive cardiomyopathy. *Acta Paediatr.* (2004) 93:1400–2. doi: 10.1111/j.1651-2227.2004.tb02943.x
43. Avenatti E, Rebellato A, Iannaccone A, Battocchio M, Dassie F, Veglio F, et al. Left ventricular geometry and 24-h blood pressure profile in Cushing's syndrome. *Endocrine.* (2017) 55:547–54. doi: 10.1007/s12020-016-0986-6
44. Walker BR, Williams BC. Corticosteroids and vascular tone: mapping the messenger maze. *Clin Sci.* (1992) 82:597–605. doi: 10.1042/cs0820597
45. Hadoke PW, Macdonald L, Logie JJ, Small GR, Dover AR, Walker BR. Intravascular glucocorticoid metabolism as a modulator of vascular structure and function. *Cell Mol Life Sci.* (2006) 63:565–78. doi: 10.1007/s00018-005-5427-2
46. Sandri M, Sandri C, Gilbert A, Skurk C, Calabria E, Picard A, et al. Foxo transcription factors induce the atrophy-related ubiquitin ligase atrogin-1 and cause skeletal muscle atrophy. *Cell.* (2004) 117:399–412. doi: 10.1016/S0092-8674(04)00400-3

Conflict of Interest: The authors declare that the research was conducted in the absence of any commercial or financial relationships that could be construed as a potential conflict of interest.

Publisher's Note: All claims expressed in this article are solely those of the authors and do not necessarily represent those of their affiliated organizations, or those of the publisher, the editors and the reviewers. Any product that may be evaluated in this article, or claim that may be made by its manufacturer, is not guaranteed or endorsed by the publisher.

frontiers in Cardiovascular Medicine

ORIGINAL RESEARCH
published: 17 December 2021
doi: 10.3389/fcvm.2021.791501

NAP1L5 Promotes Nucleolar Hypertrophy and Is Required for Translation Activation During Cardiomyocyte Hypertrophy

Ningning Guo[1,2,3†], Di Zheng[1†], Jiaxin Sun[1†], Jian Lv[1,2,3], Shun Wang[1], Yu Fang[1,2,3], Zhenyi Zhao[2,3,4], Sai Zeng[2,3], Qiuxiao Guo[2,3], Jingjing Tong[5] and Zhihua Wang[1,2,3*]*

[1] Department of Cardiology, Renmin Hospital of Wuhan University, Wuhan, China, [2] Shenzhen Key Laboratory of Cardiovascular Disease, Fuwai Hospital, Chinese Academy of Medical Sciences, Shenzhen, China, [3] State Key Laboratory of Cardiovascular Disease, Fuwai Hospital, National Center for Cardiovascular Disease, Chinese Academy of Medical Sciences and Peking Union Medical College, Beijing, China, [4] Health Science Center, School of Pharmacy, Shenzhen University, Shenzhen, China, [5] School of Life Sciences, Central China Normal University, Wuhan, China

OPEN ACCESS

Edited by:
Jin Li,
Shanghai University, China

Reviewed by:
Zhi Xin Shan,
Guangdong Provincial People's Hospital, China
Kunfu Ouyang,
Peking University, China

***Correspondence:**
Jingjing Tong
tongjj@mail.ccnu.edu.cn
Zhihua Wang
wangzhihua@fuwaihospital.org

[†] These authors have contributed equally to this work

Specialty section:
This article was submitted to General Cardiovascular Medicine, a section of the journal Frontiers in Cardiovascular Medicine

Received: *08 October 2021*
Accepted: *29 November 2021*
Published: *17 December 2021*

Citation:
Guo N, Zheng D, Sun J, Lv J, Wang S, Fang Y, Zhao Z, Zeng S, Guo Q, Tong J and Wang Z (2021) NAP1L5 Promotes Nucleolar Hypertrophy and Is Required for Translation Activation During Cardiomyocyte Hypertrophy. Front. Cardiovasc. Med. 8:791501. doi: 10.3389/fcvm.2021.791501

Pathological growth of cardiomyocytes during hypertrophy is characterized by excess protein synthesis; however, the regulatory mechanism remains largely unknown. Using a neonatal rat ventricular myocytes (NRVMs) model, here we find that the expression of nucleosome assembly protein 1 like 5 (Nap1l5) is upregulated in phenylephrine (PE)-induced hypertrophy. Knockdown of Nap1l5 expression by siRNA significantly blocks cell size enlargement and pathological gene induction after PE treatment. In contrast, Adenovirus-mediated Nap1l5 overexpression significantly aggravates the pro-hypertrophic effects of PE on NRVMs. RNA-seq analysis reveals that Nap1l5 knockdown reverses the pro-hypertrophic transcriptome reprogramming after PE treatment. Whereas, immune response is dominantly enriched in the upregulated genes, oxidative phosphorylation, cardiac muscle contraction and ribosome-related pathways are remarkably enriched in the down-regulated genes. Although Nap1l5-mediated gene regulation is correlated with PRC2 and PRC1, Nap1l5 does not directly alter the levels of global histone methylations at K4, K9, K27 or K36. However, puromycin incorporation assay shows that Nap1l5 is both necessary and sufficient to promote protein synthesis in cardiomyocyte hypertrophy. This is attributable to a direct regulation of nucleolus hypertrophy and subsequent ribosome assembly. Our findings demonstrate a previously unrecognized role of Nap1l5 in translation control during cardiac hypertrophy.

Keywords: cardiomyocyte hypertrophy, NAP1L5, translation control, nucleolar hypertrophy, ribosome assembly

INTRODUCTION

The heart develops ventricular hypertrophy to compensate for increased hemodynamic workload under various stresses, and progressively leading to heart failure (1, 2). Cardiac hypertrophy is characterized by enlarged cell size and excess protein synthesis (3–5). Protein synthesis efficiency is fine-tuned at multiple steps, such as ribosomal gene transcription, ribosome assembly, ribosome export, and translation initiation, elongation and termination (6, 7). How translation activity is regulated during cardiac hypertrophy remains largely unexplored.

Primary regulation of translation occurs in nucleolus, where ribosomal DNA is transcribed and ribosome subunits are assembled. Cardiac hypertrophy is one of the first diseases identified to be associated with ribosomal DNA transcriptional disorders (8, 9). Accelerated polymerase I (PolI) transcription rate increases ribosome numbers during the development of cardiac hypertrophy (10). Upstream binding transcription factor (UBTF) has been shown to regulate PolI transcription activity in cardiac hypertrophy (11, 12). Despite these earlier observations, however, little progression has been made about translation control in heart diseases.

The mechanistic target of rapamycin (mTOR) plays a central role in protein synthesis by phosphorylating 70 kD ribosomal protein S6 kinase 1 (S6K1) and eukaryotic translation initiation factor 4E (eIF4E)-binding protein-1 (4E-BP1), which subsequently initiate a series of signal transduction to promote the operation of ribosomes (13, 14). Though generally thought to positively correlate with the pathogenesis of cardiac hypertrophy, there are numerous mysteries about the regulation and function of mTOR. Cardiac-specific ablation of raptor, the core component of mTOR complex 1 (mTORC1), impairs adaptive hypertrophy, but causes heart failure in mice (15). Simultaneous knockout of two genes encoding for S6K1, Rps6kb1, and Rps6kb2, has no effect on pressure overload-induced cardiac hypertrophy in mice (16). Interestingly, our previous study implicated that the activation of mTOR signaling is usually transient, and quickly fades out after hypertrophic stimulation (17). To what extent do the mTOR-dependent and the mTOR-independent mechanisms contribute to translational regulation during cardiac hypertrophy remains under question.

Nucleosome assembly protein 1 like (NAP1L) protein family has been identified as evolutionarily conserved histone chaperones assisting the assembly of nucleosomes with different histone variants (18–20). It consists of five members, namely NAP1L1-5, among which NAP1L1 is the member being firstly identified and best functionally characterized (21–23). In addition to a role in assisting H2A-H2B dimer incorporation into nucleosome, NAP1L1 also participates in gene expression regulation through epigenetic mechanisms (24, 25). Recently, NAP1L family members have been found to be functionally involved in cell proliferation and differentiation during development and human diseases, such as carcinoma and virus infection (26–40). In contrast, our knowledge about other family members is still limited. NAP1L5 is the newest member firstly identified in human liver malignancy as an imprinted gene (41, 42). Chang et al. found that the gene coding for NAP1L5 was hypomethylated in congenital heart diseases (43). However, the molecular function and the role of NAP1L5 in human diseases remains largely unknown.

Here we find that NAP1L5 expression is significantly upregulated in phenylephrine (PE)-induced cardiomyocyte hypertrophy. siRNA-mediated knockdown and

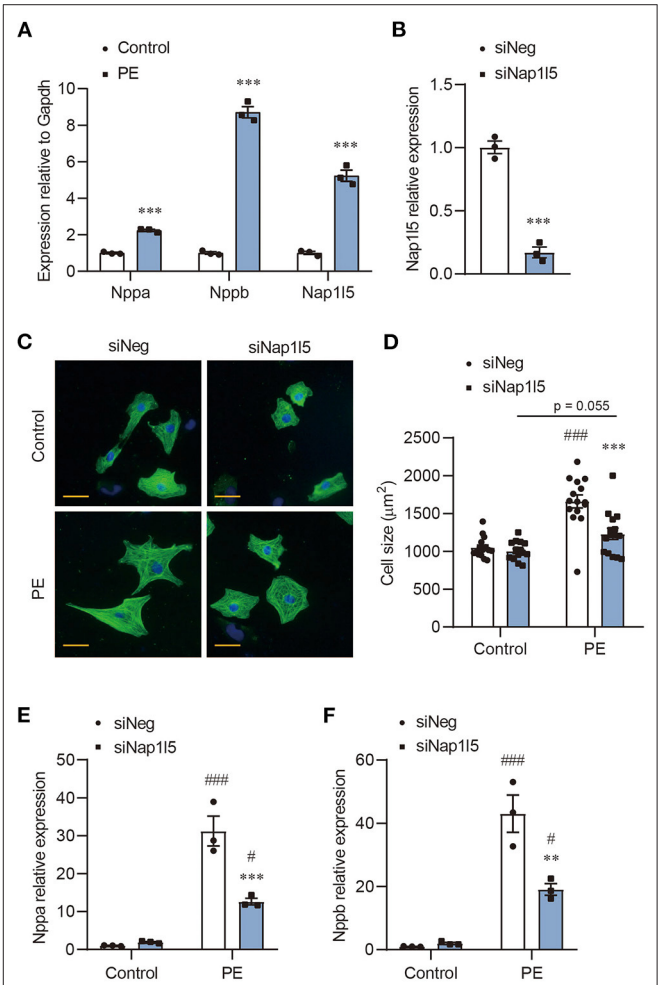

FIGURE 1 | NAP1L5 silence abolishes PE-induced cardiomyocyte hypertrophy. **(A)** Expression of Nppa, Nppb and Nap1l5 in neonatal rat ventricular myocytes (NRVMs) with and without phenylephrine (PE; 50μM) treatment measured by qRT-PCR. $^{***}P < 0.001$ vs. Control. $n = 3$. **(B)** Knockdown efficiency of Nap1l5 expression by siNap1l5 in NRVMs measured by qRT-PCR. $^{***}P < 0.001$ vs. negative control siRNA (siNeg). $n = 3$. **(C)** Representative α-actinin-staining images of NRVMs transfected with siNeg or siNap1l5, with and without PE treatment. Scale bar: 20 μm. **(D)** Quantification of cell size measured by WGA staining in NRVMs transfected with siNeg or siNap1l5, with and without PE treatment. $^{***}P < 0.001$ vs. siNeg; $^{\#\#\#}P < 0.001$ vs. Control. $n = 15$. **(E,F)** Impact of Nap1l5 knockdown on PE-induced expression of Nppa **(E)** and Nppb **(F)**. $^{**}P < 0.01$, $^{***}P < 0.001$ vs. siNeg; $^{\#}P < 0.05$, $^{\#\#\#}P < 0.001$ vs. Control. $n = 3$.

Abbreviations: 4E-BP1, eIF4E-binding protein-1; Acta1, Actin alpha 1; CHX, Cycloheximide; DAPI, 4', 6-Diamidino-2-phenylindole; DEGs, The different expression genes; eIF4E, Eukaryotic translation initiation factor 4E; GEO, Gene Expression Omnibus; GO, Gene ontology; GSEA, Gene set enrichment analysis; mTOR, The mechanistic target of rapamycin; NAP1L, Nucleosome assembly protein 1 like protein family; Nap1l5, Nucleosome assembly protein 1 like 5; NOL6, Nucleolar Protein 6; Nppa/ANF, Natriuretic peptide A; Nppb/BNP, Natriuretic peptide B; NRVMs, Neonatal rat ventricular myocytes; PCA, Principal component analysis; PE, Phenylephrine; PMSF, Phenylmethylsulfonyl fluoride; PolI, polymerase I; PRC1, Polycomb Repressive Complex 1; PRC2, Polycomb Repressive Complex 2; Rps6kb1, Ribosomal Protein S6 Kinase B1; Rps6kb2, Ribosomal Protein S6 Kinase B2; RRP7A, Ribosomal RNA Processing 7 Homolog A; S6K1, Ribosomal protein S6 kinase 1; SDAD1, SDA1 domain containing 1; UBTF, Upstream binding transcription factor; WGA, Wheat germ agglutinin.

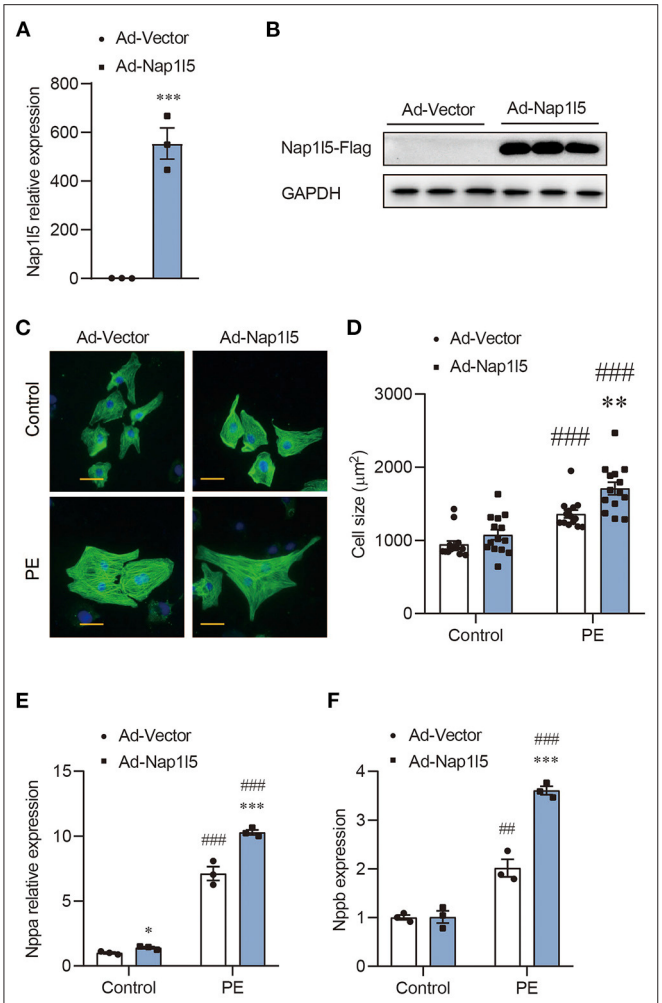

FIGURE 2 | NAP1L5 overexpression promotes PE-induced cardiomyocyte hypertrophy. **(A)** Expression of Nap1l5 in NRVMs infected with adenovirus vector (Ad-Vector) or that expressing rat Nap1l5 (Ad-Nap1l5) measured by qRT-PCR. $^{***}P < 0.001$ vs. Ad-Vector. $n = 3$. **(B)** Immuoblots showing the validation of NAP1L5 overexpression at the protein level using an anti-FLAG antibody. GAPDH was used as an internal control. $n = 3$. **(C)** Representative α-actinin-staining images of NRVMs infected with Ad-Vector or Ad-Nap1l5, with and without PE treatment. Scale bar: 20 μm. **(D)** Quantification of cell size measured by WGA staining in NRVMs infected with Ad-Vector or Ad-Nap1l5, with and without PE treatment. $^{**}P < 0.01$ vs. Ad-Vector; $^{\#\#\#}P < 0.001$ vs. Control. $n = 15$. **(E,F)** Impact of Nap1l5 overexpression on PE-induced expression of Nppa **(E)** and Nppb **(F)**. $^{**}P < 0.01$, $^{***}P < 0.001$ vs. siNeg; $^{\#}P < 0.05$, $^{\#\#\#}P < 0.001$ vs. Control. $n = 3$.

adenovirus-mediated overexpression experiments suggest that NAP1L5 is required for the development of cardiomyocyte hypertrophy. Transcriptome analysis and puromycin incorporation assay reveal a crucial regulation of nucleolus hypertrophy, ribosome assembly and protein synthesis rate by NAP1L5. Our findings demonstrate a novel role of NAP1L5 in translation control during the pathological growth of cardiomyocytes, and provide potential molecular targets to treat cardiac hypertrophy.

RESULTS

NAP1L5 Silence Abolishes PE-Induced Cardiomyocyte Hypertrophy

We previously performed an RNA-seq analysis in PE-induced cardiomyocyte hypertrophy (17). After re-evaluating the genes with altered expression, we noticed a five-fold upregulation of Nap1l5, but not other Nap1l family members, in PE-treated NRVMs compared with control, which was validated by qRT-PCR (**Figure 1A** and **Supplementary Figure 1A**). To examine whether NAP1L5 plays a role in cardiomyocyte hypertrophy, we designed a Nap1l5-specific siRNA (siNap1l5) that achieving 80% knockdown efficiency 48h after transfection in NRVMs (**Figure 1B** and **Supplementary Figure 1B**). NAP1L5 silence did not change the cell size at basal level, but significantly suppressed PE-induced cell size enlargement (**Figures 1C,D**). Consistently, NAP1L5 knockdown significantly reversed the induction of hypertrophy markers, natriuretic peptide A (Nppa; also known as ANP) and natriuretic peptide B (Nppb; also known as BNP), after PE treatment (**Figures 1E,F**). These data suggest that NAP1L5 is required for cardiomyocyte pathological growth induced by PE.

NAP1L5 Overexpression Promotes PE-Induced Cardiomyocyte Hypertrophy

We then constructed an Adenovirus carrying rat Nap1l5 gene (Ad-Nap1l5) to overexpress it in NRVMs. Both qRT-PCR and Western blot analyses confirmed the overexpression of NAP1L5 48h after infection (**Figures 2A,B**). NAP1L5 overexpression had a marginal effect on cell size at basal level; however, it significantly aggravated the cell size enlargement after PE treatment (**Figures 2C,D**). Moreover, the PE-induced expressions of Nppa and Nppb were significantly enhanced by NAP1L5 overexpression (**Figures 2E,F**). These results indicate that NAP1L5 functions as a pro-hypertrophic factor.

NAP1L5 Knockdown Reverses Hypertrophic Transcriptome Reprogramming

To explore the underlying mechanism, we performed a transcriptome analysis in NRVMs with NAP1L5 knockdown. Expression plotting confirmed the knockdown of NAP1L5 and the suppression of hypertrophy markers, including Nppa, Nppb and Acta1 (actin alpha 1, skeletal muscle), after siNap1l5 transfection (**Figure 3A**). Principal component analysis (PCA) showed that NAP1L5 knockdown alleviated the pro-hypertrophic effect of PE treatment at the transcriptome level, and also caused a special impact on global gene expression (**Figure 3B**). Venn diagram showed that the down-regulated genes after NAP1L5 knockdown shared more genes with the upregulated genes after PE treatment in comparison with the down-regulated ones, and *vice versa* (**Figure 3C**), suggesting a general anti-hypertrophic impact of NAP1L5 silence on PE-induced transcriptome reprogramming. Furthermore, heatmap of the union set between siNap1l5-sensitive and PE-sensitive genes showed that NAP1L5 knockdown was generally oppositely correlated with PE in gene expression patterns (**Figure 3D**).

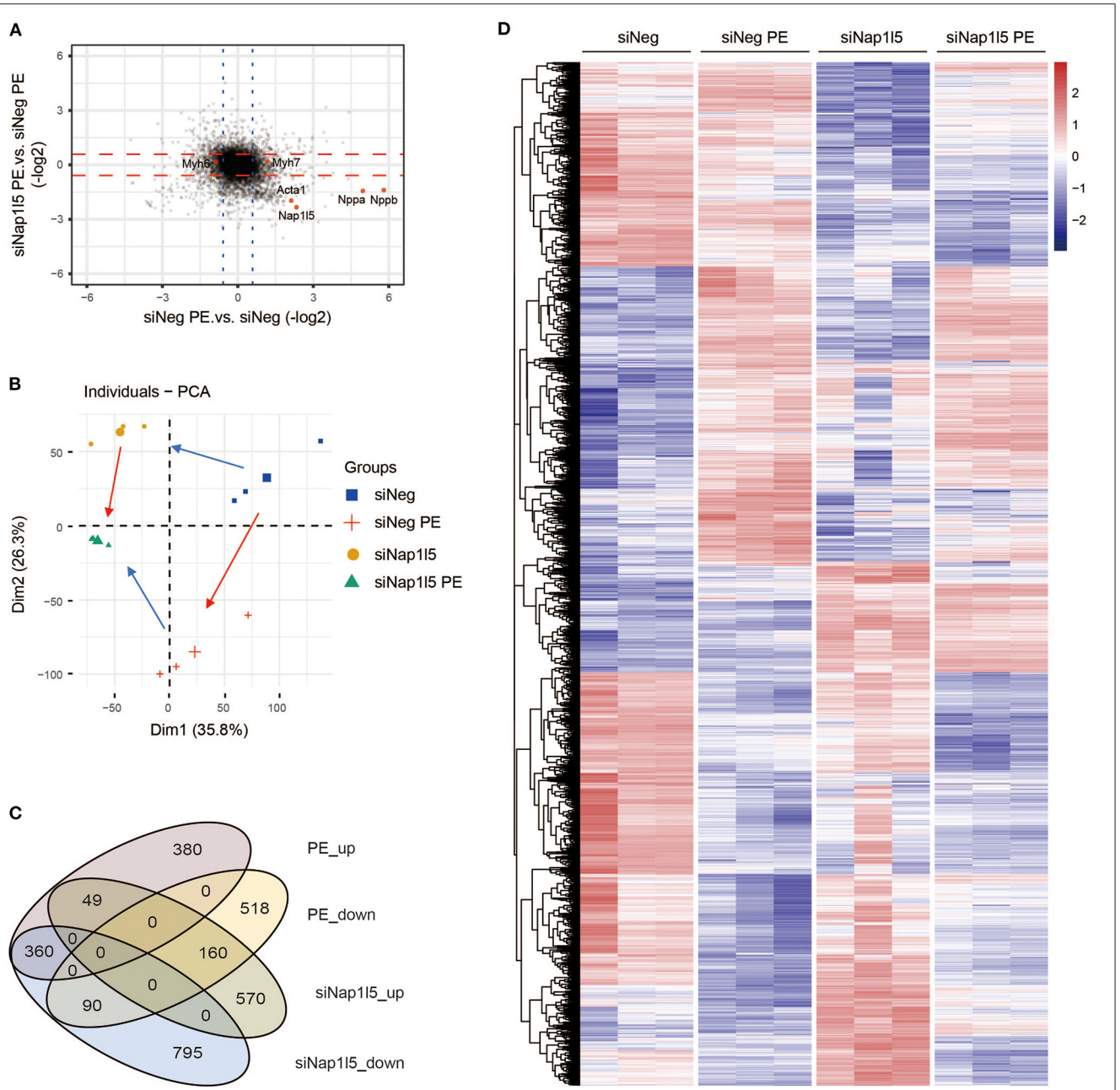

FIGURE 3 | NAP1L5 knockdown reverses hypertrophic transcriptome reprogramming. **(A)** Two-dimensional plotting showing the impact of Nap1l5 knockdown and PE treatment on gene expression. Red and blue lines indicate the threshold of 1.5-fold changes. The expressions of Nap1l5, Nppa, Nppb, Acta1, Myh6, and Myh7 are highlighted. **(B)** Principal component analysis (PCA) showing the distribution of gene profiles from NRVMs transfected with siNeg or siNap1l5, with and without PE treatment. Red arrows indicate the changes from Control to PE; blue arrows indicate changes from siNeg to siNap1l5. **(C)** Venn diagram showing the relationship among up- and down-regulated genes by PE treatment or Nap1l5 knockdown. **(D)** Heatmap of the altered genes by either PE treatment or Nap1l5 knockdown.

These data further support a crucial role of NAP1L5 in pro-hypertrophic transcriptome reprogramming.

NAP1L5 Does Not Affect Histone Methylation-Mediated Epigenetic Regulations

Gene ontology (GO) analysis showed that the upregulated genes after NAP1L5 knockdown mainly related to immune responses, whereas the down-regulated genes covered oxidative phosphorylation, cardiac muscle contraction, and ribosome (**Figures 4A,B**). Gene set enrichment analysis (GSEA) also showed that hypertrophic cardiomyopathy-related genes were enriched in the down-regulated genes after NAP1L5 knockdown (**Figure 4C**), suggesting an involvement of NAP1L5 in hypertrophic cardiomyopathy.

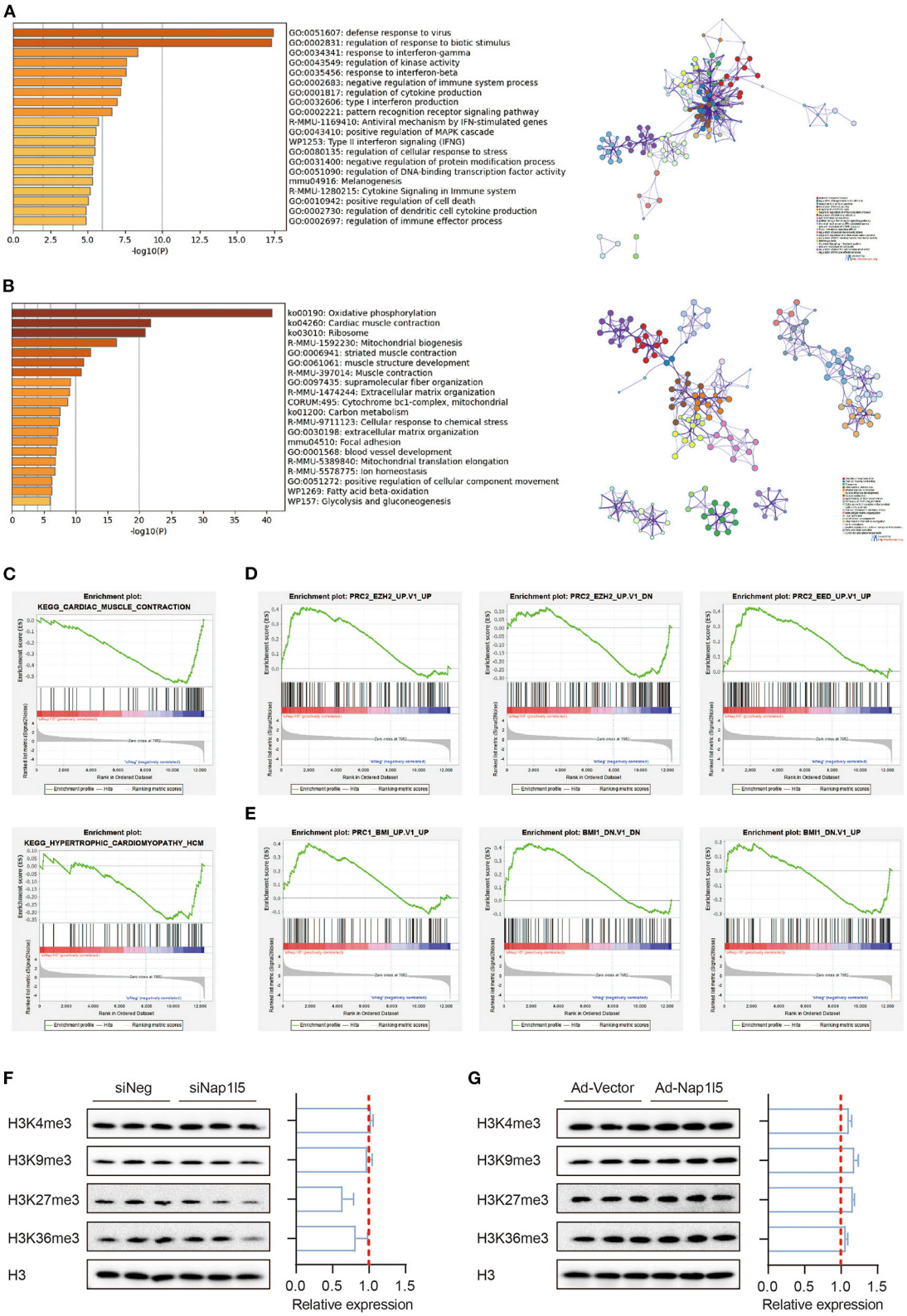

FIGURE 4 | NAP1L5 does not affect histone methylation-mediated epigenetic regulations. **(A,B)** GO analysis (left) and protein-protein interaction (PPI; right) of the upregulated **(A)** and down-regulated **(B)** genes after Nap1l5 knockdown. **(C–E)** Gene set enrichment analysis (GSEA) showing the enrichment pattern of pathways, including cardiac muscle contraction (**C**; upper), hypertrophic cardiomyopathy (**C**; lower), PRC2_EZH2_UP (**D**; left), PRC2_EZH2_DOWN (**D**: middle), PRC2_EED_UP (**D**; right), PRC1_BMI_UP (**E**; left), PRC1_BMI_DOWN (**E**; middle), and BMI1_DOWN (**E**; right) after Nap1l5 knockdown. **(F,G)** Immunoblots (left) and quantification data (right) showing the impact of Nap1l5 knockdown **(F)** and Nap1l5 overexpression **(G)** on histone methylations at H3 K4, K9, K27, and K36 sites. $n = 3$.

Interestingly, the genes altered by siNap1l5 were negatively correlated with the regulations by polycomb repressive complex II (PRC2; **Figure 4D**) and complex I (PRC1; **Figure 4E**). We became curious about a possible role of NAP1L5 in epigenetic reprogramming. However, neither NAP1L5 knockdown nor its overexpression affected global methylations at histone H3 K4, K9, K27 and K36 sites, modifications essential for transcription regulation (**Figures 4F,G**). These data implicate that epigenetic regulation might not be the key mechanism underlying NAP1L5-mediated gene regulation.

NAP1L5 Accelerates Protein Synthesis Rate

Consistently with the GO analysis results, GSEA also revealed a down-regulation of ribosomal genes after NAP1L5 knockdown (**Figure 5A**), covering nearly all the genes of large and small ribosome subunits (**Figure 5B**). This result implicates a potential role of NAP1L5 in translation control. To test this hypothesis, we performed the puromycin incorporation assay, which allowing the detection of nascently synthesized peptides using Western blot with a specific anti-puromycin antibody (17, 44). We found that NAP1L5 knockdown significantly blocked the accelerated protein synthesis rate after PE treatment (**Figure 5C**). On contrary, NAP1L5 overexpression was sufficient to increase the protein synthesis rate (**Figure 5D**), suggesting that NAP1L5 promotes translation activity during cardiomyocyte hypertrophy.

NAP1L5 Promotes Nucleolar Hypertrophy and Ribosome Assembly

We next analyzed the interactome of NAP1L5 from the String database, and found that NAP1L5 linked to core ribosomal proteins through binding to ribosome assembly or transport factors, including SDAD1, RRP7A, and NOL6 (**Figure 6A**). Interestingly, NAP1L1 also exhibited a similar interactome covering most of the NAP1L5-interacting factors (**Figure 6B**), although they share little identity in protein sequence (22.5%) or structure (**Supplementary Figure 2**). These observations implicate that NAP1L5 might participate in ribosome assembly. Nucleolus develops hypertrophy to accelerate ribosomal RNA transcription and ribosome assembly upon pro-growth stimulation (45). We found that NAP1L5 overexpression substantially increased the size of nucleolus, as evidenced by immunofluorescence of a nucleolar marker Fibrillarin (**Figure 6C**) (46). We then examined the ribosome profiles in NRVMs with NAP1L5 overexpression or knockdown. Compared with the Ad-Vector control, Ad-NAP1L5-infected NRVMs exhibited more ribosomal contents in the 40S, 60S, and 80S components (**Figures 6D,E**). Consistently, Nap1l5 knockdown in NRVMs reduced the contents of 40S, 60S and 80S components (**Figures 6F,G**), suggesting a crucial role of NAP1L5 in ribosome biogenesis.

To further explore the molecular mechanism, we tried to validate the interaction between NAP1L5 and SDAD1 or NOL6. Unfortunately, we did not observe a direct interaction between NAP1L5 and SDAD1, nor the full-length or spliced NOL6 isoforms (**Supplementary Figure 3**). These data suggest that other factors may be involved in the regulation of ribosome assembly by NAP1L5.

DISCUSSION

The pathogenesis of cardiac hypertrophy is a programmed process mediated by regulations at multiple layers such as transcription, translation, and metabolism (2, 5, 47–49). Compared with other aspects, our knowledge about translation control during cardiac hypertrophy is relatively limited. Here we find that NAP1L5 plays a key role in PE-induced cardiomyocyte hypertrophy through promoting nucleolar hypertrophy, ribosome assembly and protein synthesis.

Ribosome biogenesis is a highly energy-consuming process. After translation, ribosomal proteins need to be transported into nucleus and precisely folded with mature rRNA inside nucleolus (50). Cardiac hypertrophy is one of the first diseases identified to be associated with ribosomal DNA transcriptional disorders (8, 9). Hypertrophied cardiomyocyte is characterized by excess protein synthesis to meet the increased demand for cell function maintenance, which necessitates an accelerated ribosome biogenesis (8, 11, 51–53). Accelerated PolI transcription activity increases ribosome numbers during the development of cardiac hypertrophy (10–12). Beyond these observations, we know little about the other processes related to ribosome life cycle. Our discovery about the role of NAP1L5 in translation control accounts for a novel step toward the dynamic regulation of ribosome assembly under pathological conditions.

During evolution, higher ordered plants and mammals have acquired several paralogues of NAP1, named NAP1 like family, and five different NAP1L proteins (NAP1L1-5) have been identified. The overall structure of NAP1L proteins is highly conserved and the protein sequences of human NAP1L homologs to hNAP1L1 show identities ranging between 31% for hNAP1L5 and 64% for hNAP1L4 (54). These NAP1L proteins all contain a NAP1L motif, which is positioned within their central domain and critical for their histone chaperone activity (55). As the newest identified member of the NAP1L family, NAP1L5 has the shortest amino acid sequence (182 aa) among NAP1L family members, and its function has not been elucidated yet. Nevertheless, its homolog NAP1L1 and NAP1L2 have been reported to be histone chaperones, assisting the assembly and disassembly of nucleosome at active transcription sites (21, 23, 56–58). Okuwaki et al. (57) found that NAP1L1 was specifically responsible for the assembly and disassembly of H2A-barr body deficient variant. Tachiwana et al. (58) found that NAP1L2, but not NAP1L1, was required for the incorporation of testis-specific H3t variant into nucleosome. Attia et al. (59) reported that all five members of NAP1L family were able to interact with each other directly via their highly conserved alpha helices. Our analyses from the String database also revealed that NAP1L5 might directly interact with NAP1L2 and NAPL4 (**Figure 6A**). A series of translatome-scale affinity capture studies identified the direct interaction between NAP1L1 and NAP1L2 (60–63). Thus, our findings indicate that the NAP1L proteins might form

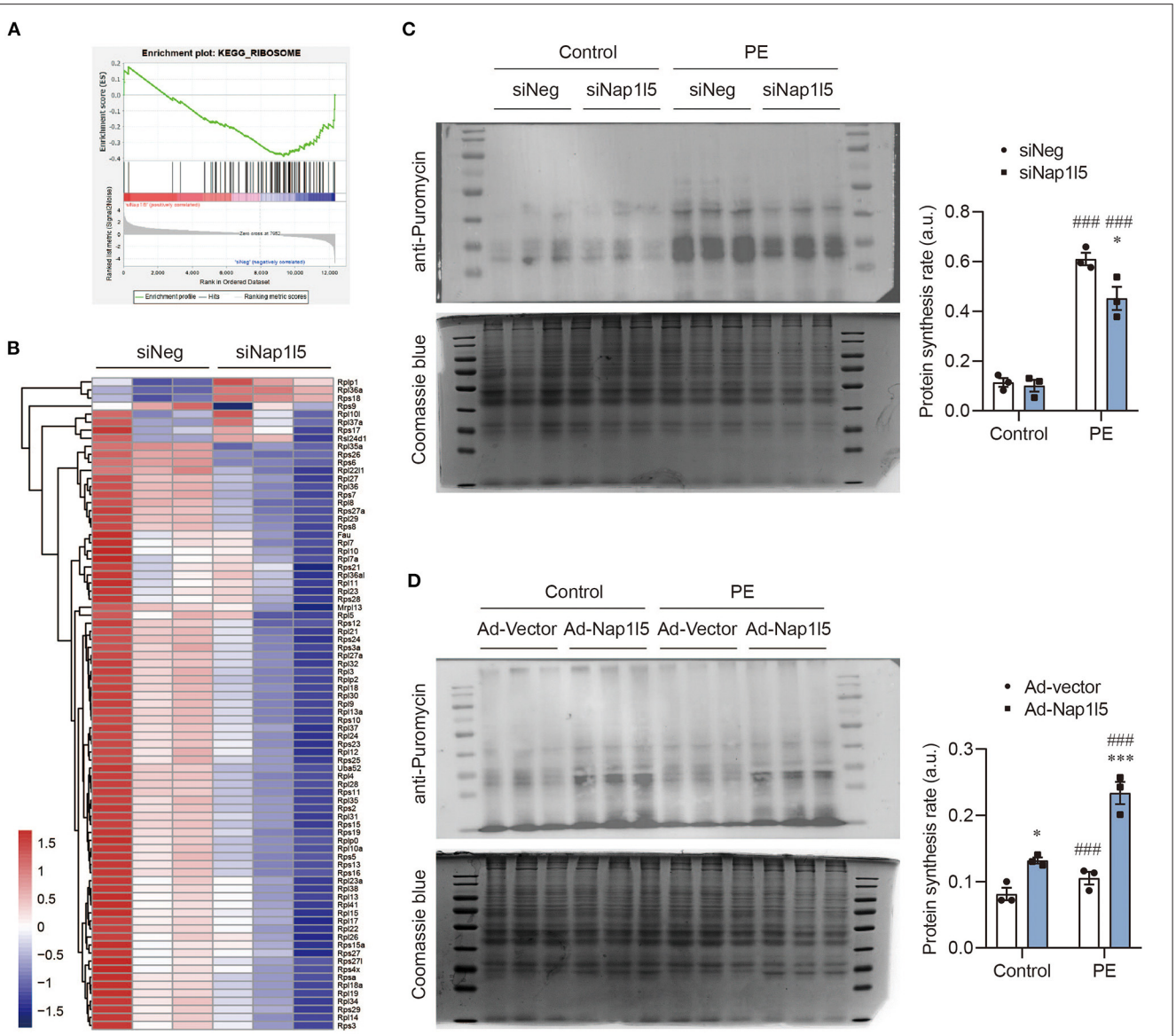

FIGURE 5 | NAP1L5 accelerates protein synthesis rate. **(A)** GSEA showing the negative enrichment of ribosome-related genes after Nap1l5 knockdown. **(B)** Heatmap showing the expression of ribosome-related genes after Nap1l5 knockdown. **(C)** Puromycin incorporation assay showing the protein synthesis rate regulated Nap1l5 knockdown in NRVMs with and without PE treatment. Quantification data were normalized to Coomassie blue staining. $^{*}P < 0.05$ vs. siNeg; $^{\#\#\#}P < 0.001$ vs. Control. $n = 3$. **(D)** Puromycin incorporation assay showing the protein synthesis rate regulated Nap1l5 overexpression in NRVMs with and without PE treatment. $^{*}P < 0.05$, $^{***}P < 0.001$ vs. siNeg; $^{\#\#\#}P < 0.001$ vs. Control. $n = 3$.

a special complex involving in the nucleosome dynamics during rRNA transcription.

SDAD1 (SDA1 domain containing 1) is a shared hub protein interacting with both NAP1L1 and NAP1L5 (**Figures 6A,B**). It has been involved in the development of cardiac hypertrophy and tumor diseases through binding with long non-coding RNAs or microRNAs (64–66). Interestingly, the yeast homolog of SDAD1 has been shown to interact with NAP1 and facilitates the export of 60S pre-ribosomal subunits from nucleus to cytoplasm (67, 68). NOL6 is a highly conserved nucleolar protein that appears to be associated with ribosome biogenesis by interacting with pre-rRNA primary transcript (69). Although interactions of NAP1L5 with SDAD1 and NOL6 have been implicated by affinity capture mass spectrum, we could not validate their direct interactions using co-IP assay (**Supplementary Figure 3**). Whether and how NAP1L5 links to the ribosome assembly process and contributes to the pathogenesis of cardiac hypertrophy need to be further investigated.

Regulation of cell growth is a fundamental process in development and disease that integrates a vast array of extra- and intra-cellular information. A central player in this

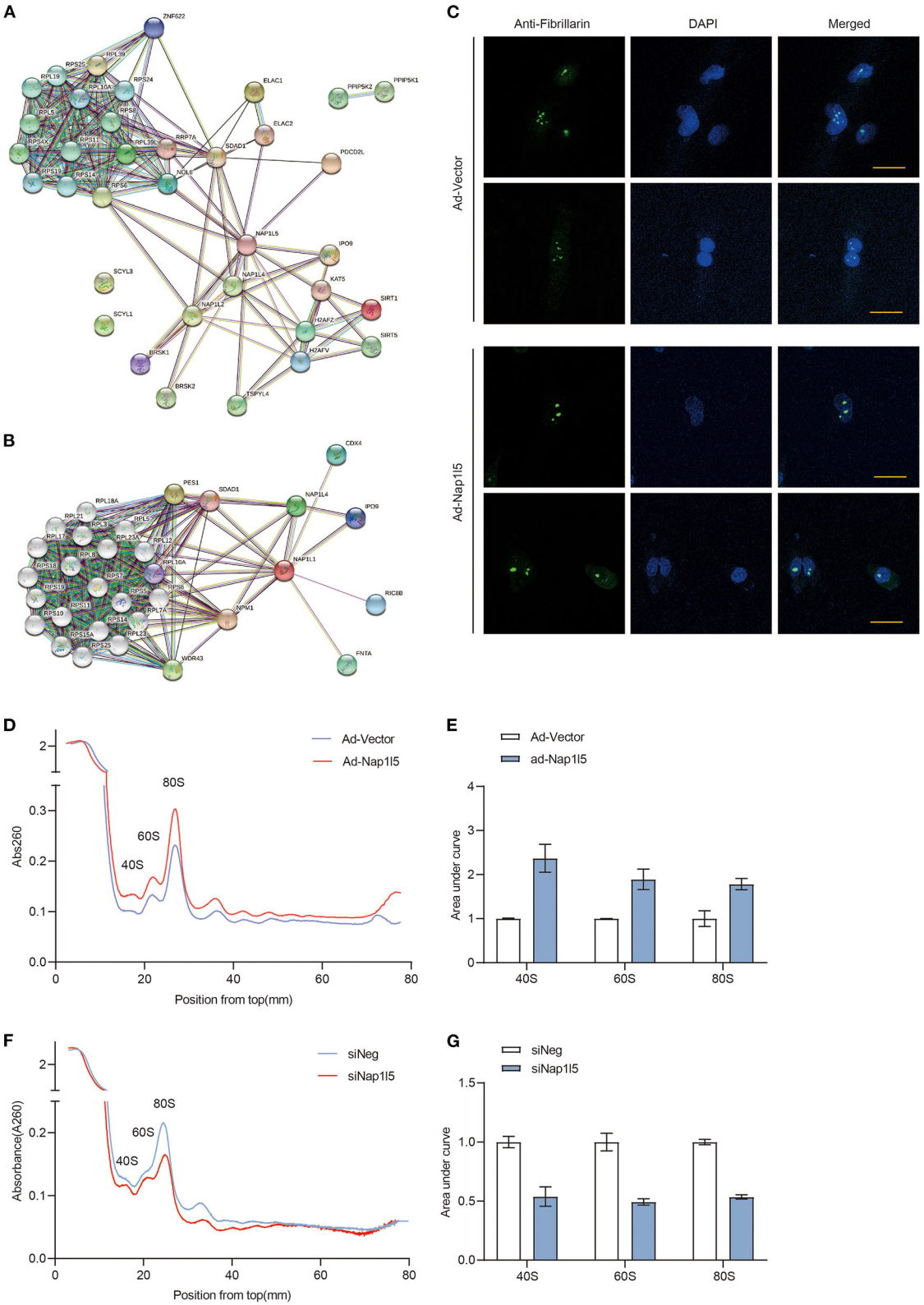

FIGURE 6 | NAP1L5 promotes nucleolar hypertrophy and ribosome assembly. **(A)** Protein-protein interaction (PPI) network of NAP1L5 organized from String database. **(B)** PPI network of NAP1L1 organized from String database. **(C)** Representative nucleolar immunofluorescence images using anti-Fibrillarin antibody in NRVMs infected with Ad-Vector or Ad-Nap1l5. $n = 15$. **(D)** Ribosome profiles from NRVMs infected with Ad-Vector or Ad-Nap1l5 using sucrose gradient and

(Continued)

FIGURE 6 | detection of absorbance at 260nm. $n = 2$. **(E)** Quantification of 40S, 60S and 80S ribosomes from the ribosome profiling assay of panel **(D)**. Data were mean ± SD. $n = 2$. **(F)** Ribosome profiles from NRVMs transfected with siNeg or siNap1l5 using sucrose gradient and detection of absorbance at 260 nm. $n = 2$. **(G)** Quantification of 40S, 60S and 80S ribosomes from the ribosome profiling assay of panel **(F)**. Data were mean ± SD. $n = 2$.

process is PolI, which transcribes ribosomal RNA (rRNA) genes in the nucleolus. Rapidly growing cancer cells are characterized by increased Pol I-mediated transcription, and consequently nucleolar hypertrophy. An aberrant increase in nucleolar size in cancer cells was documented more than a century ago. Nucleolar hypertrophy is a common feature in cancer and that nucleolar size can be used as a histopathological marker to grade the malignancy of tumors (70, 71). Despite this early association of enlarged nucleoli and cancer, little is known about nucleolar size in cardiac hypertrophy. Pathological growth of cardiomyocytes during hypertrophy is characterized by excess protein synthesis. Our data provide crucial evidence that overexpression of Nap1l5 aggravates cardiac hypertrophy along with increased ribosome assembly and translation activity. This might be attributable to its impact on PolI-mediated transcription and subsequently nucleolar hyperplasia.

mTOR is at the core of the translational regulation by converging signaling transduction from a variety of nutrients and growth factors (13, 14, 72–76). Activation of mTOR signaling has been involved in the pathogenesis of cardiac hypertrophy; however, cardiac-specific ablation of raptor impairs adaptive hypertrophy, but causes heart failure in mice (15). Moreover, simultaneous knockout of two genes encoding for S6K1, Rps6kb1 and Rps6kb2, has no effect on pressure overload-induced cardiac hypertrophy in mice (16). Interestingly, our previous study implicated that the activation of mTOR signaling is usually transient, and quickly fades out after hypertrophic stimulation (17). Due to the crucial role of mTOR in cell survival and the diverse outcomes of its inactivation (15, 16), mTOR would not be a good drug target for cardiac hypertrophy therapy. Our findings suggest that the mTOR-independent translation control might contribute even more to the accelerated protein synthesis during cardiac hypertrophy.

One limitation of this study is that all observations are from an *in vitro* cellular model induced by an α1-receptor agonist, PE. Whether this mechanism also applies *in vivo* and in human systems need to be further investigated.

CONCLUSIONS

Taken together, we demonstrate that NAP1L5 is upregulated in PE-induced cardiomyocyte hypertrophy, which functions to promote protein synthesis through facilitating ribosome assembly. Our findings provide novel insights into the translation control during cardiac hypertrophy, and provide potential molecular targets to treat cardiac hypertrophy and heart failure.

METHODS

Cell Culture

Neonatal rat ventricular myocytes (NRVMs) were isolated and cultured as described previously (17). Neonatal rat hearts (within 3 days after birth) were immediately extracted after decapitation and placed in a dish containing precooled PBS. Left ventricular tissues were dissected, finely cut into pieces, and then digested in a solution containing 0.08% type II collagenase (Sigma) and 0.125% protease (Sigma) at 37°C for 20 min/time. The supernatants were discarded at the first time and collected after that. This process continued until the heart tissues were completely digested. Cardiomyocytes were separated from fibroblasts by percoll (GE) density gradient centrifugation, and cultured in high glucose DMEM (Hyclone) containing 10% FBS (Gbico) and 1% penicillin/streptomycin. After 24 h of culture, the medium was changed to DMEM medium with 1% ITS (Invitrogen) for another 24 h before further treatment.

Plasmids

The full-length cDNA sequence of rat Nap1l5 (rNap1l5) were obtained by the National Center for Biotechnology Information (NCBI). The pcDNA3.1-rNap1l5-Flag recombinant plasmid were constructed by cloning the entire coding region of rNap1l5 into the NheI and XhoI sites of the pcDNA3.1-HA plasmid. The primer pair rNap1l5 CZF (5′- GGGAGACCCAAGCTGGCT AGC*GCCACC*atggccgaccccgagaag−3′) and rNap1l5 CZR (5′- TACGTCGTATGGGTA*TCTAGA*Tcttctcggcagagtcgggacc−3′) was used to amplify a cDNA fragment encoding the mature rNap1l5 peptide. Massive plasmid replication was performed by transforming the pcDNA3.1-rNap1l5-Flag plasmid into E. coli DH-5α. In addition, in order to overexpress Nap1l5 in NRVM, the pcDNA3.1-rNap1l5-Flag plasmid was sent to Shanghai Hanheng Biotechnology Co., Ltd. for adenovirus packaging.

The full-length cDNA sequence of rat Nol6 and SDAD1 were obtained by the National Center for Biotechnology Information (NCBI). The pcDNA3.1-SDAD1-HA recombinant plasmid were constructed by cloning the entire coding region of SDAD1 into the NheI and XhoI sites of the pcDNA3.1-Flag plasmid. The primer pair SDAD1 CZF (5′- *ACTATAGGGAGACCCAAGC TGGCTAGCGCCACCatgtccgggaggaacaac*−3′) and SDAD1 CZR (5′- *ATCTGGTACGTCGTATGGGTATCTAGActtcattcttttcctct ttttcag*−3′) was used to amplify a cDNA fragment encoding the mature SDAD1 peptide. Again, to get the mature Nol6 peptide, the primer pair Nol6 CZF (5′- *ACTCACTATAGGGAG ACCCAAGCTGGCTAGCGCCACCatgggaccagcccccgccgga*−3′) and Nol6 CZR (5′- *ATCTGGTACGTCGTATGGGTATCTAGAca cagtccacctctcacttcggg*−3′) was used to amplify a cDNA fragment encoding the mature Nol6 peptide. However, the sequencing results showed that the deletion of exon 18 of this Nol6 resulted in frameshift mutation after exon 18, so we named this spliced

NOL6 isoforms as Nol6Δ. To get the full-length Nol6, we used genomic DNA of Nol6 as a template and designed primers NOL6 gBF (tggtttgtcacctggagggcagcgg) and NOL6 gBR (cttgaggacgtcagt gtgtgtggcag) amplified in the upstream and downstream of exon 18 to obtain the missing fragment, and then the-full length Nol6 was obtained by bridging and recombination.

Cell Size Measurement

Cell size was measured using wheat germ agglutinin (WGA) staining as previously described. Briefly, cardiomyocytes were stimulated with 50 μM of PE for 48 h after transfection with different siRNA or infection with different adenoviruses for 24 h, the culture medium was discarded, washed with PBS, and fixed with 4% paraformaldehyde for 15 min at room temperature. Then 5.0 μg/mL WGA (Invitrigen) was applied to incubate with cardiomyocytes for 10 min at 37°C. When labeling was complete, removed the labeling solution, and washed cells three times with PBS. Then dyed with DAPI for 10 min at room temperature, and washed 5–7 times with PBS for 5 min each time. Finally, Images collected under a fluorescence microscope. Image Pro Plus 6.0 software was used to measure cardiomyocyte surface area. Each field of view measured more than 50 to calculate the surface area of cardiomyocytes.

Immunofluorescence

The method of immunofluorescence staining of cardiomyocytes was as described above. The cardiomyocytes used for immunofluorescence staining were cultured in a six well cell culture plate containing sterile glass slides. Cardiomyocytes were stimulated with 50 μM of PE for 48 h after transfection with different siRNA or infection with different adenoviruses for 24 h, The cells were then fixed with 4% formaldehyde in PBS for 15 min at room temperature, permeabilized with 0.1% Triton X-100 in PBS for 10 min, goat serum was blocked at room temperature for 30 min, and then incubated with α-actinin antibody (1:100, Proteintech) or Fibrillarin antibody (1:100, Abclonal) at 4°C overnight. The next day, incubated the cell sample with the corresponding secondary antibody for 1 h at room temperature. Then dyed with DAPI for 10 min at room temperature. Then washed 5–7 times with PBS for 5 min each time. Finally, removed the slides from the 6-well plate and mounted the slides. Then, the fluorescence staining pictures of cardiomyocytes were collected under a fluorescence microscope. Image Pro Plus 6.0 software was used observe and take pictures.

Immunoprecipitation

Cultured HEK293T cells co-transfected with the appropriate plasmids were collected and lysed in an IP buffer (50mM Tris-HCl (pH 8.0), 150mM NaCl, 2mM EDTA, 1% NP-40 and 5% Glycerol) supplemented with a protease inhibitor cocktail (Roche) and PMSF. After incubating for 30 min at 4°C, followed by centrifuging 13,000 g for 15 min, the cell lysates were precleared with normal mouse or rabbit immunoglobulin G and protein A/G-agarose beads (Roche) for 1h at 4°C. The precleared lysates (500 μl) were then incubated with 1 μg of antibody and 10 μl of protein A/G-agarose beads on a rocking platform at 4°C overnight. The immunocomplex was collected, washed 5–6 times with cold IP wash buffer (50mM Tris-HCl (pH 8.0), 150mM NaCl, 2mM EDTA, 0.1% NP-40) and blotted using the indicated primary antibodies.

Western Blot

Total proteins were extracted from NRVM cells. NRVM cells lysed in Radio Immunoprecipitation Assay (RIPA) lysis buffers (Beyotime, Nanjing, China). Cell lysates were centrifuged at 12,000×g for 15 min. The proteins concentration was detected by the BCA method, and equal quantities of protein extracts were loaded on a sodium dodecyl sulfate-polyacrylamide gel electrophoresis (SDS-PAGE), then transferred onto polyvinylidene fluoride (PVDF) membranes (Millipore Corp., Bedford, MA, U.S.A.). The membranes were blocked with 5% (w/v) non-fat milk for 1 h at room temperature, the membranes were incubated with specific primary antibodies overnight at 4°C. After washing 3 times with TBST, the membranes were incubated with the HRP-linked secondary antibody at room temperature for 1 h, and then washed 3 times with TBST again. Finally, the protein bands on the membranes were detected by chemiluminescent reagents (Beyotime, Nanjing, China). Chemiluminescence signals were quantified using an ECL imager, and analyzed using Quantity One software (Bio-Rad, Hercules, CA, USA). The specific primary antibodies were: anti-GAPDH (Proteintech), anti-Histone3 (Proteintech), anti-H3K4me3 (CST), anti-H3K9me3 (CST), anti-H3K27me3 (CST), anti-H3K36me3 (CST), anti-Flag (Sigma), and anti-Puromycin (Santa Cruz).

Puromycin Incorporation Assay

Different treatments of NRVM cells, 30 min before harvesting, add 1μM puromycin to each well for 30 min, then harvest the cells and extract the protein, and detect the binding level of puromycin by Western blot with anti-Puromycin antibody.

Ribosome Profiling

Ribosome profiling was performed as described. Cardiomyocytes were transfection with different siRNA or infection with different adenoviruses for 48 h, and were treated with with CHX (100 μg/mL) for 10–30 min before harvested. Cells were harvested using trypsin and then lysed in polysome extraction buffer (20 mM Tris-HCl [pH 7.0], 100 mM KCl, 5 mM $MgCl_2$, 0.5% Nonidet P-40) containing 100 μg/ml CHX, 1x protease inhibitors and 1:1,000 dilution of RiboLock RNase inhibitor for 15 min on ice. Following centrifugation, lysates were ultracentrifuged on 10–50% sucrose gradients at 190,000g for 1.5 h at 4°C. Following ultracentrifugation, fractions were collected from each sample using a BioComp Piston Gradient Fractionator instrument fitted with a TRIAX flow cell to measure absorbance.

RNA-Seq Analysis

NRVMs were transfected with siNap1l5 or siNeg using Lipofectamine RNAiMAX. After transfected 24 h, 50 μM phenylephrine (PE) were added in the media to induce cardiomyocyte hypertrophy, was performed as described previously (17). 48 h after treated with PE, NRVMs were

harvested to extracted RNA according to the manufacturer's instructions. Transcriptome sequencing of RNA was completed by Beijing Genomics Institution (BGI). Three independent biological replicate samples were sequenced for each group. (i) The different expression genes (DEGs) between groups were screened using linear models for microarray data (limma) package in R. |Fold change| >1.5 and adjusted *P*-value < 0.05 were considered the threshold. (ii) Enrichment analysis of DEGs using Metascape online database with default parameters. (iii) Gene Set Enrichment Analysis (GSEA) is used to screen significantly enriched signaling pathways and transcription factors with default parameters, was performed as described previously.

Quantitative Real-Time PCR

Total RNA was extracted from NRVM cells using the GenElute Mammalian Total RNA Miniprep Kit (Sigma-Aldrich), following the manufacturer's instructions. RNA was quantified using NanoDrop (Thermo Fisher Scientific). The cDNAs were synthesized from 1μg RNA using a RevertAid First Strand cDNA Synthesis Kit (Thermo Fisher Scientific, U.S.A.). Real-time PCR was performed using the specific primers and Ultra SYBR Mixture (Monad, Suzhou, China) on CFX96M Touch Real-Time PCR Detection System (Roche, Basel, Switzerland). The PCR primer sequences used in this study include rNap1l5-forward: GAGCACAGCAGCTGACAGAC; rNap1l5-reverse: ATGACGTCGTTCTTGGGTTC; rNppa-forward: ATACAGTG CGGTGTCCAACA; rNppa-reverse: AGCCCTCAGTTTG CTTTTCA; rNppb-forward: CAGCTCTCAAAGGACCAAGG; rNppb-reverse: GCAGCTTGAACTATGTGCCA; rGAPDH-forward: ACAGCAACAGGGTGGTGGAC; rGAPDH-reverse: TTTGAGGGTGCAGCGAACTT. Relative expression of genes was determined with GAPDH as an endogenous control.

Quantification and Statistical Analysis

Statistical analyses were performed using GraphPad Prism 8 Software. All experimental data are presented as mean ± SEM of at least three independent experiments unless denoted elsewhere. Statistical significance for multiple comparisons was determined by one-way ANOVA or two-way ANOVA followed by Tukey's test. Bonferroni adjustment was used for *post hoc* analysis. Student's *t*-test was used for comparisons between two groups. $P < 0.05$ was considered statistically significant.

DATA AVAILABILITY STATEMENT

All relevant data supporting the findings of this study are available within the article and its supplementary information or from the authors upon reasonable request. RNA-seq data have been deposited in NCBI's Gene Expression Omnibus (GEO) repository (accession code GSE173737).

ETHICS STATEMENT

The animal study was reviewed and approved by Renmin Hospital of Wuhan University.

AUTHOR CONTRIBUTIONS

ZW and JT conceptualized, designed, and supervised the study. NG, DZ, and JS performed the molecular and cellular experiments with inputs from SW. JL performed the bioinformatic analyses. YF, SZ, and QG assisted with the preparation of NRVMs. ZW and NG analyzed the data and wrote the manuscript. All authors have approved its publication.

FUNDING

This study was supported by funds from National Natural Science Foundation of China (Nos. 81722007 and 82070231), National Health Commission of China (No. 2017ZX1030440 2001-008), State Key Laboratory of Cardiovascular Disease (Nos. GZ2021015 and 2021-YJR01), and start-up funds from Fuwai Hospital Chinese Academy of Medical Sciences, Shenzhen (GSP-RC-2020002).

ACKNOWLEDGMENTS

We thank Ms. Yuan He and Mrs. Qiong Ding from Wuhan University for their technical assistance.

SUPPLEMENTARY MATERIAL

The Supplementary Material for this article can be found online at: https://www.frontiersin.org/articles/10.3389/fcvm.2021.791501/full#supplementary-material

REFERENCES

1. Marian AJ, Braunwald, E. Hypertrophic cardiomyopathy: genetics, pathogenesis, clinical manifestations, diagnosis, and therapy. *Circ Res.* (2017) 121:749–70. doi: 10.1161/CIRCRESAHA.117.311059
2. Nakamura M, Sadoshima, J. Mechanisms of physiological and pathological cardiac hypertrophy Nature reviews. *Cardiology.* (2018) 15:387–407. doi: 10.1038/s41569-018-0007-y
3. Lam MP, Wang D, Lau E, Liem DA, Kim AK, Ng DC, et al. Protein kinetic signatures of the remodeling heart following isoproterenol stimulation. *J Clin Invest.* (2014) 124:1734–44. doi: 10.1172/JCI73787
4. Lau E, Cao Q, Ng DC, Bleakley BJ, Dincer TU, Bot BM, et al. A large dataset of protein dynamics in the mammalian heart proteome. *Sci Data.* (2016) 3:160015. doi: 10.1038/sdata.2016.15
5. Maillet M, van Berlo JH, Molkentin, J. D. Molecular basis of physiological heart growth: fundamental concepts and new players. *Nat Rev Mol Cell Biol.* (2013) 14:38–48. doi: 10.1038/nrm3495
6. Xue S, Barna, M. Specialized ribosomes: a new frontier in gene regulation and organismal biology. *Nat Rev Mol Cell Biol.* (2012) 13:355–69. doi: 10.1038/nrm3359
7. Guo H. Specialized ribosomes and the control of translation. *Biochem Soc Trans.* (2018) 46:855–69. doi: 10.1042/BST20160426
8. Morgan HE, Siehl D, Chua BH, Lautensack-Belser, N. Faster protein and ribosome synthesis in hypertrophying heart. *Basic Res Cardiol.* (1985) 80:115–8.
9. Rosello-Lleti E, Rivera M, Cortes R, Azorin I, Sirera R, Martinez-Dolz L, et al. Influence of heart failure on nucleolar organization and protein

expression in human hearts. *Biochem Biophys Res Commun.* (2012) 418:222–8. doi: 10.1016/j.bbrc.2011.12.151
10. McDermott PJ, Rothblum LI, Smith SD, Morgan HE. Accelerated rates of ribosomal RNA synthesis during growth of contracting heart cells in culture. *J Biol Chem.* (1989) 264:18220–7. doi: 10.1016/S0021-9258(19)84700-2
11. Luyken J, Hannan RD, Cheung JY, Rothblum LI. Regulation of rDNA transcription during endothelin-1-induced hypertrophy of neonatal cardiomyocytes. Hyperphosphorylation of upstream binding factor, an rDNA transcription factor. *Circ Res*. (1996) 78:354–61. doi: 10.1161/01.RES.78.3.354
12. Brandenburger Y, Jenkins A, Autelitano DJ, Hannan RD. Increased expression of UBF is a critical determinant for rRNA synthesis and hypertrophic growth of cardiac myocytes. *FASEB J.* (2001) 15:2051–3. doi: 10.1096/fj.00-0853fje
13. Szwed A, Kim E, Jacinto E. Regulation and metabolic functions of mTORC1 and mTORC2. *Physiol Rev*. (2021) 101:1371–426. doi: 10.1152/physrev.00026.2020
14. Sciarretta S, Forte M, Frati G, Sadoshima, J. New insights into the role of mTOR signaling in the cardiovascular system. *Circ Res.* (2018) 122:489–505. doi: 10.1161/CIRCRESAHA.117.311147
15. Shende P, Plaisance I, Morandi C, Pellieux C, Berthonneche C, Zorzato F, et al. Cardiac raptor ablation impairs adaptive hypertrophy, alters metabolic gene expression, and causes heart failure in mice. *Circulation.* (2011) 123:1073–82. doi: 10.1161/CIRCULATIONAHA.110.977066
16. McMullen JR, Shioi T, Zhang L, Tarnavski O, Sherwood MC, Dorfman AL, et al. Deletion of ribosomal S6 kinases does not attenuate pathological, physiological, or insulin-like growth factor 1 receptor-phosphoinositide 3-kinase-induced cardiac hypertrophy. *Mol Cell Biol.* (2004) 24:6231–40. doi: 10.1128/MCB.24.14.6231-6240.2004
17. Wang Z, Zhang XJ, Ji YX, Zhang P, Deng KQ, Gong J, et al. The long noncoding RNA Chaer defines an epigenetic checkpoint in cardiac hypertrophy. *Nat Med.* (2016) 22:1131–9. doi: 10.1038/nm.4179
18. Loyola A, Almouzni, G. Histone chaperones, a supporting role in the limelight. *Biochim Biophys Acta.* (2004) 1677:3–11. doi: 10.1016/j.bbaexp.2003.09.012
19. Park YJ, Luger, K. Structure and function of nucleosome assembly proteins. *Biochem Cell Biol.* (2006) 84:549–58. doi: 10.1139/o06-088
20. Okuwaki M, Kato K, Nagata K. Functional characterization of human nucleosome assembly protein 1-like proteins as histone chaperones. *Genes Cells.* (2010) 15:13–27. doi: 10.1111/j.1365-2443.2009.01361.x
21. Ishimi Y, Hirosumi J, Sato W, Sugasawa K, Yokota S, Hanaoka F, Yamada, M. Purification and initial characterization of a protein which facilitates assembly of nucleosome-like structure from mammalian cells. *Eur J Biochem.* (1984) 142:431–9. doi: 10.1111/j.1432-1033.1984.tb08305.x
22. Ishimi Y, Kikuchi A. Identification and molecular cloning of yeast homolog of nucleosome assembly protein I which facilitates nucleosome assembly *in vitro*. *J Biol Chem.* (1991) 266:7025–9. doi: 10.1016/S0021-9258(20)89604-5
23. Fujii-Nakata T, Ishimi Y, Okuda A, Kikuchi A. Functional analysis of nucleosome assembly protein, NAP-1. The negatively charged COOH-terminal region is not necessary for the intrinsic assembly activity. *J Biol Chem*. (1992) 267:20980-6. doi: 10.1016/S0021-9258(19)36785-7
24. Asahara H, Tartare-Deckert S, Nakagawa T, Ikehara T, Hirose F, Hunter T, et al. Dual roles of p300 in chromatin assembly and transcriptional activation in cooperation with nucleosome assembly protein 1 in vitro. *Mol Cell Biol.* (2002) 22:2974–83. doi: 10.1128/MCB.22.9.2974-2983.2002
25. Sharma N, Nyborg JK. The coactivators CBP/p300 and the histone chaperone NAP1 promote transcription-independent nucleosome eviction at the HTLV-1 promoter. *Proc Natl Acad Sci USA*. (2008) 105:7959–63. doi: 10.1073/pnas.0800534105
26. Li L, Gong H, Yu H, Liu X, Liu Q, Yan G, et al. Knockdown of nucleosome assembly protein 1-like 1 promotes dimethyl sulfoxide-induced differentiation of P19CL6 cells into cardiomyocytes. *J Cell Biochem.* (2012) 113:3788–96. doi: 10.1002/jcb.24254
27. Gong H, Yan Y, Fang B, Xue Y, Yin P, Li L, et al. Knockdown of nucleosome assembly protein 1-like 1 induces mesoderm formation and cardiomyogenesis via notch signaling in murine-induced pluripotent stem cells. *Stem Cells.* (2014) 32:1759–73. doi: 10.1002/stem.1702
28. Schimmack S, Taylor A, Lawrence B, Alaimo D, Schmitz-Winnenthal H, Buchler MW, et al. A mechanistic role for the chromatin modulator, NAP1L1, in pancreatic neuroendocrine neoplasm proliferation and metastases. *Epigenetics Chromatin.* (2014) 7:15. doi: 10.1186/1756-8935-7-15
29. Gupta N, Thakker S, Verma SC. KSHV encoded LANA recruits Nucleosome Assembly Protein NAP1L1 for regulating viral DNA replication and transcription. *Sci Rep*. (2016) 6:32633. doi: 10.1038/srep32633
30. Cevik RE, Cesarec M, Da Silva Filipe A, Licastro D, McLauchlan J, Marcello A. Hepatitis C virus NS5A targets nucleosome assembly protein NAP1L1 to control the innate cellular response. *J Virol.* (2017) 91:e00880-17. doi: 10.1128/JVI.00880-17
31. Chen Z, Gao W, Pu L, Zhang L, Han G, Zuo X, et al. PRDM8 exhibits antitumor activities toward hepatocellular carcinoma by targeting NAP1L1. *Hepatology.* (2018) 68:994–1009. doi: 10.1002/hep.29890
32. Qiao H, Li Y, Feng C, Duo S, Ji F, Jiao J. Nap1l1 controls embryonic neural progenitor cell proliferation and differentiation in the developing brain. *Cell Rep*. (2018) 22:2279–93. doi: 10.1016/j.celrep.2018.02.019
33. Yin P, Li Y, Zhou L, Zhang L. NAP1L1 Regulates hepatitis C virus entry and interacts with NS3. *Virol Sin*. (2018) 33:205–8. doi: 10.1007/s12250-018-0006-5
34. Le Y, Kan A, Li QJ, He MK, Chen HL, Shi M. NAP1L1 is a prognostic biomarker and contribute to doxorubicin chemotherapy resistance in human hepatocellular carcinoma. *Cancer Cell Int*. (2019) 19:228. doi: 10.1186/s12935-019-0949-0
35. Tanaka T, Hozumi Y, Martelli AM, Iino M, Goto K. Nucleosome assembly proteins NAP1L1 and NAP1L4 modulate p53 acetylation to regulate cell fate. *Biochim Biophys Acta Mol Cell Res*. (2019) 1866:118560. doi: 10.1016/j.bbamcr.2019.118560
36. Aydin MA, Gul G, Kiziltan R, Algul S, Kemik O. Nucleosome assembly protein 1-like 1 (NAP1L1) in colon cancer patients: a potential biomarker with diagnostic and prognostic utility. *Eur Rev Med Pharmacol Sci*. (2020) 24:10512-7. doi: 10.26355/eurrev_202010_23403
37. Nagashio R, Kuchitsu Y, Igawa S, Kusuhara S, Naoki K, Satoh Y, et al. Prognostic significance of NAP1L1 expression in patients with early lung adenocarcinoma. *Biomed Res.* (2020) 41:149–59. doi: 10.2220/biomedres.41.149
38. Queiroz CJS, Song F, Reed KR, Al-Khafaji N, Clarke AR, Vimalachandran D, et al. NAP1L1: a novel human colorectal cancer biomarker derived from animal models of Apc inactivation. *Front Oncol.* (2020) 10:1565. doi: 10.3389/fonc.2020.01565
39. Dominguez F, Shiliaev N, Lukash T, Agback P, Palchevska O, Gould JR, et al. NAP1L1 and NAP1L4 binding to hypervariable domain of chikungunya virus nsP3 protein is bivalent and requires phosphorylation. *J Virol.* (2021) 95:e0083621. doi: 10.1128/JVI.00836-21
40. Zhang YW, Chen Q, Li B, Li HY, Zhao XK, Xiao YY, et al. NAP1L1 functions as a tumor promoter *via* recruiting hepatoma-derived growth factor/c-jun signal in hepatocellular carcinoma. *Front Cell Dev Biol.* (2021) 9:659680. doi: 10.3389/fcell.2021.659680
41. Harada H, Nagai H, Ezura Y, Yokota T, Ohsawa I, Yamaguchi K, et al. Down-regulation of a novel gene, DRLM, in human liver malignancy from 4q22 that encodes a NAP-like protein. *Gene.* (2002) 296:171–7. doi: 10.1016/S0378-1119(02)00855-7
42. Smith RJ, Dean W, Konfortova G, Kelsey, G. Identification of novel imprinted genes in a genome-wide screen for maternal methylation. *Genome Res.* (2003) 13:558–69. doi: 10.1101/gr.781503
43. Chang S, Wang Y, Xin Y, Wang S, Luo Y, Wang L, et al. DNA methylation abnormalities of imprinted genes in congenital heart disease: a pilot study. *BMC Med Genomics.* (2021) 14:4. doi: 10.1186/s12920-020-00848-0
44. Hidalgo San Jose L, Signer, RAJ. Cell-type-specific quantification of protein synthesis *in vivo*. *Nat Protoc.* (2019) 14:441–60. doi: 10.1038/s41596-018-0100-z
45. Kofuji S, Hirayama A, Eberhardt AO, Kawaguchi R, Sugiura Y, Sampetrean O, et al. IMP dehydrogenase-2 drives aberrant nucleolar activity and promotes tumorigenesis in glioblastoma. *Nat Cell Biol.* (2019) 21:1003–14. doi: 10.1038/s41556-019-0363-9
46. Wang T, Na J. Fibrillarin-GFP Facilitates the Identification of Meiotic Competent Oocytes Front. *Cell Dev Biol.* (2021) 9:648331. doi: 10.3389/fcell.2021.648331

47. Gibb AA, Hill, BG. Metabolic coordination of physiological and pathological cardiac remodeling. *Circ Res.* (2018) 123:107–28. doi: 10.1161/CIRCRESAHA.118.312017
48. Kolwicz SC, Purohit S, Tian R. Cardiac metabolism and its interactions with contraction, growth, and survival of cardiomyocytes. *Circ Res.* (2013) 113:603–16. doi: 10.1161/CIRCRESAHA.113.302095
49. Kimball TH, Vondriska TM. Metabolism, epigenetics, and causal inference in heart failure trends. *Endocrinol Metab.* (2020) 31:181–91. doi: 10.1016/j.tem.2019.11.009
50. Rodgers ML, Woodson SA. A roadmap for rRNA folding and assembly during transcription. *Trends Biochem Sci*. (2021) 46:889–901 doi: 10.1016/j.tibs.2021.05.009
51. Siehl D, Chua BH, Lautensack-Belser N, Morgan, H. E. Faster protein and ribosome synthesis in thyroxine-induced hypertrophy of rat heart. *Am J Physiol.* (1985) 248:C309–19. doi: 10.1152/ajpcell.1985.248.3.C309
52. Hannan RD, Stefanovsky V, Taylor L, Moss T, Rothblum LI. Overexpression of the transcription factor UBF1 is sufficient to increase ribosomal DNA transcription in neonatal cardiomyocytes: implications for cardiac hypertrophy. *Proc Natl Acad Sci USA*. (1996) 93:8750–5. doi: 10.1073/pnas.93.16.8750
53. Hannan RD, Luyken J, Rothblum LI. Regulation of ribosomal DNA transcription during contraction-induced hypertrophy of neonatal cardiomyocytes. *J Biol Chem.* (1996) 271:3213–20. doi: 10.1074/jbc.271.6.3213
54. Attia M, Rachez C, Avner P, Rogner UC. Nucleosome assembly proteins and their interacting proteins in neuronal differentiation. *Arch Biochem Biophys.* (2013) 534:20–6. doi: 10.1016/j.abb.2012.09.011
55. Mehrotra PV, Ahel D, Ryan DP, Weston R, Wiechens N, Kraehenbuehl R, et al. DNA repair factor APLF is a histone chaperone. *Mol Cell.* (2011) 41:46–55. doi: 10.1016/j.molcel.2010.12.008
56. Walter PP, Owen-Hughes TA, Cote J, Workman JL. Stimulation of transcription factor binding and histone displacement by nucleosome assembly protein 1 and nucleoplasmin requires disruption of the histone octamer. *Mol Cell Biol.* (1995) 15:6178–87. doi: 10.1128/MCB.15.11.6178
57. Okuwaki M, Kato K, Shimahara H, Tate S, Nagata, K. Assembly and disassembly of nucleosome core particles containing histone variants by human nucleosome assembly protein I. *Mol Cell Biol.* (2005) 25:10639–51. doi: 10.1128/MCB.25.23.10639-10651.2005
58. Tachiwana H, Osakabe A, Kimura H, Kurumizaka H. Nucleosome formation with the testis-specific histone H3 variant, H3t, by human nucleosome assembly proteins *in vitro*. *Nucleic Acids Res*. (2008) 36:2208–18. doi: 10.1093/nar/gkn060
59. Attia M, Forster A, Rachez C, Freemont P, Avner P Rogner UC. Interaction between nucleosome assembly protein 1-like family members. *J Mol Biol*. (2011) 407:647–60. doi: 10.1016/j.jmb.2011.02.016
60. Marcon E, Ni Z, Pu S, Turinsky AL, Trimble SS, Olsen JB, et al. Human-chromatin-related protein interactions identify a demethylase complex required for chromosome segregation. *Cell Rep.* (2014) 8:297–310. doi: 10.1016/j.celrep.2014.05.050
61. Huttlin EL, Ting L, Bruckner RJ, Gebreab F, Gygi MP, Szpyt J, et al. The BioPlex network: a systematic exploration of the human interactome. *Cell.* (2015) 162:425–40. doi: 10.1016/j.cell.2015.06.043
62. Huttlin EL, Bruckner RJ, Paulo JA, Cannon JR, Ting L, Baltier K, et al. Architecture of the human interactome defines protein communities and disease networks. *Nature.* (2017) 545:505–9. doi: 10.1038/nature22366
63. Huttlin EL, Bruckner RJ, Navarrete-Perea J, Cannon JR, Baltier K, Gebreab F, et al. Dual proteome-scale networks reveal cell-specific remodeling of the human interactome. *Cell*. (2021) 184:3022–40 e28. doi: 10.1016/j.cell.2021.04.011
64. Zeng M, Zhu L, Li L, Kang C. miR-378 suppresses the proliferation, migration and invasion of colon cancer cells by inhibiting SDAD1. *Cell Mol Biol Lett*. (2017) 22:12. doi: 10.1186/s11658-017-0041-5
65. Jing L, Li S, Wang J, Zhang G. Long non-coding RNA small nucleolar RNA host gene 7 facilitates cardiac hypertrophy *via* stabilization of SDA1 domain containing 1 mRNA. *J Cell Biochem*. (2019) 120:15089–97. doi: 10.1002/jcb.28770
66. Ding Z, Lan H, Xu R, Zhou X, Pan Y. LncRNA TP73-AS1 accelerates tumor progression in gastric cancer through regulating miR-194-5p/SDAD1 axis. *Pathol Res Pract*. (2018) 214:1993–9. doi: 10.1016/j.prp.2018.09.006
67. Zimmerman ZA, Kellogg DR. The Sda1 protein is required for passage through start. *Mol Biol Cell*. (2001) 12:201–19. doi: 10.1091/mbc.12.1.201
68. Babbio F, Farinacci M, Saracino F, Carbone ML, Privitera E. Expression and localization studies of hSDA, the human ortholog of the yeast SDA1 gene. *Cell Cycle*. (2004) 3:486–90. doi: 10.4161/cc.3.4.792
69. Utama B, Kennedy D, Ru K, Mattick JS. Isolation and characterization of a new nucleolar protein, Nrap, that is conserved from yeast to humans. *Genes Cells*. (2002) 7:115–32. doi: 10.1046/j.1356-9597.2001.00507.x
70. Pich A, Chiusa L, Margaria E. Prognostic relevance of AgNORs in tumor pathology. *Micron*. (2000) 31:133–41. doi: 10.1016/S0968-4328(99)00070-0
71. Drygin D, Rice WG, Grummt I. The RNA polymerase I transcription machinery: an emerging target for the treatment of cancer. *Annu Rev Pharmacol Toxicol.* (2010) 50:131–56. doi: 10.1146/annurev.pharmtox.010909.105844
72. Wyant GA, Abu-Remaileh M, Wolfson RL, Chen WW, Freinkman E, Danai LV, et al. mTORC1 activator SLC38A9 is required to efflux essential amino acids from lysosomes and use protein as a nutrient. *Cell*. (2017) 171:642–54 e12. doi: 10.1016/j.cell.2017.09.046
73. Kim SH, Choi JH, Wang P, Go CD, Hesketh GG, Gingras AC, et al. Mitochondrial threonyl-tRNA synthetase TARS2 is required for threonine-sensitive mTORC1 activation. *Mol Cell*. (2021). 81:398–407 e4. doi: 10.1016/j.molcel.2020.11.036
74. Rebsamen M, Pochini L, Stasyk T, de Araujo ME, Galluccio M, Kandasamy RK, et al. SLC38A9 is a component of the lysosomal amino acid sensing machinery that controls mTORC1. *Nature.* (2015) 519:477–81. doi: 10.1038/nature14107
75. Nowosad A, Jeannot P, Callot C, Creff J, Perchey RT, Joffre C, et al. p27 controls Ragulator and mTOR activity in amino acid-deprived cells to regulate the autophagy-lysosomal pathway and coordinate cell cycle and cell growth. *Nat Cell Biol.* (2020) 22:1076–90. doi: 10.1038/s41556-020-0554-4
76. Kim J, Guan KL. mTOR as a central hub of nutrient signalling and cell growth. *Nat Cell Biol.* (2019) 21:63–71. doi: 10.1038/s41556-018-0205-1

Conflict of Interest: The authors declare that the research was conducted in the absence of any commercial or financial relationships that could be construed as a potential conflict of interest.

Publisher's Note: All claims expressed in this article are solely those of the authors and do not necessarily represent those of their affiliated organizations, or those of the publisher, the editors and the reviewers. Any product that may be evaluated in this article, or claim that may be made by its manufacturer, is not guaranteed or endorsed by the publisher.

frontiers in Cardiovascular Medicine

ORIGINAL RESEARCH
published: 05 January 2022
doi: 10.3389/fcvm.2021.772815

Cardiorespiratory Responses During High-Intensity Interval Training Prescribed by Rating of Perceived Exertion in Patients After Myocardial Infarction Enrolled in Early Outpatient Cardiac Rehabilitation

Yaoshan Dun[1,2,3], *Shane M. Hammer*[2], *Joshua R. Smith*[2], *Mary C. MacGillivray*[2], *Benjamin S. Simmons*[2], *Ray W. Squires*[2], *Suixin Liu*[1,3] *and Thomas P. Olson*[2*]

[1] Division of Cardiac Rehabilitation, Department of Physical Medicine and Rehabilitation, Xiangya Hospital of Central South University, Changsha, China, [2] Division of Preventive Cardiology, Department of Cardiovascular Medicine, Mayo Clinic, Rochester, MN, United States, [3] National Clinical Research Center for Geriatric Disorders, Xiangya Hospital of Central South University, Changsha, China

OPEN ACCESS

Edited by:
Jinwei Tian,
The Second Affiliated Hospital of Harbin Medical University, China

Reviewed by:
Yuefei Liu,
University of Ulm, Germany
Zhen Zhang,
Pfizer, United States

***Correspondence:**
Thomas P. Olson
olson.thomas2@mayo.edu

Specialty section:
This article was submitted to General Cardiovascular Medicine, a section of the journal Frontiers in Cardiovascular Medicine

Received: 08 September 2021
Accepted: 14 December 2021
Published: 05 January 2022

Citation:
Dun Y, Hammer SM, Smith JR, MacGillivray MC, Simmons BS, Squires RW, Liu S and Olson TP (2022) Cardiorespiratory Responses During High-Intensity Interval Training Prescribed by Rating of Perceived Exertion in Patients After Myocardial Infarction Enrolled in Early Outpatient Cardiac Rehabilitation. Front. Cardiovasc. Med. 8:772815. doi: 10.3389/fcvm.2021.772815

Objective: We aimed to determine the cardiorespiratory responses during, and adaptations to, high-intensity interval training (HIIT) prescribed using ratings of perceived exertion (RPE) in patients after myocardial infarction (MI) during early outpatient cardiac rehabilitation (CR).

Methods: We prospectively recruited 29 MI patients after percutaneous coronary intervention who began CR within 2 weeks after hospital discharge. Eleven patients (seven men; four women; age: 61 ± 11 yrs) who completed ≥24 supervised HIIT sessions with metabolic gas exchange measured during HIIT once weekly for 8 weeks and performed pre- and post- CR cardiopulmonary exercise tests were included in the study. Each HIIT session consisted of 5–8 high-intensity intervals [HIIs, 1-min RPE 14–17 (Borg 6–20 scale)] and low-intensity intervals (LIIs, 4-min RPE < 12). Metabolic gas exchange, heart rate (HR), and blood pressure during HIIT were measured.

Results: The mean oxygen uptake ($\dot{V}O_2$) during HIIs across 88 sessions of HIITs [91 (14)% of $\dot{V}O_{2peak}$, median (interquartile range, IQR)] was significantly higher than the lower limit of target $\dot{V}O_2$ zone (75% of $\dot{V}O_{2peak}$) recommended for the HII ($p < 0.001$). Exercise intensity during RPE-prescribed HIITs, determined as $\%\dot{V}O_{2peak}$, was highly repeatable with intra-class correlations of 0.95 (95% CI 0.86– 0.99, $p < 0.001$). For cardiorespiratory adaptations from the first to the last session of HIIT, treadmill speed, treadmill grade, treadmill power, $\dot{V}O_{2HII}$, $\%\dot{V}O_{2peak}$, and V_E during HIIs were increased (all $p < 0.05$), while no difference was found for HR, $\%HR_{peak}$ and systolic blood pressure (all $p > 0.05$). $\dot{V}O_{2peak}$ increased by an average of 9% from pre-CR to post-CR. No adverse events occurred.

Conclusion: Our results demonstrate that HIIT can be effectively prescribed using RPE in MI patients during early outpatient CR. Participation in RPE-prescribed HIIT increases exercise workload and $\dot{V}O_2$ during exercise training without increased perception of effort or excessive increases in heart rate or blood pressure.

Keywords: high-intensity interval training, cardiac rehabilitation, myocardial infarction, metabolic gas exchange, rating of perceived exertion

INTRODUCTION

Exercise-based cardiac rehabilitation (CR) is a secondary prevention tool used worldwide to improve physical function and prognosis in patients after myocardial infarction (MI) (1, 2). High-intensity interval training (HIIT) has recently emerged as an alternative or adjunct strategy to traditional moderate-intensity continuous training (3). HIIT involves alternating periods ranging from a few seconds to 4 min of higher intensity exercise [high-intensity intervals, HIIs: 85 to 95% of peak heart rate (HR) corresponding to 75 to 85% of peak oxygen uptake ($\dot{V}O_2$)] with 1 to 4 min of lower intensity exercise (low-intensity intervals, LIIs: <60% of peak HR) during an exercise session (4). HIIT has been shown to result in similar or greater improvements in aerobic capacity and other health outcomes compared to moderate-intensity continuous training (4). However, the relationships between patient safety, perception of effort, and cardiorespiratory responses and adaptations during HIIT sessions in patients after MI have not been reported. Gaps in our understanding of the relationship between effort perception and cardiorespiratory responses limit our ability to provide optimal guidance for prescription, implementation, and safety of HIIT in CR.

The most common metrics to prescribe aerobic exercise intensity during CR include $\dot{V}O_2$, HR, and their derivative indicators such as percentages of predicted/peak HR and $\dot{V}O_2$; reserves of HR and $\dot{V}O_2$; and metabolic equivalents (METs) (5). During outpatient CR, continuous monitoring of $\dot{V}O_2$ is impractical and, while continuous HR monitoring is feasible, the high number of MI patients prescribed rate modulating pharmacotherapy (e.g., beta-blockers) makes HR a highly variable metric for exercise prescription (6). Furthermore, many patients who begin CR have not performed a graded exercise test, and peak HR has not been determined (7). For these patients, prescribing exercise intensity using predicted peak HR as a guide is imprecise.

Ratings of perceived exertion (RPE) are a practical alternative for prescribing exercise intensity and facilitates relative patient autonomy and progression of exercise intensity during CR (4, 8). Our CR program has used RPE, accompanied by continuous HR and periodic blood pressure monitoring, to prescribe exercise intensity for several decades (9, 10). Our CR staff are experienced in instructing patients on the proper use of the 6–20 Borg RPE scale. Patients are carefully instructed on the use of RPE as part of their baseline graded exercise test and during their first supervised exercise session in CR (10). We have previously demonstrated that RPE-prescribed HIIT improves body composition, characteristics of metabolic syndrome, and cardiorespiratory fitness in patients after MI (11, 12). However, the cardiorespiratory responses directly measured with metabolic gas exchange during, and adaptations to HIIT across several exercise sessions in MI patients have not been previously reported.

Therefore, this study aimed to determine the cardiorespiratory responses and adaptations during HIIT exercise sessions prescribed using RPE in patients with MI who participate in early outpatient CR. We hypothesized that: (1) Using RPE to prescribe exercise intensity will effectively elicit a desired HIIT cardiorespiratory response, and (2) RPE-based HIIT will result in an increasing $\dot{V}O_2$ during exercise training across exercise sessions without increased perception of effort or excessive increases in heart rate and blood pressure.

METHODS

Participants and Study Design

This prospective observational study initially recruited 29 consecutive MI patients with percutaneous coronary intervention who were referred to outpatient CR within 2 weeks of discharge from inpatient care (our traditional time to begin CR) at Mayo Clinic, Rochester, MN, USA from February 1st, 2017, to September 30^{th,} 2018. Thirteen patients who did not perform a post-CR cardiopulmonary exercise test (CPET), two who refused to wear a metabolic gas collector/mask during exercise training, and three who changed their exercise type from treadmill to recumbent stationary cycle were excluded. Eleven patients [seven men, four women; age: 62 [11] yrs, median (interquartile range, IQR); BMI: 33.0 (7.2) kg/m^2; the interval between hospital dismissal and the start of CR: 14 [4] days] who completed ≥24 sessions of supervised HIIT on a treadmill with metabolic gas exchange measured during HIIT once per week for eight consecutive weeks and who performed pre and post CR CPET were included. Cardiovascular medications were unchanged during the study period. Participants were free of angina at low exercise intensities, symptomatic arrhythmias, symptomatic heart valve disease, musculoskeletal limitations to exercise training, and significant frailty or weakness (i.e., inability to engage in HIIT). Study procedures were approved by the Institutional Review Board for Research at Mayo Clinic (Rochester, MN, USA; 15-007977) and conformed to the standards set forth by the Declaration of Helsinki. Patients were informed regarding testing procedures and potential risks of participation before providing written, informed consent.

High-Intensity Interval Training Intervention

Our protocol for HIIT has been routinely applied in CR for more than a decade and was described previously (4, 13). It was designed for routine use by patients who begin CR within 2 weeks of hospital dismissal and start HIIT after 1 week of moderate intensity aerobic exercise. Components of the exercise prescription were **F**requency: set as three sessions per week for eight consecutive weeks. **I**ntensity: HIIs lasting 1 min at an RPE 14–17 [Borg 6–20 RPE scale] followed by 4-min LIIs at RPE < 12, treadmill speed and grade were self-selected by patients themselves to achieve the target RPEs, and the RPE scores were obtained at the end of each interval. **T**ype: a treadmill was used under continuous observation by clinical exercise physiologists. **T**ime: initial time started at 30 min and gradually progressed to 40 min per session; **V**olume: at least 24 sessions of HIIT completed; **P**rogression: the number of HIIs was gradually increased from 5 to 8 throughout the study according to the patients' expectations and the judgment of clinical exercise physiologists.

Patients were carefully instructed in the proper use of the Borg RPE scale during their first supervised exercise session in outpatient CR. All patients performed adaptive exercise training during the 1st week of CR (three sessions) using RPE ratings of 11–13 to facilitate a gradual accommodation to exercise training, ensure the ability to engage in sustained exercise for a minimum of 20 min, and to become accustomed to the use of the RPE scale. Following the gradual adaptation phase (week-1), the patients started HIIT. Each exercise session began with 5–10 min of low-intensity warm-up (RPE 8–10) and ended with a 5-min low-intensity cool down.

Cardiopulmonary Exercise Testing

CPETs were conducted by clinical exercise physiologists with cardiologist oversight at the beginning and end of CR. The exercise modality and end-test criteria were consistent between pre-and post-CR tests for all patients. Our operation and interpretation procedures for CPET have been described previously (13).

Metabolic Gas Exchange Measurements During HIIT

Breath-by-breath $\dot{V}O_2$, carbon dioxide production (VCO_2), breathing frequency (f_B), and tidal volume (V_T) were measured continuously using a standard cardiorespiratory diagnostic system (Ultima Series 6 CPX^{TM}, MGC Diagnostics Corporation, Minnesota, USA) during an RPE-prescribed HIIT sessions once each week. Continuous cardiorespiratory measurements were performed during a total of 88 HIIT exercise sessions. The cardiorespiratory diagnostic system was calibrated for flow and gas concentrations before each session according to the manufacturer's recommendations using a 3-liter syringe and calibration gases of known concentration. To minimize the influence of subsidiary work, and therefore $\dot{V}O_2$ and VCO_2, patients were instructed to refrain from excessive stabilization (i.e., using handrails) during all exercise sessions. Minute V_E was calculated as the product of V_T and breathing frequency (f_B). The respiratory exchange ratio (RER) was calculated as the ratio of VCO_2 to $\dot{V}O_2$. $\dot{V}O_{2HII}$ and $\dot{V}O_{2LII}$ were calculated as the highest average $\dot{V}O_2$ of three consecutive breaths during the HIIs and LIIs (i.e., the highest single-breath $\dot{V}O_2$ value and the preceding and following breaths), respectively. Other metabolic gas exchange values (i.e., RER, VCO_2, V_E, V_E/VCO_2) were determined by averaging values of the final 15-s of HII and LII, respectively, of each HIIT session.

Heart Rate and Blood Pressure Measurements

During each HIIT session, HR and rhythm were continuously measured *via* electrocardiogram (ECG) telemetry (Q-Tel RMS, Welch Allyn, New York, USA). The HRs at the end of HIIs and LIIs were recorded. Systolic (SBP) and diastolic (DBP) blood pressures were measured *via* manual sphygmomanometer by clinical exercise physiologists at rest and during the final 15-s of HII and LII, respectively, of each HIIT session.

Sample Size Calculation

As the primary hypothesis of this study is that RPE prescribed exercise can effectively elicit the desired exercise intensity of HIIT (more than 75% $\dot{V}O_{2peak}$) in patients after MI, the $\%\dot{V}O_{2peak}$ during HIIs (VO_{2HII} / $\dot{V}O_{2peak}$ × 100), the gold standard of exercise intensity, was set as the primary endpoint. $\%\dot{V}O_{2peak}$ during HIIs was used to calculate the sample size. We applied the repeated measures analysis model of the Power Analysis & Sample Size software, version 15.0 (NCSS, LLC, USA) to calculate the sample size. The main parameters are as follows: mean $\%\dot{V}O_2$peak during HIIs was 75%, eight sessions of HIITs data from consecutive 8 weeks were collected, the mean increase of $\%\dot{V}O_{2peak}$ during HIIs was 10% across sessions, the standard deviation was 6%, autocorrelation was between 0.2 and 0.4, the dropout rate was estimated 20%. To achieve a power (1-β) of 90% with an α of 0.05, 11 participants were required.

Statistical Analysis

A minimum of five HIIs was performed by all patients during all HIIT sessions. Therefore, regardless of the number of HIIs performed (ranging from 5 to 8), the final five intervals were used to make comparisons among HIIT sessions. A familiarization HIIT session was used to ensure physiological responses were accurately characterized. The familiarization session was excluded from data analyses, and the second HIIT session was categorized as the first HIIT session. A total of 88 sessions of HIIT data (8 × 11) with gas exchange measurements were included in the analysis.

Data are presented as median [IQR] for continuous variables and frequency and percentage for categorical variables. Repeatability analysis of exercise intensity in terms of $\%\dot{V}O_{2peak}$ was performed with intra-class correlation (ICC) (14) using a random-effects model. Exercise workload (ie., treadmill speed, grade and power in watts) and cardiorespiratory variables measured during the HIIT training sessions (i.e., RPE, $\dot{V}O_2$, $\%\dot{V}O_{2peak}$, V_E, HR, %HR, BP, energy expenditure [EE] per min and per session) were compared within (HIIs vs. LIIs) and between sessions (first vs. last) using repeated-measures analysis of variance (ANOVA). Pre- and post-CR CPET measurements

TABLE 1 | Demographics and clinical characteristics.

n	11
Age (years)	62 [11]
Men	7 (64)
Body weight (kg)	98.1 [22.6]
Body mass index (kg/m^2)	33.0 [7.2]
LVEF (%)	56 [8]
Medical history, *n* (%)	
MI	11 (100)
STEMI	4 (36)
NSTEMI	7 (64)
Coronary angiography	11 (100)
One-vessel disease	5 (46)
Two-vessel disease	3 (27)
Three-vessel disease	3 (27)
Previous MI	2 (18)
Hypertension	6 (55)
Dyslipidemia	11 (100)
Smoking history	5 (45)
Medications, *n* (%)	
ACEI/ARBs	3 (27)
Anticoagulants	5 (45)
Antiplatelet agents	11 (100)
Beta-blockers	10 (91)
Calcium channel blockers	3 (27)
Diuretics	2 (18)
Nitrates	1 (9)
Digoxin	1 (9)
Statins	11 (100)
CPET parameters	
HR_{rest} (bpm)	70 [18]
HR_{peak} (bpm)	141 [54]
SBP_{rest} (mmHg)	123 [30]
DBP_{rest} (mmHg)	71 [16]
SBP_{peak} (mmHg)	180 [24]
DBP_{peak} (mmHg)	76 [20]
Respiratory exchange ratio	1.16 [0.11]
$\dot{V}O_{2peak}$ (L·min^{-1})	2.4 [0.6]
$\dot{V}O_{2peak}$ (ml·kg^{-1}·min^{-1})	24.0 [6.5]
Number of completed CR sessions	35 [1]
Days between hospital discharge and CR start	14 [4]

Data presented as median [interquartile range, IQR] for continuous variables or n (%) for categorical variables. SBP, systolic blood pressure; DBP, diastolic blood pressure; LVEF, left ventricular ejection fraction; MI, myocardial infarction; STEMI, ST-segment elevation myocardial infarction; NSTEMI, non-ST segment elevation myocardial infarction; ACEIs, angiotensin-converting enzyme inhibitors; ARBs, angiotensin II receptor blockers; CPET, cardiopulmonary exercise testing; HR, heart rate; CR, cardiac rehabilitation; $\dot{V}O_{2peak}$, peak oxygen uptake.

(i.e., $\dot{V}O_{2peak}$) were compared via Wilcoxon signed-rank test. $\%\dot{V}O_{2peak}$ and $\%HR_{peak}$ during HIITs were calculated as $(\dot{V}O_{2HIIorLII}/\dot{V}O_{2peak}) \times 100$ and $(HR_{HIIorLII}/HR_{peak}) \times 100$, respectively. $\dot{V}O_{2peak}$ and HR_{peak} values referred to pre-CR CPET. Treadmill power in watts was calculated (Watts = % treadmill grade × treadmill speed in m·min^{-1} × body weight in kg). EE per min was calculated according to the equation: calories = [$\dot{V}O_2$ in ml·kg^{-1}·min^{-1} × body weight in kilograms]/200 as described previously (15). EE per session = EE per min × exercise time. Analyses were performed with SPSS 19.0 (SPSS, Inc). Statistical significance was set at $p < 0.05$.

RESULTS

Patients' demographic and clinical characteristics are shown in **Table 1**. Among the 11 patients, four suffered ST-segment elevation MI, and seven suffered non-ST-segment elevation MI; two patients underwent double-vessel PCI, and nine performed single-vessel PCI. The interval between the hospital dismissal and the start of outpatient CR was 14 [4] [median (IQR)] days. Pre CR echocardiograms demonstrated normal left ventricular systolic function with left ventricular ejection fractions of 56% [6%] [median (IQR)]. Echocardiography was not repeated after CR.

Exercise workload and cardiorespiratory responses to RPE prescribed HIIT are presented in **Figure 1** and **Table 2**. The highest mean $\dot{V}O_2$ during HIIs of 88 sessions of HIITs [91 (14)% of $\dot{V}O_{2peak}$, median (IQR)] was significantly higher than for the target $\dot{V}O_2$ (75% of $\dot{V}O_{2peak}$) recommended for HIIs ($p < 0.001$). The ICC of exercise intensity, $\%\dot{V}O_{2peak}$, between the RPE-prescribed HIIT sessions was 0.95 (95% CI, 0.86 to 0.99, $p < 0.001$). The values of treadmill speed, treadmill grade, power, $\dot{V}O_2$, $\%\dot{V}O_{2peak}$, HR, $\%HR_{peak}$, SBP, V_E, V_T and f_B in the HIIs were significantly greater than those in the LIIs during each exercise session (all $p < 0.01$), which was consistent with the values of RPE during the HIIs vs. during the LIIs [15 (2) vs. 11 (2), median (IQR), $p < 0.001$]. A difference of 9–11% between $\%HR_{peak}$ and $\%\dot{V}O_{2peak}$ was present for the LIIs and is consistent with conventional wisdom as reported in the literature (16) that $\%HR_{peak}$ is greater than $\%\dot{V}O_{2peak}$ at a constant workrate. However, for the HIIs, $\%HR_{peak}$ was not higher than $\%\dot{V}O_{2peak}$. For the HIIs of the first HIIT session, median $\%HR_{peak}$ and $\%\dot{V}O_{2peak}$ were identical (88%), while for the final session $\%\dot{V}O_{2peak}$ was greater than $\%HR_{peak}$ (97% vs. 90%) during HIIs. No differences were found in DBP and RER between HIIs and LIIs (all $p > 0.05$).

Comparisons of the first vs. the last exercise sessions to assess cardiorespiratory adaptations during RPE-prescribed HIIT are presented in **Table 2** and **Figure 2**. No differences were found for RPE, HR, $\%HR_{peak}$, V_T, f_B, V_E/VCO_2, SBP and DBP (all $p > 0.05$) between the first and last session for both HIIs and LIIs. However, treadmill speed, treadmill grade, power, $\dot{V}O_2$, $\%\dot{V}O_{2peak}$, EE per minute and per session and V_E increased significantly from the first to the last session for the HIIs (all $p < 0.05$), while no changes were detected for the LIIs (all $p > 0.05$). No adverse events related to exercise training occurred during the study.

Body mass significantly decreased [98.1 (22.6) kg vs. 95.0 (11.0) kg, median (IQR)] with a mean decrease of 3.1 [95% CI, 0.5 to 5.7] kg ($p = 0.02$). Peak cardiorespiratory variables were determined via CPETs at the beginning and end of CR. $\dot{V}O_{2peak}$ independent of body mass was not significantly different from pre- to post-CR [2.4 (0.6) L·min^{-1} vs. 2.5 (0.7) L·min^{-1},

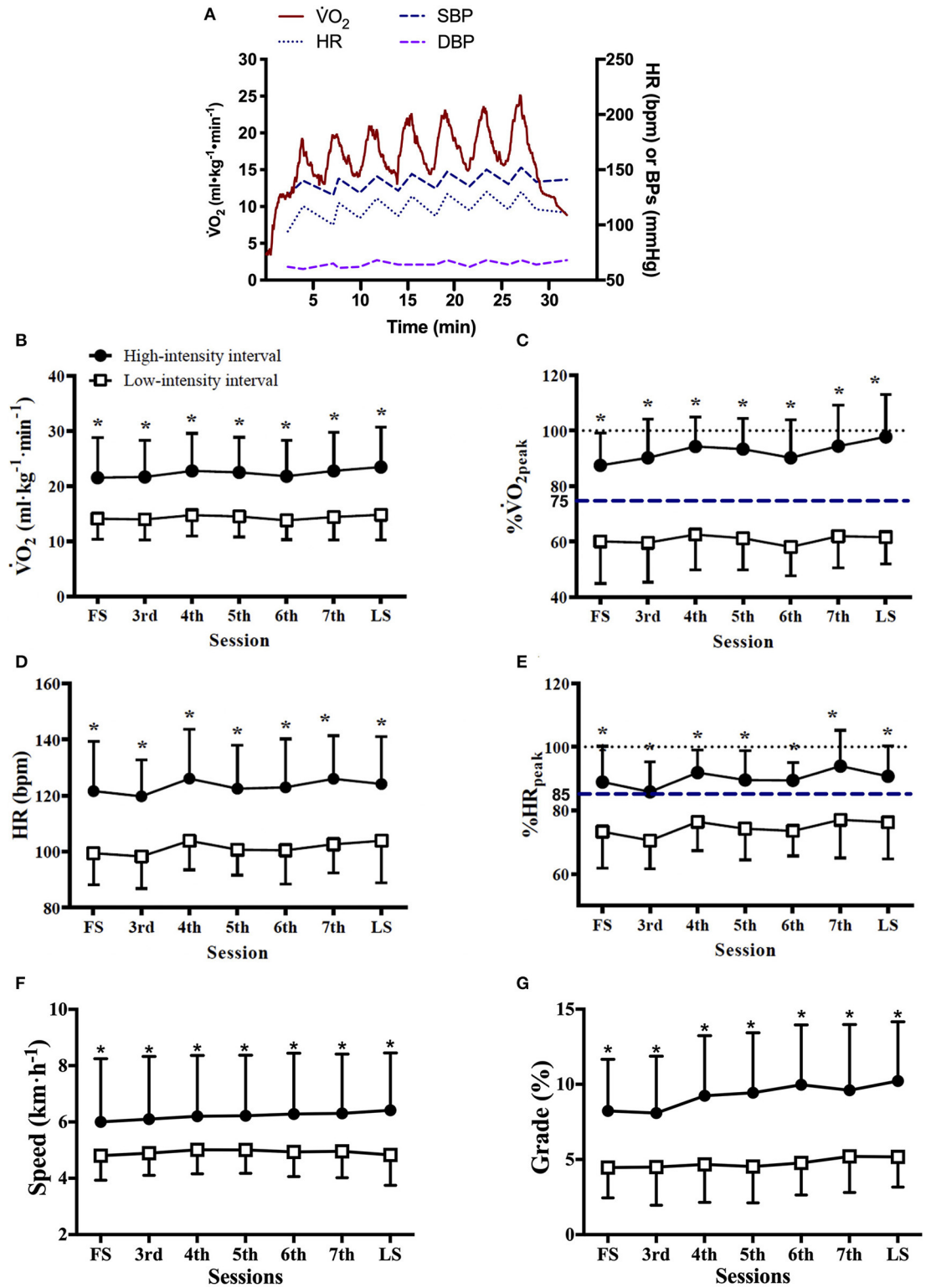

FIGURE 1 | Cardiorespiratory responses and treadmill workload during RPE-prescribed HIIT. **(A)**, a representative patient's oxygen uptake ($\dot{V}O_2$), heart rate (HR), systolic (SBP), and diastolic (DBP) blood pressure responses during a HIIT session. The average $\dot{V}O_2$ **(B)**, $\%\dot{V}O_{2peak}$ **(C)**, HR **(D)**, $\%HR_{peak}$ **(E)**, treadmill speed **(F)**, and treadmill grade **(G)** responses to the high- and low-intensity intervals over time. FS is the first exercise session. LS is the last exercise session. Repeated-measures ANOVA was used for all assessments. Data were expressed as mean + up limit of 95% confidence interval for high-intensity intervals and mean–low limit of 95% confidence interval for low-intensity intervals in **(B–G)**. *Significantly higher than low-intensity interval, $p < 0.001$.

TABLE 2 | Treadmill workload and cardiorespiratory variables during high- and low-intensity intervals.

	High-intensity intervals		Low-intensity intervals	
	First session	**Last session**	**First session**	**Last session**
Treadmill speed (km per hour)	5.9 [2.4]	6.2 [2.1]*†	4.9 [1.1]	4.9 [1.5]
Treadmill grade (%)	8.4 [2.7]	10.3 [5.8]*†	4.9 [3.2]	5.1 [2.9]†
Treadmill power (Watts)	807 [573]	1039 [707]*†	390 [211]	407 [196]
RPE	14 [2]*	15 [2]*	11 [1]	11 [2]
$\dot{V}O_2$ (ml·kg^{-1}·min^{-1})	21.1 [2.8]*	23.3 [3.0]*†	14.6 [4.6]	14.6 [2.5]
$\%\dot{V}O_{2peak}$	88 [11]*	97 [17]*†	61 [15]	61 [11]
EE per minute (kcal min^{-1})	10.4 [1.5]*	11.4 [2.0]*†	7.1 [2.0]	7.2 [1.3]
EE per 30-min session (kcal)‡	62.0 [8.8]*	68.5 [11.3]*†	170.4 [45.8]	171.7 [28.6]
RER	0.95 [0.06]	0.98 [0.07]	0.94 [0.07]	0.93 [0.08]
HR (bpm)	124 [23]*	126 [26]*	99 [17]	101 [23]
$\%HR_{peak}$	88 [8]*	90 [14]*	70 [8]	72 [11]
SBP (mmHg)	156 [18]*	148 [26]*	136 [16]	137 [16]
DBP (mmHg)	66 [8]	61 [7]	64 [14]	61 [6]
V_E (L·min^{-1})	59 [22]*	65 [24]*†	40 [12]	42 [16]
V_T (L)	1.8 [0.6]*	1.9 [0.5]*	1.4 [0.7]	1.4 [0.8]
f_B (breaths·min^{-1})	34 [8]*	36 [6]*	30 [5]	30 [6]
V_E/VCO_2	32 [5]	33 [6]*	30 [3]	31 [4]

*Data presented as median [interquartile range, IQR]. RPE, rating of perceived exertion; HR, heart rate; $\dot{V}O_2$, oxygen uptake; EE, energy expenditure; VCO_2, carbon dioxide production; RER, respiratory exchange ratio; SBP, systolic blood pressure; DBP, diastolic blood pressure; V_E, ventilation; V_T, tidal volume; f_B, breathing frequency; VCO_2, carbon dioxide output. *Significantly greater than the low-intensity interval ($p < 0.05$). †Significantly different compared to first session ($p < 0.05$). Repeated-measures ANOVA was used for all evaluations. ‡30-min session included five 1-min high-intensity intervals and five 4-min low-intensity intervals.*

median (IQR)] with a mean difference of 0.1 [95% CI, −0.1 to 0.3] L·min^{-1} ($p = 0.21$). However, $\dot{V}O_{2peak}$ dependent on body mass increased in nine of 11 subjects. $\dot{V}O_{2peak}$ relative to body mass increased [24.0 (6.5) ml·kg^{-1}·min^{-1} vs. 26.1 (8.0) ml·kg^{-1}·min^{-1}, median (IQR)] with a mean increase of 1.9 [95% CI, 0.1 to 3.8] ml·kg^{-1} · min^{-1} ($p = 0.049$). In addition, $\dot{V}O_{2peak}$ as a percentage of age, sex, and anthropometrically predicted values significantly increased from pre- to post-CR [95 (28)% vs. 100 (25)%, median (IQR)] with a mean difference of 5 [95% CI, 1 to 10] % ($p = 0.04$). No additional significant differences were detected in peak exercise cardiorespiratory variables pre- and post-CR.

DISCUSSION

Our study provided unique metabolic gas exchange data obtained during HIIT sessions and established the efficacy of using self-selected exercise intensity based on a target RPE range as a safe and practical method of prescribing HIIT for patients after MI during early outpatient CR. Our method of prescribing 5–8 one minute HIIs with RPE 14–17 interspersed with 4-min LIIs (RPE <12) during a 40-min session of training was effective in eliciting a $\dot{V}O_2$ of >95% of pre-training $\dot{V}O_{2peak}$ during the final HIIT session.

We demonstrated that over 8 weeks of HIIT, patients were able to exercise at a higher $\dot{V}O_2$ without a concurrent increase in RPE or excessive HR and blood pressure response. Patients were able to increase the rate of energy expenditure during the HIIT sessions without an increased perception of effort which is potentially clinically important for decreasing body fat stores with the attendant metabolic health benefits.

Aamot et al. (17) reported that using RPE to prescribe exercise intensity during HIIT resulted in a lower than expected intensity based on $\%HR_{peak}$, (detected 82% HR_{peak} vs expected 85% HR_{peak}) during HIIs (18) in patients with coronary artery disease in which 80% patients regularly used beta-blockers. In our study, we utilized both $\%\dot{V}O_{2peak}$ (gold standard to reflect exercise intensity) and $\%HR_{peak}$ to assess the validity of RPE-prescribed HIIT. Both $\%\dot{V}O_{2peak}$ and $\%HR_{peak}$ achieved during HIIs were more than the required levels to meet the designation of high-intensity (75% $\dot{V}O_{2peak}$ and 85% HR_{peak}) for all sessions. $\dot{V}O_{2HII}$ increased from 88% of $\dot{V}O_{2peak}$ in the first HIIT session to 97% of $\dot{V}O_{2peak}$ in the last session.

Patient progression in exercise training dose without the sacrifice of safety is a core tenet of cardiac rehabilitation. We observed that despite an increased $\dot{V}O_{2HII}$ across exercise sessions, no significant increases in HR, DBP, SBP, or perception of effort were found during RPE-prescribed HIIT. The underlying reasons for this remain unclear. $\dot{V}O_2$ is an integrated indicator of the systems that transport and utilize oxygen, including the respiratory (oxygen uptake from the atmosphere), heart (oxygen transport), peripheral vasculature (oxygen transport, tissue perfusion, tissue diffusion), and skeletal muscle (oxygen extraction and utilization) (19, 20). In the present study, HR, O_2 pulse [a surrogate for stroke volume (21)],

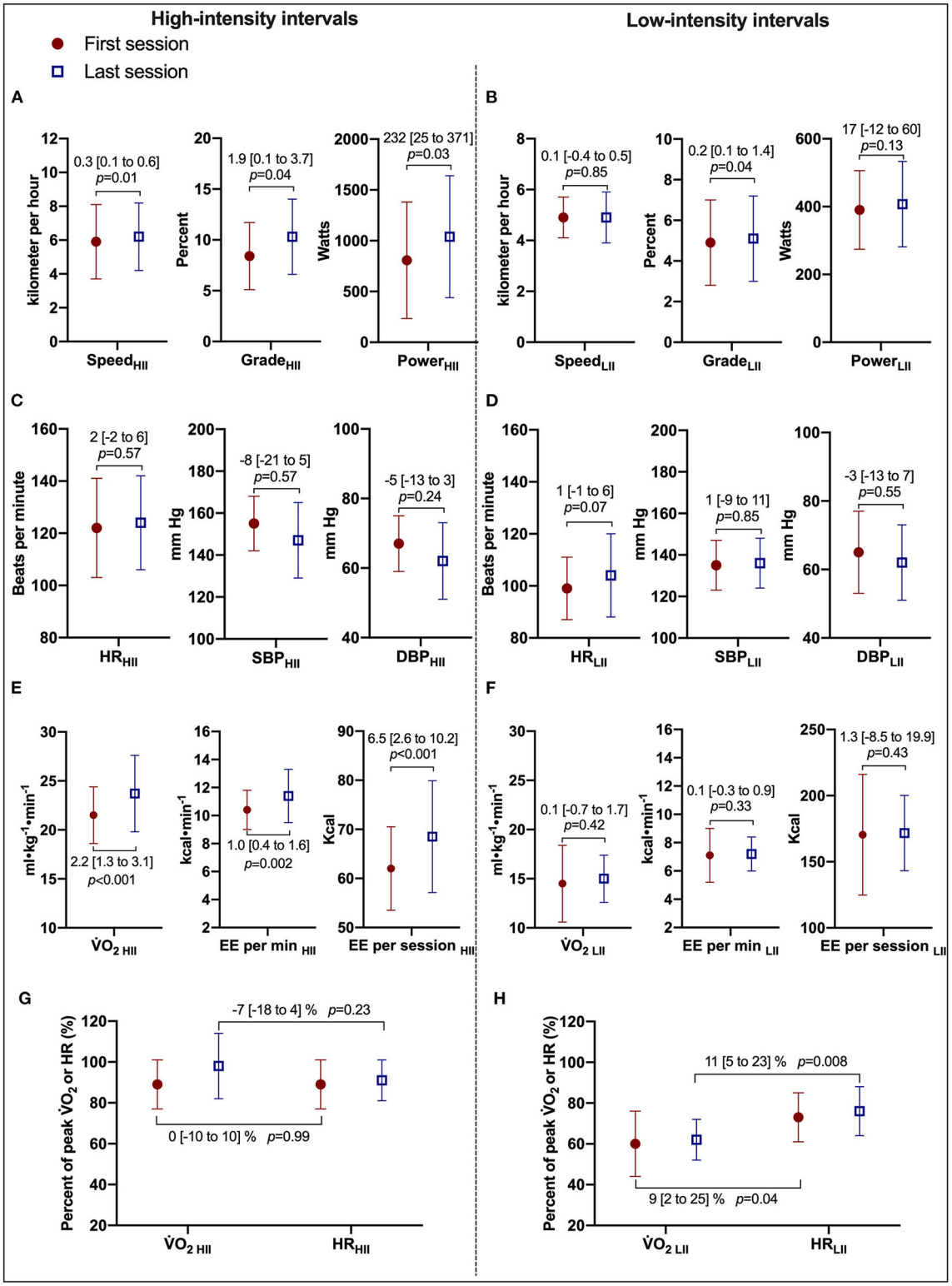

FIGURE 2 | Cardiorespiratory and treadmill workload adaptations to RPE-prescribed HIIT. **(A,B)** Present comparisons of treadmill speed, treadmill grade, and power output between the first and last HIIT sessions during high- and low-intensity intervals, respectively. **(C,D)** Present comparisons of heart rate (HR), systolic (SBP), and diastolic (DBP) blood pressure between the first and last HIIT sessions. **(E,F)** Present comparisons of oxygen uptake ($\dot{V}O_2$), energy expenditure (EE) per minute, and per session. **(G,F)** Present the changes in the relationship of $\%\dot{V}O_{2peak}$ and $\%HR_{peak}$ between the first and last HIIT sessions during high- and low-intensity intervals, respectively. HII is high-intensity interval. LII is low-intensity interval. Repeated-measures ANOVA was used for all assessments. was used for all assessments. Data were expressed as mean difference [95% confidence interval].

V_E/VCO_2 [an indicator of ventilatory efficiency (22)], RER (a variable to reflect degree of exertion) were not significantly changed during 8 weeks of RPE-prescribed HIIT sessions, which suggests that peripheral vasculature and skeletal muscle adaptations may have contributed to the increase in $\dot{V}O_{2HII}$ across sessions. This hypothesis is supported by our pre-clinical studies in mice that demonstrated regular exercise improved the structure and function of the aortic endothelium (23) and mitochondria in skeletal muscle (24, 25). However, additional research on the mechanisms responsible for these observations is needed.

In order to evaluate the cardiopulmonary adaptations during 8 weeks of HIIT sessions., we studied the relationship between $\%\dot{V}O_{2peak}$ and $\%HR_{peak}$ during the HIIT sessions. During LIIs, the values for $\%\dot{V}O_{2peak}$ were 61% for both first and last sessions, and the corresponding $\%HR_{peak}$ values were 70 and 72%, respectively. This is consistent with previous reports, where $\%HR_{peak}$ was ∼10% higher than $\%\dot{V}O_{2peak}$ (26). However, during HIIs, the $\%\dot{V}O_{2peak}$ was 88% for the first session and 97% for the last session, while the corresponding $\%HR_{peak}$ remained ∼90% for both sessions. This is a clear disconnect from the assumed relationship of $\%\dot{V}O_{2peak}$ and $\%HR_{peak}$. Though it has been assumed that the $\%HR_{peak}$-$\%\dot{V}O_{2peak}$ relationship holds during HIIT, the expected linear relationship between $\%\dot{V}O_{2peak}$ and $\%HR_{peak}$ was established during graded exercise testing with cardiopulmonary measurements and may differ during HIIT. Further studies are needed to elucidate the mechanisms responsible for these observations.

The effect of HIIT on cardiorespiratory fitness in patients with coronary artery disease has been reported, with mean $\dot{V}O_{2peak}$ increases ranging from 11 to 25% (4). A recent study from our group demonstrated that RPE-prescribed HIIT during early outpatient CR significantly improved $\dot{V}O_{2peak}$ by 18% (pre-CR vs. post-CR, 23.0 ± 6.3 vs. 28.0 ± 5.9; mean change 5.0 ± 2.5 $ml{\cdot}kg^{-1}{\cdot}min^{-1}$) in 42 MI patients (12). In the present study, HIIT improved cardiorespiratory fitness (i.e., $\dot{V}O_{2peak}$) in 9 of 11 (82%) patients, with a mean improvement of only 9%. Possibly related to the small sample size in the current study, statistically significant changes were found in $\dot{V}O_{2peak}$ related to body mass and % predicted $\dot{V}O_{2peak}$, but not in $\dot{V}O_{2peak}$ independent of body mass. The percentage of non-improvement (non-responder: failure to improve $\dot{V}O_{2peak}$) in CR was 18% in the present study, which is consistent with the data reported in the study by Savage et al. (27) in which 81 out of 385 patients (21%) failed to improve $\dot{V}O_{2peak}$ during outpatient CR using moderate-intensity continuous training. Our finding of non-improvement in $\dot{V}O_{2peak}$ with HIIT in some patients is a novel finding. Non-improvement in CR may be associated with exercise intensity, comorbidity score, self-reported physical function, diabetes, and baseline $\dot{V}O_{2peak}$ (27). In the present study, mean baseline $\dot{V}O_{2peak}$ was normal and may be a factor in our findings of a less than typical increase in $\dot{V}O_{2peak}$ and identification of non-responders with HIIT.

The present study did not assess change in left ventricular systolic or diastolic function resulting from HIIT. The literature suggested that HIIT is an effective strategy to attenuate left ventricular remodeling in clinically stable heart failure patients with reduced ejection fraction (28). The effect of HIIT on left ventricular function in heart failure with preserved ejection fraction is controversial (29), while the positive effects of HIIT on exercise capacity and quality of life in patients with MI and heart failure have been reported (4). The patients in the present study were not diagnosed with HFpEF. Further studies are warranted to investigate the effects of HIIT on cardiac function in patients after MI and heart failure with preserved ejection fraction.

LIMITATIONS

Our study examined a single, unique HIIT protocol in MI patients and may not be generalizable to other methods of prescribing HIIT or to other clinical populations. Because measuring metabolic gas exchange data during multiple 30–40 min CR exercise sessions is technically and logistically challenging, we studied only a limited number of patients. Our patients' average baseline $\dot{V}O_{2peak}$ was in the normal range for healthy individuals and our subjects are not representative of typical post-MI patients. In addition, we did not compare RPE vs. HR-based prescriptions for HIIT. While RPE certainly appears to be an effective prescriptive tool for HIIT, it remains unknown if RPE is the optimal prescription method despite its previously discussed advantages. Additionally, the cardiorespiratory assessments made during HIIT did not include direct measures of cardiac function (e.g., echocardiogram) and relied on an indirect method for cardiac adaptations (i.e., $\dot{V}O_2$ and V_E/VCO_2). As such, future studies should consider performing more comprehensive and direct measurements to identify the specific central and peripheral mechanisms responsible for the cardiorespiratory adaptations to RPE-prescribed HIIT in patients after MI.

CONCLUSIONS

RPE is an effective and safe method for prescribing HIIT for patients enrolled in early outpatient CR after uncomplicated MI. Using RPE eliminates reliance on heart rate for exercise intensity prescription and may be advantageous for patients who do not perform a pre-CR exercise test and for individuals receiving heart rate modulating medications. Using an RPE target of 14–17 during 1-min of high-intensity exercise elicits a robust $\dot{V}O_{2HII}$ of >90% of $\dot{V}O_{2peak.}$ The expected relationship between $\%HR_{peak}$ and $\%\dot{V}O_{2peak}$ ($\%HR_{peak} > \%\dot{V}O_{2peak}$) is not present during the HIIs of the HIIT. Patients are comfortable performing 5–8 one-minute intervals at >90% of $\dot{V}O_{2peak}$ during a 40-minute aerobic exercise session. Over the course of eight weeks of HIIT-based CR, patients increased treadmill speed and grade, and $\dot{V}O_{2HII}$ without an increase in perception of effort or excessive increases in heart rate and blood pressure.

DATA AVAILABILITY STATEMENT

The raw data supporting the conclusions of this article will be made available by the authors, without undue reservation.

ETHICS STATEMENT

The studies involving human participants were reviewed and approved by Mayo Clinic Institutional Review Board. The patients/participants provided their written informed consent to participate in this study.

AUTHOR CONTRIBUTIONS

YD, RS, and TO are responsible for the conception and design of the work. YD, JS, and MM contributed to the acquisition or interpretation of the work. YD, SH, JS, BS, and SL drafted the manuscript. YD, SH, JS, MM, BS, RS, SL, and TO critically revised the manuscript, gave final approval and agree to be accountable for all aspects of the work ensuring integrity and accuracy. All authors have read and approved the final manuscript.

FUNDING

The present study was supported by grants from the National Institutes of Health (HL-126638 to TO; T32 HL-07111 to SH and JS; and K12 HD-065987 to JS), National Nature Science Foundation of China (82002403 to YD), Hunan Provincial Nature Science Foundation of China (2021JJ40981 to YD), and the Youth Science Foundation of Xiangya Hospital (2019Q03 to YD).

ACKNOWLEDGMENTS

We appreciate the dedication of our patients and staff in the Cardiac Rehabilitation Center at Mayo Clinic in Rochester, MN, for their invaluable support of this study.

REFERENCES

1. Anderson JL, Adams CD, Antman EM, Bridges CR, Califf RM, Casey DE Jr, et al. 2012 ACCF/AHA focused update incorporated into the ACCF/AHA 2007 guidelines for the management of patients with unstable angina/non-ST-elevation myocardial infarction: a report of the American College of Cardiology Foundation/American Heart Association Task Force on Practice Guidelines. *Circulation*. (2013) 127:e663–828. doi: 10.1161/CIR.0b013e31828478ac
2. O'Gara PT, Kushner FG, Ascheim DD, Casey DE Jr, Chung MK, de Lemos JA, et al. 2013 ACCF/AHA guideline for the management of ST-elevation myocardial infarction: a report of the American College of Cardiology Foundation/American Heart Association Task Force on Practice Guidelines. *Circulation*. (2013) 127:e362–425. doi: 10.1161/CIR.0b013e3182742cf6
3. Piercy KL, Troiano RP, Ballard RM, Carlson SA, Fulton JE, Galuska DA, et al. The Physical Activity Guidelines for Americans. *JAMA*. (2018) 320:2020–8. doi: 10.1001/jama.2018.14854
4. Dun Y, Smith JR, Liu S, Olson TP. High-Intensity Interval Training in Cardiac Rehabilitation. *Clin Geriatr Med.* (2019) 35:469–87. doi: 10.1016/j.cger.2019.07.011
5. Mezzani A, Hamm LF, Jones AM, McBride PE, Moholdt T, Stone JA, et al. Aerobic exercise intensity assessment and prescription in cardiac rehabilitation: a joint position statement of the European Association for Cardiovascular Prevention and Rehabilitation, the American Association of Cardiovascular and Pulmonary Rehabilitation and the Canadian Association of Cardiac Rehabilitation. *Eur J Prev Cardiol.* (2013) 20:442–67. doi: 10.1177/2047487312460484
6. Diaz-Buschmann I, Jaureguizar KV, Calero MJ, Aquino RS. Programming exercise intensity in patients on beta-blocker treatment: the importance of choosing an appropriate method. *Eur J Prev Cardiol.* (2014) 21:1474–80. doi: 10.1177/2047487313500214
7. Fletcher GF, Ades PA, Kligfield P, Arena R, Balady GJ, Bittner VA, et al. Exercise standards for testing and training: a scientific statement from the American Heart Association. *Circulation.* (2013) 128:873–934. doi: 10.1161/CIR.0b013e31829b5b44
8. Iellamo F, Manzi V, Caminiti G, Vitale C, Massaro M, Cerrito A, et al. Validation of rate of perceived exertion-based exercise training in patients with heart failure: insights from autonomic nervous system adaptations. *Int J Cardiol.* (2014) 176:394–8. doi: 10.1016/j.ijcard.2014.07.076
9. Squires RW, Gau GT, Miller TD, Allison TG, Lavie CJ. Cardiovascular rehabilitation: status, 1990. *Mayo Clin Proc.* (1990) 65:731–55. doi: 10.1016/S0025-6196(12)65134-9
10. Squires RW, Gau GT. *Cardiac rehabilitation and cardiovascular health enhancement. Cardiology: Fundamentals and Practice*. Chicago: Year book Medical Publishers (1987). p. 1944–60.
11. Dun Y, Thomas RJ, Medina-Inojosa JR, Squires RW, Huang H, Smith JR, et al. High-intensity interval training in cardiac rehabilitation: impact on fat mass in patients with myocardial infarction. *Mayo Clin Proc.* (2019) 94:1718–30. doi: 10.1016/j.mayocp.2019.04.033
12. Dun Y, Thomas RJ, Smith JR, Medina-Inojosa JR, Squires RW, Bonikowske AR, et al. High-intensity interval training improves metabolic syndrome and body composition in outpatient cardiac rehabilitation patients with myocardial infarction. *Cardiovasc Diabetol.* (2019) 18:104. doi: 10.1186/s12933-019-0907-0
13. Skalski J, Allison TG, Miller TD. The safety of cardiopulmonary exercise testing in a population with high-risk cardiovascular diseases. *Circulation.* (2012) 126:2465–72. doi: 10.1161/CIRCULATIONAHA.112.110460
14. Atkinson G, Nevill AM. Statistical methods for assessing measurement error (reliability) in variables relevant to sports medicine. *Sports Med.* (1998) 26:217–38. doi: 10.2165/00007256-199826040-00002
15. Ainsworth BE, Haskell WL, Herrmann SD, Meckes N, Bassett DR Jr., Tudor-Locke C, et al. 2011 Compendium of Physical Activities: a second update of codes and MET values. *Med Sci Sports Exerc.* (2011) 43:1575–81. doi: 10.1249/MSS.0b013e31821ece12
16. Cunha FA, Midgley AW, Monteiro WD, Farinatti PT. Influence of cardiopulmonary exercise testing protocol and resting VO(2) assessment on %HR(max), %HRR, %VO(2max) and %VO(2)R relationships. *Int J Sports Med.* (2010) 31:319–26. doi: 10.1055/s-0030-1248283
17. Aamot IL, Forbord SH, Karlsen T, Stoylen A. Does rating of perceived exertion result in target exercise intensity during interval training in cardiac rehabilitation? A study of the Borg scale versus a heart rate monitor. *J Sci Med Sport.* (2014) 17:541–5. doi: 10.1016/j.jsams.2013.07.019
18. Karlsen T, Aamot IL, Haykowsky M, Rognmo O. High Intensity Interval Training for Maximizing Health Outcomes. *Prog Cardiovasc Dis.* (2017) 60:67–77. doi: 10.1016/j.pcad.2017.03.006
19. Guazzi M, Adams V, Conraads V, Halle M, Mezzani A, Vanhees L, et al. EACPR/AHA Scientific Statement. Clinical recommendations for cardiopulmonary exercise testing data assessment in specific patient populations. *Circulation.* (2012) 126:2261–74. doi: 10.1161/CIR.0b013e31826fb946
20. Guazzi M, Arena R, Halle M, Piepoli MF, Myers J, Lavie CJ. 2016 focused update: clinical recommendations for cardiopulmonary exercise testing data assessment in specific patient populations. *Circulation.* (2016) 133:e694–711. doi: 10.1161/CIR.0000000000000406
21. Bhambhani Y, Norris S, Bell G. Prediction of stroke volume from oxygen pulse measurements in untrained and trained men. *Can J Appl Physiol.* (1994) 19:49–59. doi: 10.1139/h94-003
22. Cooper DM, Kaplan MR, Baumgarten L, Weiler-Ravell D, Whipp BJ, Wasserman K. Coupling of ventilation and CO2 production during exercise in children. *Pediatr Res.* (1987) 21:568–72. doi: 10.1203/00006450-198706000-00012

23. Liu S, Zheng F, Cai Y, Zhang W, Dun Y. Effect of Long-Term Exercise Training on lncRNAs Expression in the Vascular Injury of Insulin Resistance. *J Cardiovasc Transl Res.* (2018) 11:459–69. doi: 10.1007/s12265-018-9830-0
24. Dun Y, Liu S, Zhang W, Xie M, Qiu L. Exercise combined with rhodiola sacra supplementation improves exercise capacity and ameliorates exhaustive exercise-induced muscle damage through enhancement of mitochondrial quality control. *Oxid Med Cell Longev.* (2017) 2017:8024857. doi: 10.1155/2017/8024857
25. Xie M, Jiang L, Dun Y, Zhang W, Liu S. Trimetazidine combined with exercise improves exercise capacity and anti-fatal stress ability through enhancing mitochondrial quality control. *Life Sci.* (2019) 224:157–68. doi: 10.1016/j.lfs.2019.03.027
26. Riebe D, Ehrman JK, Liguori G, Magal M. *ACSM's Guidelines for Exercise Testing and Prescription*. Tenth Edition ed Philadelphia: Wolters Kluwer (2016).
27. Savage PD, Antkowiak M, Ades PA. Failure to improve cardiopulmonary fitness in cardiac rehabilitation. *J Cardiopulm Rehabil Prev.* (2009) 29:284–91. doi: 10.1097/HCR.0b013e3181b4c8bd
28. Tucker WJ, Beaudry RI, Liang Y, Clark AM, Tomczak CR, Nelson MD, et al. Meta-analysis of exercise training on left ventricular ejection fraction in heart failure with reduced ejection fraction: a 10-year update. *Prog Cardiovasc Dis.* (2019) 62:163–71. doi: 10.1016/j.pcad.2018.08.006
29. Mueller S, Winzer EB, Duvinage A, Gevaert AB, Edelmann F, Haller B, et al. Effect of high-intensity interval training, moderate continuous training, or guideline-based physical activity advice on peak oxygen consumption in patients with heart failure with preserved ejection fraction: a randomized clinical trial. *JAMA.* (2021) 325:542–51. doi: 10.1001/jama.2020.26812

Conflict of Interest: The authors declare that the research was conducted in the absence of any commercial or financial relationships that could be construed as a potential conflict of interest.

Publisher's Note: All claims expressed in this article are solely those of the authors and do not necessarily represent those of their affiliated organizations, or those of the publisher, the editors and the reviewers. Any product that may be evaluated in this article, or claim that may be made by its manufacturer, is not guaranteed or endorsed by the publisher.

frontiers in Cardiovascular Medicine

ORIGINAL RESEARCH
published: 05 January 2022
doi: 10.3389/fcvm.2021.809689

Rutaecarpine Inhibits Doxorubicin-Induced Oxidative Stress and Apoptosis by Activating AKT Signaling Pathway

Zi-Qi Liao[1†], Yi-Nong Jiang[1†], Zhuo-Lin Su[1], Hai-Lian Bi[2], Jia-Tian Li[2], Cheng-Lin Li[1], Xiao-Lei Yang[2], Ying Zhang[1] and Xin Xie[2*]*

[1] Department of Cardiology, First Affiliated Hospital of Dalian Medical University, Dalian, China, [2] Institute of Cardiovascular Diseases, First Affiliated Hospital of Dalian Medical University, Dalian, China

OPEN ACCESS

Edited by:
Yan Zhang,
Peking University, China

Reviewed by:
Bo Sun,
Kunming University of Science and Technology, China
Guotong Fu,
St. Jude Children's Research Hospital, United States

***Correspondence:**
Xin Xie
xiexin_phd@163.com
Ying Zhang
zy114129@sina.com

[†] These authors have contributed equally to this work

Specialty section:
This article was submitted to General Cardiovascular Medicine, a section of the journal Frontiers in Cardiovascular Medicine

Received: 05 November 2021
Accepted: 23 November 2021
Published: 05 January 2022

Citation:
Liao Z-Q, Jiang Y-N, Su Z-L, Bi H-L, Li J-T, Li C-L, Yang X-L, Zhang Y and Xie X (2022) Rutaecarpine Inhibits Doxorubicin-Induced Oxidative Stress and Apoptosis by Activating AKT Signaling Pathway. Front. Cardiovasc. Med. 8:809689. doi: 10.3389/fcvm.2021.809689

Patients with cancer who receive doxorubicin (DOX) treatment can experience cardiac dysfunction, which can finally develop into heart failure. Oxidative stress is considered the most important mechanism for DOX-mediated cardiotoxicity. Rutaecarpine (Rut), a quinazolinocarboline alkaloid extracted from *Evodia rutaecarpa* was shown to have a protective effect on cardiac disease. The purpose of this study is to investigate the role of Rut in DOX-induced cardiotoxicity and explore the underlying mechanism. Intravenous injection of DOX (5 mg/kg, once a week) in mice for 4 weeks was used to establish the cardiotoxic model. Echocardiography and pathological staining analysis were used to detect the changes in structure and function in the heart. Western blot and real-time PCR analysis were used to detect the molecular changes. In this study, we found that DOX time-dependently decreased cardiac function with few systemic side effects. Rut inhibited DOX-induced cardiac fibrosis, reduction in heart size, and decrease in heart function. DOX-induced reduction in superoxide dismutase (SOD) and glutathione (GSH), enhancement of malondialdehyde (MDA) was inhibited by Rut administration. Meanwhile, Rut inhibited DOX-induced apoptosis in the heart. Importantly, we further found that Rut activated AKT or nuclear factor erythroid 2-related factor 2 (Nrf-2) which further upregulated the antioxidant enzymes such as heme oxygenase-1 (HO-1) and GSH cysteine ligase modulatory subunit (GCLM) expression. AKT inhibitor (AKTi) partially inhibited Nrf-2, HO-1, and GCLM expression and abolished the protective role of Rut in DOX-induced cardiotoxicity. In conclusion, this study identified Rut as a potential therapeutic agent for treating DOX-induced cardiotoxicity by activating AKT.

Keywords: rutaecarpine, doxorubicin, oxidative stress, apoptosis, cardiotoxicity, AKT

INTRODUCTION

Doxorubicin (DOX) is an effective chemotherapeutic drug that is widely used in treating several solid tumors and malignant hematologic diseases (1). However, DOX-induced cardiotoxicity is an insurmountable barrier that can limit its clinical application. The molecular mechanism of DOX-induced cardiotoxicity has been extensively investigated, and now oxidative stress, autophagy, mitochondrial dysfunction, and apoptosis pathways were commonly recognized as the underlying

mechanism of DOX-induced cardiotoxicity (2). Previous studies have proved that inhibition of oxidative stress dramatically alleviated DOX-induced cardiotoxicity in the heart (3). Therefore, exploring novel drugs to inhibit DOX-induced oxidative stress thereby improving patients' quality of life is urgently needed.

AKT is an essential signaling pathway regulating cell proliferation, glucose metabolism, oxidative stress, and also autophagy (4). Recent studies reported DOX inhibited PI3K/AKT signaling pathway in mice heart, and inhibition of PI3K/AKT aggravated DOX-induced cell death and heart failure (5), whereas pharmacological activation of PI3K/AKT attenuated DOX-induced cardiotoxicity (6). Nrf-2 is an essential antioxidative gene that inhibits oxidative stress *via* upregulation of the intracellular antioxidant enzymes such as HO-1 and GCLM, which promote glutathione (GSH) generation (7). Increased GSH would scavenge the excess reactive oxygen species (ROS) in DOX-treated cardiomyocytes and inhibit various forms of cell death including apoptosis and necroptosis (8, 9). The activation of PI3K/AKT is noteworthy as it was able to increase Nrf-2 and GCLM expression in the heart of DOX-treated mice (10, 11). Therefore, targeting the PI3K/AKT signaling pathway to prevent oxidative stress could be a prudent strategy in Dox-induced cardiotoxicity. Rutaecarpine (8,13-dihydroindolo-(2′,3′:3,4)pyrido(2,1-b)quinazolin-5(7H)-one) is a quinazolinocarboline alkaloid that is extracted from the traditional Chinese herb *Evodia rutaecarpa* (also named Wu Zhu Yu). It exerts beneficial roles in treating several diseases including hypertension (12), cardiac hypertrophy (13), cardiac ischemia-reperfusion injury (14), diabetes (15), and tumor (16). The cardioprotective effects of Rut were mainly attributed to its vasodilatory, antiplatelet activation, antioxidant effect, and anti-inflammatory effects (17). The antioxidant effect of Rut was to a large extent due to its regulatory role in antioxidant enzymes and NADPH oxidase. It has been reported that Rut protected hepatotoxicity by upregulating antioxidant enzymes through the Nrf-2/ARE pathway (18) and alleviated hypoxia-reoxygenation induced cardiomyocytes apoptosis through inhibiting NADPH oxidase expression (19). Since Rut has been shown to activate PI3K/AKT signaling pathway (15), and PI3K/AKT was the upstream signal of Nrf-2 (20), in this study, we investigated whether Rut protected against DOX-induced cardiotoxicity.

In this study, we showed that rutaecarpine alleviated DOX-induced cardiac dysfunction and cardiomyocyte death by inhibition of oxidative stress and the antioxidant effect of Rut probably due to the activation of the AKT/Nrf-2 signaling pathway. Thus, we concluded that Rut may become a novel potential drug to mitigate DOX-induced cardiotoxicity.

MATERIALS AND METHODS

Antibodies and Reagents

Antibodies for total AKT and phosphorylated AKT were purchased from Cell Signaling Technology (Danvers, MA, USA). Antibodies for GCLM, Nrf-2, HO-1, cleaved caspase-3, Bax, Bcl-2, and GAPDH were purchased from Proteintech (Wuhan, Hubei, China). DOX was obtained from Absin (Beijing, China), and the rutaecarpine was obtained from Chengdu Must Bio-technology (Chengdu, Sichuan, China). The AKT inhibitor (AKTi), wheat germ agglutinin (WGA), and dihydroethidium (DHE) were purchased from Sigma-Aldrich (Santa Clara, CA, USA). Hematoxylin-eosin/HE and Masson's trichrome staining kit were from Solarbio (Beijing, China). The malondialdehyde (MDA) assay kit and total SOD assay kit were purchased from Nanjing Jiancheng Bioengineering Institute (Nanjing, Jiangsu, China). The GSH assay kit was purchased from Beyotime Biotechnology (Shanghai, China). TRIzol was obtained from Invitrogen (Carlsbad, CA, USA). All primers used in our laboratory were purchased from Sangon Biotech (Shanghai, China).

Animals and Treatments

Male C57BL/6 mice aged 8–10 weeks old were purchased from Vital River Laboratory Animal Technology (Beijing, China) and were kept in pathogen-free and individual ventilated cages. All mice were grown in the standard humidity or temperature-controlled environment (70% relative humidity, 22°C) and a 12:12-h light-dark cycle. Mice were divided into six groups and subjected to the following protocols: (1) In the control group, mice were treated with saline containing 0.5% dimethyl sulfoxide(DMSO); (2) In the Rut group, Rut was dissolved in saline contained 0.5% Tween 80, and then mice received intragastric administration of 40 mg/kg Rut every day for 4 weeks; (3) In DOX group, mice were intravenously treated with DOX (5 mg/kg, dissolved in saline contained 0.5% DMSO) once per week for 2 or 4 weeks; (4) In DOX plus Rut (low dose) group, mice treated with DOX and then at the same day received intragastric administration of 20 mg/kg Rut every day for 4 weeks; (5) In DOX plus Rut (high dose) group, mice were treated with DOX and parallelly received intragastric administration of 40 mg/kg Rut every day for 4 weeks; (6) In DOX plus Rut and AKTi group, mice were intraperitoneally injected with AKTi (20 mg/kg) every other day for 4 weeks from the first day before DOX and Rut administration. Because the long-term use of DOX can result in severe side effects, we measured the changes in the food uptake, body weight, and heart function every 2 weeks. Finally, all the mice were sacrificed. The heart was harvested and then analyzed by histopathology, western blot, and real-time PCR.

Echocardiographic Assessment

After drug treatment for 2 and 4 weeks, mice were subjected to about 2% isoflurane mixed with 100% O^2 by inhalation to induce anesthesia as we described previously (21). Trans-thoracic two-dimensional M mode echocardiography at different time points was determined using a 30-MHz probe (Vevo 770 imaging system, VisualSonics, Toronto, Canada). The heart rate was maintained at 450–500 beats per min, and then the heart rate, left ventricular ejection fraction (LVEF), LV fractional shortening (LVFS), LV posterior wall (LVPW), and LV anterior wall (LVAW) at diastole and systole were measured.

Real-Time PCR

Total RNA of mice hearts was extracted using TRIzol Reagent (Invitrogen, Carlsbad, CA) according to the manufacturer's

recommendations. Double-stranded cDNA synthesis was performed using a TaKaRa cDNA synthesis kit (TaKaRa). Real-time PCR analysis was performed using the SYBR Select Master Mix according to the manufacturer's instructions (Applied Biosystems, Thermo Fischer Scientific). The mRNA of target gene expressions was normalized to GAPDH, and the relative value to sample in the control group is given by $2^{-\Delta\Delta CT}$. The primer pairs were as follows: ANF, 5′-TACAGTGCGGTG TCC AACACAG-3′ and 5′-TGCTTCCTCAGTCTGCTCACTC-3′; BNP, 5′-TCCTAGCCA GTCTCCAGAGCAA-3′ and 5′-GGT CCTTCAAGAGCTGTCTCTG-3′; collagen I, 5′-GAGTACTGG ATCG ACCCTAACCA-3′ and 5′-GACGGCTGAGTAGGGAAC ACA-3′; collagen III, 5′-TCCCCTGGAATCTGTGAATC-3′ and 5′-TGAGTCGAATTGGGGAGAAT-3′; GAPDH, 5′-AGGTCG GTGTGAACGGATTTG-3′ and 5′-TGTAGACCATGTAGT TGAGGTCA-3′.

Western Blotting

The cardiac tissue was cracked with ice-cold RIPA buffer containing a 1% protease inhibitor cocktail. Equal amounts (20–30 μg) of protein were subjected to SDS-PAGE gel for electrophoresis and transferred onto PVDF membrane by Bio-Rad western blotting system. The membranes were blocked with 5% dry milk (dissolved in PBS buffer containing 0.1% Tween 20) for 60 min at room temperature and then incubated with anti-GCLM, HO-1, p-AKT, AKT, Nrf-2, cleaved caspase-3, Bax, Bcl-2, and GAPDH overnight at 4°C. After washing by TBST buffer for 3 times, the membrane was incubated with the horseradish peroxidase-conjugated secondary antibodies for 1 h at room temperature. Finally, the immunoreactive bands were detected by Gel-Pro 4.5 Analyzer (Media Cybernetics), and the protein expression level was quantified using the ImageJ software.

Histological Analysis

The fresh hearts were fixed in a 4% paraformaldehyde solution for 24 h. After dehydration in xylene and ethanol, the heart samples were embedded in paraffin, cut into 5 μM thickness, and then subjected to hematoxylin and eosin (H&E) and Masson's trichrome staining assay kit according to the manufacturer's instruction (Solarbio, Beijing). To assess the size of cardiomyocytes, the heart sections were stained with 50 μg/ml TRITC-labeled WGA in PBS buffer at 37°C for 1 h and then subjected to three times washing. After antifluorescence quenching agent treatment, the digital images were photographed using a fluorescence microscope (BX51, OLYMPUS, Japan), and the cardiomyocyte's surface area was analyzed by Image-Pro Plus software.

TUNEL Staining

The slides obtained were processed for a TUNEL assay to detect fragmented nuclei in the myocardium. The annexin V-EGFP apoptosis detection kit was used to detect apoptotic cells according to the manufacturer's protocol. Briefly, the paraffin-sectioned tissues were dewaxed and rehydrated, and then the slides were pretreated with 3% H_2O_2 and incubated with the reaction mixture containing TdT enzyme and biotin-11-dUTP at 37°C for 1 h. One hundred microliter of horseradish peroxidase-conjugated streptavidin (HRP-labeled avidin working fluid) was added to each slide and incubated at 37°C for 30 min. Reaction products were visualized with diaminobenzidine (DAB) plus substrate–chromogen solution for an appropriate time. The sections stained were visualized using a fluorescence microscope (BX51, OLYMPUS, Japan). The apoptotic cell number in each section was calculated by counting the number of TUNEL-positive apoptotic cells in five random fields.

ROS Detection

To evaluate ROS generation in the heart, the heart sections were stained with 10 μM DHE at 37°C for 30 min. The superoxide anion (O_2^-) in the heart was able to stain red fluorescence. After the heart sections were washed three times with PBS buffer, the digital images were photographed, and the fluorescence intensity of DHE was quantified by Image-Pro Plus software.

Determination of SOD and MDA Activity

The myocardial tissue homogenate was broken by ultrasound following 2,000 g centrifugation for 5 min at 4°C, and the supernatant was prepared for the next examination. The levels of superoxide dismutase (SOD) and MDA of each group were analyzed using an automated microplate reader according to the instruction of their corresponding assay kits (Nanjing Jiancheng Bioengineering Institute, China).

GSH Content Assay

The GSH assay kit (Beyotime Biotech) was used to detect the GSH contents in the heart after drug treatments. In brief, cardiac tissue (100 μg) was lysed in the protein removal solution S provided by the kit and centrifuged at 12,000 g at 4°C for 15 min, and then the supernatant was collected. After reaction with Ellman's reagent (DTNB), GSH reductase enzyme, and NADPH, the absorbance was measured at 412 nm using a microplate reader (Tecan Infinite Pro, Switzerland).

Statistical Analysis

Data were expressed as mean ± SEM and analyzed using GraphPad Prism software version 8.0. Comparisons between multiple groups were performed using one-way multivariate ANOVA (Tukey's *post-hoc* test). The difference was considered statistically significant when the p-value was ≤ 0.05.

RESULTS

DOX-Induced Cardiac Dysfunction and Hypotrophy

Numerous studies established the mice model of DOX-induced cardiotoxicity by intraperitoneal injection of DOX. However, intraperitoneal administration of DOX resulted in several side effects that influenced the accuracy of experimental conclusions. Intraperitoneal injection of DOX in mice severely reduced the food and water intake, induced peritoneal damage, and fibrosis which subsequently led to malaise, weight loss, and finally non-cardiac death. To avoid these inadequacies, intravenous injection of low dose DOX (5 mg/kg, once a week) for 4 weeks was

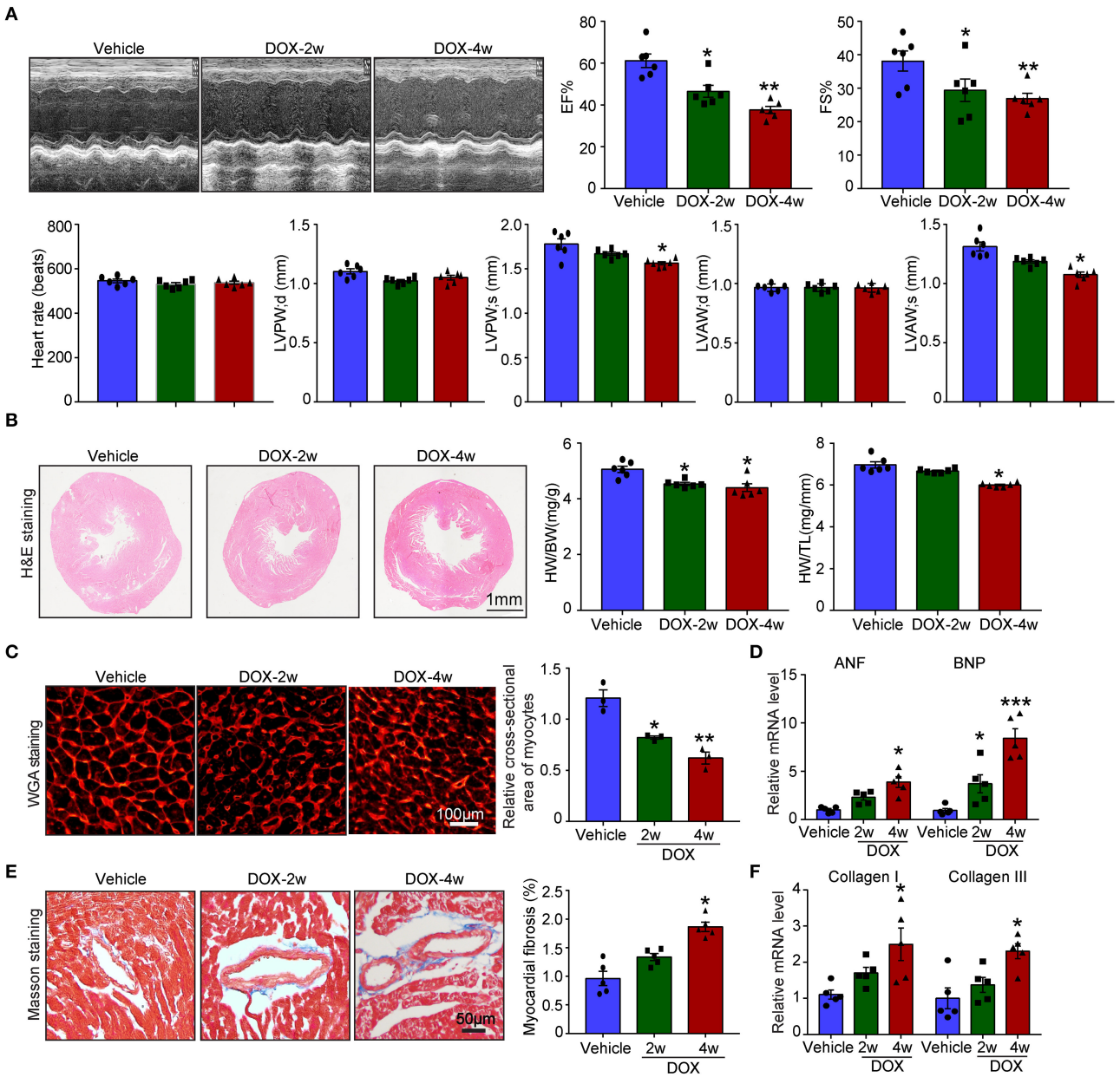

FIGURE 1 | Doxorubicin (DOX) dose-dependently induced cardiac dysfunction and cardiac fibrosis. Mice were intravenously treated with DOX (5 mg/kg) or its solvent once per week for 2 or 4 weeks. **(A)** Representative M-model echocardiography and the measurement of left ventricular EF% and FS%. The heart rate, left ventricular posterior wall (LVPW), and left ventricular anterior wall (LVAW) at diastole and systole were shown below ($n = 6$). **(B)** Representative image of hematoxylin and eosin (H and E) staining and the HW/BW and HW/TL ratios. Scale bar 1 mm. **(C)** Cardiac myocyte size was evaluated by TRITC-labeled wheat germ agglutinin (WGA) staining, and the cross-sectional area was quantified in the right panel (100 cells counted per heart, $n = 3$). **(D)** ANF and BNP mRNA expressions were determined by qRT-PCR in the heart ($n = 5$). **(E)** Cardiac fibrosis was detected by Masson's trichrome staining, and the relative fibrotic area was quantified ($n = 5$, right). Scale bar 50 μm. **(F)** The collagen I and collagen III mRNA levels in the heart ($n = 5$). Data are presented as mean ± SEM, and n represents the number of animals per group. $^{*}p < 0.05$, $^{**}p < 0.01$, $^{***}p < 0.001$ vs. vehicle.

used to induce cardiotoxicity. We found DOX time-dependently reduced cardiac function reflected by reduced LVEF, LVFS, LVPW, and LVAW during systole compared with vehicle-treated mice (**Figure 1A**). Furthermore, DOX dramatically reduced heart size, heart weight (HW) or body weight (BW), HW/tibia length (TL) ratio, and myocyte cross-sectional area (**Figures 1B,C**), whereas increased the mRNA expression of ANF and BNP (**Figure 1D**). Masson's trichrome staining showed that DOX treatment for 2- and 4-weeks time-dependently increased fibrotic area (**Figure 1E**); correspondingly, the mRNA level of fibrotic

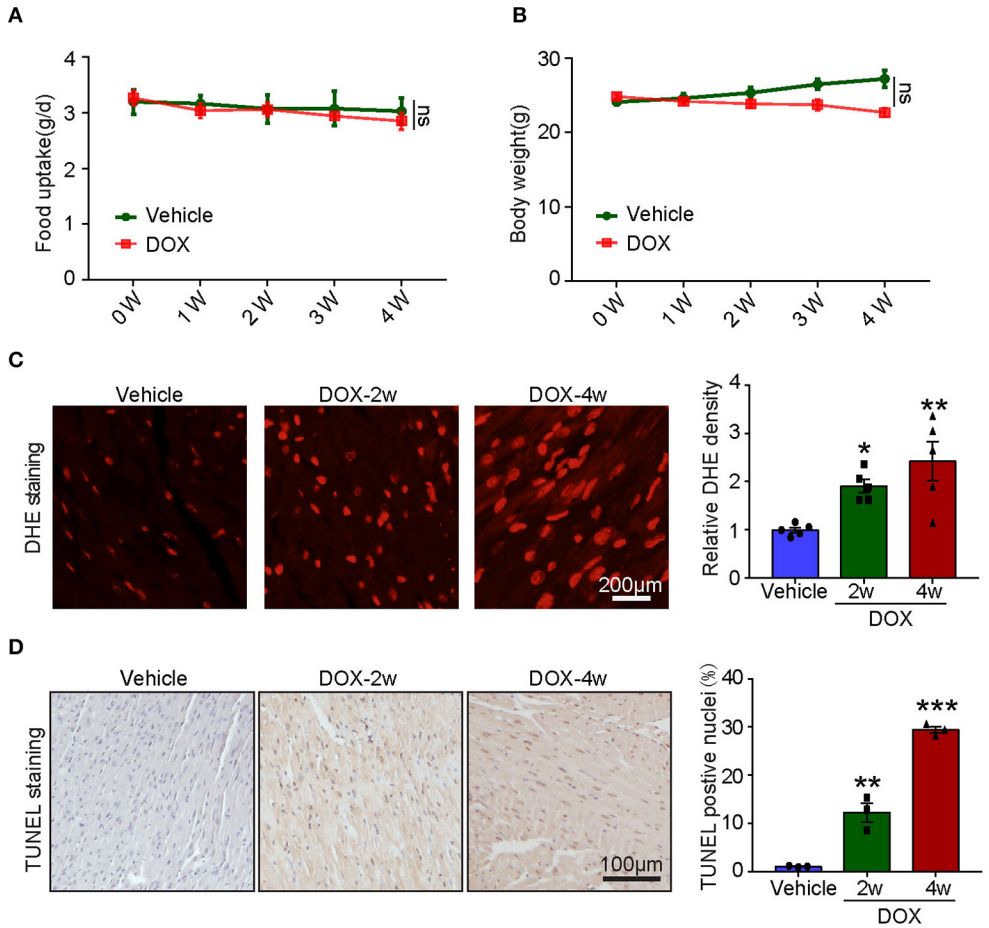

FIGURE 2 | Doxorubicin dose-dependently induced cardiac oxidative stress and apoptosis. Mice were intravenously treated with DOX (5 mg/kg) or its solvent once per week for 2 or 4 weeks. **(A,B)** The changes of food uptake and body weight after DOX treatment ($n = 4$). **(C)** Reactive oxygen species (ROS) generation was measured by dihydroethidium (DHE) staining, and the quantification of fluorescence intensity was shown right ($n = 5$). Scale bar 200 μm. **(D)** Representative TUNEL staining in the heart tissues and the TUNEL-positive nuclei were quantified ($n = 3$, right). Scale bar 100 μm. $^{*}p < 0.05$, $^{**}p < 0.01$, $^{***}p < 0.001$ vs. vehicle.

marker (collagen I and collagen III) in DOX-treated heart was also increased compared with that in the vehicle-treated heart (**Figure 1F**).

Tail Intravenous Injection of DOX-Induced Myocardial Oxidative Stress and Apoptosis With Few Systemic Side Effects

To assess the systemic side effects of DOX, the food intake and body weight of the vehicle- and DOX-treated mice were recorded. We found that intravenous administration of DOX for 1–4 weeks had little effect on food intake and body weight (**Figures 2A,B**). Next, we examined ROS generation in the heart and found DOX treatment for 2- and 4-weeks time-dependently increased ROS generation reflected by the enhanced fluorescence intensity in the heart (**Figure 2C**). Meanwhile, TUNEL staining showed DOX markedly induced myocardial apoptosis as reflected by increased TUNEL-positive nuclei in the hearts (**Figure 2D**).

Rut Inhibited DOX-Induced Cardiac Dysfunction and Fibrosis in Mice

Since intragastric administration of Rut (low dose of 20 mg/kg and high dose of 40 mg/kg) exerted beneficial effects in cardiovascular diseases (13), we selected these doses of Rut to investigate whether Rut protected against DOX-induced cardiotoxicity. Echocardiography showed DOX-treated mice developed heart failure reflected by reduced LVEF, LVFS, LVPW, and LVAW during systole compared with vehicle-treated mice, and these detrimental effects were dramatically mitigated by Rut administration (**Figure 3A**). Furthermore, Rut inhibited DOX-induced cardiac hypotrophy as reflected by the increased ratios of heart weight/body weight (HW/BW) and heart weight/tibia length (HW/TL), myocyte cross-sectional area, and decreased mRNA level of ANF and BNP (**Figures 2B–D**). Results obtained from Masson's trichrome staining and qPCR analysis revealed that the cardiac fibrosis caused by DOX was also inhibited after low and high doses of Rut administration, indicating attenuated cardiac remodeling (**Figures 3E,F**). However, there existed no

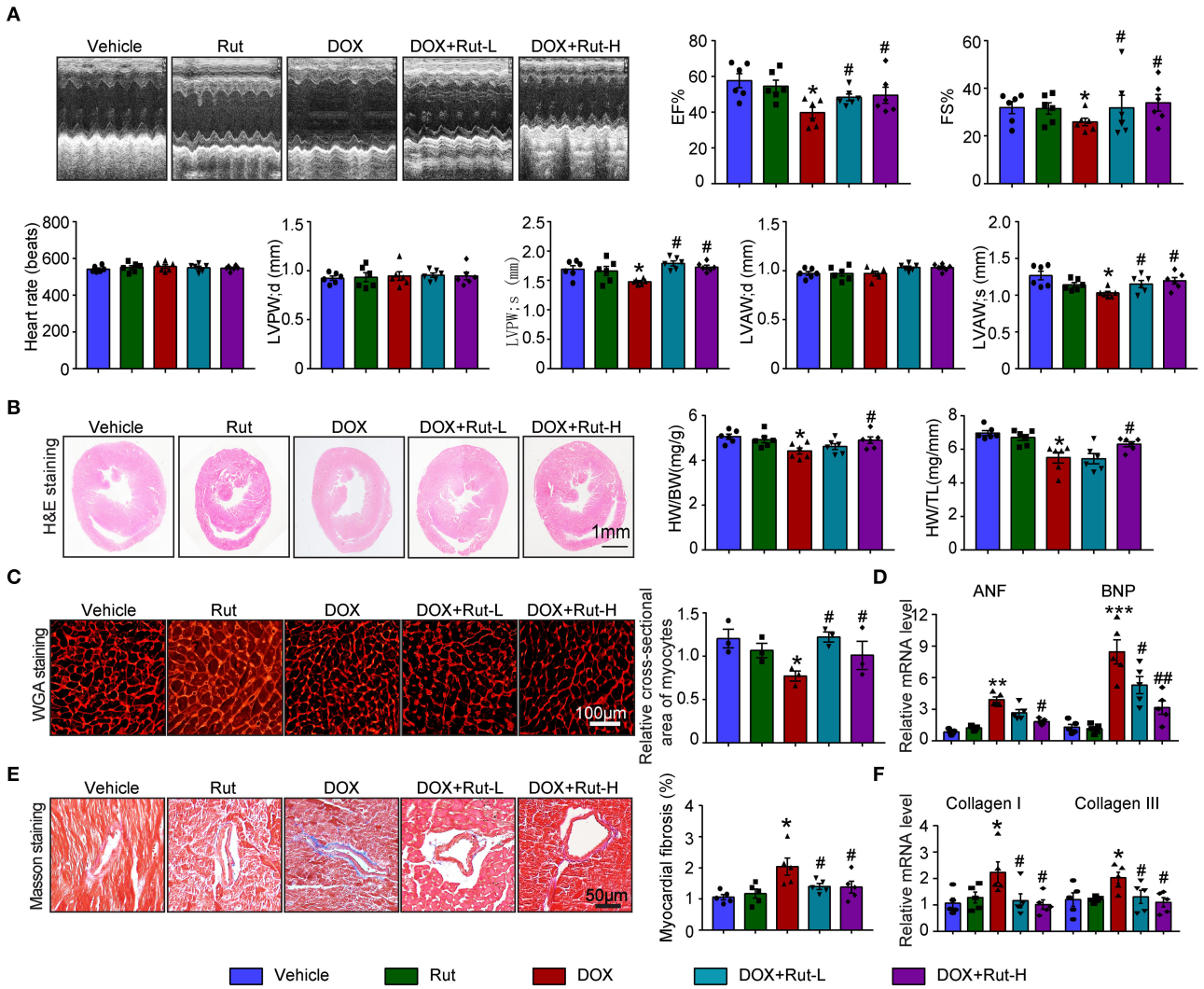

FIGURE 3 | Rutaecarpine mitigated DOX-induced cardiac dysfunction and fibrosis. Mice were treated with DOX and then on the same day received intragastric administration of 20 or 40 mg/kg Rut every day for 4 weeks. **(A)** Representative M-model echocardiography and the measurement of left ventricular EF% and FS%. The heart rate, LVPW, and LVAW at diastole and systole were shown below ($n = 6$). **(B)** Representative image of HandE staining and the HW/BW and HW/TL ratios (right, $n = 6$). Scale bar 1 mm. **(C)** Cardiac myocyte size was evaluated by TRITC-labeled WGA staining, and the cross-sectional area was quantified in the right panel (100 cells counted per heart, $n = 3$). **(D)** ANF and BNP mRNA expressions were determined by real-time quantitative PCR (qRT-PCR) in the heart ($n = 5$). **(E)** Cardiac fibrosis was detected by Masson's trichrome staining, and the relative fibrotic area was quantified ($n = 5$, right). Scale bar 50 μm. **(F)** The collagen I and collagen III mRNA levels in the heart ($n = 5$). Data are presented as mean ± SEM, and n represents the number of animals per group. $^{*}p < 0.05$, $^{**}p < 0.01$, $^{***}p < 0.001$ vs. vehicle; $^{\#}p < 0.05$, $^{\#\#}p < 0.01$ vs. DOX group.

significant changes in heart function, cardiomyocytes size, and fibrosis between the vehicle and Rut group (**Figures 3A–F**).

Rut Activated AKT/Nrf-2 Pathway and Inhibited DOX-Induced Oxidative Damage in the Heart

PI3K/AKT/Nrf-2-mediated oxidative stress was the most important mechanism of DOX-induced cardiotoxicity (10); thus, in this study, we examined ROS generation, oxidant enzymes content and AKT/Nrf-2 protein expressions in DOX-treated hearts after Rut administration. DHE and TUNEL staining showed that Rut attenuated DOX-induced ROS generation and cardiomyocytes apoptosis in the heart (**Figures 4A,B**). Meanwhile, paralleled experiments demonstrated that DOX significantly reduced SOD activity and GSH content, but increased MDA activity in the heart, and all these effects were partially inhibited by Rut (**Figures 4C–E**).

To investigate the molecular mechanism of the antioxidant effects of Rut, we examined the protein levels of p-AKT, Nrf-2, HO-1, and GCLM in DOX-treated hearts after Rut administration and found that DOX reduced the protein level of p-AKT, Nrf-2, HO-1, and GCLM compared with vehicle-treated mice (**Figure 4F**), but the reduction in these

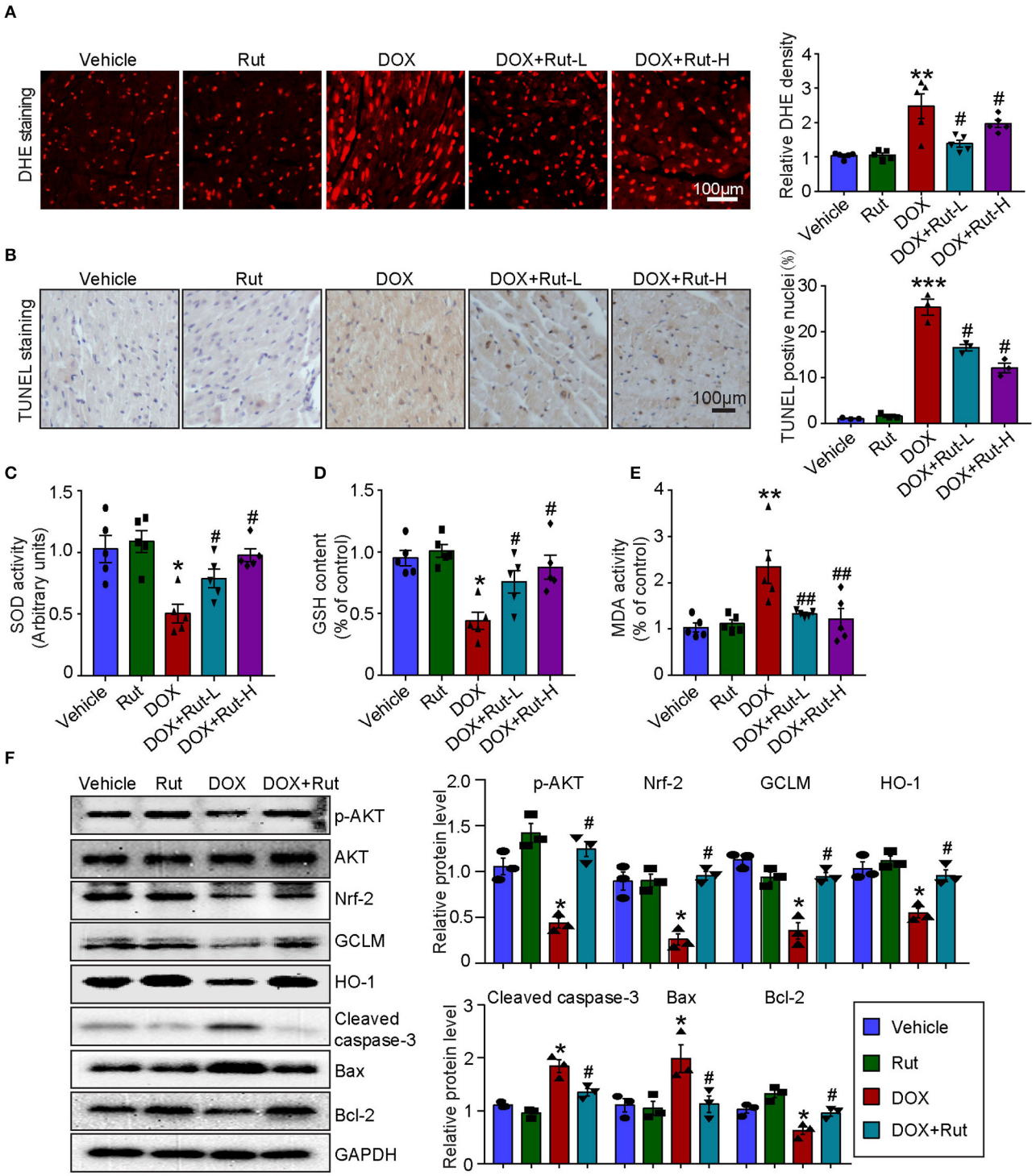

FIGURE 4 | Rutaecarpine alleviated DOX-induced oxidative stress and apoptosis. Mice were treated with DOX and then on the same day received 20 or 40 mg/kg Rut (intragastric administration) every day for 4 weeks. **(A)** ROS generation in the heart was detected by DHE staining, and the quantification of fluorescence intensity was shown right ($n = 5$). Scale bar 100 μm. **(B)** Representative TUNEL staining in the heart tissues and the TUNEL-positive nuclei were quantified ($n = 3$, right). Scale bar 100 μm. **(C–E)** Relative superoxide dismutase (SOD) activity, glutathione (GSH) content, and enhancement of malondialdehyde (MDA) activity in the heart; data in other groups were normalized to the vehicle group ($n = 5$). **(F)** Western blot analysis of p-AKT, Nrf-2, GCLM, HO-1, cleaved caspase-3, Bax, and Bcl-2 in the heart and the relevant quantification was shown right (right, $n = 3$). $^{*}p < 0.05$, $^{**}p < 0.01$, $^{***}p < 0.001$ vs. vehicle; $^{\#}p < 0.05$, $^{\#\#}p < 0.01$ vs. DOX group.

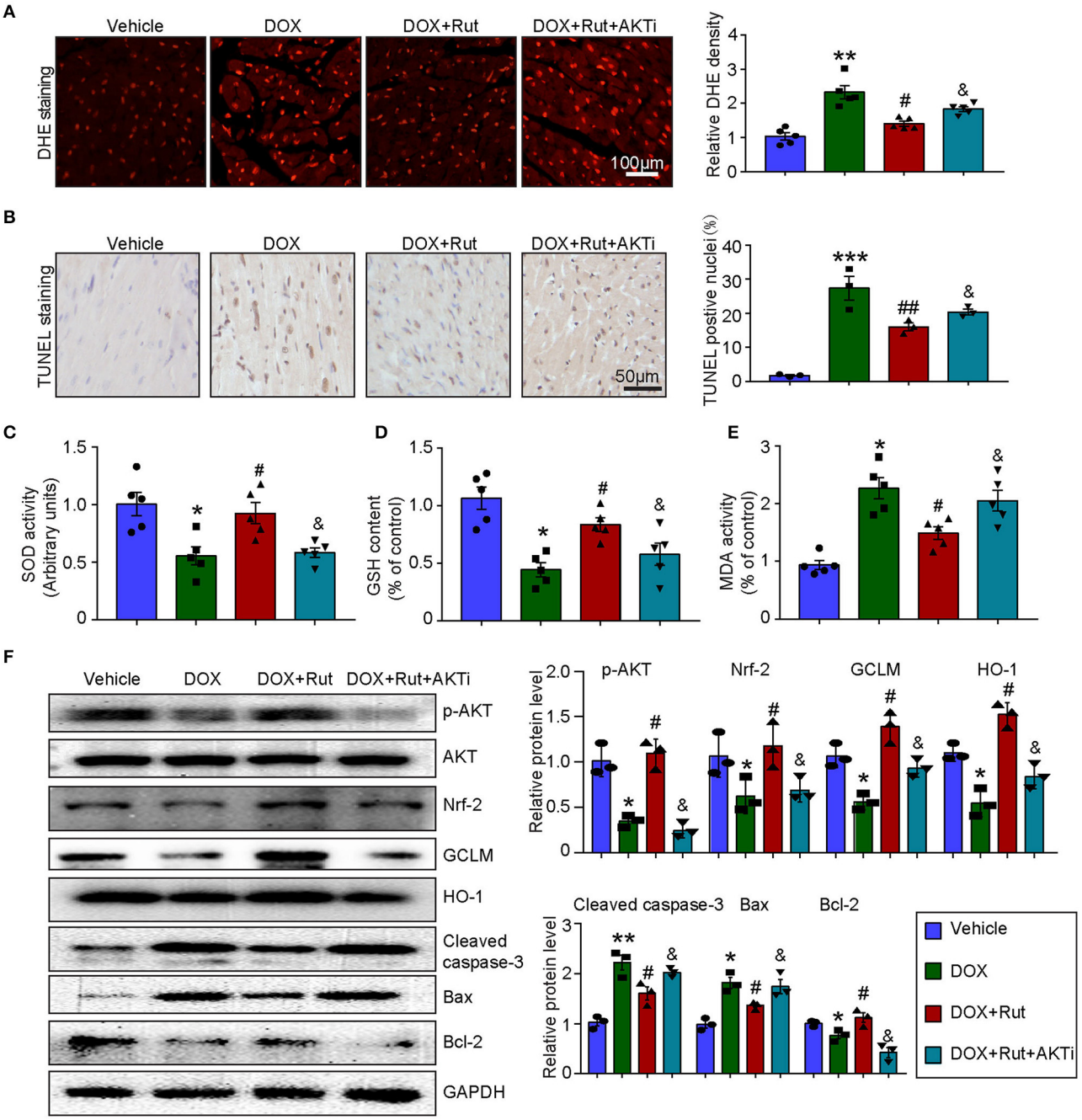

FIGURE 5 | AKT inhibitor (AKTi) abolished the antioxidant and antiapoptotic effect of rutaecarpine in DOX-treated hearts. Mice were intraperitoneally injected with AKTi (20 mg/kg) every other day for 4 weeks before DOX and Rut administration. **(A)** ROS generation in the heart was detected by DHE staining, and the quantification of fluorescence intensity was shown right ($n = 5$). Scale bar 100 μm. **(B)** Representative TUNEL staining in the heart tissues and the TUNEL-positive nuclei were quantified ($n = 3$, right). Scale bar 50 μm. **(C–E)** Relative SOD activity, GSH content, and MDA activity in the heart; data in other groups were normalized to the vehicle group ($n = 5$). **(F)** Western blot analysis of p-AKT, Nrf-2, GCLM, HO-1, cleaved caspase-3, Bax, and Bcl-2 in the heart, and the relevant quantification was shown right ($n = 3$). $^{*}p < 0.05$, $^{**}p < 0.01$, $^{***}p < 0.001$ vs. vehicle; $^{\#}p < 0.05$, $^{\#\#}p < 0.01$ vs. DOX group; $^{\&}p < 0.05$ vs. DOX plus Rut group.

protein expressions was reversed by Rut administration for 4 weeks (**Figure 4F**). In addition, the proteins involved in apoptosis were examined. Consistent with the results of TUNEL staining shown in **Figure 4B**, we found DOX enhanced the pro-apoptotic protein cleaved caspase-3 and Bax expressions, but reduced the antiapoptotic protein Bcl-2 expression (**Figure 4F**). Interestingly, these changes were all partly inhibited by Rut, suggesting the antiapoptotic effect of Rut (**Figure 4F**).

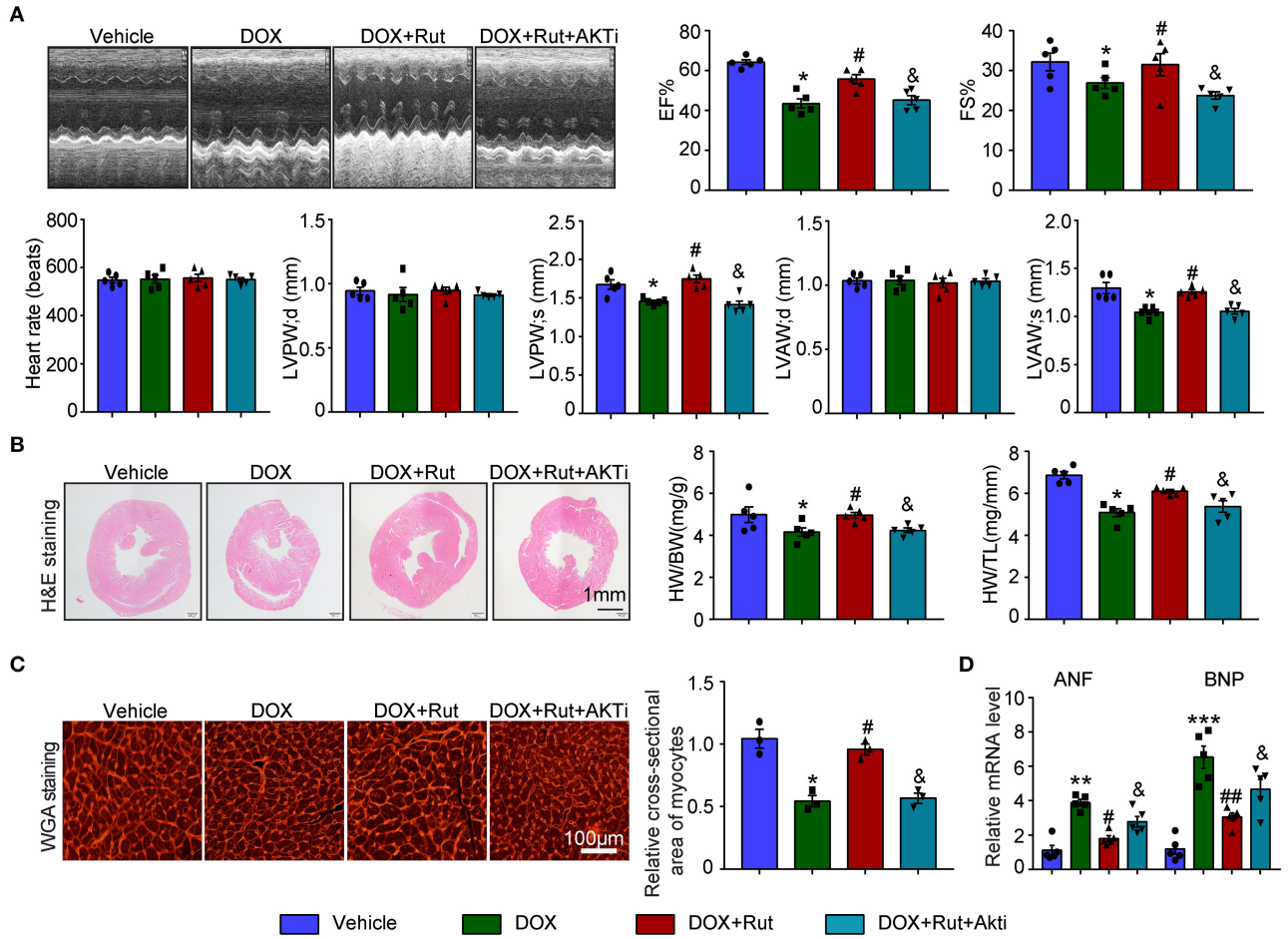

FIGURE 6 | AKT inhibitor alleviated the cardio-protective effect of rutaecarpine on DOX-induced heart failure. Mice were intraperitoneally injected with AKTi (20 mg/kg) every other day for 4 weeks from the first day before DOX and Rut administration. **(A)** Representative M-model echocardiography of the left ventricular EF% and FS%. The heart rate, LVPW, and LVAW at diastole and systole were shown below ($n = 5$). **(B)** Representative image of HandE staining and the HW/BW and HW/TL ratios (right, $n = 5$). Scale bar 1 mm. **(C)** Cardiac myocyte size was evaluated by TRITC-labeled WGA staining, and the cross-sectional area was quantified in the right panel (100 cells counted per heart) ($n = 3$, right). Scale bar 100 μm. **(D)** ANF and BNP mRNA expressions were determined by qRT-PCR in the heart ($n = 5$). $^{*}p < 0.05$, $^{**}p < 0.01$, $^{***}p < 0.001$ vs. vehicle; $^{\#}p < 0.05$, $^{\#\#}p < 0.01$ vs. DOX group; $^{\&}p < 0.05$ vs. DOX plus Rut group.

AKTi Partially Reversed the Beneficial Effect of Rut on DOX-Induced Oxidative Stress and Apoptosis in the Heart

To further confirm that the antioxidant effects of Rut were due to its ability to activate AKT/Nrf-2, the DOX combined with Rut-treated mice was subjected to AKTi. We found that the reduced ROS generation and apoptosis caused by Rut in DOX-treated heart were partially abolished by AKTi (**Figures 5A,B**). In concordance with these results, blocking AKT by its inhibitor counteracted the antioxidant effects of Rut, as demonstrated by the reduced SOD activity and GSH content, and increased MDA activity in the heart compared with DOX plus Rut group (**Figures 5C–E**). Accordingly, we examined the protein expressions which regulated oxidative stress and apoptosis in the heart and found that Rut enhanced the protein levels of p-AKT, Nrf-2, HO-1, GCLM, and Bcl-2, but inhibited cleaved caspase-3 and Bax expression compared with DOX-treated mice. Of note, all these changes in protein expressions were reversed after AKTi administration (**Figure 5F**), suggesting that the antioxidant and antiapoptotic effects of Rut were mediated by the AKT signal pathway.

AKTi Partially Abolished the Protective Effect of Rut on DOX-Induced Heart Failure

Next, the changes in cardiac function and structure were examined. We found that DOX-treated mice after Rut administration exhibited improved cardiac function, as reflected by increased LVEF, LVFS, LVPW, and LVAW during systole and also enhanced HW/BW and HW/TL ratios and myocyte size (**Figures 6A–C**), and these beneficial effects of Rut were partially inhibited by AKTi (**Figures 6A–C**). At the molecular level, we found that the biomarker of heart failure (ANF and BNP mRNA) enhanced in DOX-treated hearts was correspondingly reduced after Rut treatment, and AKTi partially reversed these

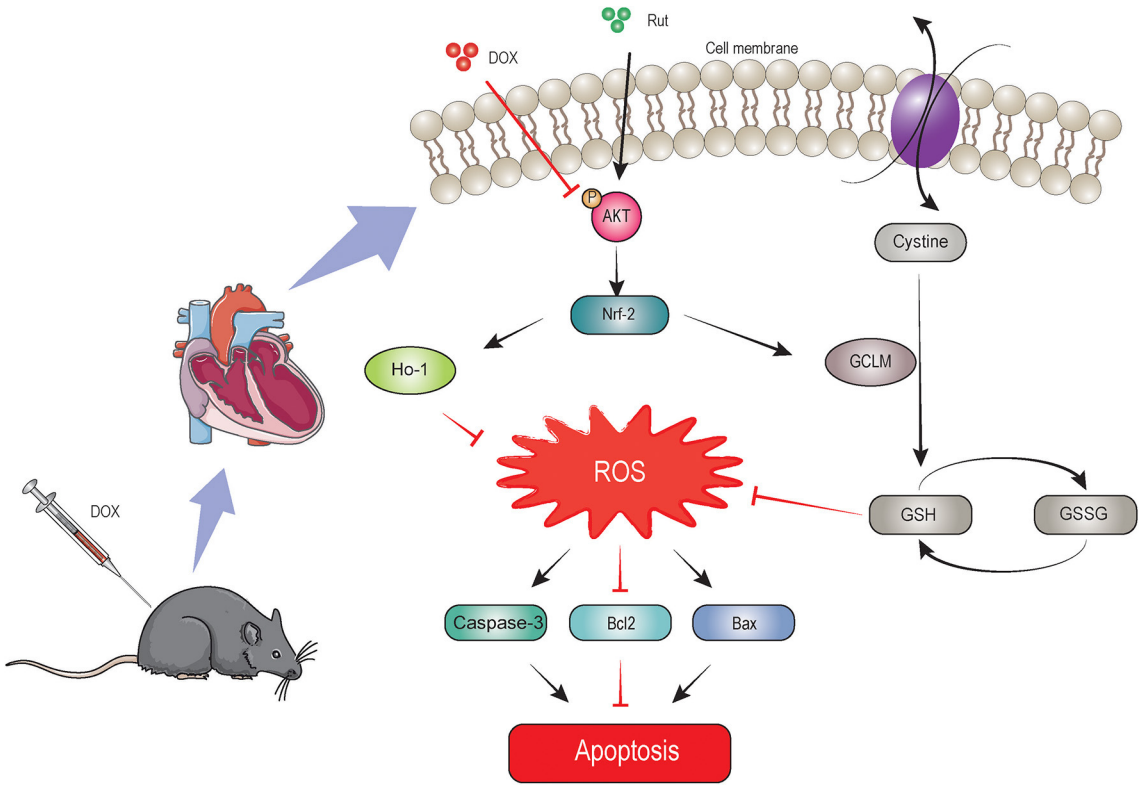

FIGURE 7 | The proposed protective mechanism by rutaecarpine on DOX-induced heart failure. Rutaecarpine activated AKT/Nrf-2 signaling pathway, which in turn inhibited DOX-induced oxidative stress and apoptosis through regulating heme oxygenase-1 (HO-1) and GSH cysteine ligase modulatory subunit (GCLM) expression.

effects (**Figure 6D**). Hence, these *in vivo* data suggested that Rut inhibited DOX-induced cardiotoxicity by activating AKT.

DISCUSSION

In this study, we identified Rut as a novel drug in treating DOX-induced cardiotoxicity, which was supported by inhibition of oxidative stress, myocardial apoptosis, fibrosis, and improvement of cardiac function. Rut enhanced HO-1 and GCLM expressions thereby leading to reduced ROS generation through activating the AKT/Nrf-2 signaling pathway, which was responsible for the beneficial effects of Rut on DOX-induced cardiotoxicity, and AKTi abolished these effects. These effects were summarized in **Figure 7**. These results highlighted that Rut may be a potential therapeutic drug for DOX-induced heart failure.

Doxorubicin is an effective chemotherapeutic drug in treating multiple cancer all over the world, but as we know, this action also comes at a price. Numerous patients who received DOX treatment developed heart failure, and this detrimental side effect even occurs many years after the cessation of DOX administration. Although there existed a cardioprotective drug that alleviated DOX-induced cardiotoxicity such as dexrazoxane, the curative effect was still not satisfactory. Thus, searching for novel drugs to mitigate the cytotoxicity of DOX and revealing the underlying mechanism is an important task. Recent studies suggested that Rut has antitumor potential by inhibiting proliferation and inducing apoptosis in multiple tumor cells, including human ovarian cancer cells (22), breast cancer cells (23), and prostate cancer cells (24). On the other side, Rut had cardioprotective roles in several cardiovascular diseases including hypertension (12), atherosclerosis (25), cardiac hypertrophy (13), and ischemia-reperfusion injury (14). However, whether Rut protected against DOX-induced cardiotoxicity remains obscure. In this study, our *in vivo* data showed that Rut inhibited DOX-induced cardiac dysfunction, oxidative stress, myocardial apoptosis, and loss of heart weight. These results indicated that Rut may be a potential drug to treat cancer and meanwhile prevent DOX-induced cardiotoxicity.

AKT signaling pathway plays an important role in regulating oxidative stress and apoptosis, and activation of AKT exerts protective effects on DOX-induced cardiotoxicity (10). Oxidative stress was able to trigger cardiomyocyte apoptosis and was one of the most important mechanisms of DOX-induced cardiotoxicity (3). Recent studies reported DOX reduced antioxidant substances such as GSH and SOD and induced apoptosis which was accompanied by increased cleaved caspase-3, Bax, and decreased Bcl-2 expression (10). GSH functions at catalyzing the reduction of peroxides, and SOD promoted the transition of O^{2-} to hydrogen peroxide (26, 27). Consistent with these reports, our results showed that the level of GSH and SOD was reduced in

DOX-treated hearts, but the level of MDA (the end product of lipid hydroperoxide) was increased. Additionally, the protein which regulated apoptosis manifested similar changes upon DOX treatment, as demonstrated by upregulation of cleaved caspase-3 and Bax and downregulation of Bcl-2 protein expressions in DOX-treated hearts. Importantly, Rut administration for 4 weeks dramatically alleviated all these effects. Of note, AKT/Nrf-2/GCLM signaling pathway inactivated by DOX was reactivated by Rut. To get deeper knowledge on the mechanism of Rut protected against DOX-induced cardiotoxicity, AKTi was then used to block AKT signaling pathway. Our results showed that AKTi inhibited AKT/Nrf-2/GCLM signaling pathway activated by Rut and further abolished the beneficial effects of Rut in DOX-induced cardiotoxicity. These results suggested that Rut may inhibit DOX-induced cardiotoxicity through AKT/Nrf-2/GCLM-mediated oxidative stress and apoptosis.

However, some limitations still existed in this study. These *in vivo* experiments only used mice to investigate the effects of Rut, and more animal models of DOX-induced cardiotoxicity and clinical experiments should be established to further confirm the protective role of Rut. In addition, although existing evidence indicated that Rut activated AKT signaling pathway through calmodulin-dependent protein kinase-II or IRS-1/PI3K in HepG2 cell or liver tissues, respectively (15, 18), whether these mechanisms were similar in the heart needs to be studied in future.

In summary, we discovered a novel drug that protected against DOX-induced cardiotoxicity. The molecular mechanism may involve the activation of the AKT/Nrf-2/GCLM signaling pathway, which alleviates DOX-induced oxidative stress and apoptosis to improve cardiac dysfunction. These findings may provide a novel therapeutic option in the treatment of DOX-induced cardiotoxicity. These findings indicated that Rut was a cardio-protective agent in treating DOX-induced cardiac toxicity.

DATA AVAILABILITY STATEMENT

The raw data supporting the conclusions of this article will be made available by the authors without undue reservation.

ETHICS STATEMENT

The animal study was reviewed and approved by the Animal Care and Use Committee of the Dalian Medical University.

AUTHOR CONTRIBUTIONS

Z-QL, Z-LS, J-TL, C-LL, and H-LB participated in most of the experiments. Z-QL, H-LB, and Z-LS performed the relevant experiment of molecular biology. X-LY, Z-QL, and Z-LS performed animal studies. XX, YZ, and Y-NJ conceived and supervised the project. XX and X-LY wrote the manuscript. All authors contributed to the article and approved the submitted version.

ACKNOWLEDGMENTS

The authors gratefully acknowledge the financial support by the National Natural Science Foundation of China (numbers XX, 81600315; Y-NJ, 82070427), the General Project of Liaoning Provincial Department of Education (YZ, LZ2019021), the Natural Science Foundation of Liaoning Province (XX, 2020-MS-269), and the Dalian youth science and technology star project (XX, 2020-RQ-069).

REFERENCES

1. Pugazhendhi A, Edison T, Velmurugan BK, Jacob JA, Karuppusamy I. Toxicity of Doxorubicin (Dox) to different experimental organ systems. *Life Sci.* (2018) 200:26–30. doi: 10.1016/j.lfs.2018.03.023
2. Renu K, Abilash VG, Thirupathi Pichiah PB, and Arunachalam S. Molecular mechanism of doxorubicin-induced cardiomyopathy - an update. *Eur J Pharmacol.* (2018) 818:241–53. doi: 10.1016/j.ejphar.2017.10.043
3. Songbo M, Lang H, Xinyong C, Bin X, Ping Z, Liang S. Oxidative stress injury in doxorubicin-induced cardiotoxicity. *Toxicol Lett.* (2019) 307:41–8. doi: 10.1016/j.toxlet.2019.02.013
4. Jafari M, Ghadami E, Dadkhah T, Akhavan-Niaki H. PI3k/AKT signaling pathway: erythropoiesis and beyond. *J Cell Physiol.* (2019) 234:2373–85. doi: 10.1002/jcp.27262
5. Kitamura Y, Koide M, Akakabe Y, Matsuo K, Shimoda Y, Soma Y, et al. Manipulation of cardiac phosphatidylinositol 3-kinase (PI3K)/Akt signaling by apoptosis regulator through modulating IAP expression (ARIA) regulates cardiomyocyte death during doxorubicin-induced cardiomyopathy. *J Biol Chem.* (2014) 289:2788–800. doi: 10.1074/jbc.M113.508143
6. Cao Y, Ruan Y, Shen T, Huang X, Li M, Yu W, et al. Astragalus polysaccharide suppresses doxorubicin-induced cardiotoxicity by regulating the PI3k/Akt and p38MAPK pathways. *Oxid Med Cell Longev.* (2014) 2014:674219. doi: 10.1155/2014/674219
7. Mirzaei S, Zarrabi A, Hashemi F, Zabolian A, Saleki H, Azami N, et al. Nrf2 signaling pathway in chemoprotection and doxorubicin resistance: potential application in drug discovery. *Antioxidants.* (2021) 10:349. doi: 10.3390/antiox10030349
8. Guo L, Zheng X, Wang E, Jia X, Wang G, Wen J. Irigenin treatment alleviates doxorubicin (DOX)-induced cardiotoxicity by suppressing apoptosis, inflammation and oxidative stress via the increase of miR-425. *Biomed Pharmacother.* (2020) 125:109784. doi: 10.1016/j.biopha.2019.109784
9. Ahmed AZ, Mumbrekar KD, Satyam SM, Shetty P, D'Souza MR, Singh VK. Chia seed oil ameliorates doxorubicin-induced cardiotoxicity in female wistar rats: an electrocardiographic, biochemical and histopathological approach. *Cardiovasc Toxicol.* (2021) 21:533–42. doi: 10.1007/s12012-021-09644-3
10. Zhang X, Hu C, Kong CY, Song P, Wu HM, Xu SC, et al. FNDC5 alleviates oxidative stress and cardiomyocyte apoptosis in doxorubicin-induced cardiotoxicity via activating AKT. *Cell Death Differ.* (2020) 27:540–55. doi: 10.1038/s41418-019-0372-z
11. Alzahrani AM, Rajendran P, Veeraraghavan VP, Hanieh H. Cardiac protective effect of kirenol against doxorubicin-induced cardiac hypertrophy in H9c2 cells through Nrf2 signaling via PI3K/AKT pathways. *Int J Mol Sci.* (2021) 22:3269. doi: 10.3390/ijms22063269
12. Ding JS, Gao R, Li D, Peng J, Ran LL, Li YJ. Solid dispersion of rutaecarpine improved its antihypertensive effect in spontaneously hypertensive rats. *Biopharm Drug Dispos.* (2008) 29:495–500. doi: 10.1002/bdd.634
13. Zeng SY, Yang L, Lu HQ, Yan QJ, Gao L, Qin XP. Rutaecarpine prevents hypertensive cardiac hypertrophy involving the inhibition of Nox4-ROS-ADAM17 pathway. *J Cell Mol Med.* (2019) 23:4196–207. doi: 10.1111/jcmm.14308

14. Xue H, Cheng Y, Wang X, Yue Y, Zhang W, Li X. Rutaecarpine and evodiamine selected as beta1-AR inhibitor candidates using beta1-AR/CMC-offline-UPLC/MS prevent cardiac ischemia-reperfusion injury via energy modulation. *J Pharm Biomed Anal.* (2015) 115:307–14. doi: 10.1016/j.jpba.2015.07.022
15. Nie XQ, Chen HH, Zhang JY, Zhang YJ, Yang JW, Pan HJ, et al. Rutaecarpine ameliorates hyperlipidemia and hyperglycemia in fat-fed, streptozotocin-treated rats via regulating the IRS-1/PI3K/Akt and AMPK/ACC2 signaling pathways. *Acta Pharmacol Sin.* (2016) 37:483–96. doi: 10.1038/aps.2015.167
16. Lin JY, Yeh TH. Rutaecarpine administration inhibits cancer cell growth in allogenic TRAMP-C1 prostate cancer mice correlating with immune balance *in vivo*. *Biomed Pharmacother.* (2021) 139:111648. doi: 10.1016/j.biopha.2021.111648
17. Tian KM, Li JJ, Xu SW. Rutaecarpine: a promising cardiovascular protective alkaloid from Evodia rutaecarpa (Wu Zhu Yu). *Pharmacol Res.* (2019) 141:541–50. doi: 10.1016/j.phrs.2018.12.019
18. Jin SW, Hwang YP, Choi CY, Kim HG, Kim SJ, Kim Y, et al. Protective effect of rutaecarpine against t-BHP-induced hepatotoxicity by upregulating antioxidant enzymes via the CaMKII-Akt and Nrf2/ARE pathways. *Food Chem Toxicol.* (2017) 100:138–48. doi: 10.1016/j.fct.2016.12.031
19. Bao MH, Dai W, Li YJ, Hu CP. Rutaecarpine prevents hypoxia-reoxygenation-induced myocardial cell apoptosis via inhibition of NADPH oxidases. *Can J Physiol Pharmacol.* (2011) 89:177–86. doi: 10.1139/Y11-006
20. Xu X, Li H, Hou X, Li D, He S, Wan C, et al. Punicalagin Induces Nrf2/HO-1 Expression via Upregulation of PI3K/AKT Pathway and Inhibits LPS-Induced Oxidative Stress in RAW264.7 Macrophages. *Mediators Inflamm.* (2015) 2015:380218. doi: 10.1155/2015/380218
21. Xie X, Bi HL, Lai S, Zhang YL, Li N, Cao HJ, et al. The immunoproteasome catalytic beta5i subunit regulates cardiac hypertrophy by targeting the autophagy protein ATG5 for degradation. *Sci Adv.* (2019) 5:eaau0495. doi: 10.1126/sciadv.aau0495
22. Chen MC, Yu CH, Wang SW, Pu HF, Kan SF, Lin LC, et al. Anti-proliferative effects of evodiamine on human thyroid cancer cell line ARO. *J Cell Biochem.* (2010) 110:1495–503. doi: 10.1002/jcb.22716
23. Guo H, Liu D, Gao B, Zhang X, You M, Ren H, et al. Antiproliferative activity and cellular uptake of evodiamine and rutaecarpine based on 3D tumor models. *Molecules.* (2016) 21:954. doi: 10.3390/molecules21070954
24. Liao Y, Liu Y, Xia X, Shao Z, Huang C, He J, et al. Targeting GRP78-dependent AR-V7 protein degradation overcomes castration-resistance in prostate cancer therapy. *Theranostics.* (2020) 10:3366–81. doi: 10.7150/thno.41849
25. Xu Y, Liu Q, Xu Y, Liu C, Wang X, He X, et al. Rutaecarpine suppresses atherosclerosis in ApoE-/- mice through upregulating ABCA1 and SR-BI within RCT. *J Lipid Res.* (2014) 55:1634–47. doi: 10.1194/jlr.M044198
26. Maejima Y, Kuroda J, Matsushima S, Ago T, Sadoshima J. Regulation of myocardial growth and death by NADPH oxidase. *J Mol Cell Cardiol.* (2011) 50:408–16. doi: 10.1016/j.yjmcc.2010.12.018
27. Zhao L, Tao X, Qi Y, Xu L, Yin L, Peng J. Protective effect of dioscin against doxorubicin-induced cardiotoxicity via adjusting microRNA-140-5p-mediated myocardial oxidative stress. *Redox Biol.* (2018) 16:189–98. doi: 10.1016/j.redox.2018.02.026

Conflict of Interest: The authors declare that the research was conducted in the absence of any commercial or financial relationships that could be construed as a potential conflict of interest.

Publisher's Note: All claims expressed in this article are solely those of the authors and do not necessarily represent those of their affiliated organizations, or those of the publisher, the editors and the reviewers. Any product that may be evaluated in this article, or claim that may be made by its manufacturer, is not guaranteed or endorsed by the publisher.

frontiers in Cardiovascular Medicine

ORIGINAL RESEARCH
published: 26 January 2022
doi: 10.3389/fcvm.2021.794957

Association of Body Weight Variability With Progression of Coronary Artery Calcification in Patients With Predialysis Chronic Kidney Disease

Sang Heon Suh[1], Tae Ryom Oh[1], Hong Sang Choi[1], Chang Seong Kim[1], Eun Hui Bae[1], Kook-Hwan Oh[2], Kyu-Beck Lee[3], Seung Hyeok Han[4], Suah Sung[5], Seong Kwon Ma[1] and Soo Wan Kim[1]* on behalf of the Korean Cohort Study for Outcomes in Patients With Chronic Kidney Disease (KNOW-CKD) Investigators*

[1] Department of Internal Medicine, Chonnam National University Medical School and Chonnam National University Hospital, Gwangju, South Korea, [2] Department of Internal Medicine, Seoul National University Hospital, Seoul, South Korea, [3] Department of Internal Medicine, Kangbuk Samsung Hospital, Sungkyunkwan University School of Medicine, Seoul, South Korea, [4] Department of Internal Medicine, College of Medicine, Institute of Kidney Disease Research, Yonsei University, Seoul, South Korea, [5] Department of Internal Medicine, Eulji Medical Center, Eulji University, Seoul, South Korea

OPEN ACCESS

Edited by:
Gian Marco Rosa, San Martino Hospital (IRCCS), Italy

Reviewed by:
Jiali Deng, Shanghai University, China
Owais Bhat, Virginia Commonwealth University, United States

***Correspondence:**
Seong Kwon Ma
drmsk@hanmail.net
Soo Wan Kim
skimw@chonnam.ac.kr

Specialty section:
This article was submitted to General Cardiovascular Medicine, a section of the journal Frontiers in Cardiovascular Medicine

Received: *14 October 2021*
Accepted: *23 December 2021*
Published: *26 January 2022*

Citation:
Suh SH, Oh TR, Choi HS, Kim CS, Bae EH, Oh K-H, Lee K-B, Han SH, Sung S, Ma SK and Kim SW (2022) Association of Body Weight Variability With Progression of Coronary Artery Calcification in Patients With Predialysis Chronic Kidney Disease. Front. Cardiovasc. Med. 8:794957. doi: 10.3389/fcvm.2021.794957

Background: We investigated whether high body weight variability (BWV) is associated with a higher prevalence of coronary artery calcification (CAC) or more rapid progression of CAC in patients with predialysis chronic kidney disease (CKD).

Methods: A total of 1,162 subjects from a nationwide prospective cohort of predialysis CKD were analyzed. The subjects were divided into the tertile (T1, T2, and T3) by BWV. CAC was assessed at the baseline and a 4-year follow-up by CT scan. Rapid progression of coronary artery calcification was defined as an increase in coronary artery calcium score (CACS) more than 200 Agatston units during a 4-year follow-up.

Results: One-way ANOVA revealed that CACS change during the follow-up period is significantly higher in the subjects with high BWV, although CACS at the baseline and 4-year follow-up was not different among the tertile groups by BWV. Logistic regression analysis revealed that compared to low BWV (T1), both moderate (T2, adjusted odds ratio (OR) 2.118, 95% CI 1.075–4.175) and high (T3, adjusted OR 2.602, 95% CI 1.304–5.191) BWV was associated with significantly increased risk of rapid progression of CAC. Importantly, the association between BWV and progression of CAC remained robust even among the subjects without significant BW gain or loss during follow-up periods (T2, adjusted OR 2.007, 95% CI 1.011–3.984; T3, adjusted OR 2.054, 95% CI 1.003–4.207).

Conclusion: High BWV is independently associated with rapid progression of CAC in patients with predialysis CKD.

Keywords: body weigh variability, cardiovascular disease, chronic kidney disease, coronary artery calcification, cardiovascular event

INTRODUCTION

Patients with chronic kidney disease (CKD) are likely to experience body weight (BW) fluctuation. Accumulation of excess extracellular fluid in patients with CKD is associated with BW gain, leading to accelerated coronary artery calcification (1), cardiovascular (CV) remodeling (2), and increase the risk of adverse renal outcome (3), and all-cause mortality (4). Conversely, malnutrition-inflammation, which is prevalent even before the commencement of renal replacement therapy (5, 6), is associated with BW loss and is ultimately associated with increased mortality (7). Diuretic use further increases the odd for BW fluctuation in patients with CKD (8). As all these conditions are likely to take place concurrently, it is expected that bodyweight variability (BWV), rather than persistent loss or gain of BW, maybe of high clinical significance, which has not been established especially in patients with predialysis CKD.

Body weight variability is an emerging surrogate of clinical outcomes. BWV is associated with a higher risk of incident diabetes mellitus (DM) (9, 10), and is also associated with adverse CV outcomes (11) and all-cause mortality (9, 12, 13) in the general population. The prognostic impact of BWV has been also validated in more specific clinical contexts, which is well illustrated in patients with DM (14–16) and coronary artery disease (CAD) (17). Moreover, it is noticeable that the association of high BWV with adverse CV outcomes is independent of traditional CV risk factors (15, 17), suggesting a potential role of BWV in the prediction of outcomes in patients with CKD. In this regard, we recently reported that high BWV is associated with adverse CV outcomes in patients with predialysis CKD (18). Despite the robust association between BWV and CV outcomes in this population, the precise mechanism of how BWV is linked to CV events was not clearly evaluated yet.

The high prevalence and prognostic role of coronary artery calcification (CAC) in patients with CKD have been investigated in several studies (19). Therefore, we here hypothesized that high BWV would be associated with a higher prevalence of CAC or more rapid progression of CAC lesions in patients with predialysis CKD, as CKD is an independent risk factor for the development of CAD (20), and CAD is the leading cause of mortality in patients with CKD (21). We analyzed the coronary artery calcium score (CACS) at the baseline and 4-year follow-up by the degree of visit-to-visit BWV in patients with predialysis CKD. To examine the clinical significance of BWV that is distinctive from longitudinal BW change, we also investigated the association of BWV with CACS progression in patients without significant BW gain or loss during follow-up periods.

METHODS

Study Designs and Participants

The Korean Cohort Study for Outcomes in Patients With Chronic Kidney Disease (KNOW-CKD) is a nationwide prospective cohort study involving nine tertiary-care general hospitals in Korea (NCT01630486 at http://www.clinicaltrials.gov) (22). Korean patients with CKD from stage 1 to predialysis stage 5, who voluntarily provided informed consent were enrolled, according to the previously described inclusion and exclusion criteria (22). This study was conducted following the principles of the Declaration of Helsinki, and the study protocol was approved by the institutional review boards of participating centers, including at the Seoul National University Hospital, the Yonsei University Severance Hospital, the Kangbuk Samsung Medical Center, the Seoul St. Mary's Hospital, the Gil Hospital, the Eulji General Hospital, the Chonnam National University Hospital, and the Busan Paik Hospital. A total of 2,238 subjects were longitudinally followed up (**Figure 1**). After excluding those lacking either the baseline or follow-up measurement of CACS, those lacking the baseline BW measurement, and those with the number of BW measurements during follow-up periods less than three times, 1,162 subjects were finally included for further analyses. The median follow-up duration was 6.940 years.

Data Collection

Demographic data, including age, gender, smoking history, medications (angiotensin-converting enzyme inhibitors and angiotensin receptor blockers (ACEi/ARBs), diuretics, number of antihypertensive drugs, and statins), and comorbid conditions, were collected at the time of screening. Anthropometric indices [height, weight, and systolic and diastolic blood pressures (SBP and DBP)] were also measured. Body mass index (BMI) was calculated as weight/height^2 (kg/m^2). Laboratory data included hemoglobin, creatinine, albumin, glucose, triglyceride, total cholesterol, low-density lipoprotein cholesterol, high-density lipoprotein cholesterol (HDL-C), 25-hydroxyvitamin D (25(OH) vitamin D), and high sensitive C-reactive protein (hs-CRP). Serum creatinine was measured by an isotope dilution mass spectrometry–traceable method, and estimated glomerular filtration rate was calculated by Chronic Kidney Disease Epidemiology Collaboration equation (23). CKD stages were determined by the Kidney Disease Improving Global Outcomes guidelines (24). Urine albumin-to-creatinine ratio (ACR) was measured in random, preferably first-voided, spot urine samples.

Determination of BWV

Body weight was measured at 0, 6, and 12 months and then yearly thereafter up to 8 years. The median number of BW measurements was seven times. Intra-individual visit-to-visit BWV is determined by average successive variability, defined as the average absolute difference between successive values (9, 14, 17, 25). The subjects were divided into the tertile by BWV, in which the 1st (T1), 2nd (T2), and 3rd (T3) tertiles were defined as low, moderate, and high BWV, respectively (**Figure 1**).

Estimation of the Rate of Longitudinal BW Change During Follow-Up Periods

The rate of longitudinal BW change for each individual was estimated using a regression model and expressed as the slope (%/year) (26). BW change less than 2.5%/year was defined as non-significant BW gain or loss (26) (**Supplementary Table S1**).

Measurement of CACS and Study Outcome

Electrocardiography-gated coronary multidetector CT scans were checked following the standard protocol of each center

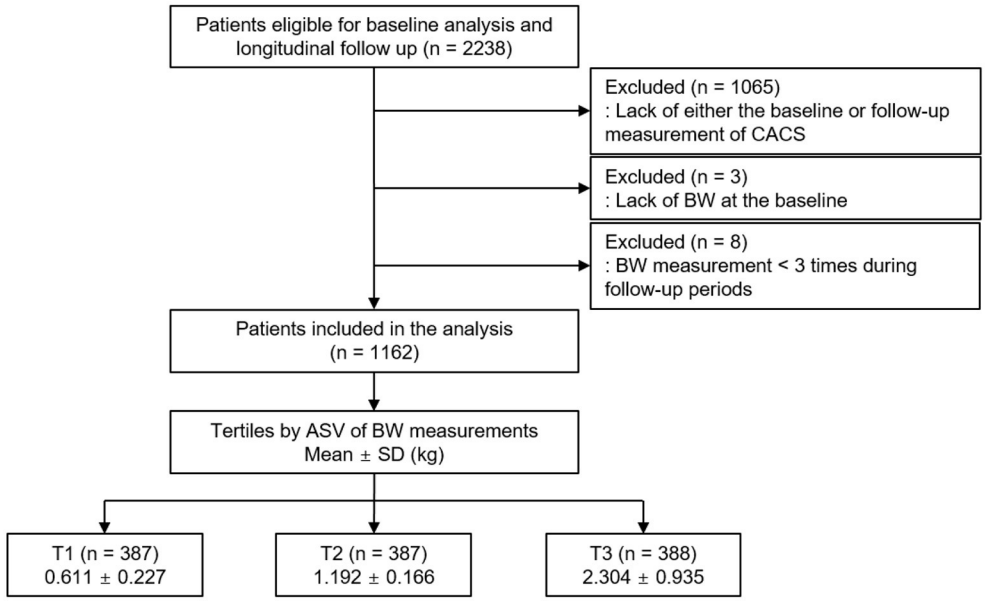

FIGURE 1 | Flow diagram of the study participants. ASV, average successive variability; BW, body weight; CACS, coronary artery calcium score; T1, 1st tertile; T2, 2nd tertile; T3, 3rd tertile.

at the baseline and year four follow-up visit. The CACS score was determined using the Agatston unit (AU) on a digital radiologic workstation (27). Rapid progression of coronary artery calcification was defined as an increase in coronary artery calcium score (CACS) more than 200 AU during a 4-year follow-up (28).

Statistical Analysis

Continuous variables were expressed as mean ± SD or median [interquartile range]. Categorical variables were expressed as the number of participants and percentage. For descriptive analyses, the Student's *t*-test or one-way ANOVA and the chi-squared test were used for continuous and categorical variables, respectively. A binary logistic regression model was analyzed to address an independent association between BWV and rapid progression of CAC, multivariate logistic regression models were analyzed. The models were adjusted for age, gender, Charlson comorbidity index, smoking history, BMI, SBP, DBP, medications (ACEi/ARBs, diuretics, total number of antihypertensive drugs, and statins), hemoglobin, albumin, HDL-C, fasting glucose, hs-CRP, 25(OH) vitamin D levels, eGFR, spot urine ACR, and baseline CACS. The results of binary logistic regression analysis were presented as odds ratios (ORs) and 95% CI. Restricted cubic splines were used to visualize the association between serum adiponectin as a continuous variable and the OR for fatal and nonfatal CV events or all-cause mortality. For sensitivity analysis, first, multivariate linear regression analysis was performed to test the linear association of BWV and CACS change during follow-up periods. Second, those with CACS < 10 AU at the baseline were excluded for binary logistic regression analysis, as the progression of CAC in the subjects was relatively rare (29). Third, as we assumed that the BWV may be exaggerated in advanced CKD, those with CKD stages 4 and 5 at the baseline were excluded for binary logistic regression analysis. Finally, to examine the clinical significance of BWV that is distinctive from longitudinal BW change, those without significant BW gain or loss during follow-up periods were excluded for binary logistic regression analysis. The results of multivariate linear regression analysis were presented as β coefficient and 95% CI. Two-sided $P < 0.05$ were considered statistically significant. Statistical analysis was performed using SPSS for Windows version 22.0 (IBM Corp., Armonk, NY, USA).

RESULTS

Baseline Characteristics

The baseline characteristics of study participants in the tertile by BWV are described in **Table 1**. The mean age, the frequency of male gender, and the burden of comorbid conditions significantly increased as BWV increased. Accordingly, the frequency of the subjects with a history of DM and the subjects on medication of no less than three antihypertensive drugs increased as BWV increased. All the other demographic data and medical history did not differ significantly across the groups. BMI also increased as BWV increased. SBP and DBP were not significantly different among the groups. Serum albumin, triglyceride, and fasting glucose levels increased as BWV increased. In contrast, HDL-C and 25(OH) vitamin D levels decreased as BWV increased. The other laboratory findings, such as spot urine ACR and eGFR, were not significantly different among the tertile groups.

Association of BWV and Rapid Progression of CAC in Patients With Predialysis CKD

To compare the CACS by BWV, a one-way ANOVA was performed (**Figure 2**). CACS at the baseline (**Figure 2A**) was

TABLE 1 | Baseline characteristics of study participants in the tertile by BWV.

	BWV			
	T1	**T2**	**T3**	***P*-value**
Follow-up duration (year)	6.466 ± 1.450	6.569 ± 1.413	6.466 ± 1.450	0.594
CACS (AU)				0.804
0	216 (55.8)	198 (51.2)	204 (52.6)	
0 <, ≤ 400	178 (38.2)	157 (40.6)	155 (39.9)	
400 <, ≤ 1000	14 (3.6)	22 (5.7)	20 (5.2)	
1,000 <	9 (2.3)	10 (2.6)	9 (2.3)	
Age (year)	54.065 ± 10.334	53.390 ± 11.171	50.353 ± 13.246	< 0.001
Male	208 (53.7)	229 (59.2)	253 (65.2)	0.005
Charlson comorbidity index				0.007
0–3	340 (87.9)	312 (80.6)	304 (78.4)	
4–5	44 (11.4)	73 (18.9)	81 (20.9)	
6–7	3 (0.8)	2 (0.5)	3 (0.8)	
DM	72 (18.6)	107 (27.6)	121 (31.2)	0.001
CAD	2 (0.5)	9 (2.3)	10 (2.6)	0.162
Arrhythmia	8 (2.1)	3 (0.8)	4 (1.0)	0.426
Medication				
ACEi/ARBs	336 (86.8)	344 (88.9)	327 (84.3)	0.167
Diuretics	91 (23.5)	91 (23.5)	108 (27.8)	0.276
Number of anti-HTN drugs ≥ 3	78 (20.2)	81 (20.9)	111 (28.6)	0.009
Statins	204 (52.7)	192 (49.6)	186 (47.9)	0.403
BMI (kg/m^2)	23.788 ± 2.2924	24.363 ± 3.058	25.616 ± 3.746	< 0.001
SBP (mmHg)	125.295 ± 14.014	125.645 ± 14.326	126.894 ± 15.551	0.279
DBP (mmHg)	77.220 ± 9.984	76.259 ± 10.358	77.090 ± 10.766	0.377
Laboratory findings				
Hemoglobin (g/dl)	13.261 ± 1.664	13.414 ± 1.887	13.408 ± 1.946	0.429
Albumin (g/dl)	4.226 ± 0.333	4.273 ± 0.335	4.296 ± 0.363	0.016
Total cholesterol (mg/dl)	174.434 ± 35.000	174.179 ± 36.672	175.917 ± 35.720	0.768
HDL-C (mg/dl)	52.278 ± 15.914	51.237 ± 15.047	48.970 ± 14.017	0.008
LDL-C (mg/dl)	95.937 ± 29.055	96.560 ± 30.792	98.829 ± 30.224	0.375
TG (mg/dl)	142.621 ± 91.443	151.832 ± 91.224	162.992 ± 101.510	0.013
Fasting glucose (mg/dl)	102.632 ± 25.048	109.135 ± 33.699	108.190 ± 31.623	0.006
25(OH) vitamin D	18.835 ± 7.286	18.854 ± 7.712	17.180 ± 6.765	0.001
hsCRP (mg/dl)	0.600 [0.200, 1.400]	0.510 [0.200, 1.400]	0.700 [0.200, 1.900]	0.809
Spot urine ACR (mg/gCr)	245.079 [42.450, 616.708]	217.470 [34.877, 597.054]	241.744 [56.312, 625.118]	0.623
eGFR (ml/min./1.73 m^2)	57.441 ± 27.405	59.227 ± 28.337	61.375 ± 30.714	0.165
CKD stages				0.167
Stage 1	72 (18.6)	79 (20.4)	100 (25.8)	
Stage 2	96 (24.8)	101 (26.1)	97 (25.0)	
Stage 3a	84 (21.7)	78 (20.2)	63 (16.2)	
Stage 3b	91 (23.5)	88 (22.7)	79 (20.4)	
Stage 4	41 (10.6)	41 (10.6)	44 (11.3)	
Stage 5	3 (0.8)	0 (0.0)	5 (1.3)	

Values for categorical variables are given as number (percentage); values for continuous variables, as mean ± SD or median (interquartile range).
ACEi, angiotensin-converting enzyme inhibitor; ACR, albumin-to-creatinine ratio; ARB, angiotensin receptor blocker; AU, Agatston unit; BMI, body mass index; BWV, body weight variability; CACS, coronary artery calcium score; CAD, coronary artery disease; CKD, chronic kidney disease; Cr, creatinine; DBP, diastolic blood pressure; DM, diabetes mellitus; eGFR, estimated glomerular filtration rate; HDL-C, high density lipoprotein cholesterol; hs-CRP, high-sensitivity C-reactive protein; HTN, hypertension; LDL-C, low-density lipoprotein cholesterol; SBP, systolic blood pressure; T1, 1st tertile; T2, 2nd tertile; T3, 3rd tertile; TG, triglyceride; 25(OH) vitamin D, 25-hydroxyvitamin D.

not significantly different among the groups. Although CACS at 4-year follow-up (**Figure 2B**) was not significantly different among the groups either, CACS at 4-year follow-up gradually increased as BWV increased. Importantly, the change of CACS during the 4-year follow-up period in subjects with high BWV (T2) was significantly larger than that in subjects with low

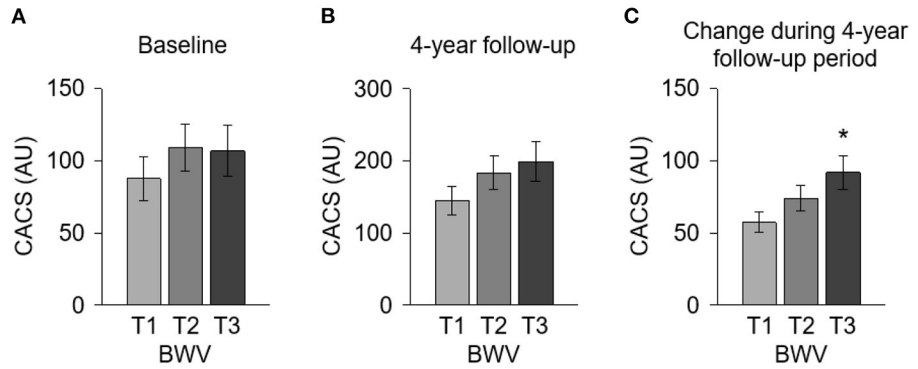

FIGURE 2 | Comparison of the CACS at the baseline and at 4-year follow-up and the CACS change during 4-year follow-up period by BWV. CACS at the baseline **(A)** and at 4-year follow-up **(B)** and the CACS change during the 4-year follow-up period **(C)** were compared by BWV. *$P < 0.05$ vs. T1 by one-way ANOVA with Scheffe's *post-hoc* test. Error bars indicate SE of means. AU, Agatston unit; BWV, body weight variability; CACS, coronary artery calcium score; T1, 1st tertile; T2, 2nd tertile; T3, 3rd tertile.

TABLE 2 | Binary logistic regression of BWV for rapid progression of CAC.

	Unadjusted		Adjusted	
	OR (95%CIs)	***P*-value**	**OR (95%CIs)**	***P*-value**
BWV, T1	Reference		Reference	
BWV, T2	2.021 (1.194, 3.422)	0.009	2.118 (1.075, 4.175)	0.030
BWV, T3	2.121 (1.259, 3.572)	0.005	2.602 (1.304, 5.191)	0.007

Models were adjusted for age, gender, Charlson comorbidity index, smoking history, BMI, SBP, DBP, medication (ACEi/ARBs, diuretics, number of antihypertensive drugs, statins), hemoglobin, albumin, HDL-C, fasting serum glucose, 25(OH) vitamin D, hs-CRP, eGFR, spot urine ACR, and baseline CACS.
BWV, body weight variability; OR, odds ratio; T1, 1st tertile; T2, 2nd tertile; T3, 3rd tertile.

BWV (T1) (**Figure 2C**). The proportion of the subjects with rapid progression of CAC during the 4-year follow-up period also increased as BWV increased (**Supplementary Figure S1**). To determine the independent association of BWV with the rapid progression of CAC, a binary logistic regression model was analyzed (**Table 2**). Compared to low BWV (T1), both moderate (T2, adjusted OR 2.118, 95% CI 1.075–4.175) and high (T3, adjusted OR 2.602, 95% CI 1.304–5.191) BWV was associated with a significantly increased risk of rapid progression of CAC. Restricted cubic spine depicted that adjusted (**Figure 2B**) OR for rapid progression of CAC is positively correlated with BWV (**Figure 3**).

Sensitivity Analysis

To test the linear association of BWV and CACS change during follow-up periods, multivariate linear regression models were analyzed (**Supplementary Table S2**). The analysis of all subjects revealed that BWV is linearly associated with CACS change during the 4-year follow-up period (adjusted β coefficient 12.098, 95% CI 1.807–22.389). Next, as the progression of CAC is dependent on the baseline CAC status, the subjects with CACS < 10 AU at the baseline ($n = 764$) were excluded for binary logistic regression analysis (**Supplementary Table S3**). Despite the substantial reduction of the number of subjects being analyzed, the analysis revealed a robust association between BWV and rapid progression of CAC (T2, adjusted OR 2.331, 95% CI 1.151–4.718; T3, adjusted OR 2.380, 95% CI 1.148–4.932). In addition, based on the assumption that BWV may be exaggerated in advanced CKD, those with CKD stages 4 and 5 at the baseline ($n = 134$) were excluded for binary logistic regression analysis (**Supplementary Table S4**). The analysis demonstrated a significant association between BWV and the rapid progression of CAC among the subjects with eGFR $\geq$ 30 ml/min/1.73 m^2 (T2, adjusted OR 2.291, 95% CI 1.078–4.867; T3, adjusted OR 3.328, 95% CI 1.529–7.242). Finally, to prove the clinical significance of BWV that is distinctive from longitudinal BW change, those without significant BW gain or loss during follow-up periods ($n = 69$) were excluded for binary logistic regression analysis (**Table 3**). The analysis reproduced a robust association between BWV and rapid progression of CAC among the subjects without significant BW gain or loss during follow-up periods (T2, adjusted OR 2.007, 95% CI 1.011–3.984; T3, adjusted OR 2.054, 95% CI 1.003–4.207).

Subgroup Analysis

To figure out whether the association of BWV with the rapid progression of CAC is modified in various clinical contexts, we conducted subgroup analyses. The subgroups were stratified by age (< 60 or ≥ 60 years), gender (male or female), Charlson comorbidity index (≤ 3 or ≥ 4), history of DM (without or with), eGFR (≥ 60 or < 60 ml/min/1.73 m^2), spot urine ACR (< 300 or ≥ 300 mg/g). Binary logistic analyses revealed that P for interactions was > 0.05 for all subgroups (**Table 4**). Linear regression analysis revealed the association is marginally more significant in those with Charlson comorbidity index ≥ 4 than in those with Charlson comorbidity index ≤ 3 (P for interaction $= 0.04$) (**Supplementary Table S2**). Age, gender, history of DM, eGFR, and albuminuria did not alter the association between BWV and rapid progression of CAC.

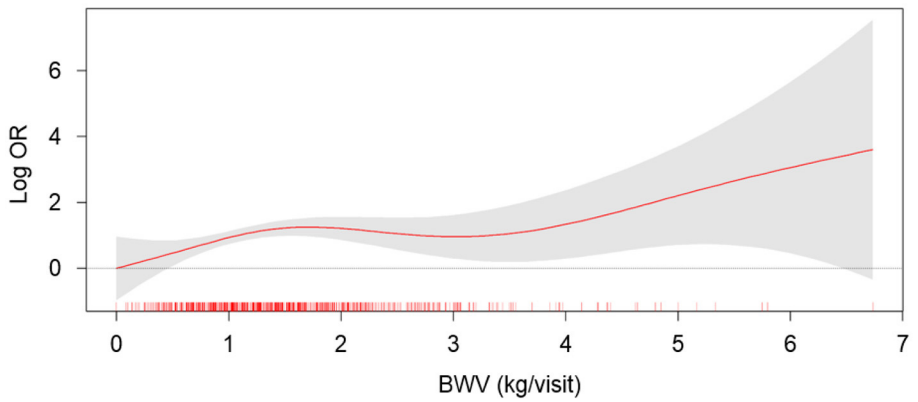

FIGURE 3 | The restricted cubic spline of BWV on the risk of rapid progression of CAC. Adjusted OR of BWV as a continuous variable for the risk of rapid progression of CAC is depicted. The model was adjusted for age, gender, Charlson comorbidity index, smoking history, BMI, SBP, DBP, medication (ACEi/ARBs, diuretics, number of antihypertensive drugs, statins), hemoglobin, albumin, HDL-C, fasting serum glucose, 25(OH) vitamin D, hs-CRP, eGFR, spot urine ACR, and baseline CACS. BWV, body weight variability; OR, odds ratio.

TABLE 3 | Binary logistic regression of BWV for rapid progression of CAC in subjects with BW maintenance during follow-up periods.

	Unadjusted		Adjusted	
	OR (95%CIs)	***P*-value**	**OR (95%CIs)**	***P*-value**
BWV, T1	Reference		Reference	
BWV, T2	1.925 (1.130, 3.280)	0.016	2.007 (1.011, 3.984)	0.046
BWV, T3	1.910 (1.110, 3.287)	0.019	2.054 (1.003, 4.207)	0.049

Models were adjusted for age, gender, Charlson comorbidity index, smoking history, BMI, SBP, DBP, medication (ACEi/ARBs, diuretics, number of antihypertensive drugs, statins), hemoglobin, albumin, HDL-C, fasting serum glucose, 25(OH) vitamin D, hs-CRP, eGFR, spot urine ACR, and baseline CACS.
BWV, body weight variability; OR, odds ratio; T1, 1st tertile; T2, 2nd tertile; T3, 3rd tertile.

DISCUSSION

In this study, we discovered that high BWV is independently associated with the rapid progression of CAC in patients with predialysis CKD. Importantly, the association between BWV and progression of CAC remains robust even among the subjects without significant BW gain or loss during follow-up periods.

Following a recent report that high BWV is associated with adverse CV outcomes in patients with predialysis CKD (18), we here suggest a rationale for the previous finding. Although BWV is associated with CV outcomes in patients with CAD (17), any direct evidence for the association between BWV and progression of CAC in patients with predialysis CKD has not been presented yet. On the other hand, compared to the patients with end-stage renal disease (ESRD), especially those under maintenance hemodialysis, the degree of BWV should be modest in patients with predialysis CKD. Intriguingly, the progression of CAC in patients with ESRD is altered by the modality of renal replacement therapy (30). A recent observational study reported that peritoneal dialysis is not associated with CAC or is associated with less CAC progression than hemodialysis (30). Provided that BWV is inevitable in most patients on hemodialysis, rather than in patients on peritoneal dialysis, primarily due to the discontinuous nature of hemodialysis leading to saw-tooth volume fluctuations (31), it is speculated that BWV may also be representative of ongoing CAC progression in patients with ESRD. Collectively, our finding expands the clinical significance of BWV as an indicator of underlying CAD in patients with predialysis CKD, which is in line with the findings both from the subjects without CKD and from the subjects with ESRD.

We are not able to present a precise mechanism of the association of BWV with the progression of CAC even in patients without significant longitudinal BW changes. One possible explanation is that BWV might be a mixed phenotype of the processes that facilitate BW gain and BW loss. As the accumulation of extracellular fluid and malnutrition-inflammation are not mutually exclusive, both of which is associated with CAC progression (1, 5, 6), a longitudinal trend of BW change may be masked if those processes concurrently take place. Therefore, a potential strength of BWV over longitudinal BW change may be a sensitive detection of vulnerable subjects who are at high risk of CAC progression, although the precise mechanism of the association of BWV with the progression of CAC should be further elucidated.

LIMITATIONS

There are a number of limitations to this study. First, we were not able to determine the causal relationship between high BWV and progression of CAC, because of the observational nature of the current study. In addition, BWV was calculated from the data up to 8 years, while CACS was collected at the baseline and 4-year follow-up. Due to the limitation of the study design, it is also possible that CAC progression might promote BW fluctuation. A more focused study should evaluate the causal relation between BWV and the progression of CAC. Second, despite the clear association of high BWV with the progression of CAC, the precise mechanism should be further clarified. Third,

TABLE 4 | Binary logistic regression of BWV for rapid progression of CAC in various subgroups.

		Unadjusted OR (95%CIs)	*P* for interaction	Adjusted OR (95%CIs)	*P* for interaction
Age < 60 years	BWV, T1	Reference	0.172	Reference	0.176
	BWV, T2	1.461 (0.663, 3.220)		1.224 (0.330, 4.533)	
	BWV, T3	1.400 (0.642, 3.053)		1.445 (0.347, 6.007)	
Age ≥ 60 years	BWV, T1	Reference		Reference	
	BWV, T2	2.676 (1.283, 5.578)		3.167 (1.237, 8.104)	
	BWV, T3	3.696 (1.767, 7.730)		4.462 (1.729, 11.517)	
Male	BWV, T1	Reference	0.435	Reference	0.719
	BWV, T2	1.674 (0.918, 3.055)		2.193 (0.996, 4.830)	
	BWV, T3	1.590 (0.880, 2.871)		2.395 (1.068, 5.371)	
Female	BWV, T1	Reference		Reference	
	BWV, T2	3.184 (0.991, 10.235)		2.428 (0.293, 20.118)	
	BWV, T3	3.748 (1.163, 12.073)		10.033 (1.088, 92.508)	
Charlson comorbidity index ≤ 3	BWV, T1	Reference	0.858	Reference	0.582
	BWV, T2	0.812 (0.297, 2.221)		1.091 (0.223, 5.343)	
	BWV, T3	0.767 (0.281, 2.097)		1.906 (0.396, 9.163)	
Charlson comorbidity index ≥ 4	BWV, T1	Reference		Reference	
	BWV, T2	2.741 (1.400, 5.370)		2.690 (1.181, 6.129)	
	BWV, T3	3.180 (1.629, 6.209)		3.216 (1.384, 7.476)	
DM (-)	BWV, T1	Reference	0.877	Reference	0.459
	BWV, T2	1.316 (0.579, 2.995)		1.709 (0.527, 5.538)	
	BWV, T3	1.345 (0.591, 3.060)		1.786 (0.521, 6.128)	
DM (+)	BWV, T1	Reference		Reference	
	BWV, T2	1.990 (0.933, 4.246)		2.235 (0.868, 5.756)	
	BWV, T3	1.894 (0.898, 3.994)		2.398 (0.928, 6.194)	
eGFR ≥ 45 ml/min./1.73 m^2	BWV, T1	Reference	0.743	Reference	0.970
	BWV, T2	1.742 (0.836, 3.631)		1.730 (0.687, 4.359)	
	BWV, T3	2.106 (1.036, 4.284)		2.513 (0.985, 6.411)	
eGFR < 45 ml/min./1.73 m^2	BWV, T1	Reference		Reference	
	BWV, T2	2.440 (1.134, 5.251)		3.071 (1.022, 9.225)	
	BWV, T3	2.237 (1.029, 4.859)		2.769 (0.895, 8.568)	
Spot urine ACR < 300 mg/g	BWV, T1	Reference	0.081	Reference	0.151
	BWV, T2	1.011 (0.469, 2.180)		1.245 (0.461, 3.365)	
	BWV, T3	1.604 (0.791, 3.254)		2.461 (0.911, 6.652)	
Spot urine ACR ≥ 300 mg/g	BWV, T1	Reference		Reference	
	BWV, T2	3.672 (1.679, 8.031)		2.633 (0.928, 7.470)	
	BWV, T3	2.846 (1.289, 6.282)		2.606 (0.895, 7.589)	

Models were adjusted for age, gender, Charlson comorbidity index, smoking history, BMI, SBP, DBP, medication (ACEi/ARBs, diuretics, number of antihypertensive drugs, statins), hemoglobin, albumin, HDL-C, fasting serum glucose, 25(OH) vitamin D, hs-CRP, eGFR, spot urine ACR, and baseline CACS.
ACR, albumin-to-creatinine ratio; BMI, body mass index; DM, diabetes mellitus; eGFR, estimated glomerular filtration rate, OR, odd ratio; T1, 1st tertile; T2, 2nd tertile; T3, 3rd tertile.

although accumulation and removal of excess fluid have been suggested as a mechanism to explain BWV in the current study, the other cause, such as diet and physical activity, should also be considered, as BW was measured as long as every 12 months. Fourth, as this cohort study enrolled only ethnic Koreans, a precaution is required to extrapolate the data in this study to other populations.

CONCLUSION

In conclusion, we report that high BWV is independently associated with the rapid progression of CAC in patients with predialysis CKD. Our results suggest that the association between BWV and progression of CAC remains robust even among the subjects without significant BW gain or loss during follow-up periods.

DATA AVAILABILITY STATEMENT

The raw data supporting the conclusions of this article will be made available by the authors, without undue reservation.

ETHICS STATEMENT

The study was conducted in accordance with the principles of the Declaration of Helsinki, and the study protocol was approved by the institutional review boards of participating centers, including at Seoul National University Hospital, Yonsei University Severance Hospital, Kangbuk Samsung Medical Center, Seoul St. Mary's Hospital, Gil Hospital, Eulji General Hospital, Chonnam National University Hospital, and Pusan Paik Hospital. The patients/participants provided their written informed consent to participate in this study.

AUTHOR CONTRIBUTIONS

SS designed and helped in the data analysis and manuscript writing. SS, TO, and HC contributed to the conception of the study. SS and CK performed the data analyses and wrote the manuscript. EB, K-HO, K-BL, SH, and SS collected the data. SM and SK helped perform the analysis with constructive discussions. All authors contributed to the article and approved the submitted version.

FUNDING

This study was supported by the Research Program funded by the Korea Centers for Disease Control and Prevention (2011E3300300, 2012E3301100, 2013E3301600, 2013E3301601, 2013E3301602, 2016E3300200, 2016E3300201, 2016E3300202, and 2019E320100) and by the National Research Foundation of Korea (NRF) funded by the Korea Government (MSIT) (NRF-2019R1A2C2086276).

SUPPLEMENTARY MATERIAL

The Supplementary Material for this article can be found online at: https://www.frontiersin.org/articles/10.3389/fcvm.2021.794957/full#supplementary-material

REFERENCES

1. Park S, Lee CJ, Jhee JH, Yun HR, Kim H, Jung SY, et al. Extracellular Fluid Excess Is Significantly Associated With Coronary Artery Calcification in Patients With Chronic Kidney Disease. *J Am Heart Assoc.* (2018) 7:e008935. doi: 10.1161/JAHA.118.008935
2. Essig M, Escoubet B, De Zuttere D, Blanchet F, Arnoult F, Dupuis E, et al. Cardiovascular remodelling and extracellular fluid excess in early stages of chronic kidney disease. *Nephrol Dial Transplant.* (2008) 23:239–48. doi: 10.1093/ndt/gfm542
3. Tai R, Ohashi Y, Mizuiri S, Aikawa A, Sakai K. Association between ratio of measured extracellular volume to expected body fluid volume and renal outcomes in patients with chronic kidney disease: a retrospective single-center cohort study. *BMC Nephrol.* (2014) 15:189. doi: 10.1186/1471-2369-15-189
4. Kim YJ, Jeon HJ, Kim YH, Jeon J, Ham YR, Chung S, et al. Overhydration measured by bioimpedance analysis and the survival of patients on maintenance hemodialysis: a single-center study. *Kidney Res Clin Pract.* (2015) 34:212–8. doi: 10.1016/j.krcp.2015.10.006
5. Zha Y, Qian Q. Protein nutrition and malnutrition in CKD and ESRD. *Nutrients.* (2017) 9. doi: 10.3390/nu9030208
6. Hanna RM, Ghobry L, Wassef O, Rhee CM, Kalantar-Zadeh K. A practical approach to nutrition, protein-energy wasting, sarcopenia, and cachexia in patients with chronic kidney disease. *Blood Purif.* (2020) 49:202–11. doi: 10.1159/000504240
7. Jagadeswaran D, Indhumathi E, Hemamalini AJ, Sivakumar V, Soundararajan P, Jayakumar M. Inflammation and nutritional status assessment by malnutrition inflammation score and its outcome in pre-dialysis chronic kidney disease patients. *Clin Nutr.* (2019) 38:341–7. doi: 10.1016/j.clnu.2018.01.001
8. Khan YH, Sarriff A, Adnan AS, Khan AH, Mallhi TH. Diuretics prescribing in chronic kidney disease patients: physician assessment versus bioimpedence spectroscopy. *Clin Exp Nephrol.* (2017) 21:488–96. doi: 10.1007/s10157-016-1303-7
9. Oh TJ, Moon JH, Choi SH, Lim S, Park KS, Cho NH, et al. Body-weight fluctuation and incident diabetes mellitus, cardiovascular disease, and mortality: a 16-year prospective cohort study. *J Clin Endocrinol Metab.* (2019) 104:639–46. doi: 10.1210/jc.2018-01239
10. Cai X, Qiu S, Liu S, Lu Y, Luo D, Li R, et al. Body-weight fluctuation and risk of diabetes in older adults: the China health and retirement longitudinal study (CHARLS). *Diabetes Res Clin Pract.* (2020) 169:108419. doi: 10.1016/j.diabres.2020.108419
11. Cologne J, Takahashi I, French B, Nanri A, Misumi M, Sadakane A, et al. Association of weight fluctuation with mortality in Japanese adults. *JAMA Netw Open.* (2019) 2:e190731. doi: 10.1001/jamanetworkopen.2019.0731
12. Lissner L, Odell PM, D'agostino RB, Stokes J 3rd, Kreger BE, Belanger AJ, et al. Variability of body weight and health outcomes in the Framingham population. *N Engl J Med.* (1991) 324:1839–44. doi: 10.1056/NEJM199106273242602
13. Zhang Y, Hou F, Li J, Yu H, Li L, Hu S, et al. The association between weight fluctuation and all-cause mortality: a systematic review and meta-analysis. *Medicine.* (2019) 98:e17513. doi: 10.1097/MD.0000000000017513
14. Bangalore S, Fayyad R, Demicco DA, Colhoun HM, Waters DD. Body weight variability and cardiovascular outcomes in patients with type 2 diabetes mellitus. *Circ Cardiovasc Qual Outcomes.* (2018) 11:e004724. doi: 10.1161/CIRCOUTCOMES.118.004724
15. Yeboah P, Hsu FC, Bertoni AG, Yeboah J. Body mass index, change in weight, body weight variability and outcomes in type 2 diabetes mellitus (from the ACCORD Trial). *Am J Cardiol.* (2019) 123:576–81. doi: 10.1016/j.amjcard.2018.11.016
16. Nam GE, Kim W, Han K, Lee CW, Kwon Y, Han B, et al. Body weight variability and the risk of cardiovascular outcomes and mortality in patients with type 2 diabetes: a nationwide cohort study. *Diabetes Care.* (2020) 43:2234–41. doi: 10.2337/dc19-2552
17. Bangalore S, Fayyad R, Laskey R, Demicco DA, Messerli FH, Waters DD. Body-weight fluctuations and outcomes in coronary disease. *N Engl J Med.* (2017) 376:1332–40. doi: 10.1056/NEJMoa1606148
18. Suh SH, Oh TR, Choi HS, Kim CS, Bae EH, Park SK, et al. Association of body weight variability with adverse cardiovascular outcomes in patients with pre-dialysis chronic kidney disease. *Nutrients.* (2021) 13:3381. doi: 10.3390/nu13103381
19. Wang XR, Zhang JJ, Xu XX, Wu YG. Prevalence of coronary artery calcification and its association with mortality, cardiovascular events in patients with chronic kidney disease: a systematic review and meta-analysis. *Ren Fail.* (2019) 41:244–56. doi: 10.1080/0886022X.2019.1595646
20. Sarnak MJ, Levey AS, Schoolwerth AC, Coresh J, Culleton B, Hamm LL, et al. Kidney disease as a risk factor for development of cardiovascular disease: a statement from the American heart association councils on kidney in cardiovascular disease, high blood pressure research, clinical cardiology, and epidemiology and prevention. *Circulation.* (2003) 108:2154–69. doi: 10.1161/01.CIR.0000095676.90936.80
21. Collins AJ, Foley RN, Chavers B, Gilbertson D, Herzog C, Johansen K, et al. 'United States renal data system 2011 annual data report: atlas of chronic

kidney disease and end-stage renal disease in the United States. *Am J Kidney Dis.* (2012) 59:e1–420. doi: 10.1053/j.ajkd.2011.11.015
22. Oh KH, Park SK, Park HC, Chin HJ, Chae DW, Choi KH, et al. KNOW-CKD (KoreaN cohort study for outcome in patients with chronic kidney disease): design and methods. *BMC Nephrol.* (2014) 15:80. doi: 10.1186/1471-2369-15-80
23. Levey AS, Stevens LA, Schmid CH, Zhang YL, Castro AF 3rd, Feldman HI, et al. A new equation to estimate glomerular filtration rate. *Ann Intern Med.* (2009) 150:604–12. doi: 10.7326/0003-4819-150-9-200905050-00006
24. Chapter 1: definition and classification of CKD. *Kidney Int Suppl.* (2013) 3:19–62. doi: 10.1038/kisup.2012.64
25. Park KY, Hwang HS, Cho KH, Han K, Nam GE, Kim YH, et al. Body weight fluctuation as a risk factor for type 2 diabetes: results from a nationwide cohort study. *J Clin Med.* (2019) 8. doi: 10.3390/jcm8070950
26. Ryu H, Hong Y, Kang E, Kang M, Kim J, Oh YK, et al. Rapid weight change over time is a risk factor for adverse outcomes in patients with predialysis chronic kidney disease: a prospective cohort study. *J Ren Nutr.* (2021) 31:569–78. doi: 10.1053/j.jrn.2021.01.026
27. Agatston AS, Janowitz WR, Hildner FJ, Zusmer NR, Viamonte MJr, Detrano R. Quantification of coronary artery calcium using ultrafast computed tomography. *J Am Coll Cardiol.* (1990) 15:827–32. doi: 10.1016/0735-1097(90)90282-T
28. Jung CY, Heo GY, Park JT, Joo YS, Kim HW, Lim H, et al. Sex disparities and adverse cardiovascular and kidney outcomes in patients with chronic kidney disease: results from the KNOW-CKD. *Clin Res Cardiol.* (2021) 110:1116–27. doi: 10.1007/s00392-021-01872-5
29. Lee MJ, Park JT, Park KS, Kwon YE, Han SH, Kang SW, et al. Normal body mass index with central obesity has increased risk of coronary artery calcification in Korean patients with chronic kidney disease. *Kidney Int.* (2016) 90:1368–76. doi: 10.1016/j.kint.2016.09.011
30. Jansz TT, Van Reekum FE, Ozyilmaz A, De Jong PA, Boereboom FTJ, Hoekstra T, et al. Coronary artery calcification in hemodialysis and peritoneal dialysis. *Am J Nephrol.* (2018) 48:369–77. doi: 10.1159/000494665
31. Charra B. Fluid balance, dry weight, and blood pressure in dialysis. *Hemodial Int.* (2007) 11:21–31. doi: 10.1111/j.1542-4758.2007.00148.x

Conflict of Interest: The authors declare that the research was conducted in the absence of any commercial or financial relationships that could be construed as a potential conflict of interest.

frontiers in Cardiovascular Medicine

ORIGINAL RESEARCH
published: 03 February 2022
doi: 10.3389/fcvm.2022.799446

Computed-Tomography as First-line Diagnostic Procedure in Patients With Out-of-Hospital Cardiac Arrest

John Adel[1†], *Muharrem Akin*[1*†], *Vera Garcheva*[1], *Jens Vogel-Claussen*[2], *Johann Bauersachs*[1], *L. Christian Napp*[1] *and Andreas Schäfer*[1]

[1] *Department of Cardiology and Angiology, Cardiac Arrest Centre, Hannover Medical School, Hannover, Germany,*
[2] *Department of Diagnostic and Interventional Radiology, Hannover Medical School, Hannover, Germany*

OPEN ACCESS

Edited by:
Robert Murray Hamilton, Hospital for Sick Children, Canada

Reviewed by:
Philipp Diehl, University Heart Center Freiburg, Germany
Christoph Sinning, University Medical Center Hamburg-Eppendorf, Germany

***Correspondence:**
Muharrem Akin
akin.muharrem@mh-hannover.de

†These authors have contributed equally to this work and share first authorship

Specialty section:
This article was submitted to General Cardiovascular Medicine, a section of the journal Frontiers in Cardiovascular Medicine

Received: *21 October 2021*
Accepted: *06 January 2022*
Published: *03 February 2022*

Citation:
Adel J, Akin M, Garcheva V, Vogel-Claussen J, Bauersachs J, Napp LC and Schäfer A (2022) Computed-Tomography as First-line Diagnostic Procedure in Patients With Out-of-Hospital Cardiac Arrest. Front. Cardiovasc. Med. 9:799446. doi: 10.3389/fcvm.2022.799446

Background: Mortality after out-of-hospital cardiac arrest (OHCA) with return of spontaneous circulation (ROSC) remains high despite numerous efforts to improve outcome. For patients with suspected coronary cause of arrest, coronary angiography is crucial. However, there are other causes and potentially life-threatening injuries related to cardiopulmonary resuscitation (CPR), which can be detected by routine computed tomography (CT).

Materials and Methods: At Hannover Medical School, rapid coronary angiography and CT are performed in successfully resuscitated OHCA patients as a standard of care prior to admission to intensive care. We analyzed all patients who received CT following OHCA with ROSC over a three-year period.

Results: There were 225 consecutive patients with return of spontaneous circulation following out-of-hospital cardiac arrest. Mean age was 64 ± 13 years, 75% were male. Of them, 174 (77%) had witnessed arrest, 145 (64%) received bystander CPR, and 123 (55%) had a primary shockable rhythm. Mean time to ROSC was 24 ± 20 min. There were no significant differences in CT pathologies in patients with or without ST-segment elevations in the initial ECG. Critical CT findings qualifying as a potential cause for cardiac arrest were intracranial bleeding ($N = 6$), aortic dissection ($N = 5$), pulmonary embolism ($N = 17$), pericardial tamponade ($N = 3$), and tension pneumothorax ($N = 11$). Other pathologies were regarded as consequences of CPR and relevant for further treatment: aspiration ($N = 62$), rib fractures ($N = 161$), sternal fractures ($N = 50$), spinal fractures ($N = 11$), hepatic bleeding ($N = 12$), and intra-abdominal air ($N = 3$).

Conclusion: Early CT fallowing OHCA uncovers a high number of causes and consequences of OHCA and CPR. Those are relevant for post-arrest care and are frequently life-threatening, suggesting that CT can contribute to improving prognosis following OHCA.

Keywords: intensive care, computed tomography, out-of-hospital cardiac arrest, resuscitation, post-resuscitation treatment, return of spontaneous circulation

INTRODUCTION

Out-of-hospital cardiac arrest (OHCA) remains a striking challenge for emergency and intensive care medicine, and constitutes one of the main causes of in-hospital mortality worldwide (1). More than 50% of OHCA cases are caused by coronary ischemia (1–4). In Europe, mortality rates after OHCA are highly variable between countries (5, 6). Overall mortality and neurologic outcome are determined by the cause of arrest and its management. Awareness for basic life support in the general population is extremely heterogeneous despite broad education programs and telephone-guided resuscitation instructions (5). While algorithms and standards of care for immediate life support are constantly progressing, in-hospital post-resuscitation care is still less standardized (7). Coronary angiography and percutaneous intervention have emerged as a central part of early in-hospital care following OHCA due to the high prevalence of myocardial infarction as cause of arrest (3, 4, 7). Urgent coronary angiography is recommended by the European Resuscitation Council (ERC) and European Society of Cardiology guidelines in case of return of spontaneous circulation (ROSC) with ST-elevation and in resuscitated patients without ST-elevation, if myocardial infarction is assumed (8, 9).

In addition to invasive assessments, an increasing number of cardiac arrest centers employ whole body computed tomography (CT) into their standard of care (10–12). However, these advanced diagnostics are not yet fully implemented as immediate post-resuscitation care by current guidelines (7, 13). The 2021 ERC guidelines recommend CT only in case of suspected non-cardiac cause of arrest or when no coronary cause of arrest could be identified during coronary angiography (7).

The Hannover Cardiac Resuscitation Algorithm (HaCRA) includes routine coronary angiography and CT immediately after hospital admission for OHCA as a standard of clinical care (14). Here, we report whether CT scans as a standard diagnostic procedure provided important additional information and improved diagnostic accuracy.

MATERIALS AND METHODS

Study Design

The HAnnover COoling REgistry -HACORE- is a prospective observational registry approved by the ethics committee at Hannover Medical School (#3567-2017) and is in accordance with the Declaration of Helsinki. HACORE includes all OHCA patients treated with therapeutic hypothermia at our institution (14).

Abbreviations: ACLS, Advanced cardiac life support; BLS, Basic life support; CPR, Cardiopulmonary resuscitation; CT, Computer tomography; ECG, Electrocardiogram; eCPR, extracorporeal cardiopulmonary resuscitation; HaCRA, Hannover Cardiac Resuscitation Algorithm; HACORE, Hannover Cooling Registry; ICU, Intensive care unit; LBBB, Left bundle branch block; MCS, Mechanic cardiac support; OHCA, Out- of- hospital cardiac arrest; PCI, Percutaneous coronary intervention; ROSC, Return of spontaneous circulation; STEMI, ST-elevation myocardial infraction.

Patient Population

From HACORE we identified all patients admitted to our center receiving immediate (<2 h after admission) CT as part of the HaCRA standard during a continuous three-year period prior to the COVID-19 pandemic (14).

Patients included were aged >18 years, had non-traumatic OHCA with successful ROSC either prior to admission or in the emergency room, 12-lead ECG following ROSC, and successful application of the HaCRA algorithm (**Figure 1**). Patients with refractory hemodynamic instability after OHCA were provided with eCPR at admission. Patients requiring early eCPR are associated with a relatively worse outcome due to their initial instability (15). In order to avoid bias by this particular collective, they were excluded from the present study. An ECG after ROSC suggestive for a coronary cause of arrest was defined by the presence of either ST-segment elevation/ depression or a new onset bundle branch block according to current guidelines (7). Written consent was obtained retrospectively by next of kin or, if not present, by legally authorized officials.

The Hannover Cardiac Resuscitation Algorithm

All patients were treated according to a local diagnostic and interventional standard procedure (14) (**Supplementary Figure 1**). In brief, the algorithm includes a multidisciplinary work-up of OHCA patients starting in the emergency room with immediate endotracheal airway management if not achieved before, continuation of mechanical CPR by an automated compression device in case of ongoing CPR, and early determination of cardiac function by transthoracic echocardiography in patients with ROSC. All patients without suspicion of obvious non-cardiac causes of arrest such as intracranial bleeding or massive pulmonary embolism were transferred to the catheterization laboratory. Diagnostic coronary angiography is performed irrespective of the presence or absence of ST-segment elevations in a 12-lead-ECG followed by revascularization of angiographically relevant coronary stenosis. In case of cardiogenic shock, complete revascularization was attempted at that time (16, 17) along with mechanical circulatory support prior to PCI (16, 18, 19). CT was performed after coronary angiography in case of a presumably cardiac cause of arrest or upfront in patients with a suspected non-cardiac cause of arrest (**Figure 1**). Thereafter, patients were transferred to the cardiac intensive care unit where therapeutic hypothermia was performed using intravascular cooling catheters (Coolguard Quattro®, ZOLL Medical, San Jose, CA, USA) for at least 24 h depending on the duration of ROSC or presence of anoxic cause of arrest. An active cooling device had been chosen to select and maintain a constant target temperature of 32°C during hypothermia followed by controlled rewarming (0.25°C per h) and maintained normothermia for at least another 72 h (14, 20). Transfer of the patient between catheterization laboratory, CT, and intensive care unit was supervised at all times by a team consisting of an anesthesiologist, intensive care physician, and an anesthetic nurse.

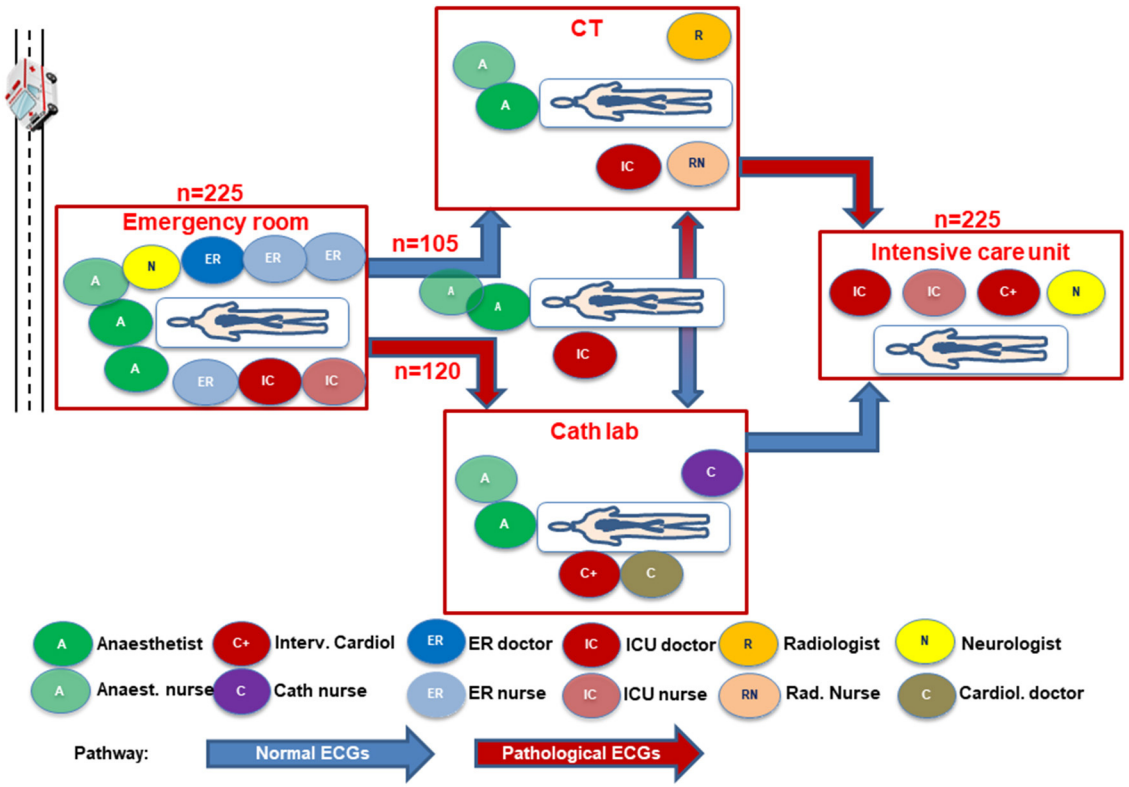

FIGURE 1 | Intrahospital patient flow and human resource allocation for patients with ROSC after OHCA depending on a suspected primary coronary or non-coronary cause of arrest; CT – computed tomography; ER, emergency room; ICU, intensive care unit.

CT Protocol

All CT-scans were conducted on a dual source dual energy CT (Somatom Force, Siemens Medical Systems, Erlangen, Germany). The CT protocol always included a native cranial CT, a native chest CT, and an arterial phase i.v. contrast enhanced chest CT with coverage of the abdomen and pelvis. For the native head CT the scan parameters were: 120 kV, 330 mAs, CareDose, rotation time 1 s, collimation 64 x 0.6 mm, 1 mm reconstructed slice thickness, pitch 0.8. For the chest, abdomen and pelvis CT the scan parameters were: 120 kV, 140 mAs, CareDose, rotation time 0.28 s, collimation 192 x 0.6 mm, 1 mm reconstructed slice thickness, pitch 2.5. For arterial phase imaging 80–100 mL of non-ionic contrast agent were injected intravenously at 5 mL/s. Bolus tracking was performed at the ascending aorta using a 250 HU trigger setting. Routinely, coronal and sagittal reconstructions were performed. A board-certified radiologist analyzed the images directly after the CT scans were performed and reported clinically relevant findings to the cardiologist in the cardiac arrest center responsible for the patient. Findings were classified as potentially life threatening in case of intracranial or intra-abdominal bleeding, free intra-abdominal air, ileus, type A aortic dissection, pericardial tamponade, central or bilateral occlusive pulmonary embolism, tension pneumothorax or pneumothorax with severely aggravated ventilation parameters with rapid improvement after chest tube insertion.

Statistics

Quantitative data are presented as mean ± standard error of mean (SEM), median and interquartile range (IQR), and ranges depending on distribution. Data were compared using the Student's *t*-test for normally distributed data or the Mann-Whitney U test for nonparametric data. Deviations from a Gaussian distribution were tested by the Kolmogorov-Smirnov test. Spearman's rank correlation for nonparametric data was used to test univariate correlations. Qualitative data are presented as absolute and relative frequencies and compared using the chi-square test or the Fisher's exact test, as appropriate. Data were analyzed using SPSS version 26.0 for Windows (SPSS Inc. Chicago, IL, USA). A $P < 0.05$ was considered statistically significant.

RESULTS

Baseline Characteristics

During the reported three-year period, 225 consecutive patients with non-traumatic OHCA and ROSC were treated per protocol and analyzed. Mean age was 64 ± 13 years and 170 (75%) patients were male. Initial rhythm after CPR was shockable in 55% (ventricular tachycardia or ventricular fibrillation, $N = 123$). Most patients (77%) had witnessed cardiac arrest and received immediate bystander CPR (64%). The average

TABLE 1 | Demographics and baseline characteristics of patients.

Characteristics	Overall *N* = 225 (100)	Pathologic ECGs* *N* = 120 (53)	Normal ECGs** *N* = 105 (47)	*P*
Male sex	170 (75)	95 (79)	75 (71)	0.178
Age (years)	64 ± 13	65 ± 13	64 ± 14	0.372
Body mass index (kg/m^2)	27 ± 7	27 ± 6	28 ± 8	0.253
Circumstance on admission				
Bystander CPR	145 (64)	77 (64)	68 (65)	0.926
Initial rhythm				
Asystole	76 (34)	30 (25)	46 (44)	0.003
Pulseless electric activity	17 (8)	9 (<1)	8 (<1)	1.000
Ventricular tachycardia/ fibrillation	123 (55)	77 (64)	46 (44)	0.002
Other	9 (4)	4 (<1)	5 (<1)	0.737
ROSC (min)	24 ±20	24 ±19	24 ±22	0.984
Ongoing resuscitation on admission	23 (10)	8 (<1)	15 (14)	0.060
Clinical chemistry on admission				
Potassium (mmol/l)	4,4 ± 1,02	4,23 ± 1,21	4,54 ± 2,21	0.841
Creatininkinase (U/l)	290 ± 191	312 ± 150	151 ± 201	0.041
Lactate (mmol/l)	8,34 ± 3,51	8,12 ± 3,12	8,71 ± 3,11	0.974
Hs-Troponin (ng/l)	690 ± 603	720 ± 513	466 ± 422	0.052
pH	7,17 ± 0,48	7,16 ± 0,43	7,17 ± 0,51	1.000
Pre-existing illness/Risk factors				
Smoking	70 (31)	40 (33)	30 (29)	0.441
Arterial hypertension	125 (55)	71 (59)	54 (51)	0.244
Hyperlipidemia	67 (30)	41 (34)	26 (25)	0.124
Positive family history for CAD	15 (7)	7 (<1)	8 (<1)	0.605
Diabetes	50 (22)	27 (23)	23 (22)	0.915
Preexisting CAD	47 (21)	26 (22)	21 (20)	0.759
Preexisting PAD	16 (7)	6 (<1)	10 (10)	0.205
Atrial fibrillation	49 (22)	26 (22)	23 (22)	0.966
Previous cerebral event (Stroke/TIA)	32 (14)	15 (13)	17 (17)	0.429
Chronic kidney disease	32 (14)	18 (15)	14 (13)	0.721
Circumstance in ICU				
Hemodialysis	67 (30)	28 (23)	39(37)	0.754
MCS	14 (6)	9 (8)	5 (5)	0.207
Mortality (30d)	113 (50)	55 (45)	58 (55)	0.913

Data are shown as mean ± standard deviation, otherwise (%) percentage of all patients with available data.

**Defined as new onset left bundle branch block, ST-elevation/-depression on admission.*

***Defined as ECG without signs suggestive for acute/chronic ischemia.*

CAD, coronary artery disease; CPR, cardio-pulmonary resuscitation; ECG, electrocardiogram; MCS, mechanic cardiac support; PAD, peripheral artery disease; ROSC, return of spontaneous circulation; TIA, transient ischemic attack.

time for reaching stable ROSC was 24 ± 20 min. ECGs after ROSC were suggestive for myocardial ischemia in 53%, and baseline characteristics of those patients were not significantly different compared to patients with non-suggestive ECGs, except for initial rhythm. A shockable rhythm was more frequent in the ischemia-suggestive ECG group (64 vs. 44%, $P = 0.002$), whereas the non-suggestive ECG group had higher numbers of asystole as initial rhythm (44 vs. 25%, $P = 0.003$) (**Table 1**).

Computed Tomography

All 225 patients received a CT of the head, chest, and abdomen/pelvis. In 120 patients (53%), CT scans were performed after coronary angiography and upfront in the remaining 105 patients. **Table 2** shows the results of cranial CT, of abdominal/pelvic CT, and those of chest CT. In the cranial CT screening a total of 17 pathological findings were described in 12 patients without ECG signs suggestive of myocardial ischemia and in five patients with ischemia-suggestive ECG patterns. The

TABLE 2 | Pathological findings on Computed tomography.

Findings	Overall $N = 225$	Pathologic ECGs* $N = 120$	Normal ECGs** $N = 105$	*P*
Cranial Computed tomography				
Intracranial bleeding	1 (<1)	0 (0)	1 (1)	0.467
Subarachnoid bleeding	4 (2)	2 (2)	2 (2)	1.000
Subdural bleeding	1 (<1)	1 (1)	0 (0)	1.000
Subgaleal bleeding	8 (4)	2 (2)	6 (6)	0.150
Skull fracture	3 (1)	0 (0)	3 (3)	0.100
Abdominal Computed tomography				
Liver bleeding	12 (5)	8 (7)	4 (4)	0.388
Liver cirrhosis	8 (4)	6 (5)	2 (2)	0.289
Intra-abdominal air	3 (1)	2 (2)	1 (1)	0.600
Mesenteric stenosis	13 (6)	10 (8)	3 (3)	0.092
Ileus	3 (1)	0 (0)	3 (3)	0.100
Invagination	2 (<1)	2 (2)	0 (0)	0.500
Chest Computed tomography				
Aortic aneurysm				
Ascending Aorta	14 (6)	8 (7)	6 (6)	0.791
Abdominal Aorta	7 (3)	5 (4)	2 (2)	0.453
Aortic dissection				
Type A	2 (<1)	2 (2)	0 (0)	0.500
Type B	3 (1)	2 (2)	1 (1)	1.000
Pericardial tamponade	3 (1)	2 (2)	1 (1)	1.000
Aspiration	62 (28)	34 (28)	28 (27)	0.780
Pulmonary embolism[a]	17 (8)	7 (6)	10 (10)	0.322
Pulmonary edema	20 (9)	11 (9)	9 (9)	0.876
Pneumothorax[b]	11 (5)	2 (2)	9 (9)	0.026
Lung mass	12 (5)	5 (4)	7 (7)	0.554
Pleural effusion	65 (29)	33 (28)	32 (30)	0.623
Rip fracture	161 (72)	88 (73)	73 (69)	0.492
Sternal fracture	50 (22)	26 (22)	24 (23)	0.830
Spinal fracture	11 (5)	4 (3)	7 (7)	0.355

Data are shown as (%) percentage of all patients with available data.

**Defined as new onset left bundle branch block, ST-elevation/-depression on admission.*

***Defined as ECG without signs suggestive for acute/chronic ischemia.*

[a]*Central or bilateral occluding embolism.*

[b]*Tension pneumothorax or aggravated ventilation parameters (↑pressure, ↓ tidal volume) with rapid improvement after chest tube insertion.*

further subdivision to intracerebral, subarachnoidal, subdural, or subgaleal bleeding showed no significant difference between the two ECG groups (**Table 2**). Abdominal CT revealed a total of 41 positive results within 28 cases with concomitant ECG signs suggestive of myocardial ischemia; only 13 cases had a non-pathological ECG, without significant differences between groups (**Table 2**). The highest number of pathological findings were made in chest CTs (**Table 2**). Overall, 438 pathologies were described with a nearly equal distribution between patients with ECGs being either suggestive or non-suggestive for coronary ischemia ($N = 229$ vs. 209).

Initially moderate pericardial effusions seen on echocardiography in the emergency room showed hemodynamic progression into pericardial tamponade in three cases as detected by CT-scan, of whom two had an ischemia-suggestive ECG. Furthermore, 17 patients suffered from central or bilateral occluding pulmonary embolism, 11 patients had pneumothoraxes, mostly represented in the patient group with ECGs non-suggestive for ischemia ($N = 9$). All of these patients showed aggravated ventilation parameters such as increased ventilatory pressures and decreased tidal volumes. One presented with a mediastinal shift and signs of tension pneumothorax that required immediate treatment. Bone fractures were located in mainly three areas: Sternal ($N = 50$), rib ($N = 161$), and spinal fractures ($N = 11$). Similarly, there was an equal distribution of fractures between groups with and without an ischemic ECG. Of all CT findings, 60 cases (27% of the total population) provided clinically relevant results, 28 (12%) in patients with ischemia-suggestive and 32 (14%) in patients with normal ECGs. Likely due to early CT diagnostics and the resulting initiation of chest drain insertions in case of pneumothorax or surgical treatment in case of aortic dissection, mortality was

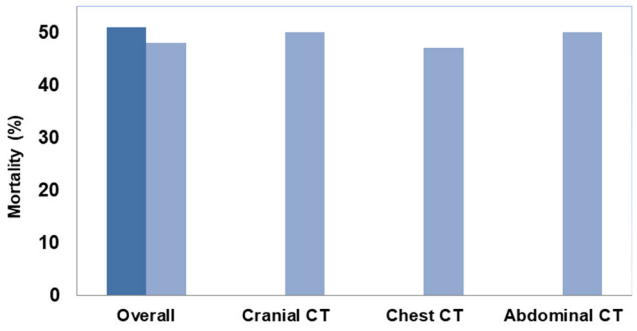

FIGURE 2 | In-hospital mortality (%) in patients with no or non-critical (dark blue) compared to critical CT-findings (light blue) including separate evaluation of critical findings with respect to the imaging area.

not increased compared to the remaining OHCA population. Overall, 113 patients (50%) died during the hospital stay. Of the 60 patients with critical CT-findings, 29 (48%) died, while 84 of the remaining 165 patients without critical pathologies in CT died (51%) (**Figure 2**). Therefore, rapid identification of potentially lethal comorbidities and subsequent causal treatment likely prevented increased mortality in this highly vulnerable subgroup [mortality 48 vs. 51%, $P = 0.7646$; relative risk 0.95 (95%-CI 0.70–1.28)].

Since prolonged time to ROSC may lead to more side effects and increased mortality, we examined whether time to ROSC was correlated with either mortality or pathological CT findings. Time to ROSC was shorter in survivors than in non-survivors (20.1 ± 1.3 min vs. 28.2 ± 2.3 min; $p = 0.003$). For most pathological CT findings there were no significant differences in time to ROSC except for patients with type A aortic dissection (65.1 ± 40.9 min vs. 23.2 ± 1.3 min; $p = 0.004$) or pericardial effusion (17.1 ± 3.4 min vs. 24.3±1.3 min; $p = 0.037$). We observed higher survival in patients with initial shockable rhythms compared to patients with non-shockable rhythms (65 vs 31%; $p < 0.001$). However, there was no significant difference in pathological CT findings with respect to the form of initial rhythm.

DISCUSSION

In this study on 225 patients with successful resuscitation after OHCA, CT on admission uncovered a substantial number of pathological and potentially life-threatening CT findings. Those were similarly distributed between patients with and those without ischemia-suggestive ECG patterns indicating a probable coronary cause of arrest. Rapid identification of potentially life-threatening conditions with subsequent intervention likely contributed to a comparable mortality compared to patients without such findings.

Results from *Coronary Angiography after Cardiac Arrest without ST-Segment Elevation (COACT)* and *Angiography after Out-of-Hospital Cardiac Arrest without ST-Segment Elevation (TOMAHAWK)* suggest that if no ST-segment elevation is present, delayed coronary angiography has no disadvantage for patients (21, 22). However, in the HACORE population we could recently show that the rate of culprit coronary stenosis was high even in patients without ST-segment elevation in first ECG after ROSC if there was an initial shockable rhythm.

There, early angiography was associated with similar favorable neurological outcome as in OHCA patients with ST-elevations (23). As supported by the trial results from COACT and TOMAHAWK and the real-world experience from HACORE, we do believe that a CT scan as initial diagnostic test should be favored in all OHCA patients without ST-segment elevations. Nevertheless, we feel that a CT does also provide valuable information in patients with ST-elevations, but the exam should be performed after successful revascularization and prior to ICU admission.

A study from the *Parisian Region out of Hospital cardiac Arrest registry (PROCAT)* found that immediate coronary angiography irrespective of ECG findings would lead to an improved outcome and hospital survival (24). This was attributed to the fact that coronary artery disease and myocardial ischemia are the most common reason for OHCA (25). However, data from the same *PROCAT* registry also demonstrated that in addition to coronary angiography, CT would be the most effective diagnostic tool to detect any other OHCA etiology. The authors concluded that only a combination between those two diagnostic modalities would lead to a clear understanding of the particular case (10). Furthermore, the presence of comorbidities on CT was associated with in-hospital mortality (10, 26), most probably due to unmasking otherwise unseen extra-coronary pathologies. Accordingly, underdiagnosing comorbidities or resuscitation-related injuries would increase morbidity and mortality, counteracting all efforts of post-resuscitation care. Missing the frequent resuscitation-related injuries might significantly affect the outcome, if they remain undetected under routine intensive care (27). In turn, recognizing those patterns may translate into better outcome or at least prevent unintended complications such as persistent bleeding, e.g., caused by intensified anti-thrombotic medications following percutaneous coronary interventions (28, 29). The observation of 438 overall pathological findings in chest CTs from 225 patients in our registry is well in line with other studies focusing on complications resulting from CPR (27, 29–32). However, even the 2020 American Heart Association (AHA) Guidelines for Cardiopulmonary Resuscitation and Emergency Cardiovascular Care mention chest radiography instead of chest CT as the essential diagnostic test for intubated patients after OHCA (25). In contrast, CT shows a clear advantage compared to simple chest radiography, since it allows higher quality imaging and multiplane anatomical reconstruction (33). Chest radiography underestimates life-threatening complications such as pneumothorax, especially in supine position single-plane images (12, 33, 34). In addition, CPR-related rib and sternal fractures are underdiagnosed by conventional chest X-ray (35). This could translate into a more complicated management of ventilation leading to ventilator-associated lung injury and worsening overall outcome. CT currently represents the only gold standard for diagnosis or rule-out of certain life-threatening pathologies such as pulmonary embolism, aortic dissection,

or intracranial bleeding (12). No other available diagnostic measure can provide rapid and definite diagnosis of potentially life-threatening pathologies in a single procedure. Measures such as sonography, echocardiography, or clinical examination are important diagnostic tools, but remain subjective, time-consuming, and insufficiently sensitive. In contrast, CT offers high quality multiplane imaging and the ability to record a whole body or larger area image in one setting. In many cases of OHCA a number of extra-cardiac pathologies detected by CT implicate an immediate threat and require adaptations of intensive care strategies in order to prevent deterioration. For instance, in cases of extracorporeal cardiopulmonary life support after OHCA, computed tomography provides sensitive information for further intensive care therapy. In a recent report in eCPR patients, routine CT diagnostic revealed a large number of relevant pathological findings similar to our observation in a broader patient cohort (36). During implementation of the 2010 American Heart Association Guidelines only 2.8% of detected pathologies were identified as directly life threating (37). However, every single cardiac arrest case has to be evaluated individually as circumstances of arrest and resuscitation differ widely. In this context, CT performed on admission provides essential information by ruling out immediately compromising conditions. Especially when considering the neurologic status after prolonged cardiopulmonary arrest in comatose patients, CT imaging helps to detect significant and irreversible pathologies on admission and may guide prognostication (28, 38). Therefore, CT imaging to detect brain injury and predict neurological outcome is, together with magnetic resonance imaging, the most studied neuroimaging modality (25). What distinguishes CT imaging from magnetic resonance imaging in the case of OHCA patients is its speed and advantageous ability in delivering additional information about structural lesions such as skull fractures. Using a radiological assessment of almost the whole body, early risk stratification for further invasive management in the intensive care setting can be planned (39). A positive finding in coronary angiography commonly represents a treatable cause of arrest and thus beneficially affects survival, also by reducing the likelihood of recurrent arrest. A "positive" finding on cranial CT scans is often associated with underlying severe damage of the brain and is most probably associated with worse outcome (10). The European Guidelines for Resuscitation Care recommend head- and thoracic- CT scans prior to ICU admission after OHCA (7). In our analysis, CT detected 496 findings with a nearly equal distribution in both pathological and normal ECG groups ($N =$ 262 vs. 234) (**Figure 3**). Even in patients with ischemic ECGs and primary PCI concomitant extra-cardiac pathologies have to be anticipated and frequently require acute treatment. Only when combining coronary angiography with whole-body CT prior to ICU admission a complete diagnostic image of the patient after OHCA will be gained. Patient recruitment for the current analysis was before the COVID-19 pandemic. Even in that non-COVID context, early CT diagnostic during initial work-up revealed important information for treatment from thoracic pathologies (40). Taking the approaching fourth wave of the pandemic into account, the likelihood of false-positive rapid PCR or MDA tests is increasing. The extremely helpful ability of chest CT to indicate a pulmonary COVID-like pattern will provide useful additive information gained from post-arrest CTs, not only influencing care of the individual patient but also impacting on strategic allocation of patients within hospitals regarding a probable or non-probable COVID-19 disease (41).

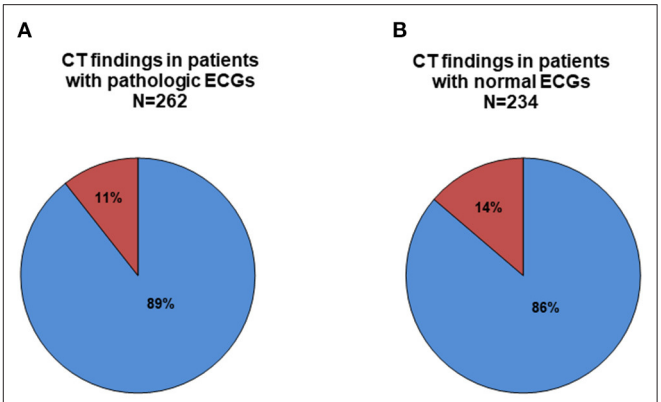

FIGURE 3 | Proportion of patients (%) with critical (red) compared to non-critical (blue) CT-findings according to the electrocardiogram (ECG) being either suggestive for coronary ischemia **(A)** or not **(B)**.

Limitations

This analysis comprises certain limitations. First, it was a retrospective single center observation. Second, it did not include other diagnostic measures that were performed immediately after admission such as echocardiography or abdominal ultrasound. Those potentially could detect pathologies or injuries secondary to CPR, either leading to a faster adjustment of management or, by missing such pathologies, emphasize the value of additional whole-body CT.

CONCLUSIONS

Immediate whole-body CT in OHCA patients provides valuable information about non-coronary causes of cardiac arrest and resuscitation-related injuries affecting further treatment. If coronary angiography is primarily used based on a suspected coronary cause of arrest, a CT should be performed afterwards. Detection of potentially life-threatening comorbidities and their causal treatment is associated with comparable mortality as in patients without life-threatening complications. Therefore, CT should be routinely included in diagnostic workup of OHCA, irrespective of the presence or absence of ischemic ECG patterns.

DATA AVAILABILITY STATEMENT

The raw data supporting the conclusions of this article will be made available by the authors, without undue reservation.

ETHICS STATEMENT

HACORE is a prospective observational registry approved by the Ethics Committee at Hannover Medical School (#3567-2017) and is in accordance with the Declaration of Helsinki.

AUTHOR CONTRIBUTIONS

AS, MA, and JB designed the registry. AS, MA, VG, LN, and JA recruited the patients and analyzed the data. AS, MA, and JA drafted the manuscript. VG, JV-C, LN, and JB critically revised the manuscript. All authors contributed to the article and approved the submitted version.

FUNDING

This study was partly supported by the Clinical Research Group (KFO) 311 of the Deutsche Forschungsgemeinschaft (DFG).

ACKNOWLEDGMENTS

The authors thank the nursing staff of the catheterization laboratory and cardiac ICU for their continuous support and care in treating OHCA patients.

SUPPLEMENTARY MATERIAL

The Supplementary Material for this article can be found online at: https://www.frontiersin.org/articles/10.3389/fcvm.2022.799446/full#supplementary-material

Supplementary Figure 1 | HaCRA work-flow for patients with out-of-hospital cardiac arrest or cardiogenic shock.

REFERENCES

1. Wong CX, Brown A, Lau DH, Chugh SS, Albert CM, Kalman JM, et al. Epidemiology of sudden cardiac death: global and regional perspectives. *Heart Lung Circ.* (2019) 28:6–14. doi: 10.1016/j.hlc.2018.08.026
2. Nadeem R, Osman H, Karaly Y, AlBakri I, Khazi F. Cardiac arrest with multi-vessel coronary artery disease and successful treatment after long conventional cardiopulmonary resuscitation: how long is too long? *Cureus.* (2019) 11:e5993. doi: 10.7759/cureus.5993
3. Bell SM, Kovach C, Kataruka A, Brown J, Hira RS. Management of out-of-hospital cardiac arrest complicating acute coronary syndromes. *Curr Cardiol Rep.* (2019) 21:146. doi: 10.1007/s11886-019-1249-y
4. Spaulding CM, Joly LM, Rosenberg A, Monchi M, Weber SN, Dhainaut JF, et al. Immediate coronary angiography in survivors of out-of-hospital cardiac arrest. *N Engl J Med.* (1997) 336:1629–33. doi: 10.1056/NEJM199706053362302
5. Grasner JT, Lefering R, Koster RW, Masterson S, Bottiger BW, Herlitz J, et al. EuReCa ONE-27 Nations, ONE Europe, ONE registry: a prospective one month analysis of out-of-hospital cardiac arrest outcomes in 27 countries in Europe. *Resuscitation.* (2016) 105:188–95. doi: 10.1016/j.resuscitation.2016.10.001
6. Grasner JT, Wnent J, Herlitz J, Perkins GD, Lefering R, Tjelmeland I, et al. Survival after out-of-hospital cardiac arrest in Europe - Results of the EuReCa TWO study. *Resuscitation.* (2020) 148:218–26. doi: 10.1016/j.resuscitation.2019.12.042
7. Nolan JP, Sandroni C, Bottiger BW, Cariou A, Cronberg T, Friberg H, et al. European Resuscitation Council and European Society of Intensive Care Medicine Guidelines 2021: Post-resuscitation care. *Resuscitation.* (2021) 161:220–69. doi: 10.1016/j.resuscitation.2021.02.012
8. Ibanez B, James S, Agewall S, Antunes MJ, Bucciarelli-Ducci C, Bueno H, et al. 2017 ESC Guidelines for the management of acute myocardial infarction in patients presenting with ST-segment elevation: The Task Force for the management of acute myocardial infarction in patients presenting with ST-segment elevation of the European Society of Cardiology (ESC). *Eur Heart J [Practice Guideline].* (2018) 39:119–77. doi: 10.1093/eurheartj/ehx393
9. Collet JP, Thiele H, Barbato E, Barthelemy O, Bauersachs J, Bhatt DL, et al. 2020 ESC Guidelines for the management of acute coronary syndromes in patients presenting without persistent ST-segment elevation. *Eur Heart J.* (2020) 41:3495-−7. doi: 10.1093/eurheartj/ehaa624
10. Chelly J, Mongardon N, Dumas F, Varenne O, Spaulding C, Vignaux O, et al. Benefit of an early and systematic imaging procedure after cardiac arrest: insights from the PROCAT (Parisian Region Out of Hospital Cardiac Arrest) registry. *Resuscitation.* (2012) 83:1444–50. doi: 10.1016/j.resuscitation.2012.08.321
11. Christ M, von Auenmueller KI, Noelke JP, Sasko B, Amirie S, Trappe HJ. Early computed tomography in victims of non-traumatic out-of-hospital cardiac arrest. *Intern Emerg Med.* (2016) 11:237–43. doi: 10.1007/s11739-015-1353-y
12. Viniol S, Thomas RP, Konig AM, Betz S, Mahnken AH. Early whole-body CT for treatment guidance in patients with return of spontaneous circulation after cardiac arrest. *Emerg Radiol.* (2020) 27:23–9. doi: 10.1007/s10140-019-01723-x
13. Lott C, Truhlar A, Alfonzo A, Barelli A, Gonzalez-Salvado V, Hinkelbein J, et al. European Resuscitation Council Guidelines 2021: Cardiac arrest in special circumstances. *Resuscitation.* (2021) 161:152–219. doi: 10.1016/j.resuscitation.2021.02.011
14. Akin M, Sieweke JT, Zauner F, Garcheva V, Tongers J, Napp LC, et al. Mortality in patients with out-of-hospital cardiac arrest undergoing a standardized protocol including therapeutic hypothermia and routine coronary angiography: experience from the HACORE registry. *JACC Cardiovasc Interv.* (2018) 11:1811–20. doi: 10.1016/j.jcin.2018.06.022
15. Sieweke JT, Akin M, Beheshty JA, Flierl U, Bauersachs J, Schafer A. Unloading in refractory cardiogenic shock after out-of-hospital cardiac arrest due to acute myocardial infarction-a propensity score-matched analysis. *Front Cardiovasc Med.* (2021) 8:704312. doi: 10.3389/fcvm.2021.704312
16. Roffi M, Patrono C, Collet JP, Mueller C, Valgimigli M, Andreotti F, et al. 2015 ESC Guidelines for the management of acute coronary syndromes in patients presenting without persistent ST-segment elevation: Task Force for the Management of Acute Coronary Syndromes in Patients Presenting without Persistent ST-Segment Elevation of the European Society of Cardiology (ESC). *Eur Heart J.* (2016) 37:267–315. doi: 10.1093/eurheartj/ehv320
17. Fillbrandt A, Frank B. Gender differences in cognitive outcome after cardiac arrest: a retrospective cohort study. *Brain Inj.* (2020) 34:122–30. doi: 10.1080/02699052.2019.1680866
18. Schafer A, Werner N, Burkhoff D, Sieweke JT, Zietzer A, Masyuk M, et al. Influence of timing and predicted risk on mortality in impella-treated infarct-related cardiogenic shock patients. *Front Cardiovasc Med.* (2020) 7:74. doi: 10.3389/fcvm.2020.00074
19. Tongers J, Sieweke JT, Kuhn C, Napp LC, Flierl U, Rontgen P, et al. Early escalation of mechanical circulatory support stabilizes and potentially rescues patients in refractory cardiogenic shock. *Circ Heart Fail.* (2020) 13:e005853. doi: 10.1161/CIRCHEARTFAILURE.118.005853
20. Akin M, Garcheva V, Sieweke JT, Adel J, Flierl U, Bauersachs J, et al. Neuromarkers and neurological outcome in out-of-hospital cardiac arrest patients treated with therapeutic hypothermia-experience from the HAnnover COoling REgistry (HACORE). *PLoS ONE.* (2021) 16:e0245210. doi: 10.1371/journal.pone.0245210
21. Lemkes JS, Janssens GN, van der Hoeven NW, Jewbali LSD, Dubois EA, Meuwissen M, et al. Coronary angiography after cardiac arrest without ST-segment elevation. *N Engl J Med.* (2019) 380:1397–407. doi: 10.1056/NEJMoa1816897
22. Desch S, Freund A, Akin I, Behnes M, Preusch MR, Zelniker TA, et al. Angiography after out-of-hospital cardiac arrest without ST-Segment elevation. *N Engl J Med.* (2021) 385:2544–53. doi: 10.1056/NEJMoa2101909
23. Garcheva V, Akin M, Adel J, Sanchez Martinez C, Bauersachs J, Schafer A. High rate of critical coronary stenosis in comatose patients with Non-ST-elevation out-of-hospital cardiac arrest (NSTE-OHCA) undergoing therapeutic hypothermia-Experience from

the HAnnover COoling REgistry (HACORE). *PLoS ONE.* (2021) 16:e0251178. doi: 10.1371/journal.pone.0251178
24. Dumas F, Cariou A, Manzo-Silberman S, Grimaldi D, Vivien B, Rosencher J, et al. Immediate percutaneous coronary intervention is associated with better survival after out-of-hospital cardiac arrest: insights from the PROCAT (Parisian Region Out of hospital Cardiac ArresT) registry. *Circ Cardiovasc Interv.* (2010) 3:200–7. doi: 10.1161/CIRCINTERVENTIONS.109.913665
25. Panchal AR, Bartos JA, Cabanas JG, Donnino MW, Drennan IR, Hirsch KG, et al. Part 3: Adult Basic and Advanced Life Support: 2020 American Heart Association Guidelines for Cardiopulmonary Resuscitation and Emergency Cardiovascular Care. *Circulation.* (2020) 142(16_suppl_2):S366–S468. doi: 10.1161/CIR.0000000000000918
26. Pell JP, Sirel JM, Marsden AK, Ford I, Walker NL, Cobbe SM. Presentation, management, and outcome of out of hospital cardiopulmonary arrest: comparison by underlying aetiology. *Heart.* (2003) 89:839–42. doi: 10.1136/heart.89.8.839
27. Beom JH, You JS, Kim MJ, Seung MK, Park YS, Chung HS, et al. Investigation of complications secondary to chest compressions before and after the 2010 cardiopulmonary resuscitation guideline changes by using multi-detector computed tomography: a retrospective study. *Scand J Trauma Resusc Emerg Med.* (2017) 25:8. doi: 10.1186/s13049-017-0352-6
28. Petek BJ, Erley CL, Kudenchuk PJ, Carlbom D, Strote J, Gatewood MO, et al. Diagnostic yield of non-invasive imaging in patients following non-traumatic out-of-hospital sudden cardiac arrest: a systematic review. *Resuscitation.* (2019) 135:183–90. doi: 10.1016/j.resuscitation.2018.09.004
29. Dunham GM, Perez-Girbes A, Bolster F, Sheehan K, Linnau KF. Use of whole body CT to detect patterns of CPR-related injuries after sudden cardiac arrest. *Eur Radiol.* (2018) 28:4122–7. doi: 10.1007/s00330-017-5117-0
30. Kashiwagi Y, Sasakawa T, Tampo A, Kawata D, Nishiura T, Kokita N, et al. Computed tomography findings of complications resulting from cardiopulmonary resuscitation. *Resuscitation.* (2015) 88:86–91. doi: 10.1016/j.resuscitation.2014.12.022
31. Kim MJ, Park YS, Kim SW, Yoon YS, Lee KR, Lim TH, et al. Chest injury following cardiopulmonary resuscitation: a prospective computed tomography evaluation. *Resuscitation.* (2013) 84:361–4. doi: 10.1016/j.resuscitation.2012.07.011
32. Choi SJ, Kim HS, Kim EY, Choi HY, Cho J, Yang HJ, et al. Thoraco-abdominal CT examinations for evaluating cause of cardiac arrest and complications of chest compression in resuscitated patients. *Emerg Radiol.* (2014) 21:485–90. doi: 10.1007/s10140-014-1218-0
33. Kim EY, Yang HJ, Sung YM, Cho SH, Kim JH, Kim HS, et al. Multidetector CT findings of skeletal chest injuries secondary to cardiopulmonary resuscitation. *Resuscitation.* (2011) 82:1285–8. doi: 10.1016/j.resuscitation.2011.05.023
34. Liu Z, Liu Q, Wu G, Li H, Wang Y, Chen R, et al. Quantitative CT assessment of lung injury after successful cardiopulmonary resuscitation in a porcine cardiac arrest model of different downtimes. *Quant Imaging Med Surg.* (2018) 8:946–56. doi: 10.21037/qims.2018.10.04
35. Lederer W, Mair D, Rabl W, Baubin M. Frequency of rib and sternum fractures associated with out-of-hospital cardiopulmonary resuscitation is underestimated by conventional chest X-ray. *Resuscitation.* (2004) 60:157–62. doi: 10.1016/j.resuscitation.2003.10.003
36. Zotzmann V, Rilinger J, Lang CN, Duerschmied D, Benk C, Bode C, et al. Early full-body computed tomography in patients after extracorporeal cardiopulmonary resuscitation (eCPR). *Resuscitation.* (2020) 146:149–54. doi: 10.1016/j.resuscitation.2019.11.024
37. Yamaguchi R, Makino Y, Chiba F, Torimitsu S, Yajima D, Inokuchi G, et al. Frequency and influencing factors of cardiopulmonary resuscitation-related injuries during implementation of the American Heart Association 2010 Guidelines: a retrospective study based on autopsy and postmortem computed tomography. *Int J Legal Med.* (2017) 131:1655–63. doi: 10.1007/s00414-017-1673-8
38. Reynolds AS, Matthews E, Magid-Bernstein J, Rodriguez A, Park S, Claassen J, et al. Use of early head CT following out-of-hospital cardiopulmonary arrest. *Resuscitation.* (2017) 113:124–7. doi: 10.1016/j.resuscitation.2016.12.018
39. Balan P, Hsi B, Thangam M, Zhao Y, Monlezun D, Arain S, et al. The cardiac arrest survival score: a predictive algorithm for in-hospital mortality after out-of-hospital cardiac arrest. *Resuscitation.* (2019) 144:46–53. doi: 10.1016/j.resuscitation.2019.09.009
40. Prokop M, van Everdingen W, van Rees Vellinga T. Quarles van Ufford H, Stoger L, Beenen L, et al. CO-RADS: A Categorical CT Assessment Scheme for Patients Suspected of Having COVID-19-Definition and Evaluation. *Radiology.* (2020) 296:E97–E104. doi: 10.1148/radiol.2020201473
41. Vogel-Claussen J, Ley-Zaporozhan J, Agarwal P, Biederer J, Kauczor HU, Ley S, et al. Recommendations of the thoracic imaging section of the german radiological society for clinical application of chest imaging and structured CT reporting in the COVID-19 pandemic. *Rofo.* (2020) 192:633–40. doi: 10.1055/a-1174-8378

Conflict of Interest: AS received modest lecture fees from Zoll regarding therapeutic hypothermia. LN received lecture/proctoring/consulting honoraria and research funding from Abiomed, and lecture honoraria from Abbott, Maquet, Orion, and Zoll.

The remaining authors declare that the research was conducted in the absence of any commercial or financial relationships that could be construed as a potential conflict of interest.

Publisher's Note: All claims expressed in this article are solely those of the authors and do not necessarily represent those of their affiliated organizations, or those of the publisher, the editors and the reviewers. Any product that may be evaluated in this article, or claim that may be made by its manufacturer, is not guaranteed or endorsed by the publisher.

frontiers in Cardiovascular Medicine

REVIEW
published: 07 February 2022
doi: 10.3389/fcvm.2021.831734

Cognitive Impairment in Heart Failure: Landscape, Challenges, and Future Directions

Mengxi Yang[1,2†], *Di Sun*[1,2†], *Yu Wang*[3], *Mengwen Yan*[1,2], *Jingang Zheng*[1,2] *and Jingyi Ren*[1,2,4*]

[1] Heart Failure Center, China-Japan Friendship Hospital, Beijing, China, [2] Department of Cardiology, China-Japan Friendship Hospital, Beijing, China, [3] Department of Neurology, China-Japan Friendship Hospital, Beijing, China, [4] Vascular Health Research Center of Peking University Health Science Center, Beijing, China

Heart failure (HF) is a major global healthcare problem accounting for substantial deterioration of prognosis. As a complex clinical syndrome, HF often coexists with multi-comorbidities of which cognitive impairment (CI) is particularly important. CI is increasing in prevalence among patients with HF and is present in around 40%, even up to 60%, of elderly patients with HF. As a potent and independent prognostic factor, CI significantly increases the hospitalization and mortality and decreases quality of life in patients with HF. There has been a growing awareness of the complex bidirectional interaction between HF and CI as it shares a number of common pathophysiological pathways including reduced cerebral blood flow, inflammation, and neurohumoral activations. Research that focus on the precise mechanism for CI in HF is still ever insufficient. As the tremendous adverse consequences of CI in HF, effective early diagnosis of CI in HF and interventions for these patients may halt disease progression and improve prognosis. The current clinical guidelines in HF have begun to emphasize the importance of CI. However, nearly half of CI in HF is underdiagnosed, and few recommendations are available to guide clinicians about how to approach CI in patients with HF. This review aims to synthesize knowledge about the link between HF and cognitive dysfunction, issues pertaining to screening, diagnosis and management of CI in patients with HF, and emerging therapies for prevention. Based on data from current studies, critical gaps in knowledge of CI in HF are identified, and future research directions to guide the field forward are proposed.

Keywords: cognitive impairment, heart failure, epidemiology, pathophysiology, diagnosis, management

OPEN ACCESS

Edited by:
Yan Zhang,
Peking University, China

Reviewed by:
Siting Feng,
Capital Medical University, China
Xiaoyan Zhao,
The First Affiliated Hospital of Zhengzhou University, China

***Correspondence:**
Jingyi Ren
renjingyi1213@hotmail.com

[†] These authors have contributed equally to this work

Specialty section:
This article was submitted to General Cardiovascular Medicine, a section of the journal Frontiers in Cardiovascular Medicine

Received: *08 December 2021*
Accepted: *30 December 2021*
Published: *07 February 2022*

Citation:
Yang M, Sun D, Wang Y, Yan M, Zheng J and Ren J (2022) Cognitive Impairment in Heart Failure: Landscape, Challenges, and Future Directions. Front. Cardiovasc. Med. 8:831734. doi: 10.3389/fcvm.2021.831734

INTRODUCTION

Both heart failure (HF) and cognitive impairment (CI) are the important health concerns for older adults and loom as the public health problems in the coming decades due to the aging global population (1, 2). The similar epidemiological trends and the bidirectional feedback interactions between the heart and the brain are expected to cause a major increase in the prevalence of CI in HF (3). HF is generally considered a leading cause of hospitalization and mortality with an estimated prevalence of >64 million individuals worldwide (4, 5). CI is a very frequent comorbidity in patients with HF and is increasingly recognized as the major cause of chronic disability. It thus confers a substantial global burden to patients and healthcare systems.

Cognitive function refers to a group of mental processes containing memory, language, executive function, visuospatial, concentration, and social cognition (6). The definition of CI is a clinical syndrome that acquires objective cognitive dysfunction affecting one or more cognitive domains. Using normative neuropsychological criteria, CI mostly refers to a performance 1.5 SD units lower than the population mean after accounting for demographics such as age and education. According to the impairment of activities of daily life, CI is classified into mild CI (MCI) and dementia (7). MCI is a stage between normal cognition and dementia that individuals, particularly, those with objective CI on neurocognitive testing and with largely preserved activities of daily living, have. Conversely, dementia is severe enough to affect independent activities of daily life (8).

Cognitive impairment (CI), including its extreme form dementia, has tremendous consequences not only for reduced HF self-care and independence, but also in limiting recognition and appropriate response to worsening HF symptoms of patients. This consequently deteriorates the prognosis of HF (9). It has been confirmed that HF contributes to cognitive decline and that the grade of CI correlates with the severity of HF. As a potent and independent prognostic factor, CI significantly increases the mortality in patients with HF (10). However, some degree of cognitive decline is typical in normal aging; hence, nearly half of CI in HF may be underdiagnosed (11). Therefore, identified CI, especially the early diagnosis of MCI in the preclinical stage, may avoid the occurrence of dementia and, by optimal therapies, revert cognition to normal which has been considered as a crucial strategy for the improvement of prognosis and quality of life in HF population.

In this review, we synthesize knowledge about the landscape of CI in HF, the latest epidemiological data on CI in HF, the current understanding of heart and brain interaction, and the clinical diagnosis and assessment of CI in HF. We also address the potential therapeutic opportunities for preventing and halting the progression of CI in patients with HF. Based on data from current studies, we identify the critical gaps in knowledge of CI in HF and propose future research directions to guide the field forward.

EPIDEMIOLOGY, PREVALENCE, AND PROGNOSTIC IMPLICATIONS OF CI IN HF

Epidemiology of CI in the General Population

Cognitive impairment (CI) remains a rising global epidemic, accounting for substantial morbidity. The prevalence rates of CI exponentially increase with increasing age, ranging from about 20% to more than 40% in general older adults (12–15). Dementia, the most severe state of CI, affects about 55 million of the adult population worldwide. The incidence of dementia in the general population is 1–2% per year. However, the incidence among patients with MCI that progressed to dementia is significantly higher, with an annual rate of 5–12%, in community-based populations without intervention (14, 16, 17) (**Figure 1**). The annual death rate was 8% among those with CI, and the rate almost doubled if patients combined with additional medical conditions, such as heart disease (14).

Prevalence of CI in Patients With HF

Cognitive impairment (CI) is overwhelmingly common and has become a severe burden in HF with a prevalence of 25–75% across population-based studies due to variation in definitions and diagnostic criteria (**Figure 2**) (10, 11, 18–23). Accounting for age, the prevalence of CI in patients with HF is significantly higher compared with the general population. A multicenter survey conducted in Italy reported that about 35% (526/1,511) of patients with HF were detected with CI, while only 29% (3,448/11,790) of patients without HF were diagnosed with CI (10). A cross-sectional analysis from communities in US recruited 6,189 patients aged ≥ 67 years. It also found that the age-adjusted prevalence of CI is about 40% in 707 patients with a moderate or high probability of HF, of which more than one third were dementia. The odds of dementia in those with HF were 1.52-fold than that of non-HF patients with the adjustment of age, race, educational level, net worth, and self-reported prior stroke (23). Gallagher R et al. studied 128 HF patients with an average age of 80 years. The odds of CI were increased more than 4-fold

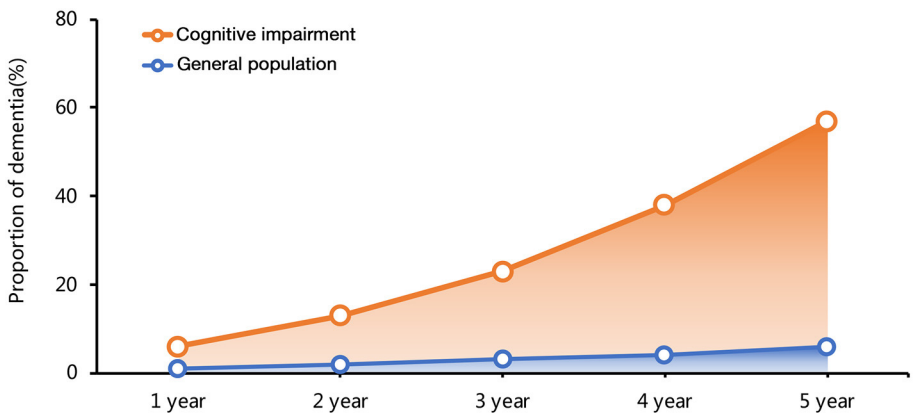

FIGURE 1 | The time curve of dementia incidence in general population and patients with cognitive impairment (CI).

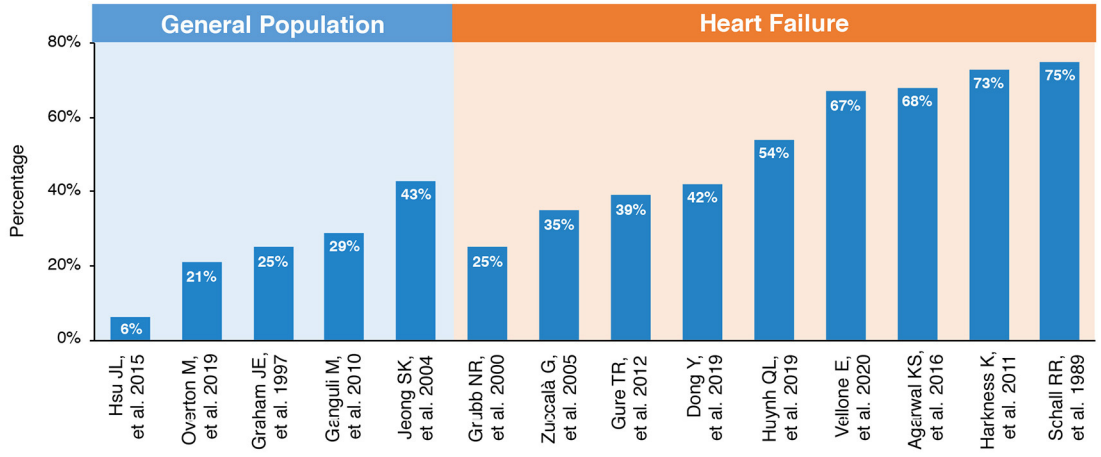

Country	Taiwan	Sweden	Canada	United States	Korean	Scotland	Italy	United States	Singapore	Australian	Global*	United States	Canada	United States
N	276	3752	1255	1982	235	20	1151	707	96	1152	605	121	44	54
Mean age	68	67	≥65	77	74	68	78	79	59	72	67	79	76	46
Mean LVEF	-	-	-	-	-	25	-	-	35	38	39	-	37	20

FIGURE 2 | Prevalence of CI in general population and patients with HF. *Including Sweden, Italy, Israel, The Netherlands, Germany, and the United States. CI, cognitive impairment; HF, heart failure; LVEF, left ventricular ejection fraction.

in HF caused by ischemic heart disease compared with non-ischemic HF (OR, 4.18; 95% confidence interval, 1.15–15.69) (24, 25). With an exception for chronic HF, the Rehabilitation Therapy for Older Acute Heart Failure Patients (REHAB-HF) study revealed that 78% elderly patients hospitalized with acute decompensated HF had broad marked impairments in cognitive function. In addition, the prevalence of CI was similar in patients with preserved vs. reduced ejection fraction [EF; HF with preserved ejection fraction (HFpEF) and HF with reduced ejection fraction (HFrEF)] when adjusted for sex, body mass index (BMI), and comorbidities (26).

Furthermore, the occurrence and deterioration of CI in patients with HF has been demonstrated in longitudinal studies. Cardiovascular Health Study (CHS) enrolled 4,864 participants without a history of HF and of clinical stroke. After a diagnosis of HF at 80 years old, 5-year decline of cognitive functions was significantly worse compared with that in participants without HF of the same age period (27). Longitudinal data with a longer 8-year period of evaluating trajectories of 457 patients also demonstrated that congestive HF predicted cognitive decline (28).

Multiple Cognitive Domain Impairments in HF

Recent studies have paid further attention to the detailed and multiple cognitive domains and spectrum of brain lesions in patients with HF. It is well-acknowledged that patients with HF typically exhibit CI in domains of memory, particularly in both verbal and visual memory, working memory, attention, processing speed, and executive function (29). A secondary analysis of Atherosclerosis Risk in Communities (ARIC) study supported that the risk of developing CI had no concern with HFpEF or HFrEF, while worse diastolic function was weakly but significantly associated with worse performance in memory, attention, and language due to abnormal cardiac hemodynamics (30). Similarly, Anna Frey et al. enrolled 148 patients with HF and determined that patients with HF exhibited cognitive deficits in the domains of attention and memory with a prevalence of 41 and 46%, respectively. Furthermore, the degree of advanced medial temporal lobe atrophy (MTA) was strongly related to CI (31). Ichijo et al. assessed the frontal brain activity by near-infrared spectroscopy (NIRS) and non-invasively measured regional cerebral bold volume in patients with HF, showing that frontal brain activity was significantly lower in the HF group than in the control subjects (28.5 vs. 88.0 mM mm; $p < 0.001$) and significantly correlated with mini-mental state examination (MMSE) ($R = 0.414$, $p = 0.017$) (32). Similar data from Asian populations indicated that the neuropsychological impairment in Asian patients with HF characterized vascular pathology with frequently impaired visuomotor speed (60%), visuoconstruction (48%), and visual memory (43%) (11).

Deterioration of Prognosis With CI in HF

Heart failure (HF) and CI accelerate each other, and CI would further worsen the cardiac function and prognosis of HF with higher mortality, hospitalization admission, and poor quality of life (QoL). As early as before the incident HF, CI is prevalent in patients with subclinical chronic heart disease at high-risk

of chronic HF. A prior study supported that patients with MCI had 2-times higher risk with diastolic dysfunction and 1.7-times greater risk with other cardiac abnormalities (33). Moreover, the development of CI in patients with HF has an adverse impact on the clinical outcomes. Previous studies confirmed that CI was an independent risk factor for death and readmission in patients with HF, which increased the risk of cardiovascular mortality by 57% and the risk of all-cause death by 50%. The prospective multi-center prevalence and prognostic value of social frailty in geriatric patients hospitalized for HF (FRAGILE-HF) study enrolled 1,180 patients with HF aged ≥65 years, and 37.1% were identified as with CI using Mini-Cog. Further, they observed that coexistence of multiple frailty domains, including cognitive dysfunction, was prevalent in patients with HF readmission and all-cause death within 1 year (34). Similarly, Patel A et al. recruited 270 patients with HF and reported that the all-cause death and readmission rates of patients with CI were twice as high as those of patients without CI (46 vs. 22%, $p < 0.0001$) (35). In line with them, Hannes H et al. further recognized that worse scores of Montreal Cognitive Assessment (MoCA) heralded increased mortality and readmission risk. A study screened HF patients aged ≥70 and found that patients with HF with CI had a significantly higher 30-day readmission rate than those without CI (26.8 vs. 12.8%; $p < 0.05$) (36). CHS study examined CI and other common comorbidities in 558 participants who developed incident HF and showed that CI was significantly associated with greater total mortality risk (37). Additional investigations regarding the cognitive functions were conducted and worse outcome were observed. Huynh QL et al. performed MoCA in 1,152 Australian patients with HF with a 12-months follow-up, suggesting that visuospatial/executive and orientation were the cognitive domains that were most predictive of post-discharge adverse outcomes in HF (18). It should also be noted that even MCI could deteriorate the prognosis of patients with HF.

It is widely endorsed that patients with HF are vulnerable to CI with serious consequences in healthcare and outcome, with interplay of poor self-care, incapacity of adhering to treatment regimens, and weakening daily living due to decreased attentions, memory, and execution abilities (38–40). On the other hand, the difficulties in describing symptoms would interfere with the recognition by doctors of worsening HF, resulting in the inability to adjust treatment strategy in time. Apart from the adverse outcome brought from poor disease management, CI also seriously impairs QoL and exercise capacity of patients. The secondary analysis of the Wii-HF trial, conducted with 605 patients, evaluated CI using MoCA and measured exercise capacity using a 6-min walk test (6MWT). It indicated that lower 6MWT scores were associated with five domains in cognitive function, including visuospatial/executive, naming, attention, language, and orientation (19).

PATHOPHYSIOLOGY, CELLULAR MECHANISM, AND RISK FACTORS OF CI IN HF

The underlying mechanism proposed for CI in HF is multifactorial but not fully elucidated. It is important to understand the pathophysiological mechanism regarding CI in HF for a promising diagnostic and therapeutic approach. Existing evidence indicated that hemodynamic alterations and molecular mechanisms may play important roles in the interaction between HF and CI. Also, common cardiovascular and non-cardiovascular comorbidities burden further link HF and CI with risk factors which have not been well established. A systematic summary addressing the potential pathophysiology and mechanisms is illustrated in **Figure 3**.

Pathophysiology of CI in HF

Reduced Cerebral Blood Flow

It has well-established that HF usually has unfavorable effect on cerebral perfusion with decreased cerebral blood flow (CBF) (41). According to previous studies, CBF could be reduced by nearly 14–30% in chronic HF depending on the severity and chronicity of HF. Despite this, it can be managed using medical treatment, cardiac resynchronization therapy, left ventricular assist devices and heart transplantation (42–46). Several factors determine the reduced CBF in patients with HF. In addition to the systematic hypoperfusion caused by reduced cardiac output (CO) and blood pressure (BP), the distortion of cerebrovascular autoregulation also appear to play critical roles in decreasing CBF (47). The cerebral autoregulation ability help maintain the adequate blood flow in the brain after using vasodilators. However, in patients with HF, microcirculatory changes, such as endothelial dysfunctions, reduced nitric oxide bioavailability, and vascular smooth muscle proliferations may lead to impaired cerebral autoregulation and abnormal cerebrovascular reactivity which appears as significant determinants of reduced CBF in HF (48).

Due to high metabolic demand and limited capacity for energy stores, the normal functions of brain highly depend on adequate perfusion to maintain normal nerve activity. Thus, the subtler alterations of CBF impairment and hypoperfusion due to cardiac dysfunctions could cause chronic brain injury, especially the vulnerable areas in the brain (49). A recent study further calculated the whole-brain CBF maps using MRI scanner and found that reduced CBF appeared in multiple areas involving bilateral prefrontal, frontal, temporal and occipital cortex, thalamus, cerebellum, corona radiate, corpus callosum, hippocampus, and amygdala, which regulate memory, decision-making executive functions, and language (50). Additionally, prior data has revealed that white matter lesions (WML) were expanded in patients with HF and was associated to CI (51, 52). This data is regarded as a manifestation of cerebral small vessels. The extensively decreased cerebral perfusion in cognitive regulatory sites is likely to contribute to cognitive deficits.

The deleterious effects of local CBF loss on cognitive function regarding molecular level have not been fully clarified, while hypoxia, reduced metabolic activity, and neurohormonal activations may play crucial roles to contribute to brain injury (53). Hypoxia caused by hypoperfusion induce the release of hypoxia inducible factor-1 (HIF-1) and increase the expression of vascular endothelial growth factor-1 (VEGF-1), resulting in increased permeability and disruption of the blood-brain barrier (BBB) by destroying the tight junctions (54, 55). Moreover, it has

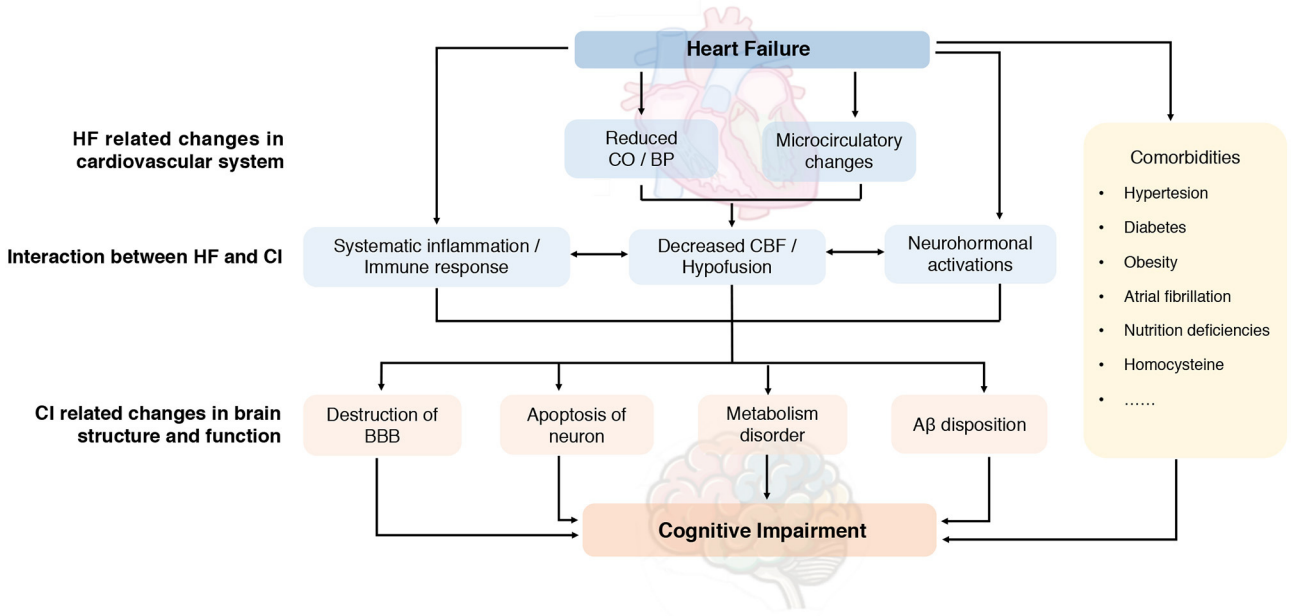

FIGURE 3 | Proposed pathophysiology of cognitive impairment in heart failure. Aβ, amyloid-β; BBB, blood-brain barrier; BP, blood pressure; CBF, cerebral blood flow; CI, cognitive impairment; CO, cardiac output; HF, heart failure.

been shown that the reduced CBF and chronic perfusion could decrease the ability of glial cells to eliminate amyloid-β (Aβ).

Even jeopardized CBF has commonly been considered to be the key explanations for CI in patients with HF as data on CBF in HFpEF with the similar manifestation of CI are still insufficient (56). Additionally, in the case of cortical gray matter loss with rich vasculature, reduced CBF did not seem to be the main causative factor (57), implying more pathological offenders should be investigated.

Inflammation, Oxidation, and Immunity

Amounting studies have shown that HF is considered as a state of systematic inflammation and that hypoperfusion in HF could contribute to local brain inflammation, which may also paly critical roles in development and deterioration of HF associated CI. Oxidative stress usually interplays with inflammation and is also proposed as one of the mechanisms in cognitive decline (58). Inflammatory factors, including interleukin-1 β (IL-1β), interleukin-6 (IL-6), tumor necrosis factor-α (TNF-α), CRP, and interleukin-17A (IL-17) have been found to be inversely associated with cognitive functions in HF patients (59) as these remain significant after changes in LVEF and symptoms of HF. Additionally, animal models of HF also demonstrated that the expression of inflammatory genes, such as toll-like receptor-4 (TLR-4), TNF-α, and IL-6, were significantly upregulated in the cortex and hippocampus, particularly in the mouse (60). Cytokines regulate cognition by altering the synaptic plasticity and neurogenesis and directly inhibit the neurotransmitter cascade involved in learning and memory (61, 62). Among the proinflammatory factors, IL-1β and TNF-α seems to be the main driver and regulator in the inflammatory response, causing cell death *via* increasing neurotoxicity. IL-1β decreases the release of glutamate, which further affects the release of brain-derived neural factors and promotes the activation of protein kinase by p38 mitogen in the hippocampus, thus interfering with the memory and consolidation ability of hippocampus (63). ASK1-p38-TNF-α is one of the key pathways involved in the disruption of the BBB, inducing the production of IL-6 (64). At the same time, IL-1β and TNF-α would upregulate the expression of CD73, which exert a protective effect on WHL by activation of glial cells and help to relieve inflammation *via* the counter-regulatory feedback (65).

Oxidative stress and immune response usually act synergistically. Increased level of circulating angiotensin II (Ang-II) during HF process induced perivascular macrophage (PVM) activation, which further regulate vascular permeability and recruit granulocyte. Upon Ang-II binds to angiotensin receptor 1 in the PVMs, the NADPH oxidase 2 is activated to promote ROS overproduction (66, 67). ROS, such as superoxide, NO, and ONOO–, increased BBB permeability *via* activating matrix metalloproteinase, producing oxidative damage to cellular molecules (68). Oxidative damage could also activate β-site amyloid precursor protein-cleaving enzyme-1 (BACE-1), resulting in increased synthesis of amyloid precursor protein (APP) and Aβ (60, 69). Meanwhile, the abnormality downregulated expressions of β-site amyloid precursor protein-cleaving enzyme-2 (BACE-2) and contribute to reduced degradation of Aβ precursor proteins.

During the process of Aβ synthesis and deposition, evidence suggest that immune mediator, such as microglia and the

macrophages in central nervous system, may contribute to the disease progression (70). Altered phenotype of microglia due to hypoperfusion result in impaired functions, which further reduce the elimination of Aβ (71). The high level of signal of translocator protein (TSPO) often indicate hyperactivated microglia. Thus, TSPO has been found as a useful marker to identify microglial activity. At the same time, active astrocytes express more amyloid precursor protein and cause an increasing Aβ production (72). Dendritic spines are important in learning and memory functions. When they are destroyed by excessive neurons, death, or Aβ, CI would occur (73).

In brief, the inflammation, oxidative stress, and immune response aggravate cognitive functions mainly *via* disruption of the BBB, damaging white matter and actitation of glial cells and, consequently, leading to CI (74).

Neurohumoral Activations

Although it has been well-documented that reduced CO and CBF are major drivers for CI in HF, interestingly, HFpEF without diminished brain perfusion has also proven to be closely and independently associated with CI. Therefore, current data support the notion that CI in HFpEF may be associated with additional mechanisms independent of hypoperfusion, of which neurohumoral activations have caught increasing attractions (75). Exacerbated neurohumoral activations may alter neuronal functions and promote productions of CI-related proteins in cognitive areas.

Sympathetic nervous system and renin-angiotensin system (RAS) activation and elevated catecholamine levels in HF were related to poor cognitive performance. On one hand, the exaggerated sympathetic activity and RAS participate in the rightward shift of the lower limit of CBF autoregulation and lead to CBF reduction in patients with HF (45). On the other hand, it is speculated that increased level of catecholamines in HF could disturb Wnt signaling *via* inducing a loss of β-adrenergic pathway. Wnt/β-catenin signaling has been implicated in the regulation of synaptic assembly, neurotransmission, and synaptic plasticity of hippocampus. Toledo et al. found that a rat with HF with normal EF displayed impaired learning process and memory loss. CI in the rats was correlated to the downregulated Wnt/β-catenin signaling, which attenuated phosphorylated glycogen synthase kinase 3β (p-GSK3β) in the hippocampus and reduced synaptic plasticity, ultimately impairing cognitive functions (76, 77).

In addition, sustaining activation of the neuroendocrine system, such as hypothalamic-pituitary-adrenal axis, was suggested to have potential effects on progression of HF and structural damages of brain by regulating the neuronal metabolism, physiologies, and gene expressions. Glucocorticoid receptors are commonly expressed in neurons and glial cells with the highest levels in the hypothalamus, hippocampus, and amygdala brain structures, while the mineralocorticoid receptors expressed most in the hippocampus, amygdala, and prefrontal cortex edge. The two kinds of cortisol receptors play vital roles for the normal cognitive functions (78).

Potential Cellular Mechanisms of CI in HF

Disruption of Blood-Brain Barrier

The complete BBB exert protective effects by preventing extravasation of toxic substances from circulation to the brain parenchyma. The increased permeability of BBB mainly caused by hypoperfusion and inflammation would lead to the influx of fluids, ions, albumin, and other proteins into neurons from the blood and cause infiltration of immune cells and secondary inflammation, further exacerbating brain edema, oxidative damage, luminal stenosis, and neuronal dysfunction, and ultimately lead to CI in patients with HF (79, 80).

Metabolism Disorder

The normal energy metabolisms in the brain are high reliant on proper cardiac function, thus poor perfusion and ischemia lead to rapid consumption of adenosine triphosphate (ATP) and subsequent ROS are produced. Oxidative damage further increases the production of cytokines to induce specific inflammatory changes and lead to Aβ deposition eventually (81). In addition, mitochondrial dysfunction has been suggested as a key mechanism during development of CI in HF, as energy deficiency would result in functional abnormalities of central neurons which are intimately linked to cognitive functions (82). Incremental evidence indicated that mitochondria are also critical for neurodevelopment and neurogenesis, while mitochondrial degeneration could mediate CI through Wnt signaling pathway (83).

Apoptosis of Neuron

Loss of brain cells has been observed in lots of neurological diseases. Bax, a member of the Bcl-2 family, plays a key role in regulating apoptosis. Prior studies have found that the expressions of Bax in the hippocampal cortex changed female mice with HF, which may affect the apoptosis process of neurons related to cognitive function in the brain (84). Furthermore, evidence have shown that the expression of caspase family, especially caspase 3 and 6, have been increased in the hippocampal tissue of mice with HF (85). Animal studies also found that the activation of the RAS in mice with HF can affect AMPK-PGC1α signaling by stimulating angiotensin II receptors and increase the apoptosis of neural stem cells in the hippocampus of rats (86).

Amyloid-β Deposition

Neuropathology of Alzheimer's disease (AD) such as Aβ deposition is closely related to chronic hypoperfusion. In patients with HF, a variety of pathways may participate in the accumulation and deposition of Aβ *via* increasing production and decreasing clearance, including CBF insufficiency, activation of microglia and astrocytes, inflammatory cascade, and oxidative imbalance. In turn, Aβ could aggravate these pathological alterations and promote neurodegenerative process, forming a vicious circle. The accumulation of Aβ ultimately leads to CI in patients with HF (87).

Risk Factors Predicting CI in Patients With HF

Although it is well-known that patients with HF are more prone to cognitive decline, the predictors of developing CI have not been fully clarified. Some earlier studies and systematic reviews revealed that left ventricular ejection fraction (LVEF) and 6-min walk tests (6MWT) were independently associated with development of CI in patients with HF. Recent work also pointed out that the high level of NT-proBNP was the independently predictor for CI in patients with HF (11, 88–90). In addition, the risk factors for dementia-related structural brain damage have also been explored. Karsten et al. observed a significant correlation between diminished gray matter density (GMD), decreased LVEF, increased NT-proBNP, and GMD in wide brain regions including the whole front median cortex along with the hippocampus and precuneus (91).

To date, the role of the well-established comorbidities in CI, such as diabetes mellitus (DM) and hypertension, has been controversial in HF-associated CI. The longitudinal time-varying analysis of Warfarin vs. Aspirin in Reduced Ejection Fraction (WARCEF) trial disclosed that higher baseline cognitive status (MMSE scores), non-white race, older age, lower education, and NYHA ≥ II were independently associated with cognitive decline in HF while traditional cardiovascular risk factors containing hypertension, DM, and smoking seemed no association with cognitive decline (92).

Besides, additional comorbidities coexisting with HF contributed to CI have become gradually recognized by exerting inflammatory, metabolic, and neurohormonal pathways (31). Obesity, as a significant contributor to HF and, especially, HFpEF, has become an established risk factor for adverse brain changes and poor cognitive outcome in HF (93). Atrial fibrillation (AF) was also demonstrated to be significantly associated with CI independent of a history of stroke, exhibiting lower total brain, gray and white matter volumes related to poorer cognition, and increased risk of dementia (94, 95). The potential mechanism includes micro-emboli and hypoperfusion resulting from abnormal heart rate and CO. Moreover, nutritional deficiencies are common in patients with HF due to absorption disorders of nutrition or diuretic use. Low level of folate, B12 vitamin, and albumin were correlated with CI and anemia (96). Animal models have demonstrated that thiamine deficiency caused brain atrophy and white matter changes, further affecting the learning ability in rats (3, 97). In addition, homocysteine levels due to renal insufficiency led to brain atrophy and brain cell apoptosis, further affecting neurogenesis and resulting in cognitive deficit (98).

CLINICAL DIAGNOSIS AND ASSESSMENT FOR CI IN HF

Subjective Assessment

Assessments, including subjective and objective, are crucial for the diagnosis of CI in HF. Whenever possible, history should be obtained both from the patient and from a family member, caregiver, or other reliable informant (99, 100). However, many patients with HF and their families accept cognitive decline as part of normal aging, and will declare themselves normal on the grounds that they are no worse than others their age. Therefore, subjective concerns alone are insufficient for diagnosis.

TABLE 1 | Screening tools used commonly in clinical practice for cognitive impairment (CI) diagnosis and assessment in general population.

Classification	Screening tools	Cut points*	Sensitivity (%)	Specificity (%)
MCI	MMSE (103)	≤22∼29	62∼85.5	53.0∼65.9
	MoCA (103)	≤22∼27	68.7∼93.0	63.9∼100.0
	Mini-Cog (109)	≤2	55	83
	CAMCOG (113)	≤94	72	76
	RCS (111)	≤7	87	70
	SLUMS (110)	≤23.5∼25.5	92∼100	55∼81
Dementia	MMSE (104–106)	≤23∼26	87∼89	82∼89
	MoCA (105)	≤17∼23	93	90
	Mini-Cog (106)	≤2	76∼99	89∼96
	CAMCOG (114)	≤92∼93	100	95
	RCS (111)	≤5	89	94
	SLUMS (110)	≤19.5∼21.5	100	91∼98

**The cut points for diagnosis of mild CI (MCI) are dependent on the population norms, age, educational level, and comorbidities, estimates of premorbid cognitive function. MMSE, mini-mental state examination; MoCA, montreal cognitive assessment; SLUMS, Saint Louis University mental status; RCS, rapid cognitive screen; CAMCOG, Cambridge cognitive examination.*

Neuropsychological Tests

The objective assessment requires to accomplish one or more standardized neuropsychological tests. Neuropsychological assessment of specific cognitive domains is preferred for both detecting mild impairments and for differential diagnosis. Diagnostic for CI in patients with HF are the same as in populations without HF. Previous studies have shown that the identification of CI by the screening tools was more accurate than the diagnosis by symptoms alone for patients with HF (101). More importantly, early diagnosis and therapy of CI could significantly reduce the 6-month readmission rate and mortality in patients with HF (101).

Multiple neuropsychological tests are available for CI assessment, including the MMSE (102–106), the MoCA (103, 105, 107), the Mini-Cog (108, 109), the Saint Louis University mental status (SLUMS) (110), the rapid cognitive screen (RCS) (111), and the Cambridge cognitive examination (CAMCOG) (112–114). MMSE and MoCA are the most frequently used tests in clinical practices. Due to different cut points, the sensitivity and specificity of screening tools are different (**Table 1**). It is critically important that the test performance of a patient be interpreted in accordance with norms for the age, educational level of that patient, and preferably for his/her cultural/linguistic group and region as well.

Nowadays, the diagnostic accuracy of neuropsychological tests to screen for CI in populations with HF varies widely in studies. In a study to evaluate the usefulness of MoCA and MMSE compared with the golden standard European Consortium

Criteria for diagnosing MCI in HF population, the sensitivity and specificity of MoCA were 82 and 91% and MMSE were 9 and 91% (115). Hawkins et al. also compared the ability of the MMSE and MoCA to detect CI in patients with HF (116). Both tests are useful in identifying the majority of patients with and without CI with the sensitivity and specificity around 60–70%. Other tests, such as the Mini-Cog and the CAMCOG, had a moderate accuracy in populations with HF (117, 118). With up and coming research investigating CI in HF, however, there is still no clear consensus regarding the optimal screening tool for the assessment of CI in HF. The evidence on how and when best to screen cognitive in patients with HF is needed.

Biomarkers

The neuropsychological tests only have a moderate accuracy for the assessment of CI, thus there is a large need of special biomarkers to support the clinical diagnosis. Cerebrospinal fluid (CSF) biomarkers that reflect the pathophysiology of CI have been increasingly used and are the most common test in neurology to identify CI. Circulating biomarkers would be preferable, as blood is more accessible than CSF. However, only a fraction of brain proteins enters the circulatory system due to the BBB. Of note, considering that patients with HF and CI have multiple pathologies, a broader panel of biomarkers reflecting neuro injury, inflammation, and oxidative stress would be needed.

Cerebrospinal Fluid Biomarkers

The exploration of biomarkers in CSF has focused on the core molecules of CI pathogenesis, including Aβ and tau proteins (119, 120). Numerous studies demonstrated that a marked decrease of Aβ42 in CSF can predict and identify CI due to cortical amyloid deposition in the brain (121, 122). In patients with AD, the degree of increase in CSF total tau is around 300% of control levels (123). A meta-analysis of 51 studies suggested that p-tau is also a satisfactory prognostic biomarker for progression of MCI (124).

However, the lumbar puncture for CSF testing is a rare to be accepted in patients with HF, although it is safe and cheap. Recent research investigated the associations of LVEF with CSF biomarkers in older adults (125). Results showed that participants with lower LVEF had higher levels of CSF t-tau and t-tau/Aβ42 ratios. There are few research focusing on the CSF biomarker in HF population. The biomarkers testing is still highly dependent on blood samples which are relatively convenient and suitable in clinical practice.

Circulating Biomarkers

Amyloid-β in Plasma

Amyloid-β 42 (Aβ42) is the most extensively studied blood biomarker for the diagnosis of symptomatic and prodromal AD and CI. Several studies reported plasma Aβ as a potentially useful biomarkers for the early diagnosis of cognitive dysfunction and for the prediction of its progression in Parkinson's disease and amnestic MCI (126, 127). However, Bayes-Genis et al. measured circulating Aβ40 in 939 consecutive patients with HF and found that there were no differences in circulating Aβ40 levels in HF patients with and without CI at baseline or during follow-up over a median of 4 years (128). Interestingly, in multivariable analysis, including relevant clinical predictors and N-terminal pro-brain natriuretic peptide (NT-proBNP), Aβ40 remained significantly associated with all-cause (HR, 1.22; 95%CI, 1.10–1.35; $p < 0.001$) and cardiovascular death (HR, 1.18; 95%CI, 1.03–1.36; $p = 0.02$), but not with HF-related death (HR, 1.13; 95%CI, 0.93–1.37; $p = 0.22$). Further studies are warranted to identify whether the bloodstream Aβ concentration results in or facilitates Aβ plaque formation in the brain in HF patients.

Inflammatory Factors in Plasma

Heart failure (HF) is considered a state of increased inflammatory responses which induce cognitive dysfunction involved in memory loss and impaired executive function. Redwine LS et al. investigated outpatients with HF and found that lower MoCA scores are associated with higher levels of plasma inflammatory biomarkers, such as interferon-γ (IFN-γ), tumor necrosis factor-α (TNF-α), and soluble vascular cell adhesion molecule-1 (sVCAM-1) (129). In an exploratory parallel design study of 69 patients with symptomatic HF, it was observed that changes in C-reactive protein (CRP) and IL-6 levels predicted alterations in MoCA scores (130).

Cortisol in Plasma

Cortisol was indicated to influence cognitive function. Elevated serum levels of cortisol were observed in patients with HF compared with healthy controls. More importantly, significantly higher levels of cortisol were found in patients with HF who had symptoms of depression and CI than those free from these symptoms. Besides, matched patients treated with cortisol performed worse on specific cognitive assessments compared with those treated with placebo, suggesting that cortisol levels in HF might influence the development of CI.

Natriuretic Peptide in Plasma

Elevated brain natriuretic peptide (BNP) and NT-proBNP are also associated with CI and increased risk for dementia in patients with HF. In recent years, there have been major advances in the development of blood-based biomarkers for CI. However, the sensitivity and specificity of a single circulating biomarker are not significant. Hence, a combination of biomarkers may offer a better diagnosis value for CI in HF.

Potential Biomarkers in Blood

Recent developments have also given some novel circulating candidate biomarkers for CI. The novel N-terminal tau fragment (NT1) in plasma is not only a biomarker to distinguish normal, MCI, and AD dementia populations with high specificity and sensitivity, but is also a strong predictor of future cognitive decline and neurodegeneration in healthy elderly individuals (131, 132). A parallel metabolomics analysis in both the brain and blood conducted by Varma et al. identified 26 metabolites from two main classes, sphingolipids and glycerophospholipids, consistently associated with severity and progression of AD (133). Abdullah et al. found that the serum flotillin levels significantly decreased in patients with AD compared with those of non-AD controls, suggesting flotillin, the abundant

exosome protein, may be a novel diagnostic marker for AD (134). However, these biomarkers mainly target in AD in the general population. Further studies are needed to validate these findings in patients with CI, especially in patients with HF and CI. Additional technical developments of novel ultrasensitive immunoassay and mass spectrometry methods show promise for blood biomarkers with potential applications as screening tools for CI in HF.

Neuroimaging

Neuroimaging has contributed to our understanding of the mechanisms by which HF may lead to CI and is recommended by guidelines for CI diagnosis. Structural changes of brain, such as increased white matter hyperintensities, gray matter loss, and brain atrophy, are frequently encountered imaging findings in patients with HF with CI and often preceded by functional changes.

Structural Brain Changes in Neuroimaging

White Matter

The increase of white matter hyperintensities (WMH) may represent underlying ischemia and impact upon the course of cognitive symptoms, which has been reported as a specific change of HF-related CI. The pathologically characteristics of WMH contains pale myelin sheath, loss of myelin sheath and axon, and mild gliosis. WMH can lead to cognitive decline and increase the risk of depression, anxiety, cerebrovascular events, dementia, and even death. These lesions usually present in small vessel diseases, which are considered to be the result of the destruction of the BBB caused by chronic cerebral hypoperfusion and the subsequent infiltration of plasma into white matter (135, 136). Brain MRI is a sensitive indicator of cerebrovascular disease and could use to image patients with HF with CI as it can reveal a number of asymptomatic findings, including WMH. Beer et al. found that left medial temporal lobe atrophy and deep WMH detected by MRI showed a negative correlation with cognitive scores in patients with HF compared with healthy controls (137). The population-based LIFE-Adult Study quantitated white matter lesions in 2,490 participants and found that the prevalence was independently associated with WML (OR 2.8, 95% CI 1.2–6.5), which was associated with cognitive dysfunction (138). Further, the longer duration of HF independently predicted WML while the duration of hypertension not.

Diffusion tensor imaging (DTI) reflects the integrity of the fiber bundle by detecting the anisotropy and degree of the water molecule diffusion in cerebral white matter fibers, which clearly display the direction and distribution of intracranial white matter fiber bundles after post-product. Kumar et al. found that the axial and radial diffusion was significantly increased and mainly existed in autonomous, analgesic, emotional, and cognitive parts in patients with HF than that in health controls, suggesting that the axon integrity and myelin were injured in patients with HF (139).

Gray Matter

The majority of imaging studies in CI have used MRI to investigate changes in gray matter structure. Almeida et al. compared the brain gray matter reduction using MRI and emotional changes between patients with chronic HF and healthy controls (140). It has demonstrated that the prevalence of depression and anxiety was much higher in patients with HF compared with that in healthy controls. Of note, gray matter loss mostly in particular parts of the brain with motional regulation, such as left and right thalamus, left caudate nucleus, left and right posterior cingulate gyrus, left and right parahippocampal gyrus, left upper middle temporal gyrus, and right lower parietal lobe.

Brain Atrophy

Studies have shown that half of patients with chronic HF has cortical brain atrophy exists, which is 10-flod higher than that in the control group (31, 91). With the advancement of imaging technologies, the detrimental effects of HF on CI have also been demonstrated with structural alterations of brain. The COGNITION.MATTERS-HF prospective cohort study quantified the concurring dynamics affecting cognitive functions in 148 patients with mild chronic HF and found that cognitive function remained stable with "intensity of attention" as the only domain declining over 3 years (141). Moreover, in patients with HF, the markedly reductions of hippocampal volume observed at baseline was more related to impaired cognitive function, while the total brain volume and the load of white matter change within the limits of normal aging.

Functional Brain Changes in Neuroimaging

The use of single photon emission computed tomography (SPECT) enables to detect the distribution of radionuclides in the body. It is widely utilized due to its great value of diagnosis for early metabolic disorder in various diseases. Alves et al. found that the regional cerebral blood flow reductions in patients with HF using SPECT was similar to the regional glucose metabolism disorder in patients with CI by positron emission tomography, which support to a view that congestion dysfunction brain changes of congestion dysfunction may develop in patients with HF, possibly as a consequence of chronic cerebral blood flow hypoperfusion (142). Recently, a prospectively study enrolled 102 patients with HF and 15 healthy controls who underwent gated 99mTc-sestamibi SPECT and found that cerebral metabolism in the whole brain was reduced, especially hippocampus and para-hippocampus areas in patients with HF, while the cerebral metabolism maintained in frontal areas due to its higher sensitivity and self-regulation (143).

Functional MRI (fMRI) is a technique highlighting regional patterns of brain activation based on little change of the deoxy/oxy-hemoglobin ratio (144). Once the neuronal activity is enhanced, the blood flow through the cortex functional region significantly increased, which results a change of deoxy/oxy-hemoglobin ratio. This ratio, due to the different magnetic properties of hemoglobin states, can be measured through MRI and reconstructed in the form of blood oxygenation level–dependent signal. Hence, fMRI has been widely used to describe the characteristics cerebral function and functional networks in CI and its related diseases. Several studies have shown the extensive activity reduction in the brain of patients with diabetes.

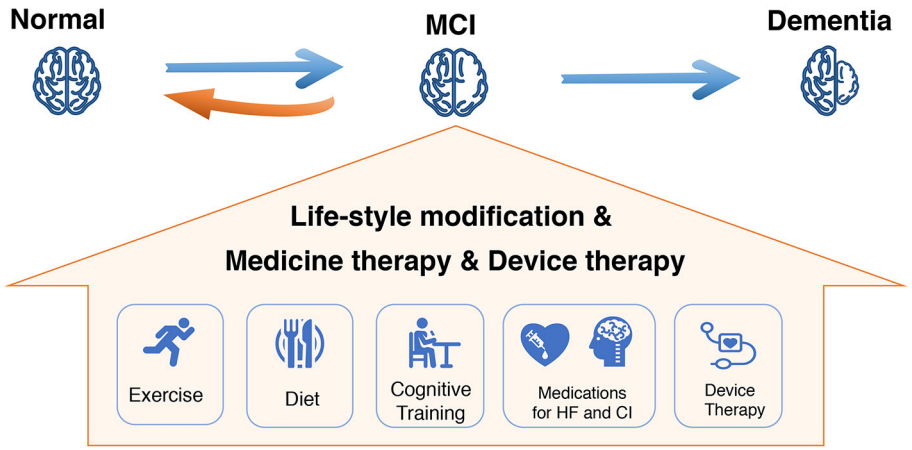

FIGURE 4 | Comprehensive management for mild CI (MCI) in HF to halt disease progression. MCI, mild cognitive impairment; HF, heart failure.

However, fMRI is rarely used in patients with HF and CI clinically and data specific for HF are currently lacking.

PREVENTION AND POTENTIAL THERAPEUTIC OPTIONS FOR CI IN HF

Improving and maintaining cardiac function should be the primary strategy for treatment of CI in patients with HF, which would have a positive impact on brain function (**Figure 4**). Although clinical guidelines in HF have recently begun to emphasize the importance of CI in HF, few recommendations are available to guide clinicians about how to approach CI in patients with HF. Contemporary HF therapies may improve or aggravate cognitive decline (**Table 2**). On the other hand, therapy for CI may also have cardiovascular side effects, which may in turn affect the treatment of HF. Furthermore, research are undergoing to develop novel potential therapeutic targets for CI and HF (**Table 3**).

Contemporary Medical Therapies

Effect of HF Medical Therapy on CI

Sodium Glucose Co-Transporter 2 Inhibitor

The novel antidiabetic agent, sodium glucose co-transporter 2 (SGLT2) inhibitor, is essential for overcoming the burden of diabetic and have beneficial cardiovascular and renal effects, especially in improving the prognosis of HF, which supports it as a foundational therapy for HF (153, 154). Evidence have shown SGLT2 inhibitor to limit or slow down brain pathology in CI among patients with diabetes. Animal studies indicated that SGLT2 significantly ameliorated cognitive decline in type 2 diabetic mice (152, 155). A recent large propensity score-matched population-based study demonstrated that patients treated with SGLT2 inhibitors were associated with lower risks of dementia compared with when treated with DPP4 inhibitors (148). Simone et al. also found that cognitive status did not change significantly during the 12 months of treatment of SGLT2 inhibitor (156). However, whether the SGLT2 inhibitor could reduce incidence of cognitive or improve the cognitive dysfunction in HF is not known and requires further confirmation.

Angiotensin Receptor Neprilysin Inhibitor

Angiotensin receptor neprilysin inhibitors (ARNIs) significantly improve the clinical outcome of patients with HFrEF as shown in PARADIGM-HF which compared the angiotensin receptor neprilysin inhibitor (ARNI) (sacubitril/valsartan) with angiotensin converting enzyme inhibitor (ACEI) (enalapril). As neprilysin is one of enzymes clearing Aβ peptides from the brain, in theory, inhibition of neprilysin may reduce Aβ degradation and accelerate its accumulation (145). Besides, inhibition of neprilysin increases bradykinin levels, which directly interacts with Aβ1-42 aggregates to generate Aβ plaques. Hence, there is a concern about how neprilysin inhibitor may cause cognitive decline in patients treated with ARNI. However, large scale randomized controlled trials, such as PARADIGM-HF, confirm that there is no adverse effect of ARNI on CI (146, 147). A possible cause may be that cognitive decline in HF is not wholly related to Alzheimer's type pathology and may also be associated with declining cardiac function and vascular abnormalities. Therefore, the long-term ARNI treatment, by improving cardiovascular function and preventing hospitalization, may have a positive effect on cognitive function in patients with HF. Further, a study, PERSPECTIVE (NCT 02884206), is undergoing to explicitly focused on whether ARNNI will lead to CI in populations with HFpEF. This study is expected to be completed in March 2022.

Angiotensin Converting Enzyme Inhibitor/Angiotensin II Receptor Blocker

Angiotensin converting enzyme inhibitors (ACEIs)/angiotensin II receptor blockers (ARBs) have been shown to improve cognitive function in patients with HF by reducing the activity of sympathetic nervous system and improving cerebral blood flow (150). In a mouse model of AD, the centrally active ACEI perindopril significantly reversed the CI, including the indices of immediate working memory and relatively long-term

TABLE 2 | Summary of trials targeting medical treatment of cognitive impairment in heart failure (HF) (completed).

Trial	Year of publication	Study design	Intervention	Study population (*n*)	Primary end point	Secondary end points	Results
ACEIs/ARBs							
The antihypertensives and vascular, endothelial and cognitive function trial (AVEC trial) (157)	2012	Randomized, controlled	Candesartan vs. lisinopril vs. hydrochlorothiazide	hypertension and cognitive impairment aged ≥60 years (53)	Changes in cognitive assessment: making test parts A and B (TMT), Hopkins verbal learning test—revised (HVLT), and the digit span test.	Change of systolic blood pressure and blood flow velocity	Candesartan improved in TMT-B ($P = 0.008$), the adjusted TMT, B-A which adjusts the test for motor speed ($P = 0.012$), and the recognition portion of the HVLT ($P = 0.034$). Blood pressure control levels and systolic blood pressure reductions were equivalent in all three groups.
Soto et al. (151)	2013	Randomized, controlled	ACEIs vs. other antihypertensive drugs	Older adults with mild to moderate Alzheimer's disease (616)	Change in MMSE score.	-	The use of ACEIs in older adults with AD is associated with a slowest rate of decline in MMSE score independent of hypertension.
Ginkgo evaluation of memory study (GEMS) (158)	2013	A *post-hoc* analysis of the randomized controlled GEMS trial.	ACEIs vs. diuretic vs. ARB vs. β-blocker vs. CCB	Older adults aged ≥75 years with normal cognition (1,928) or MCI (320)	Incidence of AD.	-	ACEI, ARB, or diuretic use was associated with reduced risk of AD among patients with normal cognition or MCI.
Zuccalà et al. (150)	2005	Observational, retrospective	With ACEIs vs. without ACEIs	Heart failure (1,220)	The improvement of cognitive performance	-	Cognitive performance improved in 30% of participants started ACEIs, but only in 22% of remaining patients ($P = 0.001$). Use of ACEIs among patients with heart failure was associated with improving cognition (odds ratio = 1.57; 95% CI 1.18–2.08) in the multivariable regression modeling, independently of baseline or discharge blood pressure levels. The probability of improving cognitive performance was higher for dosages above the median values compared with lower doses (odds ratios = 1.90 and 1.42; P for trend = 0.001), and increased with duration of treatment (odds ratios for the lower, middle, and upper tertiles = 1.25, 1.34, and 1.59; P for trend = 0.007)
Ouk et al. (160)	2021	Observational, retrospective	ACEIs vs. ARBs	Cognitively normal or AD/MCI with amyloid-β-positive aged 55–90 years (311)	Global and sub-regional amyloid-β accumulation by ^{18}F-flflorbetapir	-	In cognitively normal older adults, ARB use was associated with a lower rate of global Aβ accumulation over time compared to ACE-I users. The rates of amyloid-β accumulation had no difference between ARBs or ACEIs in amyloid-positive participants with AD dementia or MCI.

(Continued)

TABLE 2 | Continued

Trial	Year of publication	Study design	Intervention	Study population (*n*)	Primary end point	Secondary end points	Results
Hajjar et al. (159)	2020	Randomized, controlled	Candesartan vs. lisinopril	hypertension and mild cognitive impairment aged 55 years or older (141)	Change in executive function (measured using the trail making test, executive abilities: measures and instruments for neurobehavioral evaluation and research tool)	Change in episodic memory (measured using the Hopkins verbal learning test-revised) and microvascular brain injury reflected by MRI of white matter lesions.	Candesartan was superior to lisinopril on the executive function measured by Trail Making Test Part B [effect size (ES) = −12.8 (95% CI, −22.5 to −3.1)] but not executive abilities: measures and instruments for neurobehavioral evaluation and research score. Candesartan was also superior to lisinopril on the secondary outcome of Hopkins Verbal Learning Test-Revised delayed recall [ES = 0.4 (95% CI, 0.02–0.8)] and retention [ES = 5.1 (95% CI, 0.7–9.5)].
β-blockers							
Holm et al. (162)	2020	Randomized, controlled,	With β-blockers vs. without β-blockers	General population treated with β-blockers (18,063)	Incidence of dementia (developing vascular dementia, all-cause, Alzheimer's and mixed dementia)	-	β-blocker therapy was independently associated with increased risk of developing vascular dementia, regardless of confounding factors (HR: 1.72, 95%CI 1.01–3.78; P = 0.048). Conversely, treatment with β-blockers was not associated with increased risk of all-cause, Alzheimer's and mixed dementia
ARNI							
PARADIGM-HF. (146)	2017	Randomized, controlled	Sacubitril/valsartan 97/103 mg bid vs. enalapril 10 mg bid in a 1:1 ratio	Symptomatic HFrEF (8,399)	Relevant cognition- and memory-related adverse event (AE) reports	-	The incidence of dementia-related AEs in patients treated with sacubitril/valsartan was similar to that in patients treated with enalapril.
SGLT2 inhibitor							
Simone et al. (156)	2018	Randomized, controlled	Incretins vs. SGLT2 inhibitor	Elderly patients with type 2 diabetes mellitus (39)	Change of cognitive performance with the attentive matrices test, the verbal fluency test and the Babcock story recall test.	Metabolic outcomes.	Cognitive status did not change significantly during the 12 months of treatment in SGLT2 inhibitor group or incretins group. SGLT2 inhibitor resulted in a reduction in weight, in BMI, and an increase in high-density lipoprotein cholesterol.
Mui et al. (148)	2021	Retrospective, territory-wide cohort study	SGLT2I vs. DPP4I	Type 2 diabetes mellitus patients (39,828)	New-onset dementia, Alzheimer's, and Parkinson's.	All-cause, cardiovascular, and cerebrovascular mortality.	SGLT2I users had lower incidences of dementia, Alzheimer's, Parkinson's disease, all-cause, cerebrovascular, and cardiovascular mortality. SGLT2I use was associated with lower risks of dementia, Parkinson's, all-cause, cardiovascular, and cerebrovascular mortality.

Aβ, amyloid-β; ACEIs, angiotensin converting enzyme inhibitors; AD, Alzheimer's disease; ARNI, angiotensin receptor neprilysin inhibitor; ARBs, angiotensin II receptor blockers; MCI, mild CI; MRIs, magnetic resonance images; SGLT2, sodium glucose co-transporter 2.

TABLE 3 | Ongoing trials targeting medical treatment of CI in HF.

Trial	Study design	Intervention	Study population (*n*)	Primary end point	Secondary end points	ClinicalTrials.gov identifier
ACEIs/ARBs						
Candesartan's effects on Alzheimer's disease and related biomarkers (CEDAR)	Randomized, controlled	Candesartan vs. Placebo	Mild cognitive impairment; amyloid positivity determined (77)	Hypotensive episodes, symptoms of hypotension, elevated serum creatinine, hyperkalemia, discontinuing the study medication	Change in cerebrospinal fluid (CSF) Tau levels, pulse wave velocity (PWV), augmentation index (AI), brain perfusion, hippocampal volume, vasoreactivity, clinical dementia rating (CDR)	NCT02646982
Angiotensin (1–7)						
Angiotensin (1–7) treatment to improve cognitive functioning in heart failure patients	Randomized, controlled	Drug: angiotensin-(1–07) Behavioral: memory training	Adults with chronic HF; without neurologic or psychiatric disorders (16)	Changes in performance on the Memory Intentions Test (MIST)	Changes of assessment of self-reported quality of life (QoL) and systemic inflammation assay	NCT03159988
ARNI						
A multicenter, randomized, double-blind, active-controlled study to evaluate the effects of LCZ696 compared to valsartan on cognitive function in patients with chronic heart failure and preserved ejection fraction	Randomized, controlled	LCZ696 vs. valsartan vs. placebo	Patients with chronic HFpEF and cognitive function (592)	Change in the CogState global cognitive composite score (GCCS)	Change in cortical composite standardized uptake value ratio (SUVr), individual cognitive domains (memory, executive function, and attention), the summary score of the instrumental activities of daily living (IADL)	NCT02884206

recognition memory (149). In elderly patients with hypertension and CI, studies have indicated that ACEIs and ARBs could improve the cognitive function and were associated with reduced risk of AD (151, 157–159). Recently, research demonstrated that ARBs had a stronger protection against memory decline than ACEIs through its potential benefits on the inhibition of Aβ accumulation in the cortex (160).

β-Blockers

Findings of β-blockers to improve CI are heterogeneous, and some are even controversial. β-blockers may reduce the incidence of CI through the control of blood pressure. It has been first reported in *JAMA* in 1986 that β-blockers may lead to depression, which is a cause of CI. However, another study showed that there was no correlation between β-blockers and depression the next year. A meta-analysis indicated β-blockers were related to the occurrence of vascular dementia (161, 162). Thus, further investigations are warranted to identify the specific relationship between β-blockers and CI.

Mineralocorticoid Receptor Antagonists

Mineralocorticoid receptors are ubiquitously expressed in limbic brain structures such as the hippocampus, amygdala, and prefrontal cortex. Findings showed that mineralocorticoid receptor antagonists (MRAs) decreased verbal learning, verbal memory, and visuospatial memory in adult population and impaired verbal memory and executive function in young depressed patients. However, MRAs improved verbal learning and visuospatial memory in elderly depressed patients. Thus far, the relevant research of MRAs and CI is relatively limited, and the impact of MRAs on CI is still controversial (163).

Effect of CI Medical Therapy on HF

Virtually all clinical trials of HF therapy have excluded patients with CI or dementia. There is limited data pertaining to the treatment for CI in HF. As a result, current guidelines are unable to provide evidence-based recommendations for diagnosis and treatment of patients with CI in routine clinical practice (164). Acetylcholinesterase inhibitors and memantine are considered as the first-line therapy for CI due to the benefit of concentration and memory. A position paper from the Study Group on Heart and Brain Interaction of the Heart Failure Association mentioned the favorable side effect profile for CI and the potential cardiovascular adverse events. For acetylcholinesterase inhibitors co-treated with β-blockers, digoxin, amiodarone, and calcium channel blockers may increase the risk for syncope or heart block. Dizziness, hypertension, angina, bradycardia, and HF may be observed in patients treated with memantine (165, 166).

Novel Therapeutic Targets

Angiotensin-converting enzyme 2 (ACE2), angiotensin-(1-7) [Ang-(1-7)], and Mas have been identified as a new component of RAS, which constitute ACE2-Ang-(1-7)-Mas axis (167). Recently, Ang-(1-7) has showed to reverse HF-related CI in animal experiment. Ang-(1-7) is mainly produced by the hydrolysis of Ang II and the ligand for the Mas receptor. MAS is highly

expressed in the hippocampus, a brain region related to memory function. Thus, the activation of Mas by Ang-(1-7) may play a protective role in brain. Hay et al. found that following 3 weeks treatment with systemic Ang-(1-7), the HF mice novel object recognition discrimination ratios were significantly better than the performance of mice with HF treated with saline (168). Ang-(1-7) also improved spatial memory in mice with HF without effect on cardiac function. Besides, 3 weeks of Ang-(1–7) treatment in the mice with HF resulted in a significant increase in plasma IL-1a, G-CSF, IL-16, and sICAM, which have been shown a neuroprotection in animal models of head injury or brain ischemia (169). The latest study demonstrated a novel glycosylated Ang-(1-7) peptide, Ang-1-6-O-Ser-Glc-NH_2 (PNA5), which has greater brain penetration compared with the native Ang-(1-7) peptide in HF mice model. Moreover, after treatment with subcutaneous injection 1.0/mg/kg for 3 weeks, PNA5 activation of the Mas receptor reversed object recognition impairment in mice with HF and rescued spatial memory impairment. PNA5 treatment also decreased circulating pro-inflammatory cytokine, such as TNF- α, IL-7, and granulocyte cell-stimulating factor serum levels, while increasing that of the anti-inflammatory cytokine IL-10.

As an important inflammatory factor mediating the occurrence of CI in HF, TNF- α is also a potential therapeutic target. TNF-α inhibitor Etanercept improve cognitive function by increasing the density of dendritic spines in frontal and parietal cortex (76). In addition, Lidington et al. found that a TNF-α negative regulator, cystic fibrosis transmembrane conductance regulator (CFTR) may be a novel therapeutics target for CI in HF. By emulating the key features of HF-related CI, including reduced CBF and compromised neurologic function in mouse models, CFTR corrector compounds (C18) normalize pathological alterations in cerebral artery CFTR expression, vascular reactivity, and cerebral perfusion without affecting systemic hemodynamic parameters (170). Therefore, CFTR therapeutics may be a novel target to manage CI in HF.

Non-pharmacologic Approaches for CI in HF

Life-Style Modification Physical Activity and Exercise

Studies indicated that the modification of lifestyle, including exercise and diet, can potentially improve cognition in patients with HF. Higher daily steps per day predicted better cognitive function and greater subcortical volume, with specific effects for the thalamus and ventral diencephalon (171). Redwine et al. also showed a greater MoCA score increases in patients with HF with Tai Chi or resistance band exercise compared to treatment as usual. Recently, Vellone et al. found that worse CI was independently associated with lower 6MWT scores. Of note, exercise capacity was associated with various cognitive domain, including visuospatial/executive, naming, attention, language, and orientation (19). Diet modification, such as low-salt diet, Mediterranean diet, and high-fiber diet, is also a feasible approach to preserving cognitive function and reducing risk of dementia. Several observational studies reported a protective association between certain nutrients (e.g., folate, flavonoids, vitamin D, and certain lipids) or food groups (e.g., seafood, vegetables, and fruit) and cognitive outcomes in older adults. A large randomized controlled trial further demonstrated a 2-year multidomain intervention of diet, exercise, cognitive training, and vascular risk monitoring could improve or maintain cognitive function in at-risk elderly people from the general population (172).

Device Therapy

Device therapy of HF has been reported contribute to cognitive improvement by improving cardiac output. Patients with moderate to severe HF enhanced cognitive outcomes within 3 months of cardiac resynchronization therapy (CRT) due to the improved left ventricular ejection fraction (LVEF) in response to CRT (173). Patients with improved LVEF showed better outcomes on measures of executive functioning, global cognition, and visuospatial functioning. Similarly, Zimpfer et al. indicated that successful ventricular assist devices implantation contributes to cognitive improvement by increasing cerebral blood flow in patients with advanced HF (174). Besides, as a common comorbidity of HF, AF exacerbates cognitive dysfunction and cerebral perfusion in patients with HF (94). Recently, a prospective case-control study assessed changes in cognitive function in 308 patients treated with AF catheter ablation and 50 medically managed controls, finding a significant improvement in cognitive function at 3 months and 1 year after ablation but not in the control group (175). This result supported that ablation may facilitate cognitive recovery from cerebral hypoperfusion by restoring sinus rhythm.

KNOWLEDGE GAPS AND AREAS FOR FUTURE RESEARCH

The prevalent CI in patients with HF bring a greater burden to the poor outcome and worsening quality of life. Even though great efforts sought to characterize the detrimental issue the with increasing awareness and advancement of the diagnostic tools, knowledge gaps still exist in this field. First, more prospective data on the role of HF in cognitive decline await future detailed investigations. Specifically, well-designed longitudinal studies with longer follow-up are warranted to illustrate the time cure in regard of: (1) the precise progression of cognitive decline from normal to dementia in patients with HF; and (2) the deleterious effect of varying degree of CI on survivor time and clinical course of HF. Additionally, comprehensive evaluations, including treatment effectiveness, compliance, caregiver burden and frailty, should be considered. Second, further research deserves to expound the contributory mechanisms involved in the pathophysiology of CI in HF to deepen understanding of heart-brain interaction. Third, systematic assessment of CI in HF with multiple imaging and neuropsychiatric approach, risk stratifications with specific biomarker profiles, and prediction models are expected to provide more prognostic information and guide therapy decisions. Fourth, despite the growing knowledge about the mutual malignant impact of HF and CI, little is known on promising targets for novel therapeutic interventions.

In the future, research priorities outlined above will attract far more attentions in HF-CI interconnectivity. The availability of novel techniques, emerging and existing (repurposed) therapies, computational modeling and novel insights will help address these knowledge gaps.

CONCLUSIONS

Heart failure (HF) and CI are increasing in prevalence and, when present together, are associated with significant mortality and morbidity. The underlying mechanisms of the link between cardiac dysfunction and brain pathologies in HF condition are still largely elusive. While patients with HF with dementia have great difficulties in daily life and are heavily dependent on caregivers, patients with CI are more independent. Routine screening of CI is needed in HF, even from using a simple tool like MoCA, thereby improving the efficiency of HF management. In patients with HF and CI, lifestyle change and risk factor control, standard HF therapy, and appropriate medication for CI should be standard of management. Further studies are needed not only to unravel the bidirectional pathology of the heart and cognition, but also to provide more efficient interventions in the brain following HF-associated conditions. Close collaboration between the HF and neurology specialists is essential in the early recognition and appropriate management of these patients. Future research to develop a consensus management guideline for patients with HF and CI, which is not yet available, is warranted.

AUTHOR CONTRIBUTIONS

MYang and DS searched and selected the references and wrote the first draft of the review. YW and MYan contributed toward literature review and interpretation of the manuscript. JZ and JR helped to determine the content and structure of the review and contributed to the writing and revision of the manuscript. All authors approved the final version of the paper.

FUNDING

This study was supported by the National Natural Science Foundation of China (81770359 to JR), Beijing Health Technologies Promotion Program (BHTPP202004 to JR), Open Project Fund of State Key Laboratory of Molecular Developmental Biology of China (2021-MDB-KF-18 to JR), and Elite Medical Professionals Project of China-Japan Friendship Hospital (ZRJY2021-BJ01 to JR).

REFERENCES

1. Patnode CD, Perdue LA, Rossom RC, Rushkin MC, Redmond N, Thomas RG, et al. Screening for cognitive impairment in older adults: updated evidence report and systematic review for the US preventive services task force. *JAMA*. (2020) 323:764–85. doi: 10.1001/jama.2019.22258
2. Virani SS, Alonso A, Aparicio HJ, Benjamin EJ, Bittencourt MS, Callaway CW, et al. Heart disease and stroke statistics-2021 update: a report from the American Heart Association. *Circulation*. (2021) 143:e254–743. doi: 10.1161/CIR.0000000000000950
3. Havakuk O, King KS, Grazette L, Yoon AJ, Fong M, Bregman N, et al. Heart failure-induced brain injury. *J Am Coll Cardiol*. (2017) 69:1609–16. doi: 10.1016/j.jacc.2017.01.022
4. Bueno H, Moura B, Lancellotti P, Bauersachs J. The year in cardiovascular medicine 2020: heart failure and cardiomyopathies. *Eur Heart J*. (2021) 42:657–70. doi: 10.1093/eurheartj/ehaa1061
5. Metra M, Teerlink JR. Heart failure. *Lancet*. (2017) 390:1981–95. doi: 10.1016/S0140-6736(17)31071-1
6. Owens DK, Davidson KW, Krist AH, Barry MJ, Cabana M, Caughey AB, et al. Screening for cognitive impairment in older adults: US preventive services task force recommendation statement. *JAMA*. (2020) 323:757–63. doi: 10.1001/jama.2020.0435
7. Dunne RA, Aarsland D, O'Brien JT, Ballard C, Banerjee S, Fox NC, et al. Mild cognitive impairment: the Manchester consensus. *Age Ageing*. (2021) 50:72–80. doi: 10.1093/ageing/afaa228
8. Arvanitakis Z, Shah RC, Bennett DA. Diagnosis and management of dementia: review. *JAMA*. (2019) 322:1589–99. doi: 10.1001/jama.2019.4782
9. Cameron J, Worrall-Carter L, Page K, Riegel B, Lo SK, Stewart S. Does cognitive impairment predict poor self-care in patients with heart failure? *Eur J Heart Fail*. (2010) 12:508–15. doi: 10.1093/eurjhf/hfq042
10. Zuccalà G, Marzetti E, Cesari M, Lo Monaco MR, Antonica L, Cocchi A, et al. Correlates of cognitive impairment among patients with heart failure: results of a multicenter survey. *Am J Med*. (2005) 118:496–502. doi: 10.1016/j.amjmed.2005.01.030
11. Dong Y, Teo SY, Kang K, Tan M, Ling LH, Yeo PSD, et al. Cognitive impairment in Asian patients with heart failure: prevalence, biomarkers, clinical correlates, and outcomes. *Eur J Heart Fail*. (2019) 21:688–90. doi: 10.1002/ejhf.1442
12. Busse A, Hensel A, Gühne U, Angermeyer MC, Riedel-Heller SG. Mild cognitive impairment: long-term course of four clinical subtypes. *Neurology*. (2006) 67:2176–85. doi: 10.1212/01.wnl.0000249117.23318.e1
13. Di Carlo, Lamassa M, Baldereschi M, Inzitari M, Scafato E, Farchi G, et al. CIND and MCI in the Italian elderly: frequency, vascular risk factors, progression to dementia. *Neurology*. (2007) 68:1909–16. doi: 10.1212/01.wnl.0000263132.99055.0d
14. Plassman BL, Langa KM, Fisher GG, Heeringa SG, Weir DR, Ofstedal MB, et al. Prevalence of cognitive impairment without dementia in the United States. *Ann Intern Med*. (2008) 148:427–34. doi: 10.7326/0003-4819-148-6-200803180-00005
15. Lopez OL, Jagust WJ, DeKosky ST, Becker JT, Fitzpatrick A, Dulberg C, et al. Prevalence and classification of mild cognitive impairment in the cardiovascular health study cognition study: part 1. *Arch Neurol*. (2003) 60:1385–9. doi: 10.1001/archneur.60.10.1385
16. Petersen RC, Smith GE, Waring SC, Ivnik RJ, Tangalos EG, Kokmen E. Mild cognitive impairment: clinical characterization and outcome. *Arch Neurol*. (1999) 56:303–8. doi: 10.1001/archneur.56.3.303
17. Farias ST, Mungas D, Reed BR, Harvey D, DeCarli C. Progression of mild cognitive impairment to dementia in clinic- vs. community-based cohorts. *Arch Neurol*. (2009) 66:1151–7. doi: 10.1001/archneurol.2009.106
18. Huynh QL, Negishi K, De Pasquale CG, Hare JL, Leung D, Stanton T, et al. Cognitive domains and postdischarge outcomes in hospitalized patients with heart failure. *Circ Heart Fail*. (2019) 12:e006086. doi: 10.1161/CIRCHEARTFAILURE.119.006086
19. Vellone E, Chialà O, Boyne J, Klompstra L, Evangelista LS, Back M, et al. Cognitive impairment in patients with heart failure: an international study. *ESC Heart Fail*. (2020) 7:46–53. doi: 10.1002/ehf2.12542
20. Agarwal KS, Kazim R, Xu J, Borson S, Taffet GE. Unrecognized cognitive impairment and its effect on heart failure readmissions of elderly adults. *J Am Geriatr Soc*. (2016) 64:2296–301. doi: 10.1111/jgs.14471
21. Grubb NR, Simpson C, Fox KA. Memory function in patients with stable, moderate to severe cardiac failure. *Am Heart J*. (2000) 140:E1–5. doi: 10.1067/mhj.2000.106647

22. Schall RR, Petrucci RJ, Brozena SC, Cavarocchi NC, Jessup M. Cognitive function in patients with symptomatic dilated cardiomyopathy before and after cardiac transplantation. *J Am Coll Cardiol.* (1989) 14:1666–72. doi: 10.1016/0735-1097(89)90013-2
23. Gure TR, Blaum CS, Giordani B, Koelling TM, Galecki A, Pressler SJ, et al. Prevalence of cognitive impairment in older adults with heart failure. *J Am Geriatr Soc.* (2012) 60:1724–9. doi: 10.1111/j.1532-5415.2012.04097.x
24. Yaffe K, Vittinghoff E, Pletcher MJ, Hoang TD, Launer LJ, Whitmer R, et al. Early adult to midlife cardiovascular risk factors and cognitive function. *Circulation.* (2014) 129:1560–7. doi: 10.1161/CIRCULATIONAHA.113.004798
25. Gallagher R, Sullivan A, Burke R, Hales S, Gillies G, Cameron J, et al. Mild cognitive impairment, screening, and patient perceptions in heart failure patients. *J Card Fail.* (2013) 19:641–6. doi: 10.1016/j.cardfail.2013.08.001
26. Warraich HJ, Kitzman DW, Whellan DJ, Duncan PW, Mentz RJ, Pastva AM, et al. Physical function, frailty, cognition, depression, and quality of life in hospitalized adults ≥60 years with acute decompensated heart failure with preserved versus reduced ejection fraction. *Circ Heart Fail.* (2018) 11:e005254. doi: 10.1161/CIRCHEARTFAILURE.118.005254
27. Hammond CA, Blades NJ, Chaudhry SI, Dodson JA, Longstreth WT, Jr., et al. Long-term cognitive decline after newly diagnosed heart failure: longitudinal analysis in the CHS (cardiovascular health study). *Circ Heart Fail.* (2018) 11:e004476. doi: 10.1161/CIRCHEARTFAILURE.117.004476
28. Jutkowitz E, MacLehose RF, Gaugler JE, Dowd B, Kuntz KM, Kane RL. Risk factors associated with cognitive, functional, and behavioral trajectories of newly diagnosed dementia patients. *J Gerontol A Biol Sci Med Sci.* (2017) 72:251–8. doi: 10.1093/gerona/glw079
29. Ampadu J, Morley JE. Heart failure and cognitive dysfunction. *Int J Cardiol.* (2015) 178:12–23. doi: 10.1016/j.ijcard.2014.10.087
30. Faulkner KM, Dickson VV, Fletcher J, Katz SD, Chang PP, Gottesman RF, et al. Factors associated with cognitive impairment in heart failure with preserved ejection fraction. *J Cardiovasc Nurs*. (2020) 37:17–30. doi: 10.1097/JCN.0000000000000711
31. Frey A, Sell R, Homola GA, Malsch C, Kraft P, Gunreben I, et al. Cognitive deficits and related brain lesions in patients with chronic heart failure. *JACC Heart Fail.* (2018) 6:583–92. doi: 10.1016/j.jchf.2018.03.010
32. Ichijo Y, Kono S, Yoshihisa A, Misaka T, Kaneshiro T, Oikawa M, et al. Impaired frontal brain activity in patients with heart failure assessed by near-infrared spectroscopy. *J Am Heart Assoc.* (2020) 9:e014564. doi: 10.1161/JAHA.119.014564
33. Sacre JW, Ball J, Wong C, Chan YK, Stewart S, Kingwell BA, et al. Mild cognitive impairment is associated with subclinical diastolic dysfunction in patients with chronic heart disease. *Eur Heart J Cardiovasc Imaging.* (2018) 19:285–92. doi: 10.1093/ehjci/jex169
34. Matsue Y, Kamiya K, Saito H, Saito K, Ogasahara Y. Maekawa E, et al. Prevalence and prognostic impact of the coexistence of multiple frailty domains in elderly patients with heart failure: the FRAGILE-HF cohort study. *Eur J Heart Fail.* (2020) 22:2112–9. doi: 10.1002/ejhf.1926
35. Patel A, Parikh R, Howell EH, Hsich E, Landers SH, Gorodeski EZ. Mini-cog performance: novel marker of post discharge risk among patients hospitalized for heart failure. *Circ Heart Fail.* (2015) 8:8–16. doi: 10.1161/CIRCHEARTFAILURE.114.001438
36. Mamas MA, Sperrin M, Watson MC, Coutts A, Wilde K, Burton C, et al. Do patients have worse outcomes in heart failure than in cancer? A primary care-based cohort study with 10-year follow-up in Scotland. *Eur J Heart Fail.* (2017) 19:1095–104. doi: 10.1002/ejhf.822
37. Kure CE, Rosenfeldt FL, Scholey AB, Pipingas A, Kaye DM, Bergin PJ, et al. Relationships among cognitive function and cerebral blood flow, oxidative stress, and inflammation in older heart failure patients. *J Card Fail.* (2016) 22:548–59. doi: 10.1016/j.cardfail.2016.03.006
38. Alosco ML, Spitznagel MB, van Dulmen M, Raz N, Cohen R, Sweet LH, et al. Cognitive function and treatment adherence in older adults with heart failure. *Psychosom Med.* (2012) 74:965–73. doi: 10.1097/PSY.0b013e318272ef2a
39. Lovell J, Pham T, Noaman SQ, Davis MC, Johnson M, Ibrahim JE. Self-management of heart failure in dementia and cognitive impairment: a systematic review BMC. *Cardiovasc Disord.* (2019) 19:99. doi: 10.1186/s12872-019-1077-4
40. Huynh QL, Whitmore K, Negishi K, DePasquale CG, Hare JL, Leung D, et al. Cognitive impairment as a determinant of response to management plans after heart failure admission. *Eur J Heart Fail.* (2021) 23:1205–14. doi: 10.1002/ejhf.2177
41. Ovsenik A, Podbregar M, Fabjan A. Cerebral blood flow impairment and cognitive decline in heart failure. *Brain Behav.* (2021) 11:e02176. doi: 10.1002/brb3.2176
42. Rajagopalan B, Raine AE, Cooper R, Ledingham JG. Changes in cerebral blood flow in patients with severe congestive cardiac failure before and after captopril treatment. *Am J Med.* (1984) 76:86–90. doi: 10.1016/0002-9343(84)90891-X
43. Petersen P, Kastrup J, Videbaek R, Boysen G. Cerebral blood flow before and after cardioversion of atrial fibrillation. *J Cereb Blood Flow Metab.* (1989) 9:422–5. doi: 10.1038/jcbfm.1989.62
44. Cornwell WK, III, Tarumi T, Aengevaeren VL, Ayers C, Divanji P, Fu Q, et al. Effect of pulsatile and nonpulsatile flow on cerebral perfusion in patients with left ventricular assist devices. *J Heart Lung Transplant.* (2014) 33:1295–303. doi: 10.1016/j.healun.2014.08.013
45. Gruhn N, Larsen FS, Boesgaard S, Knudsen GM, Mortensen SA, Thomsen G, et al. Cerebral blood flow in patients with chronic heart failure before and after heart transplantation. *Stroke.* (2001) 32:2530–3. doi: 10.1161/hs1101.098360
46. Choi BR, Kim JS, Yang YJ, Park KM, Lee CW, Kim YH, et al. Factors associated with decreased cerebral blood flow in congestive heart failure secondary to idiopathic dilated cardiomyopathy. *Am J Cardiol.* (2006) 97:1365–9. doi: 10.1016/j.amjcard.2005.11.059
47. Stöhr EJ, McDonnell BJ, Colombo PC, Willey JZ. CrossTalk proposal: Blood flow pulsatility in left ventricular assist device patients is essential to maintain normal brain physiology. *J Physiol.* (2019) 597:353–6. doi: 10.1113/JP276729
48. Zuccalà G, Cattel C, Manes-Gravina E, Di Niro MG, Cocchi A, Bernabei R. Left ventricular dysfunction: a clue to cognitive impairment in older patients with heart failure. *J Neurol Neurosurg Psychiatry.* (1997) 63:509–12. doi: 10.1136/jnnp.63.4.509
49. Iadecola C. The neurovascular unit coming of age: a journey through neurovascular coupling in health and disease. *Neuron*. (2017) 96:17–42. doi: 10.1016/j.neuron.2017.07.030
50. Roy B, Woo MA, Wang DJJ, Fonarow GC, Harper RM, Kumar R. Reduced regional cerebral blood flow in patients with heart failure. *Eur J Heart Fail.* (2017) 19:1294–302. doi: 10.1002/ejhf.874
51. Schuff N, Matsumoto S, Kmiecik J, Studholme C, Du A, Ezekiel F, et al. Cerebral blood flow in ischemic vascular dementia and Alzheimer's disease, measured by arterial spin-labeling magnetic resonance imaging. *Alzheimers Dement.* (2009) 5:454–62. doi: 10.1016/j.jalz.2009.04.1233
52. Jefferson AL, Tate DF, Poppas A, Brickman AM, Paul RH, Gunstad J, et al. Lower cardiac output is associated with greater white matter hyperintensities in older adults with cardiovascular disease. *J Am Geriatr Soc.* (2007) 55:1044–8. doi: 10.1111/j.1532-5415.2007.01226.x
53. Leech T, Apaijai N, Palee S, Higgins LA, Maneechote C, Chattipakorn N, et al. Acute administration of metformin prior to cardiac ischemia/reperfusion injury protects brain injury. *Eur J Pharmacol.* (2020) 885:173418. doi: 10.1016/j.ejphar.2020.173418
54. Ogunshola OO, Al-Ahmad A. HIF-1 at the blood-brain barrier: a mediator of permeability? *High Alt Med Biol.* (2012) 13:153–61. doi: 10.1089/ham.2012.1052
55. Yamazaki Y, Kanekiyo T. Blood-brain barrier dysfunction and the pathogenesis of Alzheimer's disease. *Int J Mol Sci.* (2017) 18:965. doi: 10.3390/ijms18091965
56. Weber T, Wassertheurer S, O'Rourke MF, Haiden A, Zweiker R, Rammer M, et al. Pulsatile hemodynamics in patients with exertional dyspnea: potentially of value in the diagnostic evaluation of suspected heart failure with preserved ejection fraction. *J Am Coll Cardiol.* (2013) 61:1874–83. doi: 10.1016/j.jacc.2013.02.013
57. Almeida OP, Garrido GJ, Beer C, Lautenschlager NT, Arnolda L, Flicker L. Cognitive and brain changes associated with ischaemic heart disease and heart failure. *Eur Heart J.* (2012) 33:1769–76. doi: 10.1093/eurheartj/ehr467
58. Zhu X, Smith MA, Honda K, Aliev G, Moreira PI, Nunomura A, et al. Vascular oxidative stress in Alzheimer disease. *J Neurol Sci.* (2007) 257:240–6. doi: 10.1016/j.jns.2007.01.039

59. Athilingam P, Moynihan J, Chen L, D'Aoust R, Groer M, Kip K. Elevated levels of interleukin 6 and C-reactive protein associated with cognitive impairment in heart failure. *Congest Heart Fail.* (2013) 19:92–8. doi: 10.1111/chf.12007
60. Hong X, Bu L, Wang Y, Xu J, Wu J, Huang Y, et al. Increases in the risk of cognitive impairment and alterations of cerebral beta-amyloid metabolism in mouse model of heart failure. *PLoS ONE.* (2013) 8:e63829. doi: 10.1371/journal.pone.0063829
61. McAfoose J, Baune BT. Evidence for a cytokine model of cognitive function. *Neurosci Biobehav Rev*. (2009) 33:355–66. doi: 10.1016/j.neubiorev.2008.10.005
62. Tangestani Fard M, Stough C. A review and hypothesized model of the mechanisms that underpin the relationship between inflammation and cognition in the elderly. *Front Aging Neurosci*. (2019) 11:56. doi: 10.3389/fnagi.2019.00056
63. Gonzalez P, Machado I, Vilcaes A, Caruso C, Roth GA, Schiöth H, et al. Molecular mechanisms involved in interleukin 1-beta (IL-1β)-induced memory impairment Modulation by alpha-melanocyte-stimulating hormone (α-MSH). *Brain Behav Immun.* (2013) 34:141–50. doi: 10.1016/j.bbi.2013.08.007
64. Toyama K, Koibuchi N, Uekawa K, Hasegawa Y, Kataoka K, Katayama T, et al. Apoptosis signal-regulating kinase 1 is a novel target molecule for cognitive impairment induced by chronic cerebral hypoperfusion. *Arterioscler Thromb Vasc Biol.* (2014) 34:616–25. doi: 10.1161/ATVBAHA.113.302440
65. Hou X, Liang X, Chen JF, Zheng J. Ecto-5'-nucleotidase (CD73) is involved in chronic cerebral hypoperfusion-induced white matter lesions and cognitive impairment by regulating glial cell activation and pro-inflammatory cytokines. *Neuroscience.* (2015) 297:118–26. doi: 10.1016/j.neuroscience.2015.03.033
66. Faraco G, Sugiyama Y, Lane D, Garcia-Bonilla L, Chang H, Santisteban MM, et al. Perivascular macrophages mediate the neurovascular and cognitive dysfunction associated with hypertension. *J Clin Invest.* (2016) 126:4674–89. doi: 10.1172/JCI86950
67. Vanherle L, Matuskova H, Don-Doncow N, Uhl FE, Meissner A. Improving cerebrovascular function to increase neuronal recovery in neurodegeneration associated to cardiovascular disease. *Front Cell Dev Biol.* (2020) 8:53. doi: 10.3389/fcell.2020.00053
68. Pun PB, Lu J, Moochhala S. Involvement of ROS in BBB dysfunction. *Free Radic Res.* (2009) 43:348–64. doi: 10.1080/10715760902751902
69. Durrant CS, Ruscher K, Sheppard O, Coleman MP, Özen I. Beta secretase 1-dependent amyloid precursor protein processing promotes excessive vascular sprouting through NOTCH3 signalling. *Cell Death Dis.* (2020) 11:98. doi: 10.1038/s41419-020-2288-4
70. Heppner FL, Ransohoff RM, Becher B. Immune attack: the role of inflammation in Alzheimer disease. *Nat Rev Neurosci.* (2015) 16:358–72. doi: 10.1038/nrn3880
71. Rodriguez-Vieitez E, Saint-Aubert L, Carter SF, Almkvist O, Farid K, Schöll M, et al. Diverging longitudinal changes in astrocytosis and amyloid PET in autosomal dominant Alzheimer's disease. *Brain.* (2016) 139:922–36. doi: 10.1093/brain/awv404
72. Frost GR, Li YM. The role of astrocytes in amyloid production and Alzheimer's disease. *Open Biol*. (2017) 7:228. doi: 10.1098/rsob.170228
73. Gipson CD, Olive MF. Structural and functional plasticity of dendritic spines - root or result of behavior? *Genes Brain Behav*. (2017) 16:101–17. doi: 10.1111/gbb.12324
74. Morley JE, Farr SA. The role of amyloid-beta in the regulation of memory. *Biochem Pharmacol.* (2014) 88:479–85. doi: 10.1016/j.bcp.2013.12.018
75. Toledo C, Andrade DC, Díaz HS, Inestrosa NC, Del Rio R. Neurocognitive disorders in heart failure: novel pathophysiological mechanisms underpinning memory loss and learning impairment. *Mol Neurobiol.* (2019) 56:8035–51. doi: 10.1007/s12035-019-01655-0
76. Meissner A, Visanji NP, Momen MA, Feng R, Francis BM, Bolz SS, et al. Tumor necrosis factor-α underlies loss of cortical dendritic spine density in a mouse model of congestive heart failure. *J Am Heart Assoc*. (2015) 4:1920. doi: 10.1161/JAHA.115.001920
77. Toledo C, Lucero C, Andrade DC, Díaz HS, Schwarz KG, Pereyra KV, et al. Cognitive impairment in heart failure is associated with altered Wnt signaling in the hippocampus. *Aging (Albany NY).* (2019) 11:5924–42. doi: 10.18632/aging.102150
78. Gallina D, Zelinka C, Fischer AJ. Glucocorticoid receptors in the retina, Müller glia and the formation of Müller glia-derived progenitors. *Development.* (2014) 141:3340–51. doi: 10.1242/dev.109835
79. Liori S, Arfaras-Melainis A, Bistola V, Polyzogopoulou E, Parissis J. Cognitive impairment in heart failure: clinical implications, tools of assessment, therapeutic considerations. *Heart Fail Rev*. (2021). [Epub ahead of print]. doi: 10.1007/s10741-021-10118-5
80. Sfera A, Osorio C. Water for thought: is there a role for aquaporin channels in delirium? *Front Psychiatry.* (2014) 5:57. doi: 10.3389/fpsyt.2014.00057
81. Chen Z, Zhong C. Oxidative stress in Alzheimer's disease. *Neurosci Bull.* (2014) 30:271–81. doi: 10.1007/s12264-013-1423-y
82. Khacho M, Clark A, Svoboda DS, MacLaurin JG, Lagace DC, Park DS, et al. Mitochondrial dysfunction underlies cognitive defects as a result of neural stem cell depletion and impaired neurogenesis. *Hum Mol Genet.* (2017) 26:3327–41. doi: 10.1093/hmg/ddx217
83. Khacho M, Harris R, Slack RS. Mitochondria as central regulators of neural stem cell fate and cognitive function. *Nat Rev Neurosci.* (2019) 20:34–48. doi: 10.1038/s41583-018-0091-3
84. Maneechote C, Palee S, Kerdphoo S, Jaiwongkam T, Chattipakorn SC, Chattipakorn N. Balancing mitochondrial dynamics *via* increasing mitochondrial fusion attenuates infarct size and left ventricular dysfunction in rats with cardiac ischemia/reperfusion injury. *Clin Sci (Lond).* (2019) 133:497–513. doi: 10.1042/CS20190014
85. Jinawong K, Apaijai N, Chattipakorn N, Chattipakorn SC. Cognitive impairment in myocardial infarction and heart failure. *Acta Physiol (Oxf).* (2021) 232:e13642. doi: 10.1111/apha.13642
86. Kim MS, Lee GH, Kim YM, Lee BW, Nam HY, Sim UC, et al. Angiotensin II causes apoptosis of adult hippocampal neural stem cells and memory impairment through the action on AMPK-PGC1α signaling in heart failure. *Stem Cells Transl Med.* (2017) 6:1491–503. doi: 10.1002/sctm.16-0382
87. Combs CK. Inflammation and microglia actions in Alzheimer's disease. *J Neuroimmune Pharmacol*. (2009) 4:380–8. doi: 10.1007/s11481-009-9165-3
88. Gottesman RF, Grega MA, Bailey MM, Zeger SL, Baumgartner WA, McKhann GM, et al. Association between hypotension, low ejection fraction and cognitive performance in cardiac patients. *Behav Neurol.* (2010) 22:63–71. doi: 10.1155/2010/725353
89. Baldasseroni S, Mossello E, Romboli B, Orso F, Colombi C, Fumagalli S, et al. Relationship between cognitive function and 6-minute walking test in older outpatients with chronic heart failure. *Aging Clin Exp Res.* (2010) 22:308–13. doi: 10.1007/BF03324936
90. Myserlis PG, Malli A, Kalaitzoglou DK, Kalaitzidis G, Miligkos M, Kokkinidis DG, et al. Atrial fibrillation and cognitive function in patients with heart failure: a systematic review and meta-analysis. *Heart Fail Rev*. (2017) 22:1–11. doi: 10.1007/s10741-016-9587-y
91. Mueller K, Thiel F, Beutner F, Teren A, Frisch S, Ballarini T, et al. Brain damage with heart failure: cardiac biomarker alterations and gray matter decline. *Circ Res.* (2020) 126:750–64. doi: 10.1161/CIRCRESAHA.119.315813
92. Lee TC, Qian M, Liu Y, Graham S, Mann DL, Nakanishi K, et al. Cognitive decline over time in patients with systolic heart failure: insights from WARCEF. *JACC Heart Fail.* (2019) 7:1042–53. doi: 10.1016/j.jchf.2019.09.003
93. Alosco ML, Spitznagel MB, Gunstad J. Obesity as a risk factor for poor neurocognitive outcomes in older adults with heart failure. *Heart Fail Rev*. (2014) 19:403–11. doi: 10.1007/s10741-013-9399-2
94. Alosco ML, Spitznagel MB, Sweet LH, Josephson R, Hughes J, Gunstad J. Atrial fibrillation exacerbates cognitive dysfunction and cerebral perfusion in heart failure. *Pacing Clin Electrophysiol.* (2015) 38:178–86. doi: 10.1111/pace.12543
95. Stefansdottir H, Arnar DO, Aspelund T, Sigurdsson S, Jonsdottir MK, Hjaltason H, et al. Atrial fibrillation is associated with reduced brain volume and cognitive function independent of cerebral infarcts. *Stroke.* (2013) 44:1020–5. doi: 10.1161/STROKEAHA.12.679381

96. Brouwer-Brolsma EM, van de Rest O, Tieland M, van der Zwaluw NL, Steegenga WT, Adam JJ, et al. Serum 25-hydroxyvitamin D is associated with cognitive executive function in Dutch prefrail and frail elderly: a cross-sectional study exploring the associations of 25-hydroxyvitamin D with glucose metabolism, cognitive performance and depression. *J Am Med Dir Assoc*. (2013) 14:852.e859–17. doi: 10.1016/j.jamda.2013.06.010
97. Langlais PJ, Savage LM. Thiamine deficiency in rats produces cognitive and memory deficits on spatial tasks that correlate with tissue loss in diencephalon, cortex and white matter. *Behav Brain Res.* (1995) 68:75–89. doi: 10.1016/0166-4328(94)00162-9
98. Matté C, Mackedanz V, Stefanello FM, Scherer EB, Andreazza AC, Zanotto C, et al. Chronic hyperhomocysteinemia alters antioxidant defenses and increases DNA damage in brain and blood of rats: protective effect of folic acid. *Neurochem Int.* (2009) 54:7–13. doi: 10.1016/j.neuint.2008.08.011
99. Hugo J, Ganguli M. Dementia and cognitive impairment: epidemiology, diagnosis, and treatment. *Clin Geriatr Med.* (2014) 30:421–42. doi: 10.1016/j.cger.2014.04.001
100. Jessen F, Amariglio RE, Buckley RF, van der Flier WM, Han Y, Molinuevo JL, et al. The characterisation of subjective cognitive decline. *Lancet Neurol.* (2020) 19:271–8. doi: 10.1016/S1474-4422(19)30368-0
101. Dodson JA, Truong TT, Towle VR, Kerins G, Chaudhry SI. Cognitive impairment in older adults with heart failure: prevalence, documentation, and impact on outcomes. *Am J Med.* (2013) 126:120–6. doi: 10.1016/j.amjmed.2012.05.029
102. Folstein MF, Folstein SE, McHugh PR. "Mini-mental state" A practical method for grading the cognitive state of patients for the clinician. *J Psychiatr Res.* (1975) 12:189–98. doi: 10.1016/0022-3956(75)90026-6
103. Rosli R, Tan MP, Gray WK, Subramanian P, Chin AV. Cognitive assessment tools in Asia: a systematic review. *Int Psychogeriatr.* (2016) 28:189–210. doi: 10.1017/S1041610215001635
104. Mao HF, Chang LH, Tsai AY, Huang WW, Tang LY, Lee HJ, et al. Diagnostic accuracy of instrumental activities of daily living for dementia in community-dwelling older adults. *Age Ageing.* (2018) 47:551–7. doi: 10.1093/ageing/afy021
105. Huo Z, Lin J, Bat BKK, Chan JYC, Tsoi KKF, Yip BHK. Diagnostic accuracy of dementia screening tools in the Chinese population: a systematic review and meta-analysis of 167 diagnostic studies. *Age Ageing.* (2021) 50:1093–101. doi: 10.1093/ageing/afab005
106. Holsinger T, Deveau J, Boustani M, Williams JW, Jr. Does this patient have dementia? *JAMA*. (2007) 297:2391–404. doi: 10.1001/jama.297.21.2391
107. Nasreddine ZS, Phillips NA, Bédirian V, Charbonneau S, Whitehead V, Collin I, et al. The Montreal Cognitive Assessment, MoCA: a brief screening tool for mild cognitive impairment. *J Am Geriatr Soc.* (2005) 53:695–9. doi: 10.1111/j.1532-5415.2005.53221.x
108. Borson S, Scanlan J, Brush M, Vitaliano P, Dokmak A. The mini-cog: a cognitive 'vital signs' measure for dementia screening in multi-lingual elderly. *Int J Geriatr Psychiatry*. (2000) 15:1021–7. doi: 10.1002/1099-1166(200011)15:11<1021::aid-gps234>3.0.co;2-6
109. Chertkow H, Nasreddine Z, Joanette Y, Drolet V, Kirk J, Massoud F, et al. Mild cognitive impairment and cognitive impairment, no dementia: part A, concept and diagnosis. *Alzheimers Dement.* (2007) 3:266–82. doi: 10.1016/j.jalz.2007.07.013
110. Tariq SH, Tumosa N, Chibnall JT, Perry MH, III, Morley JE. Comparison of the Saint Louis University mental status examination and the mini-mental state examination for detecting dementia and mild neurocognitive disorder–a pilot study. *Am J Geriatr Psychiatry*. (2006) 14:900–10. doi: 10.1097/01.JGP.0000221510.33817.86
111. Malmstrom TK, Voss VB, Cruz-Oliver DM, Cummings-Vaughn LA, Tumosa N, Grossberg GT, et al. The rapid cognitive screen (RCS): a point-of-care screening for dementia and mild cognitive impairment. *J Nutr Health Aging.* (2015) 19:741–4. doi: 10.1007/s12603-015-0564-2
112. Radanovic M, Facco G, Forlenza OV. Sensitivity and specificity of a briefer version of the Cambridge Cognitive Examination (CAMCog-Short) in the detection of cognitive decline in the elderly: an exploratory study. *Int J Geriatr Psychiatry*. (2018) 33:769–78. doi: 10.1002/gps.4857
113. Aprahamian I, Diniz BS, Izbicki R, Radanovic M, Nunes PV, Forlenza OV. Optimizing the CAMCOG test in the screening for mild cognitive impairment and incipient dementia: saving time with relevant domains. *Int J Geriatr Psychiatry*. (2011) 26:403–8. doi: 10.1002/gps.2540
114. Nunes PV, Diniz BS, Radanovic M, Abreu ID, Borelli DT, Yassuda MS, et al. CAMcog as a screening tool for diagnosis of mild cognitive impairment and dementia in a Brazilian clinical sample of moderate to high education. *Int J Geriatr Psychiatry*. (2008) 23:1127–33. doi: 10.1002/gps.2038
115. Alagiakrishnan K, Mah D, Dyck JR, Senthilselvan A, Ezekowitz J. Comparison of two commonly used clinical cognitive screening tests to diagnose mild cognitive impairment in heart failure with the golden standard European Consortium Criteria. *Int J Cardiol.* (2017) 228:558–62. doi: 10.1016/j.ijcard.2016.11.193
116. Hawkins MA, Gathright EC, Gunstad J, Dolansky MA, Redle JD, Josephson R, et al. The MoCA and MMSE as screeners for cognitive impairment in a heart failure population: a study with comprehensive neuropsychological testing. *Heart Lung.* (2014) 43:462–8. doi: 10.1016/j.hrtlng.2014.05.011
117. Almeida OP, Beer C, Lautenschlager NT, Arnolda L, Alfonso H, Flicker L. Two-year course of cognitive function and mood in adults with congestive heart failure and coronary artery disease: the Heart-Mind Study. *Int Psychogeriatr.* (2012) 24:38–47. doi: 10.1017/S1041610211001657
118. Saito H, Yamashita M, Endo Y, Mizukami A, Yoshioka K, Hashimoto T, et al. Cognitive impairment measured by Mini-Cog provides additive prognostic information in elderly patients with heart failure. *J Cardiol.* (2020) 76:350–6. doi: 10.1016/j.jjcc.2020.06.016
119. Blennow K, Hampel H. CSF markers for incipient Alzheimer's disease. *Lancet Neurol.* (2003) 2:605–13. doi: 10.1016/S1474-4422(03)00530-1
120. Ritchie C, Smailagic N, Noel-Storr AH, Takwoingi Y, Flicker L, Mason SE, et al. Plasma and cerebrospinal fluid amyloid beta for the diagnosis of Alzheimer's disease dementia and other dementias in people with mild cognitive impairment (MCI). *Cochrane Database Syst Rev.* (2014) 2014:Cd008782. doi: 10.1002/14651858.CD008782.pub4
121. Gustafson DR, Skoog I, Rosengren L, Zetterberg H, Blennow K. Cerebrospinal fluid beta-amyloid 1-42 concentration may predict cognitive decline in older women. *J Neurol Neurosurg Psychiatry.* (2007) 78:461–4. doi: 10.1136/jnnp.2006.100529
122. Stomrud E, Hansson O, Blennow K, Minthon L, Londos E. Cerebrospinal fluid biomarkers predict decline in subjective cognitive function over 3 years in healthy elderly. *Dement Geriatr Cogn Disord.* (2007) 24:118–24. doi: 10.1159/000105017
123. Blennow K, Zetterberg H. Cerebrospinal fluid biomarkers for Alzheimer's disease. *J Alzheimers Dis.* (2009) 18:413–7. doi: 10.3233/JAD-2009-1177
124. Mitchell AJ. CSF phosphorylated tau in the diagnosis and prognosis of mild cognitive impairment and Alzheimer's disease: a meta-analysis of 51 studies. *J Neurol Neurosurg Psychiatry*. (2009) 80:966–75. doi: 10.1136/jnnp.2008.167791
125. Zheng YM, Zhao YY, Zhang T, Hou XH, Bi YL, Ma YH, et al. Left ventricular ejection fraction and cerebrospinal fluid biomarkers of Alzheimer's disease pathology in cognitively normal older adults: the CABLE study. *J Alzheimers Dis.* (2021) 81:743–50. doi: 10.3233/JAD-201222
126. Chojdak-Lukasiewicz J, Malodobra-Mazur M, Zimny A, Noga L, Paradowski B. Plasma tau protein and Abeta42 level as markers of cognitive impairment in patients with Parkinson's disease. *Adv Clin Exp Med.* (2020) 29:115–21. doi: 10.17219/acem/112058
127. Chen TB, Lee YJ, Lin SY, Chen JP, Hu CJ, Wang PN, et al. Plasma Abeta42 and total tau predict cognitive decline in amnestic mild cognitive impairment. *Sci Rep*. (2019) 9:13984. doi: 10.1038/s41598-019-50315-9
128. Bayes-Genis A, Barallat J, de Antonio M, Domingo M, Zamora E, J Vila, et al. Bloodstream amyloid-beta (1-40) peptide, cognition, and outcomes in heart failure. *Rev Esp Cardiol (Engl Ed).* (2017) 70:924–32. doi: 10.1016/j.rec.2017.02.021
129. Redwine LS, Pung MA, Wilson K, Chinh K, Duffy AR. Differential peripheral inflammatory factors associated with cognitive function in patients with heart failure. *Neuroimmunomodulation.* (2018) 25:146–52. doi: 10.1159/000493142
130. Redwine LS, Pung MA, Wilson K, Bangen KJ, Delano-Wood L, Hurwitz B. An exploratory randomized sub-study of light-to-moderate intensity exercise on cognitive function, depression symptoms and inflammation in older adults with heart failure. *J Psychosom Res.* (2020) 128:109883. doi: 10.1016/j.jpsychores.2019.109883

131. Chhatwal JP, Schultz AP, Dang Y, Ostaszewski B, Liu L, Yang HS, et al. Plasma N-terminal tau fragment levels predict future cognitive decline and neurodegeneration in healthy elderly individuals. *Nat Commun.* (2020) 11:6024. doi: 10.1038/s41467-020-19543-w
132. Chen Z, Mengel D, Keshavan A, Rissman RA, Billinton A, Perkinton M, et al. Learnings about the complexity of extracellular tau aid development of a blood-based screen for Alzheimer's disease. *Alzheimers Dement.* (2019) 15:487–96. doi: 10.1016/j.jalz.2018.09.010
133. Varma VR, Oommen AM, Varma S, Casanova R, An Y, Andrews RM, et al. Brain and blood metabolite signatures of pathology and progression in Alzheimer disease: a targeted metabolomics study. *PLoS Med.* (2018) 15:e1002482. doi: 10.1371/journal.pmed.1002482
134. Abdullah M, Kimura N, Akatsu H, Hashizume Y, Ferdous T, Tachita T, et al. Flotillin is a novel diagnostic blood marker of Alzheimer's disease. *J Alzheimers Dis.* (2019) 72:1165–76. doi: 10.3233/JAD-190908
135. Debette S, Schilling S, Duperron MG, Larsson SC, Markus HS. Clinical significance of magnetic resonance imaging markers of vascular brain injury: a systematic review and meta-analysis. *JAMA Neurol.* (2019) 76:81–94. doi: 10.1001/jamaneurol.2018.3122
136. Alosco ML, Brickman AM, Spitznagel MB, Garcia SL, Narkhede A, Griffith EY, et al. Cerebral perfusion is associated with white matter hyperintensities in older adults with heart failure. *Congest Heart Fail.* (2013) 19:E29–34. doi: 10.1111/chf.12025
137. Beer C, Ebenezer E, Fenner S, Lautenschlager NT, Arnolda L, Flicker L, et al. Contributors to cognitive impairment in congestive heart failure: a pilot case-control study. *Intern Med J.* (2009) 39:600–5. doi: 10.1111/j.1445-5994.2008.01790.x
138. Stegmann T, Chu ML, Witte VA, Villringer A, Kumral D, Riedel-Heller SG, et al. Heart failure is independently associated with white matter lesions: insights from the population-based LIFE-Adult Study. *ESC Heart Fail.* (2021) 8:697–704. doi: 10.1002/ehf2.13166
139. Kumar R, Woo MA, Macey PM, Fonarow GC, Hamilton MA, Harper RM. Brain axonal and myelin evaluation in heart failure. *J Neurol Sci.* (2011) 307:106–13. doi: 10.1016/j.jns.2011.04.028
140. Almeida OP, Garrido GJ, Etherton-Beer C, Lautenschlager NT, Arnolda L, Alfonso H, et al. Brain and mood changes over 2 years in healthy controls and adults with heart failure and ischaemic heart disease. *Eur J Heart Fail.* (2013) 15:850–8. doi: 10.1093/eurjhf/hft029
141. Frey A, Homola GA, Henneges C, Mühlbauer L, Sell R, Kraft P, et al. Temporal changes in total and hippocampal brain volume and cognitive function in patients with chronic heart failure-the COGNITIONMATTERS-HF cohort study. *Eur Heart J.* (2021) 42:1569–78. doi: 10.1093/eurheartj/ehab003
142. Alves TC, Busatto GF. Regional cerebral blood flow reductions, heart failure and Alzheimer's disease. *Neurol Res.* (2006) 28:579–87. doi: 10.1179/016164106X130416
143. Yun M, Nie B, Wen W, Zhu Z, Liu H, Nie S, et al. Assessment of cerebral glucose metabolism in patients with heart failure by (18)F-FDG PET/CT imaging. *J Nucl Cardiol.* (2020). [Epub ahead of print]. doi: 10.1007/s12350-020-02258-2
144. Fox MD, Raichle ME. Spontaneous fluctuations in brain activity observed with functional magnetic resonance imaging. *Nat Rev Neurosci.* (2007) 8:700–11. doi: 10.1038/nrn2201
145. Singh PK, Chen ZL, Ghosh D, Strickland S, Norris EH. Increased plasma bradykinin level is associated with cognitive impairment in Alzheimer's patients. *Neurobiol Dis.* (2020) 139:104833. doi: 10.1016/j.nbd.2020.104833
146. Cannon JA, Shen L, Jhund PS, Kristensen SL, Kober L, Chen F, et al. Dementia-related adverse events in PARADIGM-HF and other trials in heart failure with reduced ejection fraction. *Eur J Heart Fail.* (2017) 19:129–37. doi: 10.1002/ejhf.687
147. Poorgolizadeh E, Homayouni Moghadam F, Dormiani K, Rezaei N, Nasr-Esfahani MH. Do neprilysin inhibitors walk the line? Heart ameliorative but brain threatening! *Eur J Pharmacol.* (2021) 894:173851. doi: 10.1016/j.ejphar.2021.173851
148. Mui JV, Zhou J, Lee S, Leung KSK, Lee TTL, Chou OHI, et al. Sodium-glucose cotransporter 2 (SGLT2) inhibitors vs. dipeptidyl peptidase-4 (DPP4) inhibitors for new-onset dementia: a propensity score-matched population-based study with competing risk analysis. *Front Cardiovasc Med.* (2021) 8:747620. doi: 10.3389/fcvm.2021.747620
149. Yamada K, Uchida S, Takahashi S, Takayama M, Nagata Y, Suzuki N, et al. Effect of a centrally active angiotensin-converting enzyme inhibitor, perindopril, on cognitive performance in a mouse model of Alzheimer's disease. *Brain Res.* (2010) 1352:176–86. doi: 10.1016/j.brainres.2010.07.006
150. Zuccala G, Onder G, Marzetti E, Monaco MR, Cesari M, Cocchi A, et al. Use of angiotensin-converting enzyme inhibitors and variations in cognitive performance among patients with heart failure. *Eur Heart J.* (2005) 26:226–33. doi: 10.1093/eurheartj/ehi058
151. Soto ME, van Kan GA, Nourhashemi F, Gillette-Guyonnet S, Cesari M, Cantet C, et al. Angiotensin-converting enzyme inhibitors and Alzheimer's disease progression in older adults: results from the Reseau sur la Maladie d'Alzheimer Francais cohort. *J Am Geriatr Soc.* (2013) 61:1482–8. doi: 10.1111/jgs.12415
152. Hierro-Bujalance C, Infante-Garcia C, Del Marco A, Herrera M, Carranza-Naval MJ, Suarez J, et al. Empagliflozin reduces vascular damage and cognitive impairment in a mixed murine model of Alzheimer's disease and type 2 diabetes. *Alzheimers Res Ther.* (2020) 12:40. doi: 10.1186/s13195-020-00607-4
153. McMurray JJV, Solomon SD, Inzucchi SE, Kober L, Kosiborod MN, Martinez FA, et al. Dapagliflozin in patients with heart failure and reduced ejection fraction. *N Engl J Med.* (2019) 381:1995–2008. doi: 10.1056/NEJMoa1911303
154. Packer M, Anker SD, Butler J, Filippatos G, Pocock SJ, Carson P, et al. Cardiovascular and renal outcomes with empagliflozin in heart failure. *N Engl J Med.* (2020) 383:1413–24. doi: 10.1056/NEJMoa2022190
155. Fouchier S, Dallinga-Thie G, Meijers J, Zelcer N, Kastelein J, Defesche J, et al. Mutations in STAP1 are associated with autosomal dominant hypercholesterolemia. *Circ Res.* (2014) 115:552–5. doi: 10.1161/CIRCRESAHA.115.304660
156. Perna S, Mainardi M, Astrone P, Gozzer C, Biava A, Bacchio R, et al. 12-month effects of incretins versus SGLT2-Inhibitors on cognitive performance and metabolic profile A randomized clinical trial in the elderly with Type-2 diabetes mellitus. *Clin Pharmacol.* (2018) 10:141–51. doi: 10.2147/CPAA.S164785
157. Hajjar I, Hart M, Chen YL, Mack W, Milberg W, Chui H, et al. Effect of antihypertensive therapy on cognitive function in early executive cognitive impairment: a double-blind randomized clinical trial. *Arch Intern Med.* (2012) 172:442–4. doi: 10.1001/archinternmed.2011.1391
158. Yasar S, Xia J, Yao W, Furberg CD, Xue QL, Mercado CI, et al. Antihypertensive drugs decrease risk of Alzheimer disease: Ginkgo evaluation of memory study. *Neurology.* (2013) 81:896–903. doi: 10.1212/WNL.0b013e3182a35228
159. Hajjar I, Okafor M, McDaniel D, Obideen M, Dee E, Shokouhi M, et al. Effects of candesartan vs. lisinopril on neurocognitive function in older adults with executive mild cognitive impairment: a randomized clinical trial. *JAMA Netw Open.* (2020) 3:e2012252. doi: 10.1001/jamanetworkopen.2020.12252
160. Ouk M, Wu CY, Rabin JS, Edwards JD, Ramirez J, Masellis M, et al. Associations between brain amyloid accumulation and the use of angiotensin-converting enzyme inhibitors versus angiotensin receptor blockers. *Neurobiol Aging.* (2021) 100:22–31. doi: 10.1016/j.neurobiolaging.2020.12.011
161. Luijendijk HJ, Koolman X. The incentive to publish negative studies: how beta-blockers and depression got stuck in the publication cycle. *J Clin Epidemiol.* (2012) 65:488–92. doi: 10.1016/j.jclinepi.2011.06.022
162. Holm H, Ricci F, Di Martino G, Bachus E, Nilsson ED, Ballerini P, et al. Beta-blocker therapy and risk of vascular dementia: a population-based prospective study. *Vascul Pharmacol.* (2020) 125–126:106649. doi: 10.1016/j.vph.2020.106649
163. Wingenfeld K, Otte C. Mineralocorticoid receptor function and cognition in health and disease. *Psychoneuroendocrinology.* (2019) 105:25–35. doi: 10.1016/j.psyneuen.2018.09.010
164. Doehner W, Ural D, Haeusler KG, Celutkiene J, Bestetti R, Cavusoglu Y, et al. Heart and brain interaction in patients with heart failure: overview and proposal for a taxonomy A position paper from the Study Group on

Heart and Brain Interaction of the Heart Failure Association. *Eur J Heart Fail.* (2018) 20:199–215. doi: 10.1002/ejhf.1100

165. Wang X, Sun G, Feng T, Zhang J, Huang X, Wang T, et al. Sodium oligomannate therapeutically remodels gut microbiota and suppresses gut bacterial amino acids-shaped neuroinflammation to inhibit Alzheimer's disease progression. *Cell Res.* (2019) 29:787–803. doi: 10.1038/s41422-019-0216-x
166. Xiao S, Chan P, Wang T, Hong Z, Wang S, Kuang W, et al. A 36-week multicenter, randomized, double-blind, placebo-controlled, parallel-group, phase 3 clinical trial of sodium oligomannate for mild-to-moderate Alzheimer's dementia. *Alzheimers Res Ther.* (2021) 13:62. doi: 10.1186/s13195-021-00795-7
167. Jiang T, Gao L, Lu J, Zhang YD. ACE2-Ang-(1-7)-mas axis in brain: a potential target for prevention and treatment of ischemic stroke. *Curr Neuropharmacol.* (2013) 11:209–17. doi: 10.2174/1570159X11311020007
168. Hay M, Polt R, Heien ML, Vanderah TW, Largent-Milnes TM, Rodgers K, et al. A novel angiotensin-(1-7) glycosylated mas receptor agonist for treating vascular cognitive impairment and inflammation-related memory dysfunction. *J Pharmacol Exp Ther.* (2019) 369:9–25. doi: 10.1124/jpet.118.254854
169. Hay M, Vanderah TW, Samareh-Jahani F, Constantopoulos E, Uprety AR, Barnes CA, et al. Cognitive impairment in heart failure: a protective role for angiotensin-(1-7). *Behav Neurosci.* (2017) 131:99–114. doi: 10.1037/bne0000182
170. Lidington D, Fares JC, Uhl FE, Dinh DD, Kroetsch JT, Sauve M, et al. CFTR therapeutics normalize cerebral perfusion deficits in mouse models of heart failure and subarachnoid hemorrhage. *JACC Basic Transl Sci.* (2019) 4:940–58. doi: 10.1016/j.jacbts.2019.07.004
171. Alosco ML, Brickman AM, Spitznagel MB, Sweet LH, Josephson R, Griffith EY, et al. Daily physical activity is associated with subcortical brain volume and cognition in heart failure. *J Int Neuropsychol Soc.* (2015) 21:851–60. doi: 10.1017/S1355617715000697
172. Ngandu T, Lehtisalo J, Solomon A, Levälahti E, Ahtiluoto S, Antikainen R, et al. A 2 year multidomain intervention of diet, exercise, cognitive training, and vascular risk monitoring versus control to prevent cognitive decline in at-risk elderly people (FINGER): a randomised controlled trial. *Lancet.* (2015) 385:2255–63. doi: 10.1016/S0140-6736(15)60461-5
173. Hoth KF, Poppas A, Ellison KE, Paul RH, Sokobin A, Cho Y, et al. Link between change in cognition and left ventricular function following cardiac resynchronization therapy. *J Cardiopulm Rehabil Prev.* (2010) 30:401–8. doi: 10.1097/HCR.0b013e3181e1739a
174. Zimpfer D, Wieselthaler G, Czerny M, Fakin R, Haider D, Zrunek P, et al. Neurocognitive function in patients with ventricular assist devices: a comparison of pulsatile and continuous blood flow devices. *ASAIO J.* (2006) 52:24–7. doi: 10.1097/01.mat.0000191334.51375.7e
175. Jin MN, Kim TH, Kang KW, Yu HT, Uhm JS, Joung B, et al. Atrial fibrillation catheter ablation improves 1-year follow-up cognitive function, especially in patients with impaired cognitive function. *Circ Arrhythm Electrophysiol.* (2019) 12:e007197. doi: 10.1161/CIRCEP.119.007197

Conflict of Interest: The authors declare that the research was conducted in the absence of any commercial or financial relationships that could be construed as a potential conflict of interest.

Publisher's Note: All claims expressed in this article are solely those of the authors and do not necessarily represent those of their affiliated organizations, or those of the publisher, the editors and the reviewers. Any product that may be evaluated in this article, or claim that may be made by its manufacturer, is not guaranteed or endorsed by the publisher.

GLOSSARY

AD, Alzheimer's disease; Aβ, amyloid-β; ATP, adenosine triphosphate; ACEI, angiotensin converting enzyme inhibitor; ACE2, angiotensin-converting enzyme 2; AF, atrial fibrillation; Ang-II, angiotensin II; Ang-(1-7), angiotensin-(1-7); APP, amyloid precursor protein; ARB, angiotensin II receptor blocker; ARNI, angiotensin receptor neprilysin inhibitor; BBB, blood-brain barrier; BMI, body mass index; BNP, brain natriuretic peptide; BP, blood pressure; CAMCOG, Cambridge cognitive examination; CBF, cerebral blood flow; CFTR, cystic fibrosis transmembrane conductance regulator; CI, cognitive impairment; CO, cardiac out; CRT, cardiac resynchronization therapy; CSF, cerebrospinal fluid; DM, diabetes mellitus; DPP4, dipeptidyl peptidase-4; DTI, diffusion tensor imaging; FAQ, functional activities questionnaire; fMRI, functional magnetic resonance imaging; GMD, gray matter density; HF, heartfailure; HFpEF, heart failure with preserved ejection fraction; HFrEF, heart failure with reduced ejection fraction; HIF-1, hypoxia inducible factor-1; IL, interleukin; LVEF, left ventricular ejection fraction; MCI, mild cognitive impairment; MMSE, mini-mental state examination; MoCA, Montreal cognitive assessment; MRI, magnetic resonance imaging; MTA, medial temporal lobe atrophy; NIRS, near-infrared spectroscopy; NPI-Q, neuropsychiatric inventory questionnaire; NT-proBNP, N-terminal pro-brain natriuretic peptide; p-GSK3β, phosphorylated glycogen synthase kinase 3β; PNA5, ang-1-6-O-Ser-Glc-NH2; PVM, perivascular macrophage; QoL, quality of life; RAS, renin angiotensin system; RCS, rapid cognitive screen; SGLT2, sodium glucose co-transporter 2; SLUMS, Saint Louis University mental status; ROS, subsequent reactive oxygen species; SPECT, single photon emission computed tomography; TLR-4, toll-like receptor-4; TNF-α, tumor necrosis factor-α, TSPO, translocator protein; VEGF-1, vascular endothelial growth factor-1; WMH, white matter hyperintensities; WML, white matter lesions; BACE, β-site amyloid precursor protein-cleaving enzyme-1; 6MWT, 6-minute walk test.

frontiers in Cardiovascular Medicine

ORIGINAL RESEARCH
published: 08 February 2022
doi: 10.3389/fcvm.2022.798774

Left Ventricular Strains and Myocardial Work in Adolescents With Anorexia Nervosa

Justine Paysal[1,2], *Etienne Merlin*[3,4], *Daniel Terral*[3], *Aurélie Chalard*[5], *Emmanuelle Rochette*[3,4], *Philippe Obert*[1] *and Stéphane Nottin*[1]*

[1] Avignon University, LAPEC EA4278, Avignon, France, [2] CHU Clermont-Ferrand, Néonatologie et Réanimation Pédiatrique, Clermont-Ferrand, France, [3] CHU Clermont-Ferrand, Pédiatrie, Clermont-Ferrand, France, [4] Université Clermont Auvergne, INSERM, CIC 1405, Unité CRECHE, Clermont-Ferrand, France, [5] CHU Clermont-Ferrand, Cardiologie, Clermont-Ferrand, France

Background: Anorexia nervosa (AN) is accompanied by bradycardia, low blood pressure (BP) and cardiac morphological remodeling. Systolic and diastolic functions are relatively preserved when assessed by standard ultrasound methods. However, novel advances based on speckle tracking echocardiography (STE), that could detect subtle and early alterations of left ventricular (LV) function, remained poorly used in AN patients.

Objective: The aim of this study was to assess the cardiac function of AN patients by evaluating LV myocardial strains, myocardial work (MW) and LV mechanical dispersion. We hypothesized that LV strains and global myocardial work would be decreased and LV twisting mechanisms enhanced to preserve the systolic function.

Methods: Fifty-nine adolescents including 26 women AN patients (14.6 ± 1.9 yrs. old) with a mean duration of AN of 19 ± 9 months and 33 controls (14.1 ± 2.0 yrs. old) underwent STE to assess LV morphology and myocardial regional strains.

Results: The global longitudinal strain (GLS) was higher in AN patients compared to controls (−18.8 ± 2.0 vs. −16.9 ± 2.8%, $p = 0.006$). The area under the pressure-strain loop, representing the global MW was not altered but was shifted to the left and downwards in AN patients, due to their lower BP and higher GLS. Intraventricular mechanical dispersion was similar in both groups. Circumferential strains, twisting/untwisting mechanics were preserved.

Conclusion: Our results strongly support that the cardiac morphological remodeling observed in our AN patients was associated with normal ventricular regional myocardial functions. Only GLS was higher in AN patients, but its clinical significance remains to be demonstrated.

Keywords: myocardial strain, myocardial work, left ventricular mechanical dispersion, anorexia nervosa, left ventricular twist

OPEN ACCESS

Edited by:
Matteo Cameli, University of Siena, Italy

Reviewed by:
Serafino Fazio, Federico II University Hospital, Italy
Nazareno Paolocci, Johns Hopkins University, United States

***Correspondence:**
Stéphane Nottin
stephane.nottin@univ-avignon.fr

Specialty section:
This article was submitted to General Cardiovascular Medicine, a section of the journal Frontiers in Cardiovascular Medicine

Received: *27 October 2021*
Accepted: *10 January 2022*
Published: *08 February 2022*

Citation:
Paysal J, Merlin E, Terral D, Chalard A, Rochette E, Obert P and Nottin S (2022) Left Ventricular Strains and Myocardial Work in Adolescents With Anorexia Nervosa. Front. Cardiovasc. Med. 9:798774. doi: 10.3389/fcvm.2022.798774

INTRODUCTION

Anorexia nervosa (AN) is characterized by important weight loss, severe malnutrition and body composition abnormalities (1). Most cases are observed in females aged between 12 and 25 years (1). Cardiovascular complications in AN are frequent, occurring in up to 80% of patients, and some can be life-threatening (2). The most common abnormalities reported are sinus bradycardia,

hypotension and electrocardiographic abnormalities (3). A left ventricular (LV) remodeling has also been observed, characterized by a diminished wall thickness due to the loss of cardiac muscle (2). Regarding global diastolic function, a specific LV filling profile is usually observed, with decreased A wave and increased E/A ratio, on account very likely to sinus bradycardia (2, 4). Systolic function is often unchanged, with normal LV stroke volume and ejection fraction (EF) (5). However, most of studies in AN patients referred to standard ultrasound methods, precluding any conclusion regarding their myocardial regional function.

Myocardial strain analyses from speckle tracking echocardiography (STE) have emerged as a reliable technique for studying myocardial mechanics (6). Although they enable detecting subtle alterations in systolic function when EF is still preserved (6), their relative load dependency makes the myocardial deformation indices unable to account for changes in afterload observed in AN patients. To overcome this limitation, global myocardial work (GMW), estimated from construction of LV pressure-strain loops (LV-PSL), has recently emerged as an interesting echocardiographic tool for assessing the myocardial function (7–9). LV-PSL are strongly correlated with myocardial glucose metabolism (7) and thus could be altered in AN patients with caloric deprivations.

Non-uniform contractions of LV myocardial walls due to a decline of synchronicity affect myocardial performance. In AN patients, previous studies showed structural myocardial abnormalities with possible presence of fibrosis (10–12). Since strong interactions between myocardial fibrosis and conduction disorders have been demonstrated (13–15), we questioned a potential increase of LV mechanical dispersion in this specific population. The LV mechanical dispersion can be assessed not only from the segmental analysis of timing of LV strains (8, 13, 16), but also from the myocardial work, by differentiating the myocardial constructive work (MCW) and the myocardial wasted work (MWW) to estimate myocardial work efficiency (MWE) (7, 17).

Another important factor influencing LV myocardial performance is LV twist. During systole, contraction of the cardiomyocytes induced not only LV longitudinal, but also circumferential and radial strains (18, 19). Moreover, due to the complex orientation of the myocardial fibers, LV twists consequently to the opposing rotations of the base and the apex. Twisting of the LV, which could be assessed non-invasively by STE, is essential to maintain EF and efficiency of systolic function (20). It plays also a crucial role during diastole, with elastic energy stored during systole abruptly released during untwisting, generating an intraventricular pressure gradients very early in diastole and allowing filling to proceed at low filling pressure (18–20). It has been well-demonstrated that LV twisting mechanics was altered under various pathological states (20, 21), but its evaluation has never been done in AN patients.

In this context, the objective of the study was to compare the cardiac function of AN patients with healthy controls using novel advances in STE. We hypothesized that (1) LV strains and LV GMW would be decreased in AN patients, (2) LV intraventricular mechanical dispersion would be increased, and (3) LV twisting mechanisms would be enhanced to preserve their systolic function.

METHODS

Study Population

The study, prospective, included female patients with AN who had been diagnosed in a pediatric department of a university hospital in France between March 2019 and January 2020. All patients ranged from 10 to 18 years and fulfilled the DSM V criteria for AN (American Psychiatric Association) (22). The control group was composed of healthy adolescent girls with normal body mass and free from eating disorders. The BMI z score was calculated for all participants by specific formula (23). Patients and control subjects with chronic disease, congenital heart defect, positive family history of cardiac disease were excluded. Written informed consent was obtained from the study participants and their guardians. The Ile de France Ethics Committee approved the protocol for this study (18.12.05.66738 CAT 2).

Anthropometrical and Body Composition Assessments

Body height and body mass were measured. BMI was calculated as body mass.body height^{-2} and body surface area (BSA) was calculated according to Boyd (24). Blood pressure (BP) and HR were measured using an automatic device (General electric, Dynamap PRO 300 V2, Boston). Bradycardia was defined by HR $<$50 bpm, as in guideline on the evaluation and management of patients with bradycardia (Task force of 2018) (25). Systolic arterial hypotension was defined by systolic BP (SBP) below the 5th percentile and/or 90 mmHg (26). Body composition, including body fat mass with abdominal fat thickness (AFT) and lean mass, was evaluated by a bio-impedance system, validated for the measurement of body composition in children (27) (BioparHom, Z-Métrix, France).

Echocardiographic Recordings

Echocardiography was carried out with the subject in left lateral decubitus position, with Vivid Q ultrasound systems (GE Healthcare, Horten, Norway) using a 3.5-MHz transducer (M4S probe). Cine loops were recorded in parasternal long axis and apical (5, 4, 3 and 2 chambers) views and saved for blinded offline analysis (EchoPac, BT203 version, GE Healthcare). Grayscale images were saved at a frame rate of 80–90 frames.sec^{-1} and color tissue velocity images at a frame rate of 120–140 frames.sec^{-1}. 2D echocardiographic measurements were performed in accordance with the guidelines of the American Society of Echocardiography (28). All echocardiographic data were averaged from measurements obtained on 3–5 cardiac cycles.

LV Morphology and Global Function

LV diameters and myocardial thickness were measured from the parasternal long axis view. LV mass was estimated using Devereux formula and indexed to height$^{2.7}$ as recommended in the pediatric population (29, 30). LV diastolic function was

assessed from peak early (E wave) and atrial (A wave) transmitral flow velocities and from peak E' and A' TDI velocities, at the mitral annular level in the different apical views. LV volumes and EF were assessed using the Simpson's biplane method. Stroke volume and cardiac output (CO) were assessed from 5 chamber and parasternal long axis views, and then indexed to the BSA. Systemic vascular resistances were calculated by the formula mean arterial pressures divided by cardiac output, according the Poiseuille Law.

LV Global, Regional Strains and Dyssynchrony

Global longitudinal strain (GLS), circumferential strains (CS), diastolic longitudinal strain rate (LSr_{diast}) and twist mechanics (apical and basal rotations, peak twist and untwisting rate) were obtained as previously detailed (31). Data were normalized to percentage of systolic duration to avoid differences in heart rate and cine loop frame rates and to provide averaged strain curves during the cardiac cycle for AN and control groups. LV twist was calculated as the difference between apical and basal rotations at each percentage of systolic duration and untwist, occurring during diastole, was calculated. In order to assess the dynamics of global LV twist and its relation to radial displacement throughout the cardiac cycle, we constructed twist-displacement loops. Averaged radial displacement data from six segments in basal and in apical short-axis planes were summed and divided by 2 to obtain the mean value of radial displacement. We considered GLS, circumferential strains and LV twist as indices of myocardial systolic function, LSr_{diast} as index of LV relaxation (32) and peak untwisting rate as an index of LV diastolic suction.

LV Mechanical Dispersion and Myocardial Work Quantification

From a 17-segments model from apical 4, 3 and 2 chamber views to assess LV regional strains and time to peak (TTP) strains (18), LV mechanical dispersion was assessed by the standard deviation (SD) of the TTP (in ms) over the 17 segments (SD_{17S}).

Myocardial work (MW) and related parameters were estimated using the Automatic function imaging of the EchoPac software (**Figure 1**). MW was estimated as a function of time throughout the cardiac cycle by the combination of LV strain data (recorded on the apical 4, 3 and 2 chambers) obtained by STE and a non-invasively estimated LV pressure curve as described and validated by Russell et al. (7, 8). Peak arterial pressure measured with a cuff-manometer was assumed to be equal to peak systolic and diastolic LV pressures and to be uniform throughout the ventricle. MW was then quantified by calculating the rate of segmental shortening by differentiating the strain curve and multiplying the resulting value by the instantaneous LV pressure.

MW was calculated from mitral valve closure until mitral valve opening. During LV systole, segmental shortening contributes to the final LV ejection, whereas segmental stretch or lengthening does not contribute to LV ejection. As a result, the work performed by the myocardium during segmental shortening represents MCW, whereas the work performed by the myocardium during stretch or segmental lengthening represents energy loss, which is defined as MWW (9). During isovolumic relaxation, segmental lengthening contributes to LV relaxation, whereas segmental shortening does not. As a result, the work performed by the myocardium during segmental shortening, which does not promote LV relaxation, was considered MWW (9). On the opposite, the work performed by the myocardium during segmental lengthening was considered segmental MCW (9). The global MWE was finally obtained as follow:

$$MWE = \frac{MCW}{MCW + MWW} \times 100$$

Statistical Analysis

All values were expressed as mean ± SD. Statistical analyses were performed using Medcalc (version 19.1, Medcalc Software). One-way analysis of variance (ANOVA) was used to compare groups, after checking the normality of distribution of each variable by Shapiro-Wilk test. In the absence of normal distribution, the nonparametric Kruskal-Wallis test was used. Statistical significance for all analyses was assumed at $p < 0.05$.

RESULTS

Clinical Characteristics

Twenty-six female AN patients, with an illness duration of 19 ± 9 months, and 33 controls were included. **Table 1** shows the main clinical characteristics and the body composition of AN patients and controls. As expected, patients with AN had significantly lower body mass, BMI and BSA than controls. Percentage of body fat mass was lower and of lean mass was higher in AN patients compared to controls. AN patients showed significantly lower resting HR and lower systolic BP than the controls. Eight AN patients (30.8 %) had sinus bradycardia and 7 (26.9 %) had systolic hypotension.

Left Ventricular Morphology and Function

Data of LV morphology and function are presented in **Table 2**. LV posterior wall thickness, LV mass, LV mass index to $height^{2.7}$ were lower in AN patients compared to controls. There was no difference in the LV septum thickness, relative wall thickness (RWT), LV end-diastolic and end-systolic volume. AN patients presented with lower CO index, lower A wave with higher E/A ratio. Stroke volume index and EF were not different between groups. Systemic vascular resistances were higher in AN patients compared to controls.

Left Ventricular Strains and Myocardial Work

LV strains and MW are presented in **Figure 2** and **Table 3**. GLS was higher in AN patients compared to controls, whereas no difference were observed on circumferential strains. In AN patients, the LV-PSL was shifted to the left and downwards, consequently to the decrease of their LV pressures and the increase of their GLS. However, the area under the loop, reflecting the GMW, was similar between groups (1,657 ± 335 vs 1,737 ± 287 mmHg.% in AN patients and controls, respectively).

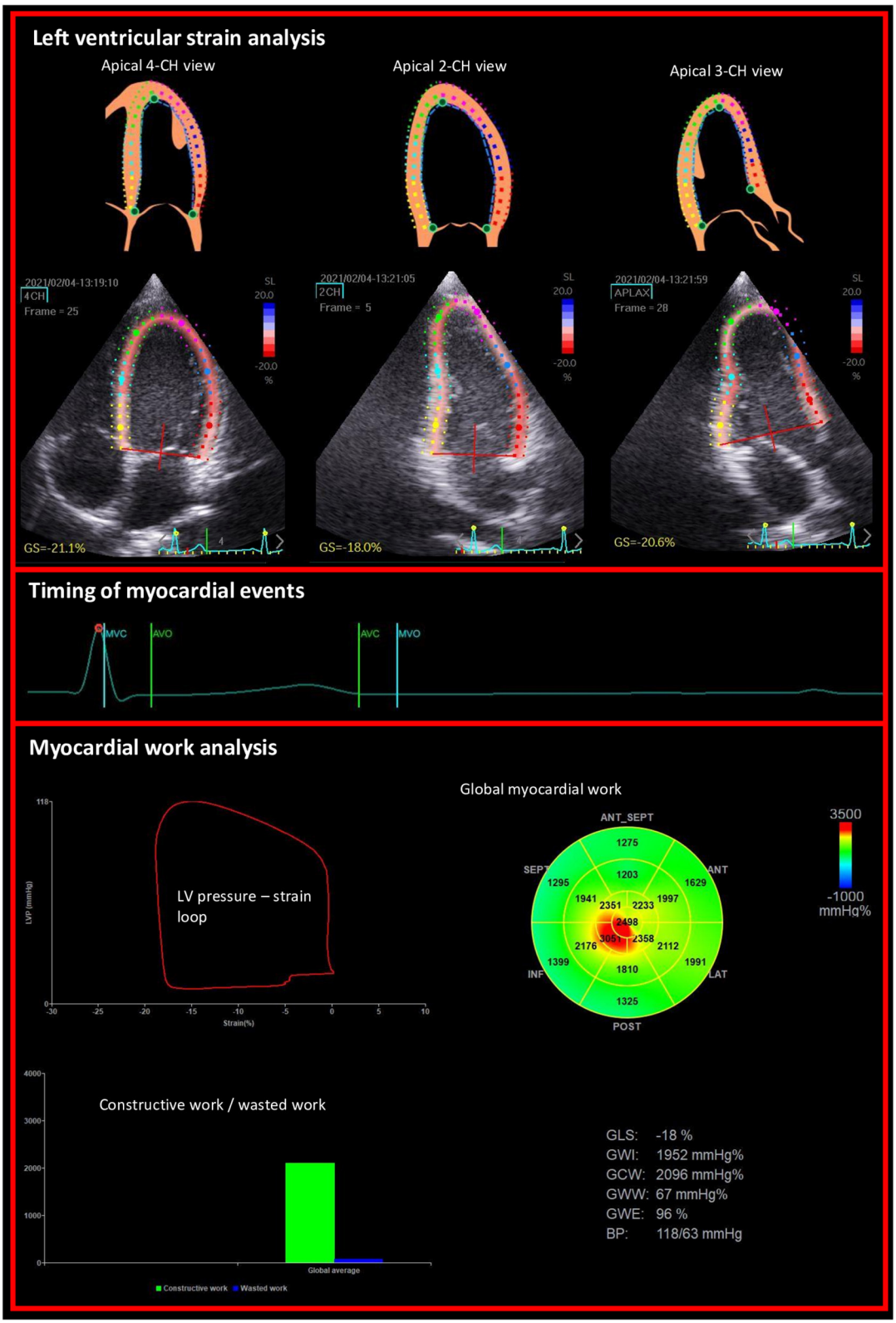

FIGURE 1 | Example of non-invasive estimation of the LV myocardial work from the left ventricular longitudinal strains on apical views and the timing of mitral and aortic valve events.

TABLE 1 | Baseline characteristics of AN patients and controls.

	AN patients ($n = 26$)	Controls ($n = 33$)
Age (years)	14.6 ± 1.9	14.1 ± 2.0
Tanner's pubertal stage	3.4 ± 1.1	4.0 ± 1.3
Anthropometry		
Height (cm)	159.8 ± 9.1	162.6 ± 10.0
Body mass (kg)	40.7 ± 8.2***	51.2 ± 9.8
BMI (kg.m^{-2})	15.8 ± 2.1***	19.2 ± 2.3
BSA (m²)	1.33 ± 0.16***	1.52 ± 0.19
Bioimpedance analysis		
AFT (mm)	8.4 ± 3.9**	14.1 ± 7.0
Body fat mass (kg)	5.1 ± 3.4***	10.5 ± 4.8
Body fat mass (%)	11.8 ± 6.2***	20.0 ± 6.6
Lean body mass (%)	85.0 ± 6.3***	76.6 ± 6.4
Hemodynamic constants		
Heart rate (bpm)	56 ± 12***	74 ± 11
Systolic BP (mmHg)	99 ± 14***	110 ± 8
Diastolic BP (mmHg)	63 ± 11	67 ± 7
Mean BP (mmHg)	75 ± 12*	81 ± 7

*AN, anorexia nervosa; BMI, body mass index; BSA, body surface area; AFT, abdominal fat thickness; BP, blood pressure; Values are mean ± SD. Significant differences with controls *$p < 0.05$; **$p < 0.01$; ***$p < 0.001$.*

TABLE 2 | Left ventricular morphology and function in AN patients and controls.

	AN patients ($n = 26$)	Controls ($n = 33$)
Morphology		
LV septum thickness (cm)	0.72 ± 0.15	0.77 ± 0.12
LV posterior wall thickness (cm)	0.67 ± 0.12*	0.75 ± 0.12
RWT	0.33 ± 0.06	0.36 ± 0.05
LV end-diastolic volume (mL)	79 ± 19	86 ± 18
LV end-systolic volume (mL)	29 ± 8	31 ± 7
LV mass (g)	79 ± 26*	96 ± 24
LV mass index to height $^{2.7}$ (g.m$^{-2.7}$)	22 ± 6*	26 ± 5
Function		
LV systolic function		
Stroke volume index (mL.m^{-2})	36.9 ± 5.9	35.6 ± 5.1
CO index (L.min^{-1}.m^{-2})	2.0 ± 0.4***	2.5 ± 0.4
EF (%)	64 ± 5	64 ± 6
LV diastolic function		
E wave (cm.s^{-1})	84 ± 17	82 ± 14
A wave (cm.s^{-1})	30 ± 6***	41 ± 7
E/A	2.9 ± 0.9***	2.0 ± 0.5
E' (cm.s^{-1})	12.8 ± 1.4	13.5 ± 1.3
A' (cm.s^{-1})	4.2 ± 0.9***	5.6 ± 1.1
E'/A'	3.2 ± 0.7***	2.5 ± 0.5
Systemic vascular resistances (AU)	30.1 ± 8.2***	21.9 ± 5.4

*Values are mean ± SD. Significant differences with controls *$p < 0.05$; **$p < 0.01$; ***$p < 0.001$.*
AN, anorexia nervosa; LV, left ventricular; RWT, relative wall thickness; CO, cardiac output; EF, ejection fraction; AU, arbitrary unit.

Left Ventricular Mechanical Dispersion

The SD_{17S}, an overall marker of intraventricular mechanical dispersion, was similar between groups (**Table 4**). No difference was observed between groups regarding MCW. The MWW was also similar and consequently the MWE was unchanged.

LV Twisting Mechanics

LV twisting mechanics are presented in **Figure 3** and **Table 3**. LV rotations and twist were similar between groups. Peak untwisting rate tended to be lower in AN patients despite difference did not reached statistical significance. Twist-radial displacement loops showed a similar pattern in both groups. After a small initial clockwise twist at the onset of ejection, twist increased linearly throughout systole. Early diastole was characterized by rapid untwisting despite small radial displacement, and then untwisting was smaller whereas displacement was larger from mid to late diastole. These results strongly supported that the untwisting efficiency and the suction effect was preserved in AN patients.

DISCUSSION

It was well-described that AN was associated with cardiac alterations (3, 5, 33). In our study, we confirmed that AN patients had lower LV mass and lower CO secondary to bradycardia. Using STE, the main objective of our study was to get insight into their regional myocardial function, including MW and LV twisting mechanics. We observed that, in AN patients, (1) GLS was higher but GMW unchanged, (2) intraventricular mechanical dispersion, assessed from time to peak strains and MWE, remained similar compared to controls, (3) twisting mechanics were preserved.

Higher Global Longitudinal Strain but Unaltered Global Myocardial Work in AN Patients

The first main result of our study was that the GLS, which allows a more sensitive analysis of systolic function than EF (34), was significant higher in AN patients compared to controls. This is an unexpected result since in various pathological states the GLS is usually decreased (35). To our knowledge, only one previous study evaluated GLS in AN patients and found a similar GLS between AN patients and controls (36). Discrepancies from our results could be explained by a different BMI z score between our group and their two groups of AN patients (i.e., −1.78 vs. −0.44 and −1.01). The severity of the disease could have an impact on the LV myocardial function.

The increase in GLS could results from a complex interplay between several factors including hypotension, low resting HR and cardiac hypotrophy. In the present study, we assessed the MW, a new echocardiographic tool based on both an assessment of LV strain and an estimation of LV intraventricular pressures (9, 37). Contrary to GLS, we did not observed difference on GMW between our AN patients and controls. Indeed, despite the different pressure-strain loops (i.e., shifted to the left and downward in AN patients due to their higher strains and their

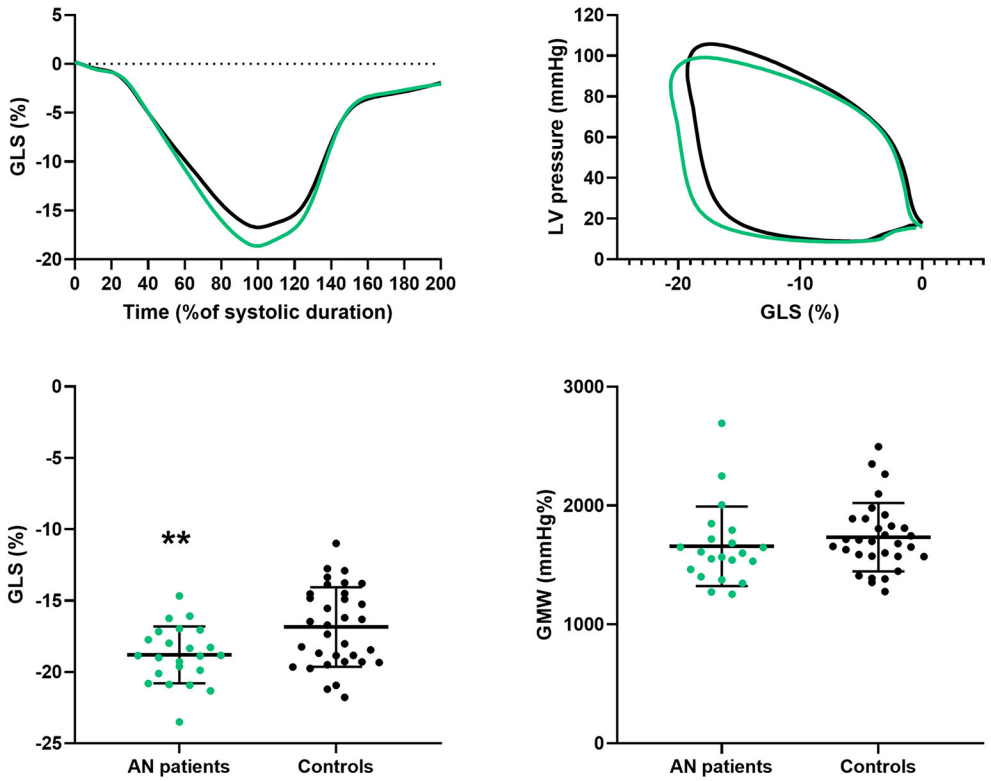

FIGURE 2 | Longitudinal strain and global myocardial work in AN patients and controls. GLS, global longitudinal strain; LV, left ventricular; GMW, global myocardial work. Difference between groups: $^{**}P < 0.01$.

TABLE 3 | Left ventricular strains and twisting mechanics in AN patients and controls.

	AN patients ($n = 26$)	Controls ($n = 33$)
Systolic strain		
GLS (%)	−18.8 ± 2.0**	−16.9 ± 2.8
CS (%)		
Basal level	−21.9 ± 2.9	−23.1 ± 3.6
Apical level	−29.6 ± 4.6	−30.9 ± 4.4
Rotation (°)		
Basal level	−3.3 ± 1.7	−3.7 ± 2.0
Apical level	5.8 ± 2.6	5.7 ± 2.1
Twist (°)	7.3 ± 3.2	7.5 ± 3.3
Diastolic strain		
LSr $_{diastolic}$	1.9 ± 0.3	1.9 ± 0.5
Untwisting rate (°.s^{-1})	−67.5 ± 31.9	−80.3 ± 31.5

*Values are mean ± SD. Significant differences with controls *p < 0.05, **p < 0.01, ***p < 0.001.*
AN, anorexia nervosa; GLS, global longitudinal strain; CS, circumferential strain; LSr, longitudinal strain rate.

TABLE 4 | LV dyssynchrony assessed by LV strains and myocardial work in AN patients and controls.

	AN patients ($n = 26$)	Controls ($n = 33$)
Myocardial work		
MCW	1,842.3 ± 336.7	2,014.0 ± 299.4
MWW	131.0 ± 78.3	173.0 ± 152.5
MWE	92.8 ± 3.8	91.9 ± 4.6
LV Dyssynchrony		
SD $_{17S}$ (ms)	42.3 ± 24.3	45.8 ± 27.0

*Values are mean ± SD. Significant differences with controls *p < 0.05; **p < 0.01; ***p < 0.001.*
AN, anorexia nervosa; MCW, myocardial constructive work; MWW, myocardial wasted work; MWE, myocardial work efficiency; SD, standard deviation.

lower SBP), area, representing the GMW, were similar between the 2 groups. This second main result strongly supported that the increase in GLS of AN patients were probably linked with their lower SBP. The key role of cardiac afterload on GLS has been demonstrated in hypertensive patients or in animals in which a decrease of GLS was observed consequently to an increase in afterload (35, 38, 39). Low HR in our AN patients could also be involved in their higher GLS, as observed in endurance athletes, in whom resting bradycardia was associated with an increase in GLS (35, 38). In pediatric populations, advancing age leads to a decrease of HR concomitantly with an increase of GLS (40), suggesting also a potential link between HR and GLS. The low LV mass of our AN patients could be another factor explaining

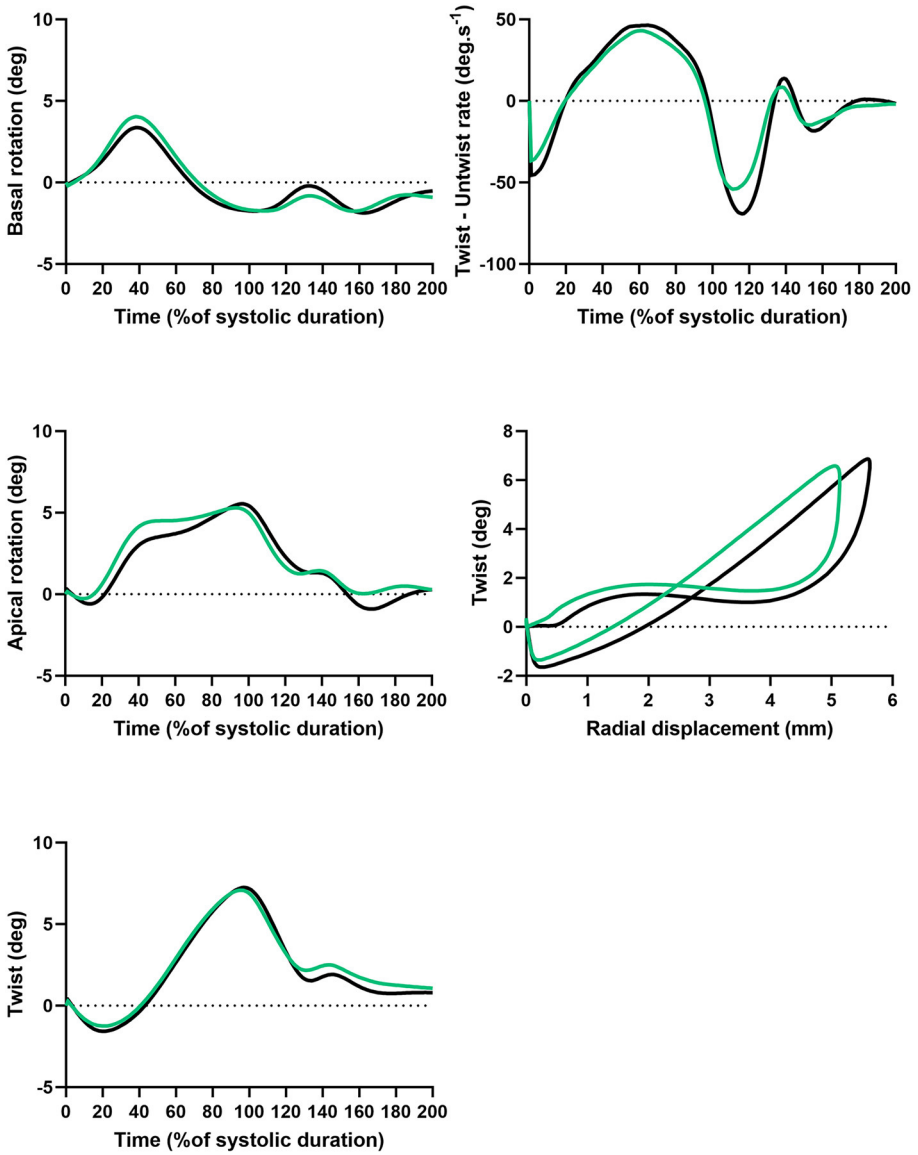

FIGURE 3 | Twist and untwist mechanisms in AN patients and controls. Basal rotation, apical rotation and twist, function of time (%of systolic duration). Twist – untwist rate, function of time (% of systolic duration). Twist function of radial displacement.

their increased GLS. Indeed, in animals, the increase in the LV dimensions was associated with an decrease in GLS (39). In our study, LV mass of patients with AN was lower compared to controls. A previous study observed that the lower LV mass in patient with AN was linked to high growth hormon, low IGF-1 and low thyroid hormon levels (41). However, our results failed to demonstrate significant correlations between GLS and posterior wall thickness, LV mass or SBP.

The clinical significance of the increased GLS remains unclear. Despite this is purely speculative, the increase in GLS at rest could act to favor the stroke volume and thus the CO despite their low LVM and resting bradycardia. We could also question their reserve of GLS during exercise and thus their effort tolerance, since it has been well-described that in response to physical activity (42, 43) or under dobutamine stress (44) the increase in LV strains acted to maintain or improved the stroke volume (42). In this context, further studies would be helpful to understand how the specific heart of AN patients respond to exercise.

Intraventricular Mechanical Dispersion in AN Patients

Several case studies based on autopsy reported cardiac fibrosis in AN patients (10, 11). Interestingly, using cardiac MRI (12) and late gadolinium enhancement, Oflaz et al. (12) observed that 23% of AN patients had a presence of myocardial fibrosis

(12). Since fibrosis is known to favor conduction abnormalities (13–15), we questioned if our AN patients had a higher LV mechanical dispersion compared to controls. Based on segmental STE analysis, we observed that the SD_{17S}, an overall index of LV mechanical dispersion remained unchanged in AN patients. Additionally, we used an up-to-date method by quantifying both MCW and MWW to calculate MWE (8, 13). In patients with increased mechanical dispersion, MWW, work that is being done by the ventricle but does not contribute to LV ejection (8, 9), is significantly increased and MWE reduced (8, 9, 13). In our study, we did not find an increase in MWW in AN patients compared to controls, highlighting that their intraventricular mechanical dispersion was not increased.

Left Ventricular Twisting Mechanics in AN Patients

During systole, contraction of the cardiomyocytes generates opposite rotations of the LV base and the apex, inducing a LV twist (18–20). Despite its key role in both systolic and diastolic performance, twist mechanics have been largely neglected in previous studies. We hypothesized that LV rotations and twist could be modified in AN patients, since it was well-demonstrated that LV twist can be affected by changes in loading conditions (21, 45). More specifically, LV twist decreased when afterload increased and/or preload decreased (21). Another major finding of our study was that LV rotations and twist was unaltered in AN patients. This could be an additional mechanism favoring the maintenance of EF and stroke volume since LV twist, helps for bringing a uniform distribution of LV fiber stress and fiber shortening across the wall, and its disappearance has been clearly shown to increase oxygen demand and reduce the efficiency of LV systolic function (20, 21).

The LV twist allows energy to be stored in elastic component during systole, energy restored very early in diastole, creating an intraventricular pressure gradient that favors LV filling (45, 46). The LV twist-untwist thus links systole to diastole (i.e., systolic-diastolic coupling). In our AN patients, LV untwisting was preserved. The twist-displacement loops highlighted that, in both groups, substantial untwisting occurred despite a relatively small radial displacement in early diastole, whereas untwisting was markedly smaller during the late phases of diastole in spite of substantial radial displacement. This result strongly supported that, in AN patients, the ventricle untwists, rapidly recoiling, creating a diastolic suction that was probably fully effective, contributing to their normal LV diastolic function.

CONCLUSION

In our study, AN was accompanied by reduced HR and SBP, associated with cardiac remodeling characterized by a decrease in LV mass and wall thickness. However, the assessment of LV strains and MW, and also of LV twisting mechanics, brought new evidences that the cardiac function of adolescent AN patients was preserved. Of note, our study population was characterized by low BMI z score, but with a relatively short illness duration. So, it would be interesting to evaluate in the future the myocardial function of AN patients with a longer illness duration.

DATA AVAILABILITY STATEMENT

The original contributions presented in the study are included in the article/supplementary material, further inquiries can be directed to the corresponding author/s.

ETHICS STATEMENT

The studies involving human participants were reviewed and approved by Ile de France Ethics Comittee (18.12.05.66738 CAT 2). Written informed consent to participate in this study was provided by the participants' legal guardian/next of kin.

AUTHOR CONTRIBUTIONS

JP: design, methodology, investigation, analysis, and writing initial manuscript. EM: investigation and supervision. DT: methodology and investigation. AC: analysis and supervision. ER: supervision. PO: methodology and analysis. SN: design, methodology, investigation, analysis, writing, and supervision. All authors contributed to the article and approved the submitted version.

FUNDING

This work was supported by the Platform 3A, funded by the European Regional Development Fund, the French Ministry of Research, Higher Education and Innovation, the Provence-Alpes-Côte-d'Azur region, the Departmental Council of Vaucluse and the Urban Community of Avignon.

ACKNOWLEDGMENTS

We gratefully thank Dominique FENEON for their contribution to patients recruitment.

REFERENCES

1. Giovinazzo S, Sukkar SG, Rosa GM, Zappi A, Bezante GP, Balbi M, et al. Anorexia nervosa and heart disease: a systematic review. *Eat Weight Disord EWD.* (2019) 24:199–207. doi: 10.1007/s40519-018-0567-1
2. Escudero CA, Potts JE, Lam PY, De Souza AM, Mugford GJ, Sandor GGS. An echocardiographic study of left ventricular size and cardiac function in adolescent females with anorexia nervosa: LV size and cardiac function in AN. *Eur Eat Disord Rev.* (2016) 24:26–33. doi: 10.1002/erv.2409
3. Sachs KV, Harnke B, Mehler PS, Krantz MJ. Cardiovascular complications of anorexia nervosa: a systematic review. *Int J Eat Disord.* (2016) 49:238–48. doi: 10.1002/eat.22481
4. Galetta F, Franzoni F, Cupisti A, Morelli E, Santoro G, Pentimone F. Early detection of cardiac dysfunction in patients with anorexia nervosa by tissue Doppler imaging. *Int J Cardiol.* (2005) 101:33–7. doi: 10.1016/j.ijcard.2004.03.006
5. Olivares JL, Vázquez M, Fleta J, Moreno LA, Pérez-González JM, Bueno M. Cardiac findings in adolescents with anorexia nervosa at

diagnosis and after weight restoration. *Eur J Pediatr.* (2005) 164:383–6. doi: 10.1007/s00431-005-1647-6
6. Potter E, Marwick TH. Assessment of left ventricular function by echocardiography: the case for routinely adding global longitudinal strain to ejection fraction. *JACC Cardiovasc Imaging.* (2018) 11:260–74. doi: 10.1016/j.jcmg.2017.11.017
7. Russell K, Eriksen M, Aaberge L, Wilhelmsen N, Skulstad H, Remme EW, et al. A novel clinical method for quantification of regional left ventricular pressure–strain loop area: a non-invasive index of myocardial work. *Eur Heart J.* (2012) 33:724–33. doi: 10.1093/eurheartj/ehs016
8. Russell K, Eriksen M, Aaberge L, Wilhelmsen N, Skulstad H, Gjesdal O, et al. Assessment of wasted myocardial work: a novel method to quantify energy loss due to uncoordinated left ventricular contractions. *Am J Physiol-Heart Circ Physiol.* (2013) 305:H996–H1003. doi: 10.1152/ajpheart.00191.2013
9. Samset E, Healthcare G. *Evaluation of Segmental Myocardial Work in the Left Ventricle.4*. Available online at: https://www.gehealthcare.com/-/media/8cab29682ace4ed7841505f813001e33.pdf
10. Lamzabi I, Syed S, Reddy VB, Jain R, Harbhajanka A, Arunkumar P. Myocardial changes in a patient with anorexia nervosa. *Am J Clin Pathol.* (2015) 143:734–7. doi: 10.1309/AJCP4PLFF1TTKENT
11. SHORT PAPERS Anorexia Nervosa and Sudden Death.
12. Oflaz S, Yucel B, Oz F, Sahin D, Ozturk N, Yaci O, et al. Assessment of myocardial damage by cardiac MRI in patients with anorexia nervosa. *Int J Eat Disord.* (2013) 46:862–6. doi: 10.1002/eat.22170
13. Nguyên UC, Verzaal NJ, van Nieuwenhoven FA, Vernooy K, Prinzen FW. Pathobiology of cardiac dyssynchrony and resynchronization therapy. *EP Eur.* (2018) 20:1898–909. doi: 10.1093/europace/euy035
14. Anderson KP, Walker R, Urie P, Ershler PR, Lux RL, Karwandee SV. Myocardial electrical propagation in patients with idiopathic dilated cardiomyopathy. *J Clin Invest.* (1993) 92:122–40. doi: 10.1172/JCI116540
15. Kawara T, Derksen R, de Groot JR, Coronel R, Tasseron S, Linnenbank AC, et al. Activation Delay After Premature Stimulation in Chronically Diseased Human Myocardium Relates to the Architecture of Interstitial Fibrosis. *Circulation*. (2001) 104:3069–75. doi: 10.1161/hc5001.100833
16. Cvijic M, Duchenne J, Ünlü S, Michalski B, Aarones M, Winter S, et al. Timing of myocardial shortening determines left ventricular regional myocardial work and regional remodelling in hearts with conduction delays. *Eur Heart J - Cardiovasc Imaging.* (2018) 19:941–9. doi: 10.1093/ehjci/jex325
17. Schrub F, Schnell F, Donal E, Galli E. Myocardial work is a predictor of exercise tolerance in patients with dilated cardiomyopathy and left ventricular dyssynchrony. *Int J Cardiovasc Imaging*. (2019) 36:45–53. doi: 10.1007/s10554-019-01689-4
18. Thomas JD, Popović ZB. Assessment of left ventricular function by cardiac ultrasound. *J Am Coll Cardiol.* (2006) 48:2012–25. doi: 10.1016/j.jacc.2006.06.071
19. Sengupta PP, Korinek J, Belohlavek M, Narula J, Vannan MA, Jahangir A, et al. Left ventricular structure and function: basic science for cardiac imaging. *J Am Coll Cardiol.* (2006) 48:1988–2001. doi: 10.1016/j.jacc.2006.08.030
20. Bloechlinger S, Grander W, Bryner J, Dünser MW. Left ventricular rotation: a neglected aspect of the cardiac cycle. *Intensive Care Med.* (2011) 37:156–63. doi: 10.1007/s00134-010-2053-8
21. Stöhr EJ, Shave RE, Baggish AL, Weiner RB. Left ventricular twist mechanics in the context of normal physiology and cardiovascular disease: a review of studies using speckle tracking echocardiography. *Am J Physiol Heart Circ Physiol.* (2016) 311:H633–644. doi: 10.1152/ajpheart.00104.2016
22. Loas G. The DSM-V : an overview. *Rev Med Brux.* (2016) 37:231–4.
23. Rolland-Cachera MF, Cole TJ, Sempé M, Tichet J, Rossignol C, Charraud A. Body Mass Index variations: centiles from birth to 87 years. *Eur J Clin Nutr.* (1991) 45:13–21.
24. Orimadegun A, Omisanjo A. Evaluation of five formulae for estimating body surface area of nigerian children. *Ann Med Health Sci Res.* (2014) 4:889–98. doi: 10.4103/2141-9248.144907
25. Kusumoto FM, Schoenfeld MH, Barrett C, Edgerton JR, Ellenbogen KA, Gold MR, et al. 2018 ACC/AHA/HRS Guideline on the Evaluation and Management of Patients With Bradycardia and Cardiac Conduction Delay: A Report of the American College of Cardiology/American Heart Association Task Force on Clinical Practice Guidelines and the Heart Rhythm Society. *Circulation*. (2019) 140:e382–e482. doi: 10.1161/CIR.0000000000000628
26. Banker A, Bell C, Gupta-Malhotra M, Samuels J. Blood pressure percentile charts to identify high or low blood pressure in children. *BMC Pediatr*. (2016) 16:98. doi: 10.1186/s12887-016-0633-7
27. Barreira TV, Staiano AE, Katzmarzyk PT. Validity assessment of a portable bioimpedance scale to estimate body fat percentage in white and African-American children and adolescents. *Pediatr Obes.* (2013) 8:e29–32. doi: 10.1111/j.2047-6310.2012.00122.x
28. Lang RM, Badano LP, Mor-Avi V, Afilalo J, Armstrong A, Ernande L, et al. Recommendations for cardiac chamber quantification by echocardiography in adults: an update from the American Society of Echocardiography and the European Association of Cardiovascular Imaging. *Eur Heart J – Cardiovasc Imaging.* (2015) 16:233–71. doi: 10.1093/ehjci/jev014
29. de Simone G, Daniels SR, Devereux RB, Meyer RA, Roman MJ, de Divitiis O, et al. Left ventricular mass and body size in normotensive children and adults: assessment of allometric relations and impact of overweight. *J Am Coll Cardiol.* (1992) 20:1251–60. doi: 10.1016/0735-1097(92)90385-Z
30. Devereux RB, Alonso DR, Lutas EM, Gottlieb GJ, Campo E, Sachs I, et al. Echocardiographic assessment of left ventricular hypertrophy: comparison to necropsy findings. *Am J Cardiol.* (1986) 57:450–8. doi: 10.1016/0002-9149(86)90771-X
31. Maufrais C, Schuster I, Doucende G, Vitiello D, Rupp T, Dauzat M, et al. Endurance training minimizes age-related changes of left ventricular twist-untwist mechanics. *J Am Soc Echocardiogr.* (2014) 27:1208–15. doi: 10.1016/j.echo.2014.07.007
32. Wang J, Khoury DS, Thohan V, Torre-Amione G, Nagueh SF. Global diastolic strain rate for the assessment of left ventricular relaxation and filling pressures. *Circulation.* (2007) 115:1376–83. doi: 10.1161/CIRCULATIONAHA.106.662882
33. Gottdiener JS, Gross HA, Henry WL, Borer JS, Ebert MH. Effects of self-induced starvation on cardiac size and function in anorexia nervosa. *Circulation.* (1978) 58:425–33. doi: 10.1161/01.CIR.58.3.425
34. Al Saikhan L, Park C, Hardy R, Hughes A. Prognostic implications of left ventricular strain by speckle-tracking echocardiography in the general population: a meta-analysis. *Vasc Health Risk Manag.* (2019) 15:229–51. doi: 10.2147/VHRM.S206747
35. *A Test in Context: Myocardial Strain Measured by Speckle-Tracking Echocardiography*. Elsevier Enhanced Reader.
36. Morris R, Prasad A, Asaro J, Guzman M, Sanders L, Hauck A, et al. Markers of Cardiovascular Dysfunction in Adolescents With Anorexia Nervosa. *Glob Pediatr Health*. (2017) 4. doi: 10.1177/2333794X17727423
37. Smiseth OA, Donal E, Penicka M, Sletten OJ. How to measure left ventricular myocardial work by pressure-strain loops. *Eur Heart J Cardiovasc Imaging.* (2020) 22:259–261. doi: 10.1093/ehjci/jeaa301
38. Iudice FL, Petitto M, Ferrone M, Esposito R, Vaccaro A, Buonauro A, et al. *Determinants of Myocardial Mechanics in Top-Level Endurance Athletes: Three-Dimensional Speckle Tracking Evaluation.7*.
39. Rösner A, Bijnens B, Hansen M, How OJ, Aarsaether E, Müller S, et al. Left ventricular size determines tissue Doppler-derived longitudinal strain and strain rate. *Eur J Echocardiogr.* (2009) 10:271–7. doi: 10.1093/ejechocard/jen230
40. Boettler P, Hartmann M, Watzl K, Maroula E, Schultemoenting J, Knirsch W, et al. Heart rate effects on strain and strain rate in healthy children. *J Am Soc Echocardiogr.* (2005) 18:1121–30. doi: 10.1016/j.echo.2005.08.014
41. Carlomagno G, Mercurio V, Ruvolo A, Senatore I, Halinskaya I, Fazio V, et al. Endocrine alterations are the main determinants of cardiac remodelling in restrictive anorexia nervosa. *ISRN Endocrinol.* (2011) 2011:171460. doi: 10.5402/2011/171460
42. Izem O, Maufrais C, Obert P, Rupp T, Schuster I, Nottin S. Kinetics of left ventricular mechanics during transition from rest to exercise. *Med Sci Sports Exerc.* (2019) 51:1838–44. doi: 10.1249/MSS.0000000000002005
43. Magne J, Mahjoub H, Dulgheru R, Pibarot P, Pierard LA, Lancellotti P. Left ventricular contractile reserve in asymptomatic primary mitral regurgitation. *Eur Heart J.* (2014) 35:1608–16. doi: 10.1093/eurheartj/eht345
44. De Luca A, Stolfo D, Caiffa T, Korcova R, Barbati G, Vitrella G, et al. Prognostic Value of global longitudinal strain-based left ventricular contractile reserve in candidates for percutaneous correction of functional

mitral regurgitation: implications for patient selection. *J Am Soc Echocardiogr.* (2019) 32:1436–43. doi: 10.1016/j.echo.2019.07.006
45. Sengupta PP, Tajik AJ, Chandrasekaran K, Khandheria BK. Twist mechanics of the left ventricle: principles and application. *JACC Cardiovasc Imaging.* (2008) 1:366–76. doi: 10.1016/j.jcmg.2008.02.006
46. Notomi Y, Popovic ZB, Yamada H, Wallick DW, Martin MG, Oryszak SJ, et al. Ventricular untwisting: a temporal link between left ventricular relaxation and suction. *Am J Physiol Heart Circ Physiol.* (2008) 294:H505–513. doi: 10.1152/ajpheart.00975.2007

Conflict of Interest: The authors declare that the research was conducted in the absence of any commercial or financial relationships that could be construed as a potential conflict of interest.

Publisher's Note: All claims expressed in this article are solely those of the authors and do not necessarily represent those of their affiliated organizations, or those of the publisher, the editors and the reviewers. Any product that may be evaluated in this article, or claim that may be made by its manufacturer, is not guaranteed or endorsed by the publisher.

frontiers in Cardiovascular Medicine

REVIEW
published: 10 February 2022
doi: 10.3389/fcvm.2022.845070

Vascular Stem/Progenitor Cells in Vessel Injury and Repair

Jiaping Tao [1,2,3†], *Xuejie Cao* [1,2,3†], *Baoqi Yu* [1,2,3*] *and Aijuan Qu* [1,2,3*]

[1] Department of Physiology and Pathophysiology, School of Basic Medical Sciences, Capital Medical University, Beijing, China, [2] The Key Laboratory of Cardiovascular Remodeling-Related Diseases, Ministry of Education, Beijing, China, [3] Beijing Key Laboratory of Metabolic Disorder-Related Cardiovascular Diseases, Beijing, China

Vascular repair upon vessel injury is essential for the maintenance of arterial homeostasis and function. Stem/progenitor cells were demonstrated to play a crucial role in regeneration and replenishment of damaged vascular cells during vascular repair. Previous studies revealed that myeloid stem/progenitor cells were the main sources of tissue regeneration after vascular injury. However, accumulating evidences from developing lineage tracing studies indicate that various populations of vessel-resident stem/progenitor cells play specific roles in different process of vessel injury and repair. In response to shear stress, inflammation, or other risk factors-induced vascular injury, these vascular stem/progenitor cells can be activated and consequently differentiate into different types of vascular wall cells to participate in vascular repair. In this review, mechanisms that contribute to stem/progenitor cell differentiation and vascular repair are described. Targeting these mechanisms has potential to improve outcome of diseases that are characterized by vascular injury, such as atherosclerosis, hypertension, restenosis, and aortic aneurysm/dissection. Future studies on potential stem cell-based therapy are also highlighted.

Keywords: vascular stem cells, atherosclerosis, restenosis, hypertension, aortic aneurysm, vascular injury, vascular remodeling

OPEN ACCESS

Edited by:
Zhanpeng Huang,
The First Affiliated Hospital of Sun Yat-sen University, China

Reviewed by:
Qingzhong Xiao,
Queen Mary University of London, United Kingdom
Zhi Xin Shan,
Guangdong Provincial People's Hospital, China

***Correspondence:**
Baoqi Yu
baoqiyu@ccmu.edu.cn
Aijuan Qu
aijuanqu@ccmu.edu.cn

† These authors have contributed equally to this work

Specialty section:
This article was submitted to General Cardiovascular Medicine, a section of the journal Frontiers in Cardiovascular Medicine

Received: *29 December 2021*
Accepted: *17 January 2022*
Published: *10 February 2022*

Citation:
Tao J, Cao X, Yu B and Qu A (2022) Vascular Stem/Progenitor Cells in Vessel Injury and Repair. Front. Cardiovasc. Med. 9:845070. doi: 10.3389/fcvm.2022.845070

INTRODUCTION

Vascular injury and repair process has been found to be associated with a variety of cardiovascular diseases, including atherosclerosis, restenosis, hypertension, and arterial aneurysm. They are mainly caused by vascular wall thickening and lumen narrowing. The main causes of the diseases are endothelial injury, vascular smooth muscle cell (VSMC) proliferation, matrix deposition induced abnormal vascular injury and repair (1). The artery wall has three layers as shown in **Figure 1**: intima, media and adventitia. The intima, which has direct access to blood flow, is mainly made up of endothelial cells (ECs) (2). The media is mainly composed of VSMCs, as well as collagen and elastic fibers. The adventitia is rich in collagen, containing a variety of cells, as well as nerves and blood vessels (3). Previous studies have shown that the occurrence and development of these diseases is due to the phenotypic transformation of VSMCs induced by a variety of factors (4, 5). But there are still unresolved disputations on the reversibility of phenotypic transformation. Recent studies suggested that VSMCs participate in pathological processes, not only through phenotypic transformation, but also from stem/progenitor cells differentiation (6). And it also found that VSMCs derived from stem/progenitor cells participate in atherosclerosis, while maintaining a contractile phenotype without phenotypic transformation (7, 8).

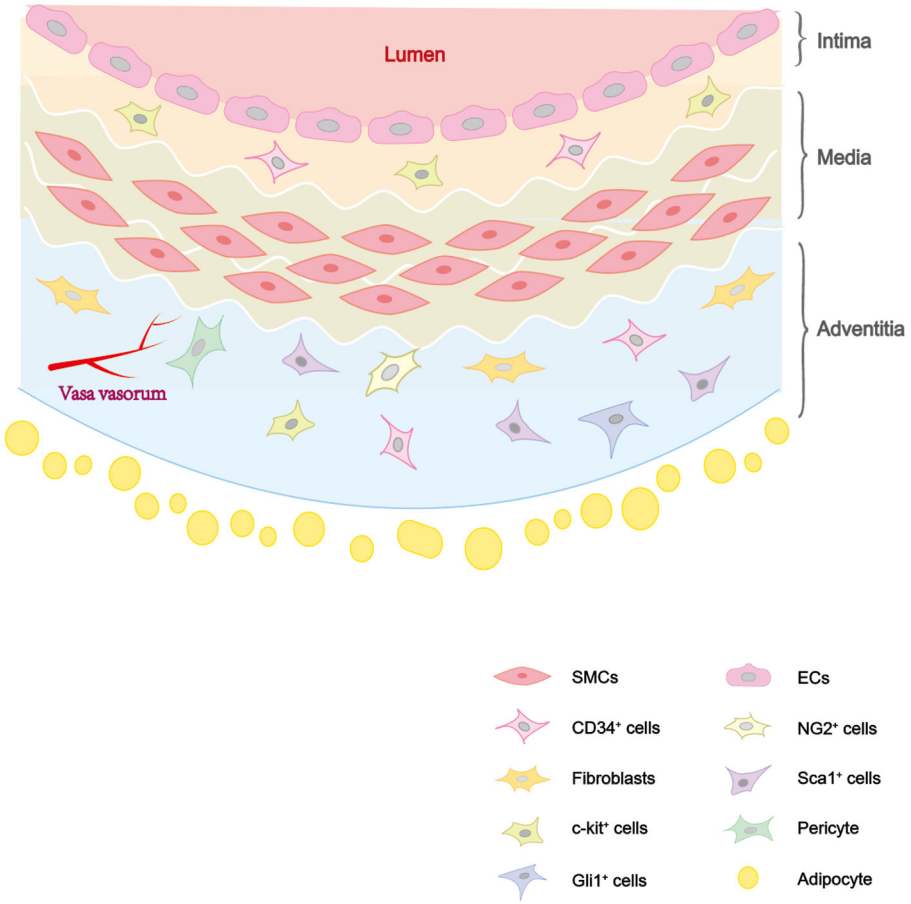

FIGURE 1 | The distribution of cells in vascular wall. The vascular wall consists of three layers: intima, media, and adventitia. The intima consists of ECs and some vascular stem cells such as c-kit$^+$ cells. The media is composed of SMCs. The adventitia is composed of vascular stem cells (Sca-1$^+$ cells, c-kit$^+$ cells, CD34$^+$ cells, pericytes, etc.) and fibroblasts.

In recent years, studies have demonstrated that resident or circulating stem/progenitor cells, such as endothelial progenitor cells (EPCs), smooth muscle progenitor cells (SMPCs), mesenchymal stem cells (MSCs), and pericytes, can differentiate into several types of vascular cells and form neointima during vascular repair (9). Vascular stem cells (VSCs) residing in blood vessels play a key role in vascular remodeling and closely related to the occurrence of vascular remodeling diseases. During embryonic development, vascular networks depend on vasculogenesis and angiogenesis. Adult VSCs are almost dormant in their niches, once blood vessels are injured, these cells can be activated to initiate neointima, with inflammatory cells infiltration and extracellular matrix (ECM) deposition (10). Perivascular tissues, including the adipose layer is also thought to be crucial in vascular development and disease progression (11).

In this review, we describe several stem/progenitor cells mainly in adventitia and their functions in development of atherosclerosis, restenosis, hypertension, and aortic aneurysm/dissection. At present, there are few studies on VSCs, and the sources of various regenerative ECs and VSMCs involved in the pathological process of vascular remodeling diseases have not been fully studied. Therefore, the mechanism of the participation of VSCs in various vascular remodeling diseases needs to be further studied. In this paper, several types of VSCs and their roles in vascular remodeling-related diseases

Abbreviations: AAA, abdominal aortic aneurysm; ADAM17, a disintigrin and metalloproteinase 17; ATF6, activating transcription factor 6; BMMSC, bone marrow mesenchymal stem cells; CCL, Chemokine (C-C motif) ligand; CXCL, Chemokine (C-X-C motif) ligand; CXCR, Chemokine (C-X-C motif) receptor; DKK3, dickkopf 3; EC, endothelial cell; ECFC, endothelial colony-forming cell; ECM, extracellular matrix; EPC, endothelial progenitor cell; Flk-1, fetal liver kinase-1; FoxM1, Forkhead box protein M1; HAECs, human aortic endothelial cells; HUVECs, human umbilical vein endothelial cells; KLF4, krüppel-like factor 4; MACs, myeloid angiogenic cells; MFAP4, microfibrillar-associated protein 4; MFS, marfan syndrome; MMP, matrix metalloproteinase; MSCs, mesenchymal stem cells; NF-κB, nuclear factor-kappa B; PDGF beta, platelets derive growth factors beta; PDGFR, platelet-derived growth factor receptor; SDF-1, stromal cell-derived factor-1; Shh, sonic hedgehog; SMPC, smooth muscle progenitor cell; STAT3, signal transducer and activator of transcription 3; TAA, thoracic aortic aneurysm; TGFβ, transforming growth factor; TNFα, tumor necrosis factor; Tsg6, TNFα-stimulated gene 6; VE-cadherin, vascular endothelial cadherin; VEGF, vascular endothelial growth factor; VSC, vascular progenitor cell; VSMCs, vascular smooth muscle cells; vWF, von willebrand factor.

are reviewed, including various vascular stem/progenitor cells in the process of vascular injury and repair as well as the key elements and important signaling pathways in the occurrence and progression of diseases. New potential targets for clinical treatment of vascular diseases are proposed.

VASCULAR STEM/PROGENITOR CELLS IN VESSEL WALL

During vascular injury, the pathological process of vascular wall changes includes ECs dysfunction, VSMCs proliferation, and inflammatory response. Many studies 'have demonstrated that vascular stem/progenitor cells can be mobilized in response to various pathological stimuli and play a key role in the vascular repair (12–15). Here we will mainly review studies on EPCs, SMPCs, MSCs, and pericytes (**Table 1**).

Resident Endothelial Progenitor Cells

Earlier studies suggested that EPCs are a group of cells mobilized from bone marrow that participate in endothelium repair after injury (35). In fact, EPCs have a variety of tissue sources, including bone marrow, spleen, blood vessel wall, lipid, and placenta (12). At present, EPCs are defined as the cell population that has the typical clonal proliferation ability and characteristics of stem cells and can differentiate into mature ECs (36).

EPCs actually consist of different cell populations, making up "early EPCs" and "late EPCs" (10). The early stage EPCs appears in early culture stage (4–7 days), its survival time is short and will not differentiate into ECs. EPCs can activate adjacent cells by releasing SDF-1 and VEGF to promote vascular growth (37). It's classical immunophenotypes are $CD45^+$,$CD14^+$, and $CD31^+$ and $CD146^-$,$CD133^-$, and $Tie2^-$ (10). The late stage EPCs can be known as endothelial colony-forming cells (ECFCs), derived from blood vessel wall, human placenta, and white adipose tissue (38). Compared with the early stage EPCs, ECFCs has a higher degree of proliferation and longer survival time, and can differentiate into mature functional ECs to participate in vascular repair (39). It's typical immunophenotypes are $CD31^+$, vWF^+, VE-cadherin$^+$, $CD146^+$, $VEGFR2^+$, and $CD45^-$, $CD14^-$.

By studying HUVECs and HAECs, it was found that the renewal of vascular wall ECs could be attributed to ECFCs (40). EPCs residing in blood vessels possess multiple abilities such as self-renewal, multi-differentiation potential, and robust proliferation (16). The research pointed out the vital role of Sox18/SoxF transcription factor in the differentiation process. The resident $CD157^+$EPCs in vascular wall of large arteries and veins showed regenerative potential of endothelial cells and vasculature (41). Animal studies have proved that EPCs can reduce the formation of neointima after artery injury and restore endothelial function (2). EPCs homing play a central role in vascular remodeling (42). Then neurotrophic factor-3 (NT-3) was proved to be able to accelerate rapid re-endothelialization of damaged carotid arteries by promoting EPCs mobilization and homing (42). It is also regulated by angiogenic chemokines (CXCL1, CXCL7, CXCL12, and CCL2), through their corresponding receptors (CXCR2, CXCR4, and CCR2) (43).

Smooth Muscle Progenitor Cells

One of the characteristics of SMPCs is the heterogeneity of their origin (44). It is believed that the regenerative VSMCs after vascular injury have several different sources (28). The main functions are contracting blood vessels, regulating angiotasis, and blood pressure (45). There are different sources of VSMCs in different segments of the aorta, expressing different molecular markers and having different functions (2).

Studies have found that if blood vessels are injured, VSMCs will migrate to the intima, changing from a higher differentiated contractile phenotype to a secretory one to initiate cell proliferation (46). It is characterized by increased proliferation, migration, ECM synthesis, along with decreased expression of contraction markers (47). The traditional view holds that imbalance of VSMC plasticity leads to maladaptive phenotypic transformation which leads to the progression of VSMC-driving vascular remodeling diseases (48). But now we found that in vascular injury and repair, sometimes only contractile VSMCs are involved in vascular remodeling process without dedifferentiating to a secretory phenotype (4). Other studies have demonstrated that VSMCs can participate in vascular remodeling process without phenotypic transition (4, 49). From the perspective of stem cell research, recent results have confirmed that VSMCs derived from VSCs can drive vascular remodeling and take part in vascular repair upon injury.

In 2004, Hu et al. (7) first confirmed the presence of Sca-1^+, c-Kit^+, $CD34^+$, and $Flk1^+$ progenitors in the aortic root of $Apoe^{-/-}$ mice (36). They found that Sca-1^+ resident adventitial progenitor cells can migrate and differentiate into VSMCs, playing an important role in atherosclerosis. Later, another group also reported that Sca-1^+, $CD34^+$, and $PDGFR\beta^+$ cells residented in the adventitia can differentiate into VSMCs *in vitro*. They also reporterd that the process is mediated by acoustic hedgehog (Shh) signaling pathway (50). Shh signaling is limited to the adventitia of the artery and may play a part in the maintenance of VPCs mainly in adventitia (50). Peripheral vascular cells (VSMC and pericytes) may share a common $FlK1^+$ progenitor cell with ECs. FlK1 is a key regulator of phenotypic transformation in VSMC which inhibits VSMC differentiation and maintains the Sca-1^+ progenitor cell phenotype, facilitating multidirectional differentiation and preventing pathological vascular remodeling (47). Based on lineage tracing study, $Gli1^+$ cells were also proved to be progenitor cells in the adventitia, expressing CD34, Sca-1, and PDGFRβ and contributing to vascular repair and related diseases (51).

Mesenchymal Stem Cells

MSCs are pluripotent stromal cells which have proliferative and immunomodulatory effects (52). MSCs from different tissues share the same triadic differentiation potential, that is, the ability to differentiate into osteoblasts, chondrocytes, and adipocytes. The cells both express typical markers CD13, CD73, and CD90 in intima as well as CD29, CD44, and CD105 in adventitia and intima. However, the differentiation tendency of

TABLE 1 | Distribution and function of vascular wall stem cells in three layers of blood vessels.

Nomenclature	Vessel wall layer	Cell markers	Function	References
EPCs	Intima	$CD31^-$, $Flk1^{lo}$	Differentiate into ECs and participate in angiogenesis	(16)
		$CD45^+$, $CD14^+$, $CD31^+$, $CD146^-$, $CD133^-$, $Tie2^-$	Release VEGF to promote angiogenesis	(17)
	Media and adventitia	$CD146^+$, $CD45^-$, $CD133^-$	Differentiate into ECs	(18, 19)
		$PW1^+$	Promote angiogenesis	(20)
		c-kit^+, $VEGFR2^+$, $CD45^-$	Differentiate into ECs, VSMCs, and cardiomyocytes	(21, 22)
		$CD34^+$, $VEGFR2^+$	Differentiate into ECs, hematopoietic cells, and macrophages	(23)
			Prevent the uncontrolled growth of VSMCs	(24–26)
SMPCs	Adventitia	Sca-1^+, c-kit^+, $CD34^+$, $Flk1^+$	Differentiate into VSMCs	(27, 28)
			Differentiate into VSMCs; neointima formation	(29)
	Media and adventitia	Lin^- Sca-1^+ c-$kit^{-/lo}$ $CD34^{-/lo}$	Differentiate into ECs and VSMCs	(30)
		$PW1^+$	Differentiate into VSMCs; promote pulmonary vascular remodeling	(20)
MSCs	Adventitia	$CD29^+$, $CD44^+$, $CD105^-$	Differentiate into osteoblasts, adipocytes, and VSMCs; promote angiogenesis	(31)
Pericytes	Media and adventitia	$PDGFR\beta^+$	Differentiate into adipocytes, osteoblasts, and chondrocytes;	(32)
		$NG2^+$,	Promote vasculogenesis and angiogenesis	(33, 34)
	Media	$CD34^+$, $CD31^+$, $CD45^+$, $CD68^+$	Differentiate into myeloid cells, osteoblasts, chondrocytes, and adipocytes	(31)

EPC, endothelial progenitor cell; SMPC, smooth muscle progenitor cell; MSC, mesenchymal stem cell.

MSCs from different sources also differ (53). Bone marrow-derived MSCs express SH2, SH3, CD29, CD44, CD71, CD90, CD106, CD120a, CD124, and easily differentiate into osteoblasts. Adipose-derived MSCs express CD34, CD13, CD45, CD14, CD144, CD31, and easily differentiate into adipocytes (14, 54). Studies found that adipose tissue stem cells are easier to isolate and more abundant compared with other types of MSCs, they can sidestep ethical issues so are widely used in stem cell studies (55).

Some research groups (56) have isolated a population of $CD34^+CD31^-$ cells expressing pericyte and mesenchymal antigens showing high proliferation and multiple-directional differentiation ability. It can have bidirectional interaction with ECs and take part in angiogenesis. It has been proved that co-culture with ECs on electrostatic spinning scaffolds can promote the differentiation of MSCs into osteoblasts (57). In the mouse model of hind limb ischemia, the researchers also found that EC-like cells derived from MSCs perform strong angiogenesis ability *in vitro* (58). Bone marrow mesenchymal stem cells (BMMSCs) can differentiate into ECs and VSMCs *in vitro* by means of growth factors modulation (59). MSCs are present in the perivascular niche of many organs, including kidneys, lungs, liver, and heart. The vascular-resident $Gli1^+$ MSCs are the main cellular source of injury-induced organ fibrosis attributed to their colony-forming activity and differentiation capacity into fibroblasts (60). The effects of these cells in vascular repair depend on their metabolic reprogramming and SMC differentiation ability *via* mir-378a-3p/TGF-β1 signaling pathway (61).

Pericytes

Pericytes are high density parietal cells located in terminal arterioles and capillaries (62, 63). Pericytes are characterized by direct contact with the underlying ECs. It can regulate capillary permeability, endothelial stability, and micro-vasoconstriction (64). In fact, there are still no specific molecular markers for pericytes. The pericyte markers currently known, such as NG2, CD146, PDGFR-B in media and adventitia, are also expressed in SMPCs and MSCs (64).

In 1992, pericyte was first reported for its osteogenic potential, it has been shown that pericytes reside in capillary and microvessels may be osteoblast progenitors (65, 66). Pericytes and MSCs derived from various human tissues are similar in their function of maintenance vascular homeostasis. Pericytes can help maintain tissue homeostasis by promoting local MSC proliferation and differentiation through the paracrine capability (67). In a systematic investigation, the researchers found the angiogenesis and multilineage differentiation potential of pericytes and MSCs from different human tissues *in vitro*, and enriched $CD34^-CD146^+$ pericytes in adipocytes and bone marrow by magnetic activated cell sorting (15). Only bone marrow-derived cells showed triadic differentiation potential, while adipocyte-derived cells exhibited poor chondrogenic differentiation under TGF-β1 stimulation. These results indicate that the regenerative potential of pericytes as stem cells depends on their tissue origins (15). Recent lineage tracing experiments using the induced Tbx18-CreERT2 cell line showed that pericytes maintained the identity under various pathological conditions such as vascular senescence and will not differentiate into other

cells. This discovery challenged the view of pericytes as stem cells (68).

VASCULAR WALL STEM/PROGENITOR CELLS IN VASCULAR DISEASES

As mentioned above, large amount of vascular stem/progenitor cells participate in the regeneration of damaged ECs and VSMCs during vascular repair upon injury. Numerous studies have confirmed the importance of VPCs in vascular remodeling diseases. Below, the roles of vascular stem/progenitor cells in atherosclerosis, restenosis, hypertension, and aneurysm/dissection, as well as their potential application in regenerative medicine will be reviewed (**Table 2**).

VPCs in Atherosclerosis

Atherosclerosis is characterized by endothelial damage, VSMC proliferation, and collagen deposition, as well as local thickening of the arterial wall caused by lipid deposition (78). Blood flow in vulnerable areas such as arterial branches has a high oscillation index and a low shear stress (79). This fluid mechanical force can directly act on ECs changing cell morphology, cytoskeleton and intercellular conjunctions, and increasing oxidative stress (80). Low density lipoprotein causes cholesterol storage when attached to the intima of the artery (81). Monocytes enter the intima from the blood, adhere to ECs and turn into macrophage. After phagocytic and ingestion of cholesterol, they form "foam cells" resulting in necrotic nuclei of atherosclerotic plaques with VSMCs (82). Fibrous cap inflammation can determine plaque stability (81). The death of VSMCs, degradation of collagen, and ECM lead to thinning of the vascular cap, resulting in increased plaque rupture with serious consequences. In fact, lumen stenosis often results from repeated ruptures and repair of complex plaques (83).

EPCs in Atherosclerosis

Decrease in EPCs predicts an increased risk of atherosclerosis. Fluid mechanical forces in arterial branches can directly affect ECs, change cell morphology and increase oxidative stress, inducing renewal of ECs (80). Shear stress is the basic driving factor of EPCs which can promote circulating EPCs homing to the injury site, inducing the anti-atherosclerotic phenotype of EPCs and promoting the differentiation process into mature ECs (84). These effects are mediated by VEGFR2, Tie2, Notch and β 1/3 integrin signaling. In 2020, a new population of EPCs have been identified in vascular walls by single-cell sequencing and lineage tracing techniques (69). The cells can differentiate into luminal and microvascular ECs and participate in endothelial homeostasis in graft sclerosis, with AKT/mTOR dependent glycolysis playing a key role in this process. SDF-1 can mobilize EPCs from bone marrow to the periphery, promote EPC regeneration and prevente cell death under pathological conditions (85). This pathway as mentioned in **Figure 2** can provide a potential target for improving the efficacy of progenitor cells in the treatment of vascular diseases (85).

SMPCs in Atherosclerosis

In recent years, the roles of SMPCs in cardiovascular diseases have been confirmed in several studies (2, 5). The adventitia progenitor cells expressing Sca-1 markers have been studied in a widespread way. In addition to regulating vascular homeostasis and pathological remodeling, these progenitor cells are also closely related to acute vascular injury in atherosclerosis (86). Initially, the Sca-1^+ and c-kit^+ adventitia progenitor cells were found to be capable of differentiating into VSMCs and participate in the formation of venous graft injury. Through the β-Gal-labeled Sca-1^+ progenitor cells to the adventitia side of vein grafts in *Apoe*$^{-/-}$ mice, the researchers found β-galactose expression in 20% of atherosclerotic lesions (7). Later in 2018, a study implanted GFP-Sca-1^+ progenitor cells into the adventitia of mice after ligation surgery and found that it could significantly reduce plaque bleeding (87). DKK3 can induce Sca-1^+ progenitor cells to differentiate into VSMCs by activating the Wnt signaling pathway, and maintain plaque stability (87). It can also induce the differentiation of Sca-1^+ progenitor cells and fibroblasts into VSMC by activating TGF-β/ATF6 and Wnt signaling pathways (87) (**Figure 2**).

MSCs in Atherosclerosis

During atherosclerosis in *Apoe* intima; these are MSC-like cells expressing Gli1 marker (51). Through acute femoral artery injury repair model, a study confirmed that Gli1$^+$MSC-like cells in the adventitia can differentiate into VSMCs. The team also found that Gli1$^+$cells can migrate to the media and intima plaques and when calcification occurs in atherosclerosis, Gli1$^+$ cells differentiate into osteoblasts (51). In addition, laminar shear stress can activate the Wnt signaling pathway of MSCs, promote β-catenin nuclear transport and activate paracrine factors under laminar shear stress (88).

Many experimental models confirmed the protective effects of MSC therapy on atherosclerosis. The production of Tsg-6, IL-10, NF-κB, and MMP from MSC can inhibit atherosclerotic plaque formation, modulate plaque cellular components and repair endothelial injury, all of which can effectively promote plaque stability (89, 90).

The functions of VPCs in vascular remodeling makes them of great significance in clinical treatment. As EPCs can induce re-endothelialization and angiogenesis of damaged arteries and have a role in regeneration of biological joint structures, they may be a promising clinical therapeutic target (79). Studies have shown a correlation between EPCs dysfunction and reduced angiogenesis in patients with coronary artery disease. As mentioned above, the c-kit^+ stem/progenitor cells can differentiate into vascular cells to promote post-injury repair. But a recent study shows that most of c-kit^+ cells differentiate into macrophages and granulocytes to reduce vascular immune inflammatory response to endothelial injury (70). This feature provides a theoretical basis for clinical improvement of vascular disease treatment. *In vitro*, high lipid levels induce MSC migration to intima, initiating the occurrence of atherosclerosis (91). Now MSC transplantation can also be a treatment direction for atherosclerosis (92).

TABLE 2 | Markers and signaling pathways of vascular wall stem cells and related diseases.

Marker	Differentiation	Animal models	Signaling pathway	Related diseases	Reference
c-Kit^{+} CD34^{+}	ECs	Aortic root of C-Kit-CreER^{T2}; Rosa26-tdTomato mice	AKT/mTOR; Smad2/3	Atherosclerosis; aortic aneurysm	(7, 69, 70)
VEGFR2^{+}	ECs	Hind limb ischemia athymic nude mice	GPR4-STAT3/VEGFA	Atherosclerosis; restenosis	(71)
Sca-1^{+}	ECs, VSMCs	DKK3$^{+/+}$and DKK3$^{-/-}$; *Apoe* $^{-/-}$ model; Lepr$^{+/+}$ and Lepr$^{-/-}$ mice	TGF-β/ATF6 and Wnt; OBR-STAT3-MAPK-Rac1/Cdc42-ERK-FAK; Hedgehog	Atherosclerosis; restenosis; hypertension; aortic aneurysm	(7, 50, 72)
CD34^{+}, αSMA^{+}	ECs, VSMCs	Patients with coronary stenting	Hedgehog; Wnt; Notch	Restenosis	(50, 73)
Pw1^{+}	VSMCs	Pw1$^{nLacZ/+}$ mouse	CXCR4; FoxM1	Hypertension	(20, 74)
KLF4	MSCs-like	TGFβR2$^{iSMC-Apoe}$ Mice	TGF-βR2-Smad2/3	Atherosclerosis; aortic aneurysm	(42, 75)
Gli1^{+}	MSCs-like	Gli1-CreER^{T2}; Ai9 mice	Indian Hedgehog; Smo-Gli12/3; TGFβR2/Smad2/3	Atherosclerosis; hypertension	(51, 60)
EGFP^{+}, CD34^{+}CD31^{-}	SVPs	Human vein	Wnt/β-catenin; Tie-2/PDGF BB; N-cadherin	Aortic aneurysm	(56, 58, 76)
CD34^{-}, CD146^{+}	PC,MSC-like	Adipocytes and bone marrow	TGF-β1	Atherosclerosis	(56)
NG2^{+}	PC,VSMC	Ng2-Cre mice	Ang/Tie2-Calpain/Akt/FOXO3A	Atherosclerosis; aortic aneurysm	(64, 77)

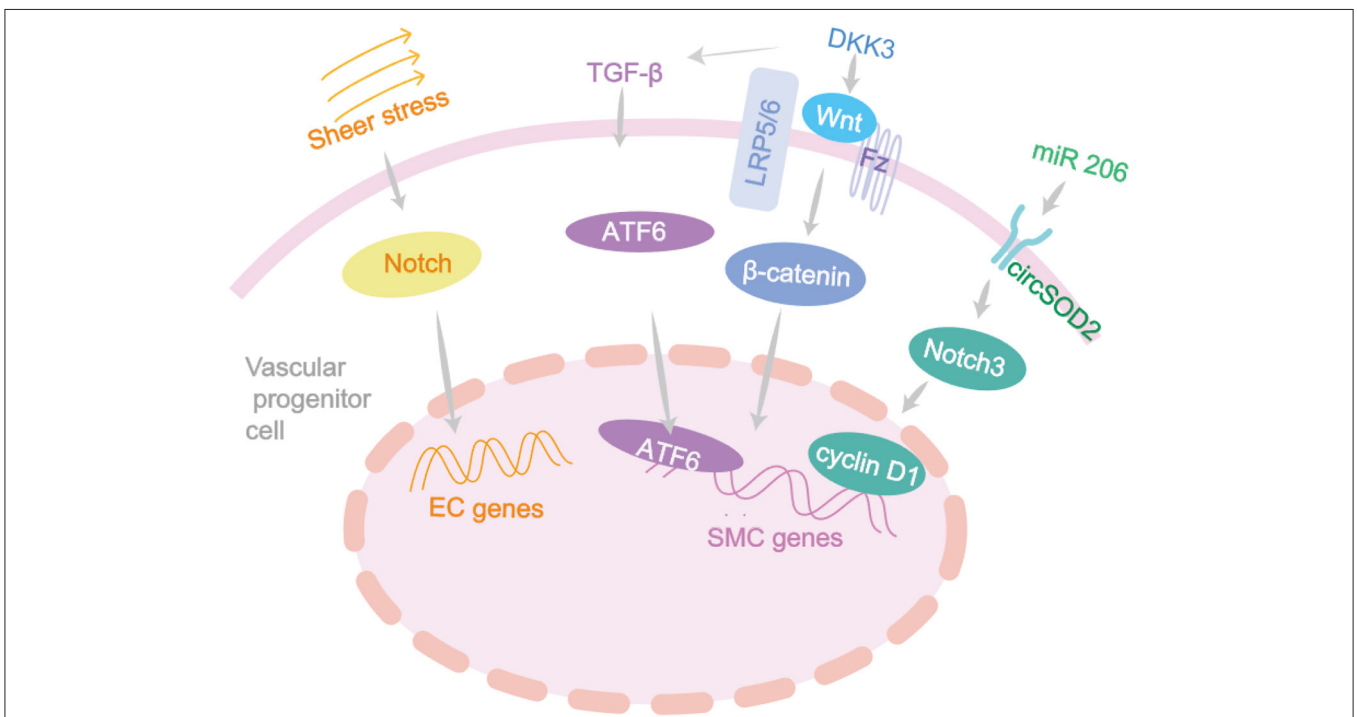

FIGURE 2 | The differentiation signaling pathway of vascular progenitor cells. Vascular development and remodeling depend on many genes and are usually initiated by fluid shear stress which acts on the Notch signaling and closely associated with the vascular remodeling diseases. DKK3 induces ECs migration through Wnt-PCP signaling pathway, accelerating re-endothelialization, and reducing neointima formation. DKK3 can induce the differentiation of Sca-1+ progenitor cells and fibroblasts into VSMC by activating TGF-β/ATF6 signaling pathways.

VPCs in Restenosis

Percutaneous coronary intervention is an effective treatment for patients with ischemic heart disease. Restenosis is the main complication of percutaneous coronary intervention (93).The main mechanisms are vascular endothelial dissection and subintimal hemorrhage caused by vascular injury after stent implantation (94, 95). Endothelial injury and other irritation can lead to a wound-healing response, while subintimal bleeding can lead to thrombosis and inflammatory cell infiltration (96). Inflammatory factors IL-1, TNF-α, and IL-6 can stimulate the proliferation of VSMCs to form neointima, lead to excessive healing of vascular wall and cause restenosis (97). Neointima is part of the injury repair response, and its formation involves inflammatory cell infiltration, matrix degradation, thrombosis, the proliferation of VSMC, and collagen secretion (98). And the proliferation of VSMCs is the main factor leading to neointima formation and restenosis (99).

The increased secretion of CCL2 and CXCL1 by VSMCs can promote Sca-1^+ progenitor cell migrate from adventitia to neointima in the injured area. Through the guide wire injury test of mouse femoral artery, the GTPase Rac1/P38 signaling pathway was found to play a key role in this process (100). A study about leptin receptor (OBR) in Sca-1^+ progenitor cells has found that the OBR-STAT3-MAPK and Rho-GTPase pathways are activated in response to leptin stimulation, inducing progenitor cell migration (72).

The regulatory role of mir-22 in the differentiation of SMPCs has been found, providing a new target for disease treatment of neointimal formation and restenosis (99). A recent study reported that $EGFP^+$ MSC in mice expressed endothelial markers and showed the ability of tube formation (58). Meanwhile, these mice showed stronger ability for blood perfusion recovery, vascular density, and improved function of ischemic limbs, providing evidence for its role in angiogenesis. These results suggest that the induction of BMMSCs may be a promising option for the treatment of ischemic diseases (58). Vascular remodeling is known to delay the progression of blood flow restriction during stenosis. However, when restenosis occurs, intimal hyperplasia can lead to lumen narrowing, with adverse effects on the body (101). After bare-metal stent implantation in mice, circulating $CD34^+$ cells have a significant increase, which also applies to patients with in-stent restenosis (73). The $CD34^+$ cells differentiated into $CD31^+$ cells and αSMA^+ cells after scaffold implantation, which may contribute to the formation of stenosis. Recently, a study found that the elimination of non-bone marrow $CD34^+$ cells could reduce the vascular lumen area and increase intima thickness (23). The non-bone marrow $CD34^+$ cells could differentiate into ECs after femoral artery injury, maintaining vascular integrity, and preventing the formation of neointima. A regulator CircSOD2, may become a new clinical drug target for inhibiting the development of hyperplastic vascular diseases such as restenosis, because its knockdown can attenuate injury-induced neointima formation and reduce VSMCs proliferation (102). The role of VPCs in vascular remodeling is crucial for improving tissue-engineered vascular grafts and designing drug-targeted therapies for angiogenesis. Dkk3 increases Sca-1^+ progenitor cell migration and contributes to VSMCs regeneration through CXCR7 activation (103). The DKK3-CXCR7 axis can mediate Sca-1^+ cell migration and *in vivo* regeneration of transplanted cells, which is of great significance in the study of artificial vascular therapy for restenosis. ETV2-mediated differentiation of exogenous Sca-1^+ cells into ECs to improve vascular remodeling and reduce neointima after injury (104). Therefore, inducing the differentiation of Sca-1^+ cells into endothelial lineages might be a therapeutic strategy for vascular diseases as summarized in **Figure 3**.

VPCs in Hypertension

Essential hypertension is defined as an unexplained increase in blood pressure that increases the risk of cardiac, brain, or kidney events. Essential hypertension is often associated with hypercholesterolemia, obesity, and diabetes. These risk factors are also present in cardiovascular disease and hypertension can worsen the symptoms (105).The pathogenesis of hypertension includes endothelial dysfunction, sympathetic nervous system activation, inflammation, oxidative stress, etc. Aldosterone can promote the polarization of macrophages to the pro-inflammatory M1 phenotype, leading to vascular dysfunction and aggravating hypertension (106). In hypertension, collagen deposition is the main factor resulting in vascular fibrosis (107). VPCs participate in the occurrence and development of hypertension and vascular fibrosis is related to a variety of signaling pathways.

In the aorta of hypertensive mice induced by Ang II, the number of Sca-1 + progenitor cells increased and the EGFP-Sca-1^+ progenitor cells co-located with the deposition areas of collagen I, III, and V in the adventitia, suggesting that Sca-1^+ progenitor cells may be the source of hypertensive vascular fibrosis (76). Lineage tracing technique displayed Adv-Sca-1 cells can differentiate into fibroblasts in the case of vascular injury, leading to vascular remodeling and sclerosis, while KLF4 may maintain the phenotype and prevent pathological vascular remodeling (13). SMPCs express PW1 in the adventitia and participate in pulmonary hypertension-related vascular remodeling (20). The number of $PW1^+$ progenitor cells increased significantly in the mouse pulmonary hypertension model under hypoxia and were able to differentiate into VSMCs through the CXCR4 pathway (20). Dysfunctional ECs can induce FoxM1 expression in VSMCs and activate FoxM1-dependent VSMC proliferation, confirming ECs and VSMCs interaction through FoxM1 signaling in vascular remodeling and promoting hypertension and fibrosis (74). Recently, a study induced perivascular fibrosis through Ang II, and found that vascular remodeling during the process was not dependent on blood pressure regulation but through ADAM17 activating PDGFR then acting on ECs (108). ADAM17 may be a new clinical target for preventing hypertension complications (109).

VPCs in Aortic Aneurysm and Dissection

Aortic aneurysm refers to local dilation of the aortic lumen ≥50% of its original diameter and structural degeneration of

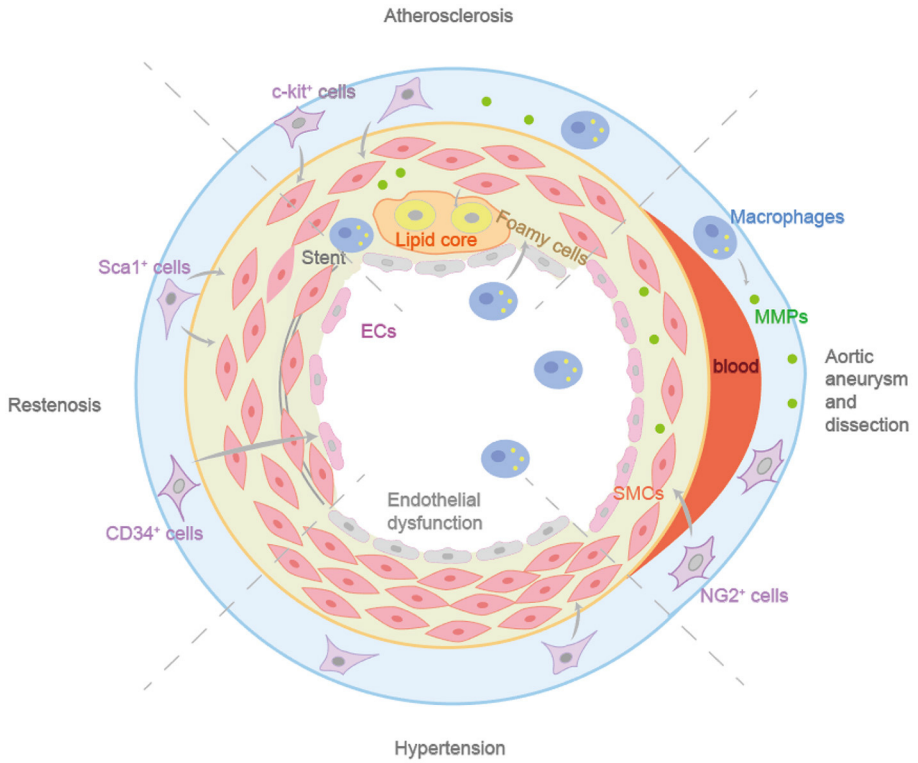

FIGURE 3 | The different roles in vascular remodeling diseases of vascular progenitor cells. c-Kit$^+$ cells can differentiate into ECs and participate in endothelial homeostasis. Sca-1$^+$ progenitor cells in adventitia can enhance the formation of neointima. Non-bone marrow CD34$^+$ cells could differentiate into ECs after femoral artery injury, maintaining vascular integrity and preventing the formation of neointima. Resident NG2$^+$ progenitor cells can differentiate into VSMCs after aortic injury during aortic aneurysm and dissection.

different segments of the aorta. Endothelial injury, VSMCs loss and ECM degradation lead to abnormal remodeling of the aortic wall resulting in aortic aneurysm and separation of layers of the aortic wall (aortic dissection) (110, 111). The composition and integrity of ECM are key determinants of the physical properties of the aortic wall (112). ECM undergoes continuous physiological remodeling and the original proteins degraded and replaced by the newly synthesized proteins. MMP plays an important role in this process. Therefore, MMPs are closely related to the pathogenesis of aortic aneurysm (113). Aortic aneurysms can progress gradually, leading to tears in the intima of the aorta or bleeding in the wall of the aorta, further leading to the formation of aortic dissection, which can be life threatening.

Aortic aneurysm formed in two main sites, thoracic aorta and abdominal aorta (114). Abdominal aortic aneurysm (AAA) is most associated with atherosclerosis, they share many common risk factors. Thoracic aortic aneurysms (TAA), located in the aortic root and ascending aorta, are more related with genetic syndromes such as Marfan syndrome (115). AAAs are marked by media and elastic fiber degradation, leading to aortic dissection (116). The pathogenesis of AAA includes VSMCs apoptosis, MMPs degradation of elastin, collagen and glycosaminoglycan, inflammatory reactions and the role of reactive oxygen species (117). Among them, apoptosis of VSMCs and degeneration of aortic media are the hallmark pathological changes of AAA. Studies have found that Il-18 receptor defect, chemokine netrin-1 deficiency, and activated transcription factor EB can reduce apoptosis of VSMCs, decrease the activity of MMP-2/9 and elastin degradation, inhibiting the occurrence and progression of AAA (118). The pathogenesis of TAA includes changes of ECM, apoptosis of VSMCs, MMPs and reactive oxygen species. Mutations of *TGFBR1*, *TGFBR2*, *SMAD3*, *TGFB2*, *COL3A1*, *FBN1*, and other genes can cause the occurrence of TAAs (119). For example, firillin-1 is the major subunit of microfibers that constitute the ECM of the thoracic aortic wall. Changes in Firillin-1 result in reduced adhesion between elastic fibers and VSMCs, thereby damaging the biomechanical integrity of the aortic wall and ultimately leading to Marfan syndrome (120). Fibrllin-1 is highly homologous to potential TGFβ binding proteins, and TGFβ gene defects are found not only in Marfan syndrome but also in Patients with Loeys-Dietz aortic aneurysm syndrome (121). A recent discovery found MFAP4 glycosylation was enhanced in MFS patients, and its expression was further enhanced in the advanced aneurysm stage (122). They also induced pluripotent stem cells to differentiate into VSMC in MFS patients and found that there was no elastin expression and the expression level of MFAP4 was unchanged.

VSMC reprogramming to a MSC-like state may play a key role in the progression of AAAs (123). During the pathogenesis of AAA, the TGF-β signaling pathway of VSMCs was inhibited. The decreased expression of TGF-βR2 could lead to reduced binding of Smad2/3 to transcription factor KLF4, leading the transformation of contractile VSMCs into MSCs-like cells. MSCs possess high plasticity and potential to differentiate into several different cell types, such as osteoblasts, chondrocytes, adipocytes, and macrophages. This characteristic has implications for aortic dilation, aortic dilation, calcification of the aortic wall, and inflammation, thereby promoting the development of aneurysms (123). Another research found *Smad3* gene mutations in the second cardiogenic SMPCs and neural crest SMPCs prevented their differentiation into VSMCs and reduced the level of proelastase. This suggests that CPC-SMPCs and NCSC-SMPCs can differentiate into VSMCs through the SMAD3-dependent TGF-β signaling pathway (124). ECs differentiation was reduced in patients with AAAs compared with healthy human MSCs, confirming that the aging MSCs impaired its original vascular repair ability, initiating the occurrence and progress of AAAs (125). Some studies have confirmed that MSCs from calcified and inflammatory aorta have high osteogenic potential and pathological angiogenesis ability under appropriate stimulation (126). Runx2 can enhance the proliferation of MSCs and induce them differentiate into osteoblast lineage cells by regulating Shh, Fgfr2/3, Wnt, and Pthlh signaling pathways (55). Runx2-mediated micro-calcification is a new pathological feature of AAA. It may be a promising strategy for clinical improvement of disease treatment regimens (127). Resident $NG2^+$ progenitor cells can differentiate into VSMCs after aortic injury during aortic aneurysm and dissection, producing growth factors that promote endothelial survival and vascular repair (77) (**Figure 3**).

CONCLUSION AND PERSPECTIVE

In this review, we provide the latest research progresses on VSCs in vascular repair upon injury. VSCs exist in the three-layers of vascular wall and play important roles in the occurrence and progression of vascular remodeling diseases such as atherosclerosis, restenosis, hypertension, aortic aneurysm, and dissection. After vascular injury, VSCs can migrate and differentiate into ECs or VSMCs, resulting in the occurrence or aggravation of vascular remodeling-related diseases. Current studies have shown that VSCs can express stem cell markers such as Sca-1 and CD34, but these markers are not specific and their roles in various diseases need to be distinguished from BMSCs or adipose stem cells. The functions of stem cells and their mechanisms in cardiovascular diseases mentioned in the text have not yet been sufficient studied, which is also the direction of further researches. Most groups are now focused on single cell sequencing and cell lineage tracing and other advanced technology to trace the source of all kinds of cells in vascular remodeling associated diseases, in order to better understand the specific role of distinct population of various vascular stem/progenitor cells in vascular remodeling which offers new potential therapeutic targets.

AUTHOR CONTRIBUTIONS

BY and AQ conceived and supervised this study. JT, XC, BY, and AQ wrote and revised the manuscript. JT and XC draw the figures and tables. All authors contributed to the article and approved the submitted version.

FUNDING

This study was supported by the Key Science and Technology Project of Beijing Municipal Institutions (KZ201910025027 and KZ202010025032); the National Natural Science Foundation of China (81870186 and 82070474); the Importation and Development of High-Caliber Talents Project of Beijing Municipal Institutions (CIT&TCD201904090; CIT&TCD20190332).

ACKNOWLEDGMENTS

We thank Dr. Qingbo Xu (Department of Cardiology, The First Affiliated Hospital of Zhejiang University School of Medicine, Hangzhou, China) and Frank J. Gonzalez (Laboratory of Metabolism, Center for Cancer Research, National Cancer Institute, National Institutes of Health, Bethesda, Maryland, USA) for the critical reading of this manuscript.

REFERENCES

1. Martínez-González J, Cañes L, Alonso J, Ballester-Servera C, Rodríguez-Sinovas A, Corrales I, et al. NR4A3: a key nuclear receptor in vascular biology, cardiovascular remodeling, and beyond. *Int J Mol Sci.* (2021) 22:11371. doi: 10.3390/ijms222111371
2. Zhang L, Issa Bhaloo S, Chen T, Zhou B, Xu Q. Role of resident stem cells in vessel formation and arteriosclerosis. *Circ Res.* (2018) 122:1608–24. doi: 10.1161/CIRCRESAHA.118.313058
3. Wang D, Li LK, Dai T, Wang A, Li S. Adult stem cells in vascular remodeling. *Theranostics.* (2018) 8:815–29. doi: 10.7150/thno.19577
4. Bkaily G, Abou Abdallah N, Simon Y, Jazzar A, Jacques D. Vascular smooth muscle remodeling in health and disease. *Can J Physiol Pharmacol.* (2021) 99:171–8. doi: 10.1139/cjpp-2020-0399
5. Owens GK, Kumar MS, Wamhoff BR. Molecular regulation of vascular smooth muscle cell differentiation in development and disease. *Physiol Rev.* (2004) 84:767–801. doi: 10.1152/physrev.00041.2003
6. Zhang Q, Chen T, Zhang Y, Lyu L, Zhang B, Huang C, et al. MiR-30c-5p regulates adventitial progenitor cells differentiation to vascular smooth muscle cells through targeting OPG. *Stem Cell Res Ther.* (2021) 12:67. doi: 10.1186/s13287-020-02127-2
7. Hu Y, Zhang Z, Torsney E, Afzal AR, Davison F, Metzler B, et al. Abundant progenitor cells in the adventitia contribute to atherosclerosis of vein grafts in ApoE-deficient mice. *J Clin Invest.* (2004) 113:1258–65. doi: 10.1172/JCI19628
8. Wang H, Zhao H, Zhu H, Li Y, Tang J, Li Y, et al. Sca-1(+) cells minimally contribute to smooth muscle cells in atherosclerosis. *Circ Res.* (2021) 128:133–5. doi: 10.1161/CIRCRESAHA.120.317972

9. Liu M, Gomez D. Smooth muscle cell phenotypic diversity. *Arterioscler Thromb Vasc Biol.* (2019) 39:1715–23. doi: 10.1161/ATVBAHA.119.312131
10. Wang X, Wang R, Jiang L, Xu Q, Guo X. Endothelial repair by stem and progenitor cells. *J Mol Cell Cardiol.* (2021) 163:133–46. doi: 10.1016/j.yjmcc.2021.10.009
11. Wu H, Zhou X, Gong H, Ni Z, Xu Q. Perivascular tissue stem cells are crucial players in vascular disease. *Free Radic Biol Med.* (2021) 165:324–33. doi: 10.1016/j.freeradbiomed.2021.02.005
12. Bianconi V, Sahebkar A, Kovanen P, Bagaglia F, Ricciuti B, Calabro P, et al. Endothelial and cardiac progenitor cells for cardiovascular repair: a controversial paradigm in cell therapy. *Pharmacol Ther.* (2018) 181:156–68. doi: 10.1016/j.pharmthera.2017.08.004
13. Majesky MW, Horita H, Ostriker A, Lu S, Regan JN, Bagchi A, et al. Differentiated smooth muscle cells generate a subpopulation of resident vascular progenitor cells in the adventitia regulated by Klf4. *Circ Res.* (2017) 120:296–311. doi: 10.1161/CIRCRESAHA.116.309322
14. Al-Nbaheen M, Vishnubalaji R, Ali D, Bouslimi A, Al-Jassir F, Megges M, et al. Human stromal (mesenchymal) stem cells from bone marrow, adipose tissue and skin exhibit differences in molecular phenotype and differentiation potential. *Stem Cell Rev Rep.* (2013) 9:32–43. doi: 10.1007/s12015-012-9365-8
15. Herrmann M, Bara JJ, Sprecher CM, Menzel U, Jalowiec JM, Osinga R, et al. Pericyte plasticity - comparative investigation of the angiogenic and multilineage potential of pericytes from different human tissues. *Eur Cell Mater.* (2016) 31:236–49. doi: 10.22203/eCM.v031a16
16. Patel J, Seppanen EJ, Rodero MP, Wong HY, Donovan P, Neufeld Z, et al. Functional definition of progenitors versus mature endothelial cells reveals key SoxF-dependent differentiation process. *Circulation.* (2017) 135:786–805. doi: 10.1161/CIRCULATIONAHA.116.024754
17. Li X, Chen C, Wei L, Li Q, Niu X, Xu Y, et al. Exosomes derived from endothelial progenitor cells attenuate vascular repair and accelerate reendothelialization by enhancing endothelial function. *Cytotherapy.* (2016) 18:253–62. doi: 10.1016/j.jcyt.2015.11.009
18. Mund JA, Estes ML, Yoder MC, Ingram DA, Case J. Flow cytometric identification and functional characterization of immature and mature circulating endothelial cells. *Arterioscler Thromb Vasc Biol.* (2012) 32:1045–53. doi: 10.1161/ATVBAHA.111.244210
19. Hassanpour M, Rezaie J, Darabi M, Hiradfar A, Rahbarghazi R, Nouri M. Autophagy modulation altered differentiation capacity of CD146(+) cells toward endothelial cells, pericytes, and cardiomyocytes. *Stem Cell Res Ther.* (2020) 11:139. doi: 10.1186/s13287-020-01656-0
20. Dierick F, Héry T, Hoareau-Coudert B, Mougenot N, Monceau V, Claude C, et al. Resident PW1+ progenitor cells participate in vascular remodeling during pulmonary arterial hypertension. *Circ Res.* (2016) 118:822–33. doi: 10.1161/CIRCRESAHA.115.307035
21. Bearzi C, Leri A, Lo Monaco F, Rota M, Gonzalez A, Hosoda T, et al. Identification of a coronary vascular progenitor cell in the human heart. *Proc Natl Acad Sci U S A.* (2009) 106:15885–90. doi: 10.1073/pnas.0907622106
22. Fang S, Wei J, Pentinmikko N, Leinonen H, Salven P. Generation of functional blood vessels from a single c-kit+ adult vascular endothelial stem cell. *PLoS Biol.* (2012) 10:e1001407. doi: 10.1371/journal.pbio.1001407
23. Jiang L, Chen T, Sun S, Wang R, Deng J, Lyu L, et al. Nonbone marrow CD34(+) cells are crucial for endothelial repair of injured artery. *Circ Res.* (2021) 129:e146–e65. doi: 10.1161/CIRCRESAHA.121.319494
24. Skrzypkowska MW, Gutknecht PG, Ryba-Stanisławowska ME, Słomiński B, Siebert J, Myśliwska JM. CD34+ and CD34+VEGFR2+ cells in poorly controlled hypertensive patients. *J Hum Hypertens.* (2019) 33:863–72. doi: 10.1038/s41371-018-0145-z
25. Wu W, Zhang J, Shao L, Huang H, Meng Q, Shen Z, et al. Evaluation of circulating endothelial progenitor cells in abdominal aortic aneurysms after endovascular aneurysm repair. *Int J Stem Cells.* (2021). doi: 10.15283/ijsc21027. [Epub ahead of print].
26. Shen Y, Wu Y, Zheng Y, Ao F, Kang K, Wan Y, et al. Responses of adventitial CD34(+) vascular wall-resident stem/progenitor cells and medial smooth muscle cells to carotid injury in rats. *Exp Mol Pathol.* (2016) 101:332–40. doi: 10.1016/j.yexmp.2016.11.004
27. Lin R-Z, Moreno-Luna R, Li D, Jaminet S-C, Greene AK, Melero-Martin JM. Human endothelial colony-forming cells serve as trophic mediators for mesenchymal stem cell engraftment via paracrine signaling. *Proc Natl Acad Sci U S A.* (2014) 111:10137–42. doi: 10.1073/pnas.1405388111
28. Tang J, Wang H, Huang X, Li F, Zhu H, Li Y, et al. Arterial Sca-1(+) vascular stem cells generate *de novo* smooth muscle for artery repair and regeneration. *Cell Stem Cell.* (2020) 26:81–96.e4. doi: 10.1016/j.stem.2019.11.010
29. Ni Z, Deng J, Potter CMF, Nowak WN, Gu W, Zhang Z, et al. Recipient c-Kit lineage cells repopulate smooth muscle cells of transplant arteriosclerosis in mouse models. *Circ Res.* (2019) 125:223–41. doi: 10.1161/CIRCRESAHA.119.314855
30. Sainz J, Al Haj Zen A, Caligiuri G, Demerens C, Urbain D, Lemitre M, et al. Isolation of "side population" progenitor cells from healthy arteries of adult mice. *Arterioscler Thromb Vasc Biol.* (2006) 26:281–6. doi: 10.1161/01.ATV.0000197793.83391.91
31. Zorzi P, Aplin AC, Smith KD, Nicosia RF. Technical advance: the rat aorta contains resident mononuclear phagocytes with proliferative capacity and proangiogenic properties. *J Leukoc Biol.* (2010) 88:1051–9. doi: 10.1189/jlb.0310178
32. Guimarães-Camboa N, Evans SM. Are perivascular adipocyte progenitors mural cells or adventitial fibroblasts? *Cell Stem Cell.* (2017) 20:587–9. doi: 10.1016/j.stem.2017.04.010
33. Teichert M, Milde L, Holm A, Stanicek L, Gengenbacher N, Savant S, et al. Pericyte-expressed Tie2 controls angiogenesis and vessel maturation. *Nat Commun.* (2017) 8:16106. doi: 10.1038/ncomms16106
34. Hesp ZC, Yoseph RY, Suzuki R, Jukkola P, Wilson C, Nishiyama A, et al. Proliferating NG2-cell-dependent angiogenesis and scar formation alter axon growth and functional recovery after spinal cord injury in mice. *J Neurosci.* (2018) 38:1366–82. doi: 10.1523/JNEUROSCI.3953-16.2017
35. Asahara T, Murohara T, Sullivan A, Silver M, van der Zee R, Li T, et al. Isolation of putative progenitor endothelial cells for angiogenesis. *Science.* (1997) 275:964–7. doi: 10.1126/science.275.5302.964
36. Psaltis PJ, Simari RD. Vascular wall progenitor cells in health and disease. *Circ Res.* (2015) 116:1392–412. doi: 10.1161/CIRCRESAHA.116.305368
37. Luo S, Xia W, Chen C, Robinson EA, Tao J. Endothelial progenitor cells and hypertension: current concepts and future implications. *Clin Sci (Lond).* (2016) 130:2029–42. doi: 10.1042/CS20160587
38. Medina RJ, Barber CL, Sabatier F, Dignat-George F, Melero-Martin JM, Khosrotehrani K, et al. Endothelial progenitors: a consensus statement on nomenclature. *Stem Cells Transl Med.* (2017) 6:1316–20. doi: 10.1002/sctm.16-0360
39. Keighron C, Lyons CJ, Creane M, O'Brien T, Liew A. Recent advances in endothelial progenitor cells toward their use in clinical translation. *Front Med (Lausanne).* (2018) 5:354. doi: 10.3389/fmed.2018.00354
40. Ingram DA, Mead LE, Moore DB, Woodard W, Fenoglio A, Yoder MC. Vessel wall-derived endothelial cells rapidly proliferate because they contain a complete hierarchy of endothelial progenitor cells. *Blood.* (2005) 105:2783–6. doi: 10.1182/blood-2004-08-3057
41. Wakabayashi T, Naito H, Suehiro JI, Lin Y, Kawaji H, Iba T, et al. CD157 marks tissue-resident endothelial stem cells with homeostatic and regenerative properties. *Cell Stem Cell.* (2018) 22:384–97.e6. doi: 10.1016/j.stem.2018.01.010
42. Chen Y, Cao J, Peng W, Chen W. Neurotrophin-3 accelerates reendothelialization through inducing EPC mobilization and homing. *Open Life Sci.* (2020) 15:241–50. doi: 10.1515/biol-2020-0028
43. Yang JX, Pan YY, Wang XX, Qiu YG, Mao W. Endothelial progenitor cells in age-related vascular remodeling. *Cell Transplant.* (2018) 27:786–95. doi: 10.1177/0963689718779345
44. Alencar GF, Owsiany KM, Karnewar S, Sukhavasi K, Mocci G, Nguyen AT, et al. Stem cell pluripotency genes Klf4 and Oct4 regulate complex SMC phenotypic changes critical in late-stage atherosclerotic lesion pathogenesis. *Circulation.* (2020) 142:2045–59. doi: 10.1161/CIRCULATIONAHA.120.046672
45. Owens GK. Regulation of differentiation of vascular smooth muscle cells. *Physiol Rev.* (1995) 75:487–517. doi: 10.1152/physrev.1995.75.3.487
46. Iyemere VP, Proudfoot D, Weissberg PL, Shanahan CM. Vascular smooth muscle cell phenotypic plasticity and the regulation of vascular calcification. *J Intern Med.* (2006) 260:192–210. doi: 10.1111/j.1365-2796.2006.01692.x

47. Frismantiene A, Philippova M, Erne P, Resink TJ. Smooth muscle cell-driven vascular diseases and molecular mechanisms of VSMC plasticity. *Cell Signal.* (2018) 52:48–64. doi: 10.1016/j.cellsig.2018.08.019
48. Wang G, Jacquet L, Karamariti E, Xu Q. Origin and differentiation of vascular smooth muscle cells. *J Physiol.* (2015) 593:3013–30. doi: 10.1113/JP270033
49. Burggren WW. Phenotypic switching resulting from developmental plasticity: fixed or reversible? *Front Physiol.* (2019) 10:1634. doi: 10.3389/fphys.2019.01634
50. Passman JN, Dong XR, Wu SP, Maguire CT, Hogan KA, Bautch VL, et al. A sonic hedgehog signaling domain in the arterial adventitia supports resident Sca-1+ smooth muscle progenitor cells. *Proc Natl Acad Sci U S A.* (2008) 105:9349–54. doi: 10.1073/pnas.0711382105
51. Kramann R, Goettsch C, Wongboonsin J, Iwata H, Schneider RK, Kuppe C, et al. Adventitial MSC-like cells are progenitors of vascular smooth muscle cells and drive vascular calcification in chronic kidney disease. *Cell Stem Cell.* (2016) 19:628–42. doi: 10.1016/j.stem.2016.08.001
52. Abedin M, Tintut Y, Demer LL. Mesenchymal stem cells and the artery wall. *Circ Res.* (2004) 95:671–6. doi: 10.1161/01.RES.0000143421.27684.12
53. Pittenger MF, Mackay AM, Beck SC, Jaiswal RK, Douglas R, Mosca JD, et al. Multilineage potential of adult human mesenchymal stem cells. *Science.* (1999) 284:143–7. doi: 10.1126/science.284.5411.143
54. Ding DC, Shyu WC, Lin SZ. Mesenchymal stem cells. *Cell Transplant.* (2011) 20:5–14. doi: 10.3727/096368910X
55. Komori T. Regulation of proliferation, differentiation and functions of osteoblasts by Runx2. *Int J Mol Sci.* (2019) 20:1694. doi: 10.3390/ijms20071694
56. Campagnolo P, Cesselli D, Al Haj Zen A, Beltrami AP, Krankel N, Katare R, et al. Human adult vena saphena contains perivascular progenitor cells endowed with clonogenic and proangiogenic potential. *Circulation.* (2010) 121:1735–45. doi: 10.1161/CIRCULATIONAHA.109.899252
57. Yao T, Chen H, Baker MB, Moroni L. Effects of fiber alignment and coculture with endothelial cells on osteogenic differentiation of mesenchymal stromal cells. *Tissue Eng Part C Methods.* (2020) 26:11–22. doi: 10.1089/ten.tec.2019.0232
58. Yao Z, Liu H, Yang M, Bai Y, Zhang B, Wang C, et al. Bone marrow mesenchymal stem cell-derived endothelial cells increase capillary density and accelerate angiogenesis in mouse hindlimb ischemia model. *Stem Cell Res Ther.* (2020) 11:221. doi: 10.1186/s13287-020-01710-x
59. Wang C, Li Y, Yang M, Zou Y, Liu H, Liang Z, et al. Efficient differentiation of bone marrow mesenchymal stem cells into endothelial cells *in vitro*. *Eur J Vasc Endovasc Surg.* (2018) 55:257–65. doi: 10.1016/j.ejvs.2017.10.012
60. Kramann R, Schneider RK, DiRocco DP, Machado F, Fleig S, Bondzie PA, et al. Perivascular Gli1+ progenitors are key contributors to injury-induced organ fibrosis. *Cell Stem Cell.* (2015) 16:51–66. doi: 10.1016/j.stem.2014.11.004
61. Gu W, Nowak WN, Xie Y, Le Bras A, Hu Y, Deng J, et al. Single-cell RNA-sequencing and metabolomics analyses reveal the contribution of perivascular adipose tissue stem cells to vascular remodeling. *Arterioscler Thromb Vasc Biol.* (2019) 39:2049–66. doi: 10.1161/ATVBAHA.119.312732
62. Armulik A, Genove G, Mae M, Nisancioglu MH, Wallgard E, Niaudet C, et al. Pericytes regulate the blood-brain barrier. *Nature.* (2010) 468:557–61. doi: 10.1038/nature09522
63. Korn J, Christ B, Kurz H. Neuroectodermal origin of brain pericytes and vascular smooth muscle cells. *J Comp Neurol.* (2002) 442:78–88. doi: 10.1002/cne.1423
64. van Dijk CG, Nieuweboer FE, Pei JY, Xu YJ, Burgisser P, van Mulligen E, et al. The complex mural cell: pericyte function in health and disease. *Int J Cardiol.* (2015) 190:75–89. doi: 10.1016/j.ijcard.2015.03.258
65. Brighton CT, Lorich DG, Kupcha R, Reilly TM, Jones AR, Woodbury RA, 2nd. The pericyte as a possible osteoblast progenitor cell. *Clin Orthop Relat Res.* 1992:287–99. doi: 10.1097/00003086-199202000-00043
66. Boström K, Watson KE, Horn S, Wortham C, Herman IM, Demer LL. Bone morphogenetic protein expression in human atherosclerotic lesions. *J Clin Invest.* (1993) 91:1800–9. doi: 10.1172/JCI116391
67. Lin CS, Lue TF. Defining vascular stem cells. *Stem Cells Dev.* (2013) 22:1018–26. doi: 10.1089/scd.2012.0504
68. Guimarães-Camboa N, Cattaneo P, Sun Y, Moore-Morris T, Gu Y, Dalton ND, et al. Pericytes of multiple organs do not behave as mesenchymal stem cells *in vivo*. *Cell Stem Cell.* (2017) 20:345–59.e5. doi: 10.1016/j.stem.2016.12.006
69. Deng J, Ni Z, Gu W, Chen Q, Nowak WN, Chen T, et al. Single-cell gene profiling and lineage tracing analyses revealed novel mechanisms of endothelial repair by progenitors. *Cell Mol Life Sci.* (2020) 77:5299–320. doi: 10.1007/s00018-020-03480-4
70. Chen Q, Yang M, Wu H, Zhou J, Wang W, Zhang H, et al. Genetic lineage tracing analysis of c-kit(+) stem/progenitor cells revealed a contribution to vascular injury-induced neointimal lesions. *J Mol Cell Cardiol.* (2018) 121:277–86. doi: 10.1016/j.yjmcc.2018.07.252
71. Ouyang S, Li Y, Wu X, Wang Y, Liu F, Zhang J, et al. GPR4 signaling is essential for the promotion of acid-mediated angiogenic capacity of endothelial progenitor cells by activating STAT3/VEGFA pathway in patients with coronary artery disease. *Stem Cell Res Ther.* (2021) 12:149. doi: 10.1186/s13287-021-02221-z
72. Xie Y, Potter CMF, Le Bras A, Nowak WN, Gu W, Bhaloo SI, et al. Leptin induces Sca-1(+) progenitor cell migration enhancing neointimal lesions in vessel-injury mouse models. *Arterioscler Thromb Vasc Biol.* (2017) 37:2114–27. doi: 10.1161/ATVBAHA.117.309852
73. Inoue T, Sata M, Hikichi Y, Sohma R, Fukuda D, Uchida T, et al. Mobilization of CD34-positive bone marrow-derived cells after coronary stent implantation: impact on restenosis. *Circulation.* (2007) 115:553–61. doi: 10.1161/CIRCULATIONAHA.106.621714
74. Dai Z, Zhu MM, Peng Y, Jin H, Machireddy N, Qian Z, et al. Endothelial and smooth muscle cell interaction *via* FoxM1 signaling mediates vascular remodeling and pulmonary hypertension. *Am J Respir Crit Care Med.* (2018) 198:788–802. doi: 10.1164/rccm.201709-1835OC
75. Shankman LS, Gomez D, Cherepanova OA, Salmon M, Alencar GF, Haskins RM, et al. KLF4-dependent phenotypic modulation of smooth muscle cells has a key role in atherosclerotic plaque pathogenesis. *Nat Med.* (2015) 21:628–37. doi: 10.1038/nm.3866
76. Wu J, Montaniel KR, Saleh MA, Xiao L, Chen W, Owens GK, et al. Origin of matrix-producing cells that contribute to aortic fibrosis in hypertension. *Hypertension.* (2016) 67:461–8. doi: 10.1161/HYPERTENSIONAHA.115.06123
77. Zou S, Ren P, Zhang L, Azares AR, Zhang S, Coselli JS, et al. Activation of bone marrow-derived cells and resident aortic cells during aortic injury. *J Surg Res.* (2020) 245:1–12. doi: 10.1016/j.jss.2019.07.013
78. Hansson GK. Inflammation, atherosclerosis, and coronary artery disease. *N Engl J Med.* (2005) 352:1685–95. doi: 10.1056/NEJMra043430
79. Baeyens N, Bandyopadhyay C, Coon BG, Yun S, Schwartz MA. Endothelial fluid shear stress sensing in vascular health and disease. *J Clin Invest.* (2016) 126:821–8. doi: 10.1172/JCI83083
80. Gimbrone MA, García-Cardeña G. Endothelial cell dysfunction and the pathobiology of atherosclerosis. *Circ Res.* (2016) 118:620–36. doi: 10.1161/CIRCRESAHA.115.306301
81. Moore KJ, Sheedy FJ, Fisher EA. Macrophages in atherosclerosis: a dynamic balance. *Nat Rev Immunol.* (2013) 13:709–21. doi: 10.1038/nri3520
82. Wolf D, Ley K. Immunity and inflammation in atherosclerosis. *Circ Res.* (2019) 124:315–27. doi: 10.1161/CIRCRESAHA.118.313591
83. Ross R, Glomset JA. Atherosclerosis and the arterial smooth muscle cell: proliferation of smooth muscle is a key event in the genesis of the lesions of atherosclerosis. *Science.* (1973) 180:1332–9. doi: 10.1126/science.180.4093.1332
84. Chistiakov DA, Orekhov AN, Bobryshev YV. Effects of shear stress on endothelial cells: go with the flow. *Acta Physiol (Oxf).* (2017) 219:382–408. doi: 10.1111/apha.12725
85. Li JH, Li Y, Huang D, Yao M. Role of stromal cell-derived factor-1 in endothelial progenitor cell-mediated vascular repair and regeneration. *Tissue Eng Regen Med.* (2021) 18:747–58. doi: 10.1007/s13770-021-00366-9
86. Jolly AJ, Lu S, Strand KA, Dubner AM, Mutryn MF, Nemenoff RA, et al. Heterogeneous subpopulations of adventitial progenitor cells regulate

vascular homeostasis and pathological vascular remodeling. *Cardiovasc Res.* (2021). doi: 10.1093/cvr/cvab174. [Epub ahead of print].
87. Karamariti E, Zhai C, Yu B, Qiao L, Wang Z, Potter CMF, et al. DKK3 (Dickkopf 3) alters atherosclerotic plaque phenotype involving vascular progenitor and fibroblast differentiation into smooth muscle cells. *Arterioscler Thromb Vasc Biol.* (2018) 38:425–37. doi: 10.1161/ATVBAHA.117.310079
88. Chen WT, Hsu WT, Yen MH, Changou CA, Han CL, Chen YJ, et al. Alteration of mesenchymal stem cells polarity by laminar shear stimulation promoting β-catenin nuclear localization. *Biomaterials.* (2019) 190–1:1–10. doi: 10.1016/j.biomaterials.2018.10.026
89. Colmegna I, Stochaj U. MSC - targets for atherosclerosis therapy. *Aging (Albany NY).* (2018) 11:285–6. doi: 10.18632/aging.101735
90. Wang SS, Hu SW, Zhang QH, Xia AX, Jiang ZX, Chen XM. Mesenchymal stem cells stabilize atherosclerotic vulnerable plaque by anti-inflammatory properties. *PLoS One.* (2015) 10:e0136026. doi: 10.1371/journal.pone.0136026
91. Tannock LR. Advances in the management of hyperlipidemia-induced atherosclerosis. *Expert Rev Cardiovasc Ther.* (2008) 6:369–83. doi: 10.1586/14779072.6.3.369
92. Chen T, Wu Y, Gu W, Xu Q. Response of vascular mesenchymal stem/progenitor cells to hyperlipidemia. *Cell Mol Life Sci.* (2018) 75:4079–91. doi: 10.1007/s00018-018-2859-z
93. Pickering JG, Ford CM, Chow LH. Evidence for rapid accumulation and persistently disordered architecture of fibrillar collagen in human coronary restenosis lesions. *Am J Cardiol.* (1996) 78:633–7. doi: 10.1016/S0002-9149(96)00384-0
94. Jukema JW, Ahmed TA, Verschuren JJ, Quax PH. Restenosis after PCI. Part 2: prevention and therapy. *Nat Rev Cardiol.* (2011) 9:79–90. doi: 10.1038/nrcardio.2011.148
95. Jukema JW, Verschuren JJ, Ahmed TA, Quax PH. Restenosis after PCI. Part 1: pathophysiology and risk factors. *Nat Rev Cardiol.* (2011) 9:53–62. doi: 10.1038/nrcardio.2011.132
96. Toutouzas K, Colombo A, Stefanadis C. Inflammation and restenosis after percutaneous coronary interventions. *Eur Heart J.* (2004) 25:1679–87. doi: 10.1016/j.ehj.2004.06.011
97. Kipshidze N, Dangas G, Tsapenko M, Moses J, Leon MB, Kutryk M, et al. Role of the endothelium in modulating neointimal formation: vasculoprotective approaches to attenuate restenosis after percutaneous coronary interventions. *J Am Coll Cardiol.* (2004) 44:733–9. doi: 10.1016/S0735-1097(04)01083-6
98. Smith SA, Newby AC, Bond M. Ending restenosis: inhibition of vascular smooth muscle cell proliferation by cAMP. *Cells.* (2019) 8:1447. doi: 10.3390/cells8111447
99. Yang F, Chen Q, He S, Yang M, Maguire EM, An W, et al. miR-22 Is a novel mediator of vascular smooth muscle cell phenotypic modulation and neointima formation. *Circulation.* (2018) 137:1824–41. doi: 10.1161/CIRCULATIONAHA.117.027799
100. Yu B, Wong MM, Potter CM, Simpson RM, Karamariti E, Zhang Z, et al. Vascular stem/progenitor cell migration induced by smooth muscle cell-derived chemokine (C-C Motif) ligand 2 and chemokine (C-X-C motif) ligand 1 contributes to neointima formation. *Stem Cells.* (2016) 34:2368–80. doi: 10.1002/stem.2410
101. Renna NF, de Las Heras N, Miatello RM. Pathophysiology of vascular remodeling in hypertension. *Int J Hypertens.* (2013) 2013:808353. doi: 10.1155/2013/808353
102. Mei X, Cui XB, Li Y, Chen SY. CircSOD2: a novel regulator for smooth muscle proliferation and neointima formation. *Arterioscler Thromb Vasc Biol.* (2021) 41:2961–73. doi: 10.1161/ATVBAHA.121.316911
103. Issa Bhaloo S, Wu Y, Le Bras A, Yu B, Gu W, Xie Y, et al. Binding of Dickkopf-3 to CXCR7 enhances vascular progenitor cell migration and degradable graft regeneration. *Circ Res.* (2018) 123:451–66. doi: 10.1161/CIRCRESAHA.118.312945
104. Le Bras A, Yu B, Issa Bhaloo S, Hong X, Zhang Z, Hu Y, et al. Adventitial Sca-1+ cells transduced with ETV2 are committed to the endothelial fate and improve vascular remodeling after injury. *Arterioscler Thromb Vasc Biol.* (2018) 38:232–44. doi: 10.1161/ATVBAHA.117.309853
105. Messerli FH, Williams B, Ritz E. Essential hypertension. *Lancet.* (2007) 370:591–603. doi: 10.1016/S0140-6736(07)61299-9
106. Drummond GR, Vinh A, Guzik TJ, Sobey CG. Immune mechanisms of hypertension. *Nat Rev Immunol.* (2019) 19:517–32. doi: 10.1038/s41577-019-0160-5
107. Intengan HD, Schiffrin EL. Vascular remodeling in hypertension: roles of apoptosis, inflammation, and fibrosis. *Hypertension.* (2001) 38(3 Pt 2):581–7. doi: 10.1161/hy09t1.096249
108. Takayanagi T, Forrester SJ, Kawai T, Obama T, Tsuji T, Elliott KJ, et al. Vascular ADAM17 as a novel therapeutic target in mediating cardiovascular hypertrophy and perivascular fibrosis induced by angiotensin II. *Hypertension.* (2016) 68:949–55. doi: 10.1161/HYPERTENSIONAHA.116.07620
109. Cardoso CRL, Salles GF. Prognostic value of changes in aortic stiffness for cardiovascular outcomes and mortality in resistant hypertension: a cohort study. *Hypertension.* (2022) 79:447–56. doi: 10.1161/HYPERTENSIONAHA.121.18498
110. Jana S, Hu M, Shen M, Kassiri Z. Extracellular matrix, regional heterogeneity of the aorta, and aortic aneurysm. *Exp Mol Med.* (2019) 51:1–15. doi: 10.1038/s12276-019-0286-3
111. Nienaber CA, Clough RE, Sakalihasan N, Suzuki T, Gibbs R, Mussa F, et al. Aortic dissection. *Nat Rev Dis Primers.* (2016) 2:16053. doi: 10.1038/nrdp.2016.71
112. Guo DC, Papke CL, He R, Milewicz DM. Pathogenesis of thoracic and abdominal aortic aneurysms. *Ann N Y Acad Sci.* (2006) 1085:339–52. doi: 10.1196/annals.1383.013
113. Wang X, Khalil RA. Matrix metalloproteinases, vascular remodeling, and vascular disease. *Adv Pharmacol.* (2018) 81:241–330. doi: 10.1016/bs.apha.2017.08.002
114. López-Candales A, Holmes DR, Liao S, Scott MJ, Wickline SA, Thompson RW. Decreased vascular smooth muscle cell density in medial degeneration of human abdominal aortic aneurysms. *Am J Pathol.* (1997) 150:993–1007.
115. Sinha S, Santoro MM. New models to study vascular mural cell embryonic origin: implications in vascular diseases. *Cardiovasc Res.* (2018) 114:481–91. doi: 10.1093/cvr/cvy005
116. Cai D, Sun C, Zhang G, Que X, Fujise K, Weintraub NL, et al. A novel mechanism underlying inflammatory smooth muscle phenotype in abdominal aortic aneurysm. *Circ Res.* (2021) 129:e202–e14. doi: 10.1161/CIRCRESAHA.121.319374
117. Quintana RA, Taylor WR. Cellular mechanisms of aortic aneurysm formation. *Circ Res.* (2019) 124:607–18. doi: 10.1161/CIRCRESAHA.118.313187
118. Pinard A, Jones GT, Milewicz DM. Genetics of thoracic and abdominal aortic diseases. *Circ Res.* (2019) 124:588–606. doi: 10.1161/CIRCRESAHA.118.312436
119. Fletcher AJ, Syed MBJ, Aitman TJ, Newby DE, Walker NL. Inherited thoracic aortic disease: new insights and translational targets. *Circulation.* (2020) 141:1570–87. doi: 10.1161/CIRCULATIONAHA.119.043756
120. Judge DP, Dietz HC. Marfan's syndrome. *Lancet.* (2005) 366:1965–76. doi: 10.1016/S0140-6736(05)67789-6
121. Yeh JSM, Rubens M, Nienaber CA. Novel reconstruction of a vascular aneurysm in Marfan syndrome. *Eur Heart J.* (2017) 38:1521. doi: 10.1093/eurheartj/ehw520
122. Yin X, Wanga S, Fellows AL, Barallobre-Barreiro J, Lu R, Davaapil H, et al. Glycoproteomic analysis of the aortic extracellular matrix in Marfan patients. *Arterioscler Thromb Vasc Biol.* (2019) 39:1859–73. doi: 10.1161/ATVBAHA.118.312175
123. Chen PY, Qin L, Li G, Malagon-Lopez J, Wang Z, Bergaya S, et al. Smooth muscle cell reprogramming in aortic aneurysms. *Cell Stem Cell.* (2020) 26:542–57.e11. doi: 10.1016/j.stem.2020.02.013
124. Gong J, Zhou D, Jiang L, Qiu P, Milewicz DM, Chen YE, et al. *In vitro* lineage-specific differentiation of vascular smooth muscle cells in response to SMAD3 deficiency: implications for SMAD3-related thoracic aortic aneurysm. *Arterioscler Thromb*

Vasc Biol. (2020) 40:1651–63. doi: 10.1161/ATVBAHA.120.313033

125. Teti G, Chiarini F, Mazzotti E, Ruggeri A, Carano F, Falconi M. Cellular senescence in vascular wall mesenchymal stromal cells, a possible contribution to the development of aortic aneurysm. *Mech Ageing Dev.* (2021) 197:111515. doi: 10.1016/j.mad.2021.111515
126. Ciavarella C, Gallitto E, Ricci F, Buzzi M, Stella A, Pasquinelli G. The crosstalk between vascular MSCs and inflammatory mediators determines the pro-calcific remodelling of human atherosclerotic aneurysm. *Stem Cell Res Ther.* (2017) 8:99. doi: 10.1186/s13287-017-0554-x
127. Li Z, Zhao Z, Cai Z, Sun Y, Li L, Yao F, et al. Runx2 (Runt-Related Transcription Factor 2)-mediated microcalcification is a novel pathological characteristic and potential mediator of abdominal aortic aneurysm. *Arterioscler Thromb Vasc Biol.* (2020) 40:1352–69. doi: 10.1161/ATVBAHA.119.314113

Conflict of Interest: The authors declare that the research was conducted in the absence of any commercial or financial relationships that could be construed as a potential conflict of interest.

frontiers in Cardiovascular Medicine

ORIGINAL RESEARCH
published: 16 February 2022
doi: 10.3389/fcvm.2022.826369

Relevance of Cor Pulmonale in COPD With and Without Pulmonary Hypertension: A Retrospective Cohort Study

Athiththan Yogeswaran[1†‡], Stefan Kuhnert[1‡], Henning Gall[1†], Marlene Faber[1], Ekaterina Krauss[1], Zvonimir A. Rako[1], Stanislav Keranov[3], Friedrich Grimminger[2†], Hossein Ardeschir Ghofrani[1†], Robert Naeije[4], Werner Seeger[1†], Manuel J. Richter[1†‡] and Khodr Tello[1‡]*

[1] Department of Internal Medicine, Member of the German Center for Lung Research, Universities of Giessen and Marburg Lung Center, Justus-Liebig-University Giessen, Giessen, Germany, [2] Department of Internal Medicine, Member of the German Center for Lung Research, Institute for Lung Health, Cardio-Pulmonary Institute, Universities of Giessen and Marburg Lung Center, Giessen, Germany, [3] Department of Cardiology and Angiology, DZHK (German Center for Cardiovascular Research), University of Giessen, Giessen, Germany, [4] Department of Pathophysiology, Faculty of Medicine, Free University of Brussels, Brussels, Belgium

Background: The relevance of cor pulmonale in COPD and pulmonary hypertension due to COPD (PH-COPD) is incompletely understood. We aimed to investigate the relationship of right ventricular-pulmonary arterial (RV-PA) uncoupling with disease severity in COPD, and the relationship of RV-PA uncoupling and use of targeted PH therapies with mortality in PH-COPD.

Methods: We retrospectively analyzed 231 patients with COPD without PH and 274 patients with PH-COPD. COPD was classified according to GOLD stages and the modified Medical Research Council dyspnoea scale. PH was categorized as mild-to-moderate or severe. RV-PA uncoupling was assessed as the echocardiographic tricuspid annular plane systolic excursion/pulmonary artery systolic pressure (TAPSE/PASP) ratio.

Results: Of the cohort with COPD without PH, 21, 58, 54 and 92 were classified as GOLD I, II, III and IV, respectively. Patients in advanced GOLD stages and those with severe dyspnoea showed significantly decreased TAPSE/PASP.
Of the PH-COPD cohort, 144 had mild-to-moderate PH and 130 had severe PH. During follow-up, 126 patients died. In univariate Cox regression, TAPSE/PASP and 6-min walk distance (6MWD; 10 m increments) predicted survival [hazard ratios (95% CI): 0.12 (0.03–0.57) and 0.95 (0.93–0.97), respectively]; notably, PH severity and simplified European Society of Cardiology/European Respiratory Society risk stratification did not. Among patients in the lowest or intermediate tertiles of TAPSE/PASP and 6MWD, those with targeted PH therapy had higher survival than those without (53 vs. 17% at 3 years).

Conclusion: Cor pulmonale (decreased TAPSE/PASP and 6MWD) is associated with disease severity in COPD and predicts outcome in PH-COPD.

Keywords: chronic obstructive pulmonary disease, cor pulmonale, pulmonary arterial hypertension, right ventricle, risk stratification

OPEN ACCESS

Edited by:
Gaurav Choudhary, Warren Alpert Medical School of Brown University, United States

Reviewed by:
Matthew Jankowich, Warren Alpert Medical School of Brown University, United States
Kurt Prins, University of Minnesota, United States

***Correspondence:**
Khodr Tello
khodr.tello@innere.med.uni-giessen.de

†ORCID:
Athiththan Yogeswaran
orcid.org/0000-0001-9505-8608
Henning Gall
orcid.org/0000-0001-7016-7373
Friedrich Grimminger
orcid.org/0000-0001-8725-6276
Hossein Ardeschir Ghofrani
orcid.org/0000-0002-2029-4419
Werner Seeger
orcid.org/0000-0003-1946-0894
Manuel J. Richter
orcid.org/0000-0003-0964-1931

‡*These authors have contributed equally to this work*

Specialty section:
This article was submitted to General Cardiovascular Medicine, a section of the journal Frontiers in Cardiovascular Medicine

Received: *30 November 2021*
Accepted: *24 January 2022*
Published: *16 February 2022*

Citation:
Yogeswaran A, Kuhnert S, Gall H, Faber M, Krauss E, Rako ZA, Keranov S, Grimminger F, Ghofrani HA, Naeije R, Seeger W, Richter MJ and Tello K (2022) Relevance of Cor Pulmonale in COPD With and Without Pulmonary Hypertension: A Retrospective Cohort Study. Front. Cardiovasc. Med. 9:826369. doi: 10.3389/fcvm.2022.826369

INTRODUCTION

Pulmonary hypertension (PH) as a complication of COPD is generally mild to moderate but can be severe in some patients (1). Mean pulmonary artery pressures (mPAP) higher than 35–40 mm Hg have been reported in 1–5% of patients with advanced COPD (2–4). PH has long been known to be associated with a reduced life expectancy in COPD, in proportion to increased PAP (5). Early studies also showed that PH due to COPD (PH-COPD) is associated with structural changes in the right ventricle or "cor pulmonale" (6). Altered right ventricular (RV) function was demonstrated by radionuclide angiography and clinicians learned that eventual systemic congestion symptomatology or "pulmonary heart disease" also heralded an increase in mortality in COPD (7–9). More recently, a validated echocardiographic measure of RV-pulmonary arterial (PA) coupling—the tricuspid annular plane systolic excursion (TAPSE)/pulmonary artery systolic pressure (PASP) ratio (10, 11)—was shown to be a strong predictor of outcome in PH on a background of either interstitial lung disease or COPD (12), as well as in heart failure (10, 13) and pulmonary arterial hypertension (PAH) (14). However, the extent to which RV dysfunction explains the altered functional state, decreased exercise capacity and decreased survival of patients with COPD is not exactly known. A risk scoring system for PAH proposed by the European Society of Cardiology and the European Respiratory Society (ESC/ERS) (15) has been successfully transposed to patients with PH due to interstitial lung disease (16) but its utility in patients with PH-COPD remains unknown. Whether targeted PH therapies (which have shown efficacy in PAH) might improve outcome in PH-COPD also remains undecided (1).

We therefore aimed to assess the relationship of disease severity with RV function in patients with COPD without PH, and the relationship of mortality with RV function, PAH-based risk scores and use of targeted PH therapies in patients with PH-COPD.

METHODS

Patients and Study Design

We performed a two-part retrospective cohort study. In the first part, we included 231 patients with COPD without PH who had TAPSE and PASP data available. Echocardiographic and lung function parameters, 6-min walk distance (6MWD), Global Initiative for Obstructive Lung Disease (GOLD) stage, COPD Assessment Test (CAT), and modified Medical Research Council (mMRC) dyspnoea score were evaluated during routine visits to the Department of Pneumology in the Universities of Giessen and Marburg Lung Center. Routine visits took place between 4 August 2010 and 16 July 2021.

In the second part of the study, we included 274 patients with PH-COPD who were enrolled in the Giessen PH registry (17) between August 1995 and December 2018 and who had not previously received targeted PH therapy; some of these patients had also been included in a previously published study (12). Right heart catheterization was performed by experts, with haemodynamic measurements assessed after a short resting period (18). All enrolled patients were followed until June 2020. Survival status was determined by contacting the patient or their physician. Use of PH-specific drugs in severe PH-COPD was decided by experts based on assessment of the individual benefit-risk ratio, as recommended in the current guidelines (15).

For patients who were diagnosed with COPD in another centre, the baseline parameters of lung function are missing due to lack of access.

All patients gave written informed consent. The study was approved by the University of Giessen institutional review board (#266/11).

Haemodynamic Classification of PH-COPD

The date of the initial right heart catheterization was taken as the date of PH diagnosis. The final diagnosis was made by a multidisciplinary board including physicians, radiologists and surgeons. PH-COPD was classified as mild-to-moderate or severe according to mPAP and cardiac index as recommended by an expert working group at the 6th World Symposium on PH (1): mPAP between 25 and 34 mm Hg alone or mPAP between 21 and 24 mm Hg with pulmonary vascular resistance (PVR) $\geq$3 Wood Units was classified as mild-to-moderate PH-COPD, and mPAP $\geq$35 mm Hg alone or mPAP $\geq$25 mm Hg with cardiac index $<$2.0 L/min/m^2 was classified as severe PH-COPD.

Risk Stratification in PH-COPD

Risk assessment in PH-COPD was performed using a validated simplified version (19) of the ESC/ERS risk stratification system (15). In brief, patients were categorized into low-, intermediate- and high-risk groups based on 6MWD, brain natriuretic peptide (BNP), right atrial pressure (RAP), cardiac index, mixed venous oxygen saturation (SvO_2), right atrial area (echocardiography), World Health Organization functional class and the presence of pericardial effusion (echocardiography), all according to the cut-offs mentioned in the ESC/ERS guidelines (15).

RV-PA coupling was assessed using the TAPSE/PASP ratio determined by echocardiography.

Statistical Analyses

Baseline characteristics are shown as mean $\pm$ standard deviation if normally distributed and as median [interquartile range (IQR)] if non-normally distributed. Comparisons between subgroups were performed using either Student's *t*-tests or non-parametric tests. Descriptive statistics and correlation analyses were used to evaluate the importance of the TAPSE/PASP ratio in COPD without PH.

In patients with PH-COPD, univariate Cox regression analysis was performed including age, PVR, BNP, 6MWD, SvO_2, RAP, cardiac index, mPAP, right atrial area, the TAPSE/PASP ratio, forced vital capacity (FVC), total lung capacity (TLC), forced expiratory volume in 1 second (FEV_1), the FEV_1/vital capacity (VC) ratio, lung diffusing capacity for carbon monoxide (DLCO), PH-COPD severity (mild-to-moderate or severe), ESC/ERS risk score and body mass index, obstruction, dyspnoea and exercise capacity (BODE) index. TAPSE or PASP alone were not added due to collinearity. All variables that showed a significant association with mortality were included in a

multivariate, stepwise, backward Cox regression model to identify independent predictors of mortality in patients with PH-COPD. Cut-off values with the highest sensitivity and specificity for predicting mortality were identified by receiver operating characteristic analysis and calculation of Youden's index. No imputation for missing data was implemented. Survival analyses were conducted using Kaplan–Meier plots (truncated at 5 years) and log-rank tests.

All analyses were performed using R 4.0 (the R Foundation, Vienna, Austria) and SPSS 26.0 (IBM, Armonk, USA). In the stepwise backward model, parameters with $p > 0.1$ were excluded. For all other analyses, $p < 0.05$ was considered significant.

RESULTS

Study Population With COPD

Baseline characteristics of the 231 patients with COPD without PH are shown in **Table 1**. The median (IQR) age was 66 (59, 72) years and 48% of the patients were female. FEV_1/VC ratio, FEV_1, TLC and FVC data were available in 226 (98%), 226 (98%), 223 (97%), and 223 (97%) patients, respectively. BNP concentration, 6MWD, CAT score and mMRC score were available in 209 (90%), 73 (32%), 179 (77%) and 119 (52%) patients, respectively. The TAPSE/PASP ratio did not differ between male and female patients ($p = 0.84$).

Relevance of TAPSE/PASP in COPD

The TAPSE/PASP ratio differed between GOLD stages I–IV (ANOVA $p < 0.001$). Patients in higher GOLD stages showed significantly lower TAPSE/PASP ratios (**Table 1**). Concordantly, patients with severe dyspnoea (mMRC grade III or IV) exhibited a significantly decreased TAPSE/PASP ratio compared with patients with less severe symptoms [mMRC III/IV: 0.61 (0.50, 0.81) mm/mm Hg; mMRC I/II: 0.75 (0.60, 0.93) mm/mm Hg; $p = 0.03$], and patients who required oxygen supplementation showed a lower TAPSE/PASP ratio than those who did not [0.59 (0.42, 0.74) mm/mm Hg vs. 0.76 (0.62, 0.95) mm/mm Hg; $p < 0.001$]. Interestingly, patients with exacerbations leading to inpatient treatment also showed a significantly lower TAPSE/PASP ratio than those without such exacerbations [0.65 (0.48, 0.77) mm/mm Hg vs. 0.76 (0.60, 0.95) mm/mm Hg; $p = 0.001$]. Patients with a higher BODE index had a significantly lower TAPSE/PASP ratio ($p = 0.034$; **Supplementary Figure 1A**).

Correlations of the TAPSE/PASP ratio with different parameters including lung function are shown in **Table 2**. The TAPSE/PASP ratio showed meaningful correlations with age, 6MWD, FEV_1 and DLCO.

Study Population With PH-COPD

Baseline characteristics of the 274 included patients with PH-COPD are shown in **Table 3**. The median (IQR) age was 70 (65, 78) years, and most of the patients (62%) were male. The FEV_1/VC ratio, FEV_1 and FVC were reduced, PH was on average mild to moderate and the 6MWD was low. In total, 144 patients (53%) had mild-to-moderate PH-COPD and 130 patients (47%) had severe PH-COPD. Patients with severe PH-COPD had normal TLC, higher FEV_1/VC ratios, FEV_1 and FVC and more severe haemodynamic impairment than patients with mild-to-moderate PH-COPD (**Table 3**). The TAPSE/PASP ratio did not differ between male and female patients ($p = 0.56$), and was slightly but non-significantly lower in patients with a higher BODE index ($p = 0.50$; **Supplementary Figure 1B**).Twenty-one patients were lost to follow-up and were therefore excluded from survival analysis.

Predictors of Mortality in PH-COPD

During follow-up (truncated at 5 years after diagnosis), 126 patients died. Median survival was 53 months. In univariate analysis, mPAP, PVR, the TAPSE/PASP ratio, 6MWD, FVC and the BODE index significantly predicted mortality whereas age, PH-COPD severity, ESC/ERS risk score, BNP, right atrial area, SvO_2, RAP, cardiac index, DLCO and other lung function tests did not (**Table 4**), although further analysis of the prognostic capability of DLCO revealed an association with short-term mortality (truncated at 2 years after diagnosis; **Supplementary Figure 3**). The TAPSE/PASP ratio correlated with mPAP, cardiac index and SvO_2 (**Supplementary Table 1**). Only the TAPSE/PASP ratio and 6MWD independently predicted mortality (**Table 4**).

Prognostic cut-off values determined by Youden's index were 0.35 mm/mm Hg for the TAPSE/PASP ratio and 299 m for 6MWD. Patients were classified into three risk groups based on the two predictors: low risk (6MWD and TAPSE/PASP above the cut-off values), intermediate risk (6MWD or TAPSE/PASP above the cut-off value), and high risk (neither 6MWD nor TAPSE/PASP above the cut-off values). As illustrated in **Figure 1**, survival at 1, 3 and 5 years was 100, 96, and 87%, respectively, in the low-risk group, 92, 74, and 62%, respectively, in the intermediate-risk group, and 75, 46, and 27%, respectively, in the high-risk group. Cox regression revealed that the risk of mortality was increased 4-fold in the intermediate-risk group [hazard ratio (HR): 3.63; 95% CI: 1.05–12.6] and 11-fold in the high-risk group (HR: 10.5; 95% CI: 3.17–34.9).

Targeted PH therapies were initiated in 57 patients with mild-to-moderate PH-COPD and 93 patients with severe PH-COPD. In both groups, survival of patients with targeted PH therapy did not differ from survival of patients without targeted PH therapy (**Figure 2**). We next evaluated survival with vs. without targeted PH therapy in the three risk groups defined by TAPSE/PASP and 6MWD. Targeted PH therapies were taken by 10 of 26 patients at low risk, 32 of 48 patients at intermediate risk, and 41 of 49 patients at high risk. Survival with vs. without targeted PH therapy showed no significant difference in any of the three risk groups (**Supplementary Figure 4**). We also classified the patients according to TAPSE/PASP tertiles (<0.28 mm/mm Hg, 0.28–0.41 mm/mm Hg and >0.41 mm/mm Hg) and 6MWD tertiles (<200, 200–300, and >300 m). In the 63 patients who were in the lowest or intermediate tertiles of TAPSE/PASP and 6MWD, those who received targeted PH therapy ($n = 50$) had a higher survival rate than those without PH therapy (**Figure 3**; log-rank $p = 0.02$; 3-year survival: 53 and 17%, respectively; HR: 0.36; 95% CI: 0.14–0.89). Of the patients receiving targeted PH therapy,

TABLE 1 | Baseline characteristics of patients with COPD without pulmonary hypertension.

	GOLD stage				
	I ($n = 21$)	**II ($n = 58$)**	**III ($n = 54$)**	**IV ($n = 92$)**	**Unknown ($n = 6$)**
Age, years	61.0 [56.0, 74.0]	67.0 [60.0, 72.8]	65.0 [60.0, 71.5]	66.0 [59.0, 71.0]	60.5 [51.3, 72.0]
n with data	21	58	54	92	6
Male sex, *n* (%)	9 (43)	27 (47)	32 (59)	47 (51)	4 (67)
n with data	21	58	54	92	6
Pack years	40.0 [30.0, 55.0]	44.5 [30.0, 50.0]	45.0 [30.0, 60.0]	40.0 [30.0, 50.0]	50.0 [35.5, 52.5]
n with data	19	52	49	73	3
BMI, kg/m^2	26.4 [24.2, 29.7]	26.8 [23.5, 30.7]	26.1 [23.5, 28.9]	23.2 [20.4, 28.9]	25.0 [23.1, 26.7]
n with data	20	58	54	92	5
FEV_1, % pred	81.8 [75.6, 87.2]	60.8 [54.0, 69.1]	40.4 [34.7, 44.8]	26.7 [22.6, 32.8]	61.4 [29.7, 98.5]
n with data	21	58	52	91	4
FEV_1/VC max	66.2 [64.1, 71.0]	55.7 [47.3, 62.3]	45.3 [38.2, 49.9]	36.2 [30.9, 44.9]	50.0 [33.8, 70.5]
n with data	21	58	52	91	4
TLC, % pred	115 [108, 121]	114 [100, 123]	118 [102, 127]	125 [112, 140]	114 [103, 124]
n with data	21	57	51	90	4
VC, % pred	98.4 [93.2, 106]	89.7 [76.2, 99.3]	72.8 [63.1, 82.0]	60.0 [49.1, 70.9]	78.3 [67.2, 99.9]
n with data	21	57	51	90	4
FVC, % pred	90.3 [81.1, 104]	78.4 [69.9, 91.5]	61.2 [54.8, 73.7]	52.0 [43.8, 60.7]	72.8 [60.0, 97.2]
n with data	20	57	52	90	4
DLCO, % pred	62.7 [50.7, 70.8]	45.5 [36.7, 69.3]	36.8 [29.5, 42.6]	22.4 [17.4, 29.4]	47.1 [45.2, 59.0]
n with data	20	52	43	46	3
TAPSE, mm	23.0 [21.0, 27.0]	22.5 [20.0, 25.0]	22.0 [20.3, 24.8]	22.0 [19.8, 25.0]	23.5 [22.0, 25.0]
n with data	21	58	54	92	6
PASP, mm Hg	24.0 [21.0, 30.0]	30.0 [25.0, 36.8]	34.5 [27.0, 39.0]	35.5 [30.0, 45.0]	33.5 [28.5, 34.0]
n with data	21	58	54	92	6
TAPSE/PASP ratio, mm/mm Hg	0.90 [0.75, 1.04]	0.76 [0.59, 0.94]	0.68 [0.57, 0.82]	0.60 [0.47, 0.76]	0.76 [0.68, 0.80]
n with data	21	58	54	92	6
BNP, pg/mL	24.5 [13.8, 58.5]	30.0 [15.3, 63.8]	22.0 [12.0, 52.3]	37.0 [18.0, 73.3]	24.0 [10.0, 89.0]
n with data	16	54	52	82	5
Creatinine, mg/dL	0.75 [0.70, 1.03]	0.80 [0.70, 1.00]	0.80 [0.70, 0.90]	0.80 [0.63, 1.00]	0.95 [0.83, 1.08]
n with data	16	55	54	90	6
6MWD, m	411 ± 145	365 ± 80.4	353 ± 91.6	257 ± 121	269 ± 148
n with data	5	13	14	39	2
mMRC dyspnoea score, *n* (%)					
0	1 (4.8)	5 (8.6)	3 (5.6)	0 (0)	1 (17)
1	3 (14)	7 (12)	5 (9.3)	2 (2.2)	0 (0)
2	2 (10)	11 (19)	6 (11)	3 (3.3)	0 (0)
3	2 (10)	11 (19)	18 (33)	18 (20)	0 (0)
4	0 (0)	0 (0)	5 (9.3)	16 (17.4)	0 (0)
CAT score	23.0 [15.5, 25.8]	22.0 [14.0, 25.0]	26.5 [19.5, 30.0]	26.0 [21.8, 30.0]	13.0 [9.50, 16.5]
n with data	18	53	46	60	2
O_2 at rest (L/min)	3.00 [3.00, 3.00]	2.00 [2.00, 3.00]	2.00 [2.00, 2.00]	2.00 [2.00, 3.00]	3.00 [3.00, 3.00]
n with data[a]	2	12	18	70	1
Long-acting beta-agonist, *n* (%)					
Unknown	0 (0)	1 (1.7)	4 (7.4)	4 (4.3)	3 (50)
No	9 (43)	10 (17)	4 (7.4)	2 (2.2)	1 (17)
Yes	12 (57)	47 (81)	46 (85)	86 (93)	2 (33)
Long-acting muscarinic antagonist, *n* (%)					
Unknown	0 (0)	2 (3.4)	4 (7.4)	4 (4.3)	3 (50)
No	6 (29)	10 (17)	4 (7.4)	5 (5.4)	1 (17)
Yes	15 (71)	46 (79)	46 (85)	83 (90)	2 (33)

(Continued)

TABLE 1 | Continued

	GOLD stage				
	I ($n = 21$)	**II ($n = 58$)**	**III ($n = 54$)**	**IV ($n = 92$)**	**Unknown ($n = 6$)**
Inhaled corticosteroids, *n* (%)					
Unknown	0 (0)	2 (3.4)	6 (11)	4 (4.3)	4 (67)
No	12 (57)	27 (47)	10 (19)	9 (9.8)	0 (0)
Yes	9 (43)	29 (50)	38 (70)	79 (86)	2 (33)
Theophylline, *n* (%)					
Unknown	4 (19)	7 (12)	8 (15)	11 (12)	3 (50)
No	17 (81)	49 (84)	42 (78)	70 (76)	3 (50)
Yes	0 (0)	2 (3.4)	4 (7.4)	11 (12)	0 (0)
Roflumilast, *n* (%)					
Unknown	5 (24)	7 (12)	9 (17)	13 (14)	3 (50)
No	16 (76)	48 (83)	34 (63)	62 (67)	3 (50)
Yes	0 (0)	1 (1.7)	10 (19)	12 (13)	0 (0)
Discontinued	0 (0)	2 (3.4)	1 (1.9)	5 (5.4)	0 (0)

Data are presented as median [interquartile range], mean ± standard deviation or n (%). Numbers of patients with available data are shown in italics. 6MWD, 6-min walk distance; % pred, % predicted; BMI, body mass index; BNP, brain natriuretic peptide; CAT, COPD Assessment Test; DLCO, lung diffusing capacity for carbon monoxide; FEV_1, forced expiratory volume in 1 s; FVC, forced vital capacity; GOLD, Global Initiative for Obstructive Lung Disease; max, maximum; mMRC, modified Medical Research Council; O_2, oxygen; PASP, pulmonary artery systolic pressure; TAPSE, tricuspid annular plane systolic excursion; TLC, total lung capacity; VC, vital capacity. [a]A total of 103 patients received O_2 supplementation; all other patients did not receive O_2 supplementation.

TABLE 2 | Correlations with the TAPSE/PASP ratio in patients with COPD without pulmonary hypertension.

Parameter	**Pearson R**	***P*-value**	**Spearman rho**	***P*-value**
Age, years	−0.316	<0.001	−0.297	<0.001
CAT score	−0.141	0.06	−0.133	0.08
Pack years	−0.153	0.03	−0.089	0.2
6MWD, m	0.314	0.007	0.326	0.005
FEV_1, % pred	0.310	<0.001	0.340	<0.001
FEV_1/VC max	0.235	<0.001	0.277	<0.001
TLC, % pred	−0.123	0.07	−0.092	0.2
VC, % pred	0.281	<0.001	0.274	<0.001
FVC, % pred	0.246	<0.001	0.254	<0.001
DLCO, % pred	0.423	<0.001	0.414	<0.001

6MWD, 6-min walk distance; % pred, % predicted; CAT, COPD Assessment Test; DLCO, lung diffusing capacity for carbon monoxide; FEV_1, forced expiratory volume in 1 s; FVC, forced vital capacity; max, maximum; PASP, pulmonary artery systolic pressure; TAPSE, tricuspid annular plane systolic excursion; TLC, total lung capacity; VC, vital capacity.

most received monotherapy (94%) with a phosphodiesterase 5 inhibitor (84%) or an endothelin receptor antagonist (16%).

DISCUSSION

The present results show that disease severity in COPD and survival in PH-COPD are predicted by cor pulmonale (assessed as RV-PA uncoupling and decreased exercise capacity) rather than severity of PH or risk scores derived from PAH research. Among patients with low TAPSE/PASP and 6MWD, those who received targeted PH therapies had better survival than those without PH therapies, although statistical significance depended on the TAPSE/PASP and 6MWD thresholds used.

The notion of a right-sided phenotype of heart failure in patients with chronic lung diseases is not new. In 1963, a World Health Organization-sponsored expert consensus conference reviewed chronic lung diseases-associated PH as a cause of heart failure, and defined "cor pulmonale" as RV hypertrophy and dilatation resulting from diseases affecting the structure or function of the lungs (6). This morphological definition proved impractical, and cor pulmonale became better understood as altered RV structure and function with eventual right heart failure symptomatology caused by PH on a background of pulmonary disease, most commonly COPD (7–9). It is interesting that echocardiographic signs of cor pulmonale may be found in patients with COPD and minimally increased PAP, suggesting that factors other than only PH alter RV-PA coupling in COPD (20).

TABLE 3 | Baseline characteristics of patients with PH due to COPD.

	Mild-to-moderate PH due to COPD (*N* = 144)	Severe PH due to COPD (*N* = 130)
Age, years	72.0 [65.0, 76.3]	69.0 [64.0, 78.0]
n with data	144	130
Male sex, *n* (%)	86 (60)	84 (65)
n with data	144	130
Body mass index, kg/m^2	24.9 [21.5, 29.6]	24.3 [22.3, 27.6]
n with data	144	130
FEV_1, % pred	39.0 [28.8, 55.7]	50.5 [32.2, 68.2]
n with data	137	128
FEV_1/VC max	48.2 [40.2, 60.0]	55.2 [47.0, 65.5]
n with data	125	115
FVC, % pred	66.3 ± 21.6	72.2 ± 23.7
n with data	116	114
TLC, % pred	114 [99.0, 125]	105 [91.5, 117]
n with data	130	123
DLCO, % pred	40.2 [27.4, 50.7]	32.3 [24.6, 43.6]
n with data	71	80
mPAP, mm Hg	28.0 [26.0, 31.0]	40.0 [36.0, 46.0]
n with data	144	130
PVR, dyn·s/cm^5	299 [248, 368]	542 [427, 699]
n with data	130	107
Cardiac index, L/min/m^2	2.84 [2.45, 3.28]	2.40 [1.90, 2.86]
n with data	144	129
SvO_2, %	68.8 [64.2, 71.9]	64.5 [58.7, 69.4]
n with data	143	128
RAP, mm Hg	4.00 [2.00, 6.00]	5.50 [3.00, 9.00]
n with data	143	128
BNP, pg/mL	55.0 [23.0, 128]	165 [57.0, 355]
n with data	122	110
6MWD, m	271 ± 102	241 ± 105
n with data	110	101
TAPSE/PASP ratio, mm/mm Hg	0.407 [0.309, 0.555]	0.286 [0.207, 0.356]
n with data	88	91
Targeted PH therapy, *n* (%)		
No	82 (57)	30 (23)
Yes	57 (40)	93 (72)
Combination therapy	3 (2.1)	4 (3.1)
Monotherapy	54 (38)	89 (68)
Phosphodiesterase 5 inhibitor		
No	2 (1.4)	17 (13)
Yes	55 (38)	76 (58)
Endothelin receptor antagonist		
No	54 (38)	75 (58)
Yes	3 (2.1)	18 (14)

Data are presented as median [interquartile range], mean ± standard deviation or n (%). Numbers of patients with available data are shown in italics. 6MWD, 6-min walk distance; % pred, % predicted; BNP, brain natriuretic peptide; DLCO, lung diffusing capacity for carbon monoxide; FEV_1, forced expiratory volume in 1 s; FVC, forced vital capacity; max, maximum; mPAP, mean pulmonary artery pressure; PASP, pulmonary artery systolic pressure; PH, pulmonary hypertension; PVR, pulmonary vascular resistance; RAP, right atrial pressure; SvO_2, mixed venous oxygen saturation; TAPSE, tricuspid annular plane systolic excursion; TLC, total lung capacity; VC, vital capacity.

TABLE 4 | Univariate and multivariate Cox regression survival analyses.

Parameter	Univariate HR (95% CI)	Multivariate HR (95% CI)
Age	0.98 (0.96–1.00)	–
PVR (per 100 dyn·s/cm^5 increase)	1.10 (1.00–1.20)	1.06 (0.92–1.22)
TAPSE/PASP ratio	0.12 (0.03–0.57)	0.27 (0.04–1.94)[a]
BNP (per 100 pg/mL)	1.00 (0.97–1.10)	–
DLCO	0.99 (0.97–1.00)	–
FEV_1/VC max (per 10 units increase)	1.00 (0.91–1.20)	–
FEV_1 (per 10% pred increase)	0.96 (0.87–1.10)	–
FVC	0.99 (0.98–1.00)	0.99 (0.98–1.00)
TLC	0.99 (0.98–1.00)	–
6MWD (per 10 m increase)	0.95 (0.93–0.97)	0.95 (0.92–0.99)[a]
SvO_2	0.98 (0.95–1.00)	–
RAP	1.00 (0.97–1.00)	–
Cardiac index	0.90 (0.69–1.20)	–
mPAP (per 5 mm Hg increase)	1.10 (1.00–1.20)	1.00 (0.80–1.30)
Right atrial area	1.00 (0.99–1.10)	–
PH-COPD severity Severe vs. mild-to-moderate	1.32 (0.88–1.99)	–
ESC/ERS risk score Intermediate vs. low	1.32 (0.91–1.93)	–
High vs. low	2.34 (0.83–6.59)	–
BODE index[b] High (>6) vs. intermediate (3–6)	0.526 (0.287–0.962)	–

*6MWD, 6-min walk distance; % pred, % predicted; BNP, brain natriuretic peptide; BODE, body mass index, obstruction, dyspnoea and exercise capacity; DLCO, lung diffusing capacity for carbon monoxide; ESC/ERS, European Society of Cardiology and European Respiratory Society; FEV_1, forced expiratory volume in 1 s; FVC, forced vital capacity; HR, hazard ratio; mPAP, mean pulmonary artery pressure; PASP, pulmonary artery systolic pressure; PH-COPD, pulmonary hypertension due to COPD; PVR, pulmonary vascular resistance; RAP, right atrial pressure; SvO_2, mixed venous oxygen saturation; TAPSE, tricuspid annular plane systolic excursion; TLC, total lung capacity; VC, vital capacity. [a]Independently predicted mortality in a stepwise backward model [Step 4, HR (95% CI): TAPSE/PASP ratio, 0.22 (0.04–1.36); 6MWD per 10 m increase, 0.95 (0.92–0.98)]. [b]Kaplan–Meier analysis revealed significant differences in survival between the three BODE index groups (**Supplementary Figure 2**), but no HR was computable for patients with a low BODE index (≤2) due to the small sample size. The BODE index was not included in the multivariate Cox regression analysis owing to a high number of missing values.*

The clinical assessment of cor pulmonale traditionally relied on radionuclide angiography for measurements of RV volumes and derived ejection fraction (EF). This approach established that RVEF is depressed and/or fails to increase during exercise in up to 50% of patients with advanced COPD, and may improve with supplemental oxygen or a variety of pulmonary vasodilating interventions including aminophylline, β2 stimulant drugs or nitrates (8, 9). Radionuclide RVEF was found in one study of 115 patients with COPD to be weakly but significantly correlated to survival (21). Radionuclide angiography has since been replaced by cardiac magnetic resonance imaging (22) or echocardiography

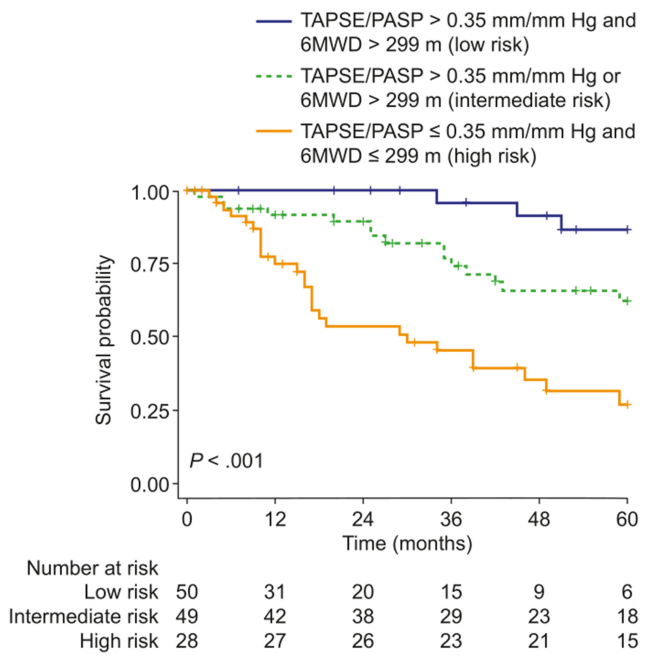

FIGURE 1 | Kaplan–Meier curves of survival probability in patients with pulmonary hypertension due to COPD stratified according to the presence/absence of two risk factors: 6MWD ≤299 m and/or TAPSE/PASP ratio ≤0.35 mm/mm Hg (thresholds determined by receiver operating characteristic analysis and Youden's index). 6MWD, 6-min walk distance; TAPSE/PASP, tricuspid annular plane systolic excursion/pulmonary artery systolic pressure.

(20) for the evaluation of cor pulmonale in COPD, but there has been no report of RVEF or any other measure of RV function as an independent predictor of outcome in patients with COPD.

In the present study, coupling of the right ventricle to afterload in COPD was assessed by simple 2D echocardiography. As recently reviewed, the right ventricle adapts to increased afterload by increasing contractility (23, 24). Therefore, correcting contractility (estimated by TAPSE) by an indirect measure of afterload (PASP) provides a more relevant assessment of RV function in patients with various forms of PH (10–14).

The present results confirm the importance of the TAPSE/PASP ratio in COPD both with and without PH. In COPD without PH, the TAPSE/PASP ratio correlated well with specific lung function parameters and 6MWD. Consistent with this finding, patients with a more advanced stage of COPD (mirrored by GOLD stages, mMRC score, need for oxygen supplementation, and presence of exacerbations leading to inpatient treatment) showed significantly reduced RV-PA coupling. In PH-COPD, the TAPSE/PASP ratio was an independent predictor of mortality, whereas the severity of PH alone was not prognostic. This may be a reason why all treatments that aim to decrease PVR or PAP have thus far failed to improve the prognosis of patients with PH-COPD (1).

The most recent proposed classification of severity of PH-COPD from the 6th World Symposium on PH attempts to identify those patients with advanced pulmonary vascular disease who might benefit from the cautious use of targeted therapies, preferably in controlled studies (1). Our patients with moderate or severe PH had a typical profile of high PAP but relatively limited alteration in lung function tests (2–4). It is therefore understandable that targeted PH therapies were prescribed for the treatment of significant pulmonary vascular disease or PAH co-morbidity (1). This strategy was not associated with a detectable effect on outcome when the patient population was analyzed as a whole. However, PH therapy was associated with increased survival in a subgroup analysis of patients in the lowest or intermediate tertiles of both TAPSE/PASP and 6MWD. These results suggest that future trials of targeted PH therapies in PH-COPD should recruit patients with more advanced RV-PA uncoupling, focusing on cor pulmonale rather than the severity of PH *per se*.

Exercise capacity is markedly reduced in COPD, in proportion to severity of the disease as assessed by the GOLD staging system (25). In a study of 365 patients with COPD, mortality was high (47% during a mean follow-up period of 5.5 years) and was predicted equally well by 6MWD and peak oxygen uptake (26). In another study of 362 patients with COPD who underwent cardiac catheterization and a 6MWD test as part of evaluation for lung transplantation, the prevalence of PH (mPAP >25 mm Hg and pulmonary arterial occlusion pressure <16 mm Hg) was 23% and 6MWD declined by 11 m for every 5 mm Hg rise in mPAP, but with borderline significance ($p = 0.04$) (27). A smaller study of 29 patients with advanced stable COPD showed no significant association between mPAP and exercise capacity (28). Decreased exercise capacity in COPD is mainly related to a ventilatory limitation (26, 28), but analysis of convective and diffusive oxygen transport mechanisms also disclosed a possible influence of cardiac output on skeletal muscle oxygen extraction (29). The present results show the relevance of RV-PA uncoupling in patients with PH-COPD; this could be a possible cause of the cardiac output limitation seen during exercise.

Recent studies have suggested that DLCO is an important predictor of mortality in patients with PH due to chronic lung disease (30, 31). However, univariate Cox regression analysis indicated that DLCO is not associated with 5-year survival in our study cohort. Although the underlying reason for the observed difference cannot be directly assessed in a retrospective cohort analysis, our study supports a role for DLCO as a predictor of short-term mortality.

There are several limitations to the present findings. The study was conducted at a single centre in Germany; the study population may therefore not be representative of the wider population with COPD. The generalizability of the results is also affected by referral bias, as the patients were evaluated at the request of their physicians for a suspicion of PH. Furthermore, only few patients in the high-risk group did not receive targeted PH therapies, and conclusions regarding the efficacy of PH therapies cannot be drawn from

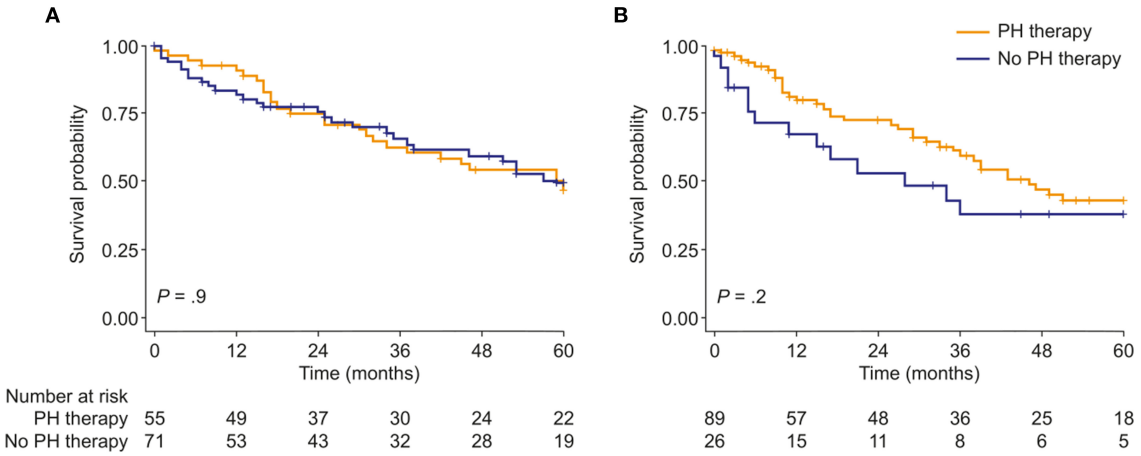

FIGURE 2 | Kaplan–Meier curves of survival probability in patients with either **(A)**, mild-to-moderate or **(B)**, severe PH due to COPD, stratified by use of targeted PH therapy. PH, pulmonary hypertension.

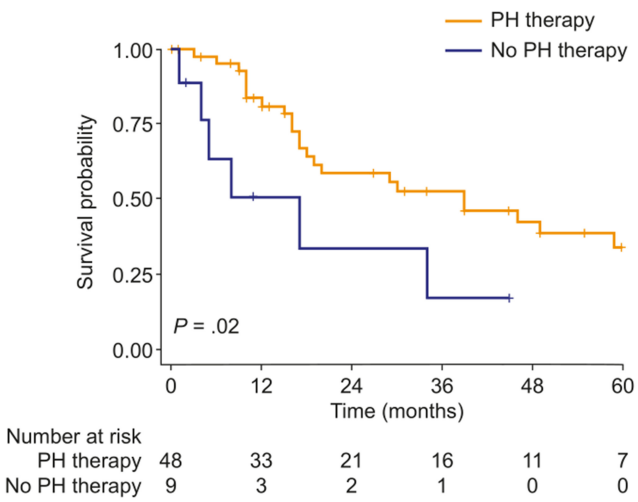

FIGURE 3 | Kaplan–Meier curves of survival probability in patients with PH due to COPD with both TAPSE/PASP and 6MWD values in the lowest or intermediate tertile, stratified by use of targeted PH therapy. 6MWD, 6-min walk distance; PH, pulmonary hypertension; TAPSE/PASP, tricuspid annular plane systolic excursion/pulmonary artery systolic pressure.

this retrospective cohort study. Nevertheless, the data draw attention to the relevance of cor pulmonale in patients with COPD, and support the enrichment of future clinical trial populations for patients with very low TAPSE/PASP and 6MWD.

Overall, we have provided evidence that cor pulmonale [assessed as RV-PA uncoupling (TAPSE/PASP ratio) and decreased exercise capacity (6MWD)] is associated with disease severity in COPD and prognosis in PH-COPD. Further studies are needed to assess the effect of targeted PH therapy in patients with PH-COPD and low TAPSE/PASP and 6MWD.

DATA AVAILABILITY STATEMENT

The raw data supporting the conclusions of this article will be made available by the authors, without undue reservation.

ETHICS STATEMENT

The studies involving human participants were reviewed and approved by University of Giessen institutional review board (#266/11), Klinikstraße 29, 35392 Gießen. The patients/participants provided their written informed consent to participate in this study.

AUTHOR CONTRIBUTIONS

AY, MR, and KT conceived the idea for the analyses detailed in this manuscript. AY undertook statistical analyses of the data in the manuscript. All authors contributed to the design, data collection in the study, drafting and critical review of the manuscript, and approved the manuscript for submission.

FUNDING

This study was funded by the Deutsche Forschungsgemeinschaft (DFG, German Research Foundation) – Projektnummer 268555672 – SFB 1213, Project B08. Editorial assistance was provided by Claire Mulligan, PhD (Beacon Medical Communications Ltd, Brighton, UK), funded by the University of Giessen.

SUPPLEMENTARY MATERIAL

The Supplementary Material for this article can be found online at: https://www.frontiersin.org/articles/10.3389/fcvm.2022.826369/full#supplementary-material

REFERENCES

1. Nathan SD, Barbera JA, Gaine SP, Harari S, Martinez FJ, Olschewski H, et al. Pulmonary hypertension in chronic lung disease and hypoxia. *Eur Respir J.* (2019) 53:1801914. doi: 10.1183/13993003.01914-2018
2. Andersen KH, Iversen M, Kjaergaard J, Mortensen J, Nielsen-Kudsk JE, Bendstrup E, et al. Prevalence, predictors, and survival in pulmonary hypertension related to end-stage chronic obstructive pulmonary disease. *J Heart Lung Transplant.* (2012) 31:373–80. doi: 10.1016/j.healun.2011.11.020
3. Chaouat A, Bugnet AS, Kadaoui N, Schott R, Enache I, Ducolone A, et al. Severe pulmonary hypertension and chronic obstructive pulmonary disease. *Am J Respir Crit Care Med.* (2005) 172:189–94. doi: 10.1164/rccm.200401-006OC
4. Thabut G, Dauriat G, Stern JB, Logeart D, Levy A, Marrash-Chahla R, et al. Pulmonary hemodynamics in advanced COPD candidates for lung volume reduction surgery or lung transplantation. *Chest.* (2005) 127:1531–6. doi: 10.1378/chest.127.5.1531
5. Bishop JM. Hypoxia and pulmonary hypertension in chronic bronchitis. *Prog Respir Res.* (1975) 9:10–6. doi: 10.1159/000398158
6. Dankmeijer J, Herles F, Ibrahim M, Reid DD, Richards DW, Stuart- Harris CH, et al. Chronic Cor Pulmonale. World health organization technical report series No. 213. *Circulation.* (1963) 27:594–615. doi: 10.1161/01.CIR.27.4.594
7. Fishman AP. State of the art: chronic cor pulmonale. *Am Rev Respir Dis.* (1976) 114:775–94. doi: 10.1164/arrd.1976.114.4.775
8. MacNee W. Pathophysiology of cor pulmonale in chronic obstructive pulmonary disease. Part One. *Am J Respir Crit Care Med.* (1994) 150:833–52. doi: 10.1164/ajrccm.150.3.8087359
9. MacNee W. Pathophysiology of cor pulmonale in chronic obstructive pulmonary disease. Part two. *Am J Respir Crit Care Med.* (1994) 150:1158–68. doi: 10.1164/ajrccm.150.4.7921453
10. Guazzi M, Dixon D, Labate V, Beussink-Nelson L, Bandera F, Cuttica MJ, et al. RV contractile function and its coupling to pulmonary circulation in heart failure with preserved ejection fraction: stratification of clinical phenotypes and outcomes. *JACC Cardiovasc Imag.* (2017) 10:1211–21. doi: 10.1016/j.jcmg.2016.12.024
11. Tello K, Wan J, Dalmer A, Vanderpool R, Ghofrani HA, Naeije R, et al. Validation of the tricuspid annular plane systolic excursion/systolic pulmonary artery pressure ratio for the assessment of right ventricular-arterial coupling in severe pulmonary hypertension. *Circ Cardiovasc Imag.* (2019) 12:e009047. doi: 10.1161/CIRCIMAGING.119.009047
12. Tello K, Ghofrani HA, Heinze C, Krueger K, Naeije R, Raubach C, et al. A simple echocardiographic estimate of right ventricular-arterial coupling to assess severity and outcome in pulmonary hypertension on chronic lung disease. *Eur Respir J.* (2019) 54:1802435. doi: 10.1183/13993003.02435-2018
13. Guazzi M, Bandera F, Pelissero G, Castelvecchio S, Menicanti L, Ghio S, et al. Tricuspid annular plane systolic excursion and pulmonary arterial systolic pressure relationship in heart failure: an index of right ventricular contractile function and prognosis. *Am J Physiol Heart Circ Physiol.* (2013) 305:H1373–81. doi: 10.1152/ajpheart.00157.2013
14. Tello K, Axmann J, Ghofrani HA, Naeije R, Narcin N, Rieth A, et al. Relevance of the TAPSE/PASP ratio in pulmonary arterial hypertension. *Int J Cardiol.* (2018) 266:229–35. doi: 10.1016/j.ijcard.2018.01.053
15. Galie N, Humbert M, Vachiery JL, Gibbs S, Lang I, Torbicki A, et al. 2015 ESC/ERS Guidelines for the diagnosis and treatment of pulmonary hypertension: the joint task force for the diagnosis and treatment of pulmonary hypertension of the European society of cardiology (ESC) and the European respiratory society (ERS): endorsed by: association for European paediatric and congenital cardiology (AEPC), international society for heart and lung transplantation (ISHLT). *Eur Respir J.* (2015) 46:903–75. doi: 10.1183/13993003.01032-2015
16. Yogeswaran A, Tello K, Faber M, Sommer N, Kuhnert S, Seeger W, et al. Risk assessment in severe pulmonary hypertension due to interstitial lung disease. *J Heart Lung Transplant.* (2020) 39:1118–25. doi: 10.1016/j.healun.2020.06.014
17. Gall H, Felix JF, Schneck FK, Milger K, Sommer N, Voswinckel R, et al. The giessen pulmonary hypertension registry: survival in pulmonary hypertension subgroups. *J Heart Lung Transplant.* (2017) 36:957–67. doi: 10.1016/j.healun.2017.02.016
18. Yogeswaran A, Richter MJ, Sommer N, Ghofrani HA, Seeger W, Gall H, et al. Evaluation of pulmonary hypertension by right heart catheterisation: does timing matter? *Eur Respir J.* (2020) 56:1901892. doi: 10.1183/13993003.01892-2019
19. Hoeper MM, Kramer T, Pan Z, Eichstaedt CA, Spiesshoefer J, Benjamin N, et al. Mortality in pulmonary arterial hypertension: prediction by the 2015 European pulmonary hypertension guidelines risk stratification model. *Eur Respir J.* (2017) 50:1700740. doi: 10.1183/13993003.00740-2017
20. Hilde JM, Skjorten I, Grotta OJ, Hansteen V, Melsom MN, Hisdal J, et al. Right ventricular dysfunction and remodeling in chronic obstructive pulmonary disease without pulmonary hypertension. *J Am Coll Cardiol.* (2013) 62:1103–11. doi: 10.1016/j.jacc.2013.04.091
21. France AJ, Prescott RJ, Biernacki W, Muir AL, MacNee W. Does right ventricular function predict survival in patients with chronic obstructive lung disease? *Thorax.* (1988) 43:621–6. doi: 10.1136/thx.43.8.621
22. Gao Y, Du X, Qin W, Li K. Assessment of the right ventricular function in patients with chronic obstructive pulmonary disease using MRI. *Acta Radiol.* (2011) 52:711–5. doi: 10.1258/ar.2011.100449
23. Sanz J, Sanchez-Quintana D, Bossone E, Bogaard HJ, Naeije R. Anatomy, function, and dysfunction of the right ventricle: JACC state-of-the-art review. *J Am Coll Cardiol.* (2019) 73:1463–82. doi: 10.1016/j.jacc.2018.12.076
24. Vonk Noordegraaf A, Chin KM, Haddad F, Hassoun PM, Hemnes AR, Hopkins SR, et al. Pathophysiology of the right ventricle and of the pulmonary circulation in pulmonary hypertension: an update. *Eur Respir J.* (2019) 53:1801900. doi: 10.1183/13993003.01900-2018
25. Pinto-Plata VM, Celli-Cruz RA, Vassaux C, Torre-Bouscoulet L, Mendes A, Rassulo J, et al. Differences in cardiopulmonary exercise test results by American thoracic society/European respiratory society-global initiative for chronic obstructive lung disease stage categories and gender. *Chest.* (2007) 132:1204–11. doi: 10.1378/chest.07-0593
26. Cote CG, Pinto-Plata V, Kasprzyk K, Dordelly LJ, Celli BR. The 6-min walk distance, peak oxygen uptake, and mortality in COPD. *Chest.* (2007) 132:1778–85. doi: 10.1378/chest.07-2050
27. Sims MW, Margolis DJ, Localio AR, Panettieri RA, Kawut SM, Christie JD. Impact of pulmonary artery pressure on exercise function in severe COPD. *Chest.* (2009) 136:412–9. doi: 10.1378/chest.08-2739
28. Pynnaert C, Lamotte M, Naeije R. Aerobic exercise capacity in COPD patients with and without pulmonary hypertension. *Respir Med.* (2010) 104:121–6. doi: 10.1016/j.rmed.2009.06.006
29. Broxterman RM, Hoff J, Wagner PD, Richardson RS. Determinants of the diminished exercise capacity in patients with chronic obstructive pulmonary disease: looking beyond the lungs. *J Physiol.* (2020) 598:599–610. doi: 10.1113/JP279135
30. Balasubramanian A, Kolb TM, Damico RL, Hassoun PM, McCormack MC, Mathai SC. Diffusing capacity is an independent predictor of outcomes in pulmonary hypertension associated with COPD. *Chest.* (2020) 158:722–34. doi: 10.1016/j.chest.2020.02.047
31. Rose L, Prins KW, Archer SL, Pritzker M, Weir EK, Misialek JR, et al. Survival in pulmonary hypertension due to chronic lung disease: influence of low diffusion capacity of the lungs for carbon monoxide. *J Heart Lung Transplant.* (2019) 38:145–55. doi: 10.1016/j.healun.2018.09.011

Conflict of Interest: AY reports non-financial support from the University of Giessen during the conduct of the study. SK reports personal fees from Chiesi, Berlin Chemie MENARINI and Insmed, and personal fees and non-financial support from GSK, Novartis and AstraZeneca outside the submitted work. HG reports grants from the German Research Foundation and non-financial support from the University of Giessen during the conduct of the study, and personal fees from Actelion, AstraZeneca, Bayer, BMS, GSK, Janssen-Cilag, Lilly, MSD, Novartis, OMT, Pfizer and United Therapeutics outside the submitted work. MF reports non-financial support from the University of Giessen during the conduct of the study. HG reports grants from the German Research

Foundation and nonfinancial support from the University of Giessen during the conduct of the study, and personal fees from Bayer, Actelion, Pfizer, Merck, GSK and Takeda, grants and personal fees from Novartis, Bayer HealthCare and Encysive/Pfizer, and grants from Aires, the German Research Foundation, Excellence Cluster Cardiopulmonary Research and the German Ministry for Education and Research outside the submitted work. RN reports relationships including consultancies, speaker's fees and membership of advisory boards with AOP Orphan Pharmaceuticals, Johnson & Johnson, Lung Biotechnology Corporation and United Therapeutics. WS reports grants from the German Research Foundation and nonfinancial support from the University of Giessen during the conduct of the study, and personal fees from Pfizer and Bayer Pharma AG outside the submitted work. MR reports grants from the German Research Foundation and non-financial support from the University of Giessen during the conduct of the study, and grants from United Therapeutics, grants and personal fees from Bayer, and personal fees from Actelion, Mundipharma, Roche and OMT outside the submitted work. KT reports grants from the German Research Foundation and non-financial support from the University of Giessen during the conduct of the study, and personal fees from Actelion and Bayer outside the submitted work.

The remaining authors declare that the research was conducted in the absence of any commercial or financial relationships that could be construed as a potential conflict of interest.

frontiers in Cardiovascular Medicine

REVIEW
published: 17 February 2022
doi: 10.3389/fcvm.2022.841928

Diabetes and Its Cardiovascular Complications: Comprehensive Network and Systematic Analyses

*Hao Wu[1†], Vikram Norton[1†], Kui Cui[1], Bo Zhu[1], Sudarshan Bhattacharjee[1], Yao Wei Lu[1], Beibei Wang[1], Dan Shan[1], Scott Wong[1], Yunzhou Dong[1], Siu-Lung Chan[1], Douglas Cowan[1], Jian Xu[2], Diane R. Bielenberg[1], Changcheng Zhou[3] and Hong Chen[1]**

[1] Department of Surgery, Vascular Biology Program, Harvard Medical School, Boston Children's Hospital, Boston, MA, United States, [2] Department of Medicine, Harold Hamm Diabetes Center, University of Oklahoma Health Sciences Center, Oklahoma, OK, United States, [3] Division of Biomedical Sciences, School of Medicine, University of California, Riverside, Riverside, CA, United States

Diabetes mellitus is a worldwide health problem that usually comes with severe complications. There is no cure for diabetes yet and the threat of these complications is what keeps researchers investigating mechanisms and treatments for diabetes mellitus. Due to advancements in genomics, epigenomics, proteomics, and single-cell multiomics research, considerable progress has been made toward understanding the mechanisms of diabetes mellitus. In addition, investigation of the association between diabetes and other physiological systems revealed potentially novel pathways and targets involved in the initiation and progress of diabetes. This review focuses on current advancements in studying the mechanisms of diabetes by using genomic, epigenomic, proteomic, and single-cell multiomic analysis methods. It will also focus on recent findings pertaining to the relationship between diabetes and other biological processes, and new findings on the contribution of diabetes to several pathological conditions.

Keywords: diabetes, comprehensive network, system analysis, cardiovascular disease complications, peripheral artery disease

OPEN ACCESS

Edited by:
Jingyan Han,
Boston University, United States

Reviewed by:
Yuqing Huo,
Augusta University, United States
Yi Tan,
University of Louisville, United States

****Correspondence:***
Hong Chen
Hong.chen@childrens.harvard.edu

[†] These authors have contributed equally to this work

Specialty section:
This article was submitted to General Cardiovascular Medicine, a section of the journal Frontiers in Cardiovascular Medicine

Received: *06 January 2022*
Accepted: *18 January 2022*
Published: *17 February 2022*

Citation:
Wu H, Norton V, Cui K, Zhu B, Bhattacharjee S, Lu YW, Wang B, Shan D, Wong S, Dong Y, Chan S-L, Cowan D, Xu J, Bielenberg DR, Zhou C and Chen H (2022) Diabetes and Its Cardiovascular Complications: Comprehensive Network and Systematic Analyses. Front. Cardiovasc. Med. 9:841928. doi: 10.3389/fcvm.2022.841928

INTRODUCTION

Diabetes mellitus is a critical public health issue that causes incapacitation and mortality in both acute and chronic complications of the disease. It affects various races and populations. The prevalence of diabetes in adults globally was ∼6.4% in 2010 and was predicted to rise to 7.7% in 2030 (1). Diabetes in general is a chronic metabolic disease, characterized by β-cell dysfunction and/or insulin resistance and hyperglycemia.

Diabetes mellitus is classified as a spectrum of metabolic disorders in which the American Diabetes Association (ADA) divides into four categories: type 1 diabetes (T1D), type 2 diabetes (T2D), monogenic diabetes (MD) and gestational diabetes (GD). T1D is an autoimmune illness that is caused by the beta cells of the pancreas' Langerhans islets being destroyed. These beta cells secrete insulin, and thus insulin has to be used throughout T1D patient lives. T1D accounts for around 5–10% of all diabetic cases. Insulin resistance and impaired secretion, as well as increased hepatic glucose synthesis, are all pathological symptoms of T2D. Approximately 90% of diabetics have T2D (2). In fact, over 29 million people in the US have T2D. Many risk factors, both genetic and non-genetic, have been identified that play a role in the process of T2D. For example: obesity, physical inactivity, advanced age, hypertension, hyperlipidemia, and family history are all risk

factors. Furthermore, cardiovascular disease, stroke, periodontal disease, neuropathy, retinopathy, foot ulcers, and amputations are well studied complications associated with T2D (3).

Monogenic diabetes is caused by a defect in a single gene and often has a similar clinical presentation to T1D and T2D. Gestational diabetes was once considered to be an early stage of T2D (3). Now it is thought that there is increased susceptibility to T2D enabled by pregnancy-induced insulin resistance which is characteristic of gestational diabetes. After the patient has given birth, typically their glucose levels will return to normal.

The significant health consequences of diabetes have led to an emphasis on early identification, management and treatment strategies for diabetic patients. In this review, we will summarize recent findings on the mechanisms of diabetes that have used genomic, epigenomic, proteomic, and multiomics single-cell analysis methods (4, 5). Given the huge contribution of cardiovascular complications to the severity in outcome of diabetes, we will also discuss recent findings on the relationship between diabetes and the physiological systems it affects, such as lymphangiogenesis, angiogenesis, gut microbiota diversity, and more. With further research being done in these areas, we will be better equipped to therapeutically intervene in the development of diabetes and its associated cardiovascular complications.

ADVANCEMENT IN ELUCIDATING THE MECHANISMS OF DIABETES

Genomics Research

Genomic analysis to detect risks for chronic diseases such as diabetes is quickly progressing in the clinical setting, thanks to the use of next-generation sequencing technology including whole-genome sequencing.

T1D is a multifaceted disorder with genetic and environmental risk factors. In the last several decades, numerous studies have been conducted to identify T1D-susceptibility genes in which more than 40 different genetic loci associated with T1D have been identified (6, 7). The human leukocyte antigen (HLA) area on chromosome 6p21, protein tyrosine phosphatase non-receptor type 22 (PTPN22) on 1p13, interleukin 2 receptor subunit alpha (IL2RA) on 10p15, the insulin gene (INS-VNTR) locus on 11p15, as well as the cytotoxic T-lymphocyte associated protein 4 (CTLA4) locus on 2q33 are all among the different genetic loci associated with T1D (8). CTLA4 is an immunoglobulin that plays an important role in the pathogenesis of autoimmune disorders like T1D (9). The interleukin-2 receptor complex's -chain is encoded by the IL2RA gene, which has eight exons. In regulatory T-cells, the expression of IL2RA is essential in controlling the immune response and preventing autoimmune disease (10). Recently, several studies have been conducted and found the frequency of them in different populations to be very different (11, 12).

T2D is a complex disease that leads to serious consequences. Thus, there has been an emphasis on early identification of individuals at high risk for T2D. Several clinical factors correlated with T2D risk that can be identified early on include body mass index (BMI), age, and family history. With the advancement in genomics, including genomic factors in risk assessment and management could make risk prediction and treatment of T2D more precise.

Around 40% of the risk, onset, and progression of diabetes is due to genetic factors, which varies from person to person (13). There have been more than 50 loci associated with T2D risk identified by the Genome Wide Association Studies (GWAS) since 2007 (14–17). Several genes associated in insulin production, glucose metabolism, and beta-cell activity have been identified. One study (18) found the association of 21 genetic variants with T2D and confirmed that individuals with a high genetic score had an increased risk of T2D. The study (18) looked at 65 single nucleotide polymorphisms (SNPs), seven of which were found in four genes which are Gli-similar 3 (GLIS3), transcription factor-7–like 2 (TCF7L2), leucine rich repeat containing G protein-coupled receptor 5 (LGR5), and protein tyrosine phosphatase receptor type D (PTPRD). These 7 SNPs were strongly associated with T2D. GLIS3 is a diabetes susceptibility gene that participates in the propagation of pancreatic beta cells. TCF7L2 was observed to have a relationship with BMI and has been demonstrated to affect β-cell responsiveness to insulin.

Furthermore, because oral anti-hyperglycemic drugs are affected by pharmacogenomic variation in a high number of T2D patients, research suggests genomics could play a role in choosing the most successful therapy (19). Several studies have revealed that genetic variations are involved in drug absorption, transport, metabolism, and action, and that these variations may alter drug pharmacokinetics or pharmacodynamics (20, 21). Since the susceptibility loci, identified by GWAS, for T2D mellitus alter insulin secretion and/or sensitivity, they may also influence the efficacy of the insulin secretagogue and/or sensitizer. The potassium voltage-gated channel subfamily Q member 1 (KCNQ1) gene, for example, has been linked to repaglinide and rosiglitazone efficacy in East Asians and at the same time confers the highest risk of T2D Mellitus in East Asians (22, 23).

In overall, existing knowledge of the role of genetic variables in diabetes supports the notion that diabetes is a complicated disease that differs from person to person. In addition, important information on the genetic underpinnings for various therapeutic responses to pharmacologic therapy is now being discovered. With increasing knowledge about the importance of genetic information in the onset, progression and treatment of diabetes, genome-based strategies can be considered to improve the risk prediction and customized management of individual patients. Both of which will contribute to better health outcomes for diabetic patients.

Epigenetics Research

In the past few years it has been determined that mainly environmental factors have been considered as predisposing factors for weight gain or the development of T2D (24). Despite significant efforts to find genetic susceptibility variations, little progress has been made, and the common genetic variables that cause diabetes susceptibility can only account for a small portion of individual risk variants. In addition, there is evidence

that the current diabetes epidemic is driven by environmental factors. Recent studies have shown that in addition to a good balance between energy intake and energy expenditure, normal metabolic regulation in adulthood is also affected by the pre- and post-natal environment. In fact, maternal calorie restriction during pregnancy can alter the metabolic phenotype of their children by epigenetic control of certain genes, which can be passed down to future generations. Thus, it is important to identify the epigenetic markers of diabetes and the methylation and/or histone acetylation levels of genes involved in metabolic processes. Recent studies have pointed out that endocrine disruptors, which are chemicals that interfere with many homeostatic mechanisms, play a role in the high incidence of diabetes. Given the existing data on the effects of endocrine disruptors such as obesogens, it seems that exposure to these disruptors may play an important role in the diabetes pandemic (24).

Epigenetics has been defined as a heritable change in gene function without changes in the nucleotide sequence, however this is not a universal definition (25). Epigenetic changes can be handed down from one cell generation to the next (mitotic inheritance) as well as between generations of species (meiotic inheritance). Epigenetics can be affected by the environment, which makes it a potentially important pathogenic mechanism for complex multifactorial diseases such as T2D (**Figure 1**). DNA methylation, histone modification, and microRNA are all epigenetic factors that can help explain how cells with the same DNA differentiate into different cell types with different phenotypes (26), all of which aid in explaining how cells with identical DNA differentiate into different cell types with different phenotypes. DNA methylation and histone modification, in particular, are important in the pathogenesis of T2D.

DNA methylation necessitates the activity of methyltransferases, of which there are two types: DNA methyltransferase 1 (DNMT1), which replicates the DNA methylation pattern (maintains methylation) between cell generations during replication, and DNA methyltransferase 3A (DNMT3a) and DNA methyltransferase 3 beta (DNMT3b), which are both responsible for DNA de novo methylation (27). The way in which this DNA methylation occurs is still poorly understood and needs further research if we are to understand the mechanisms behind the pathogenesis of T2D. For recent research on DNA methylation, see Patra et al. (28). Examples of ways to determine these genetic signals include using the Chromatin analysis methods, such as ATAC-seq and DNase-seq, which have been applied to a large number of islets to generate aggregated spectra that mask important cells and regulate heterogeneity (29, 30). In addition, GWAS have been able to identify >400 independent signals that encode genetic predispositions for T2D (31). Finally, more than 90% of linked SNPs are found in non-coding regions and contain chromatin-defined islet enhancer elements, indicating the presence of significant transcriptional regulatory components for diabetes disease risk (32).

Histone modification starts with the formation of chromatin. The nucleosome, which consists of around 147 DNA base pairs surrounding histone octamers, is the most fundamental component of chromatin. Histone octamers are composed of H3-H4 tetramers, with one H2A-H2B dimer on each side. Although the core histones are densely packed, histone modifying enzymes can alter their NH2 terminal tails, causing acetylation, methylation, phosphorylation, SUMO acylation, or ubiquitination (33). An example of this modification involves histone modifying enzyme HDAC which has been shown to remove histone acetyltransferase (HAT) and add acetyl groups (33–35) to lysine residues in the tail of histones. Although enhanced HAT activity and histone acetylation have been linked to increased gene transcription, the exact mechanism that promotes transcription is unknown (36). On top of this, histone methyltransferases and histone demethylases have been shown to mediate HAT activity (37). Taken together, understanding how histone modification and acetylation are regulated is important for determining the transcription mechanism's access to DNA, as well as DNA replication, recombination, and chromosomal organization, all of which are crucial in understanding its relationship to T2D.

Proteomics Research

Integrative profiling of proteins expressed in cells, tissues, and organs has been done using proteomics. Proteomics research has provided potential tools for the systematic investigation of proteins that are differently expressed between healthy individuals and cancer patients (38), as well as Alzheimer's disease (39) and diabetes patients (40). Proteomics has been widely used in diabetes studies focusing on different stages of diabetes with diverse sample sources.

A longitudinal study of the human plasma proteome discovered possible protein indicators in T1D progression, resulting in a promising list of protein markers that dysregulate temporally before islet autoimmunity develops. (41). Key enzymes against oxidative stress, CAT and SOD1, were identified (41). Eri Takahashi et al. (42) carried out serum proteomics using a T2D mouse model and identified differentially expressed proteins in the prediabetic state, among which the level of serine protease inhibitor (SERPIN)A3 was found to be elevated significantly. This change was also confirmed to be increased in T2D patients, indicating SERPINA3 could be used for the early detection of type 2 diabetes mellitus (42).

Proteomic analysis of human islets from patients with T1D was also carried out (43). Upon human pancreatic islets being exposed to palmitate, lipidomics and proteomics were done which revealed proteins implicated in the action of saturated fatty acids as well as potential pathways for how chronic saturated free fatty acids disrupt beta-cells and lead to the development of T2D mellitus (44).

Adipose tissue is an endocrine organ secreting multiple bioactive factors such as leptin, tumor necrosis factor-α and interleukin-6, all of which influence insulin resistance and β-cell dysfunction (45). White adipose tissue (WAT) and brown adipose tissue (BAT) are two types of adipose tissue that are linked to the development of metabolic diseases. As a result of these studies, differentially expressed proteins involved in cytoskeleton function and structure, oxidative stress,

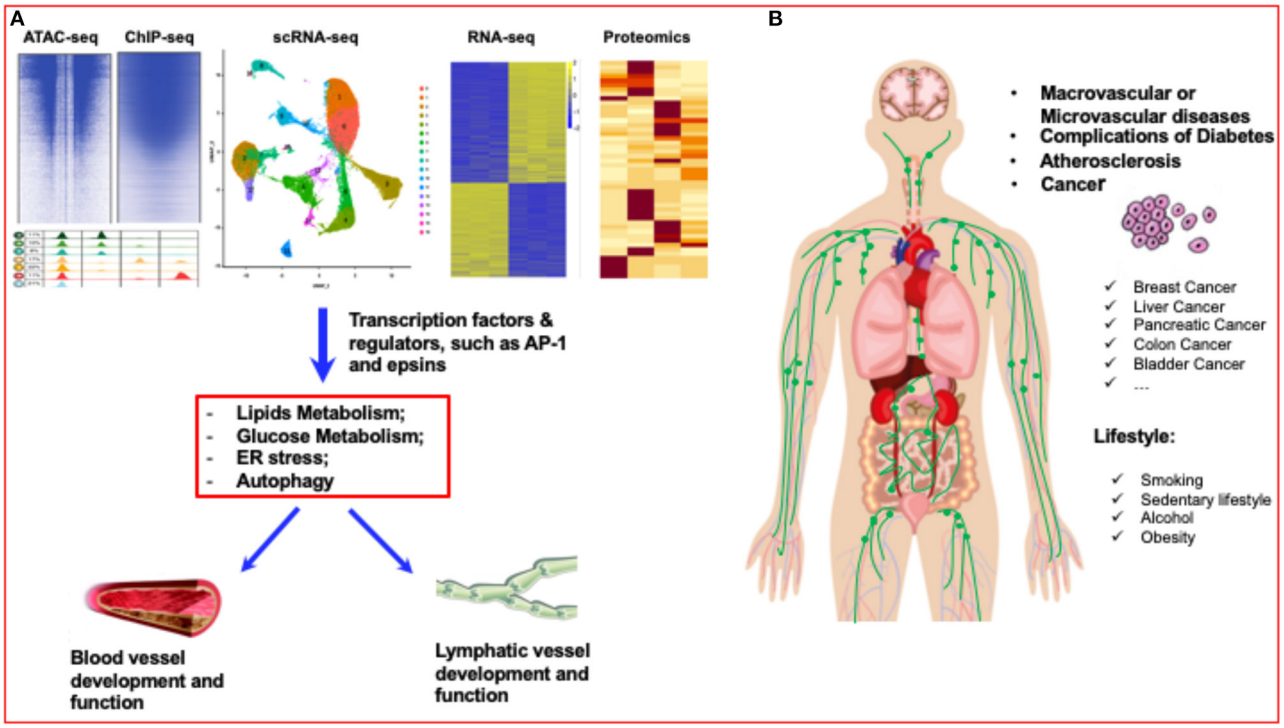

FIGURE 1 | Diabetes research has entered a new era of single-cell biology. **(A)** Single-cell analysis has entered the multiomics age. By using multiomics single-cell analysis, such as ATAC-seq, ChIP-seq, scRNA-seq, RNA-seq and proteomics analysis, the transcriptome factors or regulators of blood vessels and lymphatic vessels can be accurately identified. **(B)** Lifestyles, such as smoking, sedentary lifestyle, alcohol, and obesity can significantly affect the vascular diseases, such as atherosclerosis, diabetes, even including different cancers.

inflammation, and retinoid metabolism have been identified in TD-related adipose tissues (46–48).

Proteomic analysis of protein expression in diabetic patient samples provides detailed qualitative and quantitative information on the proteins implicated in the course of diabetes. This could potentially yield pathomechanistic insights and lead to the development of new therapeutic targets for diabetes intervention. The importance of such promising potential markers warrants greater investigation and research.

Single-Cell Multiomic Analysis

Characterizing the transcriptome profile of a single cell through single-cell RNA sequencing (scRNA-Seq) has become a universal tool for identifying known and new cell types, as well as understanding tissue structure and function, ushering in a new era of single-cell biology (4, 5, 49) (**Figure 1**). This has been shown to be especially true in complex organs and tissues with a high degree of cellular heterogeneity, such as mammalian brains and tumors (50, 51).

In the past few years, using scRNA-Seq to analyze pancreas cells at the individual level has made great strides. Among them, exciting discoveries have been made in the immunology of T1D and T2D. For example, scRNA-Seq analysis has shown that increased expression of the anion transporter SLC26A9 delayed the onset of cystic fibrosis diabetes, a unique type of diabetes that has similar characteristics to T1D and T2D (52).

ScRNA-seq has also been shown to be useful in the cellular characteristics of human *in vitro* β cell differentiation, providing a perspective for the use of human stem cell differentiation as a useful therapeutic that could guide future efforts to focus on islet cell differentiation and regeneration in diabetic models (53). The single-cell transcriptome analysis of the human ductal tree indicates that progenitors might be activated *in situ* for therapeutic purposes (54). Other successful examples include a study done by Baron and Muraro et al. who used scRNA-Seq to deconvolute a large number of human and mouse pancreas gene expression samples to detect disease-related differential expression. The data set provided resources for discovering new cell type-specific transcription factors, signal receptors, and medical-related genes in human and mouse pancreases (55, 56). Another research team conducted single-cell transcriptomics analysis of the human endocrine pancreas and also demonstrated the powerful functions of single-cell RNA-seq (57).

T2D is a complex disease characterized by pancreatic islet dysfunction, insulin resistance, and blood sugar level disturbances (**Figure 2**). Pancreatic islets are a mixture of cell types expressing different hormonal programs, so each cell type may contribute differently to the underlying regulatory processes that regulate T2D-related transcription circuits. There are many ways to use genetic signals of T2D to identify the type of activity undergone by islet cells and to provide higher-resolution mechanical insights into genetically encoded risk pathways for

T2D. Single-cell genomics has exploded in popularity during the last decade. The most prevalent technique is single-cell RNA sequencing (RNA-seq), which assesses gene expression. Other approaches examine methylation, genetic variation, protein abundance, and chromatin accessibility, among other things. To date, single-cell analysis has entered the multiomics age (4, 5). Some research has combined these methodologies—and the associated layers of data—with "multiomics" investigations. In a technique called scNMT-seq, Argelaguet integrated gene expression profiling, methylation, and chromatin accessibility. Another technique called CITE-seq profiles both transcription and protein abundance. An additional technique known as G&T-seq captures both genomic DNA and RNA (5, 58, 59). A recent multiomics single-cell analysis identifies new cell types and processes that may contribute to the pathogenesis of T1D immunity as well as provide new cellular and molecular insights into human pancreatic function (bioRxiv, 2021, doi: 10.1101/2021.01.28.42859). In addition, due to the rapidly growing suite of software tools, there will be more and more applications of multiomics single-cell analysis in diabetes research (**Figure 1**).

While genomic analysis on diabetic risk prediction and pharmacological responses in the clinic suggests the importance for the development of individual/personal-based diabetic medicine, epigenetics research has generated new knowledge about one of the most important environmental risk factors for diabetes. Advances in proteomics research and single-cell multiomic analysis have been providing unpreceded insights into specific cell-type and molecular networks involved in the pathogenesis of diabetes. In overall, mechanistic findings in these areas will help to better understand the mechanisms of diabetes, which would lead to identifying new therapeutic targets in the pathophysiological systems that cause diabetic complications.

DIABETES AND CARDIOVASCULAR SYSTEMS AND BEYOND

Angiogenesis and Diabetes

Angiogenesis is a well-studied process that entails the formation of new blood vessels from existing blood vessels and is involved in a large number of physiological and pathological conditions. During embryonic development, wound healing, menstruation, and angiogenesis must occur to provide adequate blood flow and oxygenation to growing tissues (60). Vascular disease associated with aberrant angiogenesis is a feature of some long-term diabetic consequences. Diabetic retinopathy and nephropathy are both linked to excessive angiogenesis. Inhibition of angiogenesis can lead to impaired wound healing, impaired development of coronary collateral vessels, embryonic vascular disease in pregnancy with maternal diabetes, and transplant rejection in diabetic recipients (60).

The majority of the vasculature in a healthy adult is dormant, with only 0.01 percent of endothelial cells undergoing division. Excessive or insufficient vascular growth as in the case of pathological angiogenesis contributes to numerous non-neoplastic disorders. In some diseases, vessels do not grow, but rather abnormally remodel (61). Angiogenesis has been recognized as a hallmark of cancer and various metabolic and inflammatory diseases, such as obesity, T2D, atherosclerosis and NAFLD (61). Both physiological and pathological angiogenic variants are controlled by carefully orchestrated, temporally and spatially controlled signals from surrounding tissues, and it is the sum of these signals that causes the sequential release of angiogenic stimulators (e.g., VEGF, bFGF, PDGF) and inhibitors (e.g., endostatin, angiostatin, thrombospondin). In the past decade, research in molecular mechanisms underlining pathological angiogenesis (blood vessel growth) has grown at an explosive rate, and has led to the approval of anti-angiogenic drugs for the treatment of cancer and eye diseases (62).

Endothelial progenitor cells (EPCs) are a subtype of progenitor cells, which are first isolated in the circulation (63), and have the capacity to differentiate into mature ECs *in vitro* and *in vivo* (64). Dysfunctional EPCs with impaired vascular repairing capacity have been reported in diabetes (65). In a small clinical study of cardiovascular disease patients with or without diabetes, an increase in EPC numbers was promoted by statin administration, which was associated with HDL changes (66). Although large clinical trials are needed to validate EPCs as independent indicators of cardiovascular risk (67), several recent pre-clinical studies support its role in restoring angiogenesis in diabetes. For example, EC-specific overexpression of metallothionein (MT), an antioxidant protein, prevented impairment of angiogenesis in a hind limb Ischemia model of mice fed a high-fat diet (HFD) or treated with streptozotocin (STZ) (68). The protection was likely due to the preserved function of EPC, attributable to a reduction in oxidative stress and an enhanced expression of hypoxia-inducible factor 1a (HIF-1a), stromal cell–derived factor (SDF-1), and VEGF in ischemic tissues (68). Endothelial-colony-forming cells (ECFCs) are isolated as a novel type of progenitor cells (69). Like EPCs, ECFCs have the potential capacity to promote angiogenesis *in vitro* and *in vivo* which could be impaired by diabetes with similar mechanisms (70). ECFCs, which are of endothelial origin, are believed to be a better cell therapy tool for vascular regeneration in ischaemic models (70) because ECFCs express $CD31^+$, $CD34^+$, $CD146^+$, $VEGFR2^+$, and von Willebrands factor (69). On the other hand, EPCs are of myeloid origin and express $CD31^+$, $CD34^+$, $CD45^+$, $VEGFR2^+$, and $Tie\text{-}2^+$, with a low proliferative capacity. Further investigation, however, needs to be done to prove the applicability of ECFCs in pre-clinical and clinical settings (70).

Although diabetes can cause a variety of pathologies, vascular complications account for most of the morbidity and mortality of diabetes (71). Furthermore cardiovascular disease causes 75% of the deaths of diabetic patients (71). Diabetes can cause macrovascular and microvascular problems characterized by endothelial dysfunction, which can have serious consequences for wound healing (72, 73). Inhibition of the vascular endothelial growth factor (VEGF-VEGFR2) signal axis is related to endothelial dysfunction typical of diabetes (74, 75). Under high glucose exposure, VEGFR2 ligand and intrinsic kinase-independent phosphorylation occurs in the Golgi apparatus of endothelial cells, thereby impairing

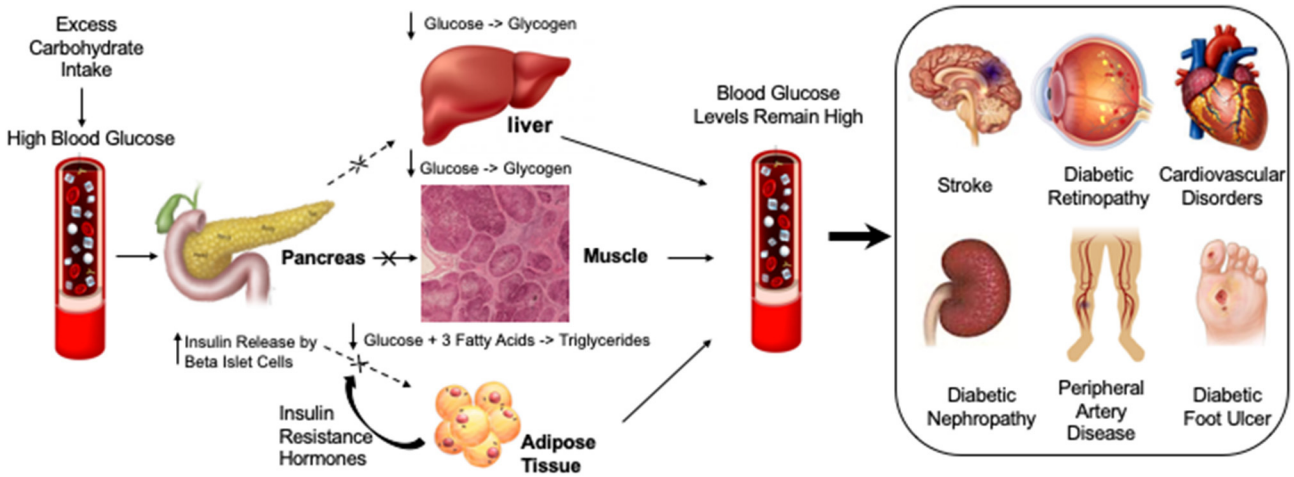

FIGURE 2 | Diabetic compilations are caused by insulin resistance leading to persistently elevated glucose levels or hyperglycemia. Different factors that may cause or exacerbate blood glucose levels are highlighted under "Lifestyle." High levels of blood glucose in diabetic vessels can cause different diabetic complications such as Diabetic Foot Ulcer, Diabetic Nephropathy, Cardiovascular Disorders, Diabetic Retinopathy, Peripheral artery disease and Stroke.

transport of receptors to the cell surface. The result is that VEGFR2 on the plasma membrane of endothelial cells gradually decreases, thereby weakening the angiogenic response of diabetes.

There is evidence that beta cells are an important ally of islet endothelial cells (EC). In addition, ECs seem to directly affect the expression and secretion of insulin genes and the survival of β cells. Pancreatic islet EC is an important partner for β cell function (76). This dynamic relationship is very important in the context of type 1 and type 2 diabetes and has been shown to establish the potential of EC or its progenitor cells to enhance the reconstitution of blood glucose control after islet transplantation in animal models (76, 77). Dysfunctional islet endothelium may lead to the progression of type 1 diabetes, the deterioration of type 2 diabetes, and the failure of islet transplantation (76). Treatments that prevent the breakdown of the complex β-cell/EC axis in pancreatic islets or restore this crosstalk may improve the prognosis of diabetic patients in the future.

In order to assess pathological or diabetic angiogenesis, there are many *in vivo, ex vivo,* and *in vitro* bioassays that are available for proper evaluation of angiogenesis (78). *In vitro* bioassays are used to detect EC cells proliferation, tube formation and migration, and *in vivo* bioassays, such as the corneal micropocket assay, matrigel plug assay, tail edema, and dermal punch biopsy wound healing assays are all used to evaluate angiogenesis and lymphangiogensis (78). Abnormal angiogenesis contributes to vascular disorders in diabetes. Provided the distinct role of angiogenesis in macrovascular and microvascular complications of diabetes, future studies should identify tissue-specific regulators of angiogenesis and their underlying mechanisms by using conventional approaches coupled with single-cell multiomic analysis and other integrative methodologies.

Lymphangiogenesis and Diabetes

Lymphatic vessels and blood vessels create an intricate system that aids in the management of tissue pressure and the production of edema. Lymphatic endothelial cells and lymphangiogenesis play critical roles of homeostasis, metabolism and immunity in both physiological and pathological angiogenesis. Except for the reproductive organs during ovarian cycles and pregnancy, the majority of lymphatic vessels in adult tissues are dormant (79). A variety of pathological conditions such as inflammation and tumor formation promote lymphangiogenesis and lymphatic vessel remodeling in the adult (80). In addition, lymphangiogenesis is enhanced post organ transplantation for inducing immune system reactivation in the draining lymph node, resulting in organ rejection (81). In general, a consequence of chronic complicated disorders, such as diabetes, is poor lymphangiogenesis (82) (**Figure 1**).

Recently, studies have suggested the therapeutic roles of lymphangiogenesis in various pathological conditions. For example, excess lymphangiogenesis favors metastasis and inflammation, however insufficient lymphangiogenesis can cause lymphedema (82, 83). The reasons and effects of adult lymphangiogenesis is still up for debate for whether it is beneficial or detrimental. Enhancing lymphangiogenesis protects against diabetes and other metabolic diseases (82). Obesity and diabetes have been linked to a lack of lymphatic architecture and impaired lymphatic function (84–89). Diet-induced obesity impairs lymphangiogenesis as indicated by decreased LYVE1 positive lymphatic vessel density (87), and corroborating impaired lymphangiogenesis in diabetic mice (82, 90). Transcription factor prospero homebox 1 (Prox1) is one of the key regulators of lymphangiogensis (46). Disturbed lymphangiogenesis in *Prox1*$^{+/-}$ mice induced obesity, coupled with decreased lymph flow in adult mouse models (91, 92). Obesity is considered to make up 80–85% of the risk of developing T2D. Recent

studies have shown that obese people are 80 times more likely to develop T2D than people with a BMI below 22 (https://www.diabetes.co.uk/diabetes-and-obesity.html). Enhancing VEGFR3 expression and VEGFR3 signaling by depleting epsins modulates VEGFR2/3 in endothelial cells promotes lymphangiogenesis and augments lymph flow in type 2 diabetic mice (82, 93) (**Figure 1**). LEC specific epsin depletion increased VEGFR3 expression and reduced VEGFR3 endocytosis and degradation resulting in enhanced wound-healing and surgery-induced lymphedema resolutions in diabetic mice (82). Since the animal model was in stage III of diabetic progression via STZ injection combined with HFD, the promoting lymphangiogenesis in the diabetic mouse did not increase insulin sensitivity. This might be due to damaged pancreatic β-cells having no response to any excess glucose which would usually decrease insulin responsiveness. In HFD-induced obese mice, overexpressing VEGF-D increases lymphatic density in adipose tissue, which lowers local immune cell buildup and improves systemic metabolic response by reducing insulin resistance and enhancing insulin sensitivity (94). There are little lymphatic vessels in mice white adipose tissue and promoting *de novo* lymphangiogenesis in adipose tissue enhanced insulin sensitivity in HFD mice treated for 16 weeks. Even if the body weight was similar between adipose tissue-VEGF-D-overexpressed mice and littermate controls, enhanced lymphangiogenesis in adipose tissue increased insulin sensitivity and reduced insulin resistance compared to the controls. Lymphatic vessels play a role in glycerol clearance and removal of infiltrated immune cells which improves metabolism in obese mice (94). Different fat pads develop and mature at different rates (95). For example, epididymal adipose tissue exhibits very little lipid component until P4 while other fat pads (e.g., subcutaneous, retroperitoneal adipose tissue) display high lipid component on postnatal day 1 (95). VEGFR3 and Prox1 show a significant percentage of distribution in the epididymal adipose tissue until postnatal day 5, indicating lymphangiogenesis may play an inhibitory role in lipid deposition in adipose tissues. Notably, angiogenesis contributes to adipose tissue development (95) while lymphatics might play an inhibitory role in lipid deposition in the adipose tissue. While VEGF-D also promotes angiogenesis via VEGFR2 (96), there is no significant increase in angiogenesis by VEGF-D overexpression in adipose tissues (94, 97). Hence, there is a protective effect via adipose tissue-VEGF-D-overexpression due to enhanced lymphangiogenesis.

Although human adipose tissue shows noticeable expression of lymphatic vessels (98), very little lymphatics are expressed in murine adipose tissues controversially (95, 97). What are the specific roles of lymphatics in adipose tissues? Which regions of adipose tissues express lymphatics? To further substantiate these findings and questions, future studies utilizing genetically modified mouse models should be used to identify the spatiotemporal and distinct roles of lymphatics in various adipose tissues. In addition, the role of lymphangiogenesis in other metabolic tissues, including liver and skeletal muscle, warrant further investigation.

Tumorigenesis and Diabetes

Tumor angiogenesis is distinct from other kinds of angiogenesis in terms of timing (99). Angiogenesis is unusually prolonged in some non-malignant processes, however it is still self-limited, such as in pyogenic granuloma or keloid development. Diabetes has been linked to an increased risk of cancer, according to extensive studies (100–102) and increased mortality of cancer patients (103). Previous research on the link between diabetes and cancer has found that diabetics are more prone to develop malignancies of the liver, pancreas, endometrial, colon, rectum, breast, and bladder (104) (**Figure 1**).

The mechanism of such an increased risk in these patients remains unclear whether: (i) the association is mainly due to shared risk factors such as obesity (105); (ii) diabetes itself alters cancer risk which may be related to insulin resistance (106), hyperinsulinemia (107–109), proinflammatory status and increased oxidative stress (1–35) (110); (iii) the risk of cancer is modified with medications administered to combat diabetes; or (iv) a combination of all these assumptions.

More observational studies have been accumulating with regard to the effects of diabetes treatment in cancer incidence. Insulin growth factor (IGF) is an important hormone for normal and transformed cell growth, development, differentiation and survival, which may play an important role in mammary tumorigenesis and diabetes (111). Several studies have found that anti-hyperglycemic drugs for diabetes treatment may be associated with either an increased or reduced risk of cancer (112, 113). Meta-analysis of observational studies found that while treatments with metformin decrease insulin resistance, it may also reduce the risk of colorectal and hepatocellular cancer in diabetic patients (114, 115), but sulfonylureas and insulin, which may cause hyperinsulinemia, did not show a significant influence. In pancreatic cancer, metformin, thiazolidinediones and insulin use had no significant effect while sulfonylurea use was associated with a 70% increase in the odds of having pancreatic cancer (116). Remaining concerns were expressed for a potential link between pioglitazone (117) and a novel class of oral glucose-lowing drug Sodium-glucose cotransporter 2 (SGLT2) inhibitors (118) with bladder cancer. Besides glucose-lowing drugs, a retrospective study of 92,366 women with newly diagnosed T2D observed a decrease in risk of endometrioid cancer in diabetic patients treated with statins (119). Long-term prospective trials and post-marketing surveillance studies are, however, required in the future.

In addition to increased incidence of cancer, diabetes also has deleterious effects on cancer prognosis. Diabetes was found to be strongly related with an increased risk of death from overall cancer in a study (120) in more than 771,297 Asians with pathologies of the endometrium, liver, thyroid, kidney, breast, ovary, pancreas, and prostate [hazard ratio 1.26 (CI 1.21–1.31)]. Extensive studies have provided the mechanism in which diabetes influences a poor cancer prognosis, including strengthening metastatic potential of cancer, favoring cancer growth (121). Also, impaired immune function in diabetes possibly results in a more aggressive cancer course. At the same time, researchers are trying to use probiotics, especially microbial short-chain fatty

acids (SCFAs) to fight against inflammation and protect from tumorigenesis in people with diabetes (122).

Preexisting diabetes is linked to an increased risk of morbidity and mortality in cancer patients, according to all of these studies. There are also studies that investigated the impact of cancer on long term outcomes of diabetes (123). Researchers followed three cohorts of diabetes patients subsequently diagnosed with breast, colorectal or prostate cancer for 10 years, and they found that in the UK, incidence of cancer appears to have little adverse impact on diabetes-related mortality (123).

These findings are clinically meaningful which point to the importance of appropriate cancer screening among diabetic patients and management of diabetic patients with cancer.

Gut Microbiota Homeostasis and Diabetes

All organisms that live in the gastrointestinal (GI) tract are referred to as gut microbiota. The human body is home to trillions of microorganisms (124), all of which serve a crucial part in normal intestinal function and the host's overall health. Some studies linked gut microbiota with diabetes (**Figure 1**).

The gut microbiota is mostly formed of four phyla: *Firmicutes, Bacteroidetes, Actinobacteria,* and *Proteobacteria*. Each individual has a unique microbiota composition (125). Diet, disease status, drugs, and host genetics will all have an impact on the composition. Among them, diet is the main contributor to the diversity of microbiota. It has been suggested that diet accounts for 57% of the variations while host genetics only account for 13% (126). Diet has been shown to affect the content and function of the gut microbiome in both animal and human studies. One study (127) switched mice from low-fat, plant polysaccharide–rich diet to a high fat and sugar diet, which altered the composition of the microbiota within a single day. Mice fed a high-fat, high-sugar diet showed a higher number of *Erysipelotrichi* class bacteria in the *Firmicutes phylum* and a lower number of *Bacteroides* spp. (127). *Bacteroides* spp., *E. coli*, and other bacteria were found in reduced numbers in mice on a vegetarian diet (127).

It's becoming clear that gut microbiota has a role in a variety of disorders, including type 1 and type 2 diabetes. T1D is an autoimmune illness caused by the immune system's destruction of pancreatic β-cells. It is mainly caused by a genetic defect as well as epigenetic and environmental factors. Increased rates of T1D incidence in recent years have been attributed to genetic factors as well as changes in lifestyle, such as nutrition, hygiene, and antibiotic use, all of which can have a direct impact on microbiota (128). Several studies have found changes in gut microbiota composition between people with T1D and healthy people. Compared with age matched healthy controls, gut microbiota in children with high genetic risk for T1D showed less diverse and less dynamic microbiota (129). These findings underscore the importance of learning more about the function bacteria may have in the development of T1D (128–131).

Obesity and T2D are also linked to dysbiosis of the gut microbiota, according to extensive research conducted in animal models and humans. Studies in germ-free mice revealed changes in the gut microbiome makeup that could have a role in disease development, including obesity and diabetes (132–134). *AKKermansia muciniphila*, a mucin-degrading bacteria found in the mucus layer, was isolated in one study. In rodents and humans, it has an inverse relationship with body weight. This study found that the abundance of *AKKermansia muciniphila* was reduced in obese and type 2 diabetic mice, and that prebiotic feeding restored *AKKermansia muciniphila* abundance, which was linked to improvements in metabolic diseases such as fat mass gain, adipose tissue and insulin resistance. Butyrate-producing *Roseburia intestinalis* and *Faecalibacterium prausnitzii* concentrations were found to be lower in T2D patients, but *Lactobacillus gasseri* and *Streptococcus mutans*, Proteobacteria, and some Clostridiales were found to be greater among 345 Chinese individuals (135). T2D is also linked to increased bacterial expression of oxidative stress-related genes, resulting in a proinflammatory signature in the gut microbiome (135). All of these studies point to a link between the gut microbiome's makeup and T2D.

For the mechanisms of how gut bacteria affect T2D, most studies focused on the involvement of microbiota in obesity and their role in insulin signaling and low grade inflammation. High-calorie diets contribute to obesity and T2D has been demonstrated by numerous studies (136, 137) and increasing evidence suggests that the link between diet and obesity lies in the gut microbiota (125, 138, 139). One study in mice found that the abundance of *A. muciniphila* decreased in obese and T2D mice. Prebiotic feeding of *A. muciniphila* improved metabolic profiles, and reduced fat mass and insulin resistance induced by high fat diet (140). Qin et al. (135) showed T2D patients had a moderate degree of gut microbial dysbiosis, a decrease in universal butyrate-producing bacteria, which play a role in regulating important T2D pathways including insulin signaling, inflammation and glucosehomeostasis (135, 141, 142). On the other hand, gut microbiota has been shown to affect the production of key insulin signaling molecules such as GLP-1 and PYY through SCFA and its binding to FFAR2 (143). Interestingly, recent studies reported that administration of metformin, the routinely used drug to control hyperglycemia in T2D, alters the composition of the microbiota (144–146).

Numerous studies have suggested that gut microbiota may have a role in the development of diabetes, as well as the importance of gut microbiota in metabolic illnesses that affect key pathways such as energy balance and inflammation. As a result, a better understanding of the relationships between gut microbiota may provide novel therapeutic interventions of diabetes the future.

CARDIOVASCULAR AND OTHER COMPLICATIONS IN DIABETES

Diabetic Retinopathy

Studies divide diabetic retinopathy (DR) into two progressive stages: non-proliferative retinopathy (NPDR) and proliferative diabetic retinopathy (PDR) (147). Non-proliferative retinopathy is characterized by high glucose which induces dysfunction and structural damage to the retina blood vessels, causing them to leak and dilate (148). At the NPDR stage, vision isn't significantly

altered and the condition is asymptomatic (149). PDR on the other hand can result in aberrant, fragile retinal neovessel formation and blindness (150, 151). The vision loss can occur from proliferation of new immature retinal vessels as well as increased leakage and permeability of retinal blood vessels (151). Pericyte loss, which is a hall mark early risk factor for DR, results in local outpouching of capillary walls which is used as a diagnostic for DR (152). Capillary obstruction and ischemia result from a significant loss of pericytes. When pericytes are lost, hypoxia-inducible factor 1 is activated, which causes VEGF to be upregulated (153–155) (**Figures 2**, **3**). Therapeutic drugs such as Pegaptanib, Bevacizumab, Ranibizumab and Aflibercept have been implanted to target VEGF to inhibit its expression since this factor has been found to be highly upregulated in patients with retinopathy (156, 157). These anti-VEGF therapies significantly reduce retinal inflammation, growth of neovessels, and when combined with Ang-2 produces an enhanced effect in reducing retinal inflammation, retinal apoptosis and neovascular leakage (157, 158).

Studies also report that hyperglycemia is a known treatable risk factor for DR. It has been studied that cellular elements in microvasculature are particularly sensitive to damage from hyperglycemia (159). Hyperglycemia is also responsible for apoptosis of pericytes as well as retinal inflammation (160). More importantly however, hyperglycemia plays a broader role in various metabolic pathways, such as upregulated VEGF, increased polyol and PKC pathway activity, chronic oxidative damage, increased activation of renin angiotensin, chronic inflammation and abnormal clumping of leukocytes, which are all involved in the progression of diabetic retinopathy (161–164).

Diabetic Nephropathy

The thickening of the glomerular basement membrane is a common early change in both type 1 and type 2 diabetic nephropathy, according to studies (165). A related consequence is the expansion of cellular and matrix components in the mesangium which ultimately restricts and distorts glomerular capillaries which diminishes the capillary filtration surface (165). In combination with mesangial expansion, other mechanisms that inhibit glomerular filtration rate include the excess secretion of Semaphorin3a (sema3a) from podocytes (166). Excess sema3a exacerbates other diabetic nephropathy (DN) risk factors such as the development of kimmelstiel-wilson lesions and podocyte effacement and injury (166, 167). Thus, many studies have focused on developing therapeutics to inhibit signaling pathways that promote sema3a such as the JNK and Rac1/NF-κB p65 signaling pathways (167, 168). Oher well known risk factors that are critical to the pathogenesis of DN include deposition of extracellular matrix proteins (ECM), which include collagen, laminin and fibronectin, in the mesangial and the glomerular basement membrane.

Studies have also focused on the ambiguous role of circular RNAs in signaling pathways that result in the promotion of ECMs such as circRNA_010383, circRNA_15698, and circRNA CDR1as/ciRS-7 (169–171). In addition, signaling pathways such as Notch, Wnt, mToR, epac-rpa-1 may all play critical roles in the accumulation of ECMs as well as renal fibrosis (172). Further research should be done on how these signaling pathways are related to ECM accumulation. However, some of those signaling pathways have been shown to have independent roles in DN development and podocyte apoptosis.

For example, in addition to various downstream transcription factors that are thought to regulate the Notch signaling pathway, a recent study has found an additional regulating mechanism via cross talk between miRNAs and the Notch pathway (173). Under high-glucose condition models, overexpression of miR-145-5p inhibited high glucose-induced podocyte cell apoptosis and it was found that the direct target of miR-145-5p was Notch1 (173). Thus, inactivation of the Notch signaling pathway by overexpressing miR-145-5p could attenuate podocyte death in DN. It has also been established that the Wnt pathway plays an independent role in the progression of DN (174). In a study focusing on panax notoginseng (PN), it was concluded that PN plays a role in inhibiting wnt1 in the Wnt/β-catenin signaling pathway which causes a downstream effect of reducing epithelial-mesenchymal transition (EMT), which contributes to podocyte dysfunction, as well as restoring normal protein expression of nephrin (174).

In addition to the critical role of inhibiting Notch and Wnt, inhibition of the mTOR pathway has been studied as a target to ameliorate DN. A recent study found that sperm-associated antigen 5 (SPAG5) plays a role in activating the AKT/mTOR signaling pathway by forming a positive feedback loop with SPAG5-AS1, miR-769-5p and transcriptional repressor YY1 (175). Furthermore, it was concluded that regulating expression of SPAG5 could regulate podocyte injury under high glucose conditions since SPAG5 directly regulates the AKT/mTOR pathway (175). Another study demonstrated that transplantation of adipose-derived stem cells (ADSC) derived from exosome (ADSC-exo), attenuated podocyte damage in DN (176). The mechanism being that ADSCs-exo mediates the transport of miR-486 to podocytes by regulating activation of the mTOR pathway, leading to decreased podocyte injury (176).

Other critical pathways that lead to podocyte injury and dysfunction involve KDM6A and KLF10 which present a positive feedback loop in podocytes causing podocyte dysfunction under diabetic conditions (177). This pathway is so critical that mouse models were protected against diabetic induced treatment once this pathway was inactivated (177). Other pathologies that lead to podocyte dysfunction include nephrin down-regulation (178). Involved in nephrin downregulation is PACSIN2 which has been found to be highly expressed in podocytes of diabetic animal models (178). Though the relationship between PACSIN2 and nephrin is till speculative, studies have shown that nephrin relies on a complex of PACSIN2 and rabenosyn-5 for nephrin endocytosis and recycling (178, 179). Thus, overexpression of PACSIN2 combined with rabenosyn-5 could increase nephrin endocytosis resulting in a breakdown of podocyte effacement, ultimately leading to podocyte dysfunction and death.

Cell senescence could be another mechanism in which DN occurs according to some studies. Conversely, the disease conditions presented by DN also most likely accelerate the progression of the disease (180). Cell senescence has been found to cause a loss of self-repair in cells as well as their regenerative

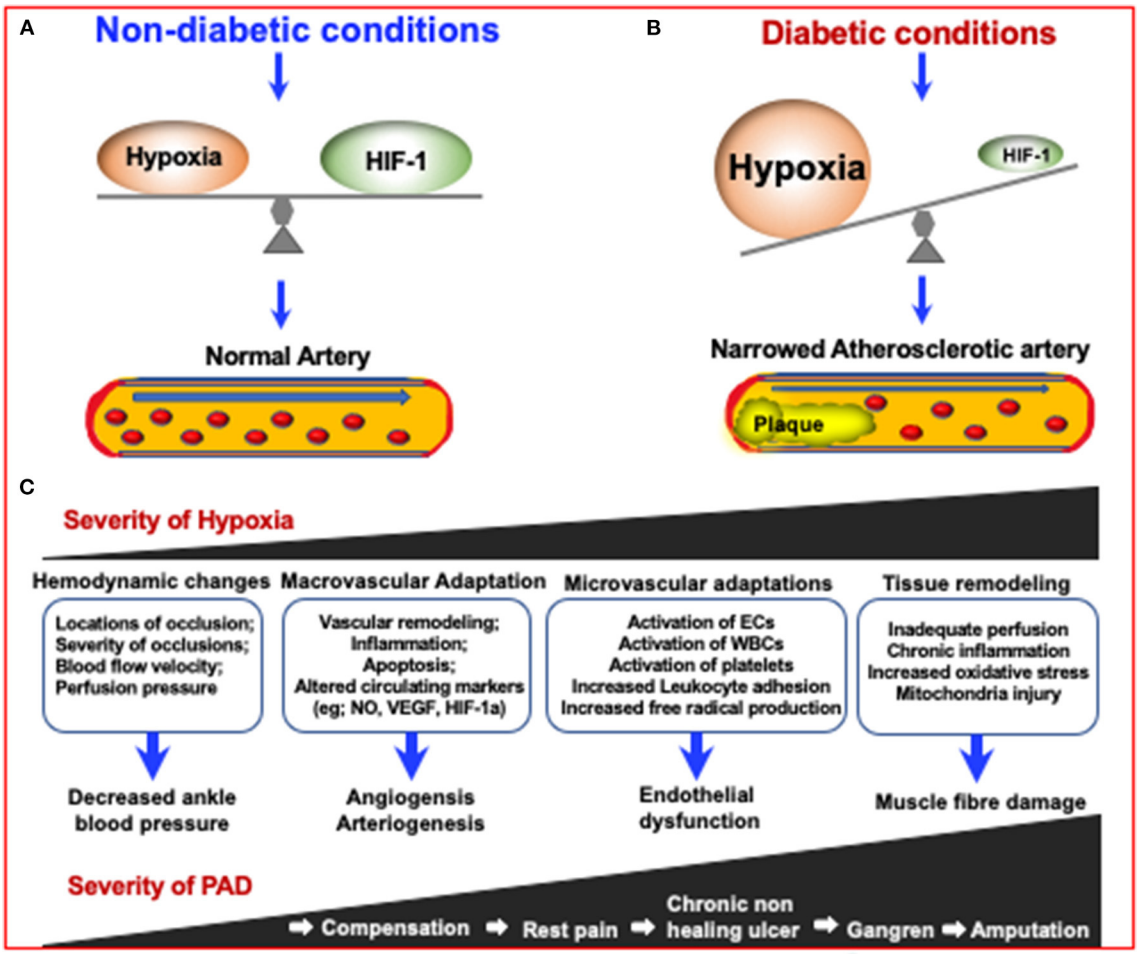

FIGURE 3 | The mechanisms in which diabetes can increase the severity of Peripheral Artery Disease (PAD) *via* increasing the severity of hypoxia which results in narrowing of arteries. Due to the inhibition of HIF-1 in diabetes, an impaired response to hypoxia can lead to diabetes and diabetic complications. **(A)** Under non-diabetic conditions, HIF-1 signaling responds to reduced oxygen levels, resulting in a steady state of hypoxia. **(B)** In the case of diabetes, although the tissue is more hypoxic, HIF-1 signal transduction is inhibited, resulting in impaired adaptive response to hypoxia, leading to the development of diabetes and its complications (155). **(C)** The consequences of increased PAD severity and hypoxia severity are highlighted in the boxes and describe the consequences respective to the degree of PAD severity.

ability (180). This would be particularly pathological to renal cells leading to accelerated aging of the kidney. Hyperglycemia in diabetic patients is related to the production of reactive oxygen species (ROS) that cause oxidative stress resulting in activation of pathways which cause renal damage and onset cell senescence (181). Similarly, studies have found that overproduction of mitochondiral reactive oxygen species (mtROS) in DN due to excessive metabolic demand could also be mechanism that could lead to damaged renal cells (182).

Diabetic nephropathy is a progressive kidney disease affecting kidney glomeruli, arterioles, tubules and the interstitium. Dapagliflozin and Prevention of Adverse outcomes in Chronic Kidney Disease (DAPA-CKD), a randomized controlled trial (183, 184), demonstrated beneficial kidney and cardiovascular outcomes with dapagliflozin vs. placebo in participants with Chronic Kidney Disease (CKD) with and without diabetes (185). More prespecified analyses from this landmark trial have confirmed dapagliflozin's cardio-renal protective effects, in favor of combined therapy (186). In light of the mechanistic findings presented in this review, future studies should test integrative approaches to identify dual or multiple targets to deal with this complex disease.

Diabetic Cardiomyopathy

There is a significant relationship between the prevalence of heart failure and diabetes. In the absence of other traditional cardiac risk factors such as coronary artery disease, hypertension, and valvular heart disease, diabetes alone can cause heart failure, namely diabetic cardiomyopathy (DCM), presenting pathological changes in cardiac structure, metabolism, and function (187). In fact, diabetes is prevalent in anywhere between 10 and 40% of heart failure subjects due to cardiomyopathy (188). The major manifestations include cardiac stiffness, myocardial fibrosis, and hypertrophy, eventually progressing to clinical heart

failure (189). Due to its' significant impacts on human health, the mechanisms behind the pathogenesis of DCM have been a hot topic of research.

The pathological factors of diabetes relevant to the pathogenesis of cardiomyopathy include hyperlipidemia, hyperglycemia and systemic insulin resistance (190). Hyperlipidemia and hyperglycemia were discussed in a recent study in their relationship to inhibiting expression of transcription factor Sp1 which was shown to be involved in downregulating mitochondrial calcium uptake 1 (MICUI1) (191). More specifically, restoring normal function of mitochondrial calcium uptake 1 (MICU1), which was confirmed to be downregulated in the hearts of diabetic mice via hyperlipidemia and hyperglycemia, was important for inhibiting the progression of cardiomyopathy (191). Thus, confirming with previous studies, it was concluded that reduced mitochondrial Ca^{2+} uptake *via* downregulated MICU1 caused dysfunction in diabetic hearts (191). Hyperglycemia and hyperlipidemia also play crucial pathological roles in cardiomyopathy via hyperglycemia-induced oxidative stress and fibrosis development due to increased ROS generation (192). Sirtuin 1 (SIRT1) is a deacetylase that has been previously shown to have a protective effect against cardiovascular disease in the context of resisting sustained oxidative stress (193). Thus, it would be very therapeutically beneficial to target SIRT1 as a means of reducing or preventing cardiomyopathy. This rational was implemented in this study focusing on the role of Tetrahydrocannabinol (THC) in mitigating oxidative stress caused by hyperglycemia by activating SIRT1 (192). The study confirmed with past research that SIRT1 is inhibited due to high glucose levels in the mouse hearts of diabetic cardiomyopathy models. The study also confirmed that superoxide Dismutase 2 (SOD2) is a product of SIRT1 activation and plays the main role in regulating ROS homeostasis when deacetylated. Interestingly, SIRT1 was dramatically upregulated when THC was administered and any pathological downstream transformations, such as reduction of deacetylation SOD2, were shown to be reversed (192). This is a novel therapeutic finding that hasn't been demonstrated before. It is also worth noting that activation of SIRT3 combined with administration of melatonin had a similar protective effect in reducing oxidative stress brought on by hyperglycemia (194). However, SIRT4 did not have these same protective effects and in fact was found to promote cardiac dysfunction by increasing ROS levels (195).

Although hyperglycemia, systemic insulin resistance, and hyperinsulinemia are regarded as the key etiological factors of DCM (187), multiple mechanisms may act at systemic, myocardial, and cellular/molecular levels, including metabolic abnormalities (e.g., lipotoxicity and glucotoxicity), mitochondrial damage and dysfunction, oxidative stress, abnormal calcium signaling, inflammation and epigenetic factors. For example, recent studies demonstrated in diabetic animal models that decreased cardiomyocyte function is a potential mechanism leading to DCM, which could result from decreased AMPK signaling, or increased AMP-activated protein kinase (MPK) signaling and increased protein kinase C (PKC) and mitogen-activated protein kinase (MAPK) signaling. Upregulation of double-stranded RNA-activated protein kinase (PKR) pathway also caused glucolipotoxicity in DCM (196). A new study using multi-omics technology in a HFD-STZ model showed that the formation of short-chain acylcarnitine species in T2D mouse hearts activated networks to redistribute excess acetyl-CoA toward ketogenesis and incomplete β-oxidation, resulting in loss of metabolic flexibility and the capacity of the heart to respond to subsequent cardiovascular events (197). Clearly, these disturbances would predispose the heart to extracellular remodeling and hypertrophy, both eventually leading to heart failure (187). Along with the deleterious hyperglycemic and hyperlipidemic effects on DCM, immerging research has analyzed the impact of HFD-induced diabetes on cardiac dysfunction in the context of lipotoxicity (198). The transcription factor studied was PPAR-γ, which has been demonstrated to regulate the expression of genes related to lipid metabolism (198). Consistent with previous studies, PPAR-γ was found to be highly expressed in diabetic heart models, however this study first demonstrated that PPAR-γ was directly associated with upregulation of ketogenic enzymes HMGCS2, PDK4 and BDH1 all of which are involved in controlling lipotoxicity and subsequent cardiac dysfunction (198–200). Therefore, ablation of PPAR-γ in diabetic-heart mouse models lead to improvements in cardiac contraction and prevention of fibrosis development both of which are suggestive of better cardiac function (198).

Some research has been done on the expression of non-coding RNAs (LncRNAs) and their involvement in the pathogenesis of DCM. To highlight a single study, it was found that LncRNA Kcnq1ot1 was significantly upregulated in high glucose cardiac fibroblasts as well as diabetic myocardial tissues (201). The main pathological pathway discussed in relation to DCM involved regulating caspase-1, the hypothesis being that downregulating Kcnq1ot1 repressed activation of miR-214-3p which reduced expression of caspase-1 and its downstream inflammatory cytokines such as interleukin 6, interleukin 10, and the IL-1 family, all of which are involved in DCM induced heart failure (202). Other studies that focused on lncRNAs, such as myocardial infarction–associated transcript (MIAT) (203), myosin heavy-chain-associated RNA transcripts (Mhrt) (204), and H19/miR-675 (205), all similarly found that forced expression or overexpression of these lncRNAs lead to preservation of cardiomyocyte apoptosis involved in the pathogenesis of DCM. Thus, there is therapeutic protentional in knocking out these specific lncRNAs in ameliorating DCM.

Taken together, it is clear that there is emerging research in the area of therapeutically treating DCM. As described above, numerous findings have been made that deal with the mechanisms behind DCM, such as targeting certain transcription factors like Sp1, deacetylases such as SIRT1 and oxidative stress (206). There are also some findings dealing with blocking long non-coding RNA (207) like Kcnq1ot1, Mhrt, and exsosomal miRNAs, like H19/miR-675 all of which have been demonstrated to promote DCM (208). Future studies should show additional mechanistic findings through the use of advanced and integrative methodologies.

Diabetic Complications in Peripheral Artery Disease

Peripheral artery disease (PAD) by itself affects 27 million individuals in both Europe and North America annually (209). The known risk factors of PAD are old age, risk of cardiovascular disease, and ethnicity, specifically if one is of Hispanic or African American descent (210). Diabetes in relation to PAD has been studied and has been shown to exacerbate PAD. For example, a 20 year follow up study found a significant increased risk of death for patients with diabetes and PAD compared to patients without diabetes (211). Thus, research in how diabetes contributes as a risk factor for PAD-associated mortality is critical (**Figure 3**).

The main mechanisms in which diabetes fosters the development of PAD are mainly through the same mechanisms that cause cardiovascular disease. Derangements in the vessel wall caused by vascular inflammation and endothelial cell dysfunction, aberrant blood cells, and an increase in reactive oxygen species are among these mechanisms (155, 212) (**Figure 3**). Hyperglycemia, a pathological consequence of diabetes, causes damage to the vascular endothelium in a variety of pathways such as the protein kinase C and advanced glycation end products pathways all of which lead to dysregulation of growth factors, cytokines, epigenetic changes, and abnormality of non-coding RNAs leading to macrovascular complications such as PAD (213). Another way in which hyperglycemia can cause damage to the vascular system is by inducing hypoxia which leads to oxidative stress (OxS) and subsequent vascular damage (214). This mechanism is illustrated in **Figure 3**. Moreover, oxidative stress (OxS) seems to play a pathophysiological role in PAD and atherosclerosis via its association with the production of reactive oxygen species ROS. Production of ROS from OxS is caused by OxS impairing nitric oxide (NO) synthesis (215). Over production of ROS, which at low levels act as signaling molecules that mediate vascular cell proliferation, migration, and differentiation, can be detrimental to microvascular angiogenesis (216). Therefore, it is clear there is some sort of cascading affect between OxS and cardiovascular diseases such as PAD, and oxidative stress biomarkers are key for identifying their progression (215).

However, there are some studies that speculate alternative mechanisms in which diabetes causes PAD. For example, one study found that serum levels of omentin-1, an adipocytokine, were significantly lower in diabetic patients with PAD compared to diabetic controls without PAD and that these levels significantly dropped as disease severity progressed (217). This is the first study to assess reduced serum omentin-1 levels as being a potential biomarker for PAD and thus should be researched more (217). Hyperglycemia was reported to hyperphosphorylated PKCβ in diabetic animal models resulting in impaired ischemia-induced activation of the canonical NF-κβ signaling pathway and inferior experimental PAD outcomes (218). Interestingly, both omentin-1 and PKCβ expression levels had significant correlations with severity of PAD in diabetic models. Another potential useful biomarker that was studied included prolonged heart rate-corrected QT interval (QTc) which was found to have a significant positive association with severity of PAD in patients that have diabetic foot ulcers (219). Additionally, there is some evidence that links elevated leptin levels with the presence and severity of PAD and diabetes (220).

To further highlight potential therapeutic targets, one study concluded that glucose normalization could be targeted as a therapeutic in diabetic patients to ameliorate PAD (221). Specifically, this study showed that impaired VEGFR expression, via greater ubiquitination under high glucose conditions, was linked to impaired perfusion recovery in Type 1 diabetes. Another study focused on acylated ghrelin (AG) and found that plasma AG was significantly lower in animal models with diabetes and PAD (222). By modulating specific miRNAs such as miRNA 126 and 132, they were able to influence the expression levels of AG which promoted a proangiogenic response. In other words, restoring AG to normal plasma levels lead to revascularization in diabetic and PAD models which means that exogenous AG could be a promising therapeutic for treating PAD in diabetic patients (222).

Micro RNAs (miRs) seem to play an independent role in diabetic PAD; however, more research needs to be done on the specific mRNAs that affect diabetic PAD. To exemplify a few, diabetes-induced upregulation of mRNA-133a was found to impair angiogenesis in PAD by reducing nitrogen oxide synthesis in endothelial cells (223). Conversely, inhibiting expression of miR-133a resulted in improved angiogenesis after experimental post-ischemic inducement in diabetic mice (223). Another miR identified as miR-93 enhanced blood perfusion after experimental hind limb ischemia, making it a valuable target for modulation in promoting angiogenesis particularly in ischemic tissue (224). Thus, there is some evidence to support that miRs play an important role in recovering from PAD reduced blood perfusion; however, more investigation is warranted.

Studies have shown that diabetes accelerates atherosclerosis and that peripheral artery disease is a marker of advanced atherosclerosis (225). Patients with PAD and diabetes were found to have an increased risk of cardiovascular death or ischemic stroke as well as a higher risk for lower extremity amputations compared to patients with PAD and no diabetes (226). More specifically, patients with T2D and PAD had lower heart rate variability which is indicative of autonomic dysfunction (227). Furthermore, autonomic cardiovascular dysfunction in relationship with atherosclerosis has been studied. Specifically it was found that diabetic patients with low heart rate variability had higher levels of inflammatory markers such carotid intima-media thickness (IMT) (228).

Concerning the lower extremity amputation risk, advanced PAD can result in chronic limb threatening ischemia (CLTI) which is associated with a higher risk of lower limb loss (229). Since amputation risk of lower extremities is a common complication of patients with PAD and diabetes (230), it is important to be able to assess PAD risk among diabetic patients before they develop diabetic foot ulcers in which amputation then becomes more necessary. One major indicator of amputation risk that can be non-invasively assessed is by determining the ankle brachial index (231). The results of this study showed that patients who exhibited a lower ankle brachial index were at a higher risk for a foot ulcer and thus an amputation.

An emerging method that could be more predictive include ultrasound measurement methods that, for example, can be used in plantar soft tissues in order to predict diabetic related changes in the foot (232). In one study, it was found that Sub-MTH fat pads were significantly thinner and subhalangeal fat pads were significantly thicker in diabetic neuropathic feet compared to neuropathic controls (233). Another study conducted in China used similar ultrasonographic methods to detect foot muscle atrophy in Chinese patients with type 2 diabetes mellitus. The extensor digitorum brevis muscles (EDB) as well as the muscles of the first interstitium (MILs) had a reduced transverse diameter, thickness, and cross sectional area in all of the patients' nondominant feet, according to this study (234). In other studies, it has been found that the use of ultrasound can assess a significant reduction in the thickness of the intrinsic foot muscles and plantar tissues in patients with T2D (235). There is also evidence that people with T2D have stiffer heel pads (236). Taken together, these studies represent useful data for using ultrasonography as a noninvasive and cost effective way to detect early diabetic complications in the foot. Advancement in this technology would be critical for patients who have diabetes and PAD in order to prevent or reduce their need for amputation (**Figure 3**).

PERSPECTIVES

Currently the incidence and prevalence of diabetes mellitus around the world is very high and diabetes has become a threat to mankind globally. With the advancement of genomics, epigenomics, proteomics, and multiomics single-cell analyses, more promising and powerful approaches for mechanistic studies of diabetes have come to fruition. Also, the association between diabetes and other physiological systems, especially the cardiovascular system, revealed more potential pathways and targets involved in the progression of diabetes. Therapeutically intervening in these pathways will also help us to mitigate the effects that diabetes has on other pathologies described in this review such as retinopathy, nephropathy, peripheral artery disease, and cardiomyopathy. The information described in this paper would present a tremendous leap forward in predicting, diagnosing, managing and treating diabetes.

AUTHOR CONTRIBUTIONS

HW, VN, and HC proposed the conception. HW, VN, KC, BZ, SB, YWL, BW, DS, SW, S-LC, YD, DC, JX, DRB, CZ, and HC performed the literature search complied and wrote the manuscript. HW, VN, and HC proofed the manuscript and figures. All authors contributed to manuscript draft and revision.

FUNDING

This work was supported in part by NIH Grants R01HL093242, R01HL130845, R01HL133216, R01HL137229, R01HL156362, and R01HL158097 and American Heart Association Established Investigator Award to HC, R01HL141858 to DRB, NIH R01ES023470, NIH R01HL131925 to CZ, and Scientist Development Grant 17SDG33410868 and NIH T32 to HW.

REFERENCES

1. Shaw JE, Sicree RA, Zimmet PZ. Global estimates of the prevalence of diabetes for 2010 and 2030. *Diabetes Res Clin Pract.* (2010) 87:4–14. doi: 10.1016/j.diabres.2009.10.007
2. Rubino F. Is type 2 diabetes an operable intestinal disease? A provocative yet reasonable hypothesis. *Diabetes Care.* (2008) 31 Suppl 2:S290–296. doi: 10.2337/dc08-s271
3. Tamas G, Kerenyi Z. Current controversies in the mechanisms and treatment of gestational diabetes. *Curr Diab Rep.* (2002) 2:337–46. doi: 10.1007/s11892-002-0024-3
4. Macaulay IC, Ponting CP, Voet T. Single-cell multiomics: multiple measurements from single cells. *Trends Genet.* (2017) 33:155–68. doi: 10.1016/j.tig.2016.12.003
5. Perkel JM. Single-cell analysis enters the multiomics age. *Nature.* (2021) 595:614–6. doi: 10.1038/d41586-021-01994-w
6. Barrett JC, Clayton DG, Concannon P, Akolkar B, Cooper JD, Erlich HA, et al. Genome-wide association study and meta-analysis find that over 40 loci affect risk of type 1 diabetes. *Nat Genet.* (2009) 41:703–7. doi: 10.1038/ng.381
7. Todd JA, Walker NM, Cooper JD, Smyth DJ, Downes K, Plagnol V, et al. Robust associations of four new chromosome regions from genome-wide analyses of type 1 diabetes. *Nat Genet.* (2007) 39:857–64. doi: 10.1038/ng2068
8. Vella A, Cooper JD, Lowe CE, Walker N, Nutland S, Widmer B, et al. Localization of a type 1 diabetes locus in the IL2RA/CD25 region by use of tag single-nucleotide polymorphisms. *Am J Hum Genet.* (2005) 76:773–9. doi: 10.1086/429843
9. Nisticò L, Buzzetti R, Pritchard LE, Van der Auwera B, Giovannini C, Bosi E, et al. The CTLA-4 gene region of chromosome 2q33 is linked to, and associated with, type 1 diabetes. *Belgian Diabetes Registry Hum Mol Genet.* (1996) 5:1075–80. doi: 10.1093/hmg/5.7.1075
10. Krönke M, Leonard J, Depper M, Greene W. Structure and function of the human interleukin 2 receptor gene. *Behring Inst Mitt.* (1987) 1987:60–72
11. Gale EA. The rise of childhood type 1 diabetes in the 20th century. *Diabetes.* (2002) 51:3353–61. doi: 10.2337/diabetes.51.12.3353
12. Steck AK, Rewers MJ. Genetics of type 1 diabetes. *Clin Chem.* (2011) 57:176–85. doi: 10.1373/clinchem.2010.148221
13. Markowitz SM, Park ER, Delahanty LM, O'Brien KE, Grant RW. Perceived impact of diabetes genetic risk testing among patients at high phenotypic risk for type 2 diabetes. *Diabetes Care.* (2011) 34:568–73. doi: 10.2337/dc10-1960
14. Steinthorsdottir V, Thorleifsson G, Reynisdottir I, Benediktsson R, Jonsdottir T, Walters GB, et al. A variant in CDKAL1 influences insulin response and risk of type 2 diabetes. *Nat Genet.* (2007) 39:770–5. doi: 10.1038/ng2043
15. Lindgren CM, Heid IM, Randall JC, Lamina C, Steinthorsdottir V, Qi L, et al. Genome-wide association scan meta-analysis identifies three Loci influencing adiposity and fat distribution. *PLoS Genet.* (2009) 5:e1000508. doi: 10.1371/journal.pgen.1000508
16. Morris AP, Voight BF, Teslovich TM, Ferreira T, Segrè AV, Steinthorsdottir V, et al. Large-scale association analysis provides insights into the genetic architecture and pathophysiology of type 2 diabetes. *Nat Genet.* (2012) 44:981–90.
17. Voight BF, Scott LJ, Steinthorsdottir V, Morris AP, Dina C, Welch RP, et al. Twelve type 2 diabetes susceptibility loci identified through large-scale association analysis. *Nat Genet.* (2010) 42:579–89. doi: 10.1038/ng.609
18. Lebrón-Aldea D, Dhurandhar EJ, Pérez-Rodríguez P, Klimentidis YC, Tiwari HK, Vazquez AI. Integrated genomic and BMI analysis for type 2 diabetes risk assessment. *Front Genet.* (2015) 6:75. doi: 10.3389/fgene.2015.00075

19. Chen M, Zhang R, Jiang F, Wang J, Peng D, Yan J, et al. Joint effects of diabetic-related genomic loci on the therapeutic efficacy of oral anti-diabetic drugs in Chinese type 2 diabetes patients. *Sci Rep.* (2016) 6:23266. doi: 10.1038/srep23266
20. Kleinberger JW, Pollin TI. Personalized medicine in diabetes mellitus: current opportunities and future prospects. *Ann N Y Acad Sci.* (2015) 1346:45–56. doi: 10.1111/nyas.12757
21. Liao WL, Tsai FJ. Personalized medicine in type 2 diabetes. *Biomedicine (Taipei).* (2014) 4:8. doi: 10.7603/s40681-014-0008-z
22. Cho YS, Chen CH, Hu C, Long J, Ong RT, Sim X, et al. Meta-analysis of genome-wide association studies identifies eight new loci for type 2 diabetes in east Asians. *Nat Genet.* (2011) 44:67–72. doi: 10.1038/ng.1019
23. Dai XP, Huang Q, Yin JY, Guo Y, Gong ZC, Lei MX, et al. KCNQ1 gene polymorphisms are associated with the therapeutic efficacy of repaglinide in Chinese type 2 diabetic patients. *Clin Exp Pharmacol Physiol.* (2012) 39:462–8. doi: 10.1111/j.1440-1681.2012.05701.x
24. Ling C, Groop L. Epigenetics: a molecular link between environmental factors and type 2 diabetes. *Diabetes.* (2009) 58:2718–25. doi: 10.2337/db09-1003
25. Bird A. Perceptions of epigenetics. *Nature.* (2007) 447:396–8. doi: 10.1038/nature05913
26. Ling C, Ronn T. Epigenetics in human obesity and type 2 diabetes. *Cell Metab.* (2019) 29:1028–44. doi: 10.1016/j.cmet.2019.03.009
27. Clouaire T, Stancheva I. Methyl-CpG binding proteins: specialized transcriptional repressors or structural components of chromatin? *Cell Mol Life Sci.* (2008) 65:1509–22. doi: 10.1007/s00018-008-7324-y
28. Patra SK, Patra A, Rizzi F, Ghosh TC, Bettuzzi S. Demethylation of (Cytosine-5-C-methyl) DNA and regulation of transcription in the epigenetic pathways of cancer development. *Cancer Metastasis Rev.* (2008) 27:315–34. doi: 10.1007/s10555-008-9118-y
29. Hesselberth JR, Chen X, Zhang Z, Sabo PJ, Sandstrom R, Reynolds AP, et al. Global mapping of protein-DNA interactions in vivo by digital genomic footprinting. *Nat Methods.* (2009) 6:283–9. doi: 10.1038/nmeth.1313
30. Buenrostro JD, Giresi PG, Zaba LC, Chang HY, Greenleaf WJ. Transposition of native chromatin for fast and sensitive epigenomic profiling of open chromatin, DNA-binding proteins and nucleosome position. *Nat Methods.* (2013) 10:1213–8. doi: 10.1038/nmeth.2688
31. Mahajan A, Taliun D, Thurner M, Robertson NR, Torres JM, Rayner NW, et al. Fine-mapping type 2 diabetes loci to single-variant resolution using high-density imputation and islet-specific epigenome maps. *Nat Genet.* (2018) 50:1505–13. doi: 10.1038/s41588-018-0241-6
32. Rai V, Quang DX, Erdos MR, Cusanovich DA, Daza RM, Narisu N, et al. Single-cell ATAC-Seq in human pancreatic islets and deep learning upscaling of rare cells reveals cell-specific type 2 diabetes regulatory signatures. *Mol Metab.* (2020) 32:109–21. doi: 10.1016/j.molmet.2019.12.006
33. Kouzarides T. Chromatin modifications and their function. *Cell.* (2007) 128:693–705. doi: 10.1016/j.cell.2007.02.005
34. Haberland M, Montgomery RL, Olson EN. The many roles of histone deacetylases in development and physiology: implications for disease and therapy. *Nat Rev Genet.* (2009) 10:32–42. doi: 10.1038/nrg2485
35. Avvakumov N, Cote J. The MYST family of histone acetyltransferases and their intimate links to cancer. *Oncogene.* (2007) 26:5395–407. doi: 10.1038/sj.onc.1210608
36. Shahbazian MD, Grunstein M. Functions of site-specific histone acetylation and deacetylation. *Annu Rev Biochem.* (2007) 76:75–100. doi: 10.1146/annurev.biochem.76.052705.162114
37. Marmorstein R, Trievel RC. Histone modifying enzymes: structures, mechanisms, and specificities. *Biochim Biophys Acta.* (2009) 1789:58–68. doi: 10.1016/j.bbagrm.2008.07.009
38. Lin LL, Huang HC, Juan HF. Discovery of biomarkers for gastric cancer: a proteomics approach. *J Proteomics.* (2012) 75:3081–97. doi: 10.1016/j.jprot.2012.03.046
39. Ho L, Sharma N, Blackman L, Festa E, Reddy G, Pasinetti GM. From proteomics to biomarker discovery in Alzheimer's disease. *Brain Res Brain Res Rev.* (2005) 48:360–9. doi: 10.1016/j.brainresrev.2004.12.025
40. Ma Y, Yang C, Tao Y, Zhou H, Wang Y. Recent technological developments in proteomics shed new light on translational research on diabetic microangiopathy. *FEBS J.* (2013) 280:5668–81. doi: 10.1111/febs.12369
41. Liu CW, Bramer L, Webb-Robertson BJ, Waugh K, Rewers MJ, Zhang Q. Temporal expression profiling of plasma proteins reveals oxidative stress in early stages of Type 1 Diabetes progression. *J Proteomics.* (2017) 172:100–10. doi: 10.1016/j.jprot.2017.10.004
42. Takahashi E, Unoki-Kubota H, Shimizu Y, Okamura T, Iwata W, Kajio H, et al. Proteomic analysis of serum biomarkers for prediabetes using the Long-Evans Agouti rat, a spontaneous animal model of type 2 diabetes mellitus. *J Diabetes Investig.* (2017) 8:661–71. doi: 10.1111/jdi.12638
43. Nyalwidhe JO, Grzesik WJ, Burch TC, Semeraro ML, Waseem T, Gerling IC, et al. Comparative quantitative proteomic analysis of disease stratified laser captured microdissected human islets identifies proteins and pathways potentially related to type 1 diabetes. *PLoS ONE.* (2017) 12:e0183908. doi: 10.1371/journal.pone.0183908
44. Roomp K, Kristinsson H, Schvartz D, Ubhayasekera K, Sargsyan E, Manukyan L, et al. Combined lipidomic and proteomic analysis of isolated human islets exposed to palmitate reveals time-dependent changes in insulin secretion and lipid metabolism. *PLoS ONE.* (2017) 12:e0176391. doi: 10.1371/journal.pone.0176391
45. Ouchi N, Parker JL, Lugus JJ, Walsh K. Adipokines in inflammation and metabolic disease. *Nat Rev Immunol.* (2011) 11:85–97. doi: 10.1038/nri2921
46. Berti DA, Russo LC, Castro LM, Cruz L, Gozzo FC, Heimann JC, et al. Identification of intracellular peptides in rat adipose tissue: Insights into insulin resistance. *Proteomics.* (2012) 12:2668–81. doi: 10.1002/pmic.201200051
47. Ota A, Kovary KM, Wu OH, Ahrends R, Shen WJ, Costa MJ, et al. Using SRM-MS to quantify nuclear protein abundance differences between adipose tissue depots of insulin-resistant mice. *J Lipid Res.* (2015) 56:1068–78. doi: 10.1194/jlr.D056317
48. Murri M, Insenser M, Bernal-Lopez MR, Perez-Martinez P, Escobar-Morreale HF, Tinahones FJ. Proteomic analysis of visceral adipose tissue in pre-obese patients with type 2 diabetes. *Mol Cell Endocrinol.* (2013) 376:99–106. doi: 10.1016/j.mce.2013.06.010
49. Bakken TE, van Velthoven CT, Menon V, Hodge RD, Yao Z, Nguyen TN, et al. Single-cell and single-nucleus RNA-seq uncovers shared and distinct axes of variation in dorsal LGN neurons in mice, non-human primates, and humans. *Elife.* (2021) 10:e64875. doi: 10.7554/eLife.64875
50. Gonzalez-Silva L, Quevedo L, Varela I. Tumor functional heterogeneity unraveled by scRNA-seq technologies. *Trends Cancer.* (2020) 6:13–9. doi: 10.1016/j.trecan.2019.11.010
51. Hodge RD, Bakken TE, Miller JA, Smith KA, Barkan ER, Graybuck LT, et al. Conserved cell types with divergent features in human versus mouse cortex. *Nature.* (2019) 573:61–8. doi: 10.1038/s41586-019-1506-7
52. Lam AN, Aksit MA, Vecchio-Pagan B, Shelton CA, Osorio DL, Anzmann AF, et al. Increased expression of anion transporter SLC26A9 delays diabetes onset in cystic fibrosis. *J Clin Invest.* (2020) 130:272–86. doi: 10.1172/JCI129833
53. Veres A, Faust AL, Bushnell HL, Engquist EN, Kenty JH, Harb G, et al. Charting cellular identity during human in vitro beta-cell differentiation. *Nature.* (2019) 569:368–73. doi: 10.1038/s41586-019-1168-5
54. Qadir MMF, Alvarez-Cubela S, Klein D, van Dijk J, Muniz-Anquela R, Moreno-Hernandez YB, et al. Single-cell resolution analysis of the human pancreatic ductal progenitor cell niche. *Proc Natl Acad Sci USA.* (2020) 117:10876–87. doi: 10.1073/pnas.19183 14117
55. Baron M, Veres A, Wolock SL, Faust AL, Gaujoux R, Vetere A, et al. A single-cell transcriptomic map of the human and mouse pancreas reveals inter- and intra-cell population structure. *Cell Syst.* (2016) 3:346–60e344. doi: 10.1016/j.cels.2016.08.011
56. Muraro MJ, Dharmadhikari G, Grun D, Groen N, Dielen T, Jansen E, et al. A single-cell transcriptome atlas of the human pancreas. *Cell Syst.* 3:385–394.e383. doi: 10.1016/j.cels.2016.09.002
57. Wang YJ, Schug J, Won KJ, Liu C, Naji A, Avrahami D, et al. Single-cell transcriptomics of the human endocrine pancreas. *Diabetes.* (2016) 65:3028–38. doi: 10.2337/db16-0405
58. Cao J, O'Day DR, Pliner HA, Kingsley PD, Deng M, Daza RM, et al. A human cell atlas of fetal gene expression. *Science.* (2020) 370:aba7721. doi: 10.1126/science.aba7721

59. Argelaguet R, Clark SJ, Mohammed H, Stapel LC, Krueger C, Kapourani CA, et al. Multi-omics profiling of mouse gastrulation at single-cell resolution. *Nature.* (2019) 576:487–91. doi: 10.1038/s41586-019-1825-8
60. Johnson KE, Wilgus TA. Vascular endothelial growth factor and angiogenesis in the regulation of cutaneous wound repair. *Adv Wound Care.* (2014) 3:647–61. doi: 10.1089/wound.2013.0517
61. Carmeliet P, Jain RK. Angiogenesis in cancer and other diseases. *Nature.* (2000) 407:249–57. doi: 10.1038/35025220
62. Carmeliet P, Jain RK. Molecular mechanisms and clinical applications of angiogenesis. *Nature.* (2011) 473:298–307. doi: 10.1038/nature10144
63. Asahara T, Murohara T, Sullivan A, Silver M, van der Zee R, Li T, et al. Isolation of putative progenitor endothelial cells for angiogenesis. *Science.* (1997) 275:964–7. doi: 10.1126/science.275.5302.964
64. Medina RJ, Barber CL, Sabatier F, Dignat-George F, Melero-Martin JM, Khosrotehrani K, et al. Endothelial progenitors: a consensus statement on nomenclature. *Stem Cells Transl Med.* (2017) 6:1316–20. doi: 10.1002/sctm.16-0360
65. Fadini GP, Avogaro A. Potential manipulation of endothelial progenitor cells in diabetes and its complications. *Diabetes Obes Metab.* (2010) 12:570–83. doi: 10.1111/j.1463-1326.2010.01210.x
66. Jaumdally RJ, Goon PK, Varma C, Blann AD, Lip GY. Effects of atorvastatin on circulating $CD34^+/CD133^+/CD45^-$ progenitor cells and indices of angiogenesis (vascular endothelial growth factor and the angiopoietins 1 and 2) in atherosclerotic vascular disease and diabetes mellitus. *J Intern Med.* (2010) 267:385–93. doi: 10.1111/j.1365-2796.2009.02151.x
67. Fadini GP, Mehta A, Dhindsa DS, Bonora BM, Sreejit G, Nagareddy P, et al. Circulating stem cells and cardiovascular outcomes: from basic science to the clinic. *Eur Heart J.* (2020) 41:4271–82. doi: 10.1093/eurheartj/ehz923
68. Wang K, Dai X, He J, Yan X, Yang C, Fan X, et al. Endothelial overexpression of metallothionein prevents diabetes-induced impairment in ischemia angiogenesis through preservation of HIF-1alpha/SDF-1/VEGF signaling in endothelial progenitor cells. *Diabetes.* (2020) 69:1779–92. doi: 10.2337/db19-0829
69. Ingram DA, Mead LE, Tanaka H, Meade V, Fenoglio A, Mortell K, et al. Identification of a novel hierarchy of endothelial progenitor cells using human peripheral and umbilical cord blood. *Blood.* (2004) 104:2752–60. doi: 10.1182/blood-2004-04-1396
70. Lyons CJ, O'Brien T. The functionality of endothelial-colony-forming cells from patients with diabetes mellitus. *Cells.* (2020) 9:1731. doi: 10.3390/cells9071731
71. Carmeliet P. Angiogenesis in health and disease. *Nat Med.* (2003) 9:653–60. doi: 10.1038/nm0603-653
72. Swift MR, Weinstein BM. Arterial-venous specification during development. *Circ Res.* (2009) 104:576–88. doi: 10.1161/CIRCRESAHA.108.188805
73. Wang R, Chadalavada K, Wilshire J, Kowalik U, Hovinga KE, Geber A, et al. Glioblastoma stem-like cells give rise to tumour endothelium. *Nature.* (2010) 468:829–33. doi: 10.1038/nature09624
74. Herbert SP, Huisken J, Kim TN, Feldman ME, Houseman BT, Wang RA, et al. Arterial-venous segregation by selective cell sprouting: an alternative mode of blood vessel formation. *Science.* (2009) 326:294–8. doi: 10.1126/science.1178577
75. Fischer C, Mazzone M, Jonckx B, Carmeliet P. FLT1 and its ligands VEGFB and PlGF: drug targets for anti-angiogenic therapy? *Nat Rev Cancer.* (2008) 8:942–56. doi: 10.1038/nrc2524
76. Peiris H, Bonder CS, Coates PT, Keating DJ, Jessup CF. The beta-cell/EC axis: how do islet cells talk to each other? *Diabetes.* (2014) 63:3–11. doi: 10.2337/db13-0617
77. Penko D, Rojas-Canales D, Mohanasundaram D, Peiris HS, Sun WY, Drogemuller CJ, et al. Endothelial progenitor cells enhance islet engraftment, influence beta-cell function, and modulate islet connexin 36 expression. *Cell Transplant.* (2015) 24:37–48. doi: 10.3727/096368913X673423
78. Nowak-Sliwinska P, Alitalo K, Allen E, Anisimov A, Aplin AC, Auerbach R, et al. Consensus guidelines for the use and interpretation of angiogenesis assays. *Angiogenesis.* (2018) 21:425–532. doi: 10.1007/s10456-018-9613-x
79. Rutkowski JM, Ihm JE, Lee ST, Kilarski WW, Greenwood VI, Pasquier MC, et al. VEGFR-3 neutralization inhibits ovarian lymphangiogenesis, follicle maturation, and murine pregnancy. *Am J Pathol.* (2013) 183:1596–607. doi: 10.1016/j.ajpath.2013.07.031
80. Nihei M, Okazaki T, Ebihara S, Kobayashi M, Niu K, Gui P, et al. Chronic inflammation, lymphangiogenesis, and effect of an anti-VEGFR therapy in a mouse model and in human patients with aspiration pneumonia. *J Pathol.* (2015) 235:632–45. doi: 10.1002/path.4473
81. Kim H, Kataru RP, Koh GY. Regulation and implications of inflammatory lymphangiogenesis. *Trends Immunol.* (2012) 33:350–6. doi: 10.1016/j.it.2012.03.006
82. Wu H, Rahman HNA, Dong Y, Liu X, Lee Y, Wen A, et al. Epsin deficiency promotes lymphangiogenesis through regulation of VEGFR3 degradation in diabetes. *J Clin Invest.* (2018) 128:4025–43. doi: 10.1172/JCI96063
83. Wong BW, Wang X, Zecchin A, Thienpont B, Cornelissen I, Kalucka J, et al. The role of fatty acid beta-oxidation in lymphangiogenesis. *Nature.* (2017) 542:49–54. doi: 10.1038/nature21028
84. Lee Y, Chakraborty S, Meininger CJ, Muthuchamy M. Insulin resistance disrupts cell integrity, mitochondrial function and inflammatory signaling in lymphatic endothelium. *Microcirculation.* (2018) 2018:e12492. doi: 10.1111/micc.12492
85. Lee Y, Fluckey JD, Chakraborty S, Muthuchamy M. Hyperglycemia- and hyperinsulinemia-induced insulin resistance causes alterations in cellular bioenergetics and activation of inflammatory signaling in lymphatic muscle. *FASEB J.* (2017) 31:2744–59. doi: 10.1096/fj.201600887R
86. Scallan JP, Hill MA, Davis MJ. Lymphatic vascular integrity is disrupted in type 2 diabetes due to impaired nitric oxide signalling. *Cardiovasc Res.* (2015) 107:89–97. doi: 10.1093/cvr/cvv117
87. Garcia Nores GD, Cuzzone DA, Albano NJ, Hespe GE, Kataru RP, Torrisi JS, et al. Obesity but not high-fat diet impairs lymphatic function. *Int J Obesity.* (2016) 40:1582–90. doi: 10.1038/ijo.2016.96
88. Nitti MD, Hespe GE, Kataru RP, Garcia Nores GD, Savetsky IL, Torrisi JS, et al. Obesity-induced lymphatic dysfunction is reversible with weight loss. *J Physiol.* (2016) 594:7073–87. doi: 10.1113/JP273061
89. Weitman ES, Aschen SZ, Farias-Eisner G, Albano N, Cuzzone DA, Ghanta S, et al. Obesity impairs lymphatic fluid transport and dendritic cell migration to lymph nodes. *PLoS ONE.* (2013) 8:e70703. doi: 10.1371/journal.pone.0070703
90. Maruyama K, Asai J, Ii M, Thorne T, Losordo DW, D'Amore PA. Decreased macrophage number and activation lead to reduced lymphatic vessel formation and contribute to impaired diabetic wound healing. *Am J Pathol.* (2007) 170:1178–91. doi: 10.2353/ajpath.2007.060018
91. Escobedo N, Proulx ST, Karaman S, Dillard ME, Johnson N, Detmar M, et al. Restoration of lymphatic function rescues obesity in Prox1-haploinsufficient mice. *JCI Insight.* (2016) 1:e85096. doi: 10.1172/jci.insight.85096
92. Harvey NL, Srinivasan RS, Dillard ME, Johnson NC, Witte MH, Boyd K, et al. Lymphatic vascular defects promoted by Prox1 haploinsufficiency cause adult-onset obesity. *Nat Genet.* (2005) 37:1072–81. doi: 10.1038/ng1642
93. Morris A. Epsins as a target for wound-healing therapeutics. *Nat Rev Endocrinol.* (2018) 14:566. doi: 10.1038/s41574-018-0090-5
94. Chakraborty A, Barajas S, Lammoglia GM, Reyna AJ, Morley TS, Johnson JA, et al. Vascular endothelial growth factor-D (VEGF-D) overexpression and lymphatic expansion in murine adipose tissue improves metabolism in obesity. *Am J Pathol.* (2019) 189:924–39. doi: 10.1016/j.ajpath.2018.12.008
95. Han J, Lee JE, Jin J, Lim JS, Oh N, Kim K, et al. The spatiotemporal development of adipose tissue. *Development.* (2011) 138:5027–37. doi: 10.1242/dev.067686
96. Achen MG, Jeltsch M, Kukk E, Mäkinen T, Vitali A, Wilks AF, et al. Vascular endothelial growth factor D (VEGF-D) is a ligand for the tyrosine kinases VEGF receptor 2 (Flk1) and VEGF receptor 3 (Flt4). *Proc Natl Acad Sci USA.* (1998) 95:548–53. doi: 10.1073/pnas.95.2.548
97. Lammoglia GM, Van Zandt CE, Galvan DX, Orozco JL, Dellinger MT, Rutkowski JM. Hyperplasia, de novo lymphangiogenesis, and lymphatic regression in mice with tissue-specific, inducible overexpression of murine VEGF-D. *Am J Physiol Heart Circul Physiol.* (2016) 311:H384–394. doi: 10.1152/ajpheart.00208.2016
98. Redondo PAG, Gubert F, Zaverucha-do-Valle C, Dutra TPP, Ayres-Silva JP, Fernandes N, et al. Lymphatic vessels in human adipose tissue. *Cell Tissue Res.* (2020) 379:511–20. doi: 10.1007/s00441-019-03108-5
99. Folkman J. Tumor angiogenesis. *Adv Cancer Res.* (1985) 43:175–203. doi: 10.1016/S0065-230X(08)60946-X

100. Wang P, Kang D, Cao W, Wang Y, Liu Z. Diabetes mellitus and risk of hepatocellular carcinoma: a systematic review and meta-analysis. *Diabetes Metab Res Rev*. (2012) 28:109–22. doi: 10.1002/dmrr.1291
101. Zhu Z, Wang X, Shen Z, Lu Y, Zhong S, Xu C. Risk of bladder cancer in patients with diabetes mellitus: an updated meta-analysis of 36 observational studies. *BMC Cancer*. (2013) 13:310. doi: 10.1186/1471-2407-13-310
102. Deng L, Gui Z, Zhao L, Wang J, Shen L. Diabetes mellitus and the incidence of colorectal cancer: an updated systematic review and meta-analysis. *Dig Dis Sci*. (2012) 57:1576–85. doi: 10.1007/s10620-012-2055-1
103. Barone BB, Yeh HC, Snyder CF, Peairs KS, Stein KB, Derr RL, et al. Long-term all-cause mortality in cancer patients with preexisting diabetes mellitus: a systematic review and meta-analysis. *JAMA*. (2008) 300:2754–64. doi: 10.1001/jama.2008.824
104. Margel D, Urbach D, Lipscombe LL, Bell CM, Kulkarni G, Austin PC, et al. Association between metformin use and risk of prostate cancer and its grade. *J Natl Cancer Inst*. (2013) 105:1123–31. doi: 10.1093/jnci/djt170
105. Klil-Drori AJ, Azoulay L, Pollak MN. Cancer, obesity, diabetes, and antidiabetic drugs: is the fog clearing? *Nat Rev Clin Oncol*. (2017) 14:85–99. doi: 10.1038/nrclinonc.2016.120
106. Perseghin G, Calori G, Lattuada G, Ragogna F, Dugnani E, Garancini MP, et al. Insulin resistance/hyperinsulinemia and cancer mortality: the Cremona study at the 15th year of follow-up. *Acta Diabetol*. (2012) 49:421–8. doi: 10.1007/s00592-011-0361-2
107. Azar M, Lyons TJ. Diabetes, insulin treatment, and cancer risk: what is the evidence? *F1000 Med Rep*. (2010) 2:M2-4. doi: 10.3410/M2-4
108. Bonelli L, Aste H, Bovo P, Cavallini G, Felder M, Gusmaroli R, et al. Exocrine pancreatic cancer, cigarette smoking, and diabetes mellitus: a case-control study in northern Italy. *Pancreas*. (2003) 27:143–9. doi: 10.1097/00006676-200308000-00007
109. Maisonneuve P, Lowenfels AB, Bueno-de-Mesquita HB, Ghadirian P, Baghurst PA, Zatonski WA, et al. Past medical history and pancreatic cancer risk: results from a multicenter case-control study. *Ann Epidemiol*. (2010) 20:92–8. doi: 10.1016/j.annepidem.2009.11.010
110. Garg SK, Maurer H, Reed K, Selagamsetty R. Diabetes and cancer: two diseases with obesity as a common risk factor. *Diabetes Obes Metab*. (2014) 16:97–110. doi: 10.1111/dom.12124
111. Cocca C, Nunez M, Gutierrez A, Martin G, Cricco G, Medina V, et al. IGF-I in mammary tumorigenesis and diabetes. *Anticancer Res*. (2004) 24:2953–65.
112. Lee MS, Hsu CC, Wahlqvist ML, Tsai HN, Chang YH, Huang YC. Type 2 diabetes increases and metformin reduces total, colorectal, liver and pancreatic cancer incidences in Taiwanese: a representative population prospective cohort study of 800,000 individuals. *BMC Cancer*. (2011) 11:20. doi: 10.1186/1471-2407-11-20
113. Chaiteerakij R, Yang JD, Harmsen WS, Slettedahl SW, Mettler TA, Fredericksen ZS, et al. Risk factors for intrahepatic cholangiocarcinoma: association between metformin use and reduced cancer risk. *Hepatology*. (2013) 57:648–55. doi: 10.1002/hep.26092
114. Singh S, Singh PP, Singh AG, Murad MH, Sanchez W. Anti-diabetic medications and the risk of hepatocellular cancer: a systematic review and meta-analysis. *Am J Gastroenterol*. (2013) 108:881–91; quiz 892. doi: 10.1038/ajg.2013.5
115. Singh S, Singh H, Singh PP, Murad MH, Limburg PJ. Antidiabetic medications and the risk of colorectal cancer in patients with diabetes mellitus: a systematic review and meta-analysis. *Cancer Epidemiol Biomarkers Prev*. (2013) 22:2258–68. doi: 10.1158/1055-9965.EPI-13-0429
116. Singh S, Singh PP, Singh AG, Murad MH, McWilliams RR, Chari ST. Anti-diabetic medications and risk of pancreatic cancer in patients with diabetes mellitus: a systematic review and meta-analysis. *Am J Gastroenterol*. (2013) 108:510–19; quiz 520. doi: 10.1038/ajg.2013.7
117. Tuccori M, Filion KB, Yin H, Yu OH, Platt RW, Azoulay L. Pioglitazone use and risk of bladder cancer: population based cohort study. *BMJ*. (2016) 352:i1541. doi: 10.1136/bmj.i1541
118. Tang H, Dai Q, Shi W, Zhai S, Song Y, Han J. SGLT2 inhibitors and risk of cancer in type 2 diabetes: a systematic review and meta-analysis of randomised controlled trials. *Diabetologia*. (2017) 60:1862–72. doi: 10.1007/s00125-017-4370-8
119. Arima R, Marttila M, Hautakoski A, Arffman M, Sund R, Ilanne-Parikka P, et al. Antidiabetic medication, statins and the risk of endometrioid endometrial cancer in patients with type 2 diabetes. *Gynecol Oncol*. (2017) 146:636–41. doi: 10.1016/j.ygyno.2017.06.011
120. Chen Y, Wu F, Saito E, Lin Y, Song M, Luu HN, et al. Association between type 2 diabetes and risk of cancer mortality: a pooled analysis of over 771,000 individuals in the Asia Cohort Consortium. *Diabetologia*. (2017) 60:1022–32. doi: 10.1007/s00125-017-4229-z
121. Habib SL, Rojna M. Diabetes and risk of cancer. *ISRN Oncol*. (2013) 2013:583786. doi: 10.1155/2013/583786
122. Yang Q, Ouyang J, Sun F, Yang J. Short-chain fatty acids: a soldier fighting against inflammation and protecting from tumorigenesis in people with diabetes. *Front Immunol*. (2020) 11:590685. doi: 10.3389/fimmu.2020.590685
123. Griffiths RI, Valderas JM, McFadden EC, Bankhead CR, Lavery BA, Khan NF, et al. Outcomes of preexisting diabetes mellitus in breast, colorectal, and prostate cancer. *J Cancer Surviv*. (2017) 11:604–13. doi: 10.1007/s11764-017-0631-2
124. Ng M, Fleming T, Robinson M, Thomson B, Graetz N, Margono C, et al. Global, regional, and national prevalence of overweight and obesity in children and adults during 1980-2013: a systematic analysis for the Global Burden of Disease Study 2013. *Lancet*. (2014) 384:766–81. doi: 10.1016/S0140-6736(14)60460-8
125. Musso G, Gambino R, Cassader M. Obesity, diabetes, and gut microbiota: the hygiene hypothesis expanded? *Diabetes Care*. (2010) 33:2277–84. doi: 10.2337/dc10-0556
126. Brown K, DeCoffe D, Molcan E, Gibson DL. Diet-induced dysbiosis of the intestinal microbiota and the effects on immunity and disease. *Nutrients*. (2012) 4:1095–119. doi: 10.3390/nu4081095
127. Turnbaugh PJ, Ridaura VK, Faith JJ, Rey FE, Knight R, Gordon JI. The effect of diet on the human gut microbiome: a metagenomic analysis in humanized gnotobiotic mice. *Sci Transl Med*. (2009) 1:6ra14. doi: 10.1126/scitranslmed.3000322
128. Gülden E, Wong FS, Wen L. The gut microbiota and Type 1 Diabetes. *Clin Immunol*. (2015) 159:143–53. doi: 10.1016/j.clim.2015.05.013
129. Murri M, Leiva I, Gomez-Zumaquero JM, Tinahones FJ, Cardona F, Soriguer F, et al. Gut microbiota in children with type 1 diabetes differs from that in healthy children: a case-control study. *BMC Med*. (2013) 11:46. doi: 10.1186/1741-7015-11-46
130. Burrows MP, Volchkov P, Kobayashi KS, Chervonsky AV. Microbiota regulates type 1 diabetes through Toll-like receptors. *Proc Natl Acad Sci U S A*. (2015) 112:9973–7. doi: 10.1073/pnas.1508740112
131. Yang C, Fei Y, Qin Y, Luo D, Yang S, Kou X, et al. Bacterial flora changes in conjunctiva of rats with streptozotocin-induced type i diabetes. *PLoS ONE*. (2015) 10:e0133021. doi: 10.1371/journal.pone.0133021
132. Goodrich JK, Waters JL, Poole AC, Sutter JL, Koren O, Blekhman R, et al. Human genetics shape the gut microbiome. *Cell*. (2014) 159:789–99. doi: 10.1016/j.cell.2014.09.053
133. Turnbaugh PJ, Ley RE, Mahowald MA, Magrini V, Mardis ER, Gordon JI. An obesity-associated gut microbiome with increased capacity for energy harvest. *Nature*. (2006) 444:1027–31. doi: 10.1038/nature05414
134. Koren O, Goodrich JK, Cullender TC, Spor A, Laitinen K, Bäckhed HK, et al. Host remodeling of the gut microbiome and metabolic changes during pregnancy. *Cell*. (2012) 150:470–80. doi: 10.1016/j.cell.2012.07.008
135. Qin J, Li Y, Cai Z, Li S, Zhu J, Zhang F, et al. A metagenome-wide association study of gut microbiota in type 2 diabetes. *Nature*. (2012) 490:55–60. doi: 10.1038/nature11450
136. Field AE, Willett WC, Lissner L, Colditz GA. Dietary fat and weight gain among women in the Nurses' Health Study. *Obesity*. (2007) 15:967–76. doi: 10.1038/oby.2007.616
137. Mozaffarian D, Hao T, Rimm EB, Willett WC, Hu FB. Changes in diet and lifestyle and long-term weight gain in women and men. *N Engl J Med*. (2011) 364:2392–404. doi: 10.1056/NEJMoa1014296
138. Graf D, Di Cagno R, Fåk F, Flint HJ, Nyman M, Saarela M, et al. Contribution of diet to the composition of the human gut microbiota. *Microb Ecol Health Dis*. (2015) 26:26164. doi: 10.3402/mehd.v26.26164
139. Sonnenburg ED, Smits SA, Tikhonov M, Higginbottom SK, Wingreen NS, Sonnenburg JL. Diet-induced extinctions in the gut microbiota compound over generations. *Nature*. (2016) 529:212–5. doi: 10.1038/nature16504

140. Everard A, Belzer C, Geurts L, Ouwerkerk JP, Druart C, Bindels LB, et al. Cross-talk between Akkermansia muciniphila and intestinal epithelium controls diet-induced obesity. *Proc Natl Acad Sci USA.* (2013) 110:9066–71. doi: 10.1073/pnas.1219451110
141. Tai N, Wong FS, Wen L. The role of gut microbiota in the development of type 1, type 2 diabetes mellitus and obesity. *Rev Endocr Metab Disord.* (2015) 16:55–65. doi: 10.1007/s11154-015-9309-0
142. Cani PD, Osto M, Geurts L, Everard A. Involvement of gut microbiota in the development of low-grade inflammation and type 2 diabetes associated with obesity. *Gut Microbes.* (2012) 3:279–88. doi: 10.4161/gmic.19625
143. Cani PD, Delzenne NM. The role of the gut microbiota in energy metabolism and metabolic disease. *Curr Pharm Des.* (2009) 15:1546–58. doi: 10.2174/138161209788168164
144. Forslund K, Hildebrand F, Nielsen T, Falony G, Le Chatelier E, Sunagawa S, et al. Disentangling type 2 diabetes and metformin treatment signatures in the human gut microbiota. *Nature.* (2015) 528:262–6. doi: 10.1038/nature15766
145. Lee H, Ko G. Effect of metformin on metabolic improvement and gut microbiota. *Appl Environ Microbiol.* (2014) 80:5935–43. doi: 10.1128/AEM.01357-14
146. Shin NR, Lee JC, Lee HY, Kim MS, Whon TW, Lee MS, et al. An increase in the Akkermansia spp. population induced by metformin treatment improves glucose homeostasis in diet-induced obese mice. *Gut.* (2014) 63:727–35. doi: 10.1136/gutjnl-2012-303839
147. Wang W, Lo ACY. Diabetic retinopathy: pathophysiology and treatments. *Int J Mol Sci.* (2018) 19. doi: 10.3390/ijms19061816
148. Xiao Z, Zhang X, Geng L, Zhang F, Wu J, Tong J, et al. Automatic non-proliferative diabetic retinopathy screening system based on color fundus image. *Biomed Eng Online.* (2017) 16:122. doi: 10.1186/s12938-017-0414-z
149. Sivaprasad S, Pearce E. The unmet need for better risk stratification of non-proliferative diabetic retinopathy. *Diabet Med.* (2019) 36:424–33. doi: 10.1111/dme.13868
150. Ghamdi AHA. Clinical predictors of diabetic retinopathy progression; a systematic review. *Curr Diabetes Rev.* (2020) 16:242–7. doi: 10.2174/1573399815666190215120435
151. Chen L, Cui Y, Li B, Weng J, Wang W, Zhang S, et al. Advanced glycation end products induce immature angiogenesis in in vivo and ex vivo mouse models. *Am J Physiol Heart Circ Physiol.* (2020) 318:H519–33. doi: 10.1152/ajpheart.00473.2019
152. Beltramo E, Porta M. Pericyte loss in diabetic retinopathy: mechanisms and consequences. *Curr Med Chem.* (2013) 20:3218–25. doi: 10.2174/09298673113209990022
153. Campochiaro PA. Molecular pathogenesis of retinal and choroidal vascular diseases. *Prog Retin Eye Res.* (2015) 49:67–81. doi: 10.1016/j.preteyeres.2015.06.002
154. Zimna A, Kurpisz M. Hypoxia-inducible factor-1 in physiological and pathophysiological angiogenesis: applications and therapies. *Biomed Res Int.* (2015) 2015:549412. doi: 10.1155/2015/549412
155. Catrina SB, Zheng X. Hypoxia and hypoxia-inducible factors in diabetes and its complications. *Diabetologia.* (2021) 64:709–16. doi: 10.1007/s00125-021-05380-z
156. Apte RS, Chen DS, Ferrara N. VEGF in signaling and disease: beyond discovery and development. *Cell.* (2019) 176:1248–64. doi: 10.1016/j.cell.2019.01.021
157. Zhao Y, Singh RP. The role of anti-vascular endothelial growth factor (anti-VEGF) in the management of proliferative diabetic retinopathy. *Drugs Context.* (2018) 7:212532. doi: 10.7573/dic.212532
158. Foxton RH, Uhles S, Gruner S, Revelant F, Ullmer C. Efficacy of simultaneous VEGF-A/ANG-2 neutralization in suppressing spontaneous choroidal neovascularization. *EMBO Mol Med.* (2019) 11. doi: 10.15252/emmm.201810204
159. Barrett EJ, Liu Z, Khamaisi M, King GL, Klein R, Klein BEK, et al. Diabetic microvascular disease: an endocrine society scientific statement. *J Clin Endocrinol Metab.* (2017) 102:4343–410. doi: 10.1210/jc.2017-01922
160. Shin ES, Sorenson CM, Sheibani N. Diabetes and retinal vascular dysfunction. *J Ophthalmic Vis Res.* (2014) 9:362–73. doi: 10.4103/2008-322X.143378
161. Rubsam A, Parikh S, Fort PE. Role of inflammation in diabetic retinopathy. *Int J Mol Sci.* (2018) 19. doi: 10.3390/ijms19040942
162. Sahajpal NS, Goel RK, Chaubey A, Aurora R, Jain SK. Pathological perturbations in diabetic retinopathy: hyperglycemia, AGEs, oxidative stress and inflammatory pathways. *Curr Protein Pept Sci.* (2019) 20:92–110. doi: 10.2174/1389203719666180928123449
163. Kang Q, Yang C. Oxidative stress and diabetic retinopathy: Molecular mechanisms, pathogenetic role and therapeutic implications. *Redox Biol.* (2020) 37:101799. doi: 10.1016/j.redox.2020.101799
164. Volpe CMO, Villar-Delfino PH, Dos Anjos PMF, Nogueira-Machado JA. Cellular death, reactive oxygen species (ROS) and diabetic complications. *Cell Death Dis.* (2018) 9:119. doi: 10.1038/s41419-017-0135-z
165. Marshall CB. Rethinking glomerular basement membrane thickening in diabetic nephropathy: adaptive or pathogenic? *Am J Physiol Renal Physiol.* (2016) 311:F831–43. doi: 10.1152/ajprenal.00313.2016
166. Aggarwal PK, Veron D, Thomas DB, Siegel D, Moeckel G, Kashgarian M, et al. Semaphorin3a promotes advanced diabetic nephropathy. *Diabetes.* (2015) 64:1743–59. doi: 10.2337/db14-0719
167. Sang Y, Tsuji K, Inoue-Torii A, Fukushima K, Kitamura S, Wada J. Semaphorin3A-inhibitor ameliorates doxorubicin-induced podocyte injury. *Int J Mol Sci.* (2020) 21. doi: 10.3390/ijms21114099
168. Tian X, Gan H, Zeng Y, Zhao H, Tang R, Xia Y. Inhibition of semaphorin-3a suppresses lipopolysaccharide-induced acute kidney injury. *J Mol Med (Berl).* (2018) 96:713–24. doi: 10.1007/s00109-018-1653-6
169. Hu W, Han Q, Zhao L, Wang L. Circular RNA circRNA_15698 aggravates the extracellular matrix of diabetic nephropathy mesangial cells via miR-185/TGF-beta1. *J Cell Physiol.* (2019) 234:1469–76. doi: 10.1002/jcp.26959
170. Zou Y, Zheng S, Deng X, Yang A, Xie X, Tang H, et al. The role of circular RNA CDR1as/ciRS-7 in regulating tumor microenvironment: a pan-cancer analysis. *Biomolecules.* (2019) 9. doi: 10.3390/biom9090429
171. Peng F, Gong W, Li S, Yin B, Zhao C, Liu W, et al. circRNA_010383 acts as a sponge for miR-135a, and its downregulated expression contributes to renal fibrosis in diabetic nephropathy. *Diabetes.* (2021) 70:603–15. doi: 10.2337/db20-0203
172. Zeng LF, Xiao Y, Sun L. A glimpse of the mechanisms related to renal fibrosis in diabetic nephropathy. *Adv Exp Med Biol.* (2019) 1165:49–79. doi: 10.1007/978-981-13-8871-2_4
173. Wei B, Liu YS, Guan HX. MicroRNA-145-5p attenuates high glucose-induced apoptosis by targeting the Notch signaling pathway in podocytes. *Exp Ther Med.* (2020) 19:1915–24. doi: 10.3892/etm.2020.8427
174. Xie L, Zhai R, Chen T, Gao C, Xue R, Wang N, et al. Panax notoginseng ameliorates podocyte EMT by targeting the Wnt/beta-catenin signaling pathway in STZ-induced diabetic rats. *Drug Des Devel Ther.* (2020) 14:527–38. doi: 10.2147/DDDT.S235491
175. Xu J, Deng Y, Wang Y, Sun X, Chen S, Fu G. SPAG5-AS1 inhibited autophagy and aggravated apoptosis of podocytes via SPAG5/AKT/mTOR pathway. *Cell Prolif.* (2020) 53:e12738. doi: 10.1111/cpr.12738
176. Jin J, Shi Y, Gong J, Zhao L, Li Y, He Q, et al. Exosome secreted from adipose-derived stem cells attenuates diabetic nephropathy by promoting autophagy flux and inhibiting apoptosis in podocyte. *Stem Cell Res Ther.* (2019) 10:95. doi: 10.1186/s13287-019-1177-1
177. Lin CL, Hsu YC, Huang YT, Shih YH, Wang CJ, Chiang WC, et al. A KDM6A-KLF10 reinforcing feedback mechanism aggravates diabetic podocyte dysfunction. *EMBO Mol Med.* (2019) 11. doi: 10.15252/emmm.201809828
178. Dumont V, Tolvanen TA, Kuusela S, Wang H, Nyman TA, Lindfors S, et al. PACSIN2 accelerates nephrin trafficking and is up-regulated in diabetic kidney disease. *FASEB J.* (2017) 31:3978–90. doi: 10.1096/fj.201601265R
179. Nakamichi R, Hayashi K, Itoh H. Effects of high glucose and lipotoxicity on diabetic podocytes. *Nutrients.* (2021) 13. doi: 10.3390/nu13010241
180. Xiong Y, Zhou L. The signaling of cellular senescence in diabetic nephropathy. *Oxid Med Cell Longev.* (2019) 2019:7495629. doi: 10.1155/2019/7495629
181. Sapian S, Budin SB, Taib IS, Mariappan V, Zainalabidin S, Chin KY. Role of polyphenol in regulating oxidative stress, inflammation, fibrosis, and apoptosis in diabetic nephropathy. *Endocr Metab Immune Disord Drug Targets.* (2021). doi: 10.2174/1871530321666211119144309. [Epub ahead of print].

182. Zhao M, Wang Y, Li L, Liu S, Wang C, Yuan Y, et al. Mitochondrial ROS promote mitochondrial dysfunction and inflammation in ischemic acute kidney injury by disrupting TFAM-mediated mtDNA maintenance. *Theranostics.* (2021) 11:1845–63. doi: 10.7150/thno.50905
183. Heerspink HJL, Stefansson BV, Chertow GM, Correa-Rotter R, Greene T, Hou FF, et al. Rationale and protocol of the dapagliflozin and prevention of adverse outcomes in chronic kidney disease (DAPA-CKD) randomized controlled trial. *Nephrol Dial Transplant.* (2020) 35:274–82. doi: 10.1093/ndt/gfz290
184. Wheeler DC, Stefansson BV, Batiushin M, Bilchenko O, Cherney DZI, Chertow GM, et al. The dapagliflozin and prevention of adverse outcomes in chronic kidney disease (DAPA-CKD) trial: baseline characteristics. *Nephrol Dial Transplant.* (2020) 35:1700–11. doi: 10.1093/ndt/gfaa234
185. Persson F, Rossing P, Vart P, Chertow GM, Hou FF, Jongs N, et al. Efficacy and safety of dapagliflozin by baseline glycemic status: a prespecified analysis from the DAPA-CKD trial. *Diabetes Care.* (2021) 44:1894–7. doi: 10.2337/dc21-0300
186. Fioretto P, Pontremoli R. Expanding the therapy options for diabetic kidney disease. *Nat Rev Nephrol.* (2021) 2021:1–2. doi: 10.1038/s41581-021-00522-3
187. Prandi FR, Evangelista I, Sergi D, Palazzuoli A, Romeo F. Mechanisms of cardiac dysfunction in diabetic cardiomyopathy: molecular abnormalities and phenotypical variants. *Heart Fail Rev.* (2022) 2022:1–10. doi: 10.1007/s10741-021-10200-y
188. Paolillo S, Marsico F, Prastaro M, Renga F, Esposito L, De Martino F, et al. Diabetic cardiomyopathy: definition, diagnosis, and therapeutic implications. *Heart Fail Clin.* (2019) 15:341–7. doi: 10.1016/j.hfc.2019.02.003
189. Jia G, Hill MA, Sowers JR. Diabetic cardiomyopathy: an update of mechanisms contributing to this clinical entity. *Circ Res.* (2018) 122:624–38. doi: 10.1161/CIRCRESAHA.117.311586
190. Poornima IG, Parikh P, Shannon RP. Diabetic cardiomyopathy: the search for a unifying hypothesis. *Circ Res.* (2006) 98:596–605. doi: 10.1161/01.RES.0000207406.94146.c2
191. Ji L, Liu F, Jing Z, Huang Q, Zhao Y, Cao H, et al. MICU1 Alleviates diabetic cardiomyopathy through mitochondrial Ca(2+)-dependent antioxidant response. *Diabetes.* (2017) 66:1586–600. doi: 10.2337/db16-1237
192. Li K, Zhai M, Jiang L, Song F, Zhang B, Li J, et al. Tetrahydrocurcumin ameliorates diabetic cardiomyopathy by attenuating high glucose-induced oxidative stress and fibrosis via activating the SIRT1 pathway. *Oxid Med Cell Longev.* (2019) 2019:6746907. doi: 10.1155/2019/6746907
193. Karbasforooshan H, Karimi G. The role of SIRT1 in diabetic cardiomyopathy. *Biomed Pharmacother.* (2017) 90:386–92. doi: 10.1016/j.biopha.2017.03.056
194. Zhai M, Li B, Duan W, Jing L, Zhang B, Zhang M, et al. Melatonin ameliorates myocardial ischemia reperfusion injury through SIRT3-dependent regulation of oxidative stress and apoptosis. *J Pineal Res.* (2017) 63. doi: 10.1111/jpi.12419
195. Luo YX, Tang X, An XZ, Xie XM, Chen XF, Zhao X, et al. SIRT4 accelerates Ang II-induced pathological cardiac hypertrophy by inhibiting manganese superoxide dismutase activity. *Eur Heart J.* (2017) 38:1389–98. doi: 10.1093/eurheartj/ehw138
196. Mangali S, Bhat A, Jadhav K, Kalra J, Sriram D, Vamsi Krishna Venuganti V, et al. Upregulation of PKR pathway mediates glucolipotoxicity induced diabetic cardiomyopathy in vivo in wistar rats and in vitro in cultured cardiomyocytes. *Biochem Pharmacol.* (2020) 177:113948. doi: 10.1016/j.bcp.2020.113948
197. Li DK, Smith LE, Rookyard AW, Lingam SJ, Koay YC, McEwen HP, et al. Multi-omics of a pre-clinical model of diabetic cardiomyopathy reveals increased fatty acid supply impacts mitochondrial metabolic selectivity. *J Mol Cell Cardiol.* (2021) 164:92–109. doi: 10.1016/j.yjmcc.2021.11.009
198. Sikder K, Shukla SK, Patel N, Singh H, Rafiq K. High fat diet upregulates fatty acid oxidation and ketogenesis via intervention of PPAR-gamma. *Cell Physiol Biochem.* (2018) 48:1317–31. doi: 10.1159/000492091
199. Lopaschuk GD, Karwi QG, Ho KL, Pherwani S, Ketema EB. Ketone metabolism in the failing heart. *Biochim Biophys Acta Mol Cell Biol Lipids.* (2020) 1865:158813. doi: 10.1016/j.bbalip.2020.158813
200. Shukla SK, Liu W, Sikder K, Addya S, Sarkar A, Wei Y, et al. HMGCS2 is a key ketogenic enzyme potentially involved in type 1 diabetes with high cardiovascular risk. *Sci Rep.* (2017) 7:4590. doi: 10.1038/s41598-017-04469-z
201. Yang F, Qin Y, Lv J, Wang Y, Che H, Chen X, et al. Silencing long non-coding RNA Kcnq1ot1 alleviates pyroptosis and fibrosis in diabetic cardiomyopathy. *Cell Death Dis.* (2018) 9:1000. doi: 10.1038/s41419-018-1029-4
202. Li H, Chen C, Wang DW. Inflammatory cytokines, immune cells, and organ interactions in heart failure. *Front Physiol.* (2021) 12:695047. doi: 10.3389/fphys.2021.695047
203. Zhou X, Zhang W, Jin M, Chen J, Xu W, Kong X. lncRNA MIAT functions as a competing endogenous RNA to upregulate DAPK2 by sponging miR-22-3p in diabetic cardiomyopathy. *Cell Death Dis.* (2017) 8:e2929. doi: 10.1038/cddis.2017.321
204. Li HQ, Wu YB, Yin CS, Chen L, Zhang Q, Hu LQ. Obestatin attenuated doxorubicin-induced cardiomyopathy via enhancing long noncoding Mhrt RNA expression. *Biomed Pharmacother.* (2016) 81:474–81. doi: 10.1016/j.biopha.2016.04.017
205. Li X, Wang H, Yao B, Xu W, Chen J, Zhou X. lncRNA H19/miR-675 axis regulates cardiomyocyte apoptosis by targeting VDAC1 in diabetic cardiomyopathy. *Sci Rep.* (2016) 6:36340. doi: 10.1038/srep36340
206. Byrne NJ, Rajasekaran NS, Abel ED, Bugger H. Therapeutic potential of targeting oxidative stress in diabetic cardiomyopathy. *Free Radic Biol Med.* (2021) 169:317–42. doi: 10.1016/j.freeradbiomed.2021.03.046
207. Guo Y, Feng X, Wang D, Kang X, Zhang L, Ren H, et al. Long non-coding RNA: a key regulator in the pathogenesis of diabetic cardiomyopathy. *Front Cardiovasc Med.* (2021) 8:655598. doi: 10.3389/fcvm.2021.655598
208. Zhang T, Gao Z, Chen K. Exosomal microRNAs: potential targets for the prevention and treatment of diabetic cardiomyopathy. *J Cardiol.* (2022) S0914-5087(21)00376-2. doi: 10.1016/j.jjcc.2021.12.013
209. Norgren L, Hiatt WR, Dormandy JA, Nehler MR, Harris KA, Fowkes FG, et al. Inter-society consensus for the management of peripheral arterial disease (TASC II). *J Vasc Surg.* (2007) 45 Suppl S:S5–67. doi: 10.1016/j.jvs.2006.12.037
210. Selvin E, Erlinger TP. Prevalence of and risk factors for peripheral arterial disease in the United States: results from the National Health and Nutrition Examination Survey, 1999–2000. *Circulation.* (2004) 110:738–43. doi: 10.1161/01.CIR.0000137913.26087.F0
211. Leibson CL, Ransom JE, Olson W, Zimmerman BR, O'Fallon WM, Palumbo PJ. Peripheral arterial disease, diabetes, and mortality. *Diabetes Care.* (2004) 27:2843–49. doi: 10.2337/diacare.27.12.2843
212. Thiruvoipati T, Kielhorn CE, Armstrong EJ. Peripheral artery disease in patients with diabetes: epidemiology, mechanisms, and outcomes. *World J Diabetes.* (2015) 6:961–9. doi: 10.4239/wjd.v6.i7.961
213. Paul S, Ali A, Katare R. Molecular complexities underlying the vascular complications of diabetes mellitus—a comprehensive review. *J Diabetes Comp.* (2020) 34:107613. doi: 10.1016/j.jdiacomp.2020.107613
214. Paneni F, Beckman JA, Creager MA, Cosentino F. Diabetes and vascular disease: pathophysiology, clinical consequences, and medical therapy: part I. *Eur Heart J.* (2013) 34:2436–43. doi: 10.1093/eurheartj/eht149
215. Signorelli SS, Scuto S, Marino E, Xourafa A, Gaudio A. Oxidative stress in peripheral arterial disease (PAD) mechanism and biomarkers. *Antioxidants.* (2019) 8:antiox8090367. doi: 10.3390/antiox8090367
216. Fadini GP, Spinetti G, Santopaolo M, Madeddu P. Impaired regeneration contributes to poor outcomes in diabetic peripheral artery disease. *Arterioscler Thromb Vasc Biol.* (2020) 40:34–44. doi: 10.1161/ATVBAHA.119.312863
217. Biscetti F, Nardella E, Bonadia N, Angelini F, Pitocco D, Santoliquido A, et al. Association between plasma omentin-1 levels in type 2 diabetic patients and peripheral artery disease. *Cardiovasc Diabetol.* (2019) 18:74. doi: 10.1186/s12933-019-0880-7
218. Alleboina S, Wong T, Singh MV, Dokun AO. Inhibition of protein kinase C beta phosphorylation activates nuclear factor-kappa B and improves postischemic recovery in type 1 diabetes. *Exp Biol Med.* (2020) 245:785–96. doi: 10.1177/1535370220920832
219. Hong J, Liu WY, Hu X, Jiang FF, Xu ZR, Li F, et al. Association between heart rate-corrected QT interval and severe peripheral arterial disease in patients with type 2 diabetes and foot ulcers. *Endocr Connect.* (2021) 10:845–51. doi: 10.1530/EC-21-0140

220. Katsiki N, Mikhailidis DP, Banach M. Leptin, cardiovascular diseases and type 2 diabetes mellitus. *Acta Pharmacol Sin.* (2018) 39:1176–88. doi: 10.1038/aps.2018.40
221. Dokun AO, Chen L, Lanjewar SS, Lye RJ, Annex BH. Glycaemic control improves perfusion recovery and VEGFR2 protein expression in diabetic mice following experimental PAD. *Cardiovasc Res.* (2014) 101:364–72. doi: 10.1093/cvr/cvt342
222. Neale JPH, Pearson JT, Thomas KN, Tsuchimochi H, Hosoda H, Kojima M, et al. Dysregulation of ghrelin in diabetes impairs the vascular reparative response to hindlimb ischemia in a mouse model; clinical relevance to peripheral artery disease. *Sci Rep.* (2020) 10:13651. doi: 10.1038/s41598-020-70391-6
223. Chen L, Liu C, Sun D, Wang T, Zhao L, Chen W, et al. MicroRNA-133a impairs perfusion recovery after hindlimb ischemia in diabetic mice. *Biosci Rep.* (2018) 38. doi: 10.1042/BSR20180346
224. Hazarika S, Farber CR, Dokun AO, Pitsillides AN, Wang T, Lye RJ, et al. MicroRNA-93 controls perfusion recovery after hindlimb ischemia by modulating expression of multiple genes in the cell cycle pathway. *Circulation.* (2013) 127:1818–28. doi: 10.1161/CIRCULATIONAHA.112.000860
225. Hamburg NM, Creager MA. Pathophysiology of intermittent claudication in peripheral artery disease. *Circ J.* (2017) 81:281–9. doi: 10.1253/circj.CJ-16-1286
226. Barnes JA, Eid MA, Creager MA, Goodney PP. Epidemiology and risk of amputation in patients with diabetes mellitus and peripheral artery disease. *Arterioscler Thromb Vasc Biol.* (2020) 40:1808–17. doi: 10.1161/ATVBAHA.120.314595
227. Chen SC, Chen CF, Huang JC, Lee MY, Chen JH, Chang JM, et al. Link between peripheral artery disease and heart rate variability in hemodialysis patients. *PLoS ONE.* (2015) 10:e0120459. doi: 10.1371/journal.pone.0120459
228. Kadoya M, Koyama H. Sleep, Autonomic nervous function and atherosclerosis. *Int J Mol Sci.* (2019) 20. doi: 10.3390/ijms20040794
229. Tay S, Abdulnabi S, Saffaf O, Harroun N, Yang C, Semenkovich CF, et al. Comprehensive assessment of current management strategies for patients with diabetes and chronic limb-threatening ischemia. *Clin Diabetes.* (2021) 39:358–88. doi: 10.2337/cd21-0019
230. Rodionov RN, Peters F, Marschall U, L'Hoest H, Jarzebska N, Behrendt CA. Initiation of SGLT2 inhibitors and the risk of lower extremity minor and major amputation in patients with type 2 diabetes and peripheral arterial disease: a health claims data analysis. *Eur J Vasc Endovasc Surg.* (2021) 62:981–90. doi: 10.1016/j.ejvs.2021.09.031
231. Yang MC, Huang YY, Hsieh SH, Sun JH, Wang CC, Lin CH. Ankle-brachial index is independently associated with cardiovascular outcomes and foot ulcers in asian patients with type 2 diabetes mellitus. *Front Endocrinol.* (2021) 12:752995. doi: 10.3389/fendo.2021.752995
232. Morrison T, Jones S, Causby RS, Thoirs K. Can ultrasound measures of intrinsic foot muscles and plantar soft tissues predict future diabetes-related foot disease? A systematic review. *PLoS ONE.* (2018) 13:e0199055. doi: 10.1371/journal.pone.0199055
233. Bus SA, Maas M, Cavanagh PR, Michels RP, Levi M. Plantar fat-pad displacement in neuropathic diabetic patients with toe deformity: a magnetic resonance imaging study. *Diabetes Care.* (2004) 27:2376–81. doi: 10.2337/diacare.27.10.2376
234. Wang X, Chen L, Liu W, Su B, Zhang Y. Early detection of atrophy of foot muscles in Chinese patients of type 2 diabetes mellitus by high-frequency ultrasonography. *J Diabetes Res.* (2014) 2014:927069. doi: 10.1155/2014/927069
235. Kumar CG, Rajagopal KV, Hande HM, Maiya AG, Mayya SS. Intrinsic foot muscle and plantar tissue changes in type 2 diabetes mellitus. *J Diabetes.* (2015) 7:850–7. doi: 10.1111/1753-0407.12254
236. Chatzistergos PE, Naemi R, Sundar L, Ramachandran A, Chockalingam N. The relationship between the mechanical properties of heel-pad and common clinical measures associated with foot ulcers in patients with diabetes. *J Diabetes Complications.* (2014) 28:488–93. doi: 10.1016/j.jdiacomp.2014.03.011

Conflict of Interest: The authors declare that the research was conducted in the absence of any commercial or financial relationships that could be construed as a potential conflict of interest.

Publisher's Note: All claims expressed in this article are solely those of the authors and do not necessarily represent those of their affiliated organizations, or those of the publisher, the editors and the reviewers. Any product that may be evaluated in this article, or claim that may be made by its manufacturer, is not guaranteed or endorsed by the publisher.

frontiers in Cardiovascular Medicine

POLICY AND PRACTICE REVIEWS
published: 24 February 2022
doi: 10.3389/fcvm.2022.762443

The Post-thrombotic Syndrome-Prevention and Treatment: VAS-European Independent Foundation in Angiology/Vascular Medicine Position Paper

Benilde Cosmi[1,2], Agata Stanek[3], Matja Kozak[4], Paul W. Wennberg[5], Raghu Kolluri[6], Marc Righini[7], Pavel Poredos[8], Michael Lichtenberg[9], Mariella Catalano[2], Sergio De Marchi[2,10], Katalin Farkas[11], Paolo Gresele[12], Peter Klein-Wegel[13], Gianfranco Lessiani[14], Peter Marschang[15], Zsolt Pecsvarady[16], Manlio Prior[2,10], Attila Puskas[17] and Andrzej Szuba[18]*

[1] Division of Angiology and Blood Coagulation, Department of Specialty, Diagnostic and Experimental Medicine, S. Orsola Malpighi University Hospital Research Institute IRCSS, University of Bologna, Bologna, Italy, [2] Inter-University Research Center on Vascular Diseases & Angiology Unit, University of Milan, L Sacco Hospital, VAS-European Independent Foundation in Angiology/Vascular Medicine, Milan, Italy, [3] Department of Internal Medicine, Angiology and Physical Medicine, Faculty of Medical Sciences in Zabrze, Medical University of Silesia, Bytom, Poland, [4] Department for Vascular Diseases, Medical Faculty of Ljubljana, University Medical Center Ljubljana, Ljubljana, Slovenia, [5] Department of Cardiovascular Medicine, Gonda Vascular Center, Mayo Clinic, Rochester, MN, United States, [6] Cardiovascular Medicine, OhioHealth/Riverside Methodist Hospital, Columbus, OH, United States, [7] Division of Angiology and Hemostasis, Geneva University Hospitals and Faculty of Medicine, Geneva, Switzerland, [8] Department for Vascular Disease, University Medical Center Ljubljana, Ljubljana, Slovenia, [9] Michael Lichtenberg, Klinikum Hochsauerland, Arnsberg, Germany, [10] Unit of Angiology, Department of Medicine - University of Verona, Cardiovascular and Thoracic Department, Verona University Hospital, Verona, Italy, [11] Department of Angiology, Szent Imre University Teaching Hospital, Budapest, Hungary, [12] Department of Medicine and Surgery, University of Perugia, Perugia, Italy, [13] Angiologic Clinic, Interdisciplinary Center of Vascular Medicine, Klinikum Ernst von Bergmann, Potsdam, Germany, [14] Angiology Unit, Department of Internal Medicine, Città Sant'Angelo Hospital, Pescara, Italy, [15] Department of Internal Medicine, Central Hospital of Bolzano (SABES-ASDAA), Bolzano, Italy, [16] 2nd Department of Internal Medicine - Vascular Center, Flor Ferenc Teaching Hospital, Kistarcsa, Hungary, [17] Angio Center-Vascular Medicine Private Clinic, Tirgu Mures, Romania, [18] Department of Angiology, Hypertension and Diabetology, Wroclaw Medical University, Wroclaw, Poland

OPEN ACCESS

Edited by:
Pietro Enea Lazzerini, University of Siena, Italy

Reviewed by:
Per Morten Sandset, University of Oslo, Norway
Alejandro Lazo-Langner, Western University, Canada

***Correspondence:**
Benilde Cosmi
benilde.cosmi@unibo.it; vas@unimi.it

Specialty section:
This article was submitted to General Cardiovascular Medicine, a section of the journal Frontiers in Cardiovascular Medicine

Received: *21 August 2021*
Accepted: *10 January 2022*
Published: *24 February 2022*

Citation:
Cosmi B, Stanek A, Kozak M, Wennberg PW, Kolluri R, Righini M, Poredos P, Lichtenberg M, Catalano M, De Marchi S, Farkas K, Gresele P, Klein-Wegel P, Lessiani G, Marschang P, Pecsvarady Z, Prior M, Puskas A and Szuba A (2022) The Post-thrombotic Syndrome-Prevention and Treatment: VAS-European Independent Foundation in Angiology/Vascular Medicine Position Paper. Front. Cardiovasc. Med. 9:762443. doi: 10.3389/fcvm.2022.762443

Importance: The post-thrombotic syndrome (PTS) is the most common long-term complication of deep vein thrombosis (DVT), occurring in up to 40–50% of cases. There are limited evidence-based approaches for PTS clinical management.

Objective: To provide an expert consensus for PTS diagnosis, prevention, and treatment.

Evidence-Review: MEDLINE, Cochrane Database review, and GOOGLE SCHOLAR were searched with the terms "post-thrombotic syndrome" and "post-phlebitic syndrome" used in titles and abstracts up to September 2020.

Filters Were: English, Controlled Clinical Trial / Systematic Review / Meta-Analysis / Guideline. The relevant literature regarding PTS diagnosis, prevention and treatment was reviewed and summarized by the evidence synthesis team. On the basis of this review, a panel of 15 practicing angiology/vascular medicine specialists assessed the appropriateness of several items regarding PTS management on a Likert-9 point scale, according to the RAND/UCLA method, with a two-round modified Delphi method.

Findings: The panelists rated the following as appropriate for diagnosis: 1-the Villalta scale; 2- pre-existing venous insufficiency evaluation; 3-assessment 3–6 months after diagnosis of iliofemoral or femoro-popliteal DVT, and afterwards periodically, according to a personalized schedule depending on the presence or absence of clinically relevant PTS. The items rated as appropriate for symptom relief and prevention were: 1- graduated compression stockings (GCS) or elastic bandages for symptomatic relief in acute DVT, either iliofemoral, popliteal or calf; 2-thigh-length GCS (30–40 mmHg at the ankle) after ilio-femoral DVT; 3- knee-length GCS (30–40 mmHg at the ankle) after popliteal DVT; 4-GCS for different length of times according to the severity of periodically assessed PTS; 5-catheter-directed thrombolysis, with or without mechanical thrombectomy, in patients with iliofemoral obstruction, severe symptoms, and low risk of bleeding. The items rated as appropriate for treatment were: 1- thigh-length GCS (30–40 mmHg at the ankle) after iliofemoral DVT; 2-compression therapy for ulcer treatment; 3- exercise training. The role of endovascular treatment (angioplasty and/or stenting) was rated as uncertain, but it could be considered for severe PTS only in case of stenosis or occlusion above the inguinal ligament, followed by oral anticoagulation.

Conclusions and Relevance: This position paper can help practicing clinicians in PTS management.

Keywords: post-thrombotic syndrome, post-phlebitic syndrome, deep vein thrombosis, prevention, diagnosis, treatment

INTRODUCTION

Post-thrombotic syndrome (PTS) is the most common long-term complication of deep vein thrombosis (DVT) occurring in up to 40–50% of patients, primarily due to impaired thrombus resolution with persistent venous outflow obstruction and secondary valvular incompetence (1). PTS has not been routinely considered as an outcome of the large number of randomized clinical trials which have investigated pharmacological strategies for the prevention and treatment of venous thromboembolism (VTE), which includes DVT and PE in the last 30 years (2–4) and only secondary *post-hoc* analyses are available (5). Unfortunately there is very limited evidence regarding a number of issues in PTS management, and what evidence exists is of very low quality.

The limited evidence available and the many areas of uncertainty also imply a wide spectrum of variations and heterogeneity in PTS clinical management across different countries.

This prompted VAS-European Independent Foundation in Angiology/Vascular Medicine to launch a project for a position paper on the appropriateness of interventions for PTS involving practicing expert clinicians from many different countries.

The concept of appropriateness refers to the relative weight of the benefits and harms of a medical or surgical intervention (6). An appropriate procedure is one in which "the expected health benefit (e.g., increased life expectancy, relief of pain, reduction in anxiety, improved functional capacity) exceeds the expected negative consequences (e.g., mortality, morbidity, anxiety, pain, time lost from work) by a sufficiently wide margin that the procedure is worth doing, exclusive of cost" (6).

VAS-European Independent Foundation in Angiology/Vascular Medicine is a non-profit scientific organization (Transparency European Union Register Number: 818165941069-15) which was established in 1991 (as European Working Group). VAS established programs on European education and training (UEMS accreditation), promoting collaborative research as well as awareness in the area of vascular medicine/angiology (www.vas-int.net). To enforce stable collaborations in Europe and internationally, VAS defined stable partnerships with >50 scientific societies organizations and Universities in Europe and at international level. VAS is present in more than 40 countries and it has established networks focused on actions and campaigns, aimed at improving and qualifying competences and attention on vascular disease, as well as suggesting concrete changes on health systems approach to vascular diseases and their prevention for the benefit of patients and populations.

The aim of VAS position paper was to provide practical indications to the busy clinician for diagnosis, prevention, and treatment of PTS after DVT of the lower limbs.

METHODS

We used the RAND/UCLA appropriateness method and a two-round modified Delphi method (6). A multidisciplinary group of expert practicing clinicians were recruited to conduct a literature review (evidence synthesis team) composed of eight practicing angiology/vascular medicine specialists from seven different European Countries and from USA. MEDLINE, Cochrane Database review and GOOGLE SCHOLAR were

searched from up to September 2020 with terms used in titles and abstracts: "post-phlebitic syndrome," "diagnosis," "prevention," and "treatment." Filters were: English, Controlled Clinical Trial / Systematic Review / Meta-Analysis / Guideline. Only prospective clinical trials examining PTS diagnosis, and randomized clinical trials and systematic reviews that examined prevention and treatment of PTS, published in the English language, were included. Abstracts, conference proceedings, review paper, observational or retrospective cohort studies for prevention or treatment, editorials and commentaries were excluded.

Following the search, duplicates were removed. Titles and abstracts were screened for assessment against review inclusion criteria. Full text of selected citations was assessed in detail against the inclusion criteria and, out of 496 citations, three prospective studies for diagnosis, five systematic reviews, and four randomized clinical trials not included in the systematic reviews were selected. Any disagreements that arose between the reviewers were resolved through discussion.

Methodological assessment was conducted according to the American College of Cardiology Foundation/ American Heart Association Task Force on Practice Guidelines (7) and The Rational Clinical Examination (8). Methodological assessment was completed for systematic reviews and primary studies not included in the systematic reviews. In fact primary studies included in the systematic reviews had been assessed for risk of bias when included in the original systematic reviews. **Appendix 1** reports the results of this review.

Based on this review, a Likert 9-point scale was constructed for each of 29 items regarding PTS diagnosis, prevention and treatment. Forms were sent to a 15 member expert panel *via* e-mail. The expert panel was composed of 13 angiology/vascular medicine specialists and two internal medicine specialists from seven different European countries, some of them also members of the VAS Advisory board with a large clinical experience in qualified centers.

Each panelist rated each item separately and e-mailed the rated items to the moderator (BC) (first round). Items were classified into three levels of appropriateness (**Table 1**).

Indications were classified into three levels of appropriateness, using the following definitions (6):

- *Appropriate*: panel median of 7–9, without disagreement on the final appropriateness scale. It would be considered improper care not to provide this service, and there is a reasonable chance that this procedure will benefit the patient (A procedure could be appropriate if it had a low likelihood of benefit but few risks; such procedures would not be necessary). The benefit to the patient is not small (A procedure could be appropriate if it had a minor but almost certain benefit, but it would not be necessary).
- *Uncertain*: panel median of 4–6 OR any median with disagreement
- *Inappropriate*: panel median of 1–3, without disagreement

And the agreement of all ratings was calculated with the Interpercentile Range Adjusted for Symmetry (IPRAS) (6). If the Interpercentile Range of a particular indication is larger than the IPRAS of that particular indication, it is rated with disagreement. This method allows for any number of participant responses and better accounts for dispersion and higher weights on the extremes than traditional methods (9).

The second round involved a face-to-face web-based virtual meeting of panelists with the moderator to debate the median ratings and disagreements from all panelists and to propose items for the final statements.

RESULTS

Table 1 shows ratings and disagreements. During the second round, of the 26 items for which there was agreement, 15 were accepted with no change, two were modified and retained, and nine were deleted. The three items for which there was disagreement were deleted. The final total was 17 items.

VAS Position Statements

PTS Diagnosis and Surveillance

1- The Villata Scale (VS) is appropriate for the diagnosis and classification of PTS severity.

2- It is appropriate to assess pre-existing venous insufficiency (e.g., contralateral limb) for classifying PTS severity after DVT.

3- It is appropriate to assess PTS at least 3–6 months after the diagnosis of iliofemoral or femoro-popliteal DVT, and afterwards according to a personalized schedule depending on the presence or absence of clinically relevant PTS at these time-points.

There is no specific recommended time limit to diagnose PTS and studies have followed up patients for two 2 years or longer. Initial symptoms and signs of the acute phase may require sometime to subside. As a result, the diagnosis of PTS should be deferred until 3–6 months. Afterwards, the timing of surveillance is also related to the severity of PTS at these time points, also considering risk factors for PTS and patients' characteristics (DVT initial extension, BMI, life style).

PTS Symptom Management

1- Graduated compression stockings (GCS) or elastic bandages are appropriate for symptomatic relief in acute DVT, either iliofemoral, popliteal, or calf.

Compression can ameliorate limb pain and swelling in both proximal and calf DVT. Ideally, elastic bandages are more appropriate in severely swollen limbs in the first few days, although not always feasible. After reducing the swelling with compression bandages, GCS can be applied. The size of compression stockings should be taken on the limb contralateral to the DVT to avoid stockings becoming too large after oedema has subsided.

2- Catheter-directed thrombolysis, with or without mechanical thrombectomy, is appropriate in patients with iliofemoral obstruction, severe symptoms, and a low risk of bleeding.

TABLE 1 | Ratings of proposed items with medians and disagreement.

PTS diagnosis and surveillance	Median	Disagreement
1- The Villalta scale is recommended for diagnosis and severity classification of PTS	7	No
2- The Ginsberg scale is recommended for diagnosis and severity classification of PTS	5	Yes
3- The Brandjes scale is recommended for diagnosis and severity classification of PTS	5	No
4- The CEAP scale is recommended for diagnosis and severity classification of PTS	5	No
5- Preexisting venous insufficiency (e.g., contralateral limb) should be taken into account for classifying PTS severity after DVT	7	No
6- PTS should be assessed 1 month after the diagnosis of iliofemoral DVT	4	Yes
7- PTS should be assessed 1 month after the diagnosis of popliteal or calf DVT	4	Yes
8- PTS should be assessed 6 months after the diagnosis of iliofemoral DVT	8	No
9- PTS should be assessed 6 months after the diagnosis of popliteal or calf DVT	7	No
10- PTS should be assessed periodically (e.g., 6 months) and for at least 2 years since the diagnosis of proximal or calf DVT	7	No
PTS symptom mangement and prevention	**Median**	**Disagreement**
1- Graduated compression stockings (GCS) or elastic bandages are recommended for symptomatic relief in acute DVT	8	No
2- Knee length GCS (40 mmHg at the ankle) are recommended after iliofemoral DVT	6	No
3- Thigh-length GCS (40 mmHg at the ankle) are recommended after iliofemoral DVT	7	No
4- Knee length GCS (40 mmHg at the ankle) are recommended after popliteal or calf DVT	7	No
5- Thigh length GCS (40 mmHg at the ankle) are recommended after popliteal or calf DVT	4	No
6- GCS are recommended for different lengths of time according to the severity of periodically assessed PTS	7	No
7- Catheter-directed thrombolysis, with or without mechanical thrombectomy, are appropriate in patients with iliofemoral obstruction, severe symptoms, and a low risk of bleeding	7	No
8- Catheter-directed thrombolysis, with or without mechanical thrombectomy, are appropriate in patients with popliteal obstruction, severe symptoms, and a low risk of bleeding	4	No
PTS Treatment	**Median**	**Disagreement**
1- Thigh length GCS (30–40 mmHg at the ankle) are recommended after iliofemoral DVT	7	No
2- Knee length GCS (30–40 mmHg at the ankle) are recommended after iliofemoral DVT	6	No
3- Thigh-length GCS (30–40 mmHg at the ankle) are recommended after popliteal or calf DVT	3	No
4- Knee length GCS (30–40 mmHg at the ankle) are recommended after popliteal or calf DVT	7	No
5- Compression therapy is recommended for ulcer treatment	9	No
6- Exercise training is recommended for PTS treatment	7	No
7- Endovascular treatment (angioplasty and/or stenting) is recommended for the treatment of severe PTS	6	No
8- Oral anticoagulation is recommended after endovascular treatment with stenting	7	No
9- Long term oral anticoagulation is recommended after endovascular treatment with stenting	6	No
10- Open surgical reconstruction and hybrid operations are appropriate for the treatment of severe PTS	4	No
11- Veno-active drugs are recommended	6	No

Appropriate: panel median of 7–9, without disagreement on the final appropriateness scale: it would be considered improper care not to provide this service, and there is a reasonable chance that this procedure will benefit the patient. The benefit to the patient is not small.

Uncertain: panel median of 4–6 OR any median with disagreement; Inappropriate: panel median of 1–3, without disagreement.

It is appropriate, especially in young subjects with iliofemoral DVT, for symptomatic relief (especially in Iliac Vein Compression syndrome) and improvement of quality of life.

The CaVent study on CDT had a long follow-up and reported a significant reduction in PTS in subjects with iliofemoral DVT treated with CDT albeit with an increased risk of bleeding.

PTS Prevention

1- Thigh-length GCS (30–40 mmHg at the ankle) are appropriate for the prevention of PTS after iliofemoral DVT.

Studies on the use of GCS for PTS prevention have produced conflicting results and a Cochrane meta-analysis concluded that the use of GCS led to a clinically significant, although non statistically significant, reduction in the incidence of PTS albeit with no reduction in the incidence of severe PTS and no clear difference in DVT recurrence or PE.

Studies have evaluated knee-high GCS to prevent PTS, as they are more comfortable and easy to wear. Thigh-high GCS are also available, although less comfortable, and they may be employed during the initial 6–12 months, while knee-high GCS could be employed afterward. A personalized choice of stockings could be considered according to DVT extension and development of PTS.

2- Knee-length GCS (30–40 mmHg at the ankle) are appropriate for the prevention of PTS after popliteal DVT.

Knee-length stockings are more comfortable, and they increase patient compliance with GCS.

The correct information and continuous guidance of the patient is paramount to increase compliance. A reduction of the degree of compression may be considered to improve

compliance. Calf DVT does not deserve stockings for prevention, but only for symptom relief.

3- GCS are appropriate for different lengths of time according to the severity of periodically assessed PTS.

The duration of compression stockings should be individualized according to the severity of PTS as assessed over time. Thigh-high GCS could be used in certain patients, such as those with extensive iliofemoral DVT, skin induration, or secondary lymphedema ("phlebolymphedema").

PTS Treatment

1- Thigh length GCS (30–40 mmHg at the ankle) are appropriate for PTS treatment after iliofemoral DVT.
2- Knee length GCS (30–40 mmHg at the ankle) are appropriate for PTS treatment after popliteal DVT.
3- Compression therapy is appropriate for ulcer treatment.

Treatment of ulcers due to PTS with different types of bandages/stockings is a broader topic, also applying to ulcers due to chronic venous insufficiency, deserving to be addressed separately.

4- Exercise training is appropriate for PTS treatment. Exercise training such as walking is addressed in very few studies, as well as lifestyle changes such as weight loss in overweight or obese subjects.
5- The role of endovascular treatment (angioplasty and/or stenting above the inguinal ligament) is uncertain for the treatment of severe PTS. Such an approach can be considered only in stenosis or occlusion, without severe valve incompetence, and only above the inguinal ligament.
6- Oral anticoagulation is appropriate after endovascular treatment with stenting for PTS treatment.

However, the type and optimal length of anticoagulation is uncertain and still a debated issue.

DISCUSSION

PTS is the most common complication of DVT; however, many uncertainties remain regarding its diagnosis, prevention, and treatment. This consensus paper provides a framework for the busy clinician, addressing several practical issues of PTS management.

The methodological assessment of the existing studies on PTS rated most of them of low or very low quality. As a result, many issues regarding PTS management deserve further investigation.

PTS diagnosis itself needs further research efforts as more recent studies raise concerns with VS scale, although externally validated and endorsed by scientific societies. Limitations include the subjective measures of its components, the presence of all items in patients with chronic venous insufficiency (CVI) due to primary valvular reflux or secondary superficial venous insufficiency unrelated to DVT (9) and the lack of evaluation of ulcer severity. Since the prevalence of primary CVI is higher in the general population, a significant proportion of DVT patients have pre-existing primary CVI. However, CVI cannot be correctly evaluated at the time of DVT diagnosis although the examination of the contralateral limb could help. The presence of pre-existing VCI could worsen PTS signs and symptoms and lead to overestimation of the severity of PTS during follow-up.

VS has the potential to misclassify or overestimate pre-existing venous disease as PTS (10). However, there is no formal method to account for pre-existing venous insufficiency in the VS. In another study, the authors concluded that common patient complaints and the impact of PTS are not well-reflected in the VS (11). Most recently, Ning et al. noted that VS misclassified those with primary CVI and a history of DVT as having PTS by 42.3% (12). The VS plus revised CEAP could be investigated to incorporate previous venous insufficiency (13).

The timing of PTS surveillance is also not well-defined. Studies have usually evaluated PTS every 6 months after diagnosis for 2 years. Assessment at 1 month after diagnosis is too early, as there might still be symptoms of the acute phase, although one study showed that persisting symptoms after 1 month are associated with a higher risk of PTS. Another option is the SOX-PTS scale combining the VS with BMI plus anatomical extension of PTS at the time of DVT diagnosis which was developed and externally validated to predict PTS occurrence at the time of DVT diagnosis (14). This scale could help identify those subjects who may need more strict surveillance to detect PTS development. Whole leg color Duplex scan ultrasound may be performed at each time point of follow-up (in lying and standing position with standardized provocative maneuvers) but only the basis of worsening symptoms, also to exclude recurrent DVT. Still, it may not reflect the clinical stage of PTS, which requires a physical examination. A Choose Wisely statement of the Society of Vascular Medicine partnered with American Board of Internal Medicine came out with—do not repeat DUS unless there are changes in clinical symptoms (15). Moreover, ultrasound modalities to assess recanalization (e.g., presence of residual thrombosis) and venous reflux are not incorporated in formal scales and not standardized. Methods to standardize the ultrasound results should also require further investigation.

Surveillance with telemedicine to avoid office visits with the self-assessment of VS and quality of life assessment could also be further explored. PTS prevention is still a major debated issue, especially in case of extensive DVT when the interventional approach can be considered. The CaVent study had a long follow-up and reported a significant reduction in PTS in subjects with iliofemoral DVT treated with CDT albeit with an increased risk of bleeding (16).

However, only a minority of the overall population presenting with iliofemoral DVT was enrolled into interventional studies for PTS prevention with pharmacomechanical thrombectomy (PMT) adjunctive to standard anticoagulant treatment vs. standard anticoagulant treatment alone such as in the ATTRACT trial (17), as <2.5% of the screened population were enrolled. Suboptimal technical success rates were observed and this could explain poor outcomes in the intervention arms. However, in these multicentre studies, the technical outcomes could be interpreted as more reflective of routine practice than selected centers of excellence. Several limitations of the ATTRACT study should also be considered, such as a significant heterogeneity

of devices and methods employed for clot removal, no clear indication for stenting, the use of only arterial stents were, a long interval between symptom onset and onset of therapy.

In conclusion, the results of the interventional randomized clinical trials such as ATTRACT and CAVA (17, 18) indicate that at the moment, PMT cannot be recommended routinely for DVT of the lower limbs, for which anticoagulation remains the standard treatment. However, the role of interventional therapy for PTS has evolving evidence. The relationship between the technical success of early thrombus removal (and persistent deep venous patency) and clinical outcomes deserves further investigation.

The role of DOACs for PTS prevention is emerging in recent studies and in *post-hoc* analyses evaluating PTS in trials of DVT treatment with DOAC vs. VKA (19). Despite several limitations, in studies on DOACs more than 60–70% of patients were free of PTS and severe manifestations such as skin ulcer and/or other severe and, by definition, intractable manifestations, were observed only in a minority (<5–6%) of subjects after an average of 30-month follow-up in both DOAC and VKA treated patients. These PTS rates at long-term follow-up are similar to those of studies in which thrombolytic therapies were used, such as in the ATTRACT study and are possibly related to a less variable anticoagulant activity in the acute phase of DVT, thus favoring vein recanalization (20). There are no randomized trials comparing interventional approaches to conservative approaches for PTS treatment, and only observational studies are available on the use of venous stents, which therefore cannot be recommended routinely.

In addition, the optimal antithrombotic treatment after venous stenting is still not clearly defined and varies among different studies. As a result, firm indications cannot be extrapolated from such studies. General recommendations include anticoagulant therapy during the intervention and continued after the intervention, usually for 3–6 months. DOACs are being used to an increasing extent, but there is a lack of sufficient experience with these agents (20).

Lifestyle changes such as exercise and BMI control in case of overweight or obesity should also be considered, although very limited evidence exists on these approaches for both PTS prevention and treatment.

CONCLUSION

PTS is the most common long term complication of DVT, regular surveillance and conservative medical approach with standard anticoagulation and graduated compression stockings are indicated for PTS prevention in the majority of subjects. Interventional and endovascular approaches for prevention and treatment have limited evidence and should be considered in selected subjects. The statements of this position paper merely reflect the consensus opinion of experts based on low quality evidence in most cases.

AUTHOR CONTRIBUTIONS

BC and MC: conception and design, construction of Likert 9-point scale items. BC, AS, MK, PW, RK, MR, PP, ML, and MC: literature search, review with methodological assessments, and evidence synthesis. BC, MC, SD, KF, PG, PW, MK, GL, PM, ZP, PP, MP, AP, MR, ASt, and ASz: rating of items and participation to the two-round modified Delphi consensus. BC and ASt: drafting the article. All authors: critical revision of the article for important intellectual content and final approval. All authors contributed to the article and approved the submitted version.

SUPPLEMENTARY MATERIAL

The Supplementary Material for this article can be found online at: https://www.frontiersin.org/articles/10.3389/fcvm.2022.762443/full#supplementary-material

REFERENCES

1. Vazquez SR, Kahn SR. Advances in the diagnosis and management of postthrombotic syndrome. *Best Pract Res Clin Haematol.* (2012) 25:391–402. doi: 10.1016/j.beha.2012.06.006
2. Geerts WH, Bergqvist D, Pineo GF, Heit JA, Samama CM, Lassen MR, et al. Prevention of venous thromboembolism: American College of Chest Physicians Evidence-Based Clinical Practice Guidelines (8th Edition). *Chest.* (2008) 133(6 Suppl.):381S–453S. doi: 10.1378/chest.08-0656
3. Kearon C, Akl EA, Ornelas J, Blaivas A, Jimenez D, Bounameaux H, et al. Antithrombotic therapy for VTE disease: CHEST guideline and expert panel report. *Chest.* (2016) 149:315–52. doi: 10.1016/j.chest.2015.11.026
4. Kahn SR, Galanaud JP, Vedantham S, Ginsberg JS. Guidance for the prevention and treatment of the post-thrombotic syndrome. *J Thromb Thrombolysis.* (2016) 41:144–53. doi: 10.1007/s11239-015-1312-5
5. Cheung YW, Middeldorp S, Prins MH, Pap AF, Lensing AW, Ten Cate-Hoek AJ, et al. Post-thrombotic syndrome in patients treated with rivaroxaban or enoxaparin/vitamin K antagonists for acute deep-vein thrombosis: a *post-hoc* analysis. *Thromb Haemost.* (2016) 116:733–8. doi: 10.1160/TH16-01-0041
6. Fitch K. *Rand/UCLA Appropriateness Method User's Manual*. RAND. Available online at: http://www.rand.org (acessed April 20, 2021).
7. Jacobs AK, Kushner FG, Ettinger SM, Guyton RA, Anderson JL, Ohman EM, et al. ACCF/AHA clinical practice guideline methodology summit report: a report of the American College of Cardiology Foundation/American Heart Association Task Force on Practice Guidelines. *J Am Coll Cardiol.* (2013) 61:213–65. doi: 10.1016/j.jacc.2012.09.025
8. Simel D. A primer on the precision and accuracy of the clinical examination. Update. In: Simel DL, Rennie D, editors, *The Rational Clinical Examination*. New York, NY: Mcgraw- Hill (2009). Available online at: http://www.jamaevidence.com/content/347002 (acessed April 20, 2021).
9. Strijkers RH, Wittens CH, Kahn SR. Villalta scale: goals and limitations. *Phlebology.* (2012) 27(Suppl.1):130–5. doi: 10.1258/phleb.2011.012s02
10. Soosainathan A, Moore HM, Gohel MS, Davies AH. Scoring systems for the post-thrombotic syndrome. *J Vasc Surg.* (2013) 57:254–61. doi: 10.1016/j.jvs.2012.09.011
11. Engeseth M, Enden T, Andersen MH, Sandset PM, Wik HS. Does the Villalta scale capture the essence of postthrombotic syndrome? A qualitative study of patient experience and expert opinion. *J Thromb Haemost.* (2019) 17:1707–14. doi: 10.1111/jth.14557

12. Ning J, Ma W, Fish J, Trihn F, Lurie F. Biases of Villalta scale in classifying post-thrombotic syndrome in patients with pre-existing chronic venous disease. *J Vasc Surg Venous Lymphat Disord.* (2020) 8:1025–30. doi: 10.1016/j.jvsv.2020.01.018
13. Lurie F, Passman M, Meisner M, Dalsing M, Masuda E, Welch H, et al. The 2020 update of the CEAP classification system and reporting standards. *J Vasc Surg Venous Lymphat Disord.* (2020) 8:342–52. doi: 10.1016/j.jvsv.2019.12.075
14. Rabinovich A, Gu CS, Vedantham S, Kearon C, Goldhaber SZ, Gornik HL et al. External validation of the SOX-PTS score in a prospective multicenter trial of patients with proximal deep vein thrombosis. *J Thromb Haemost.* (2020) 18:1381–9. doi: 10.1111/jth.14791
15. Five things physicians and patients should question in vascular medicine. *Choosing Wisely*. Available online at: https://www.vascularmed.org/i4a/pages/index.cfm?pageID=3398&activateFull=tru
16. Haig Y, Enden T, Grøtta O, Kløw NE, Slagsvold CE, Ghanima W, et al. Post-thrombotic syndrome after catheter-directed thrombolysis for deep vein thrombosis (CaVenT): 5-year follow-up results of an open-label, randomised controlled trial. *Lancet Haematol.* (2016) 3:e64–71. doi: 10.1016/S2352-3026(15)00248-3
17. Vedantham S, Goldhaber SZ, Julian JA, Kahn SR, Jaff MR, Cohen DJ, et al. Pharmacomechanical catheter-directed thrombolysis for deep-vein thrombosis. *N Engl J Med.* (2017) 377:2240–52. doi: 10.1056/NEJMoa1615066
18. Notten P, Ten Cate-Hoek AJ, Arnoldussen CWKP, Strijkers RHW, de Smet AAEA, Tick LW, et al. Ultrasound-accelerated catheter-directed thrombolysis versus anticoagulation for the prevention of post-thrombotic syndrome (CAVA): a single blind, multicentre, randomised trial. *Lancet Haematol.* (2020) 7:e40–9. doi: 10.1016/S2352-3026(19)30209-1
19. Palareti G, Cosmi B. The direct oral anticoagulants may also be effective against the risk of postthrombotic syndrome. *Intern Emerg Med.* (2020) 15:365–7. doi: 10.1007/s11739-019-02251-9
20. Jalaie H, Arnoldussen C, Barbati M, Kurstjens R, de Graaf R, Grommes J, et al. What predicts outcome after recanalization of chronic venous obstruction: hemodynamic factors, stent geometry, patient selection, anticoagulation or other factors? *Phlebology*. (2014) 29(1Suppl):97–103. doi: 10.1177/0268355514529510

Conflict of Interest: BC declares speakers's fees from Instrumentation Laboratory, Werfen IL, Sanofi, Aspen, Bristol-Myers-Squibb, advisory board fees for Viatris, Techdow Farma Italy. ASt declares receiving grants from Metrum Cryoflex, honorario for lectures from Alfa Sigma, President of the Polish Society of Cryotherapy, unpaid. GL reports Leadership or fiduciary role in other board, society, committee or advocacy group, paid or unpaid: Vice President of Italian Society of Angiology and Vascular Disease (2018–2021); consulting fees from Alfa Sigma. PM declares Payment for a lecture from Bayer (2018), President of the Austrian Society of Vascular Medicine (ÖGIA) 2018–2019, unpaid. MP declares payment or honoraria for lectures of Alfa Sigma, Aspen, BMS Pfizer, support for travel from Alfa Sigma. MC Honorary President UEMS, Division of Angiology unpaid. PG is President of the Italian Society for the Study of Haemostasis and Thrombosis (SISET: 2020–2022) unpaid.

The remaining authors declare that the research was conducted in the absence of any commercial or financial relationships that could be construed as a potential conflict of interest.

Publisher's Note: All claims expressed in this article are solely those of the authors and do not necessarily represent those of their affiliated organizations, or those of the publisher, the editors and the reviewers. Any product that may be evaluated in this article, or claim that may be made by its manufacturer, is not guaranteed or endorsed by the publisher.

frontiers in Cardiovascular Medicine

ORIGINAL RESEARCH
published: 09 March 2022
doi: 10.3389/fcvm.2022.813904

Determination of Agrin and Related Proteins Levels as a Function of Age in Human Hearts

Katie L. Skeffington[1], *Ffion P. Jones*[1], *M. Saadeh Suleiman*[1], *Massimo Caputo*[1], *Andrea Brancaccio*[2,3*†] and *Maria Giulia Bigotti*[1,3*†]

[1] Bristol Heart Institute, Research Floor Level 7, Bristol Royal Infirmary, Bristol, United Kingdom, [2] Institute of Chemical Sciences and Technologies "Giulio Natta" (SCITEC)-CNR, Rome, Italy, [3] School of Biochemistry, University of Bristol, Bristol, United Kingdom

Background: Mature cardiomyocytes are unable to proliferate, preventing the injured adult heart from repairing itself. Studies in rodents have suggested that the extracellular matrix protein agrin promotes cardiomyocyte proliferation in the developing heart and that agrin expression is downregulated shortly after birth, resulting in the cessation of proliferation. Agrin based therapies have proven successful at inducing repair in animal models of cardiac injury, however whether similar pathways exist in the human heart is unknown.

Methods: Right ventricular (RV) biopsies were collected from 40 patients undergoing surgery for congenital heart disease and the expression of agrin and associated proteins was investigated.

Results: Agrin transcripts were found in all samples and their levels were significantly negatively correlated to age ($p = 0.026$), as were laminin transcripts ($p = 0.023$), whereas no such correlation was found for the other proteins analyzed. No significant correlations for any of the proteins were found when grouping patients by their gender or pathology. Immunohistochemistry and western blots to detect and localize agrin and the other proteins under analysis in RV tissue, confirmed their presence in patients of all ages.

Conclusions: We show that agrin is progressively downregulated with age in human RV tissue but not as dramatically as has been demonstrated in mice; highlighting both similarities and differences to findings in rodents. Our results lay the groundwork for future studies exploring the potential of agrin-based therapies in the repair of damaged human hearts.

Keywords: agrin, proliferation, dystroglycan, extracellular matrix, myocardial infarction

OPEN ACCESS

Edited by:
Andrew Landstrom,
Duke University, United States

Reviewed by:
Rachel Sarig,
Weizmann Institute of Science, Israel
Sayan Chakraborty,
*Institute of Molecular and Cell Biology (A*STAR), Singapore*

***Correspondence:**
Maria Giulia Bigotti
g.bigotti@bristol.ac.uk
Andrea Brancaccio
andrea.brancaccio@cnr.it

†These authors share last authorship

Specialty section:
This article was submitted to General Cardiovascular Medicine, a section of the journal Frontiers in Cardiovascular Medicine

Received: *12 November 2021*
Accepted: *11 February 2022*
Published: *09 March 2022*

Citation:
Skeffington KL, Jones FP, Suleiman MS, Caputo M, Brancaccio A and Bigotti MG (2022) Determination of Agrin and Related Proteins Levels as a Function of Age in Human Hearts. Front. Cardiovasc. Med. 9:813904. doi: 10.3389/fcvm.2022.813904

INTRODUCTION

One major challenge in cardiovascular medicine is the loss of proliferative capacity of mammalian cardiomyocytes shortly after birth, rendering the adult heart unable to repair itself following an injury such as a myocardial infarction (1, 2). Much interest has therefore been focused on gaining a better understanding of the factors which prevent adult cardiomyocytes from proliferating, and whether it may be possible to positively affect cardiac repair by inducing their re-entry into the cell cycle. In an elegant series of experiments, Bassat and colleagues demonstrated that the cardiac

extracellular matrix (ECM) plays an important role in controlling cardiomyocyte proliferation and identified the ECM proteoglycan agrin as a critical component of this process (3). Using a mouse model they found that the expression of agrin, a protein known to play a vital role in cardiac development (4, 5), is highest in the first days of postnatal life and significantly downregulated by day 7, which would exactly correspond to the timeframe over which murine cardiomyocytes lose the ability to proliferate (3, 6). Excitingly, administration of agrin to both murine and piglet models of myocardial infarction have been demonstrated to reactivate cardiomyocyte proliferation and promote cardiac repair (3, 7).

Agrin is primarily known for its fundamental role in recruiting/clustering of acetylcholine receptors at the neuromuscular junction (8, 9) and also for its genetic variants causing several forms of congenital myasthenia (10). However it has also been found to be involved in cancer pathogenesis, where it is thought to form a mechanotransductive link between the ECM and transcription factors YAP (Yes associated protein) and TAZ (transcriptional co-activator with PDZ binding motif), thus contributing to uncontrolled cell proliferation [reviewed in (11)]. The transcription factor YAP also promotes growth in cardiac tissue (12), and the work of Bassat and coworkers (3) suggests that, in neonatal cardiomyocytes, agrin plays a vital role in promoting cardiomyocyte proliferation through binding to the ECM protein dystroglycan (DG). DG is part of a larger transmembrane complex, the dystrophin-glycoprotein complex, and is composed by two subunits, the highly glycosylated extracellular α-DG and the transmembrane β-DG, that interact non-covalently to form a bridge between the ECM and the actin cytoskeleton (13, 14). It was hypothesized (3) that binding of agrin to α-DG in the myocardium causes a conformational change in the dystrophin-glycoprotein complex, which in turn prevents β-DG from binding YAP intracellularly, thus allowing its localization to the nucleus, where YAP can then exert its co-transcriptional activity and promote proliferation [reviewed in (15)]. Conversely, it has been demonstrated that in mature murine cardiomyocytes, YAP establishes a strong interaction with β-DG and is thus sequestered to the plasma membrane: the lack of nuclear localization impairs YAP co-transcriptional activity, resulting in loss of cardiomyocyte proliferation capacity (12). The mechanisms which cause YAP to become membrane bound and thus prevent proliferation are uncertain, but agrin expression has been observed to decrease significantly in the first days of postnatal life in murine species (3), in a timeframe that coincides with the loss of cardiomyocyte replicative capacity. It has been suggested that this may result in agrin being out-competed for binding to the DG receptor by another, more abundant protein such as the extracellular protein laminin [reviewed in (15)]. Replacement of agrin with a different interactor would trigger, in ways yet unknown, β-DG binding to YAP and its tethering at the cell periphery.

Whilst there are still many questions regarding the exact mechanisms of action involved, the possibility to harness the pro-proliferative capacity of agrin for regenerative purposes shows great potential. Crucially, all the work described has been performed in animal models, and currently nothing is known on whether similar pathways exist in human cardiac tissue, and how they are modulated during growth. A thorough analysis of the levels of agrin and of the proteins implicated in this proliferative axis at different ages in the human heart is the first necessary step to understand the potential of agrin for therapies to aid cardiac regeneration in humans. Such an analysis is hindered by the intrinsic difficulties connected to the collection of healthy human cardiac samples. In this study we have used right ventricular biopsies collected from patients undergoing cardiac surgery to investigate for the first time how the levels of agrin, DG, laminin and YAP change with age in human heart tissue.

Abbreviations: DG, Dystroglycan; ECM, Extracellular matrix; IHC, Immunohistochemistry; RV, Right ventricle; YAP, Yes associated protein.

MATERIALS AND METHODS

Sample Collection

Waste right ventricular tissue was collected from 40 patients undergoing cardiac surgery at the Bristol Royal infirmary for a variety of congenital cardiac conditions (**Table 1**). Full informed consent was obtained prior to surgery from the patients or their parents as appropriate. The study was conducted in accordance with the declaration of Helsinki, and the protocol was approved by the North Somerset and South Bristol Research Ethics Committee (REC 07/H0106/172). Half of the collected tissue from each patient was fixed in 10% formalin before being transferred to PBS for storage at 4°C. The other half of the tissue was stored at −20°C in Allprotect Tissue Reagent (Qiagen). Heart tissue lysates for 0 days old and adult mice were purchased from Leinco Technologies (cat.# M1135 and M1013, respectively). Formalin-fixed mid-cardiac section from 3 month old adult mice were obtained from Insight Biotechnologies (cat.# MoFPT016).

mRNA Analysis

Total RNA was extracted from tissue samples stored as described above using the RNeasy Mini Kit. Specifically, 5–15 mgs of RV tissue from each patient were homogenized according to the manufacturer instructions using PowerBead Tubes filled with 0.7 mm garnets (Qiagen) to efficiently break the tissue by 4–6 × 1 min cycles in a mechanic vertical shaking homogenator (Minilys, Bertin Technologies) at 4°C. The integrity of the RNA thus prepared was confirmed by the Agilent Tape station RNA assays on an Agilent 2,200 TapeStation instrument, and RNA Integrity Numbers (RIN) were calculated by the machine software. The quantity of extracted RNA was determined by measuring the absorbance at 260 nm on a nanodrop (Thermo Scientific), and RNA quality was deemed good for downstream analysis when Abs260 nm/Abs280 $\geq$ 1.8 and Abs260 nm/Abs230 $\geq$ 2. 0.5–1 μg of total RNA from each patient were reverse transcribed using the QuantiTect Reverse Transcription Kit (Qiagen). When necessary, the RNA was concentrated before reverse transcription (GeneJET RNA Cleanup and Concentration Micro Kit, Thermo Scientific).

RT-PCR reactions were run on a QuantStudio5 Real Time PCR machine (ThermoFisher Scientific), using the QuantiFast SYBR Green PCR Kit (Qiagen). Target and housekeeping

TABLE 1 | Patient characteristics.

Pathology	Number of patients	Age in years (mean ± SEM, median, max, min)	Gender (M/F)
TOF	15	1.03 ± 0.22, 0.59, 2.79, 0.23	8/7
VSD	8	0.27 ± 0.05, 0.32, 0.38, 0.02	4/4
PVR	9	12.16 ± 1.97, 12.66, 24.29, 4.25	8/1
Other	8	7.85 ± 5.50, 0.11, 43.93, 0.003	4/4
All	**40**	**4.75 ± 1.37, 0.57, 43.93, 0.003**	**24/16**

Patients characterized by prevalent diagnosis/surgery.
TOF, Tetralogy of Fallot; VSD, ventricular septal defect; PVR, pulmonary valve replacement.
"Other" includes patients undergoing Ross-Konno procedures and patients with cardiac tumors, Truncus Arteriosus or Total Anomalous Pulmonary Venous Drainage.

RNAs were amplified with the following QuantiTect Primer Assay primer mixes (Qiagen): Hs_AGRN_va.1_SG (agrin), Hs_DAG1_1_SG (DG), Hs_LAMA2_1_SG (laminin-α2), Hs_YAP1_1_SG (YAP), Hs_GAPDH_1_SG (GAPDH), HS_IPO8_1_SG (IPO8) and HS_POLR2A_1_SG. The α2 chain was chosen as representative of laminin in the heart, where it is one of the most populated forms (16). Five nanograms of cDNA from the retrotranscribed material were used in each reaction, and all reactions were performed in triplicate in each experiment. The data reported in the results were averaged over a minimum of 2 RT-PCR reactions for each patient. To take into account the heterogeneity of the RV samples, based on the work of Molina and colleagues (17) three different genes stably expressed in human cardiac tissue were chosen as reference for determining all the ΔCt values, namely glyceraldehyde 3-phosphate dehydrogenase (*GAPDH*), importin 8 (*IPO8*) and RNA polymerase II subunit A (*POLR2A*). Comparative quantification was used to identify whether the target genes were up- or down-regulated relative to the two oldest patients under analysis. Relative expression of all genes was calculated by the ΔΔCt method. Specifically, if Ct(TP) is the Ct value measured for a target gene in a patient (TP), and Ct(AvgeRP) is the averaged Ct of the 3 reference genes for that patient, then the relative expression for the patient (ΔCtTP) is calculated as:

$$\Delta CtTP = Ct\,(TP) - Ct(AvgeRP)$$

Up- or down-regulation of target genes were assessed relative to the average expression in the two oldest patients (P'), aged 43 and 24, so that:

$$\Delta\Delta CtTP = \Delta CtTP - \Delta CtTP'$$

Throughout the paper, transcripts levels are expressed as fold changes relative to the average expression of the two oldest patients, as calculated from the expression:

$$Fold\ change = 2^{-\Delta\Delta CtTP}$$

Immunohistochemistry (IHC)

The fixed tissue was embedded in paraffin and sectioned at 4 μm thickness. The sections on the slides were deparaffinized and antigen retrieval performed using 10 mM citrate buffer, pH 6.4, at 95°C. The slides were washed in PBS, endogenous peroxidase activity inhibited by a 10 min incubation with Bloxall (Vector Laboratories), and the slides rewashed. The sections were then incubated for 30 min at room temperature in 10% donkey serum (Sigma Aldrich) to block non-specific antigens, followed by incubation in primary antibody (agrin: GTX54904, GeneTex, laminin-α2: STJ93889, St John's Laboratory, DG: 11017-1-AP, Proteintech) or PBS (negative control) overnight at 4°C. The sections were then washed in PBS and exposed to secondary antibody (ECL anti-rabbit IgG, NA934, GE Healthcare) for 1 h at room temperature before another wash and exposure to DAB (Vector Laboratories) for 20 min. Finally, the slides were counterstained with Mayer's Haemotoxylin and images were taken using an O8 slidescanner (Precipoint).

Proteins Identification

Total proteins were extracted from samples stored at −20°C in Allprotect Tissue Reagent (Qiagen). RIPA lysis buffer with freshly added phosStop (Roche 04906837001), cOmplete protease inhibitors cocktail (Roche 11836170001) and benzonase (Thermo Scientific) was added to 10–20 mg of samples into gentleMACS M Tubes with strainers (Miltenyi Biotech). The tissue was then homogenized into a gentleMACS Dissociator instrument (Miltenyi Biotech). Insoluble material in the homogenates was spun down by centrifugation (5 min at 4,000 xg, 4°C), the supernatants were checked for total protein content (see below) and stored at −80°C. The extracted proteins in each sample were quantified with the Pierce™ Rapid Gold BCA Protein Assay Kit (Thermo scientific: A53225) following the manufacturer instructions.

Blotting

Total proteins for each sample were diluted to load an amount of 20 μg/gel lane and denatured by adding LDS loading buffer (Invitrogen). Samples were loaded on 4–12% Bis-Tris Gels (Invitrogen) and SDS-PAGE were run at 100V in MES SDS running buffer. The Spectra Multicolour Broad Range Protein ladder was used as a molecular weight marker (Thermo Scientific). Proteins were transferred on activated PVDF membranes (Thermo scientific) at 250 mA for 1.30 h at room temperature (RT). After blocking and washing, blots were hybridized with primary antibodies overnight at 4°C; see **Supplementary Table 1** for details on the antibodies used. To note, due to inefficient probing with the anti-laminin-α2 Ab, an anti-laminin-γ1 Ab was used

instead (see **Supplementary Table 1**). Blots were then washed and incubated 1 h with the secondary antibodies indicated in **Supplementary Table 1**. Blots were developed using 1 ml of Immobilon Forte Western HRP substrate (Millipore-WBLUF0500) for 1 min. For each membrane both colorimetric and chemiluminescence images were taken on a ChemiDoc MP imaging system (BioRad) and analyzed with the BioRad Image Lab software. When necessary, membranes were stripped using Restore^{TM} Plus Western blot stripping buffer (Thermo scientific) according to the protocol provided and re-probed with the antibodies of choice. Densitometric analysis, when possible, was conducted using ImageJ.

Liquid Chromatography Mass Spectrometry

A total of 50 ug of total protein extract from each RV tissue lysate were subjected to tryptic digestion followed by a LC-MS run on an Orbitrap Fusion Tribrid Mass Spectrometer with ETD instrument (Thermo Scientific) operated with up-stream Ultimate 3,000 nano-LC system at the Proteomic Facility at the University of Bristol. The resulting data were analyzed with a Sequest search against the Uniprot Human database and against an in house database of common contaminants, and the results have been filtered using a 5% FDR cut-off.

Statistics

Correlations between RNA expression and age were assessed using two-tailed Pearson correlation coefficient. Gender differences were assessed using unpaired Student's *t*-tests and differences between pathologies using one-way ANOVA. Regression analysis was used to find the unstandardised regression coefficient β and it's standard error for agrin expression in each pathology group. All statistics were performed in SPSS Version 26 (IBM Analytics, New York, NY) and significance was accepted when $p < 0.05$.

RESULTS

Forty patients [mean age 4.7 ± 1.4 years (mean ± SEM)] undergoing cardiac surgery for a variety of conditions were recruited (**Table 1**). The RNA obtained from the tissue was of high quality, with RIN values in the range of 8–9. The expression of agrin, laminin-α2, DG and YAP were very similar between the 24 year old and 43 year old (**Figure 1**), and the results of the other patients were normalized to the average expression in these two adult patients. The agrin gene was found to be expressed in the right ventricle of all patients, with its transcript levels (expressed both as ΔΔCts relative to the adult controls and as individual ΔCts) significantly negatively correlated to the patient age at the time of operation ($p = 0.026$, **Figure 1A** and **Supplementary Figure 1B**, respectively). As an immediate measure, upon correction/normalization against the housekeeping controls, the number of RT-PCR cycles of neonates (highest expression, i.e., lowest RT-PCR cycles) is 1.55 times lower than those of the two adults (lowest expression, i.e., highest RT-PCR cycles).

Splitting the pediatric cases into two age groups (0–1 years and 1–15 years) demonstrates that it is not only babies who have higher agrin expression than adults; agrin levels also remain elevated in older children (**Supplementary Figure 1A**). The α2 chain was chosen as representative of laminin in the heart, where it is one of the most populated forms (16), and its expression also demonstrated a significant negative correlation with patient age ($p = 0.023$, **Figure 1B** and **Supplementary Figure 1C**). The expression of DG and YAP, on the other hand, did not correlate with age (**Figures 1C,D** and **Supplementary Figures 1D,E**).

The relative transcript levels of agrin, laminin, DG or YAP were not significantly different between male and female patients (**Figure 2A**), nor any significant difference was found between groups of patients with different pathologies (**Figure 2B**). In this respect, it has to be noted that the distribution of ages in the 4 main categories of pathology, although partially overlapping, is different, with patients with ventricular septal defects being the youngest, followed by Tetralogy of Fallot patients and with the eldest patients grouped in the pulmonary valve replacement and "other" categories (see **Table 1**). Remarkably, the levels of agrin decrease with age in each of the categories (**Figure 2C**), thus strongly indicating that the phenomenon is independent from pathology in the cohort of patients under consideration. Furthermore, analysis of the other clinical data available for the whole cohort of patients highlighted the absence of significant correlation between agrin levels and any of the collected clinical parameters.

To investigate the presence and possible age-dependence of agrin, laminin and DG at the protein level, total protein extracts from the 40 human RV samples were analyzed by western blotting. **Figure 3** reports western blots of representative samples set out in increasing age order from left to right for the three proteins (**Figures 3A,C**). The blots support the qPCR results, showing that agrin is expressed in human heart throughout life, as shown by the presence of clearly defined bands from the youngest representative (2 months) RV sample all the way through to the oldest (43 years). For comparison, **Figure 3B** shows a western blot on heart extracts from mice, whereby agrin is present in neonatal heart but undetectable in adult. Laminin and dystroglycan are also abundant in all the samples, with no significant variability in the amount of both proteins across different age groups. Although a proper quantification was hindered by a considerable heterogeneity in the agrin bands (due to extensive glycosylation and possibly to a certain amount of degradation upon samples preparation) the protein was consistently detected in replicate WB experiments in all the patients. Moreover, a high molecular weight band, representing the fully glycosylated form of agrin (∼400 kDa, see black asterisk in **Figure 3A**) was detected in samples of all ages and, although not properly quantifiable by densitometry, a trend of decreasing levels from youngest to oldest patients is evident, Notably, agrin has been found to be intrinsically prone to proteolysis in skeletal muscle atrophy/wasting induced by stroke (18) and chronic heart failure (19) and the 110 kDa C-terminal agrin fragment thus produced constitutes a biomarker of muscle wasting. Interestingly, one of the populated bands in our agrin western blots has an apparent molecular weight of ∼110 kDa (**Figure 3**), compatible with that of the C-terminal agrin fragment. Although no obvious effect of age on the levels

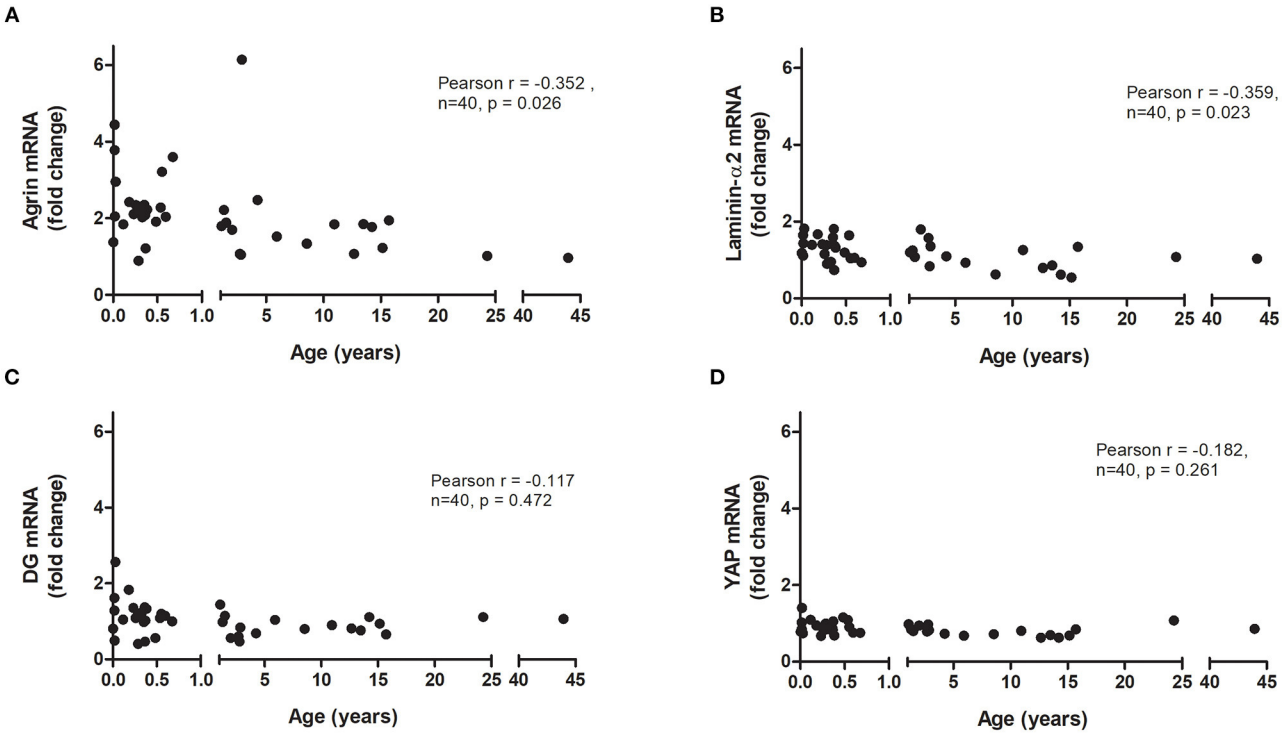

FIGURE 1 | Relative mRNA expression of agrin and associated proteins in human hearts. Correlation of the transcript levels of agrin **(A)**, laminin **(B)**, dystroglycan (DG; **C**) and YAP **(D)** with age in right ventricular biopsies from patients undergoing cardiac surgery ($n = 40$). Fold changes were calculated relative to the mRNA levels of two adult patients (24 and 43 years). Significant correlations were tested for using two-tailed Pearson correlation coefficient.

of the 110 kDa fragment is evident, other factors could affect this and other fragment populations, including any prior heart injuries and the variable degree of degradation of the samples, thus making any effect of age less detectable. Since sample extracts from the 40 RV samples analyzed in this study presented different degrees of degradation, densitometric analysis based on all of the detectable bands could not be conclusive, and no direct comparison could be drawn with transcriptomic results. Also interestingly, inspection of the α-DG bands detected on the blot reveals an opposite trend of glycosylated protein as compared to agrin, i.e., α-DG appears to be more glycosylated with age. Lastly, since the laminin signal in the blots shown in **Figure 3C** appeared the most reliable in terms of opportunity to quantify it, a densitometric analysis was conducted and confirmed that laminin levels (at least those of laminin-γ1, as probed on the western blots) decrease with age of a factor of 3.5 folds (see also **Supplementary Figure 2**), which is in line, although slightly higher, with the transcripts evidences.

LC-MS has also been employed in an attempt to identify and make a semi-quantitative assessment of the proteins under analysis. Due to the scarcity of the starting material for all the samples, no pre-fractionation of the protein extracts was possible, hindering a precise quantification. Nonetheless, protein lysates of RV tissue from 2 representative patients (2 months and 24 years old) were subjected to a LC-MS analysis upon proteolytic digestion. The results, summarized in **Supplementary Table 2**, show how agrin, laminin and α-DG were all identified with a high degree of confidence in both samples, despite ECM proteins being notoriously difficult to characterize with this kind of technique. Interestingly, although the hits for α-DG are comparable in the two samples analyzed, the number of peptides identified for agrin and laminin (and thus the total sequence coverage for both) are much higher in the RV sample from the infant than that from the adult patient. Specifically, although no definitive conclusions can be drawn for laminin, the sensibly smaller representation of agrin peptides in the older patient might indicate a smaller amount of full-length protein, possibly due to a lower level of expression as well as a higher degree of degradation with respect to the younger patient.

IHC staining aimed at identifying on-tissue the proteins under analysis, found evidence of the expression of agrin within the ECM in tissue from patients of all ages (**Figure 4**). The protein appears to have a wide distribution, with staining of cardiomyocytes particularly evident in adult human samples. For comparison, we performed similar IHC experiments in adult mice hearts (**Figure 4**, bottom panels), where we found very little evidence of agrin staining. **Supplementary Figures 3, 4** show a similar distribution of laminin and DG mainly within the ECM of cardiomyocytes in samples of the whole age range. It is important to stress that, like western blots in the specific conditions here described, IHC can only be used as a qualitative indicator of the presence and localization of the three proteins

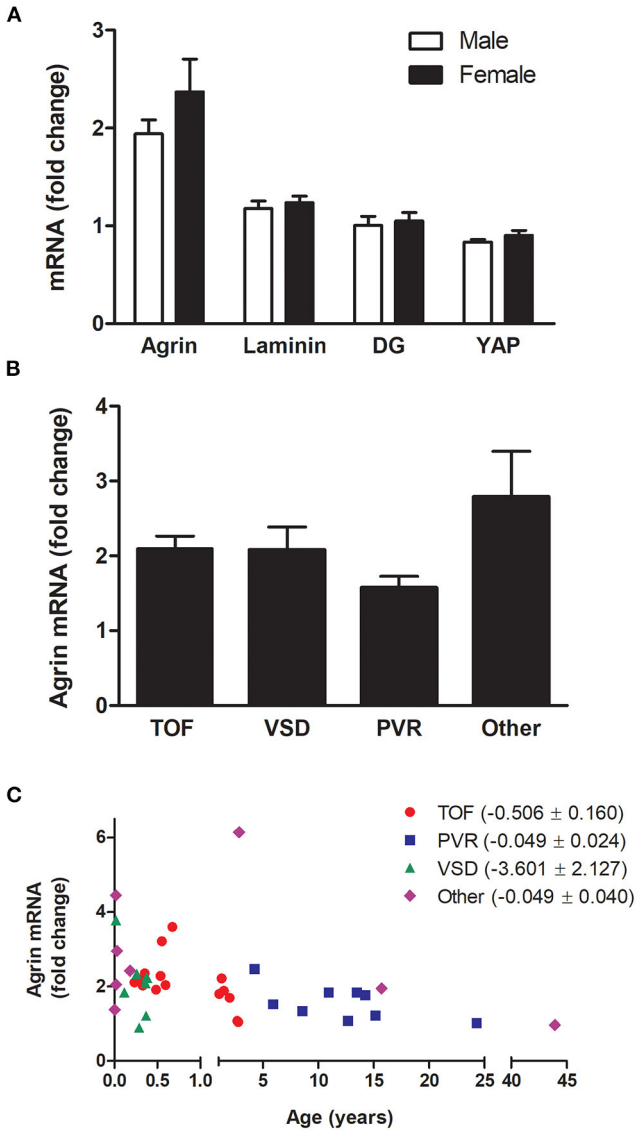

FIGURE 2 | mRNA expression of agrin and associated proteins by gender and pathology. Transcript levels for agrin, laminin, DG and YAP in male patients compared to females **(A)** and transcript levels of agrin in patients with different pathologies **(B,C)** $n = 40$. In particular, **(C)** shows the agrin levels dependence on age as broken down according to pathology. TOF, Tetralogy of Fallot; VSD, ventricular septal defect; PVR, pulmonary valve replacement. "Other" includes patients undergoing Ross-Konno procedures and patients with cardiac tumors, Truncus Arteriosus or Total Anomalous Pulmonary Venous Drainage. The bracketed numbers in the legend are the unstandardised coefficient β ± SEM. Fold changes were calculated relative to the mRNA levels of two adult patients (24 and 43 years old). Student's *t*-tests for unpaired data **(A)** or one-way ANOVA **(B)** revealed no significant differences.

in the tissues under analysis and as such could not provide information to complement (or otherwise) the quantitative transcriptomic results. Nevertheless, the results of transcripts and proteins analysis are consistent in showing how agrin is the least populated of the proteins under investigation, as indicated by the higher ΔCt values (indicative of lower mRNA levels, see **Supplementary Figure 1**) and the relatively fainter signals in western blots (see **Figure 3**) as well as IHC (**Figure 4** vs. **Supplementary Figures 3, 4**, respectively) for agrin relative to both DG and laminin. Finally, although little is known about agrin presence in the heart in locations other than the ECM of the cardiac muscle, it is likely that, by analogy to skeletal muscle, there may also be agrin at neuromuscular junctions. Since the cardiac muscle, which is the source of the samples used in this work, is mainly composed of cardiomyocytes [70% of myocardium volume (20)], it is reasonable to assume that the agrin analyzed in this work comes from the ECM of cardiomyocytes and from neuromuscular junctions.

DISCUSSION

Our study is the first to collect data on the transcription/expression levels of agrin and associated proteins in human cardiac tissue at different stages of development. Previous work from a different laboratory demonstrates that, in mice, agrin transcript levels halve in the first week of postnatal life and continue to decrease into adulthood (3); an even stronger negative time dependency was shown for the protein product, with agrin protein expression in adult mice around one tenth of that found in neonates. However, a study by a different group using only immunofluorescence staining reported similar levels of agrin expression in adult and embryonic mouse hearts (21). Our own results in mice suggest a decrease in expression of the agrin protein with age and very little agrin presence at the protein level in adult mice as measured both by IHC and western blotting. Our transcripts results on human cardiac tissue demonstrate that there is also a decrease in agrin expression with age in human hearts. This finding lays the groundwork for a molecular analysis aimed at understanding whether this change in agrin expression with age is associated with a role for this protein in cardiac regeneration, similarly to what has been described in mice. Such an important analogy, however, has its counterpart in the evidence that agrin expression, crucially, does not decrease with age in humans as dramatically as it has been described in mice. Indeed we measured an agrin transcripts fold change in neonates that is 2.3x the levels found in adults, suggesting a reduction of agrin expression of only slightly more than half with growth to adulthood in humans. Furthermore, the reduction in agrin expression with age is even less apparent at the protein level, with agrin being clearly present in tissue sections of adult controls, where staining for agrin in IHC is comparable to that recorded on samples from much younger patients (see **Figure 4**); this is in striking contrast with the almost complete lack of agrin signal we measured in RV sections from adult mice. The results of the western blot go in the same direction, with comparable levels of protein measured in samples of all ages, irrespective of the degradation pattern, which appears to be rather sporadic and non-specific within the wide age range considered. On the other hand in mice, similarly to the IHC data, there is almost no agrin detectable by western blot at adulthood (**Figure 3B**). Thus our data demonstrate a less

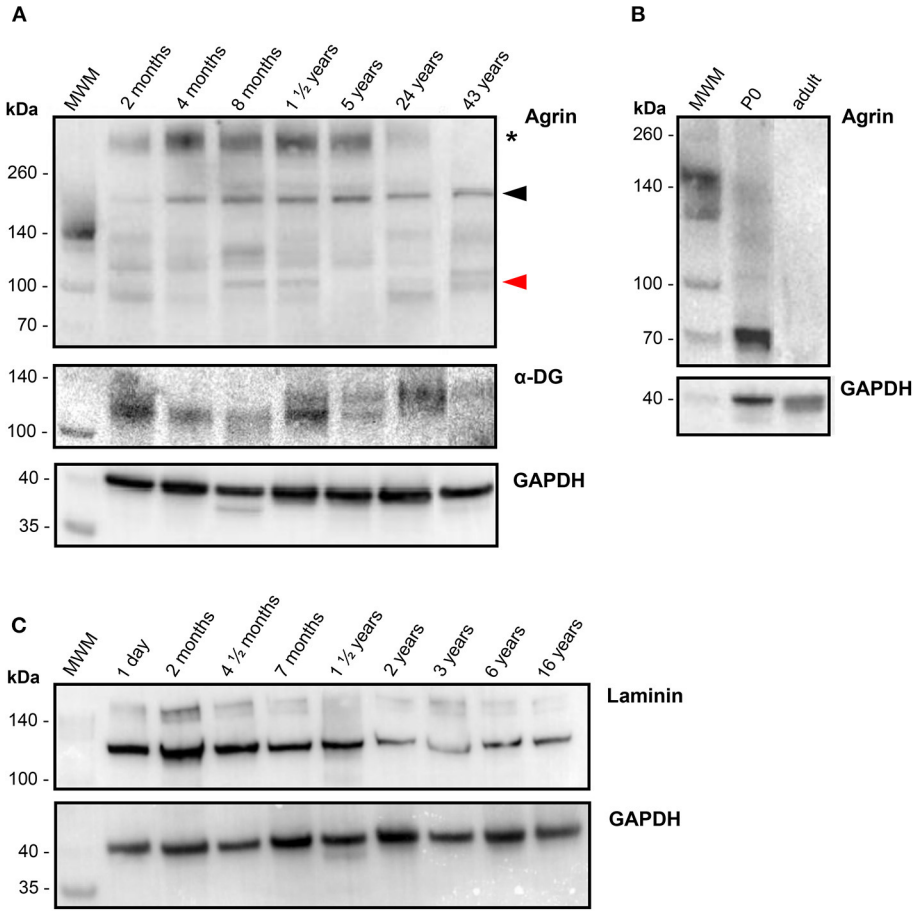

FIGURE 3 | Protein levels of agrin and related proteins in human hearts. **(A)** Western blots of the proteins indicated, as detected in RV samples collected from representative patients ($n = 7$) of different ages, in increasing order from left (2 months old) to right (43 years old) as identified on top of each lane. For comparison, a western blot of agrin detected in commercial mouse heart tissue lysates (Leinco Technologies) from 0 days old (P0) and adult mice is reported in **(B)**, together with the corresponding loading control GAPDH at the bottom. **(C)** Western blots of laminin (plus loading control), as detected in RV samples collected from representative patients ($n = 9$) of different ages, in increasing order from left (1 day old) to right (16 years old) as identified on top of each lane Proteins extracted from human RV samples as well as the commercial mice heart samples were probed with the antibodies specified in **Supplementary Table 1**, and bands of the correct molecular weight have been identified for laminin-γ1 (∼160 kDa), α-DG (110-130 kDa) and the housekeeping protein GAPDH (36 kDa). The series of bands identified for human agrin originate from differential glycosylation and proteolytic degradation: the asterisk indicate the fully glycosylated form (∼400 kDa), the black arrowhead points to a band that could represent the unglycosylated form (∼220 kDa) and the red arrowhead indicates the ∼110 kDa band that could represent a C-terminal agrin fragment (CAF), see Results for details.

dramatic reduction in agrin expression with age than is seen in mice, both at the transcript level and even more so at the protein level. If a role for agrin in a possible regenerative program was confirmed in humans, these results may point to important differences in how it is controlled in rodent vs. human hearts.

It has been suggested that, with age, the binding of agrin to the α-DG receptor may be increasingly outcompeted by another extracellular protein, and laminin has been put forward as a potential candidate for this (15). Laminin is known to play an important role in promoting cardiac muscle stability (22) as well as being crucial for cardiomyocyte differentiation (23, 24) and maturation (25). Laminin and agrin show a similar affinity for α-DG (26), and a slight increase in laminin expression has been demonstrated between postnatal days 1 and 2 in mice (6). However, results in the current study suggest that in human cardiac tissue (similarly to what was found with agrin) the expression of laminin in the right ventricle is negatively correlated with age. Interestingly, using an analogous approach to the one we have employed (but relying on post-mortem myocardial biopsies), it was shown that, irrespective of the presence of a cardiac pathology, there was a negative correlation between age and laminin-α2 transcripts in a cohort of human subjects between 9 and 58 years old (27). The correlation we found of laminin expression with age was indeed more significant than the correlation of agrin with age ($p = 0.023$ and $p = 0.026$, respectively), however this comparison is affected by the presence of one patient who had unusually high agrin expression for their age (**Figure 1A**), weakening the strength of the correlation. As

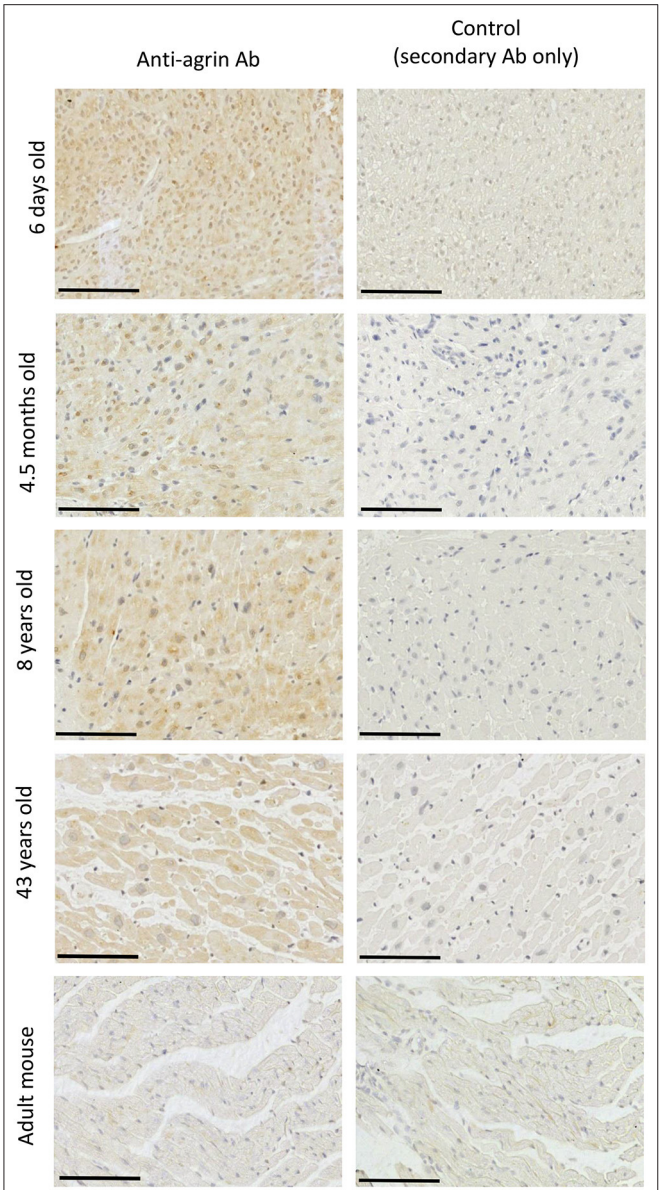

FIGURE 4 | Identification of agrin in RV tissue sections. Immunohistochemical staining for agrin in the RV of four patients aged between 6 days and 43 years and in the RV of an adult mouse (9 weeks). Each scale bar represents 100 μm. A negative control for each image is found in the right-hand column.

a matter of fact, the decrease in laminin-α2 transcript levels with age in our study was fairly modest, and it is unclear how much functional significance it would have. On the other hand, quantification at the protein level shows a decrease of about 3.5 folds in the adults relative to infants, which needs to be further investigated. Although purely observational in nature, our findings would not seem to confirm the hypothesis formulated by Bassat and coworkers (3), that a simultaneous reduction in agrin expression and increase in laminin levels with age results in the latter out-competing agrin in binding to α-DG. However, we show that the negative correlation of agrin expression with age is steeper than that of laminin in human RV (**Figures 1A,B**), and since the measured α-DG binding affinities of the two proteins are very similar (26), this could account for a possible replacement of agrin with laminin as early in life as by the first year of age. Notably, our results also show for the first time that, although α-DG expression in RV tissue is not significantly correlated with age, its level of glycosylation might be, as demonstrated by the higher apparent molecular weight of the glycosylated species of adults as compared to children in our western blot analysis. Taken together with the finding that the trend in glycosylated agrin with age is the opposite, i.e., adults show a less glycosylated protein than children, this observation could suggest a possible role of the reciprocal glycosylation states of α-DG and agrin in their interaction along the growth of individuals.

Our investigation of the protein levels by IHC and western blots, although less quantitative than our transcriptomic analysis, confirms that agrin is present in the cardiac tissues of all the patients analyzed, therefore also suggesting that the agrin/laminin expression levels during cardiac muscle development and in adulthood are not controlled in the "all or nothing" way described in mice. Moreover, our western blot analysis confirms the relatively high susceptibility of the C-terminal portion of agrin to proteolysis, as has been previously shown in skeletal muscle (18, 19). It could be hypothesized that such degradation, by negatively affecting the interaction of agrin with DG, is a factor in the loss of pro-proliferative capacity of this protein along the lifetime of an individual, although such an hypothesis is possibly too simplistic, based on the evidence of the efficacy of recombinant agrin (composed exclusively of the ∼100 kDa C-terminal) in regenerating the heart of animal models (3, 7).

It is possible that additional factors are involved which favor the binding of the α-DG receptor to laminin over agrin. For example, in skeletal muscle, changes in the degree of glycosylation of the α-DG receptor can affect the affinity of laminin for the receptor, resulting in muscular dystrophy (28, 29). Despite our preliminary evidences of a possible positive trend of glycosylation with age, it is fundamentally unknown whether the degree of glycosylation of the α-DG receptor in cardiac tissue changes with age, and to what extent this might affect the binding of agrin or laminin. Alternatively, laminin may not be the only other key player at all and other, as yet unidentified, proteins or factors that influence the binding affinity of agrin to the α-DG receptor may be involved. Interestingly, DG has been shown to also play a fundamental role in actively inhibiting the spread of myocardial damage from cardiomyocytes to neighboring cells (30), which points to the capacity of this receptor to sense the extracellular environment and respond to the cellular needs and might hint to its direct involvement in controlling the expression/action of agrin. Additionally, it has been demonstrated that cardiac maturation also results in the phosphorylation of YAP via its interaction with proteins in upstream pathways such as the Hippo pathway (31, 32), and the relative importance of YAP phosphorylation vs. the interaction of agrin with α-DG in leading to the sequestration of YAP at the cell periphery is unknown.

There has been much interest in the potential use of agrin based therapies in cardiac regeneration. Until now all work has however been carried out in animal models. This study demonstrates for the first time that agrin is actively expressed in human cardiac tissue in an age-dependent way, with a transcripts peak very early in life and a steady decrease toward adulthood, echoing the pattern of expression observed in rodents (3). Future work is necessary to identify a possible agrin-driven regenerative program, elucidate the molecular mechanisms involved and investigate whether these pathways could be harnessed therapeutically to promote cardiac regeneration in humans. In this respect, our finding that agrin is clearly detectable at the protein level in adult human heart shows how, unlike what described for rodent hearts, if an agrin-driven proliferative program exists in humans, it does not fully switch off with aging, opening up new therapeutic scenarios. Indeed, a potential pharmacological re-activation of the endogenous agrin-DG axis could constitute an alternative/complementary approach to the direct administration of exogenous agrin proven to be effective in cardiac repair of murine (3) and porcine (7) models.

One limitation of this study is that all the cardiac tissue analyzed came from patients with diseased hearts, since for obvious ethical reasons it is not possible to obtain fresh cardiac tissue (*ex-vivo*) from healthy human hearts. However, as discussed above the patients involved in this study suffered from a variety of cardiac conditions, and there was no evidence of an association of altered agrin expression with any particular pathology, nor with gender or any of the recorded clinical parameters. Another limitation is that all samples came from the right ventricles of patients. Although it cannot be ruled out that the scenario described here may be different in the left ventricle, studies that have investigated the differential characteristics of left and right ventricles at the molecular level have not highlighted any major differences between the two in the agrin related pool of proteins that are the object of this analysis (33).

DATA AVAILABILITY STATEMENT

The original contributions presented in the study are included in the article/**Supplementary Material**, further inquiries can be directed to the corresponding authors.

ETHICS STATEMENT

The studies involving human participants were reviewed and approved by North Somerset and South Bristol Research Ethics Committee (REC 07/H0106/172). Written informed consent to participate in this study was provided by the participants' legal guardian/next of kin.

AUTHOR CONTRIBUTIONS

MB and AB conceived the project. MB, AB, MS, and MC conceptualized and designed the research. MC collected the clinical samples. KS, FJ, and MB performed the research. KS, FJ, AB, and MB analyzed the data. KS and MB drafted the manuscript, which was edited and approved by all authors. All authors contributed to the article and approved the submitted version.

FUNDING

This work was supported by grants from the Sir Jules Thorn Charitable Trust (MC) and the British Heart Foundation, grant no. CH/1/32804 (KS, MB, and MC). FJ is the recipient of a British Heart Foundation PhD studentship in Integrative Cardiovascular Sciences. The Cardiovascular theme of NIHR Bristol Biomedical Research Centre also supported this work. The funders played no role in the design of the study, in the collection, analysis and interpretation of data, or in the decision to submit the manuscript for publication.

ACKNOWLEDGMENTS

We would like to acknowledge Eva Jover Garcia (IdiSNA, Pamplona, Spain) for helpful discussions on qPCR experiments setup and interpretation, Ahmed Gamal Thabet Ahmed for his help with finding the clinical data, Kate Heesom for her assistance with the LC-MS, and Elisa Avolio for her advice during the revision.

SUPPLEMENTARY MATERIAL

The Supplementary Material for this article can be found online at: https://www.frontiersin.org/articles/10.3389/fcvm.2022.813904/full#supplementary-material

REFERENCES

1. Bergmann O, Zdunek S, Felker A, Salehpour M, Alkass K, Bernard S, et al. Dynamics of cell generation and turnover in the human heart. *Cell*. (2015) 161:1566–75. doi: 10.1016/j.cell.2015.05.026
2. Oparil S, Bishop SP, Clubb FJ Jr. Myocardial cell hypertrophy or hyperplasia. *Hypertension*. (1984) 6(6 Pt 2):III38–43. doi: 10.1161/01.HYP.6.6_Pt_2.III38
3. Bassat E, Mutlak YE, Genzelinakh A, Shadrin IY, Baruch Umansky K, Yifa O, et al. The extracellular matrix protein agrin promotes heart regeneration in mice. *Nature*. (2017) 547:179–84. doi: 10.1038/nature22978
4. Jing X, Liu B, Deng S, Du J, She Q. Agrin yes-associated protein promotes the proliferation of epicardial cells. *J Cardiovasc Pharmacol*. (2021) 77:94–9. doi: 10.1097/FJC.0000000000000926
5. Sun X, Malandraki-Miller S, Kennedy T, Bassat E, Klaourakis K, Zhao J, et al. The extracellular matrix protein agrin is essential for epicardial epithelial-to-mesenchymal transition during heart development. *Development*. (2021) 148:dev197525. doi: 10.1242/dev.197525
6. Notari M, Ventura-Rubio A, Bedford-Guaus SJ, Jorba I, Mulero L, Navajas D, et al. The local microenvironment limits the regenerative potential of the mouse neonatal heart. *Sci Adv*. (2018) 4:eaao5553. doi: 10.1126/sciadv.aao5553

7. Baehr A, Umansky KB, Bassat E, Jurisch V, Klett K, Bozoglu T, et al. Agrin promotes coordinated therapeutic processes leading to improved cardiac repair in pigs. *Circulation*. (2020) 142:868–81. doi: 10.1161/CIRCULATIONAHA.119.045116
8. Jacobson C, Cote PD, Rossi SG, Rotundo RL, Carbonetto S. The dystroglycan complex is necessary for stabilization of acetylcholine receptor clusters at neuromuscular junctions and formation of the synaptic basement membrane. *J Cell Biol*. (2001) 152:435–50. doi: 10.1083/jcb.152.3.435
9. Gesemann M, Cavalli V, Denzer AJ, Brancaccio A, Schumacher B, Ruegg MA. Alternative splicing of agrin alters its binding to heparin, dystroglycan, and the putative agrin receptor. *Neuron*. (1996) 16:755–67. doi: 10.1016/S0896-6273(00)80096-3
10. Engel AG, Shen XM, Selcen D, Sine SM. Congenital myasthenic syndromes: pathogenesis, diagnosis, and treatment. *Lancet Neurol*. (2015) 14:420–34. doi: 10.1016/S1474-4422(14)70201-7
11. Chakraborty S, Hong W. Linking extracellular matrix agrin to the hippo pathway in liver cancer and beyond. *Cancers*. (2018) 10:45. doi: 10.3390/cancers10020045
12. Morikawa Y, Heallen T, Leach J, Xiao Y, Martin JF. Dystrophin-glycoprotein complex sequesters Yap to inhibit cardiomyocyte proliferation. *Nature*. (2017) 547:227–31. doi: 10.1038/nature22979
13. Barresi R, Campbell KP. Dystroglycan: from biosynthesis to pathogenesis of human disease. *J Cell Sci*. (2006) 119(Pt 2):199–207. doi: 10.1242/jcs.02814
14. Bozzi M, Morlacchi S, Bigotti MG, Sciandra F, Brancaccio A. Functional diversity of dystroglycan. *Matrix Biol*. (2009) 28:179–87. doi: 10.1016/j.matbio.2009.03.003
15. Bigotti MG, Skeffington KL, Jones FP, Caputo M, Brancaccio A. Agrin-mediated cardiac regeneration: some open questions. *Front Bioeng Biotechnol*. (2020) 8:594. doi: 10.3389/fbioe.2020.00594
16. Boland E, Quondamatteo F, van Agtmael T. The role of basement membranes in cardiac biology and disease. *Biosci Rep*. (2021) 41:BSR20204185. doi: 10.1042/BSR20204185
17. Molina CE, Jacquet E, Ponien P, Munoz-Guijosa C, Baczko I, Maier LS, et al. Identification of optimal reference genes for transcriptomic analyses in normal and diseased human heart. *Cardiovasc Res*. (2018) 114:247–58. doi: 10.1093/cvr/cvx182
18. Scherbakov N, Knops M, Ebner N, Valentova M, Sandek A, Grittner U, et al. Evaluation of C-terminal agrin fragment as a marker of muscle wasting in patients after acute stroke during early rehabilitation. *J Cachexia Sarcopenia Muscle*. (2016) 7:60–7. doi: 10.1002/jcsm.12068
19. Steinbeck L, Ebner N, Valentova M, Bekfani T, Elsner S, Dahinden P, et al. Detection of muscle wasting in patients with chronic heart failure using C-terminal agrin fragment: results from the Studies Investigating Co-morbidities Aggravating Heart Failure (SICA-HF). *Eur J Heart Fail*. (2015) 17:1283–93. doi: 10.1002/ejhf.400
20. Zhou P, Pu WT. Recounting cardiac cellular composition. *Circ Res*. (2016) 118:368–70. doi: 10.1161/CIRCRESAHA.116.308139
21. Hilgenberg LGW, Pham B, Ortega M, Walid S, Kemmerly T, O'Dowd DK, et al. Agrin regulation of α3 sodium-potassium ATPase activity modulates cardiac myocyte contraction. *J Biol Chem*. (2009) 284:16956–65. doi: 10.1074/jbc.M806855200
22. Nguyen Q, Lim KRQ, Yokota T. Current understanding and treatment of cardiac and skeletal muscle pathology in laminin-α2 chain-deficient congenital muscular dystrophy. *Appl Clin Genet*. (2019) 12:113–30. doi: 10.2147/TACG.S187481
23. Wang D, Wang Y, Liu H, Tong C, Ying Q, Sachinidis A, et al. Laminin promotes differentiation of rat embryonic stem cells into cardiomyocytes by activating the integrin/FAK/PI3K p85 pathway. *J Cell Mol Med*. (2019) 23:3629–40. doi: 10.1111/jcmm.14264
24. Yap L, Tay HG, Nguyen MTX, Tjin MS, Tryggvason K. Laminins in cellular differentiation. *Trends Cell Biol*. (2019) 29:987–1000. doi: 10.1016/j.tcb.2019.10.001
25. Chanthra N, Abe T, Miyamoto M, Sekiguchi K, Kwon C, Hanazono Y, et al. A novel fluorescent reporter system identifies laminin-511/521 as potent regulators of cardiomyocyte maturation. *Sci Rep*. (2020) 10:4249. doi: 10.1038/s41598-020-61163-3
26. Sciandra F, Bozzi M, Bigotti MG, Brancaccio A. The multiple affinities of α-dystroglycan. *Curr Protein Pept Sci*. (2013) 14:626–34. doi: 10.2174/1389203711209070644
27. Oliviero P, Chassagne C, Salichon N, Corbier A, Hamon G, Marotte F, et al. Expression of laminin α2 chain during normal and pathological growth of myocardium in rat and human. *Cardiovasc Res*. (2000) 46:346–55. doi: 10.1016/S0008-6363(00)00034-1
28. Brancaccio A. A molecular overview of the primary dystroglycanopathies. *J Cell Mol Med*. (2019) 23:3058–62. doi: 10.1111/jcmm.14218
29. Falsaperla R, Pratico AD, Ruggieri M, Parano E, Rizzo R, Corsello G, et al. Congenital muscular dystrophy: from muscle to brain. *Ital J Pediatr*. (2016) 42:78. doi: 10.1186/s13052-016-0289-9
30. Michele DE, Kabaeva Z, Davis SL, Weiss RM, Campbell KP. Dystroglycan matrix receptor function in cardiac myocytes is important for limiting activity-induced myocardial damage. *Circ Res*. (2009) 105:984–93. doi: 10.1161/CIRCRESAHA.109.199489
31. von Gise A, Lin Z, Schlegelmilch K, Honor LB, Pan GM, Buck JN, et al. YAP1, the nuclear target of Hippo signaling, stimulates heart growth through cardiomyocyte proliferation but not hypertrophy. *Proc Natl Acad Sci USA*. (2012) 109:2394–9. doi: 10.1073/pnas.1116136109
32. Xin M, Kim Y, Sutherland LB, Murakami M, Qi X, McAnally J, et al. Hippo pathway effector Yap promotes cardiac regeneration. *Proc Natl Acad Sci USA*. (2013) 110:13839–44. doi: 10.1073/pnas.1313192110
33. Mohenska M, Tan NM, Tokolyi A, Furtado MB, Costa MW, Perry AJ, et al. 3D-cardiomics: a spatial transcriptional atlas of the mammalian heart. *J Mol Cell Cardiol*. (2021) 163:20–32. doi: 10.1016/j.yjmcc.2021.09.011

Conflict of Interest: The authors declare that the research was conducted in the absence of any commercial or financial relationships that could be construed as a potential conflict of interest.

Publisher's Note: All claims expressed in this article are solely those of the authors and do not necessarily represent those of their affiliated organizations, or those of the publisher, the editors and the reviewers. Any product that may be evaluated in this article, or claim that may be made by its manufacturer, is not guaranteed or endorsed by the publisher.

frontiers in Cardiovascular Medicine

ORIGINAL RESEARCH
published: 18 March 2022
doi: 10.3389/fcvm.2022.803532

Valosin Containing Protein as a Specific Biomarker for Predicting the Development of Acute Coronary Syndrome and Its Complication

Chenchao Xu[1†], Bokang Yu[1†], Xin Zhao[2†], Xinyi Lin[1], Xinru Tang[1], Zheng Liu[1], Pan Gao[2], Junbo Ge[2], Shouyu Wang[1] and Liliang Li[1*]*

[1] Department of Forensic Medicine, School of Basic Medical Sciences, Fudan University, Shanghai, China, [2] Department of Cardiology, Shanghai Institute of Cardiovascular Diseases, Zhongshan Hospital, Fudan University, Shanghai, China

OPEN ACCESS

Edited by:
Saskia CA De Jager,
Utrecht University, Netherlands

Reviewed by:
Ning Zhou,
Huazhong University of Science and Technology, China
Yuling Zhang,
Sun Yat-sen Memorial Hospital, China

***Correspondence:**
Shouyu Wang
shouyu_wang@fudan.edu.cn
Liliang Li
liliangli11@fudan.edu.cn

[†]These authors have contributed equally to this work and share first authorship

Specialty section:
This article was submitted to General Cardiovascular Medicine, a section of the journal Frontiers in Cardiovascular Medicine

Received: 28 October 2021
Accepted: 04 February 2022
Published: 18 March 2022

Citation:
Xu C, Yu B, Zhao X, Lin X, Tang X, Liu Z, Gao P, Ge J, Wang S and Li L (2022) Valosin Containing Protein as a Specific Biomarker for Predicting the Development of Acute Coronary Syndrome and Its Complication. Front. Cardiovasc. Med. 9:803532. doi: 10.3389/fcvm.2022.803532

Background: Acute coronary syndrome (ACS) consists of a range of acute myocardial ischemia-related manifestations. The adverse events of ACS are usually associated with ventricular dysfunction (VD), which could finally develop to heart failure. Currently, there is no satisfactory indicator that could specifically predict the development of ACS and its prognosis. Valosin-containing protein (VCP) has recently been proposed to protect against cardiac diseases. Hence, we aimed to assess whether VCP in serum can serve as a valuable biomarker for predicting ACS and its complication.

Methods: Human serum samples from 291 participants were collected and classified into four groups based on their clinical diagnosis, namely healthy control ($n = 64$), ACS ($n = 40$), chronic coronary syndrome (CCS, $n = 99$), and nonischemic heart disease (non-IHD, $n = 88$). Clinical characteristics of these participants were recorded and their serum VCP levels were detected by enzyme-linked immunosorbent assay (ELISA). Association of serum VCP with the development of ACS and its complication VD was statistically studied. Subsequently, GWAS and eQTL analyses were performed to explore the association between *VCP* polymorphism and monocyte count. A stability test was also performed to investigate whether VCP is a stable biomarker.

Results: Serum VCP levels were significantly higher in the ACS group compared with the rest groups. Besides, the VCP levels of patients with ACS with VD were significantly lower compared to those without VD. Multivariate logistic regression analysis revealed that VCP was associated with both the risk of ACS ($P = 0.042$, OR = 1.222) and the risk of developing VD in patients with ACS ($P = 0.035$, OR = 0.513) independently. The GWAS analysis also identified an association between *VCP* polymorphism (rs684562) and monocyte count, whereas the influence of rs684562 on *VCP* mRNA expression level was further verified by eQTL analysis. Moreover, a high stability of serum VCP content was observed under different preservation circumstances.

Conclusion: Valosin-containing protein could act as a stable biomarker in predicting the development of ACS and its complication VD.

Keywords: valosin-containing protein, acute coronary syndrome, ventricular dysfunction, prognosis prediction, serological biomarker

INTRODUCTION

Acute coronary syndrome (ACS) represents a series of acute myocardial ischemia-related symptoms caused by disruption of coronary artery plaque and consequent thrombosis-induced severe coronary artery stenosis or occlusion (1, 2). Depending on its severity, ACS could mainly lead to three manifestations: unstable angina pectoris, acute myocardial infarction (AMI), and sudden cardiac death (SCD) (3, 4). Given its high morbidity and mortality, ACS has long been considered as a life threat and a great burden to healthcare system worldwide. It is estimated that 40% of patients who experienced such a coronary event may die within 5 years. Moreover, the risk of death for those who suffered from recurrent cardiac events could be 5–6 times higher than general population (5–7).

Previous studies have demonstrated that the adverse prognostic events of ACS are mainly associated with ventricular dysfunction (VD), which may finally lead to heart failure of the patients (8, 9). Hence, the early treatment of ACS, which includes thrombolytic therapy and anticoagulant therapy, could be essential for better prognosis (10). To achieve that purpose, accurate indicators for the early diagnosis and prognosis estimation are required. Cardiac biomarkers, such as creatine kinase MB (CK-MB) and cardiac troponin T (cTnT), have been proved to be useful in predicting ACS, particularly non-ST segment elevated myocardial infarction (non-STEMI) (11–13). Due to the application of these biomarkers, the diagnostic efficiency of ACS has been significantly improved (14, 15). However, most of these biomarkers are not specific indicators for ACS, or rather a reflection of the established fact of myocardial infarction (16–21). Moreover, estimation of the long-term outcomes, which can be negatively affected by VD, remains to be further improved due to the lack of valid prognostic indicators. Therefore, an effective indicator that can be used to predict both the development of ACS and its complication in a convenient way is urgently needed.

Valosin-containing protein (VCP), also known as p97, is a conserved type II AAA+ (ATPases associated with diverse cellular activities) family protein abundantly expressed in cardiac tissues. The biological functions of VCP range from protein metabolism to intracellular homeostasis. The disruption of protein homeostasis has been proved to involve in various cardiac diseases, which includes heart failure, myocardial infarction, and diabetic cardiomyopathy (22). As an important maintainer of protein homeostasis in cardiovascular system, VCP has been suggested to have a protective role toward ischemia–reperfusion injury and VD (23–25). In our recent study, a significant increase in serum VCP concentration was observed in early myocardial ischemia-induced SCD cases, which further verified the activation of VCP expression toward acute myocardial ischemia (26). In addition, experiments on transgenic mice revealed that disruption of VCP activity could lead to the development of cardiomyopathy and defects in cardiomyocyte nuclear morphology, which suggests the pleiotropic functions of VCP in cardiac homeostasis (27). Though VCP has been considered to be a crucial cardiac protective factor, it remains obscure whether VCP is related to the development of VD in patients with ACS. Besides, the content changes of secretory VCP in ACS also deserve to be clarified.

In this research, the serum VCP levels among several different groups, namely healthy control group, ischemic heart disease (IHD) group, and non-IHD group, were investigated. For a better comparison, the IHD group was further subdivided into ACS group and chronic coronary syndrome (CCS) group. In addition, association between serum VCP levels and the development of ACS, along with its most common complication—VD—were statistically analyzed. The aim was to explore whether VCP could serve as a specific biomarker to predict both ACS and its complication.

MATERIALS AND METHODS

Ethical Statement

Human serum samples were collected from participants who were admitted to Zhongshan Hospital affiliated to Fudan University (Shanghai, China) during the period August 2020 to August 2021. Sampling and study design was in agreement with the ethical principles stated in the Declaration of Helsinki of the World Medical Association (28) and approved by the Ethics Committee at Zhongshan Hospital, Fudan University (approval number: B2020-078R).

Sample Classification

Human serum samples from 291 participants were collected and classified into four groups: healthy control group ($n = 64$), ACS group ($n = 40$), CCS group ($n = 99$), and non-IHD group ($n = 88$). Grouping was performed based on symptoms, diagnosis, medical history, and laboratory information. Individuals with none or mild diseases irrelevant to cardiac function were allocated into healthy control group. Individuals with IHD were subdivided into ACS and CCS groups according to the ESC and JCS guidelines (3, 29). The rest cases, which include arrhythmia, valvular heart disease, congenital heart disease, and cardiomyopathy, were pooled into non-IHD group. Demographic information of the donors, which includes age, sex, history of smoking, and drinking, and also their echocardiographic parameters and blood–urine biochemistry test results were collected. For the purpose of this study, whether patients developed VD following diagnosis of ACS was also retrieved from medical records. Based on the clinical practice, the diagnosis of VD is based on interpretation of combined qualitative and quantitative echocardiographic parameters by an experienced operator who classifies the cardiac function as "normal" and "dysfunction" (30). Patients who developed VD preceding the diagnosis of ACS were excluded from this study. Depending on the presence of VD, the ACS group was subdivided into two cohorts, namely "ACS + VD" ($n = 14$) and "ACS + non-VD" ($n = 26$). Serum samples were collected immediately after admission before the first medical intervention.

Preparation of Serum Samples

A total of 5 mL peripheral blood was acquired from each donor and coagulated at room temperature (RT) for 30 min, followed by

centrifugation at 12,000 rpm for 10 min at 4°C. Separated serum samples were stored at −80°C until use.

Serum VCP Level Detection

Samples were initially diluted with saline by a serial dilution of 2-, 5-, 10-, and 100-folds. The preliminary experiment suggests that a dilution of 5-folds yielded good results within the range of standards. Hence, all serum samples were diluted in a ratio of 1:5 for further assay in this study. Procedure of the two-site sandwich assay is demonstrated as previously described (26). VCP was separated by binding to the corresponding dendrimer-linked monoclonal antibody on the microplate. Additionally, a horse radish peroxidase (HRP)-conjugated secondary monoclonal antibody was applied to form an antibody-antigen-labeled antibody sandwich. Finally, unbound, labeled antibody was removed by elution.

The serum VCP detection was conducted using a commercial kit from Shanghai YuBo Biotechnology (catalog no.: YB-VCP-Hu, Shanghai, China) for enzyme-linked immune sorbent assay (ELISA) purposes. Briefly, an aliquot of 50 μL diluted sample or the standards was added to a 96-well microplate and incubated with 100 μL rabbit antimouse HRP-conjugated secondary antibody at 37°C for 1 h. Subsequently, the unbound antibody was washed for five times. The microplates were then incubated with 100 μL/well enzyme substrates and kept in dark at 37°C to allow immunoreaction. Finally, the reaction was quenched by the addition of 50 μL stop solution. Signal intensity was detected of the absorbance at the wavelength of 450 nm using the BioTek Epoch Microplate Spectrophotometer (Biotek, Winooski, VT, USA). The concentration of VCP in each sample was determined based on the calibration curve generated with the human full-length VCP protein standard. Sample diluent was made of 10% NBS, 0.05% Tween-20, 0.2% procline-300, and PBS with pH 7.2–7.4. As per the manufacturer's instructions, crossreaction with other nonspecific analytes and the influence of a spectrum of other biological substances and drugs were negligible due to the use of specific monoclonal antibodies in this system. The specificity of this commercial kit was also verified in our previous study (26).

Stability Test

To test the stability of VCP in human serum, two groups of serum samples were exposed at 4°C or RT for up to 6 days, respectively. Meantime, aliquots from 6 time points (1, 3, 6 h, 1, 3, and 6 d) were collected for VCP assay. Serum samples in both two groups were collected from two individuals and treated under 3 different conditions: (A) original serum sample without treatment, (B) original serum sample supplemented with 1,500 pg/mL human VCP standard, (C) original serum sample supplemented with 750 pg/mL human VCP standard. In addition, a third group that consists of serum samples from another four individuals was applied to investigate the possible effect of multigelation. Specifically, five aliquots from each sample were thawed and frozen repeatedly for 1 to 5 times, respectively. In each thaw–frozen cycle, samples were frozen at −20 °C for 20 min and then brought back to RT for 1 h.

Genome-Wide Association Study (GWAS) Analysis of *VCP* Polymorphisms and Monocyte Count

Genome-wide association study summary data of 145 K individuals from the UK Biobank release (https://www.ukbiobank.ac.uk/) were used to explore the association between the *VCP* polymorphisms and monocyte count. Specifically, variants with a minor allele frequency greater or equal to 1% and an imputation info score greater or equal to 0.5 were kept for association analysis. A Bonferroni-corrected *p*-value of 5.00E-8 was used as the threshold to assess the statistical significance. Eventually, variants that reached genome-wide significance were annotated using HaploReg v4.1 (31). The regional plot was generated using LocusZoom (https://my.locuszoom.org/).

Expression Quantitative Trait Loci (EQTL) Analysis of Rs684562 and *VCP* MRNA Expression Level

To further explore the association between *VCP* mRNA expression levels and the polymorphism identified by GWAS, an eQTL analysis was performed with R software (version 4.0.5) by employing the 1000 Genomes Project Phase 3 genotype data from the Ensembl database (http://www.ensembl.org/) and the deep RNA-sequencing data of lymphoblastoid cell lines (LCLs) collected from 462 individuals of five populations genotyped in the 1000 Genomes Project (32, 33).

Statistical Analysis

Statistical analyses were performed with R software (version 4.0.5) and GraphPad Prism software v 8.3.0 (La Giolla, CA, USA). Continuous variables, such as serum VCP levels, were presented as mean ± standard error of mean (SEM). Categorical variables, such as female gender, were exhibited as numbers or proportions. Differences among groups were compared using one-way ANOVA test for normally distributed continuous variables with homogeneous variance; otherwise, Kruskal–Wallis test were used. Pearson's chi-squared test was used for categorical variables. For comparisons between two groups, parametric Student's *t*-test or nonparametric Mann–Whitney *U*-test was performed, which depends on the group size. Univariate logistic regression analysis was initially performed to screen risk factors for ACS or VD in patients with ACS. Variables with significance were further investigated with multivariate logistic stepwise regression analysis. All statistical tests were two-sided, and $p < 0.05$ was considered statistically significant.

RESULTS

Clinical Characteristics of Study Population

Of the 291 participants enrolled in this study, no significant difference was observed among different groups concerning their gender, drinking habit, and the blood level of some

biochemistry indicators, such as hemoglobin, creatine, eGFR, HbA1c, triglyceride, and urine pH. However, there was statistically significant difference in terms of their age, smoking habit, along with the level of the rest biochemistry indicators. The blood levels of several indicators, such as fasting plasma glucose (FPG), cTnT, N-terminal pro-B-type natriuretic peptide (NT-proBNP), CK-MB, creatine kinase MM (CK-MM), and high-sensitive C-reactive protein (hs-CRP), were substantially raised in ACS group compared to the rest groups. Meanwhile, the glycosylated albumin (GA-L) level was remarkably raised in non-IHD, CCS, and ACS groups, whereas the total cholesterol (TC), low-density lipoprotein cholesterol (LDL-C), and high-density lipoprotein cholesterol (HDL-C) levels were reduced in these three groups (**Table 1**). In terms of echocardiographic parameters, patients with ACS exhibited significantly reduced left ventricular ejection fraction (LVEF) compared to the rest groups. Besides, increased left atrium diameter (LAD) and left ventricular end diastolic diameter (LVDd) were observed in ACS, CCS, and non-IHD groups, compared to the healthy control group (**Table 2**).

Significantly Increased Serum VCP Level in ACS Group

Serum VCP levels of the four groups were exhibited in **Figure 1**. Mean ± SEM of the VCP level for each group was also plotted (ACS: 1,213.00 ± 40.36, Ctrl: 1,111.00 ± 21.62, non-IHD: 1,124.00 ± 20.66, CCS: 1,111.00 ± 23.23). As can be seen, serum VCP level is significantly increased in the ACS group compared with the healthy control group ($P = 0.030$), the non-IHD group ($P = 0.031$), and the CCS group ($P = 0.023$), whereas there was no significant difference neither between the healthy control group and the non-IHD group ($P = 0.680$), or between the healthy control group and the CCS group ($P = 0.987$). Besides, there is also no significant difference between the CCS group and the non-IHD group ($P = 0.677$).

Statistical and Genetic Association Between VCP and ACS

According to the univariate logistic regression analysis based on data from all 291 participants, the odds ratios (OR) with

TABLE 1 | Demographic and laboratory information of the study population.

	Control ($n = 64$)	Non-IHD ($n = 88$)	CCS ($n = 99$)	ACS ($n = 40$)	*P*-value
Demographic characteristic					
Age (years)	58 (48.0–68.0)	63 (51.8–71.3)	67 (60.3–72.0)	67 (57.5–75.3)	**0.002**
Gender (female%)	23 (35.9)	32 (36.4)	32 (32.7)	7 (17.5)	0.168
Smoking [*n*(%)]	2 (3.1)	19 (21.6)	22 (22.4)	15 (37.5)	**<0.001**
Drinking [*n*(%)]	1 (1.6)	9 (10.2)	11 (11.2)	4 (10.0)	0.095
Biochemistry indicators					
Hemoglobin (g/L)	130 (118.0–149.0)	124 (106.8–135.0)	127 (104.3–138.8)	125 (108.0–134.0)	0.095
Albumin (g/L)	45 (38.0–48.0)	40 (36.0–42.0)	39 (37.0–42.8)	36 (34.0–41.0)	**<0.001**
Creatinine	80 (66.8–102.0)	84 (73.8–115.0)	87 (68.3–113.8)	89 (76.0–124.8)	0.522
eGFR (mL/min/1.73 m^2)	90 (44.0–102.0)	77 (53.5–96.5)	74 (52.3–94.8)	77 (48.8–88.3)	0.404
FPG (mmol/L)	5.2 (4.8–5.9)	5.4 (4.7–7.0)	5.6 (4.9–7.4)	6.7 (5.4–9.1)	**0.002**
GA-L (%)	13.3 (12.0–15.5)	15.5 (13.0–18.6)	15.1 (13.4–16.6)	15.1 (13.7–19.3)	**0.001**
HbA1c (%)	5.7 (5.4–5.9)	5.9 (5.4–7.1)	5.8 (5.6–7.1)	6.0 (5.6–7.8)	0.094
cTnT (ng/mL)	0.012 (0.006–0.049)	0.043 (0.014–0.124)	0.040 (0.010–0.121)	0.536 (0.075–1.842)	**<0.001**
Log(NT-proBNP)(pg/mL)	4.947 (3.694–6.280)	6.963 (6.076–7.935)	6.572 (4.908–7.886)	7.477 (6.482–8.765)	**<0.001**
CK-MB (U/L)	15 (12.0–20.0)	15 (12.0–18.0)	15 (13.0–22.0)	20 (14.8–44.3)	**0.001**
CK-MM (U/L)	62 (41.0–96.0)	59 (34.0–108.0)	52 (33.3–83.8)	171 (44.5–488.5)	**0.004**
hs-CRP (mg/L)	1.1 (0.4–3.2)	2.0 (0.6–10.6)	1.4 (0.5–8.3)	6.4 (1.9–36.3)	**<0.001**
TC (mmol/L)	4.930 (4.165–5.490)	3.780 (3.220–4.610)	3.310 (2.870–3.890)	3.410 (2.850–4.170)	**<0.001**
Triglyceride (mmol/L)	1.480 (1.095–2.078)	1.260 (0.907–1.755)	1.310 (0.930–1.940)	1.190 (0.780–1.910)	0.320
LDL-C (mmol/L)	2.795 (1.990–3.327)	2.070 (1.640–2.810)	1.620 (1.290–2.130)	1.560 (1.340–2.220)	**<0.001**
HDL-C (mmol/L)	1.210 (1.012–1.490)	1.010 (0.860–1.250)	1.040 (0.840–1.160)	1.030 (0.830–1.170)	**0.004**
UA	328(265–409)	379(302–483)	339(291–399)	398(314–462)	**0.003**
Urine pH	5.5 (5.5–6.1)	6.0 (5.5–6.0)	5.5 (5.5–6.5)	5.5 (5.1–6.0)	0.637
Proteinuria					**0.001**
−	38 (66.7)	69 (83.1)	73 (80.2)	19 (50.0)	
+	10 (17.5)	8 (9.6)	10 (11.0)	14 (36.8)	
≥ + +	9 (15.9)	6 (7.2)	8 (8.8)	5 (13.2)	

eGFR, estimated glomerular filtration rate; FPG, fasting plasma glucose; GA-L, glycosylated albumin; HbA_{1c}, glycosylated hemoglobin; cTnT, cardiac troponin T; NT-proBNP, amino terminal probrain natriuretic peptide; CK-MB, creatine kinase MB; CK-MM, creatine kinase MM; hs-CRP, high-sensitivity C-reactive protein; TC, total cholesterol; LDL-C, low-density lipoprotein cholesterol; HDL-C, high-density lipoprotein cholesterol; UA, uric acid. Bold value indicates the statistical significance.

TABLE 2 | Medical history and echocardiography of the study population.

	Control ($n = 64$)	Non-IHD ($n = 88$)	CCS ($n = 99$)	ACS ($n = 40$)	*P*-value
History of cardiovascular disease					
Arrhythmia	0 (0.0)	52 (59.1)	23 (23.2)	5 (12.5)	**<0.001**
Cardiomyopathy	0 (0.0)	9 (10.2)	7 (7.1)	0 (0.0)	**0.009**
Valvular disease	0 (0.0)	29 (33.0)	5 (5.1)	2 (5.0)	**<0.001**
Congenital heart disease	0 (0.0)	11 (12.5)	0 (0.0)	0 (0.0)	**<0.001**
Hypertension	28 (43.8)	38 (43.2)	71 (72.4)	30 (75.0)	**<0.001**
Dyslipidemia	28 (43.8)	38 (43.2)	71 (72.4)	30 (75.0)	**<0.001**
Diabetes	7 (10.9)	3 (3.4)	7 (7.1)	4 (10.0)	0.298
Medication received before admission					
ACEI/ARBs	6 (9.4)	19 (22.1)	39 (40.6)	16 (40.0)	**<0.001**
CCB	11 (17.2)	22 (25.0)	29 (30.2)	11 (27.5)	0.314
β blockers	6 (9.4)	23 (26.1)	37 (38.5)	14 (35.0)	**0.001**
diuretics	4 (6.2)	29 (33.0)	29 (30.2)	5 (12.5)	**<0.001**
Digoxin	0 (0.0)	7 (8.0)	5 (5.2)	0 (0.0)	**0.040**
Statins	12 (18.8)	5 (5.7)	52 (54.2)	21 (52.5)	**<0.001**
Antithrombotics	7 (10.9)	12 (13.6)	72 (75.0)	34 (85.0)	**<0.001**
Anticoagulation	2 (3.1)	22 (25.0)	10 (10.4)	9 (22.5)	**0.001**
Nitrate esters	1 (1.6)	9 (10.2)	18 (18.8)	18 (45.0)	**<0.001**
Trimetazidine	0 (0.0)	2 (2.3)	3 (3.1)	0 (0.0)	0.530
Insulin	2 (3.1)	6 (6.8)	14 (14.6)	1 (2.5)	**0.033**
OAD	2 (3.1)	12 (13.6)	12 (12.5)	6 (15.0)	0.090
Echocardiographic parameters					
ARD (mm)	34 (31–37)	33 (32–37)	33 (31–35)	34 (32–36)	0.324
LAD (mm)	38 (36–40)	44 (41–50)	41 (39–45)	41 (38–42)	**<0.001**
LVDd (mm)	46 (44–49)	49 (45–54)	48 (44–52)	49 (45–55)	**0.005**
IVS (mm)	10 (9–11)	10 (9–12)	10 (9–12)	10 (10–12)	0.068
LVPW (mm)	9 (9–10)	10 (9–11)	10 (9–10)	10 (9–10)	0.345
PAP (mmHg)	30 (30–34)	35 (31–44)	33 (31–38)	32 (30–35)	**<0.001**
LVEF (%)	65 (63–67)	64 (58–66)	60 (50–66)	54 (43–62)	**<0.001**

ACEI, angiotensin-converting enzyme inhibitors; ARB, angiotensin receptor blockers; CCB, calcium channel blocker; OAD, oral antidiabetic drugs; ARD, aortic root diameter; LAD, left atrial diameter; LVDd, left ventricular end diastolic diameter; IVS, interventricular septal thickness; LVPW, posterior wall thickness of left ventricle; PAP, pulmonary arterial systolic pressure; LVEF, left ventricular ejection fraction. Bold value indicates the statistical significance.

its 95% confidence intervals (CIs) for 36 possible indicators are presented in **Table 3**. As can be seen, VCP, along with several other indicators, which include FPG, cTnT, NT-proBNP, CK-MB, CK-MM, uric acid (UA), and proteinuria (+), is positively correlated with the risk of ACS, whereas albumin and LVEF were negatively correlated with the risk of ACS. To further verify the association between VCP and the risk of ACS, a multivariate logistic stepwise regression analysis was performed for the above 10 identified indicators. The statistical results revealed that VCP, along with cTnT and UA, was independent variables in the optimized model (**Table 4**). Taken together, these findings suggest that VCP level is strongly related to the risk of ACS.

To further investigate the potential role of VCP in the occurrence of ACS at a genetic level, a GWAS analysis that focusses on genetic variants associated with monocyte count was performed. As shown in **Figure 2A**, a common SNP (rs684562) located on the *VCP* gene, which is indicated by a purple rhombic dot, was significantly associated with human monocyte count ($P = 2.20E\text{-}14$). In addition, the eQTL analysis further revealed that *VCP* mRNA level was associated with the genotype of rs684562 (**Figure 2B**). Individuals carrying the T allele on the rs684562 locus tend to have decreased *VCP* levels as compared to the C allele. Taken together, these findings imply that gene polymorphism might affect the VCP expression that consequently modulates peripheral blood monocyte count and inflammation and regulates the development of ACS.

Decreased Serum VCP Level in Patients With ACS With VD

Since the long-term prognosis of ACS is closely reflected by the presence of VD, we then subdivided the ACS group into 2 cohorts depending on whether or not the patient developed VD and then compared the serum VCP level between the two cohorts. Our results showed that patients with ACS who developed VD exhibited significantly decreased serum VCP levels compared to those who did not develop VD ($P = 0.014$) (**Figure 3**).

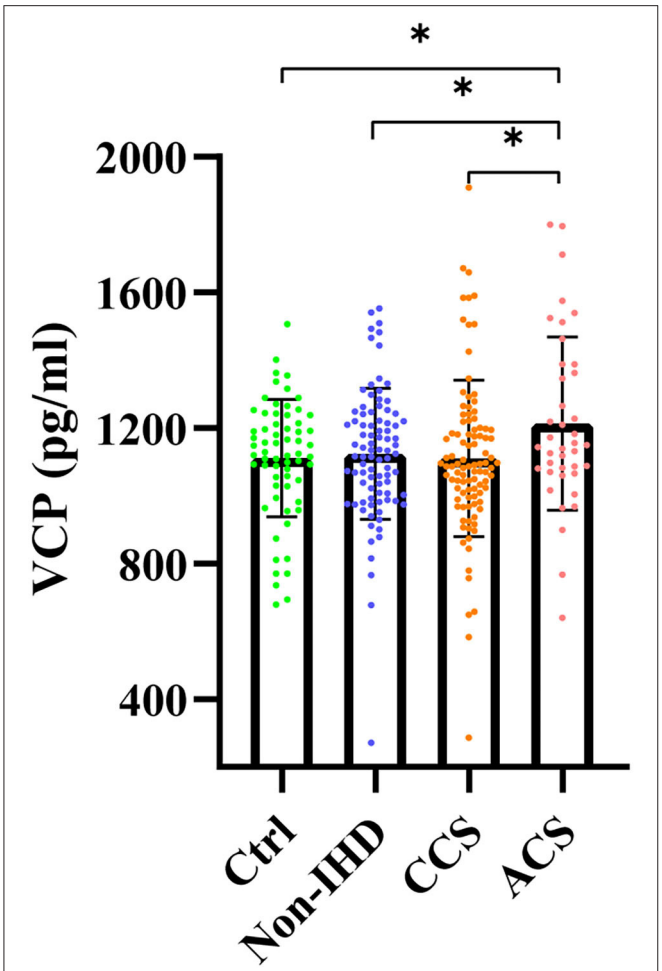

FIGURE 1 | Serum VCP levels of healthy control group (Ctrl), nonischemic heart disease group (non-IHD), chronic coronary syndrome group (CCS), and acute coronary syndrome group (ACS) (*$p < 0.05$).

Association Between VCP and the Risk of Developing VD in Patients With ACS

According to the univariate logistic regression analysis based on data from the 40 patients with ACS, the ORs with its 95% CI for 36 possible indicators are presented in **Table 5**. Among the indicators, only VCP, UA, left ventricular diameter in systole (LVDs), and interventricular septal thickness (IVS) are statistically correlated with the risk of developing VD in the ACS cohort.

To further confirm the association between VCP and the risk of developing VD, a multivariate logistic stepwise regression analysis was again performed for the above 4 identified indicators. Statistical results revealed that VCP, LVDs, and IVS were independent variables in the optimized model (**Table 6**), which suggest that VCP is significantly associated with the development of VD in patients with ACS. In addition, the OR (0.513) with its 95% CI (0.276–0.954) indicated that the risk of developing VD tends to reduce as the serum VCP level increases. Similarly, it can be inferred that increased IVS and decreased LVD are significantly related to reduced odds of developing VD in the patients with ACS.

TABLE 3 | Univariate logistic regression analysis of ACS and possible indicators (all indicators increase by 1 unit unless otherwise specified).

Indicator	OR (95% CI)	*P*-value
VCP[a]	1.234 (1.044, 1.459)	**0.014**
Age	0.999 (0.968, 1.032)	0.975
Gender	0.437 (0.175, 1.096)	0.078
Smoking	2.073 (0.934, 4.598)	0.073
Drinking	0.879 (0.262, 2.943)	0.834
Hemoglobin	0.996 (0.981, 1.012)	0.647
Albumin	0.923 (0.854, 0.998)	**0.045**
Creatinine	1.001 (0.999, 1.003)	0.487
eGFR	0.996 (0.983, 1.009)	0.508
FPG	1.113 (1.003, 1.235)	**0.045**
GA-L	1.038 (0.958, 1.124)	0.361
HbA1c	1.045 (0.775, 1.410)	0.772
cTnT[b]	1.052 (1.018, 1.088)	**0.003**
log(NT-proBNP)	1.353 (1.103, 1.659)	**0.004**
CK-MB	1.034 (1.011, 1.058)	**0.004**
CK-MM	1.003 (1.001, 1.004)	**0.003**
hs-CRP	1.009 (1.000, 1.019)	0.062
TC	1.177 (0.752, 1.844)	0.476
Triglyceride	1.089 (0.776, 1.529)	0.622
LDL-C	1.155 (0.685, 1.948)	0.590
HDL-C	0.592 (0.204, 1.717)	0.334
UA	1.004 (1.001, 1.006)	**0.007**
Urine pH	0.709 (0.417, 1.205)	0.204
Proteinuria +[c]	5.379 (2.068, 13.988)	**<0.001**
Proteinuria ≥ ++[d]	2.401 (0.705, 8.183)	0.161
Hypertension	1.141 (0.492, 2.647)	0.759
Dyslipidemia	1.444 (0.399, 5.235)	0.576
Diabetes	1.292 (0.614, 2.718)	0.500
ARD	1.093 (0.986, 1.212)	0.090
LAD	0.955 (0.887, 1.028)	0.219
LVDd	1.037 (0.989,1.087)	0.137
LVDs	1.037 (0.993, 1.082)	0.099
IVS	1.037 (0.850, 1.266)	0.719
LVPW	1.000 (0.843, 1.185)	0.997
PAP	0.974 (0.923, 1.028)	0.335
LVEF	0.969 (0.940, 0.998)	**0.037**

[a] *VCP increases by 100 units.*
[b] *cTnT increases by 0.003 units.*
[c] *Compared with nonproteinuria group.*
[d] *Compared with nonproteinuria group.*
Bold value indicates the statistical significance.

Stability of VCP in Serum

Given the fact that optimal storage and handling condition of serum samples cannot always be achieved during clinical practice, we have tested the stability of VCP upon three different circumstances. The results showed that after 6 days, the final VCP content slightly declined to 94.11% and 95.19% of its initial level when stored at 4°C or RT, respectively (**Figure 4A**). In addition, the VCP content in repeatedly thawed and frozen

samples also maintained at a stable level after five freeze–thaw cycles (**Figure 4B**). These findings suggest that neither long-term storage at 4°C or RT nor multigelation could seriously affect serum VCP quantity.

DISCUSSION

In this study, serum VCP level was found to be significantly increased in the ACS group compared with the healthy control, CCS, and non-IHD groups. Meanwhile, statistical results from the multivariate logistic regression models also demonstrated that the serum VCP level is an independent risk factor for ACS ($P = 0.042$, OR = 1.222). More importantly, by dividing the ACS cohort into "ACS + VD" and "ACS + non-VD" subgroups, we have further observed that during progression of ACS, patients who developed VD exhibited significantly decreased serum VCP levels compared to those who did not develop VD. Multivariate logistic regression analysis showed that serum VCP was an independent variable that significantly correlated with the risk of VD in patients with ACS ($P = 0.035$, OR = 0.513). These outcomes suggest that VCP could be an effective biomarker for the prediction of both ACS and its complication.

To explore the possible mechanism behind the correlation between serum VCP level and the occurrence of ACS, a

TABLE 4 | Multivariate logistic stepwise regression analysis of ACS and candidate indicators (all indicators increase by 1 unit unless otherwise specified).

Indicator	OR (95% CI)	*P* value
VCP[a]	1.222 (1.008, 1.482)	**0.042**
cTnT[b]	1.054 (1.015, 1.093)	**0.006**
UA	1.004 (1.001, 1.007)	**0.007**
FPG	1.121 (0.960, 1.310)	0.150
CK-MM	1.002 (0.998, 1.006)	0.286
CK-MB	1.014 (0.959, 1.073)	0.520
Albumin	0.957 (0.830, 1.113)	0.570
LVEF	1.014 (0.959, 1.073)	0.620
Proteinuria	1.193 (0.508, 2.804)	0.686
NT-proBNP	0.970 (0.616, 1.528)	0.896

[a] *VCP increases by 100 units.*
[b] *cTnT increases by 0.003 units.*
Bold value indicates the statistical significance.

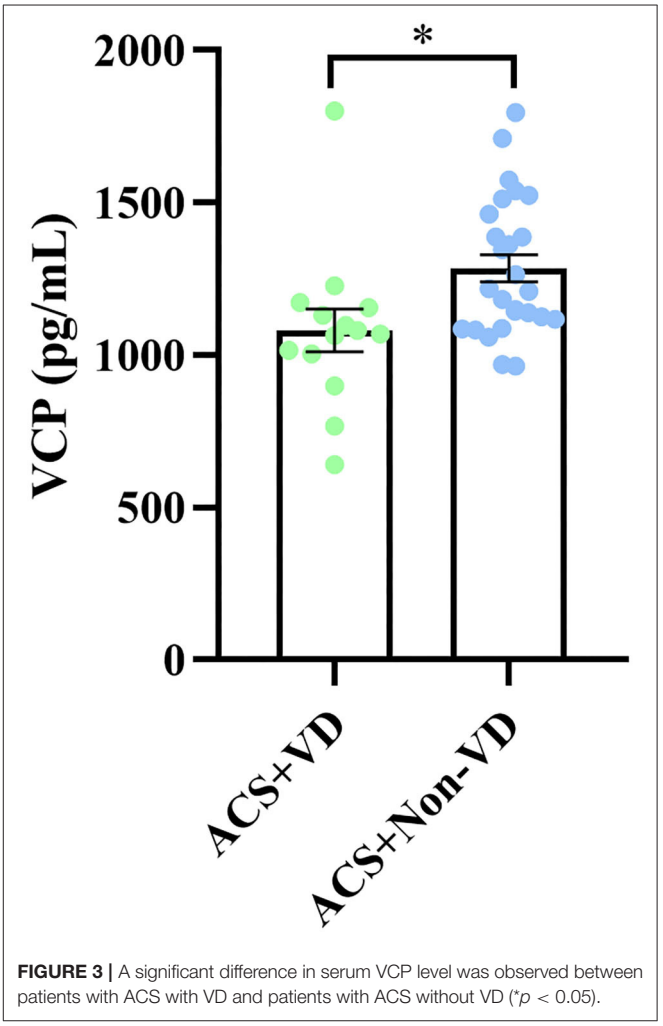

FIGURE 3 | A significant difference in serum VCP level was observed between patients with ACS with VD and patients with ACS without VD (*$p < 0.05$).

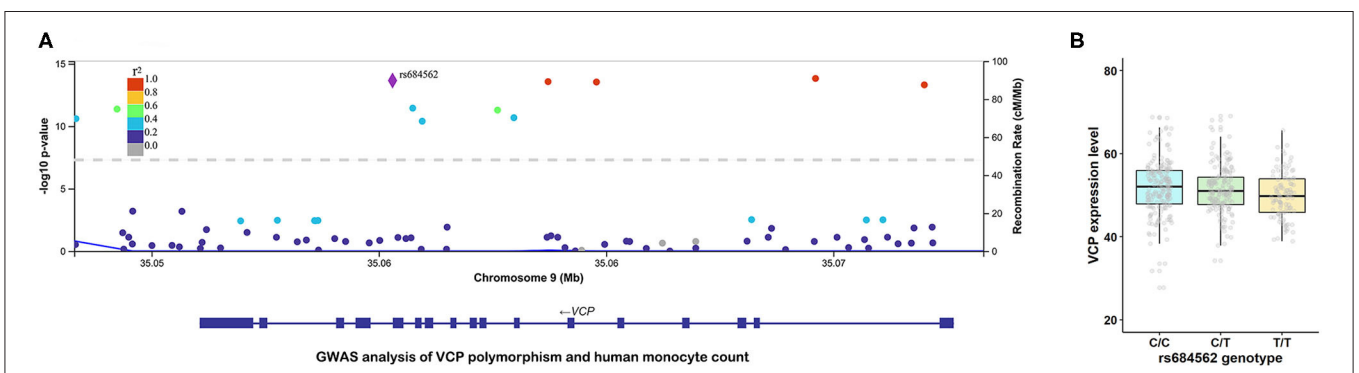

FIGURE 2 | *VCP* polymorphism is correlated with human monocyte count and *VCP* mRNA expression level. **(A)** Association between rs684562 and human monocyte count revealed by GWAS ($P = 2.20E-14$). **(B)** Association between *VCP* mRNA expression level and the genotype of rs684562 revealed by eQTL analysis.

TABLE 5 | Risk factors for VD in patients with ACS evaluated by univariate logistic regression analysis (all indicators increases by 1 unit unless otherwise specified).

Indicator	OR (95% CI)	*P*-value
VCP[a]	0.651 (0.442, 0.957)	**0.029**
Gender	0.256 (0.028, 2.383)	0.231
Age	1.033 (0.979, 1.089)	0.236
Smoking	0.889 (0.231, 3.425)	0.864
Drinking	0.590 (0.056, 6.266)	0.661
Hemoglobin	0.980 (0.951, 1.010)	0.199
Albumin	0.997 (0.866, 1.147)	0.966
Creatinine	1.000 (0.996, 1.003)	0.775
eGFR	0.983 (0.961, 1.006)	0.148
FPG	1.193 (0.993, 1.432)	0.059
GA-L	1.144 (0.968, 1.351)	0.114
HbA1c	1.833 (0.985, 3.414)	0.056
cTnT[b]	0.989 (0.975, 1.003)	0.129
log(NT-proBNP)	1.578 (0.987, 2.523)	0.057
CK-MB	0.973 (0.939, 1.009)	0.139
CK-MM	0.998 (0.996, 1.001)	0.176
hs-CRP	1.000 (0.985, 1.015)	0.976
TC	0.496 (0.201, 1.221)	0.127
Triglyceride	1.169 (0.720, 1.900)	0.528
LDL-C	0.270 (0.067, 1.080)	0.064
HDL-C	0.105 (0.005, 2.032)	0.136
UA	1.005 (1.000, 1.009)	**0.033**
Urine pH	0.784 (0.255, 2.412)	0.672
Proteinuria +	0.562 (0.194, 1.628)	0.288
Proteinuria ≥ ++	0.344 (0.032, 3.688)	0.378
Hypertension	1.351 (0.289, 6.320)	0.702
Dyslipidemia	0.590 (0.056, 6.266)	0.661
Diabetes	3.400 (0.873, 13.239)	0.078
ARD	1.224 (0.994, 1.508)	0.057
LAD	1.053 (0.913, 1.215)	0.480
LVDd	1.097 (0.999, 1.205)	0.052
LVDs	1.131 (1.028, 1.244)	**0.012**
IVS	0.507 (0.292, 0.879)	**0.016**
LVPW	0.641 (0.343, 1.200)	0.165
PAP	1.052 (0.952, 1.162)	0.318
LVEF	0.952 (0.900, 1.007)	0.086

[a]*VCP increases by 100 units.*
[b]*cTnT increases by 0.003 units.*
[c]*Compared with proteinuria negative group.*
[d]*Compared with proteinuria negative group.*
Bold value indicates the statistical significance.

TABLE 6 | Risk factors for VD in patients with ACS evaluated by multivariate logistic stepwise regression analysis (all indicators increase by 1 unit unless otherwise specified).

Indicator	OR (95% CI)	*P*-value
VCP[a]	0.513 (0.276, 0.954)	**0.035**
LVDs	1.315 (1.031, 1.677)	**0.028**
IVS	0.272 (0.094, 0.786)	**0.016**
UA	1.003 (0.996, 1.011)	0.394

[a]*VCP increases by 100 units.*
Bold value indicates the statistical significance.

GWAS analysis that focusses on genetic variants associated with monocyte count was performed. Accordingly, rs684562, which is a common SNP located on the *VCP* gene, was found to be significantly associated with human monocyte count. The eQTL analysis further suggested that *VCP* mRNA expression level was associated with the genotype of rs684562, since individuals carrying the T allele tended to have a lower *VCP* level compared with those carrying the C allele. Inflammation with monocyte aggregation plays an important role in the development and progression of atherosclerosis and other cardiovascular diseases (34). It is now widely accepted that inflammation dysfunction is one of the main mechanisms of ACS (35). Thus, our findings indicated that the upregulation of VCP in ACS might be related to its participation in modulating monocyte count and inflammation. Moreover, previous studies have revealed that elevated levels of inflammatory markers produced by enhanced inflammation, along with increased white blood cell counts, are not only associated with a higher ACS incidence, but also a sign of poor prognostic events, which include VD and heart failure (36–39). According to a recent study, sufficient VCP in the heart could prevent pressure overload-induced heart failure by rectifying the inflammatory signaling and enhancing the cardiac resistance to oxidative stress (40). Therefore, the antiinflammatory function of VCP might explain its upregulation in the "ACS + non-VD" group. In addition, overexpression of VCP has been proposed to protect the cardiac function from negative effects of pathological Ca^{2+} overload by modulating Ca^{2+} uptake proteins (41), which we assume might also be a pathway for VCP to work against the development of VD.

Except for the predictive value of a biomarker, its stability is also a critical concern for clinical use. Our stability test results revealed that serum VCP level merely slightly decreased by 5.89 and 4.81% after 6 days when stored at 4°C or RT, respectively. This finding suggests that the stability of VCP is similar to several previously proposed biomarkers for the diagnosis of ACS, such as aspartate aminotransferase (AST) (reduced by 2.1%, 4°C, 7d), CK-MB (increased by 1.9%, 4°C, 7d) and cTnT (increased by 0.6%, 4°C, 7d), and better than some others, such as cardiac troponin I (cTnI) (reduced by 19.3%, 4°C, 7d) (42). Furthermore, no significant fraction reduction was observed in terms of the serum VCP level even after 5 freeze–thaw cycles. These indicate that VCP is stable in serum under different storage circumstances and thus could be applied as a suitable serological biomarker. During clinical practice, such kind of stable indicators should be of great value, as their expression levels in blood samples could be accurately quantified even after long-term storage.

Apart from VCP, some common indicators, which include albumin, FPG, UA, proteinuria, LVEF, cTnT, NT-proBNP, CK-MB, and CK-MM, were also identified to be the independent risk factors for ACS in this study. Among these indicators, the last four has previously been reported to be applied in diagnosis of ACS. From our laboratory test results, it can be observed that the serum levels of cTnT, CK-MB, and CK-MM were indeed notably

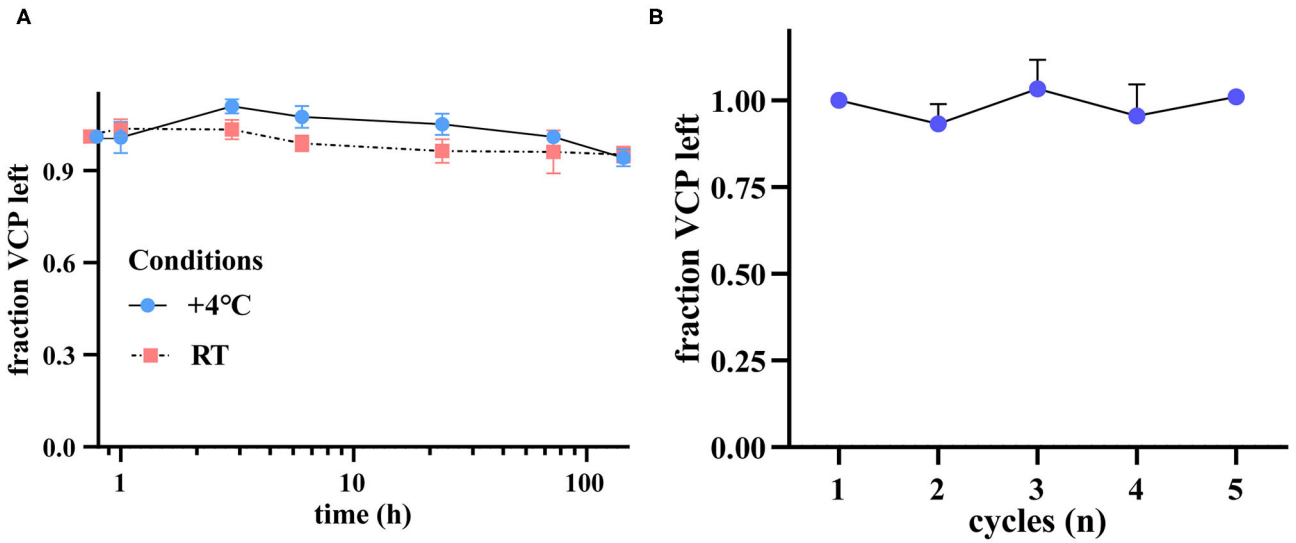

FIGURE 4 | VCP is a stable serological biomarker under different preservation circumstances. **(A)** VCP content left after 1, 3, 6 h, 1, 3, and 6 d, illustrated by fraction change ($n = 6$). **(B)** VCP content left after 1–5 cycles of freezing and thawing ($n = 4$).

elevated in the ACS group. However, previous studies also revealed their limitations in the diagnosis of ACS. Taking cTnT, the most representative one, for example, its elevation reflects the "fait accompli" of myocardial infarction, rather than progression of ACS (16, 17). As for the other indicators, their elevations are most likely to be physiological compensation effects, which are not specific secondary reactions to ACS. For example, an increased FPG level could be explained by hyperglycemia under the stress of ACS, known as stress induced hyperglycemia (SIH) (18, 19), whereas the elevation of UA is possibly due to the fact that UA level is closely related to oxidative stress, endothelial dysfunction, inflammation, and vasoconstriction, which are the common features in the episode of ACS (20, 21). In the recent years, the development of omics technology like metabolomics has also been proposed to promote the diagnosis of ACS. However, its clinical application has not yet been guaranteed due to problems concerning technical challenges and data interpretation (43). In view of feasibility, promising biomarkers that can be assayed using simple detection methods are currently still preferentially considered. Recently, serum CCL21 level was found to be independently associated with outcome after ACS (44), which has highlighted the potential of applying gene expression pattern to promote clinical evaluation. Similarly, the inclusion of VCP in routine serum test should significantly improve the diagnostic accuracy of ACS in the early stage. Besides, detection of serum VCP could also be beneficial to patients with ACS due to its informative role in prognosis estimation. In clinical practice, Killip classification is widely used to evaluate the severity of pump failure and guide the therapy selection (45). Nevertheless, the assessment is based on clinical findings, which can be subjective and interfered by respiratory infection symptoms, not to mention that it is unable to reflect the development of VD. On the other hand, existing indicators, such as CK-MB and cTnT for the diagnosis of ACS, or NT-proBNP for the diagnosis of heart failure, are all released passively after ischemia-induced myocardial cell injury, myocardial ventricle wall stress, or tissue hypoxia and therefore could not be applied as specific and valuable prognostic indicators during progression of ACS (46, 47). In this study, two morphological indicators, LVDs and IVS, were also identified to be significantly correlated with the risk of developing VD; however, these are not suitable for clinical application. Blood biochemistry test is currently an important procedure during the clinical evaluation of ACS. As a molecular indicator that can be quantified by the broadly used ELISA, VCP could be easily integrated with some existing biochemical indicators without the requirement of additional pretreatment for the blood samples. More importantly, an advantage of VCP is that it allows a much earlier prediction of prognosis compared to other morphological changes that may only take place in severe phase, which could be helpful in assessing whether some early interventions are needed to prevent poor prognosis of ACS.

The main strengths of our study are 3 folds: (1) we discovered the dual function of serum VCP as it predicts both the development of ACS and its complication. The versatility of VCP suggested its superiority over the current clinical markers; (2) we performed the GWAS and eQTL analyses to explore the potential mechanisms behind the VCP function; (3) we also validated VCP stability under different storage conditions, which might increase the feasibility and practicability of translating VCP into clinical use. However, several limitations should be noted. First, the prognosis prediction role of VCP deserves to be verified in a larger size of samples, since there are currently only 14 serum samples from the "ACS + VD" subgroup, which makes our conclusion lack of confidence. Second, stratification of the VD in patients with ACS based on the degrees of their cardiac dysfunction or physical activity condition was not performed in this study due to the relative small sample size. Hence, further

research with more samples consisting of patients with different severities of complications are required to explicit the dynamic expression changes of VCP during the development of VD.

CONCLUSION

Overall, the serum level of VCP was found to be positively correlated with the risk of ACS. Higher serum VCP level was significantly related to reduced odds of developing VD in patients with ACS. Serum VCP was stable under different preservation conditions. Our study suggests that VCP is a promising and stable biomarker that can be used to predict both the development of ACS and its complication.

DATA AVAILABILITY STATEMENT

Publicly available datasets were analyzed in this study. This data can be found here: http://www.ensembl.org/. The datasets generated and analyzed for this study can be obtained by contacting the corresponding authors.

ETHICS STATEMENT

The studies involving human participants were reviewed and approved by Ethics Committee at Zhongshan Hospital, Fudan University. The patients/participants provided their written informed consent to participate in this study.

AUTHOR CONTRIBUTIONS

CX and BY performed the experiments, data analysis, and drafted the manuscript. XZ and PG prepared the serum samples. XZ collected the clinical data for all participants. XL, XT, and ZL helped in serum preparation, provided technical assistance in GWAS analysis, and statistical analysis. JG supervised this study. SW and LL conceived and supervised this study and revised the manuscript. All authors contributed to the article and approved the submitted version.

FUNDING

This study was financially supported by the National Natural Science Foundation of China (grant nos. 81871527 and 82070285), the Shanghai Health Committee Research Foundation (20194Y0066), the Zhengyi Scholar Foundation of School of Basic Medical Sciences, Fudan University (no. S25-15), and the Fudan Junzheng Scholar Foundation (no. 2193101011003).

ACKNOWLEDGMENTS

We are grateful to UK Biobank and Gleb Kichaev et al. for the public GWAS data of a large-scale prospective cohort study (UK Biobank, http://www.ukbiobank.ac.uk/).

REFERENCES

1. Amsterdam EA, Wenger NK, Brindis RG, Casey DE Jr, Ganiats TG, Holmes DR Jr, et al. 2014 AHA/ACC Guideline for the Management of Patients with Non-ST-Elevation Acute Coronary Syndromes: a report of the American College of Cardiology/American Heart Association Task Force on Practice Guidelines. *J Am Coll Cardiol.* (2014) 64:e139–e228. doi: 10.1016/j.jacc.2014.09.017
2. Fanaroff AC, Rymer JA, Goldstein SA, Simel DL, Newby LK. Does This Patient With Chest Pain Have Acute Coronary Syndrome?: The Rational Clinical Examination Systematic Review. *JAMA.* (2015) 314:1955–65. doi: 10.1001/jama.2015.12735
3. Kimura K, Kimura T, Ishihara M, Nakagawa Y, Nakao K, Miyauchi K, et al. JCS 2018 guideline on diagnosis and treatment of acute coronary syndrome. *Circ J.* (2019) 83:1085–196. doi: 10.1253/circj.CJ-19-0133
4. Corbett SJ, Ftouh S, Lewis S, Lovibond K, Guideline C. Acute coronary syndromes: summary of updated NICE guidance. *BMJ.* (2021) 372:m4760. doi: 10.1136/bmj.m4760
5. Rogers WJ, Canto JG, Lambrew CT, Tiefenbrunn AJ, Kinkaid B, Shoultz DA, et al. Temporal trends in the treatment of over 1.5 million patients with myocardial infarction in the U.S. from 1990 through 1999. *J Am Coll Cardiol.* (2000) 36:2056–63. doi: 10.1016/S0735-1097(00)00996-7
6. Makki N, Brennan TM, Girotra S. Acute coronary syndrome. *J Intensive Care Med.* (2013) 30:186–200. doi: 10.1177/0885066613503294
7. Virani SS, Alonso A, Benjamin EJ, Bittencourt MS, Callaway CW, Carson AP, et al. Heart Disease and Stroke Statistics-2020 Update: a report from the american heart association. *Circulation.* (2020) 141:e139–596. doi: 10.1161/CIR.0000000000000757
8. Harjola VP, Parissis J, Bauersachs J, Brunner-La Rocca HP, Bueno H, Celutkiene J, et al. Acute coronary syndromes and acute heart failure: a diagnostic dilemma and high-risk combination. A statement from the Acute Heart Failure Committee of the Heart Failure Association of the European Society of Cardiology. *Eur J Heart Fail.* (2020) 22:1298–314. doi: 10.1002/ejhf.1831
9. Tsutsui H, Isobe M, Ito H, Ito H, Okumura K, Ono M, et al. JCS 2017/JHFS 2017 Guideline on Diagnosis and Treatment of Acute and Chronic Heart Failure- Digest Version. *Circ J.* (2019) 83:2084–184. doi: 10.1253/circj.CJ-19-0342
10. Ponikowski P, Voors AA, Anker SD, Bueno H, Cleland JG, Coats AJ, et al. 2016 ESC Guidelines for the diagnosis and treatment of acute and chronic heart failure: The Task Force for the diagnosis and treatment of acute and chronic heart failure of the European Society of Cardiology (ESC). Developed with the special contribution of the Heart Failure Association (HFA) of the ESC. *Eur J Heart Fail.* (2016) 18:891–975. doi: 10.1002/ejhf.592
11. Collet JP, Thiele H, Barbato E, Barthelemy O, Bauersachs J, Bhatt DL, et al. 2020 ESC Guidelines for the management of acute coronary syndromes in patients presenting without persistent ST-segment elevation. *Eur Heart J.* (2021) 42:1289–367. doi: 10.1093/eurheartj/ehaa575
12. Ibanez B, James S, Agewall S, Antunes MJ, Bucciarelli-Ducci C, Bueno H, et al. 2017 ESC Guidelines for the management of acute myocardial infarction in patients presenting with ST-segment elevation. *Rev Esp Cardiol (Engl Ed).* (2017) 70:1082. doi: 10.1016/j.rec.2017.11.010
13. Guedeney P, Collet JP, Diagnosis and Management of Acute Coronary Syndrome: What is New and Why? Insight From the 2020 European Society of Cardiology Guidelines. *J Clin Med.* (2020) 9:3474. doi: 10.3390/jcm9113474
14. van Beek DE, van Zaane B, Buijsrogge MP, van Klei WA. Implementation of the third universal definition of myocardial infarction after coronary artery bypass grafting: a survey study in Western Europe. *J Am Heart Assoc.* (2015) 4:e001401. doi: 10.1161/JAHA.114.001401
15. Gavard JA, Chaitman BR, Sakai S, Stocke K, Danchin N, Erhardt L, et al. Prognostic significance of elevated creatine kinase MB after coronary bypass surgery and after an acute coronary syndrome: results from the GUARDIAN trial. *J Thorac Cardiovasc Surg.* (2003) 126:807–13. doi: 10.1016/S0022-5223(03)00735-9

16. Libby P, Pasterkamp G, Crea F, Jang IK. Reassessing the mechanisms of acute coronary syndromes. *Circ Res.* (2019) 124:150–60. doi: 10.1161/CIRCRESAHA.118.311098
17. Silvestre JS. CCL21 in Acute Coronary Syndromes: Biomarker of the 21st Century? *J Am Coll Cardiol.* (2019) 74:783–5. doi: 10.1016/j.jacc.2019.06.029
18. Li M, Chen G, Feng Y, He X. Stress Induced Hyperglycemia in the Context of Acute Coronary Syndrome: Definitions, Interventions, and Underlying Mechanisms. *Front Cardiovasc Med.* (2021) 8:676892. doi: 10.3389/fcvm.2021.676892
19. Bellis A, Mauro C, Barbato E, Ceriello A, Cittadini A, Morisco C. Stress-Induced Hyperglycaemia in Non-Diabetic Patients with Acute Coronary Syndrome: From Molecular Mechanisms to New Therapeutic Perspectives. *Int J Mol Sci.* (2021) 22:775. doi: 10.3390/ijms22020775
20. Kanbay M, Segal M, Afsar B, Kang DH, Rodriguez-Iturbe B, Johnson RJ. The role of uric acid in the pathogenesis of human cardiovascular disease. *Heart.* (2013) 99:759–66. doi: 10.1136/heartjnl-2012-302535
21. He C, Lin P, Liu W, Fang K. Prognostic value of hyperuricemia in patients with acute coronary syndrome: a meta-analysis. *Eur J Clin Invest.* (2019) 49:e13074. doi: 10.1111/eci.13074
22. Gouveia M, Xia K, Colon W, Vieira SI, Ribeiro F. Protein aggregation, cardiovascular diseases, and exercise training: Where do we stand? *Ageing Res Rev.* (2017) 40:1–10. doi: 10.1016/j.arr.2017.07.005
23. Lizano P, Rashed E, Stoll S, Zhou N, Wen H, Hays TT, et al. The valosin-containing protein is a novel mediator of mitochondrial respiration and cell survival in the heart in vivo. *Sci Rep.* (2017) 7:46324. doi: 10.1038/srep46324
24. Ide Y, Horie T, Saito N, Watanabe S, Otani C, Miyasaka Y, et al. Cardioprotective Effects of VCP Modulator KUS121 in Murine and Porcine Models of Myocardial Infarction. *JACC Basic Transl Sci.* (2019) 4:701–14. doi: 10.1016/j.jacbts.2019.06.001
25. Shu H, Peng Y, Hang W, Zhou N, Wang DW. Emerging role of VCP/p97 in cardiovascular diseases: novel insights and therapeutic opportunities. *Biochem Soc Trans.* (2021) 49:485–94. doi: 10.1042/BST20200981
26. Yu B, Xu C, Tang X, Liu Z, Lin X, Meng H, et al. Endoplasmic reticulum stress-related secretory proteins as biomarkers of early myocardial ischemia-induced sudden cardiac deaths. *Int J Legal Med.* (2021). 136:159–168. doi: 10.1007/s00414-021-02702-z
27. Brody MJ, Vanhoutte D, Bakshi CV, Liu R, Correll RN, Sargent MA, et al. Disruption of valosin-containing protein activity causes cardiomyopathy and reveals pleiotropic functions in cardiac homeostasis. *J Biol Chem.* (2019) 294:8918–29. doi: 10.1074/jbc.RA119.007585
28. World Medical Association. World Medical Association Declaration of Helsinki: Ethical Principles for Medical Research Involving Human SubjectsWorld Medical Association Declaration of HelsinkiSpecial Communication. *JAMA.* (2013) 310:2191–4. doi: 10.1001/jama.2013.281053
29. Knuuti J, Wijns W, Saraste A, Capodanno D, Barbato E, Funck-Brentano C, et al. 2019 ESC Guidelines for the diagnosis and management of chronic coronary syndromes: the Task Force for the diagnosis and management of chronic coronary syndromes of the European Society of Cardiology (ESC). *Eur Heart J.* (2020) 41:407–77. doi: 10.1093/eurheartj/ehz425
30. Patel N, Lally PA, Kipfmueller F, Massolo AC, Luco M, Van Meurs KP, et al. Ventricular dysfunction is a critical determinant of mortality in congenital diaphragmatic hernia. *Am J Respir Crit Care Med.* (2019) 200:1522–30. doi: 10.1164/rccm.201904-0731OC
31. Ward LD, Kellis M. HaploReg: a resource for exploring chromatin states, conservation, and regulatory motif alterations within sets of genetically linked variants. *Nucleic Acids Res.* (2012) 40:D930–934. doi: 10.1093/nar/gkr917
32. McVean GA, Altshuler DM, Durbin RM, Abecasis GR, Bentley DR, Chakravarti A, et al. An integrated map of genetic variation from 1,092 human genomes. *Nature.* (2012) 491:56–65. doi: 10.1038/nature11632
33. Lappalainen T, Sammeth M, Friedländer MR. t Hoen PAC, Monlong J, Rivas MA, et al. Transcriptome and genome sequencing uncovers functional variation in humans. *Nature.* (2013) 501:506–11. doi: 10.1038/nature12531
34. Prabhu SD, Frangogiannis NG. The biological basis for cardiac repair after myocardial infarction: from inflammation to fibrosis. *Circ Res.* (2016) 119:91–112. doi: 10.1161/CIRCRESAHA.116.303577
35. Lawler PR, Bhatt DL, Godoy LC, Luscher TF, Bonow RO, Verma S, et al. Targeting cardiovascular inflammation: next steps in clinical translation. *Eur Heart J.* (2021) 42:113–31. doi: 10.1093/eurheartj/ehaa099
36. Swiatkiewicz I, Magielski P, Kubica J, Zadourian A, DeMaria AN, Taub PR. Enhanced Inflammation is a Marker for Risk of Post-Infarct Ventricular Dysfunction and Heart Failure. *Int J Mol Sci.* (2020) 21:807. doi: 10.3390/ijms21030807
37. Anzai T. Post-infarction inflammation and left ventricular remodeling: a double-edged sword. *Circ J.* (2013) 77:580–7. doi: 10.1253/circj.CJ-13-0013
38. Seropian IM, Sonnino C, Van Tassell BW, Biasucci LM, Abbate A. Inflammatory markers in ST-elevation acute myocardial infarction. *Eur Heart J Acute Cardiovasc Care.* (2016) 5:382–95. doi: 10.1177/2048872615568965
39. Wu TT, Zheng YY, Xiu WJ, Wang WR, Xun YL, Ma YY, et al. White Blood Cell Counts to High-Density Lipoprotein Cholesterol Ratio, as a Novel Predictor of Long-Term Adverse Outcomes in Patients After Percutaneous Coronary Intervention: a retrospective cohort study. *Front Cardiovasc Med.* (2021) 8:616896. doi: 10.3389/fcvm.2021.616896
40. Zhou N, Chen X, Xi J, Ma B, Leimena C, Stoll S, et al. Genomic characterization reveals novel mechanisms underlying the valosin-containing protein-mediated cardiac protection against heart failure. *Redox Biol.* (2020) 36:101662. doi: 10.1016/j.redox.2020.101662
41. Stoll S, Xi J, Ma B, Leimena C, Behringer EJ, Qin G, et al. The valosin-containing protein protects the heart against pathological Ca2+ overload by modulating Ca2+ uptake proteins. *Toxicol Sci.* (2019) 171:473–84. doi: 10.1093/toxsci/kfz164
42. Woltersdorf WW, Bayly GR, Day AP. Practical implications of in vitro stability of cardiac markers. *Ann Clin Biochem.* (2001) 38:61–3. doi: 10.1258/0004563011900146
43. Pouralijan Amiri M, Khoshkam M, Salek RM, Madadi R, Faghanzadeh Ganji G, Ramazani A. Metabolomics in early detection and prognosis of acute coronary syndrome. *Clin Chim Acta.* (2019) 495:43–53. doi: 10.1016/j.cca.2019.03.1632
44. Caidahl K, Hartford M, Ravn-Fischer A, Lorentzen E, Yndestad A, Karlsson T, et al. Homeostatic chemokines and prognosis in patients with acute coronary syndromes. *J Am Coll Cardiol.* (2019) 74:774–82. doi: 10.1016/j.jacc.2019.06.030
45. Takasaki A, Kurita T, Hirabayashi Y, Matsuo H, Tanoue A, Masuda J, et al. Prognosis of acute myocardial infarction in patients on hemodialysis stratified by Killip classification in the modern interventional era (focus on the prognosis of Killip class 1). *Heart Vessels.* (2021) 37:208–218.doi: 10.1007/s00380-021-01919-7
46. Brown AM, Sease KL, Robey JL, Shofer FS, Hollander JE. The impact of B-type natriuretic peptide in addition to troponin I, creatine kinase-MB, and myoglobin on the risk stratification of emergency department chest pain patients with potential acute coronary syndrome. *Ann Emerg Med.* (2007) 49:153–63. doi: 10.1016/j.annemergmed.2006.08.024
47. Shrivastava A, Haase T, Zeller T, Schulte C. Biomarkers for Heart Failure Prognosis: Proteins, Genetic Scores and Non-coding RNAs. *Front Cardiovasc Med.* (2020) 7:601364. doi: 10.3389/fcvm.2020.601364

Conflict of Interest: LL, CX, BY, ZL, and XT are inventors on a patent application 202110561991.0 submitted by Fudan University that covers A novel application of serum LMAN2, CAPN-1, and VCP in diagnosing early myocardial ischemia-induced sudden cardiac death.

The remaining authors declare that the research was conducted in the absence of any commercial or financial relationships that could be construed as a potential conflict of interest.

Publisher's Note: All claims expressed in this article are solely those of the authors and do not necessarily represent those of their affiliated organizations, or those of the publisher, the editors and the reviewers. Any product that may be evaluated in this article, or claim that may be made by its manufacturer, is not guaranteed or endorsed by the publisher.

frontiers in Cardiovascular Medicine

BRIEF RESEARCH REPORT
published: 22 March 2022
doi: 10.3389/fcvm.2022.802183

Diagnostic and Therapeutic Management of the Thoracic Outlet Syndrome. Review of the Literature and Report of an Italian Experience

Giuseppe Camporese[1], Enrico Bernardi[2], Andrea Venturin[3], Alice Pellizzaro[3], Alessandra Schiavon[3], Francesca Caneva[3], Alessandro Strullato[3], Daniele Toninato[3], Beatrice Forcato[3], Andrea Zuin[4], Francesco Squizzato[5,6], Michele Piazza[5,6], Roberto Stramare[7], Chiara Tonello[1], Pierpaolo Di Micco[8], Stefano Masiero[3], Federico Rea[4], Franco Grego[5,6] and Paolo Simioni[9]*

[1] Angiology Unit, Department of Cardiac, Thoracic and Vascular Sciences and Public Health, Padua University Hospital, Padua, Italy, [2] Department of Emergency and Accident Medicine, Hospital of Treviso, Treviso, Italy, [3] Physical Medicine and Rehabilitation Unit, Department of Neurosciences, Padua University Hospital, Padua, Italy, [4] Thoracic Surgery, Department of Cardiac, Thoracic and Vascular Sciences and Public Health, Padua University Hospital, Padua, Italy, [5] Vascular Surgery, Department of Cardiac, Thoracic and Vascular Sciences and Public Health, Padua University Hospital, Padua, Italy, [6] Department of Medicine DIMED, Institute of Radiology, Padua University Hospital, Padua, Italy, [7] Unit of Advanced Clinical and Translational Imaging, Department of Medicine, University Hospital of Padua, Padua, Italy, [8] Department of Internal Medicine and Emergency Room, Naples Buon Consiglio Fatebenefratelli Hospital, Naples, Italy, [9] Department of Internal Medicine, General Medicine Unit, Thrombotic and Haemorrhagic Disorders Unit, University Hospital of Padua, Padua, Italy

OPEN ACCESS

Edited by:
Avi Leader,
Rabin Medical Center, Israel

Reviewed by:
Torsten Willenberg,
Consultant, Bern, Switzerland
Orly Avnery,
Meir Medical Center, Israel

***Correspondence:**
Giuseppe Camporese
giuseppe.camporese@aopd.veneto.it

Specialty section:
This article was submitted to General Cardiovascular Medicine, a section of the journal Frontiers in Cardiovascular Medicine

Received: *26 October 2021*
Accepted: *28 February 2022*
Published: *22 March 2022*

Citation:
Camporese G, Bernardi E, Venturin A, Pellizzaro A, Schiavon A, Caneva F, Strullato A, Toninato D, Forcato B, Zuin A, Squizzato F, Piazza M, Stramare R, Tonello C, Di Micco P, Masiero S, Rea F, Grego F and Simioni P (2022) Diagnostic and Therapeutic Management of the Thoracic Outlet Syndrome. Review of the Literature and Report of an Italian Experience. Front. Cardiovasc. Med. 9:802183. doi: 10.3389/fcvm.2022.802183

The Thoracic Outlet Syndrome is a clinical potentially disabling condition characterized by a group of upper extremity signs and symptoms due to the compression of the neurovascular bundle passing through the thoracic outlet region. Because of the non-specific nature of signs and symptoms, to the lack of a consensus for the objective diagnosis, and to the wide range of etiologies, the actual figure is still a matter of debate among experts. We aimed to summarize the current evidence about the pathophysiology, the diagnosis and the treatment of the thoracic outlet syndrome, and to report a retrospective analysis on 324 patients followed for 5 years at the Padua University Hospital and at the Naples Fatebenefratelli Hospital in Italy, to verify the effectiveness of a specific rehabilitation program for the syndrome and to evaluate if physical therapy could relieve symptoms in these patients.

Keywords: diagnosis, treatment, thoracic outlet syndrome, surgery, rehabilitation

INTRODUCTION

The Thoracic Outlet Syndrome (TOS) is a clinical potentially disabling condition characterized by a group of upper extremity signs and symptoms due to the compression of the neurovascular bundle passing through the thoracic outlet region, an anatomical site enclosed among the anterior middle scalene muscles, the clavicle, and the first rib.

According to the pathophysiology, TOS can be classified in: neurogenic (nTOS), arterial (aTOS), and venous (vTOS). Each one of these may recognize either a congenital (cervical ribs or anomalous first rib), or traumatic (whiplash injuries, falls), or functionally acquired (active and vigorous repetitive sport- and/or work-related activities) cause (1–4).

The incidence of TOS ranges from 3 to 80/1,000 people; nonetheless, due to the non-specific nature of signs and symptoms, to the lack of a consensus for the objective diagnosis, and to the wide range of etiologies, the actual figure is still a matter of debate (1–4).

In 2016, the Society for Vascular Surgery issued a consensus document attempting to standardize the terminology, definitions, diagnostic criteria, reporting standards and therapeutic options for each type of TOS (1).

This article summarizes the current evidence about the epidemiology and the pathophysiology of TOS, and its diagnostic and therapeutic approach at the Padua University Hospital and at the Naples Fatebenefratelli Hospital in Italy together with a report of our personal experience in this setting.

Epidemiology

nTOS accounts for 90–95% of cases, vTOS for 3–5%, and aTOS for the remaining 1–2%. Signs and symptoms most often occur between 20 and 50 years and are usually unilateral, especially involving the dominant arm. While nTOS is more prevalent in women, aTOS equally affects both genders, and vTOS is more frequent in men. Both aTOS and nTOS share common etiologies causing artery and/or nerve compression, such as trauma (whiplash injury), or anatomic abnormalities (cervical ribs, anterior and/or middle scalene hypertrophy, tumors, or fibrous bands). vTOS is more common in athletes (e.g., volley, baseball, swimming, body-building, etc.), manual workers or subjects performing vigorous activity (2–6).

Anatomy

The superior thoracic outlet is the anatomical area crossed by the brachial plexus, and by the subclavian artery and vein. It lies between the anterior and middle scalene muscles, superiorly to the first rib, posteriorly to the clavicle, laterally to the sternal manubrium.

The brachial plexus is formed by the anterior branches of cervical roots C5 to C8, the anterior branch of the first thoracic nerve (T1) and the anastomotic branches of C4 and T2. It supplies nerve fibers to the thorax and upper limb.

The thoracic outlet includes three distinct anatomical spaces where a compression of the neurovascular structures may occur (**Figure 1**):

- *Triangle of the scalenes*: most frequently involved in the compression of the brachial plexus and of the subclavian artery. It is formed anteriorly by the anterior scalene muscle, and posteriorly by the middle scalene muscle; the base of the triangle is made up by the first rib.
- C*osto-clavicular space*: most frequently involved in the compression of the subclavian vein. It is outlined anteriorly by the middle third of the clavicle, and postero-medially by the first rib and by the aponeurosis of the subclavian muscle.
- S*ubpectoral space*: the entire brachial plexus may be compressed at this level (5, 7). It is bordered anteriorly by the tendon of the pectoralis minor muscle and the coracoid process, and posteriorly by the thoracic wall.

Pathophysiology

A list of the most common congenital or acquired causes of TOS is reported in **Table 1** (8–12).

Congenital Factors

The prevalence of a cervical rib accounts for 1–2% in the general population, women being most frequently affected. About 20% of nTOS cases are attributable to this anomaly, that also constitutes a risk factor for the development of aTOS (9, 10).

Acquired Factors

Acquired causes of TOS include: consolidation defects of the first rib and of the clavicle, and muscular hypertrophy due to physical or professional repetitive activities involving lifting weights. Also, postural disorders and scapular girdle dysfunction may lead to narrowing of the costoclavicular angle, resulting in compression of the neck vascular bundle (13). Acute symptoms may develop following traumatic events, such as whiplash or a fall on an outstretched arm (14). Other causes are Pancoast tumor, hereditary multiple exostosis, and osteochondromas.

CLINICAL DIAGNOSIS

Clinical Features and Physical Examination

It is essential to collect an accurate medical history describing symptoms, their onset and duration, the presence of aggravating/alleviating factors, and the associated degree of disability. Pain in the neck, occipital region, chest, shoulders and upper limbs is frequently reported. Other symptoms are: paraesthesia, hypoesthesia or anesthesia, weakness, heaviness, dyschromia and dystermia (5, 15, 16). A complete list of TOS-related signs and symptoms is reported in **Supplementary Table 1S** (see **Supplementary Material**).

Provocative Maneuvers

These maneuvers (see **Supplementary Table 2S**) may evoke TOS typical symptoms (10). Simultaneous positivity of several maneuvers may increase specificity; for instance, in a study by Gillard et al. the specificity of the Adson and Roos tests ranged from 30 to 72% when used alone, increasing to 82% when both were performed (5, 17–20).

IMAGING

Plethysmography

Finger plethysmography may detect a subclavian artery compression displaying both a delayed upslope of the sphygmic wave, and a loss of the dicrotic notch during provocative maneuvers. These findings, however, are also common in the normal population, mandating further diagnostic testing (1, 4, 21).

Ultrasound Assessment

In our Institutions, patients with suspected vascular TOS undergo dynamic bilateral Color-Coded Doppler Ultrasonography (CCDU). CCDU allows for non-invasive real-time visualization, as well as for pulsed Doppler waveform analysis and blood-flow velocity evaluation, of the subclavian

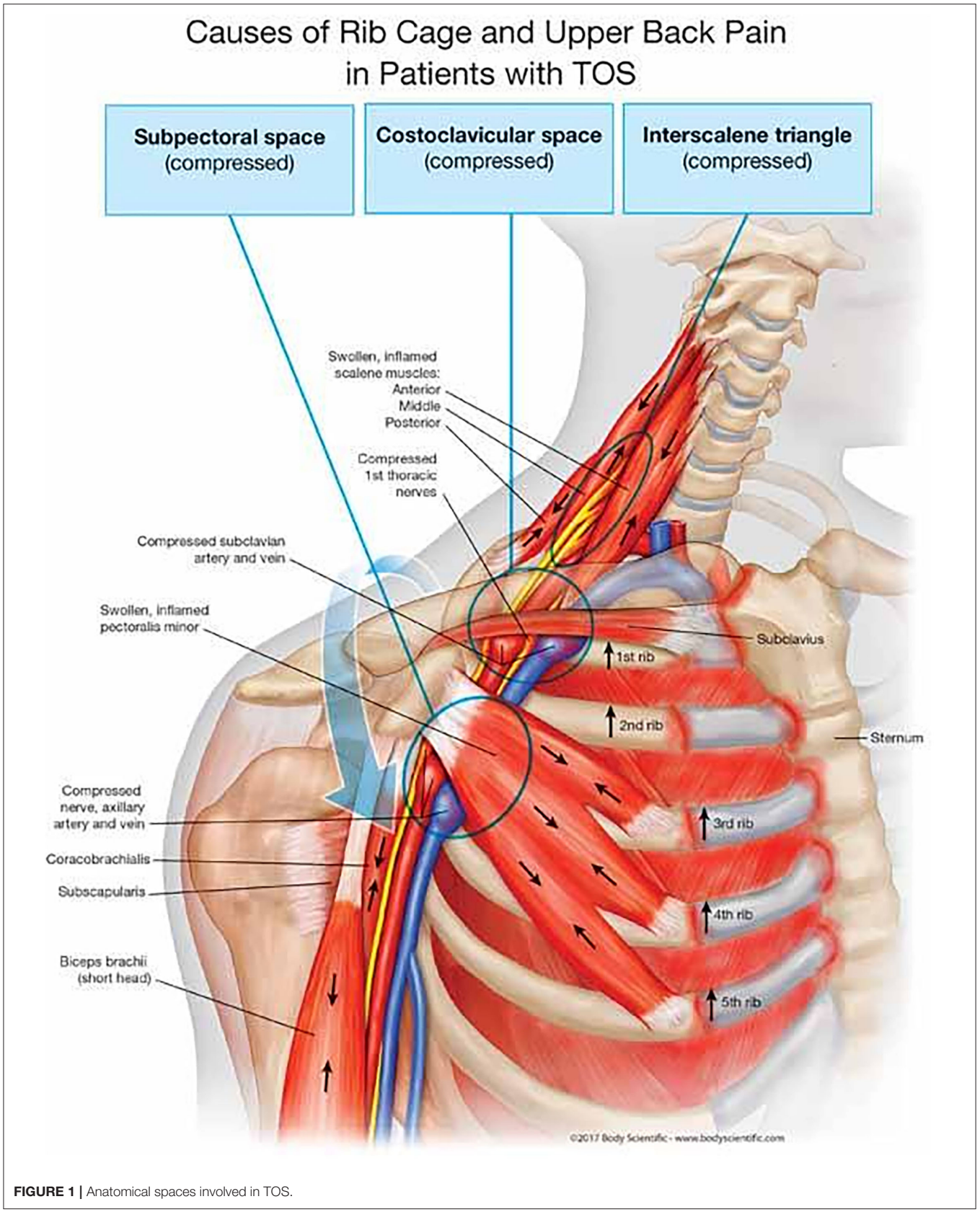

FIGURE 1 | Anatomical spaces involved in TOS.

TABLE 1 | Common causes of TOS.

Congenital factors	Acquired abnormalities
Cervical rib	Postural factors
1st rib anomaly	Fall injuries to upper limb
C7 transverse process abnormalities	Clavicular Fracture
Fibrous bundles between transverse process of C7 and the 1st rib	1st rib fracture
Supernumerary rib	Whiplash injury
Anomalies of scalene muscle insertion	Repetitive stress injuries
Supernumerary scalene muscle	Hypertrophy of the scalene muscles
Exostosis of the first rib	Decrease trapezius, scapulae elevator, rhomboides muscles tone
Cervicodorsal scoliosis	Shortening of the scalene, trapezius, elevator scapulae, pectoralis muscles

and axillary vessels, both at rest and during provocative maneuvers (1, 21–23). Currently, a consensus on the preferred technique to evaluate suspected TOS by ultrasonography is lacking. In our Institutions, all sonographic examinations are performed with last generation ultrasound equipment, using a 3–13 MHz multifrequency linear-array probe for higher accuracy, according to a standardized technique (see Section 1, **Supplementary Material**).

Chest and/or Cervical X-Ray

Plain chest and/or cervical X-ray films should be obtained in all patients with suspected TOS, being a sensitive and low-cost modality to identify major bone abnormalities potentially causing TOS (**Table 1**). In doubtful cases, contrast-enhanced computed tomography angiography (CTA) or magnetic resonance angiography (MRA) may be performed, as they provide a more detailed survey of the anatomy, especially useful to diagnose TOS subtypes (21, 24–26).

CTA

Detailed methodology is reported in Section 2 of the **Supplementary Material**.

CTA is especially useful in symptomatic patients without skeletal anomalies at conventional radiography (27). Several studies have focused on the efficacy of 3-D reconstructions, which can define the anatomical details, highlight anatomical relationships between vascular and bone structures, and allow surgery planning.

CTA can detect deep-vein thrombosis and venous collateral circuits, both consequences of venous compression. CTA is the preferred choice for the evaluation of patients with suspected anomalous ribs or fractures, and it is also useful in postoperative patients with suspected remnant 1st rib (**Supplementary Figure 1S**).

Among CTA limitations are: ionizing radiation exposure, scarce visualization of brachial plexus, mandatory supine position, and poor arm/shoulder hyperabduction due to the gantry size (28, 29).

MRA

Detailed methodology is reported in Section 3 of the **Supplementary Material**.

MRA with provocative maneuvers is the cross-sectional imaging test of choice in patients with suspected TOS, allowing for careful study of all the anatomical components of the thoracic outlet (30). Even without contrast media, MRA can show arterial and neural plexus compression, venous thrombosis and venous collateral circuits, muscle hyperthrophy and hypotrophy, accessories muscles, and anomalous fibrous bands (**Supplementary Figure 2S**). T1-weighted sagittal sequences are useful for assessing vascular and neural compression and for revealing post-stenotic dilation; instead, coronal sequences supply good views of the brachial plexus, and may highlight fibrous bands. All sequences should be acquired during bilateral arm abduction with the head and neck in the neutral position, and repeated during arm adduction with additional contrast administration (31–34).

MRA has some advantages over CTA, such as multi-planar analysis, optimal small parts visualization, and lack of ionizing radiation, the latter being of particular interest in the generally young patient population affected by TOS. However, when MRA cannot be performed due to claustrophobia or implanted devices, CTA remains the study of choice.

Both MRA and CTA are difficult to perform in patients with severe or dialysis-dependent renal failure.

Venography and Arteriography

Both venography and arteriography have been historically considered the diagnostic "gold standard", but due to single-plane resolution and invasiveness, they have been widely replaced by CTA and MRA, and currently have a very limited use (e.g., severe arterial insufficiency or ischemia, aneurysms, extended thrombosis or vein fibrosis; see **Supplementary Figure 3S**) (2, 21).

ELECTRODIAGNOSTICS

True nTOS is a plexopathy caused by a fibrous band from a rudimentary cervical rib to the first thoracic rib, trapping the lower trunk of the brachial plexus and developing a sensory and motor deficit in the C8-T1 distribution territory. nTOS is often confused clinically with ulnar neuropathy at the elbow, or with C8-T1 radiculopathy (35). In nTOS, T1 fibers tend to be preferentially affected, leading to a distinctive pattern. In most cases, the ulnar sensory nerve action potential (SNAP) amplitude is low but not absent, the medial antebrachial cutaneous SNAP amplitude is also usually low or absent, and the median SNAP is normal. Additionally, the axonal loss is characterized by a low compound muscle action potential (CMAP) amplitude in both the median and ulnar motor nerves, typically with a more profound decrease in the median response affecting the median-innervated thenar muscles (5, 36). Needle electromyography

abnormalities are found in median- more than in ulnar-innervated C8–T1 muscles, and less so in radial innervated C8 muscles; in particular, the thenar muscles are more severely involved than the hypothenar ones. Such abnormalities may include fibrillation potentials, positive sharp waves, and long duration motor unit potentials (MUPs). The abductor pollicis brevis is preferentially innervated by the T1 root, and is most commonly affected in nTOS (37).

TREATMENT

Initial management of TOS is usually conservative (dedicated physical therapy, addressing muscle imbalance, postural abnormalities and neural mobilities). Patients are taught that overhead activity, heavy lifting, repetitive motions or use of vibratory tools will aggravate their symptoms, and play against good long-term physical or surgical results.

Although a consensus on the appropriate conservative regimen for nTOS remains controversial, a multimodal approach including patient education, TOS-specific rehabilitation and drug therapies has shown positive results in 60–70% of cases.

If symptoms persist after at least 3–6 months of rehabilitation and patients are experiencing some degree of disability at work, sleep, recreation, or daily living activities, a surgical approach should be considered, and treatment choice is usually related to surgeon experience, kind of involved anatomical district, extent of surgical procedure, and exposure needs (38, 39). Other indications for surgery include arterial and/or venous compression with or without parietal damages, thrombosis or aneurysms.

Medical Therapy

Pharmacological interventions often provide symptom relief, and mainly include analgesics (non-steroidal anti-inflammatory drugs and/or opioids) for neuropathic pain, as well as muscle relaxants, anticonvulsants and/or antidepressants as adjuvants.

Parenteral Treatment

Symptomatic patients with scalene muscles contracture who fail to respond to conservative approach may benefit from botulinum toxin injection (BTX-A), though its efficacy is still controversial. Some studies suggest that BTX-A injections are associated with significant pain and symptoms reduction in up to 70% of patients, for up to 3 months. Injection of steroids and local anesthetics (bupivacaine, lidocaine, triamcinolone and ropivacaine) has also shown good clinical efficacy (40, 41).

Conservative Rehabilitative Treatment

The main purpose of rehabilitative treatment is to restore the width of anatomical spaces, whose compression is at the basis of the pathology; moreover, rehabilitation treatment can support the diagnosis of TOS, if symptom improvement is observed. Physical therapy is associated with significant symptom improvement in 50 to 90% of patients (42).

There is lack of consensus on the duration and the timing of the rehabilitation process, even within the TOS subtypes, according to the degree of disability and other individual factors. Revaluation and adaption of therapy must be ongoing, and dictated by symptoms status. A 6-month physical therapy program consisting of home-exercises, stretching, postural corrections, and muscle recruitment patterns, primarily focusing on the neck and shoulder, can alleviate symptoms associated with TOS. Generally, patients with mild TOS are expected to improve within 6 weeks (43, 44). In refractory cases undergoing decompressive surgery, post-surgical rehabilitation plays a key role in the recovery of autonomy and upper limb range of motion, and in the improvement of the patients' quality of life (45–47).

Key points of rehabilitative treatment are: postural education (e.g., avoid carrying heavy weights and prolonged hyperabduction of the upper limbs); cervico-dorsal and scapular girdle massage (to resolve contractures); diathermy or laser therapy (for antalgic purposes); kinesiotherapy (to restore the balance between muscles opening and closing thoracic egress).

The rehabilitation course should be scheduled as follows: postural exercises; static reinforcement of the muscles that open the strait; stretching of the muscles that close the strait; kinesiotherapy of the cervical spine; breathing exercises to lessen the overload of scalene muscles and to lower the first rib.

The rehabilitation program must be guided by a physiotherapist specialized in TOS treatment (see Section 4 in **Supplementary Material** for details) (43, 44). A summary of exercises targeting the shoulder muscles are shown in **Supplementary Figure 4S** and **Supplementary Table 3S**.

SURGICAL TREATMENT

Thoracic Surgery

With proper and accurate patient selection and compliance, the surgical management of TOS may have excellent outcomes. The various syndromes are similar and the specific compression mechanism is often difficult to identify; however, the first rib seems to be a common denominator along which most compressive factors operate (**Supplementary Figure 5S**) (41, 48, 49).

Many authors think that resection of the first rib, with cervical rib when present, is best performed through the trans-axillary approach (see Section 5, **Supplementary Material**) for complete removal with subclavian vascular decompression, while the supraclavicular approach (see Section 6, **Supplementary Material**) is often preferred in nTOS, but may be appropriate in any combinations of these clinical syndromes (50, 51).

In properly selected patients, clinical results of first rib resection may be considered good (complete relief of symptoms) in 85% of patients, fair (improvement with some residual or recurrent mild symptoms) in 10% and poor (no change from preoperative status) in 5% (50, 52, 53).

Recently, removal of the first rib on total videothoracoscopic or robotic approach was described, but the outcomes are yet to be completely determined (51, 54).

Considering the peculiar anatomical district, there are many possible complications and, although rarely, they may also be very serious (55, 56).

Among these are:

- *Brachial plexus injury*, due to excessive traction to the roots of the plexus during mobilization of first rib; to reduce this risk, it is useful to raise the shoulder and to bend the head toward the operative side.
- *Phrenic nerve injury*, may occur with just minor traction or during a lifting with a forceps, so every contact should be avoided or limited, even with a vessel loop. Another kind of damage is the contact with the cautery, uni- or bipolar.
- *Long thoracic nerve injury*, may occur by cutting one of branches of the nerve, usually running near the lateral side of middle scalene muscle, causing a winged scapula.
- *Thoracic duct injury*, the thoracic duct may lie in the middle of the scalene fat pad in the lower left portion of the neck; injury at this level causes milky (or clear) fluid leaking in the operative field. If a leak is evident, damage is managed by ties, clips or bipolar cautery.
- *Vascular injury*, an injury to the subclavian artery or vein may occur, that can be more easily controlled through the supraclavicular approach.

Based on this consideration, a thoughtful, well-articulated, informed consent is mandatory.

Vascular Surgery

The three main concepts of vascular surgical treatment are: relieving the arterial compression (the trigger of the disease), repairing the damaged subclavian artery (local complication), and restoring the distal circulation (distal complication) (57).

The indications for vascular surgery are: failure of conservative therapy with persisting disabling symptoms that interfere with daily life activities; or with vascular (arterial) complications: stenosis, thrombosis, distal embolization or aneurysm.

Transaxillary first rib resection (as originally described by Roos) (2) is the gold standard for the treatment of aTOS (see Section 5, **Supplementary Material**) (58). The rationale of first rib resection is that it guarantees a decompression of the neurovascular bundle in all cases of costoclavicular space narrowing (59). Roos rib resection seems to be more effective in preventing symptoms recurrence compared to scalenectomy, because also in those cases of anterior scalene hypertrophy/anatomic variation, TOS is still determined by the reduction of the costoclavicular space, that is corrected by the resection of the first rib (**Supplementary Figure 5S**) (59). Transaxillary rib resection carries the disadvantage of a limited subclavian artery exposure, therefore other access (typically supra-clavicular) are needed if an arterial intervention is needed.

Surgical Treatment of the Damaged Artery

Subclavian artery impingement may occasionally result in local arterial complications, such as stenosis or chronic occlusion, post-stenotic dilatation or aneurysm formation (60).

Subclavian/axillary artery stenosis or occlusion may be the consequence of the chronic mechanical stress at the level of the costo-clavicular space. This may rarely result in chronic upper limb ischemia with claudication, rest pain or ischemic tissue loss. The gold standard for treatment in these cases is represented by surgical by-pass. The by-pass sources of inflow and outflow depend on the specific anatomical situation, that is preoperatively planned according to the CTA/MRA or arteriography.

In case of subclavian artery aneurysm, the rational for the surgical treatment is to eliminate the source of chronic embolization. Surgery consists in arterial resection and substitution with a vascular graft, performed via a supraclavicular approach. The preferred conduit in this case is represented by heparinized polytetrafluorethylene (PTFE), anastomosed in an end-to-end fashion (60, 61).

There have been scattered reports of endovascular repair of the subclavian artery combined with surgical decompression of the thoracic outlet and more data are needed to assess the role of endovascular solutions in aTOS (57).

Restoration of the Distal Circulation

Acute Limb Ischemia

The clinical presentation is characterized by pulselessness, acute pain, pallor, paresthesia, paralysis or paresis, and hypothermia of the hand. This clinical situation warrants an emergent treatment to preserve the hand function and viability. Acute limb ischemia in aTOS may be related to subclavian artery thrombosis, embolization from the subclavian artery (due to presence of an aneurysm or arterial wall thrombosis), or both. The treatment is typically based on Fogarty thrombo-embolectomy and/or catheter-directed thrombolysis (61).

Fogarty thrombo-embolectomy is performed through an oblique incision at the level of the cubital fossa. The bicipital aponevrosis is divided exposing the distal brachial artery and its bifurcation into the radial and ulnar arteries. A transverse arteriotomy is performed and the Fogarty catheter is advanced through the proximal and distal arterial axis.

Fogarty thrombo-embolectomy is effective in restoring the patency of acutely occluded arteries; however this may not be always sufficient in aTOS, where microembolization may be responsible for distal circulation impairment. Distal bypasses are sometimes necessary in patients with chronically occluded arteries of the upper limb due to chronic embolization from aTOS. Intra-arterial thrombolysis is based on loco-regional infusion of thrombolytic agents (typically urokinase) through a multi-hole catheter placed at the level of the arterial thrombosis. It has the advantage to be effective also on smaller distal vessels that are not affected by surgery, but it may take 12–72 h to achieve an optimal result, therefore its use alone is not recommended in acute limb ischemia with threatened limb. In our experience, we use thrombolysis after Fogarty thrombo-embolectomy, in those cases where surgery alone is not sufficient to restore an adequate blood flow, because of distal arterial branches (i.e., interdigital) occlusion. In any case, revascularization does not eliminate the cause of arterial compression, thus physical therapy or/and surgical first rib resection are still indicated after the acute event.

Chronic Limb Ischemia

Chronic distal embolization from the damaged subclavian artery may determine chronic occlusion of the arteries of the arm or

forearm. In case of disabling claudication, rest pain, or tissue loss, a peripheral revascularization is indicated. This typically consists in a surgical bypass; also in this case the precise inflow and outflow sources depend on the specific case. If available, a saphenous vein graft is preferred in this anatomical region (60–62).

PERSONAL EXPERIENCE

Study Cohort and Methods

In 2019 we started a retrospective survey to verify the effectiveness of a specific rehabilitation program for TOS, and to evaluate if physical therapy could relieve symptoms of TOS. We assessed 324 patients referred to our Institutions between 2004 and 2019, 270 females (83%) and 54 males (17%), aged between 12 and 59, with an average age of 38 years (SD 12). Data were collected from patients attending the outpatient clinic of the Clinic of Physical and Rehabilitative Medicine, Thoracic Surgery, Angiology and Occupational Medicine. Patients were classified on the basis of job categories, and of TOS subtype: aTOS 4%; vTOS 7%; vascular TOS (venous and arterial) 13%; nTOS 29%; miscellaneous TOS 47%. The following comorbidities were recorded in our cohort: C7 abnormalities (15%); shoulder disorders (i.e.: rotator-cuff tendinopathies, impingement syndrome, or other) (14%); history of whiplash (13%); previous episodes of deep venous thrombosis of the upper limbs (24%). All patients underwent diagnostic imaging procedures, such as cervical spine radiograms, basal and contrast-enhanced cervical CTA/MRA, CCDU, and electromyography.

All 324 patients were offered a specific rehabilitation protocol in appropriately trained centers, 285 (88%) of them accepted, and 39 (12%) refused any type of treatment. Patients rejecting treatment were much alike patients who underwent rehabilitation (**Table 2**), but declined because they either could not afford enough time to follow the complex rehabilitation program, or had geographic inaccessibility to the rehabilitation centers who were chosen for the study.

Treated and untreated patients were evaluated by the Numeric Pain Rating Scale (NRS) to assess pain burden, either at baseline (T0), after 6 months (T1), and at the last available follow-up visit (T2). Three groups of patients were identified: worsened symptoms (NRS value at T-2 greater than at T-0); stationary symptoms (no difference between T-2 and T-0 NRS values); improved symptoms (NRS value at T-2 lower than at T-0). All data were compared by Chi-square test, Fisher-Freeman-Halton exact test or Student' *t*-test, where appropriate. The effect of treatment on the temporal trend of NRS-score was evaluated by repeated measures analysis of variance (ANOVA) using NRS-scores at T0, T1, and T2 as within-subjects factor, and treatment as between-subjects factor.

TABLE 2 | Demographics of the investigated population.

		Treatment		
		No (39)	**Yes (285)**	***p***
Age	(years, mean + SD)	39.6 ± 11.7	37.9 ± 11.7	0.405
Sex	F	32 (82.1)	238 (83.5)	0.820
	M	7 (17.9)	47 (16.5)	
TOS variant	aTOS	1 (2.6)	12 (4.2)	0.254
	vTOS	1 (2.6)	22 (7.7)	
	vaTOS	4 (10.3)	38 (13.3)	
	nTOS	17 (43.6)	77 (27.0)	
	mTOS	16 (41.0)	136 (47.7)	
Job	High risk workers[a]	9 (23.1)	101 (35.4)	0.151
	Low risk workers[b]	30 (76.9)	184 (64.6)	
Comorbidities	C7 abnormalities	6 (15.3)	42 (14.7)	0.991
	Shoulder disorders	6 (15.3)	39 (13.7)	
	Whiplash	5 (12.8)	36 (12.6)	
	Previous dvt upper limbs	9 (23.1)	68 (23.9)	
Conservative treatment	Massages		20 (7.0)	
	Massages + specific TOS m&ph rehab protocol		74 (26.0)	
	CTEN stimulation		17 (6.0)	
	CTEN stimulation + specific TOS m&ph rehab protocol		60 (21.1)	
	hydrogalvanotherapy		15 (5.3)	
	Hydrogalvanotherapy + specific TOS m&ph rehab protocol		53 (18.6)	
	Specific TOS m&ph rehab protocol		46 (16.1)	
Surgical Treatment	Cervical rib resection		4 (1.4)	
	Cervical rib resection + neurolysis		3 (1.1)	
	Cervical rib resection + scalenectomy		2 (0.7)	
	First rib resection		11 (3.9)	
	First rib resection + neurolysis		2 (0.7)	
	First rib resection + scalenectomy		1 (0.4)	
	Neurolysis		1 (0.4)	
	Other surgery		3 (1.1)	
	Scalenectomy		2 (0.7)	

[a] *Video-terminalists, clerks, teachers.*
[b] *Other jobs.*

RESULTS

The patients' characteristics are summarized in **Table 2**. Overall, a statistically significant higher number of patients undergoing a specific rehabilitation protocol reported either improved or stationary symptoms as compared to untreated patients, at the last available follow-up visit (T2) (**Figure 2**). Namely, of 285 patients in the TOS specific rehabilitative program, 192 (67%) had improved symptoms; 72 (25%) were stationary; and 21 (7%) had worsened symptoms at T-2 (**Table 3**; $p < 0.01$). A detailed description of NRS scores at the three time-points in the two patient groups is reported in **Supplementary Table 4S**.

Worsened symptoms occurred more frequently in workers of the services industry (computer users, teachers, clerks), as compared to other workers at lower risk of TOS ($p = 0.046$); and in patients with shoulder disorders as compared to those

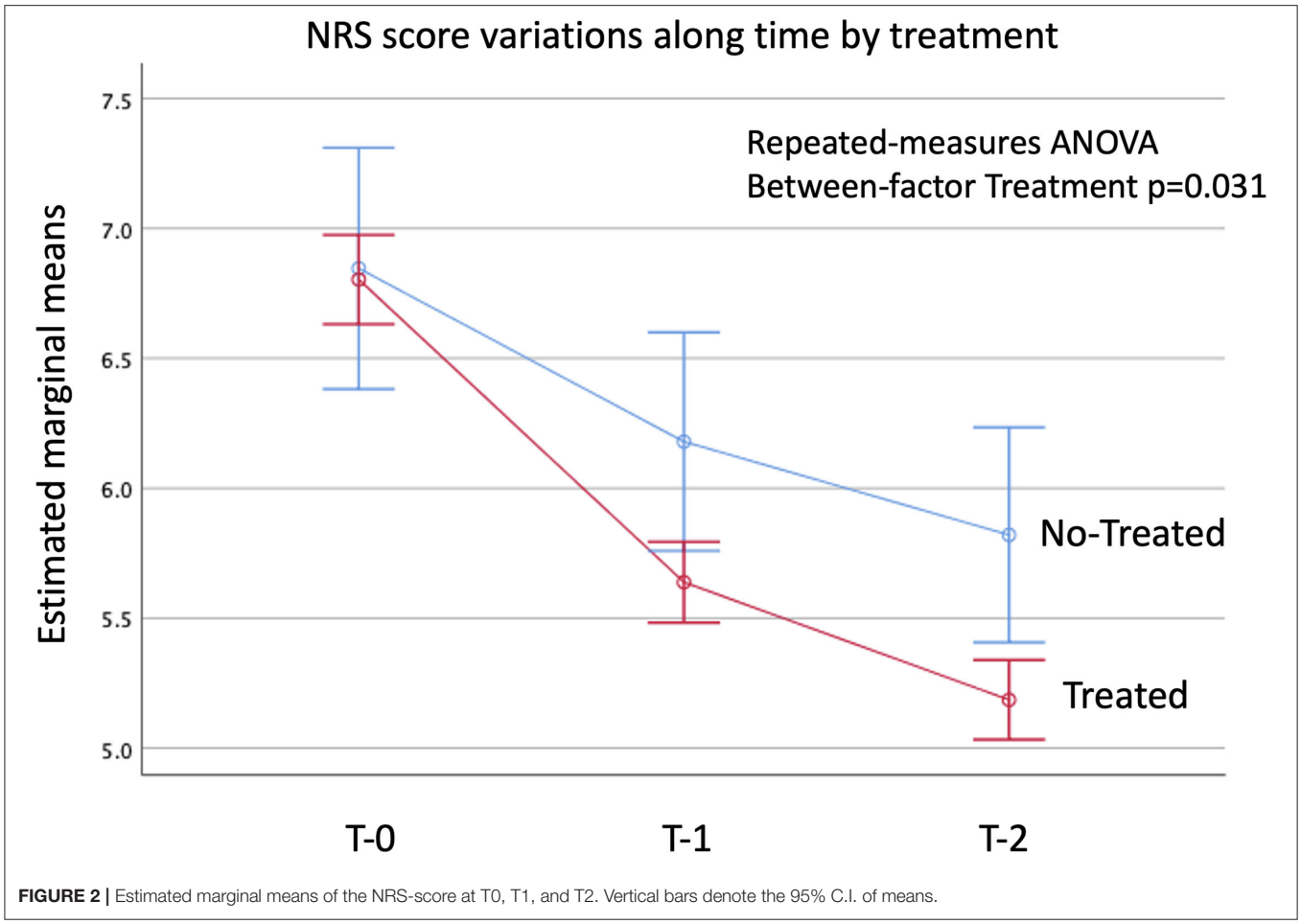

FIGURE 2 | Estimated marginal means of the NRS-score at T0, T1, and T2. Vertical bars denote the 95% C.I. of means.

TABLE 3 | Symptoms variation in patients undergoing a specific rehabilitation protocol vs. those refusing treatment at the last available follow-up visit.

	Control group (39)	TOS specific rehabilitation protocol (285)	*p* value*
Improved, *n* (%)	21 (53.8%)	192 (67.4%)	<0.01
Stationary, *n* (%)	0	72 (25.3%)	
Worsened, *n* (%)	18 (46.2%)	21 (7.4%)	

**Fisher-Freeman-Halton exact test.*

without ($p = 0.04$) (see **Supplementary Table S5**). On the contrary, a history of C7 abnormalities or of whiplash did not impact on symptoms. Of the 285 patients participating in the rehabilitation protocol, 19% underwent hydro-galvanotherapy, massages, or cervical transcutaneous electrical nerve stimulation only; while 81% had one or more of the aforementioned interventions plus a specific TOS manual and physical rehabilitation training.

Only 29 (10%) out of 285 patients, all 21 patients with worsened symptoms plus 8 patients with stationary symptoms underwent surgical treatment (single or combined surgical procedures). Of them, 50% underwent first rib resection, 30% cervical rib resection, 20% scalenectomy, 20% neurolysis; and 10% other surgery.

Interestingly, no significant differences in terms of NRS scores were found at T-2 between patients who underwent surgery vs. patients who did not (**Supplementary Table S6**).

COMMENT

Our results emphasize the importance of rehabilitative treatment as a first-line therapeutic approach in the management of patients with TOS. Indeed, according to the NRS scores provided by our patients, a structured rehabilitation program is associated with a statistically significant better outcome ($p = 0.03$) than no rehabilitation.

We observed a higher incidence of TOS among patients working in activities involving intensive computer use, such as video-terminal workers, office workers, teachers (34% of patients); and in activities involving the mobilization of disabled patients, such as social-health workers and/or nurses, subjected to repeated efforts of the upper limbs in an abducted position (12% of patients). Our findings confirm the important role that work activity plays in the development of TOS, in line with what reported in the literature (57, 63). Despite the higher incidence

of TOS found in the female sex, we didn't observe sex-related differences in terms of efficacy of rehabilitative treatment, as well as in terms of symptoms improvement.

A situation potentially influencing the outcome of rehabilitative treatment in TOS patients is the presence of concomitant diseases. The rehabilitation program did not result in a better outcome in patients with previous cervical trauma or whiplash, or with supernumerary cervical ribs or C7 anomalies ($p = 0.4$ and $p = 0.8$, respectively). However, significant differences in the rehabilitation outcome were found in patients presenting with musculo-tendon pathologies of the shoulder and TOS vs. patients with TOS but without shoulder pathologies ($p = 0.04$). This difference is likely due to the fact that the rehabilitative pathway performed by the patients is focused only on treating TOS-symptoms.

CONCLUSIONS

The objective diagnosis of TOS is a continuous challenge due to the wide variety of non-specific symptoms and of differential diagnosis. Despite several progresses in the diagnostic process in the last 20 years, significant technical issues and controversies still persist. In this sense, clinical suspicion should be confirmed by objective (instrumental) diagnosis, in order to achieve prompt recognition of the syndrome and a swift start of the treatment for rapid and successful results.

We believe that a structured and standardized rehabilitative process should represent the initial treatment for TOS, leaving surgery only for patients who failed to improve after a conservative management program or with refractory or recurrent symptoms.

Albeit encouraging and in line with the literature, our results require confirmation coming from properly designed studies on a larger patient cohort.

DATA AVAILABILITY STATEMENT

The raw data supporting the conclusions of this article will be made available by the authors, without undue reservation.

ETHICS STATEMENT

Ethical review and approval was not required for the study on human participants in accordance with the local legislation and institutional requirements. Written informed consent for participation was not required for this study in accordance with the national legislation and the institutional requirements.

AUTHOR CONTRIBUTIONS

GC and AV gave substantial contributions to the conception or design of the work. GC, AV, AP, ASc, ASt, FC, PD, AZ, RS, FS, and MP provided the acquisition and analysis or interpretation of data for the work. GC, EB, SM, FR, FG, and PS drafting the work or revising it critically for important intellectual content. GC, AV, AP, ASc, ASt, FC, AZ, FS, MP, RS, EB, PD, SM, FR, FG, and PS provided approval for publication of the content. GC, AV, AP, ASc, ASt, FC, AZ, FS, MP, RS, EB, PD, SM, FR, FG, and PS agree to be accountable for all aspects of the work in ensuring that questions related to the accuracy or integrity of any part of the work are appropriately investigated and resolved. All authors contributed to the article and approved the submitted version.

SUPPLEMENTARY MATERIAL

The Supplementary Material for this article can be found online at: https://www.frontiersin.org/articles/10.3389/fcvm.2022.802183/full#supplementary-material

REFERENCES

1. Illig KA, Donahue D, Duncan A, Freischlag J, Gelabert H, Johansen K, et al. Reporting standards of the society for vascular surgery for thoracic outlet syndrome. *J Vasc Surg*. (2016) 64:e23–35. doi: 10.1016/j.jvs.2016.04.039
2. Sanders RJ, Hammond SL, Rao NM. Diagnosis of thoracic outlet syndrome. *J Vasc Surg*. (2007) 46:601–4. doi: 10.1016/j.jvs.2007.04.050
3. Hwang JH, Ku S, Jeong JH. Traditional medicine treatment for thoracic outlet syndrome: a protocol for systematic review of randomized controlled trials. *Medicine*. (2020) 99:e21074. doi: 10.1097/MD.0000000000021074
4. Povlsen S, Povlsen B. Diagnosing thoracic outlet syndrome: current approaches and future directions. *Diagnostics*. (2018) 8:21. doi: 10.3390/diagnostics8010021
5. Jones MR, Prabhakar A, Viswanath O, Urits I, Green JB, Kendrick JB, et al. Thoracic outlet syndrome: a comprehensive review of pathophysiology, diagnosis, and treatment. *Pain Ther*. (2019) 8:5–18. doi: 10.1007/s40122-019-0124-2
6. Li N, Dierks G, Vervaeke HE, Jumonville A, Kaye AD, Myrcik D, et al. Thoracic outlet syndrome: a narrative review. *J Clin Med*. (2021) 10:962. doi: 10.3390/jcm10050962
7. Sanders RJ, Annest SJ, editors. Anatomy of the thoracic outlet and related structures. In: *Thoracic Outlet Syndrome*. Cham: Springer (2021). p. 37–44.
8. Brantigan CO, Roos DB. Etiology of neurogenic thoracic outlet syndrome. *Hand Clin*. (2004) 20:27–36. doi: 10.1016/S0749-0712(03)00080-5
9. Chernoff N, Rogers JM. Supernumerary ribs in developmental toxicity bioassays and in human populations: incidence and biological significance. *J Toxicol Environ Health B Crit Rev*, (2004) 7:437–49. doi: 10.1080/10937400490512447
10. Laulan J, Fouquet B, Rodaix C, Jauffret P, Roquelaure Y, Descatha A. Thoracic outlet syndrome: definition, aetiological factors, diagnosis, management and occupational impact. *J Occup Rehabil*. (2011) 3:366–73. doi: 10.1007/s10926-010-9278-9
11. Merks JH, Smets AM, van Rijn RR, Kobes J, Caron HN, Maas M, et al. Prevalence of rib anomalies in normal Caucasian children and childhood cancer patients. *Eur J Med Genet*. (2005) 48:113–29. doi: 10.1016/j.ejmg.2005.01.029
12. Brewin J, Hill M, Ellis H. The prevalence of cervical ribs in a London population. *Clin Anat*. (2009) 22:331–6. doi: 10.1002/ca.20774
13. Sanders RJ, Rao NM. The forgotten pectoralis minor syndrome: 100 operations for pectoralis minor syndrome alone or accompanied by neurogenic thoracic outlet syndrome. *Ann Vasc Surg*. (2010) 24:701–8. doi: 10.1016/j.avsg.2010.02.022
14. Sanders RJ, Haug CE. *Thoracic Outlet Syndrome: A Common Sequela of Neck Injuries*. Philadelphia: Lippincott. (1991) p. 237.
15. Fugate MW, Rotellini-Coltvet L, Freischlag JA. Current management of thoracic outlet syndrome. *Curr Treat Options Cardiovasc Med*. (2009) 2:176–83. doi: 10.1007/s11936-009-0018-4

16. AW Nichols. Diagnosis and management of thoracic outlet syndrome. *Curr Sports Med Rep*. (2009) 8:240–9. doi: 10.1249/JSR.0b013e3181b8556d
17. Gillard J, Pérez-Cousin M, Hachulla E, Remy J, Hurtevent JF, Vinckier L, et al. Diagnosing thoracic outlet syndrome: contribution of provocative tests, ultrasonography, electrophysiology, and helical computed tomography in 48 patients. *Joint Bone Spine*. (2001) 68:416–24. doi: 10.1016/S1297-319X(01)00298-6
18. Plewa MC, Delinger M. The false-positive rate of thoracic outlet syndrome shoulder maneuvers in healthy subjects. *Acad Emerg Med*. (1998) 4:337–42. doi: 10.1111/j.1553-2712.1998.tb02716.x
19. Kuhn JE, Lebus VGF, Bible JE. Thoracic outlet syndrome. *J Am Acad Orthop Surg*. (2015) 4:222–32. doi: 10.5435/JAAOS-D-13-00215
20. Ozoa G, Alves D, Fish DE. Thoracic outlet syndrome. *Phys Med Rehabil Clin N Am*. (2011) 22:473–83. doi: 10.1016/j.pmr.2011.02.010
21. Nguyen LL, Soo Hoo AJ. Evaluation and management of arterial thoracic outlet syndrome. *Thoracic Surg Clin*. (2021) 31:45–54. doi: 10.1016/j.thorsurg.2020.09.006
22. Cook JR, Thompson RW. Evaluation and management of venous thoracic outlet syndrome. *Thoracic Surg Clin*. (2021) 31:27–44. doi: 10.1016/j.thorsurg.2020.08.012
23. Longley DG, Yedlicka JW, Molina EJ, Schwabacher S, Hunter DW, Letourneau JG. Thoracic outlet syndrome: evaluation of the subclavian vessels by color Doppler ultrasonography. *AJR*. (1992) 158:623–30. doi: 10.2214/ajr.158.3.1739007
24. Weber AE, Criado E. Relevance of bone anomalies in patients with thoracic outlet syndrome. *Ann Vasc Surg*. (2014) 28:924–32. doi: 10.1016/j.avsg.2013.08.014
25. Moriarty JM, Bandyk DF, Broderick DF, Cornelius RS, Dill KE, Francois CJ, et al. ACR appropriateness criteria imaging in the diagnosis of thoracic outlet syndrome. *J Am Coll Radiol*. (2015) 12:438–44. doi: 10.1016/j.jacr.2015.01.016
26. Chang KZ, Likes K, Davis K, Demos J, Freischlag JA. The significance of cervical ribs in thoracic outlet syndrome. *J Vasc Surg*. (2013) 57:771–5. doi: 10.1016/j.jvs.2012.08.110
27. Bilbey JH, Müller NL, Connell DG, Luoma AA, Nelems B. Thoracic outlet syndrome: evaluation with CT. *Radiology*. (1989) 171:381–4. doi: 10.1148/radiology.171.2.2704801
28. Khalilzadeh O, McKinley G, Torriani M, Gupta R. Imaging assessment of thoracic outlet syndrome. *Thorac Surg Clin*. (2021) 31:19–25. doi: 10.1016/j.thorsurg.2020.09.002
29. Gillet R, Teixeira P, Meyer JB, Rauch A, Raymond A, Dap F, et al. Dynamic CT angiography for the diagnosis of patients with thoracic outlet syndrome: correlation with patient symptoms. *J Cardiovasc Comput Tomogr*. (2018) 12:158–65. doi: 10.1016/j.jcct.2017.11.008
30. Blair BN, Rapaport S, Dirk Sostman H, Blaie DC. Normal brachial plexus: MR imaging. *Radiology*. (1987) 165:763–67. doi: 10.1148/radiology.165.3.3685357
31. Demondion X, Bacqueville E, Paul C, Duquesnoy B, Huchulla E, Cotton A. Thoracic outlet: assessment with MR imaging in asymptomatic and symptomatic populations. *Radiology*. (2003) 227:461–8. doi: 10.1148/radiol.2272012111
32. Matsumura JS, Rilling WS, Pearce WH, Nemcek AA, Vogelzang RL, Yao JST. Helical computed tomography of the normal thoracic outlet. *J Vasc Surg*. (1997) 26:776–83. doi: 10.1016/S0741-5214(97)70090-9
33. Demondion X, Bountry N, Drizenko A, Paul C, Francke JP, Cotton A. Thoracic outlet. Anatomic correlation with MR imaging. *AJR*. (2000) 175:417–22. doi: 10.2214/ajr.175.2.1750417
34. Demirbag D, Unlu U, Ozdemir F, Genchellac H, Temnzoz O, Ozdemur H, et al. The relationship between magnetic resonance imaging and postural maneuver and physical examination tests in patients with thoracic outlet syndrome: results of a double-blind, controlled study. *Arch Phys Med Rehabil*. (2007) 88:844–51. doi: 10.1016/j.apmr.2007.03.015
35. Shapiro D, Preston B, editors. *Electromyography and Neuromuscular Disorders*. 4th ed. London: Elsevier (2020).
36. Sanders RJ, Annest SJ. Pectoralis minor syndrome: subclavicular brachial plexus compression. *Diagnostics*. (2017) 7:1–12. doi: 10.3390/diagnostics7030046
37. Rubin DI. Brachial and lumbosacral plexopathies: a review. *Clin Neurophysiol Pract*. (2020) 5:173–93. doi: 10.1016/j.cnp.2020.07.005
38. Sanders RJ, Hammond SL, Rao NM. Thoracic outlet syndrome: a review. *Neurologist*. (2008) 14:365–73. doi: 10.1097/NRL.0b013e318176b98d
39. Crosby CA, Wehbé MA. Conservative treatment for thoracic outlet syndrome. *Hand Clin*. (2004) 20:43–9. doi: 10.1016/S0749-0712(03)00081-7
40. Foley JM, Finlayson H, Travlos A. A review of thoracic outlet syndrome and the possible role of botulinum toxin in the treatment of this syndrome. *Toxins*. (2012) 4:1223–35. doi: 10.3390/toxins4111223
41. Finlayson HC, O'Connor RJ, Brasher PMA, Travlos A. Botulinum toxin injection for management of thoracic outlet syndrome: a double-blind, randomized, controlled trial. *Pain*. (2011) 9:2023–28. doi: 10.1016/j.pain.2011.04.027
42. Vanti C, Natalini L, Romeo A, Tosarelli D, Pillastrini P. Conservative treatment of thoracic outlet syndrome. a review of the literature. *Eura Medicophys*. (2007) 43:55–70.
43. Watson LA, Pizzari T, Balster S. Thoracic outlet syndrome Part 2: conservative management of thoracic outlet. *Man Ther*. (2010) 15:305–14. doi: 10.1016/j.math.2010.03.002
44. Balakatounis KC, Angoules AG, Panagiotopoulou KA. Conservative treatment of thoracic outlet syndrome (TOS): creating an evidence-based strategy through critical research appraisal. *Current Orthopaedics*. (2007) 21:471–76. doi: 10.1016/j.cuor.2007.11.006
45. Levine NA, Rigby BR. Thoracic outlet syndrome: biomechanical and exercise considerations. *Healthcare*. (2018) 6:68. doi: 10.3390/healthcare6020068
46. Hanif S, Tassadaq N, Rathore MFA, Rashid P, Ahmed N, Niazi F. Role of therapeutic exercises in neurogenic thoracic outlet syndrome. *J Ayub Med Coll Abbottabad*. (2007) 19:85–88.
47. Novak CB, Collins ED, Mackinnon SE. Outcome following conservative management of thoracic outlet syndrome. *J Hand Surg Am*. (1995) 4:542–8. doi: 10.1016/S0363-5023(05)80264-3
48. Kuwayama DP, Lund JR, Brantigan CO, Glebova NO. Choosing surgery for neurogenic TOS: the role of physical exam, physical therapy and imaging. *Diagnostic*. (2017) 7:37–50. doi: 10.3390/diagnostics7020037
49. Ferrante MA, Ferrante ND. The thoracic outlet syndromes: part 2. The arterial, venous, neurovascular, and disputed thoracic outlet syndromes. *Muscle Nerve*. (2017) 56:663–73. doi: 10.1002/mus.25535
50. Stilo F, Montelione N, Benedetto F, Spinelli D, Vigliotti RC, Spinelli F. Thirty-year experience of transaxillary resection of first rib for thoracic outlet syndrome. *Int Angiol*. (2020) 39:82–8. doi: 10.23736/S0392-9590.19.04300-1
51. Ojanguren A, Krueger T, Gonzalez M. First rib resection by VATS for thoracic outlet syndrome. *Multimed Man Cardiothorac Surg*. (2020). doi: 10.1510/mmcts.2020.027
52. Karamustafaoglu YA, Yoruk Y, Tarladacalisir T, Kuzucuoglu M. Transaxillary approach for thoracic outlet syndrome: results of surgery. *Thorac Cardiovasc Surg*. (2011) 59:349–52. doi: 10.1055/s-0030-1250480
53. Akkuş M, Kose S, Sönmezoglu Y. Transaxillary first rib resection for treatment of the thoracic outlet syndrome. *J Vis Exp*. (2020). doi: 10.3791/59659
54. Martinez BD, Albeshri H, Chulkov M, Alharthi S, Nazzal MMS, Sferra J. Development and evolution of a robotic surgical technique for the treatment of thoracic outlet syndrome. *J Vasc Surg*. (2021) 74:938–45.e1. doi: 10.1016/j.jvs.2021.02.013
55. Sanders RJ, Hammond SL. Supraclavicular first rib resection and total scalenectomy: technique and results. *Hand Clin*. (2004) 20:61–70. doi: 10.1016/S0749-0712(03)00093-3
56. Thompson RW, Petrinec D, Toursarkissian B. Surgical treatment of thoracic outlet compression syndromes. II. Supraclavicular exploration and vascular reconstruction. *Ann Vasc Surg*. (1997) 11:442–51. doi: 10.1007/s100169900074
57. Povlsen B, Hansson T, Povlsen SD. Treatment for thoracic outlet syndrome. *Cochrane Database Syst Rev*. (2014) CD007218. doi: 10.1002/14651858.CD007218.pub3
58. Roos DB. Experience with first rib resection for thoracic outlet syndrome. *Ann Surg*. (1971) 173:429–42. doi: 10.1097/00000658-197103000-00015
59. Deriu GP, Battaglia L. La sindrome dell'egresso toracico. In: Luigi Pozzi, editor. *Atti del IX corso di Agg.to in chirurgia generale*. Roma, Dic (1982).

60. Davidovic LB, Kostic DM, Jakovljevic NS, Kuzmanovic IL, Simic TM. Vascular thoracic outlet syndrome. *World J Surg*. (2003) 27:545–50. doi: 10.1007/s00268-003-6808-z
61. Vemuri C, McLaughlin LN, Abuirqeba AA, Thompson RW. Clinical presentation and management of arterial thoracic outlet syndrome. *J Vasc Surg*. (2017) 65:1429–39. doi: 10.1016/j.jvs.2016.11.039
62. Hussain MA, Aljabri B, Al-Omran M. Vascular thoracic outlet syndrome. *Semin Thorac Cardiovasc Surg*. (2016) 28:151–7. doi: 10.1053/j.semtcvs.2015.10.008
63. Franklin GM. Work-related neurogenic thoracic outlet syndrome: diagnosis and treatment. *Phys Med Rehabil Clin N Am*. (2015) 26:551–61. doi: 10.1016/j.pmr.2015.04.004

Conflict of Interest: The authors declare that the research was conducted in the absence of any commercial or financial relationships that could be construed as a potential conflict of interest.

frontiers | Frontiers in Cardiovascular Medicine

ORIGINAL RESEARCH
published: 06 April 2022
doi: 10.3389/fcvm.2022.793535

Comparability of Heart Rate Turbulence Methodology: 15 Intervals Suffice to Calculate Turbulence Slope – A Methodological Analysis Using PhysioNet Data of 1074 Patients

Valeria Blesius[1]*, *Christopher Schölzel*[1], *Gernot Ernst*[2,3] and *Andreas Dominik*[1]

[1] Life Science Informatics Group, Department of Mathematics, Natural Sciences and Informatics, Technische Hochschule Mittelhessen (THM) University of Applied Sciences, Giessen, Germany, [2] Department of Anaesthesiology, Kongsberg Hospital, Vestre Viken Hospital Trust, Kongsberg, Norway, [3] Psychological Institute, University of Oslo, Oslo, Norway

Heart rate turbulence (HRT) is a characteristic heart rate pattern triggered by a ventricular premature contraction (VPC). It can be used to assess autonomic function and health risk for various conditions, e.g., coronary artery disease or cardiomyopathy. While comparability is essential for scientific analysis, especially for research focusing on clinical application, the methodology of HRT still varies widely in the literature. Particularly, the ECG measurement and parameter calculation of HRT differs, including the calculation of turbulence slope (TS). In this article, we focus on common variations in the number of intervals after the VPC that are used to calculate TS (#TSRR) posing two questions: 1) Does a change in #TSRR introduce noticeable changes in HRT parameter values and classification? and 2) Do larger values of turbulence timing (TT) enabled by a larger #TSRR still represent distinct HRT? We compiled a free-access data set of 1,080 annotated long-term ECGs provided by Physionet. HRT parameter values and risk classes were determined both with #TSRR 15 and 20. A standard local tachogram was created by averaging the tachograms of only the files with the best heart rate variability values. The shape of this standard VPC sequence was compared to all VPC sequences grouped by their TT value using dynamic time warping (DTW) in order to identify HRT shapes. When calculated with different #TSRR, our results show only a little difference between the number of files with enough valid VPC sequences to calculate HRT (<1%) and files with different risk classes (5 and 6% for HRT0-2 and HRTA-C, respectively). In the DTW analysis, the difference between averaged sequences with a specific TT and the standard sequence increased with increasing TT. Our analysis suggests that HRT occurs in the early intervals after the VPC and TS calculated from late intervals reflects common heart rate variability rather than a distinct response to the VPC. Even though the differences in classification are marginal, this can lead to problems in clinical application and scientific research. Therefore, we recommend uniformly using #TSRR 15 in HRT analysis.

Keywords: heart rate turbulence (HRT), noninvasive risk stratification, heart rate variability (HRV), heart failure, myocardial infarction, methodology, standardization

OPEN ACCESS

Edited by:
Maurizio Acampa,
Siena University Hospital, Italy

Reviewed by:
Akiomi Yoshihisa,
Fukushima Medical University, Japan
Axel Bauer,
Medical University of Innsbruck, Austria

***Correspondence:**
Valeria Blesius
hrt@blesius.eu

Specialty section:
This article was submitted to Original Research Article, a section of the journal Frontiers in Cardiovascular Medicine

Received: *12 October 2021*
Accepted: *07 February 2022*
Published: *06 April 2022*

Citation:
Blesius V, Schölzel C, Ernst G and Dominik A (2022) Comparability of Heart Rate Turbulence Methodology: 15 Intervals Suffice to Calculate Turbulence Slope – A Methodological Analysis Using PhysioNet Data of 1074 Patients. Front. Cardiovasc. Med. 9:793535. doi: 10.3389/fcvm.2022.793535

1. INTRODUCTION

1.1. Heart Rate Turbulence

With a simple point-of-care investigation of the heart rate, it is possible to estimate the condition and prognosis of patients. A possible method is HRT, which is a naturally occurring phenomenon that arises after a VPC (2): The characteristic pattern comprises an initial drop of interval length (IL) followed by slowly increasing and afterward decreasing length (refer to the **Supplementary Figure 1** for a visual representation). This heart rate fluctuation is provoked by the ineffectiveness of the premature beat, which leads to a drop of blood pressure and activates the baroreflex (3, 4).

Because of this dependency on the autonomic nervous system (ANS), HRT can be used as a marker for autonomic health (5). Studies have shown that HRT parameters can be useful risk indicators for all-cause mortality after myocardial infarction or chronic heart failure (5, 6). In combination with other risk indicators, HRT can be used in clinical diagnostics to make therapeutic decisions (7–9). Several methods for the inclusion of HRT in implantable cardioverter defibrillators have already been suggested (10–12). Similarly, GE Healthcare implemented HRT assessment in their Holter analysis software tools *MARS* and *CardioDay*, which both have already been used for HRT analysis (13–15).

For HRT, there are three main parameter values that can be calculated (check the **Supplementary Figure 1** for a graphical depiction): turbulence onset (TO) describes the first drop of the IL after the VPC compared to the intervals before the VPC. It is, therefore, a marker for the parasympathetic response. TS describes the steepest slope of the tachogram after the compensatory interval (compI). The third parameter TT is the index of the first interval that shows TS (4). Both TS and TT are markers for the sympathetic and parasympathetic activity.

Although the #TSRR was described in the standards as being 15 (16), many studies use 20 instead as suggested in the first description of HRT (17). The first article to give 15 as #TSRR is Barthel et al. (18) but without giving a reason for changing the original method. In reviews about HRT, there is a switch of suggesting #TSRR 20 at first (19–21) and then #TSRR 15 in recent years (2, 5, 22–25). However, many publications of late still use #TSRR 20 (26–30).

1.2. Rationale and Scope

Comparability is one of the key factors of scientific research, especially when developing techniques and workflows used in clinical medicine. Methodological variance diminishes comparable data and can lead to seemingly contradictory results, which make it difficult to assess the usefulness of a technique for a particular use case. For HRT, a standard methodology has been published in the "International Society for Holter and Noninvasive Electrocardiology (ISHNE)" Consensus (16). However, many studies still use different methods to assess HRT (31) causing the aforementioned difficulties.

Until now, no study has analyzed the difference in HRT parameter values when calculated from different #TSRRs. A higher #TSRR increases the risk of artifacts and other arrhythmias to lie in the required calculation range which leads to an exclusion of the VPCSs (VPC snippet, i.e., all RR intervals surrounding the VPC 78 used for HRT calculation). Conversely, with a lower #TSRR, these compromising intervals may lie outside of the needed calculation range for some VPC snippet, i.e. all RR intervals surrounding the VPC used for HRT calculations (VPCSs) which would make them shorter but valid sequences for HRT assessment. In consequence, a change in #TSRR can lead to a selection of different sets of VPCSs and, therefore, affect all HRT parameter values of a person.

Since HRT is triggered by a VPC *via* the baroreflex, it is plausible that the reaction should arise without any delay. This means that the slope that represents the turbulence should arise first in direct proximity to the compI and second always after a similar time period. Accordingly, TS calculated from either only late intervals or intervals with widely differing indices may only describe random fluctuation rather than a reaction of the ANS. Because TT describes the localization of TS, it can be used to test this assumption.

In this article, we analyze two hypotheses:

- Hypothesis 1: *There is a distinct difference in HRT parameters when calculating HRT with #TSRR 15 or 20.*
  We test this on a large free-access data set from Physionet and compare the resulting HRT parameters and classes.
- Hypothesis 2: *Persons with a high TT value or a high TT variability do not show HRT, but seemingly random fluctuations, i.e., heart rate variability (HRV).*

We, therefore, create an averaged ideal standard VPCS (stVPCS) with distinct HRT by filtering the Physionet data set *via* HRV parameters. This standard VPCS is then compared with sequences that have been averaged from VPCSs sorted for their respective TT value.

2. MATERIALS AND METHODS

2.1. Materials

2.1.1. Data

We used databases available on physionet.org (32). The databases had to include annotations of long-term electrocardiograms

Abbreviations: ANS, autonomic nervous system; compI, compensatory interval; couplI, coupling interval; CRAN, The Comprehensive R Archive Network; DTW, dynamic time warping; ECG, electrocardiogram; HRT, heart rate turbulence; HRV, heart rate variability; IL, interval length; IQR, interquartile range, i.e., the difference between the upper and lower quartiles; ISHNE, International Society for Holter and Noninvasive Electrocardiology; NR, not reliable; nRMSSD, RMSSD normalized for heart rate; nTS, TS normalized after (1); numTSRR[#TSRR], number of RR intervals in which TS is calculated; postRRs, RR intervals in a VPCS following the compI; preRRs, RR intervals in a VPCS before the couplI; refI, reference interval; RMSSD, square root of the mean of the squared successive differences between adjacent RR intervals; SD, standard deviation; SD1, SD of data points in poincare plot projected to the axis perpendicular to the line of identity; SD2, SD of data points in poincare plot projected to the line of identity; SDANN, standard deviation of the averages of all normal sinus rhythm intervals in any 5 min segments; SDNN, standard deviation of the averages of all normal sinus rhythm intervals; stVPCS, standard VPCS; TO, turbulence onset; TS, turbulence slope; TT, turbulence timing; TTSD, SD of TT; VPCS, VPC snippet, i.e., all RR intervals surrounding the VPC used for HRT calculation; VPC, ventricular premature contraction.

(ECGs) specifying the beat types. All databases that fit those criteria at the time of analysis (15.01.2021) are summed up in **Table 1**.

Since our analysis should be independent of the medical background of measurements, we did not exclude databases based on their scope. In sum, our analysis included 1,080 annotation files. If possible, we preferred annotations that were manually corrected, although most of the databases only included automatically generated annotations.

2.1.2. The RHRT Package

For the calculation of the HRT parameter values of each annotation file, we used our R package *RHRT* (v. 1.1) (38). *RHRT* provides functions to find VPCSs in time intervals and calculate HRT parameter values with customisable filtering criteria, order of calculation and normalization. The package can be found on The Comprehensive R Archive Network (CRAN) (https://CRAN.R-project.org/package=RHRT) and on github (https://github.com/VBlesius/RHRT). The default methodology of filtering, calculation, and classification is done as suggested in Blesius et al. (31), which mostly follows the ISHNE consensus (16). In contrast to the standards, we use 5 instead of 2 RR intervals in a VPCS before the couplI (preRRs), because the preceding intervals are used to calculate the reference interval (refI) and must, therefore, be included in the filtering process. Furthermore, we use TS normalized after (1) (nTS) which is TS normalized for heart rate and #TSRR. A detailed description can be found in the **Supplementary Data Sheet 1** and the documentation of the package.

TABLE 1 | Overview of the used databases.

ID	Full name	ECGs	Length	Corrected	Scope
chfdb	BIDMC Congestive Heart Failure Database (33)	15	20	no	severe congestive heart failure (NYHA class 3-4)
chf2db	Congestive Heart Failure RR Interval Database	29	23	yes	congestive heart failure (NYHA classes 1-3)
crisdb	CAST RR Interval Sub-Study Database (34)	762	23.9	no	myocardial infarction
excluded	Recordings excluded from the NSRDB	2	22.7	unknown	low-grade arrhythmias
ltafdb	Long Term AF Database (35)	84	23.8	yes	paroxysmal or sustained atrial fibrillation
ltdb	MIT-BIH Long-Term ECG Database	7	22.2	yes	unknown
ltstdb	Long Term ST Database (36)	86	23.4	yes	variety of events of segment changes
nsrdb	MIT-BIH Normal Sinus Rhythm Database	18	21.1	unknown	no significant arrhythmias
nsr2db	Normal Sinus Rhythm RR Interval Database	54	24	yes	normal sinus rhythm
sddb	Sudden Cardiac Death Holter Database (37)	23	23.5	(yes)	sustained ventricular tachyarrhythmia, mostly with actual cardiac arrest

The IDs correspond to the URLs under which the databases are accessible online. The number of ECGs mostly matches the number of recorded persons in each database, only for ltstdb four of the 80 persons were recorded multiple times. The columns Length and corrected give the median length of the records and whether the annotations were manually corrected, respectively. For sddb, only a part of the records had manually corrected annotations. Information that could not be found, i.e., whether annotations were corrected or the scope of the study, was marked as "unknown." The version of all databases is 1.0.0, and they can be found on https://physionet.org/about/database/ (32).

2.1.3. Other R Packages

Statistical differences between data sets were calculated with the *stats* package (v 4.1.1). *RHRV* version 4.2.6 was used to calculate HRV parameter values. For the Poincaré filter and the data preparation of the HRV calculation, we used the packages, *geometry* (v. 0.4.5), *smoother* (v. 1.1), and *purrr* (v. 0.3.4). To compare the stVPCS with the averaged VPCSs *dtw* (v. 1.22.3) was used. This package provides functions for DTW, which is an algorithm to compare similarities of two sequences: All points of the first sequence are matched to the points of the second one whereas points can be matched to multiple other points. The only limitation is that the first and last points have to be matched to each other, respectively, and mapped indices have to be increasing, meaning that there may not be overlapping matches. Dynamic time warping (DTW) can calculate a matching score, which was used in this analysis.

2.2. Methods

2.2.1. Comparing Data With #TSRR 15 and 20

We assessed HRT of all files twice with the default parameters of *RHRT* and the settings numPostRRs = 15 (TSRR15) and numPostRRs = 20 (TSRR20). Additionally, we created a data set from the valid VPCs included in the analysis with #TSRR 20, but calculated HRT results with numPostRRs = 15 (TSRR15∩). This leads to a data set with identical VPCs but shorter VPCSs that allows comparison without considering filtering effects. We then calculated the arithmetic mean and SD of HRT parameter values and classified the data into HRT0-2 and HRTA-C. Depending on the number of files with enough valid VPCSs, either a Welch's unequal variances *t*-test or a paired Student's *t*-test (both with *t.test* of the *stats* package) were used to detect differences between the sets of parameter values.

2.2.2. Creating a stVPCS

The purpose of the analysis was to compare VPCSs sorted on the basis of TT with an stVPCS. Since HRT is most pronounced in persons without autonomic dysfunction as reviewed in Bauer et al. (16), we needed to select files of supposedly healthy persons. However, the databases used do not include data from persons labeled as healthy. It may be assumed that NSRDB and NSR2DB are comprised of such data, but manual inspection of Poincaré plots revealed abnormal patterns throughout both databases. Therefore, we used HRV to filter the files of all databases that have the most sound values of these autonomic markers. The filtering process included three steps:

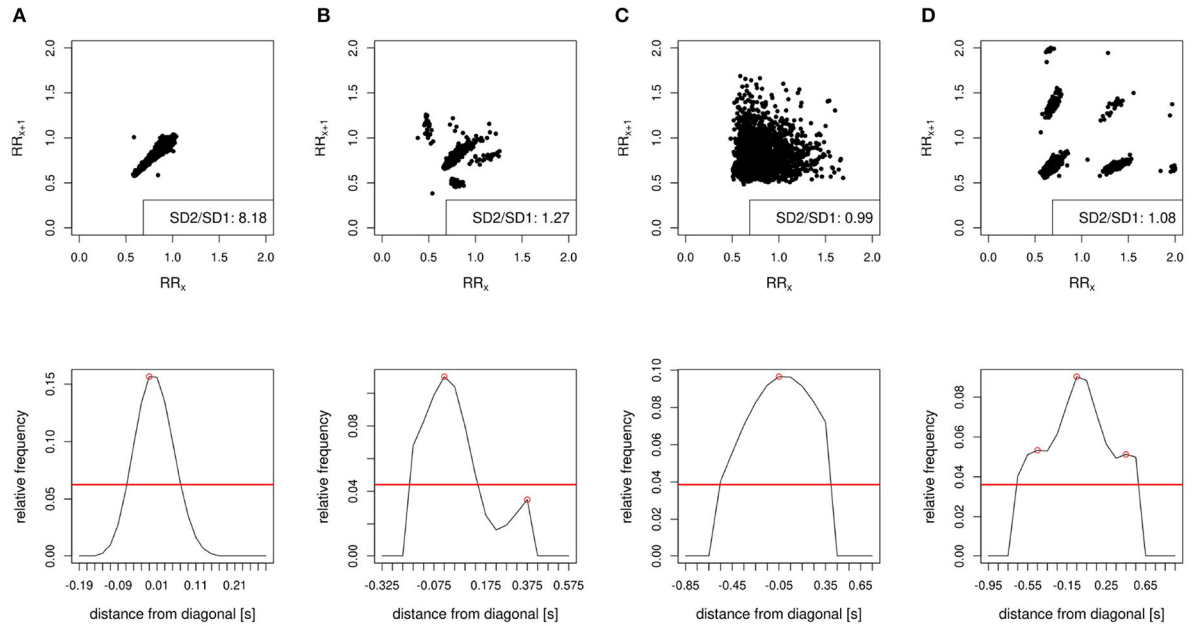

FIGURE 1 | Lorenz plot patterns and their corresponding smoothed histograms of SD1. The plots show 30-min chunks of different measurements that were used in the analysis as an example of different Lorenz plot patterns. The Poincaré plots in the top show a **(A)** comet, **(B)** side lobe pattern, **(C)** fan pattern, and **(D)** island pattern. The corresponding plots below show the histograms after smoothing. The lobe, fan, and island patterns have an SD2/SD1 ratio of less than 1.5 and would, therefore, be excluded. The histogram of the island patterns includes more than one local maximum, which is another criterion for exclusion. Data: **(A)** *nsr008* from *NSR2DB*, **(B)** *nsr018* from *NSR2DB*, **(C)** *01* from *LTAFDB*, and **(D)** *f018* from *CRISDB*.

2.2.2.1. Length of Files

At first, all files that were shorter than 20 h or longer than 28 h were discarded. Since HRT is correlated with the circadian rhythm of the ANS, it should be calculated from measurements with a length as close as possible to 24 h or its multiple if procurable.

Applying the following filters—especially the Poincaré filter—to full measurements can lead to the discarding of basically valid data due to temporary irregularities in heart rhythm. Furthermore, variability in the length of the measurements can lead to a bias in HRV parameter values (39). Therefore, we cut the measurements into snippets of 30 min and applied the following filters to these chunks. Only data files with at least 75% valid chunks were passed on by the Poincaré filter to the next step. In the HRV filter, the mean of all chunks was calculated for every parameter, respectively, before ranking the measurements.

2.2.2.2. Poincaré Filter

As a next step, we used a filter that quantifies the data distribution within a Poincaré plot: this non-linear method of HRV analysis plots data points of a time series against their respective successors to visualize the beat-to-beat variability of RR intervals. Any pathology that affects the length of RR-intervals causes distinct patterns in the Poincaré plots. These patterns have been systematically analyzed and categorized by Esperer et al. (40) and were called lorenz plot patterns. Plots from persons with sinus rhythm show so-called "comets" or "torpedos," which are shaped as long cones or ellipses, respectively (Refer to **Figure 1A**). Other lorenz plot patterns are:

- "island" patterns consisting of four or nine roundly shaped clusters that are connected to atrial tachycardia or atrial flutter, both with the atrioventricular block (**Figure 1D**).
- "fan" patterns which look like broader spread torpedos or triangles and occur in persons with atrial fibrillation or multifocal atrial tachycardia (**Figure 1C**).
- "lobe" patterns consisting of one central and several eccentric clusters which occur due to frequent VPCs or atrial premature contractions (**Figure 1B**).

For our analysis, we focused on filtering out Poincaré plots with island and fan patterns since they are specific for different kinds of atrial arrhythmia and atrioventricular block. This leaves torpedos, comets, and lobe patterns that show sinus rhythm or possible VPCs. Since high-frequent VPCs are an indicator for high risk (41–43), we focused on plots that show mostly comets and torpedos. The chunk-wise analysis of the plots left enough VPCs in the resulting data. In contrast to most other shapes, torpedos and comets consist of just one evenly shaped cluster. We use this fact for two conditions of our filter: First, we projected all data points onto the axis perpendicular to the line of identity and analyzed their distribution. After taking the logarithm and smoothing, histograms with more than one extremum exceeding 40% of the maximum were excluded to rule out strong side lobe and island patterns (refer to **Figure 1**). Second, we calculated the SD of the projected points which is the HRV parameter SD1. Analogously, we calculated SD2 from the diagonal. The ratio of SD1 with SD2 had to exceed 1.5 since a lower ratio proved to be indicative of broader spread patterns like islands or fans. This cut-off was deduced from Esperer et al. (40), who showed that

especially fans have a ratio of the length and the width of the central cluster of less than 1. We used SD1 and SD2 here since they are more commonly known and the exact methodology to create a cluster has not been described in the article.

2.2.2.3. HRV Filter

The last filtering step is based on the HRV time and frequency domain of the data. We calculated the following HRV parameters with the RHRV package: SD of the averages of all normal sinus rhythm intervals (SDNN), SD of the averages of all normal sinus rhythm intervals in any 5 min segments (SDANN), triangular index, i.e., the total number of all normal sinus rhythm intervals divided by the maximum of the interval frequency distribution, square root of the mean of the squared successive differences between adjacent RR intervals (RMSSD), very low frequency power, low frequency power, high frequency power, and the ratio of low and high frequency power. For every parameter, all files were ranked for their HRV values, respectively: Files with a value that exceeded three times the interquartile range, i.e. the difference between the upper and lower quartiles (IQR), were considered to be outliers. If their values were greater or less than the median±3·IQR they were given the penalty score "−1." For all HRV parameters, high values were assumed to be better, only for triangular index lower values were scored higher. Accordingly, the files were sorted by their HRV value and the best 20% received the score "1," while the remaining received "0." After this scoring process for every HRV parameter, the scores were summed up for every file, leading to possible scores from −8 (all parameter values are outliers) to 8 (all parameter values are in the top for their respective parameter). On the basis of the scores, the highest ranking 20% of the files were used to create the stVPCS.

Heart rate turbulence of all top ranking files was calculated with the *RHRT* package. All HRT calculations were done with the default settings of the *RHRT* package except for "numPostRRs" (#TSRR) for which we used 20 intervals because the longer range is the maximum of commonly used #TSRR and provided more intervals for later comparisons. For each file, the averaged VPCS was used as the basis to calculate an overall averaged VPCS (stVPCS).

2.2.3. Comparing VPCSs Based on TT

2.2.3.1. HRT Values

We calculated the HRT parameter values of every file in our databases with the default settings of the *RHRT* package except "numPostRRs" for which we used 30 intervals to ensure a wide range of possible TT values.

2.2.3.2. DTW With stVPCS

We extracted the RR intervals in a VPCS following the compI (postRRs) of every averaged VPCS, grouped them based on their respective TT, and calculated an averaged postRRs sequence for every TT. For the next step of matching the postRRs of the stVPCS to every averaged postRRs sequence *via* DTW, we tested two methods: First, we matched the standard sequence dynamically to the averaged sequences with the default step pattern "symmetric2" of the *dtw* function. Second, we removed the leading intervals of the standard sequence before the TT to receive a sequence that only consists of the intervals that shape the TS and all following intervals. The averaged sequences were cut accordingly and shortened to fit the standard sequence. The standard sequence was matched to all averaged sequences index by index with the *dtw* step pattern *rigid*.

TABLE 2 | HRT0-2 classes of files before and after changing #TSRR from 15 (columns) to 20 (rows) during HRT assessment.

TSRR20 \ TSRR15	*HRT0*	*HRT1*	*HRT2*	*NR*
HRT0	386	15	0	3
HRT1	9	118	0	3
HRT2	0	0	0	0
NR	7	6	0	315

Of the 682 files that could be calculated in both TSRR15 and TSRR20, 43 files are classified differently. NR, not reliable.

TABLE 3 | HRTA-C classes of files before and after changing #TSRR from 15 (columns) to 20 (rows) during HRT assessment.

TSRR20 \ TSRR15	*HRTA*	*HRTB*	*HRTC*	*NR*
HRTA	372	11	0	2
HRTB	6	118	0	3
HRTC	0	0	0	0
NR	18	15	0	317

Of the 682 files that could be calculated in both TSRR15 and TSRR20, 55 files are classified differently. Most of the files that could be classified with #TSRR 15 are marked NR with #TSRR 20. NR, not reliable.

2.2.3.3. Intra-Subject Variability of TT

As a measure of the variability of TT within a file, we calculated the SD of TT (TTSD) and the Pearson correlation coefficient for TT and TTSD.

3. RESULTS

3.1. Comparing Data With #TSRR 15 and 20

The number of files that included enough VPCs to calculate HRT was similar with #TSRR 15 (870 files) and #TSRR 20 (862). Similarly, the number of files sorted in different HRT classes were similar with #TSRR 15 and 20 for HRT0-2 (HRT0 402 vs. 404, HRT1 139 vs. 130, and NR 321 vs. 328) as well as HRTA-C (HRTA 396 vs. 385, HRTB 144 vs. 127, and NR 322 vs. 350). Of the 862 files from which HRT parameters could be calculated in both analyzes, 43 and 55 files were differently classified into HRT classes HRT0-2 and HRTA-C, respectively (refer to **Tables 2**, **3**).

When comparing the HRT parameters of TSRR15, TSRR20, and TSRR15∩ (data in TSRR20 recalculated with #TSRR 15), the most influenced parameter is TT with 5.47 ± 2.38 (TSRR15∩) and 5.75 ± 3 (TSRR20) (refer to **Table 4**). The TO values of TSRR15∩ and TSRR20 were identical, while the mean difference of the TS and TT values were 0.06 (CI 0.03 to 0.09, $p = 4.9 \cdot 10^{-4}$) and 0.4 (CI 0.28–0.53, $p = 2.9 \cdot 10^{-10}$), respectively. The most

differing values of the unpaired *t*-tests were the TT values of TSRR15 and TSRR20 with CI −0.5 to 0.03 and $p = 0.08$. The *p*-values of all other unpaired *t*-tests ranged from 0.71 to 0.99 with differences of the arithmetic means between 0.001 and 0.043. A noticeable difference is the high number of TT values that were NR with #TSRR 20 (79) compared to both #TSRR 15 analyzes (9 and 6, respectively).

3.2. Creating a stVPCS

Of the 1,080 annotation files included in the analysis, 70 files were shorter than 20 h and 1 file longer than 28 h. Thus, they were excluded.

TABLE 4 | Heart rate turbulence parameters calculated with different #TSRR.

	TO		TS		TT	
	Mean ± SD	**NR**	**Mean ± SD**	**NR**	**Mean ± SD**	**NR**
TSRR20	−2.19 ±1.51	327	4.39 ± 4.43	8	5.75 ± 3	79
TSRR15	−2.19 ±1.51	327	4.39 ± 4.41	20	5.25 ± 2.41	9
TSRR15∩	−2.19 ±1.51	327	4.39 ± 4.43	19	5.47 ± 2.38	6

Calculations were done with 1) #TSRR 20 on all files, 2) #TSRR 15 on all files, and 3) #TSRR 15 on the intersection (∩) of the files and ventricular premature contractions (VPCs) of TSRR15 and TSRR20.

Of the 1,009 remaining files, 652 were removed through the Poincaré filter, leaving 357 files.

After HRV parameter calculation and averaging 33 of the files contained at least one outlier. The median score of the files was 1 with a minimum of −7 and a maximum of 7.

From the best 20% (71 files), HRT was calculated. In 24 files, no or too few valid VPCSs could be found. While most of the remaining 47 files showed a distinct HRT pattern (refer to **Figure 2**), some did not (refer to **Figure 3**). **Table 5** shows a detailed overview of the number of filtered files broken down by databases.

After classification, 41 of the files used for the stVPCS had HRT class HRT0, 5 files had HRT1, and 1 file HRT2. Of these files, 7 (2 HRT0, 4 HRT1, 1 HRT2) are marked as not reliable by the *RHRT* package. When adding TT to the classification, 40 files had HRT class HRTA and 7 files HRTB, whereas the classification from 10 files (4 of HRTA, 6 of HRTB) are marked as unreliable.

Because stVPCS should be used for comparison as the ideal HRT shape, it is important that it shows a pronounced reaction to the VPC and low risk HRT parameters. The sequence averaged from all 47 VPCSs showed a distinct HRT pattern (refer to **Figure 4** with TO = 3.12%, TS = 7.85 ms/RR, and TT = 3. Therefore, it falls in the lowest risk categories HRT0 and HRTA. The parameter nTS could not be calculated

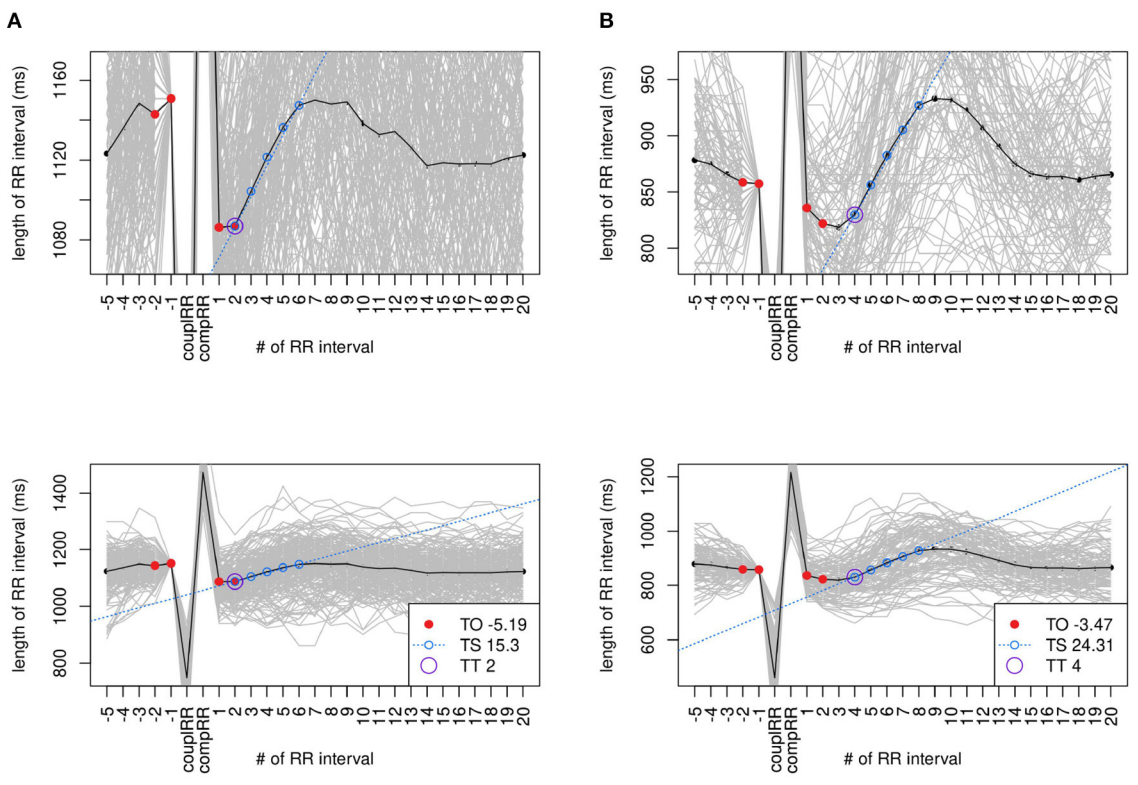

FIGURE 2 | Standard VPCS (stVPCS) files with distinct heart rate turbulence (HRT). Exemplary tachograms of two files used to calculate the stVPCS that show distinct HRT. Both files are in class HRTA. The upper row shows a zoomed in tachogram, the row below the respective tachogram zoomed out. Data: **(A)** *e145a* from *CRISDB* and **(B)** *nsr010* from *NSR2DB*.

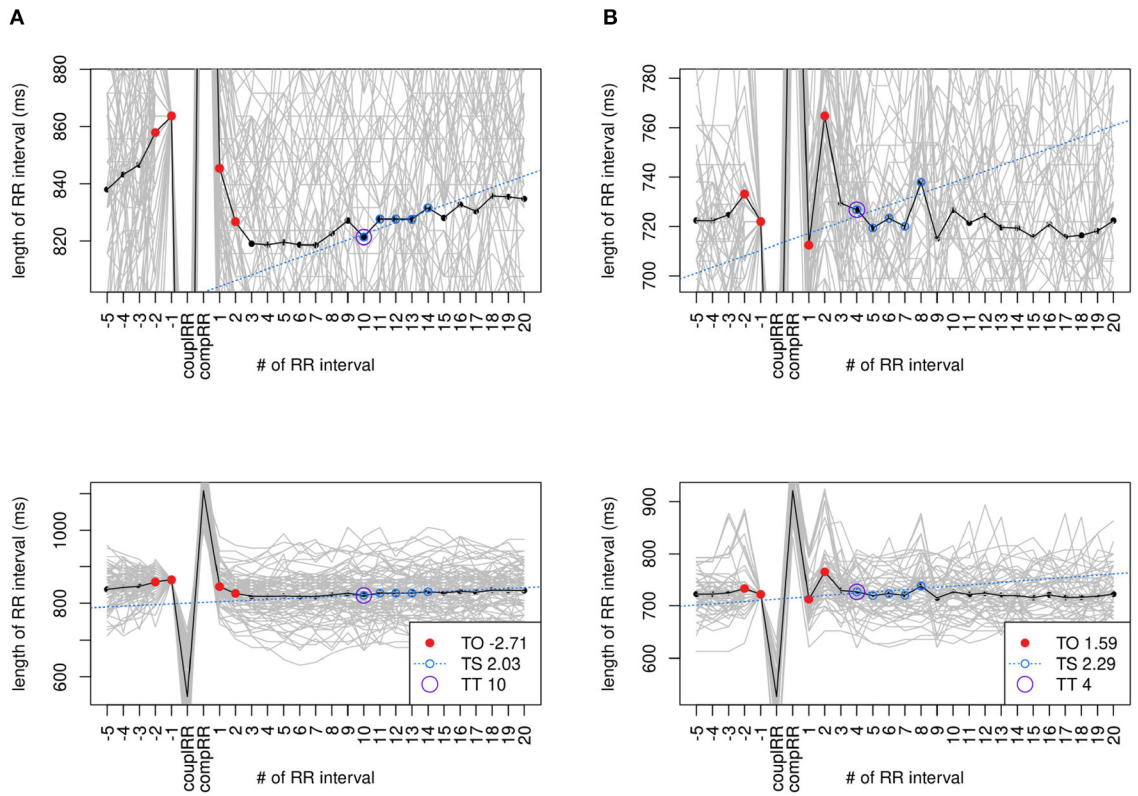

FIGURE 3 | stVPCS files without distinct HRT. Exemplary tachograms of two files used to calculate the stVPCS that do not show distinct HRT. Both files are in class HRTB. The upper row shows a zoomed in tachogram, the row below the respective tachogram zoomed out. Data: **(A)** *s20491* from *LTSTDB* and **(B)** *chf202* from *CHF2DB*.

TABLE 5 | Overview of the number of files remaining after every analysis step sorted by their databases.

DB	Input	Length	Poincaré	HRV	HRT
CHFDB	15	0	0	0	0
CHF2DB	29	26	9	2	1
CRISDB	762	731	210	38	36
excluded	2	2	1	0	0
LTAFDB	84	76	11	3	1
LTDB	7	6	0	0	0
LTSTDB	86	81	54	13	7
NSRDB	18	17	17	6	0
NSR2DB	54	54	52	9	2
SDDB	23	16	3	0	0
Sum	1,080	1,009	357	71	47

The different steps are Input (before any filtering), Length (after filtered for measurement length), Poincaré (after Poincaré filter), HRV (after HRV filter), and HRT (files with enough valid VPCSs to calculate HRT). DB, database.

for stVPCS because RMSSD needs to be calculated from a respective long-term measurement, which is not applicable for the averaged VPCS.

3.3. Comparing VPCSs Based on TT

3.3.1. HRT Values

The HRT parameter values of all files sorted by TT can be seen in **Figure 5** and in the **Supplementary Table 1** in more detail. Half of the files have a TT between 4 and 8. The median TS is above the threshold of 2.5 ms/RR for TT values 6 and lower and under the threshold for most higher TT values. For high TT values, the median of TS varies, whereas the number of files in these groups is considerably lower. Unequal distribution is noticeable since the groups with more than 20 files (TT of 2 to 10) include 82% of all files. Analogously to TS, the median of TO is below the threshold for low TT values (1 to 11) and varies with increasing TT.

The parameter values of nTS worsen clearly and the pattern changes compared to the TS values: Only the medians of nTS from a TT of 2–4 still lie above the threshold. The nTS medians of all other TT values including 1 lie below the threshold. For many TT values, no file has an nTS value that exceeds the threshold.

3.3.2. DTW With stVPCS

The results of the DTW analysis are shown in **Figures 6**, **7**. The plots for all TT values can be found in the **Supplementary Figures 2** and **3**. The averaged VPCS that matched the stVPCS the best was TT 3. Apart from TT 1, with

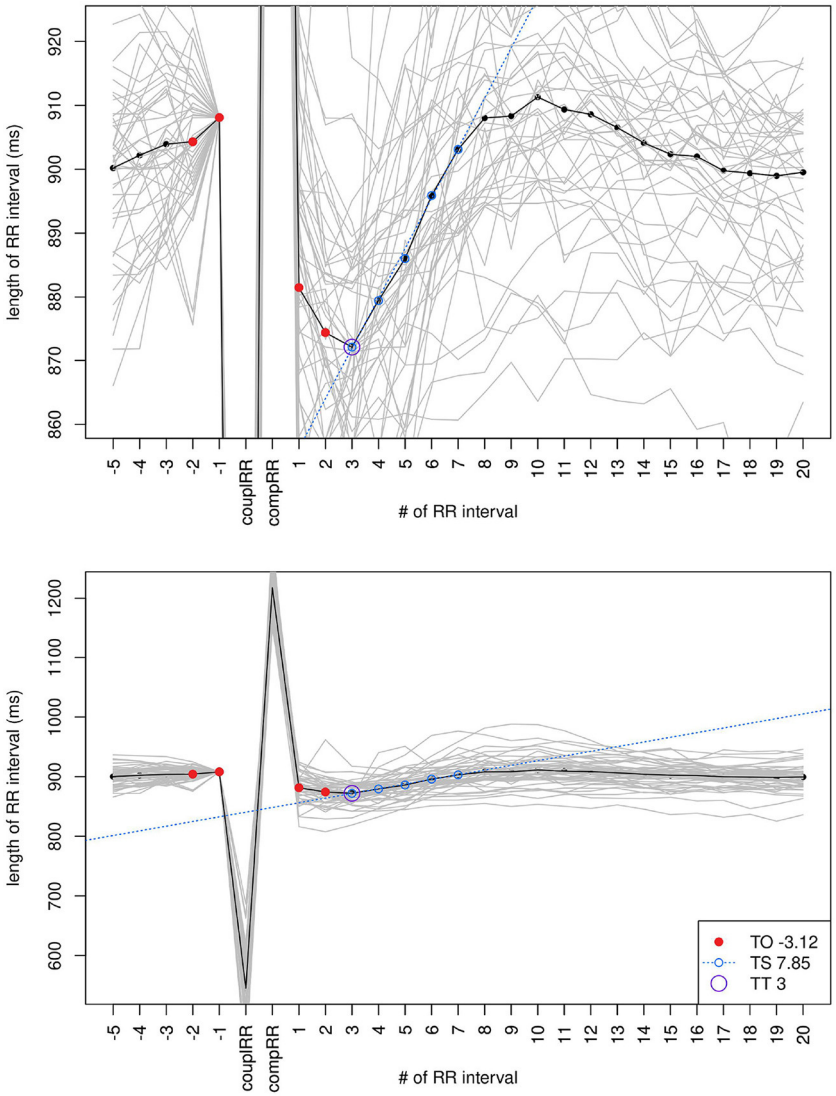

FIGURE 4 | The stVPCS calculated from 47 files that matched all filter criteria and had the best HRV parameters.

rising TT, the difference between VPCS and stVPCS increased. The averaged VPCS with TT 1 lacked the characteristic delayed IL decrease but showed an immediate IL rise followed only by a shallow IL decline.

Analogously to the comparison with the full sequences, the averaged VPCS with TT 3 matched the best with the stVPCS after cutting. The difference of the VPCS of TT 1 to the best sequence is similar to the analysis without cutting (full VPCSs: Diff^{TT1} 82, Diff^{TT3} 31; with cutting: Diff^{TT1} 60, Diff^{TT3} 22). The sequences with TT 2 to 4 considerably line with the stVPCS, while the sequences flatten out continuously with rising TT.

3.3.3. Intra-Subject Variability of TT

The TT and TTSD within a file were significantly correlated ($\rho = 0.26, p < 0.005$, refer to **Figure 8**).

4. DISCUSSION

4.1. Differences in Classification

In our analysis of 1,080 files, only 8 could additionally be classified when using a lower #TSRR. Furthermore, there were 43 and 55 files that changed classification due to #TSRR in the classification systems HRT0-2 and HRTA-C, respectively. The switches were both within HRT classes as well as between an HRT class and NR. Interestingly, a high number of these files switched from an HRT class when calculated with #TSRR 15 to NR with #TSRR 20, meaning that a higher #TSRR leads to more variability in the data.

The same can be seen for TT values, where a higher amount of values was NR with #TSRR 20. This can be explained by the majority of the files with not reliable TT values showing a very shallow tachogram in visual analysis. With no distinct

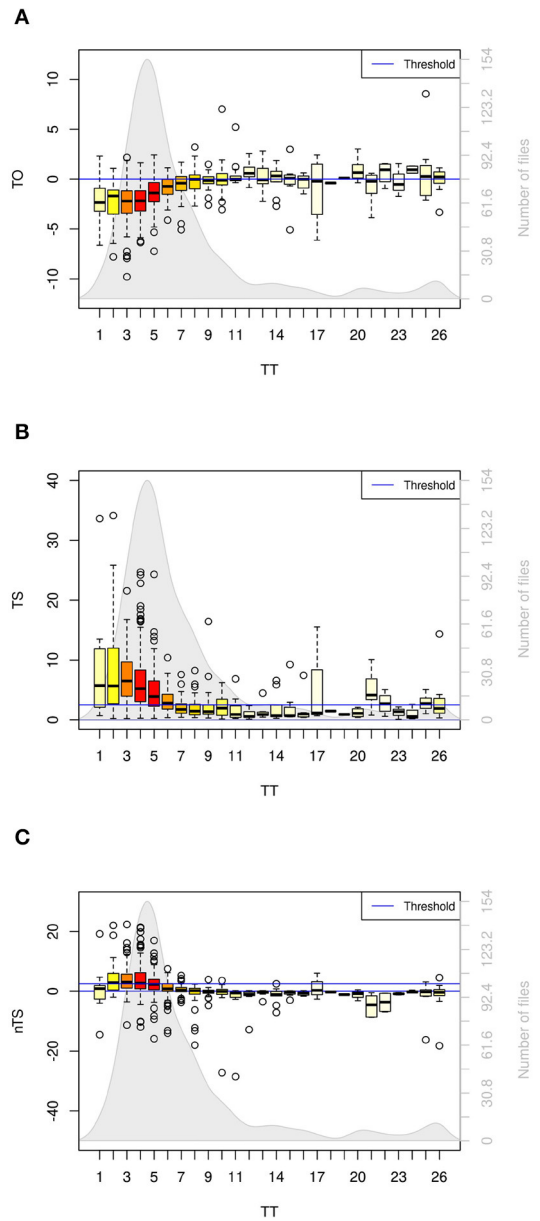

FIGURE 5 | Averaged HRT parameter values of all files grouped by the respective turbulence timing (TT) value. The color of the boxes and the gray background graph illustrate the number of files in the different groups. The common threshold of TO (0%) **(A)** and TS (2.5 ms/RR) **(B)** is represented as a blue line. The common cut-off of TS is used for nTS, because no threshold for nTS has been established yet **(C)**. The median of the groups with low TT (TT $\leq$ 10 for TO and TT $\leq$ 6 for TS) lie on the low-risk side of the threshold. For nTS, only the medians of the groups with a TT of 2–4 lie above the threshold.

IL increase, random fluctuations have a stronger influence on the location of the steepest slope, thus increasing the variability of TT. Furthermore, longer VPCSs lead to a higher number of possible TT values and therefore higher variability. This high variability combined with a lower number of VPCSs results in non-significant results in the reliability check and, thus, a higher number of files with NR TT.

The only HRT parameter with distinctly differing values is TT which is to be expected with higher #TSRR. This leads to the differences in classification being marginal with less than 1% more classifiable files and 5–6% files changing the resulting classes. However, in clinical settings, even small numbers of patients that cannot be classified or are differently classified based on methodological variances are unfavorable-especially if this could be avoided by uniformly adjusting one parameter.

4.2. stVPCS

The stVPCS received through our pipeline shows a distinct HRT pattern with the HRT classes of HRT0 and HRTA, which imply the least possible risk. The tachogram of our stVPCS is similar to tachograms showing characteristic HRT patterns in reviews (16, 19, 22). Although the databases used to consist of files from subjects with severe diseases, with the filtering pipeline, we were able to find a set of files without pathological abnormalities based on their sound HRT parameter values. The resulting stVPCS seemed to be a feasible approximation of a healthy HRT reaction that could be used as a template for the following analysis.

4.3. Random Fluctuation With High TTs

Apart from TT 1, the tachograms with low TTs showed a similar pattern to the stVPCS (check the **Supplementary Data Sheet 2** for a discussion of VPCS with TT 1). With increasing TT the tachograms get more shallow meaning the reaction to the VPC becomes less distinct with increasing distance to the VPC. Especially with high TT values, the tachograms show no distinct pattern but apparently random fluctuation. This can also be seen in the mean HRT values grouped by TT. As expected, the VPCSs with a low TT show the best TS values. The same can be seen for TO. With high TT values, however, the medians for both TS and TO vary, which implies common HRV rather than HRT. Still, the number of VPCSs used to calculate the medians decreases with increasing TT, which may bias this observation.

Nevertheless, TTSD is lower with lower TT values meaning that in persons with low TT the fastest slope occurs in a narrower range. Again, a narrower range implies a steady underlying mechanism that causes turbulence within a distinct time interval while a high fluctuation of TT values within a person suggests randomness. Therefore, TTSD may possibly be used as a measurement for the reliability of TT as well as TS and nTS.

Our data suggest, that only measurements with TT 2 to approximately 6 show distinct HRT. This can be seen in the DTW plots in combination with the median values of the HRT parameters grouped by TT. We recommend visually inspecting all measurements with TT 1 or higher than 7 to ensure the validity of the HRT parameters. Admittedly, manual visual inspection introduces unpreventable human error and, thus, variability to the analyzes, which should be avoided wherever possible. Therefore, DTW may be a method to ensure a reliable reaction to the VPC by comparing the progress of the tachogram of a person to a standard tachogram established from a healthy peer group. Additionally, stVPCS could be generated for different pathological conditions, which would enable using HRT not only

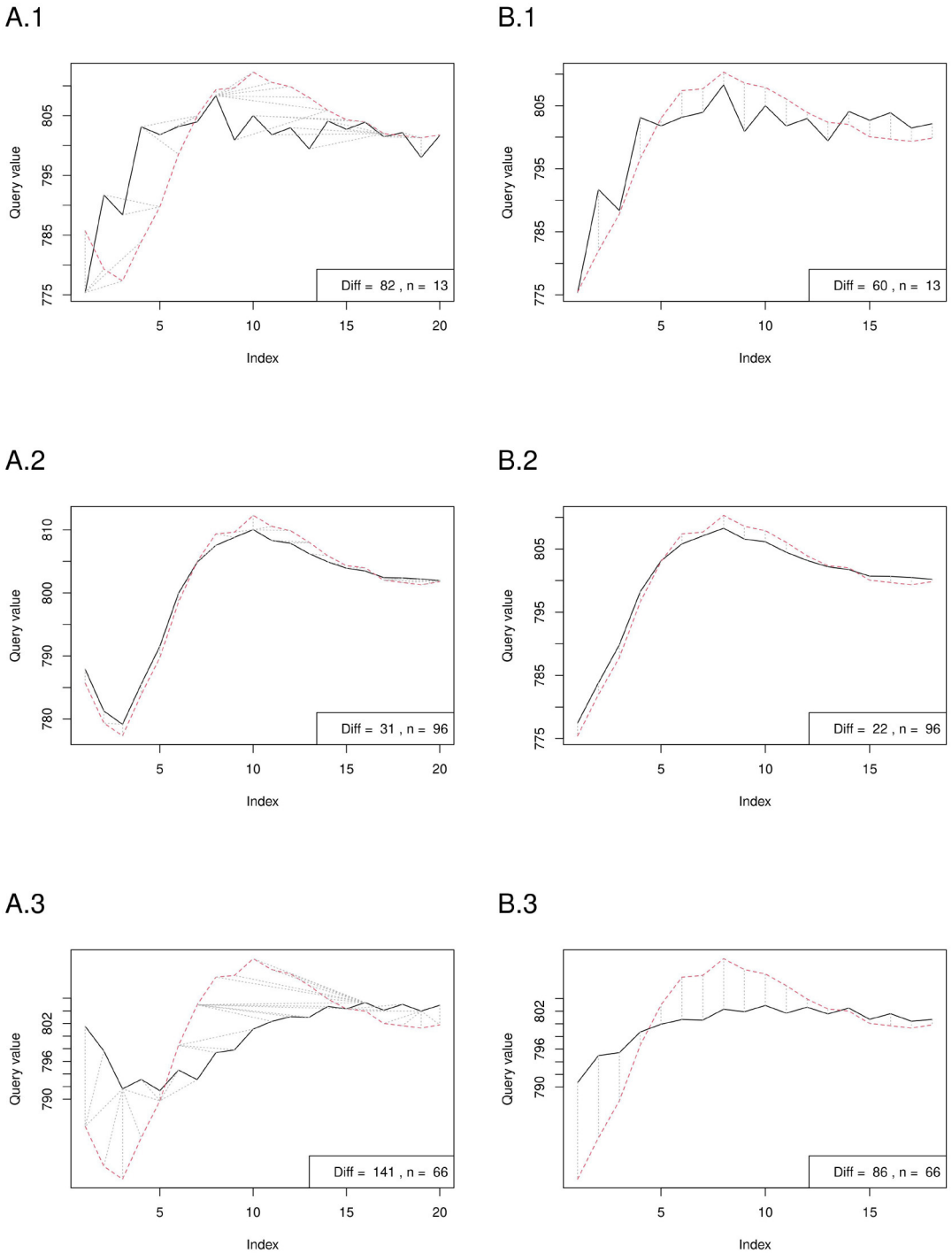

FIGURE 6 | Dynamic time warping (DTW) analysis of exemplary postRRs grouped by their respective TT. The left side **(A)** shows the analysis of the stVPCS with the full postRRs sequences, the right side **(B)** with the cut sequences. From up to down the plots show the comparisons for TT 1 (1), 3 (2), and 7 (3). The full averaged sequence of TT 1 **(A.1)** lacks the initial bend and shows an immediate IL incline. The sequence of TT = 3 fits the stVPCS the best, both in the full **(A.2)** and in the cut version **(B.2)**.

for risk assessment but also as part of diagnostics. Possibly, DTW could replace the original HRT parameters, because it analyzes the tachogram as a whole instead of reducing it to selective parameters that can be biased as seen in this study with TS. Using DTW for HRT analysis needs establishing the mentioned stVPCSs through a sufficiently large data set with fitting health conditions and with respect to factors influencing HRT like age or circadian rhythm (31). A similar approach has already been

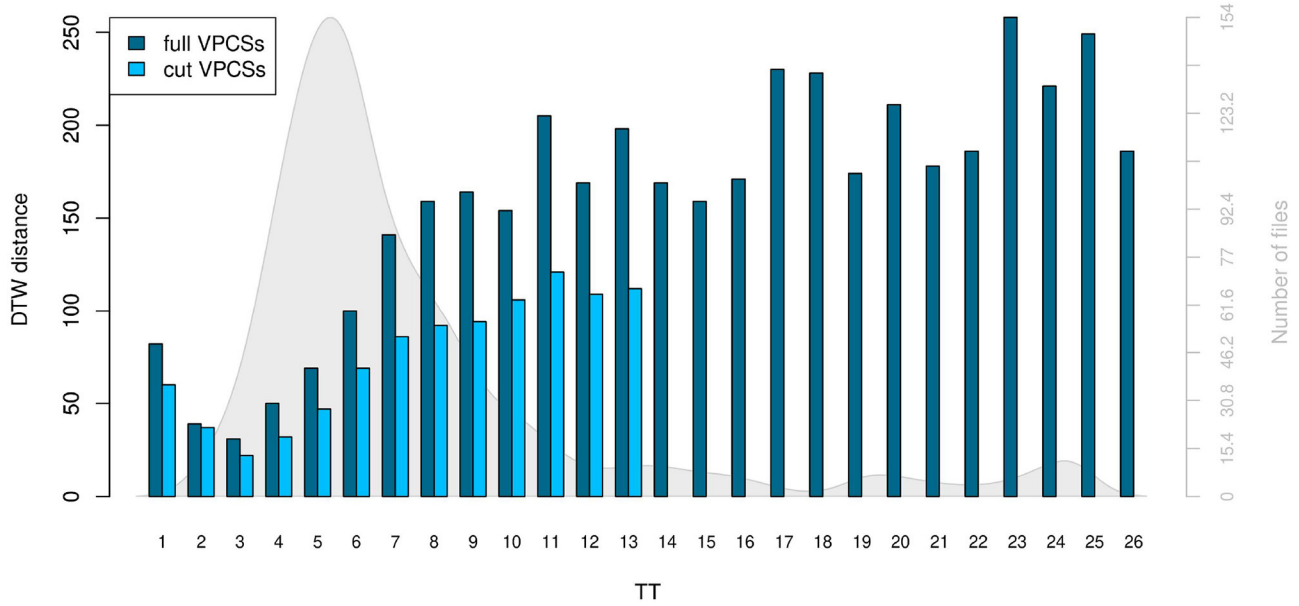

FIGURE 7 | Distances calculated by DTW. The differences between stVPCS and the averaged VPCSs of all files grouped by their respective TT are shown in dark blue (full sequences) and light blue (cut sequences). The distances of the cut sequences are lower than the distances of the full sequences. In both TT 3 has the lowest distance to the stVPCS. The gray background graph and the corresponding axis on the right illustrate the number of files in the different groups.

done by Martínez et al. (44) based on a Neyman-Pearson detector (44) that compares a VPCS to the first three functions of a Karhunen-Loève transform expansion (45, 46). Under certain circumstances, this assessment is more robust regarding noise than TO and TS and needs fewer VPCSs to reach a high probability of detecting distinct HRT (46), which shows that comparison of shape patterns as a whole instead of reducing them to restricted aspects of the curve progression offers promising risk assessment parameters.

4.4. Hypotheses

Our first hypothesis suggested a distinct difference in HRT values when calculated with different #TSRRs. Although we could show a difference in the number of assessable HRT values and HRT classes, the differences are not as distinct as we expected with < 1% and 5–6% affected files, respectively. However, no variable risk assessment is obstructive in clinical diagnostics, especially if the results obtained from the same person vary solely based on a difference in methodology. Consequentially, the question remains which of the commonly used #TSRR are optimal for the analysis.

Therefore, our second hypothesis tackled the question of whether high TT or TTSD values do not show actual HRT but random fluctuation. The tachograms of the files with different parameter values based on #TSRR show, that these differences are mainly based on variability due to different sets of VPCSs used for calculation instead of actual HRT at the end of the VPCSs. Furthermore, the comparison of the stVPCS with averaged VPCSs grouped by TT verifies that with increasing TT the response to the VPCs decreases considerably. The same result is implied by HRT values passing their respective thresholds to an increasing degree with rising TT.

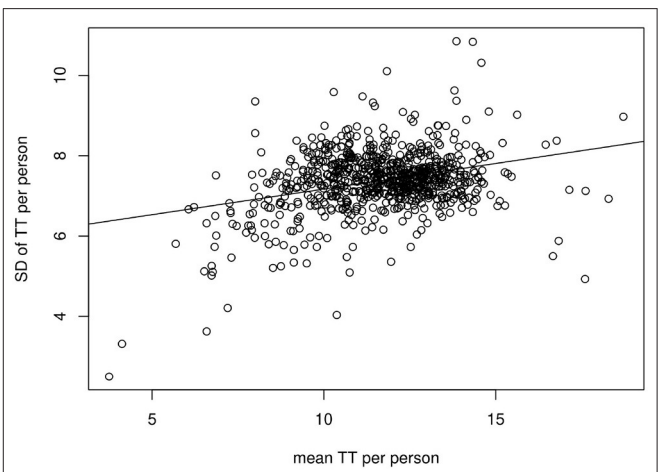

FIGURE 8 | Linear regression analysis of TT and its respective TTSD of all files included in the analysis.

4.5. Limitations

While some of the files included in the stVPCS derive from NSR2DB that is defined as subjects with "normal sinus

rhythm," the vast majority of files belong to the CRISDB, LTSTDB, LTAFDB, and CHF2DB that include ECGs of persons after myocardial infarction, with ST-segment anomalies, atrial fibrillation, and congestive heart failure, respectively. Therefore, it is probable that files were included from persons with diagnosed pathologies that are not visible in the used autonomic markers and may bias our results. It would be interesting to repeat the analysis with data from healthy subjects to examine a possible difference in the stVPCSs.

Due to the lack of meta-data in the user databases, we did not analyze any influence of medication on #TSRR. To our knowledge, a temporal change in the HRT response has not been studied so far. The focus of HRT research rather lies on the strength of the response than its delay. The same goes for any response of the baroreflex: Baroreflex sensitivity has been shown to change with antihypertensive medication (47, 48), but its temporal aspect has not been studied. Since the baroreflex response latency can be influenced through short directed intervention such as tilt or atropine administration (49), it is possible that drugs influencing the sympathovagal balance like beta-blockers can change the response delay as well. However, the temporal scale of the difference does not exceed 1 s which amounts to approximately two intervals (49) and is likely to be less with long-term medication and adapted baroreceptor sensitivity. Therefore, we expect that any medication influencing HRT does not influence our results, but this also should be investigated with appropriate data.

It is important to mention that our results allow conclusions about the behavior of the autonomic marker but not its predictive power. Since HRT is a risk marker for major adverse cardiac events, analysis without meta-data about the outcome of the studied patients can only be the first step and must be verified with appropriate clinical data.

5. CONCLUSION

We recommend using #TSRR 15 for HRT analysis. The lower number of valid intervals results in a higher amount of VPCSs that can be used in the analysis as well as discarding of intervals that show random fluctuation instead of HRT. Therefore, it leads to more reliable data.

DATA AVAILABILITY STATEMENT

Publicly available datasets were analyzed in this study. This data can be found at: https://physionet.org/content/chfdb/1.0.0/; https://physionet.org/content/chf2db/1.0.0/; https://physionet.org/content/crisdb/1.0.0/; https://physionet.org/content/excluded/1.0.0/; https://physionet.org/content/ltafdb/1.0.0/; https://physionet.org/content/ltdb/1.0.0/; https://physionet.org/content/ltstdb/1.0.0/; https://physionet.org/content/nsrdb/1.0.0/; https://physionet.org/content/nsr2db/1.0.0/; https://physionet.org/content/sddb/1.0.0.

ETHICS STATEMENT

Ethical review and approval was not required for the study on human participants in accordance with the local legislation and institutional requirements. Written informed consent for participation was not required for this study in accordance with the national legislation and the institutional requirements.

AUTHOR CONTRIBUTIONS

VB conceived the project, implemented the analysis pipeline and performed all analyzes and literature research, created all figures and tables, and wrote the initial draft of the manuscript and revised it. CS provided technical advice in the implementation of the analysis pipeline. CS, GE, and AD reviewed the manuscript. AD supervised the project. All authors contributed to the article and approved the submitted version.

SUPPLEMENTARY MATERIAL

The Supplementary Material for this article can be found online at: https://www.frontiersin.org/articles/10.3389/fcvm.2022.793535/full#supplementary-material

REFERENCES

1. Hallstrom AP, Stein PK, Schneider R, Hodges M, Schmidt G, Ulm K. Structural relationships between measures based on heart beat intervals: potential for improved risk assessment. *IEEE Trans Biomed Eng*. (2004) 51:1414–20. doi: 10.1109/TBME.2004.828049
2. Lombardi F, Stein PK. Origin of heart rate variability and turbulence: an appraisal of autonomic modulation of cardiovascular function. *Front Physiol*. (2011) 2:95. doi: 10.3389/fphys.2011.00095
3. Wichterle D, Melenovsky V, Malik M. Mechanisms involved in heart rate turbulence. *Card Electrophysiol Rev*. (2002) 6:262–6. doi: 10.1023/A:1016385126668
4. Watanabe MA, Marine JE, Sheldon R, Josephson ME. Effects of ventricular premature stimulus coupling interval on blood pressure and heart rate turbulence. *Circulation*. (2002) 106:325–30. doi: 10.1161/01.CIR.0000022163.24831.B5
5. Cygankiewicz I. Heart rate turbulence. *Prog Cardiovasc Dis*. (2013) 56:160–71. doi: 10.1016/j.pcad.2013.08.002
6. Disertori M, Masè M, Rigoni M, Nollo G, Ravelli F. Heart rate turbulence is a powerful predictor of cardiac death and ventricular arrhythmias in postmyocardial infarction and heart failure patients: a systematic review and meta-analysis. *Circ Arrhythm Electrophysiol*. (2016) 9:e004610. doi: 10.1161/CIRCEP.116.004610
7. Golukhova EZ, Gromova O, Grigoryan M, Merzlyakov V, Shumkov K, Bockeria L, et al. Noninvasive predictors of malignant arrhythmias. *Cardiology*. (2016) 135:36–42. doi: 10.1159/000445881
8. Lin K, Wei L, Huang Z, Zeng Q. Combination of Ewing test, heart rate variability, and heart rate turbulence analysis for early diagnosis

of diabetic cardiac autonomic neuropathy. *Medicine*. (2017) 96:e8296. doi: 10.1097/MD.0000000000008296
9. Bugan B, Cekirdekci EI. Prognostic significance of heart rate turbulence parameters in patients with noncompaction cardiomyopathy. *Cardiology*. (2019) 142:56–62. doi: 10.1159/000499408
10. Gimeno-Blanes FJ, Blanco-Velasco M, Barquero-Pérez Ó, García-Alberola A, Rojo-Álvarez JL. Sudden cardiac risk stratification with electrocardiographic indices - a review on computational processing, technology transfer, and scientific evidence. *Front Physiol*. (2016) 7:82. doi: 10.3389/fphys.2016.00082
11. Frolov AV, Vaikhanskaya TG, Melnikova OP, Vorobiev AP, Guel LM. Risk stratification personalised model for prediction of life-threatening ventricular tachyarrhythmias in patients with chronic heart failure. *Kardiol Pol*. (2017) 75:682–8. doi: 10.5603/KP.a2017.0060
12. Soguero-Ruiz C, Mora-Jiménez I, Ramos-López J, Quintanilla Fernández T, García A, Díez-Mazuela D, et al. An interoperable system toward cardiac risk stratification from ECG monitoring. *Int J Environ Res Public Health*. (2018) 15:428. doi: 10.3390/ijerph15030428
13. Fazio G, Sarullo FM, D'Angelo L, Lunetta M, Visconti C, Di Gesaro G, et al. Heart rate turbulence for guiding electric therapy in patients with cardiac failure. *J Clin Monit Comput*. (2010) 24:125–9. doi: 10.1007/s10877-009-9218-4
14. Kaplan RM, Herzog CA, Larive B, Subacius H, Nearing BD, Verrier R, et al. T-Wave alternans, heart rate turbulence, and ventricular ectopy in standard versus daily hemodialysis: results from the FHN daily trial. *Ann Noninvasive Electrocardiol*. (2016) 21:566–71. doi: 10.1111/anec.12354
15. Uznańska-Loch B, Wikło K, Trzos E, Wierzbowska-Drabik K, Chrzanowski Ł, Kasprzak JD, et al. Advanced and traditional electrocardiographic risk factors in pulmonary arterial hypertension: the significance of ventricular late potentials. *Kardiol Pol*. (2018) 76:586–93. doi: 10.5603/KP.a2017.0257
16. Bauer A, Malik M, Schmidt G, Barthel P, Bonnemeier H, Cygankiewicz I, et al. Heart rate turbulence: standards of measurement, physiological interpretation, and clinical use: international society for Holter and Noninvasive electrophysiology consensus. *J Am Coll Cardiol*. (2008) 52:1353–65. doi: 10.1016/j.jacc.2008.07.041
17. Schmidt G, Malik M, Barthel P, Schneider R, Ulm K, Rolnitzky L, et al. Heart-rate turbulence after ventricular premature beats as a predictor of mortality after acute myocardial infarction. *Lancet*. (1999) 353:1390–6. doi: 10.1016/S0140-6736(98)08428-1
18. Barthel P, Schneider R, Bauer A, Ulm K, Schmitt C, Schömig A, et al. Risk stratification after acute myocardial infarction by heart rate turbulence. *Circulation*. (2003) 108:1221–6. doi: 10.1161/01.CIR.0000088783.34082.89
19. Guzik P, Schmidt G. A phenomenon of heart-rate turbulence, its evaluation, and prognostic value. *Card Electrophysiol Rev*. (2002) 6:256–61. doi: 10.1023/A:1016333109829
20. Bauer A, Schmidt G. Heart rate turbulence. *J Electrocardiol*. (2003) 36(Suppl.):89–93. doi: 10.1016/j.jelectrocard.2003.09.020
21. Watanabe MA. Heart rate turbulence: a review. *Indian Pacing Electrophysiol J*. (2003) 3:10–22.
22. Watanabe MA, Schmidt G. Heart rate turbulence: a 5-year review. *Heart Rhythm*. (2004) 1:732–8. doi: 10.1016/j.hrthm.2004.09.003
23. Francis J, Watanabe MA, Schmidt G. Heart rate turbulence: a new predictor for risk of sudden cardiac death. *Ann Noninvasive Electrocardiol*. (2005) 10:102–9. doi: 10.1111/j.1542-474X.2005.10102.x
24. Bauer A, Zürn CS, Schmidt G. Heart rate turbulence to guide treatment for prevention of sudden death. *J Cardiovasc Pharmacol*. (2010) 55:531–8. doi: 10.1097/FJC.0b013e3181d4c973
25. Zuern CS, Barthel P, Bauer A. Heart rate turbulence as risk-predictor after myocardial infarction. *Front Physiol*. (2011) 2:99. doi: 10.3389/fphys.2011.00099
26. Yamada S, Yoshihisa A, Hijioka N, Kamioka M, Kaneshiro T, Yokokawa T, et al. Autonomic dysfunction in cardiac amyloidosis assessed by heart rate variability and heart rate turbulence. *Ann Noninvasive Electrocardiol*. (2020) 25:e12749. doi: 10.1111/anec.12749
27. Oyelade T, Canciani G, Bottaro M, Zaccaria M, Formentin C, Moore K, et al. Heart rate turbulence predicts survival independently from severity of liver dysfunction in patients with cirrhosis. *Front Physiol*. (2020) 11:602456. doi: 10.3389/fphys.2020.602456
28. Yamada S, Yoshihisa A, Sato Y, Sato T, Kamioka M, Kaneshiro T, et al. Utility of heart rate turbulence and T-wave alternans to assess risk for readmission and cardiac death in hospitalized heart failure patients. *J Cardiovasc Electrophysiol*. (2018) 29:1257–64. doi: 10.1111/jce.13639
29. Yildiz C, Yildiz A, Tekiner F. Heart rate turbulence analysis in subclinical hypothroidism heart rate turbulence in hypothyroidism. *Acta Cardiologica Sinica*. (2015) 31:444–8. doi: 10.6515/acs20150428a
30. Soylu MO, Altun I, Basaran O, Uzun Y, Dogan V, Ergun G, et al. Impact of QRS morphology on heart rate turbulence and heart rate variability after cardiac resynchronization therapy in patients with heart failure. *Eur Rev Med Pharmacol Sci*. (2016) 20:317–22.
31. Blesius V, Schölzel C, Ernst G, Dominik A. HRT assessment reviewed: a systematic review of heart rate turbulence methodology. *Physiol Meas*. (2020) 41:08TR01. doi: 10.1088/1361-6579/ab98b3
32. Goldberger AL, Amaral LA, Glass L, Hausdorff JM, Ivanov PC, Mark RG, et al. PhysioBank, physiotoolkit, and physionet: components of a new research resource for complex physiologic signals. *Circulation*. (2000) 101:E215–20. doi: 10.1161/01.CIR.101.23.e215
33. Baim DS, Colucci WS, Monrad ES, Smith HS, Wright RF, Lanoue A, et al. Survival of patients with severe congestive heart failure treated with oral milrinone. *J Am Coll Cardiol*. (1986) 7:661–70. doi: 10.1016/S0735-1097(86)80478-8
34. Stein PK, Domitrovich PP, Kleiger RE, Schechtman KB, Rottman JN. Clinical and demographic determinants of heart rate variability in patients post myocardial infarction: insights from the cardiac arrhythmia suppression trial (CAST). *Clin Cardiol*. (2000) 23:187–94. doi: 10.1002/clc.4960230311
35. Petrutiu S, Sahakian AV, Swiryn S. Abrupt changes in fibrillatory wave characteristics at the termination of paroxysmal atrial fibrillation in humans. *EP Europace*. (2007) 9:466–70. doi: 10.1093/europace/eum096
36. Jager F, Taddei A, Moody GB, Emdin M, Antolič G, Dorn R, et al. Long-term ST database: a reference for the development and evaluation of automated ischaemia detectors and for the study of the dynamics of myocardial ischaemia. *Med Biol Eng Comput*. (2003) 41:172–82. doi: 10.1007/BF02344885
37. Greenwald SD. *The Development and Analysis of a Ventricular Fibrillation Detector* (Master's thesis) (1986). Available online at: https://dspace.mit.edu/handle/1721.1/92988
38. Blesius V, Dominik A. RHRT: an R package to assess heart rate turbulence. *J Open Source Softw*. (2021) 6:3540. doi: 10.21105/joss.03540
39. Malik M, Bigger JT, Camm AJ, Kleiger RE, Malliani A, Moss AJ, et al. Heart rate variability-Standards of measurement, physiological interpretation, and clinical use. *Eur Heart J*. (1996) 17:354–81. doi: 10.1093/oxfordjournals.eurheartj.a014868
40. Esperer HD, Esperer C, Cohen RJ. Cardiac arrhythmias imprint specific signatures on lorenz plots. *Ann Noninvasive Electrocardiol*. (2008) 13:44–60. doi: 10.1111/j.1542-474X.2007.00200.x
41. Lown B, Wolf M. Approaches to sudden death from coronary heart disease. *Circulation*. (1971) 44:130–42. doi: 10.1161/01.CIR.44.1.130
42. Kostis JB, McCrone K, Moreyra AE, Gotzoyannis S, Aglitz NM, Natarajan N, et al. Premature ventricular complexes in the absence of identifiable heart disease. *Circulation*. (1981) 63:1351–6. doi: 10.1161/01.CIR.63.6.1351
43. Latchamsetty R, Bogun F. Premature ventricular complexes and premature ventricular complex induced cardiomyopathy. *Curr Probl Cardiol*. (2015) 40:379–422. doi: 10.1016/j.cpcardiol.2015.03.002
44. Martínez JP, Laguna P, Solem K, Sörnmo L. Evaluation of a Neyman-Pearson heart-rate turbulence detector. *Annu Int Conf IEEE Eng Med Biol Soc*. (2008). 2008:4407–10. doi: 10.1109/IEMBS.2008.4650188
45. Smith D, Solem K, Laguna P, Martínez JP, Sörnmo L. Model-based detection of heart rate turbulence using mean shape information. *IEEE Trans Biomed Eng*. (2010) 57:334–42. doi: 10.1109/TBME.2009.2030669
46. Martínez JP, Cygankiewicz I, Smith D, Bayés de Luna A, Laguna P, Sörnmo L. Detection performance and risk stratification using a model-based shape index characterizing heart rate turbulence. *Ann Biomed Eng*. (2010) 38:3173–84. doi: 10.1007/s10439-010-0081-8

47. Berdeaux A, Giudicelli Jf. Antihypertensive drugs and baroreceptor reflex control of heart rate and blood pressure. *Fundamental Clin Pharmacol*. (1987). 1:257–82. doi: 10.1111/j.1472-8206.1987.tb00565.x
48. Grassi G, Trevano FQ, Seravalle G, Scopelliti F, Mancia G. Baroreflex function in hypertension: consequences for antihypertensive therapy. *Prog Cardiovasc Dis*. (2006) 48:407–15. doi: 10.1016/j.pcad.2006.03.002
49. Keyl C, Schneider A, Dambacher M, Bernardi L. Time delay of vagally mediated cardiac baroreflex response varies with autonomic cardiovascular control. *J Appl Physiol*. (2001) 91:283–9. doi: 10.1152/jappl.2001.91.1.283

Conflict of Interest: The authors declare that the research was conducted in the absence of any commercial or financial relationships that could be construed as a potential conflict of interest.

frontiers | Frontiers in Cardiovascular Medicine

ORIGINAL RESEARCH
published: 07 April 2022
doi: 10.3389/fcvm.2022.840485

A Novel Risk Score to Predict In-Hospital Mortality in Patients With Acute Myocardial Infarction: Results From a Prospective Observational Cohort

Lulu Li[1,2], Xiling Zhang[2], Yini Wang[2], Xi Yu[2], Haibo Jia[2], Jingbo Hou[2], Chunjie Li[3], Wenjuan Zhang[4], Wei Yang[5], Bin Liu[6], Lixin Lu[7], Ning Tan[8], Bo Yu[2] and Kang Li[1]**

[1] Department of Biostatistics, School of Public Health, Harbin Medical University, Harbin, China, [2] Department of Cardiology, Second Affiliated Hospital of Harbin Medical University, Harbin, China, [3] Department of Emergency, Tianjin Chest Hospital, Tianjin, China, [4] Department of Cardiology, Tianjin Medical University General Hospital, Tianjin, China, [5] Department of Cardiology, Fourth Affiliated Hospital of Harbin Medical University, Harbin, China, [6] Department of Cardiology, The Second Hospital of Jilin University, Changchun, China, [7] Department of Cardiology, Daqing Long Nan Hospital, Daqing, China, [8] Department of Cardiology, Guangdong General Hospital, Guangzhou, China

OPEN ACCESS

Edited by:
Lilei Yu,
Wuhan University, China

Reviewed by:
Stefano Carugo,
IRCCS Ca 'Granda Foundation Maggiore Policlinico Hospital, Italy
Andrea Passantino,
ICS Maugeri spa SB (IRCCS), Italy

***Correspondence:**
Kang Li
likang@ems.hrbmu.edu.cn
Bo Yu
dryu_hmu@163.com

Specialty section:
This article was submitted to General Cardiovascular Medicine, a section of the journal Frontiers in Cardiovascular Medicine

Received: 21 December 2021
Accepted: 18 February 2022
Published: 07 April 2022

Citation:
Li L, Zhang X, Wang Y, Yu X, Jia H, Hou J, Li C, Zhang W, Yang W, Liu B, Lu L, Tan N, Yu B and Li K (2022) A Novel Risk Score to Predict In-Hospital Mortality in Patients With Acute Myocardial Infarction: Results From a Prospective Observational Cohort. Front. Cardiovasc. Med. 9:840485. doi: 10.3389/fcvm.2022.840485

Objectives: The aim of this study was to develop and validate a novel risk score to predict in-hospital mortality in patients with acute myocardial infarction (AMI) using the Heart Failure after Acute Myocardial Infarction with Optimal Treatment (HAMIOT) cohort in China.

Methods: The HAMIOT cohort was a multicenter, prospective, observational cohort of consecutive patients with AMI in China. All participants were enrolled between December 2017 and December 2019. The cohort was randomly assigned (at a proportion of 7:3) to the training and validation cohorts. Logistic regression model was used to develop and validate a predictive model of in-hospital mortality. The performance of discrimination and calibration was evaluated using the Harrell's c-statistic and the Hosmer-Lemeshow goodness-of-fit test, respectively. The new simplified risk score was validated in an external cohort that included independent patients with AMI between October 2019 and March 2021.

Results: A total of 12,179 patients with AMI participated in the HAMIOT cohort, and 136 patients were excluded. In-hospital mortality was 166 (1.38%). Ten predictors were found to be independently associated with in-hospital mortality: age, sex, history of percutaneous coronary intervention (PCI), history of stroke, presentation with ST-segment elevation, heart rate, systolic blood pressure, initial serum creatinine level, initial N-terminal pro-B-type natriuretic peptide level, and PCI treatment. The c-statistic of the novel simplified HAMIOT risk score was 0.88, with good calibration (Hosmer–Lemeshow test: $P = 0.35$). Compared with the Global Registry of Acute Coronary Events risk score, the HAMIOT score had better discrimination ability in the training (0.88 vs. 0.81) and validation (0.82 vs. 0.72) cohorts. The total simplified HAMIOT risk score ranged from

0 to 121. The observed mortality in the HAMIOT cohort increased across different risk groups, with 0.35% in the low risk group (score $\leq$ 50), 3.09% in the intermediate risk group (50 $<$ score $\leq$ 74), and 14.29% in the high risk group (score $>$ 74).

Conclusion: The novel HAMIOT risk score could predict in-hospital mortality and be a valid tool for prospective risk stratification of patients with AMI.

Clinical Trial Registration: [https://clinicaltrials.gov], Identifier: [NCT03297164].

Keywords: acute myocardial infarction, in-hospital mortality, risk score, logistic regression model, net reclassification improvement, integrated discrimination index

INTRODUCTION

Patients with acute myocardial infarction (AMI) have a wide range of risks for immediate and long-term mortality worldwide. The in-hospital mortality of patients with AMI has decreased because of improved therapies over the past decades, such as early reperfusion, primary percutaneous coronary intervention (PCI), antithrombotic medication, and secondary prevention. However, the mortality rate of patients with AMI in China continues to substantial increase, at approximately 60 per 100,000 population annually (1). Thus, a potential risk stratification tool provides an opportunity to identify high risk patients and those who will benefit from appropriate decision-making on treatment strategy, level of care or length of hospital stay.

Over the last two decades, several risk scores have been developed to predict in-hospital mortality in patients with acute coronary syndrome (ACS) or AMI (2–12). Among them, the Global Registry of Acute Coronary Events (GRACE) (2) risk score is the most popular and widely recommended model for risk assessment and adjustment in patients with ACS/AMI in the guidelines of the European Society of Cardiology (ESC) (13, 14) and American College of Cardiology/American Heart Association (ACC/AHA) (15). Several other risk score models, such as the Acute Coronary Treatment and Intervention Outcomes Network (ACTION) Registry–Get With The Guidelines (GWTG) mortality risk score (4, 6) from the United States, the China Acute Myocardial Infarction (CAMI) registry (8, 9) or the Improving Care for Cardiovascular Disease in China-Acute Coronary Syndrome (CCC-ACS) project (10), were also derived to predict in-hospital mortality. However, these risk score models have some limitations (16–19). First, some of the excluded patients had a high risk, and some were modeled after selected populations that enrolled non-consecutive patients. Second, most risk scores were established in an era when the treatment strategy and patient characteristics were relatively different. Third, most of the published risk scores seldom contained patients from developing countries, especially in China.

Therefore, we aimed to develop and validate a novel in-hospital mortality risk model for patients with AMI from the Heart failure after Acute Myocardial Infarction with Optimal Treatment (HAMIOT) cohort in China. We also sought to build a simple risk score tool for in-hospital mortality that could be used prospectively for risk stratification.

MATERIALS AND METHODS

Study Population

With the support of National Key Research and Development Program of China, the HAMIOT cohort was a multicenter, prospective, observational cohort study that included consecutive patients with AMI in China[1] (NCT03297164). From December 2017 to December 2019, a total of 12,179 patients aged 18 years or older with symptoms or signs of ST-segment elevation or non-ST-segment elevation were enrolled, in which 136 patients were excluded because of prior chronic heart failure or tumors. The cohort was randomly assigned into the training (n = 8,431) and validation (n = 3,612) cohorts. The proportion was 7:3. The overall study design and flow chart were presented in **Figure 1**. The study was evaluated in an external validation cohort (n = 3,095), with prospectively enrolled patients with AMI in the Second Affiliated Hospital of Harbin Medical University from October 2019 to March 2021.

In this study, variables such as demographic characteristics, medical history, presentation with electrocardiogram and echocardiography findings, laboratory examinations, and treatment strategies were collected during hospitalization. ST-segment elevation myocardial infarction (STEMI) and non-ST-segment elevation myocardial infarction (NSTEMI) were defined according to the ESC guidelines (11, 12). The endpoint was in-hospital all-cause mortality in patients with AMI. The data was collected and the patients were interviewed by a group of trained clinical research coordinators, cardiologists and nurses through an electronic data collection platform.

The study protocol was approved by the ethics or institutional review board of the hospitals participating in the study, and all procedures were in accordance with the Declaration of Helsinki. Each eligible patient signed an informed consent form and agreed to a follow-up after discharge either through over the telephone, inpatient, or outpatient interview.

Statistical Methods

Generally, continuous variables were presented as median (25th and 75th percentiles), and were tested with the Student's t-test or the Mann–Whitney U test. Categorical variables were expressed as counts and percentages (%), and were compared using the Chi-square(χ^2) test or Fisher's exact test. The

[1]https://clinicaltrials.gov

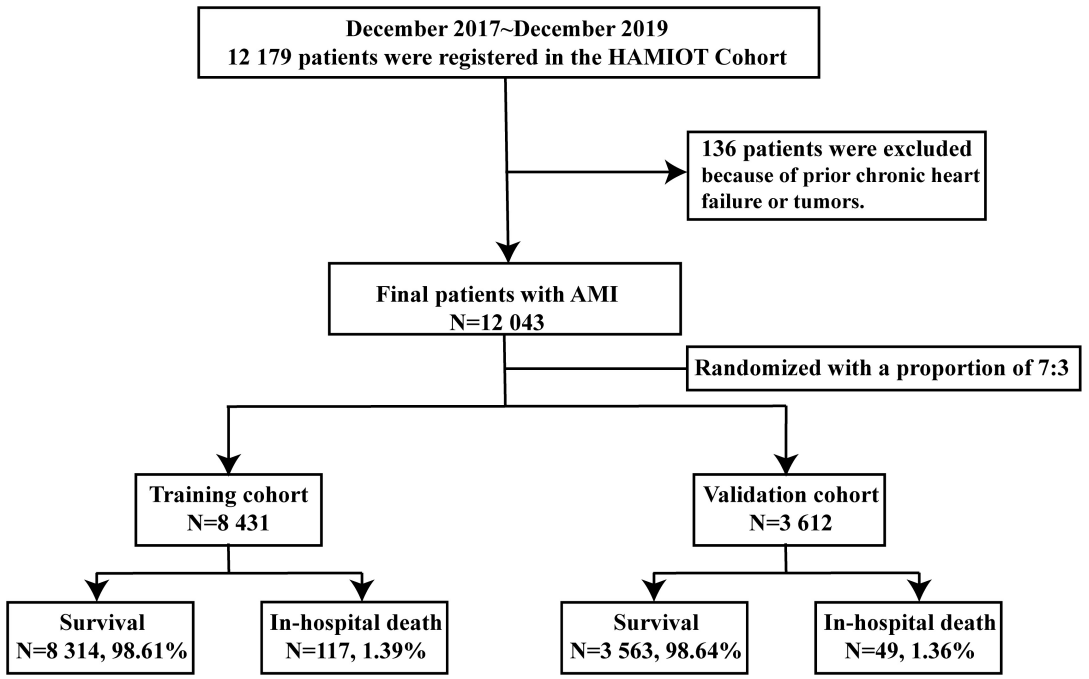

FIGURE 1 | Study flow chart of the HAMIOT Cohort Study. From December 2017 to December 2019, 12,043 patients with AMI were randomly assigned into the training (n = 8,431) and validation (n = 3,612) cohorts. HAMIOT, the Heart failure after Acute Myocardial Infarction with Optimal Treatment; AMI, acute myocardial infarction.

training and validation cohorts were randomly divided using the method of Proc Surveyselect in SAS 9.3 (SAS Institute, Cary, NC, United States).

The unadjusted associations between candidate variables and in-hospital mortality were analyzed using the univariate logistic regression model. Variables, presented as $P < 0.20$ in the univariate logistic regression analysis, were included in the multivariate logistic regression analysis, and they were then evaluated by the stepwise selection approach for model building. The final logistic regression model contained variables with P values < 0.05. The associations between the candidate risk predictors and in-hospital mortality were presented as odds ratios (ORs) with 95% confidence intervals (CIs).

A novel simplified risk score was developed according to the final logistic regression model. For continuous variables, stratification was performed using certain thresholds, and the simplified risk score was re-evaluated. In the final logistic regression model, continuous variables were age, heart rate, systolic blood pressure (SBP), initial serum creatinine level and initial N-terminal pro-B-type natriuretic peptide (NT-proBNP) level. They were categorized as: (1) age (<60, 60–70, 70–80, ≥80 years); (2) heart rate (<60, 60–100, ≥100 beats/min), (3) SBP (<100, 100–120, 120–140, 140–160, ≥160 mmHg), (4) initial serum creatinine level (<1.3, ≥1.3 mg/dL), and (5) initial NT-proBNP level (<125, 125–2,000, >2,000 pg/mL). The risk score of each predictor was calculated on the basis of the beta (β) coefficient of the re-evaluated model (20).

Discrimination and calibration were evaluated using the c-statistic or receiver operating characteristic (ROC) curve and the Hosmer–Lemeshow goodness-of-fit test, respectively. Internal validation was evaluated using the bootstrap techniques (1,000 replications) to obtain optimism corrected c-statistics (21). External validation of the HAMIOT risk score was assessed using a prospectively subsequent AMI cohort from the Second Affiliated Hospital of Harbin Medical university. In addition, the performance of the HAMIOT risk score was assessed in selected subgroups, including age (<60 vs. ≥60 years), sex (female vs. male), body mass index (BMI) (<25 vs. ≥25 kg/m^2), presentation with ST-segment elevation (STEMI vs. NSTEMI), current smoking (yes vs. no), history of stroke (yes vs. no), Killip class (I vs. II–IV), cardiac arrest (yes vs. no), and PCI treatment during hospitalization (yes vs. no). Moreover, the novel HAMIOT risk score was compared to the GRACE risk score in the training, validation and subgroup cohorts. Finally, we calculated the net reclassification improvement (NRI), which focused on the improvement that patients were appropriately assigned to different risk groups (low risk, score ≤ 50; intermediate risk, 50 < score ≤ 74; high risk, score > 74), and the integrated discrimination index (IDI), which evaluated how well the HAMIOT risk score increased prognostic accuracy (22).

The initial NT-proBNP level and cardiac enzymes were normalized using $\log_{10}$ transformation. The missing values of some prognostic variables were simply arranged according to the corresponding median or mode values. All statistical analysis were performed using the SAS 9.3 or R (version 4.1.0) software. All reported P-values were based on two-sided tests, and statistical significance was set at $P < 0.05$.

TABLE 1 | Characteristics of baseline in the training and validation cohorts.

Variables	All population	Training cohort	Validation cohort
Number of patients	12,043	8,431	3,612
Demographic characteristics			
Age, years	62.33(53.84,69.58)	62.21(53.60,69.48)	62.59(54.28,69.76)
Sex			
Male	8,758(72.72%)	6,172(73.21%)	2,586(71.59%)
Female	3,285(27.28%)	2,259(26.79%)	1,026(28.41%)
BMI, kg/m^2	24.74(22.83,27.04)	24.77(22.84,27.05)	24.54(22.74,27.04)
Medical history			
Current smoking	4,952(41.12%)	3,482(41.30%)	1,470(40.70%)
History of diabetes	2,890(24.00%)	2,091(24.80%)	799(22.12%)
History of hypertension	6,167(51.21%)	4,340(51.48%)	1,827(50.58%)
History of CABG	51(0.42%)	40(0.47%)	11(0.30%)
History of PCI	781(6.49%)	542(6.43%)	239(6.62%)
History of stroke	1,634(13.57%)	1,109(13.15%)	525(14.53%)
Presentation characteristics			
Presentation with STEMI			
STEMI	8,434(70.03%)	5,913(70.13%)	2,521(69.80%)
NSTEMI	3,609(29.97%)	2,518(29.87%)	1,091(30.20%)
SBP, mmHg	130(116.00,148.00)	130(116.00,148.00)	130(116.00,149.00)
DBP, mmHg	80(70.00,90.00)	80(70.00,90.00)	80(70.00,90.00)
Heart rate, beats/min	75(65.00,86.00)	75(65.00,86.00)	75(65.00,87.00)
LVEF, %	58(50.00,62.00)	58(50.00,62.00)	58(50.00,62.00)
Cardiac arrest	105(0.87%)	76(0.9%)	29 (0.8%)
Killip class			
I	8,468(92.92%)	5,950(93.13%)	2,518(92.44%)
II–IV	645(7.08%)	439(6.87%)	206(7.56%)
Laboratory examinations			
White blood cell, $10^9/L$	9.8(7.82,12.20)	9.77(7.81,12.20)	9.81(7.84,12.19)
Red blood cell, $10^9/L$	4.62(4.24,5.00)	4.63(4.24,5.01)	4.6(4.23,4.98)
Hemoglobin, g/L	144(131.00,156.00)	144(131.00,156.00)	143(131.00,156.00)
Urea, mmol/L	5.60(4.54,6.90)	5.58(4.50,6.93)	5.64(4.60,6.90)
Serum creatinine, mg/dL	0.86(0.74,1.03)	0.86(0.74,1.03)	0.87(0.74,1.03)
ALT, U/L	27(18.00,42.00)	27(18.00,42.70)	26(17.00,42.00)
AST, U/L	47(25.50,117.00)	47(25.40,119.00)	47(25.80,113.20)
TG, mmol/L	1.46(1.03,2.11)	1.47(1.04,2.11)	1.45(1.01,2.09)
TC, mmol/L	4.53(3.86,5.26)	4.53(3.86,5.26)	4.52(3.88,5.27)
HDL-C, mmol/L	1.10(0.92,1.35)	1.10(0.92,1.34)	1.11(0.93,1.37)
LDL-C, mmol/L	2.72(2.09,3.39)	2.72(2.09,3.40)	2.71(2.09,3.38)
Fasting blood glucose, mg/dL	6.36(5.28,8.39)	6.38(5.29,8.44)	6.30(5.25,8.29)
NT-proBNP, pg/mL	602.15(180.00,1611.00)	606(182.00,1609.00)	598.6(173.00,1636.00)
CK, U/L	251(108.00,773.80)	248.5(107.00,778.00)	254(110.00,764.00)
CKMB, ng/mL	10.10(2.50,51.60)	10.20(2.50,51.60)	10.00(2.50,51.51)
cTn I, μg/L	1.98(0.28,11.60)	1.95(0.28,11.14)	2.05(0.30,12.60)
Treatment during hospitalization			
Aspirin	11,151(92.59%)	7,795(92.46%)	3,356(92.91%)
Clopidogrel/Ticagrelor	11,206(93.05%)	7,834(92.92%)	3,372(93.36%)
Statins	11,120(92.34%)	7,761(92.05%)	3,359(93.00%)
Absence of PCI treatment	3,356(27.87%)	2,337(27.72%)	1,019(28.21%)
Primary endpoint			
In-hospital mortality	166(1.38%)	117(1.39%)	49(1.36%)

Continuous variables were presented as median (Q1, Q3 quantiles), and categorical variables were presented as number (%). BMI, body mass index; CABG, coronary artery bypass graft; PCI, percutaneous coronary intervention; STEMI, ST-segment elevation myocardial infarction; NSTEMI, non-ST-segment elevation myocardial infarction; SBP, systolic blood pressure; DBP, diastolic blood pressure; LVEF, left ventricular ejection fraction; ALT, alanine transaminase; AST, aspartate aminotransferase; TG, triglyceride; TC, total cholesterol; HDL-C, high-density lipoprotein cholesterol; LDL-C, low-density lipoprotein cholesterol; NT-proBNP, N-terminal pro-B-type natriuretic peptide; CK, creatine kinase; CK-MB, creatine kinase-MB; cTn I, cardiac troponin I.

TABLE 2 | Univariate analysis between baseline characteristics (continuous variables) and in-hospital mortality in the training cohort.

Variables	Patients alive	Patients died	OR (95%CI)	*P*-value
Number of patients	8,314	117	–	–
Age, years	62.06(53.50,69.30)	73.63(66.03,80.72)	1.11(1.08,1.13)	<0.01
BMI, kg/m^2	24.79(22.86,27.06)	23.55(21.88,26.12)	0.93(0.88,0.98)	0.01
SBP, mmHg	130(116.00,148.00)	122(106.00,140.00)	0.98(0.98,0.99)	<0.01
DBP, mmHg	80(70.00,90.00)	77(65.50,85.00)	0.98(0.97,0.99)	<0.01
Heart rate, beats/min	75(65.00,86.00)	83(68.00,98.00)	1.02(1.01,1.03)	<0.01
LVEF,%	58(50.00,62.00)	46.4(40.00,57.00)	0.95(0.93,0.96)	<0.01
WBC, 10^9/L	9.76(7.81,12.18)	10.35(7.90,14.15)	1.06(1.02,1.1)	<0.01
RBC, 10^9/L	4.64(4.25,5.01)	4.29(3.92,4.64)	0.4(0.3,0.53)	<0.01
Hemoglobin, g/L	145(131.50,157.00)	133(123.00,148.00)	0.99(0.98,1)	0.02
Urea, mmol/L	5.57(4.50,6.90)	7.4(5.33,9.12)	1.00(1.00,1.01)	0.23
Serum creatinine, mg/dL	0.86(0.74,1.02)	0.96(0.76,1.36)	1.83(1.53,2.18)	<0.01
ALT, U/L	27(18.00,42.00)	37.65(21.00,61.00)	1.03(1.02, 1.04)‡	<0.01
AST, U/L	46.3(25.00,117.00)	86(37.00,222.30)	1.02(1.01, 1.03)‡	<0.01
TG, mmol/L	1.47(1.04,2.12)	1.35(1.02,1.84)	0.72(0.56,0.94)	0.01
TC, mmol/L	4.54(3.86,5.26)	4.23(3.41,4.89)	0.79(0.65,0.96)	0.02
HDL-C, mmol/L	1.10(0.92,1.34)	1.07(0.85,1.37)	0.55(0.32,0.95)	0.03
LDL-C, mmol/L	2.72(2.09,3.40)	2.54(1.92,3.26)	0.87(0.70,1.07)	0.17
Fasting blood glucose, mg/dL	6.37(5.29,8.42)	7.49(6.10,11.04)	1.09(1.05,1.14)	<0.01
NT-proBNP, pg/mL	592(180.00,1564.93)	3600(1377.00,9080.00)	2.16(1.87,2.49)*	<0.01
CK, U/L	245(107.00,769.00)	508(186.00,1725.00)	2.28(1.59,3.27)*	<0.01
CKMB, ng/mL	10(2.50,50.90)	29(8.20,181.80)	2.06(1.42, 2.97)*	<0.01
cTn I, μg/L	1.9(0.27,11.00)	5.77(1.08,29.53)	1.44(1.17,1.77)*	<0.01

‡*Odds ratio of per-10 unit increase with 95% confidence interval.*
**Odds ratio of log$_{10}$ transformation with 95% confidence interval.*
OR, odds ratio; other abbreviations are in ***Table 1****.*

RESULTS

Baseline Characteristic

From December 2017 to December 2019, a total of 12,179 patients with AMI (STEMI and NSTEMI) participated in the HAMIOT cohort. Among them, 136 patients were excluded because of prior chronic heart failure or tumors. In total, our study consisted of 12,043 eligible patients with AMI. The in-hospital mortality rate of these patients was 166 (1.38%). The median age was 62 years, 73% were male, and 70% presented with ST-segment elevation. The patients were randomly divided into the training (n = 8,431) and validation (n = 3,612) cohorts with in-hospital mortalities of 117 (1.39%) and 49 (1.36%), respectively. Demographic characteristics, medical history, presentation characteristics, laboratory examination results, medication and PCI treatment during hospitalization were described in **Table 1**. There were no significant differences between the training and validation cohorts (each $P > 0.05$).

The external validation cohort contained 3,095 independent patients with AMI from the Second Affiliated Hospital of Harbin Medical University. Among them, 32 (1.03%) patients died in the hospital. Baseline characteristics were provided in **Supplementary Material** (**Supplementary Table 1**).

Predictors of In-Hospital Mortality

In the training cohort, the association between each baseline characteristic and in-hospital mortality was analyzed using the univariate logistic regression model and was presented in **Table 2** (for continuous variables) and **Table 3** (for categorical variables). Patients who died in the hospital were more likely to be old, female, and had an elevated heart rate, low SBP and diastolic blood pressure, high incidence of previous diseases (diabetes, hypertension, coronary artery bypass graft, PCI treatment, and stroke), low rate of treatment with medication (aspirin, clopidogrel or ticagrelor, and statins) and PCI treatment (each $P < 0.05$). For laboratory findings, alanine transaminase, aspartate aminotransferase, and fasting plasma glucose were higher, and triglyceride, total cholesterol, and high-density lipoprotein cholesterol were lower in dead patients compared to survival patients (each $P < 0.05$). The initial levels of serum creatinine, NT-proBNP and cardiac enzymes (creatine kinase, creatine kinase-MB and cardiac troponin I) were high in the non-survival patients (each $P < 0.05$).

In the multivariate logistic regression analysis, variables presented as $P < 0.20$ in the univariate analysis (**Tables 2**, **3**) were included. Ten predictors were found to be independently associated with in-hospital mortality: age, sex, history of PCI treatment, history of stroke, presentation with ST-segment elevation, heart rate, SBP, initial serum creatinine level, initial NT-proBNP level, and PCI treatment. The results of the multivariate logistic regression analyses were displayed in **Figure 2**. The performance of discrimination and calibration were 0.88 (c-statistic) and $P = 0.16$ (Hosmer–Lemeshow goodness-of-fit test), respectively.

TABLE 3 | Univariate analysis between baseline characteristics (categorical variables) and in-hospital mortality in the training cohort.

Variables		n	In-hospital mortality,%	OR (95%CI)	*P*-value
Demographic characteristics					
Sex	Male	6172	0.97	Ref	Ref
	Female	2259	2.52	2.64(1.83, 3.80)	<0.01
Medical history					
Current smoking	No	4949	1.72	Ref	Ref
	Yes	3482	0.92	0.53(0.35,0.8)	0.02
History of diabetes	No	6340	1.21	Ref	Ref
	Yes	2091	1.91	1.59(1.08,2.33)	0.02
History of hypertension	No	4091	1.08	Ref	Ref
	Yes	4340	1.68	1.57(1.08,2.29)	0.02
History of CABG	No	8391	1.37	Ref	Ref
	Yes	40	5	3.79(0.9,15.89)	0.07
History of PCI	No	7889	1.24	Ref	Ref
	Yes	542	3.51	2.89(1.75,4.76)	<0.01
History of stroke	No	7322	1.22	Ref	Ref
	Yes	1109	2.52	2.11(1.37,3.23)	0.01
Presentation characteristics					
Presentation with STEMI	NSTEMI	2518	1.11	Ref	Ref
	STEMI	5913	1.51	1.36(0.89, 2.08)	0.16
Cardiac arrest	No	8355	1.38	Ref	Ref
	Yes	76	2.63	0.94(0.47,7.99)	0.36
Killip class	I	5950	1.46	Ref	Ref
	II–IV	439	4.33	3.05(1.84,5.06)	<0.01
Treatment during hospitalization					
Aspirin	No	636	3.3	Ref	Rref
	Yes	7795	1.23	0.37(0.23,0.59)	<0.01
Clopidogrel/Ticagrelor	No	597	3.18	Ref	Ref
	Yes	7834	1.25	0.39(0.23,0.63)	<0.01
Statins	No	670	2.84	Ref	Ref
	Yes	7761	1.26	0.44(0.27,0.72)	0.01
Absence of PCI treatment	No	6094	0.64	Ref	Ref
	Yes	2337	3.34	5.36(3.64,7.90)	<0.01

*Abbreviations are in **Tables 1, 2**.*

HAMIOT Risk Score

The novel HAMIOT risk score compromised predictors identified in the multivariate logistic regression model and was re-evaluated by categorical predictors, including age, heart rate, SBP, initial serum creatinine level and initial NT-proBNP level. The score of each predictor was built on the basis of estimated β coefficient parameter. The results with simple inter score were shown in **Figure 3A**. The c-statistic of the simplified HAMIOT risk score was 0.88. **Figure 3B** showed the distribution of individual scores along with the relationship between the patient risk score and the probability of in-hospital mortality in the training cohort. **Figure 3C** presented the corresponding relationship between the observed and expected in-hospital mortality across deciles of risk, in which the Hosmer–Lemeshow goodness-of-fit test was $P = 0.35$.

Discrimination of the HAMIOT risk score was validated both internally and externally. The new simplified risk score was validated in the validation cohort (n = 3,612), and the discrimination ability was 0.82 with good calibration ($P = 0.64$). Internal validation was also evaluated using bootstrap techniques (1,000 replications) to obtain the optimism corrected c-statistic, which was 0.85. The discrimination ability was 0.82 (c-statistic) in the external validation cohort, and the ROC curve was presented in **Supplementary Figure 1**. In addition, the c-statistic values of the selected subgroups were calculated, and they performed well, as seen in **Table 4**.

Furthermore, the total risk score of the established HAMIOT risk score model ranged from 0 to 121. The novel HAMIOT risk score of in-hospital mortality was stratified into three risk groups: low risk(score $\leq$ 50); intermediate risk(50<score $\leq$ 74); and high risk(score $>$ 74). **Figure 3D** described the observed in-hospital mortality across each risk group in the HAMIOT and external cohorts. The observed in-hospital mortality rates were 0.35, 3.09, and 14.29% in the HAMIOT cohort, and 0.31, 2.21, and 11.39% in the external cohort, respectively.

Comparision With Grace Risk Score

Compared with the GRACE risk score, the c-statistic of the HAMIOT risk score was 0.88 vs. 0.81 (**Figure 4A**) in the training cohort and 0.82 vs. 0.72 (**Figure 4B**) in the validation cohort,

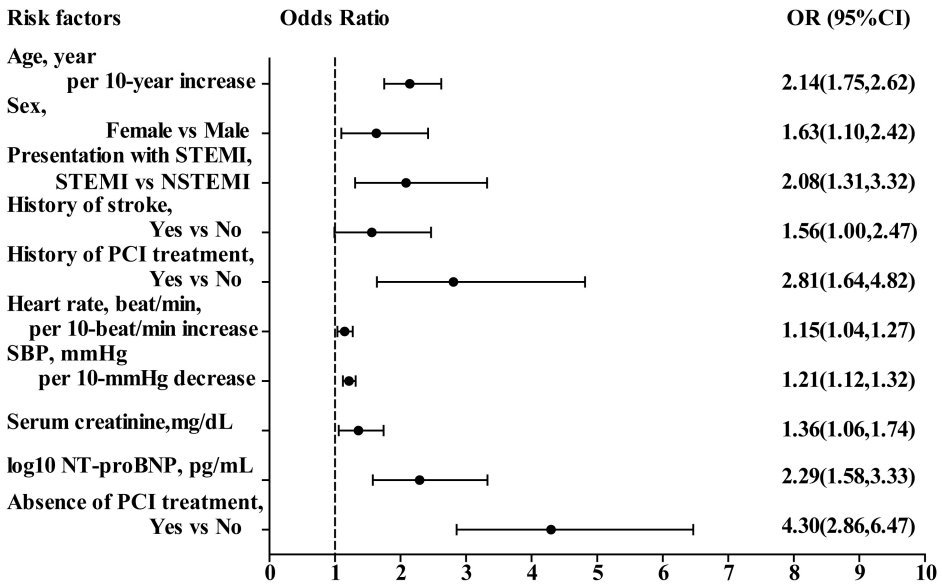

FIGURE 2 | Odds ratio of in-hospital mortality in multivariate logistic regression model. OR, odds ratio; CI, confidence interval; STEMI, ST-segment elevation myocardial infarction; NSTEMI, non-ST-segment elevation myocardial infarction; SBP, systolic blood pressure; NT-proBNP, N-terminal pro-B-type natriuretic peptide; PCI, percutaneous coronary intervention.

presenting a significantly improved discrimination ability. The improved reclassification and discrimination were evaluated using NRI and IDI, and they were 30.81 and 4.9% (each $P < 0.01$), respectively. For subgroups, such as age (≥60 years), presentation with STEMI, BMI (<25 kg/m^2), absence of previous stroke, Killip class(I level), and presentation without cardiac arrest, the c-statistic values were higher than the GRACE risk score (each $P < 0.05$). The other subgroups presented comparable discrimination ability with the GRACE risk score.

DISCUSSION

The present study extended clinical understanding of AMI risk and provided a novel simplified HAMIOT risk score of in-hospital mortality of 12,043 consecutive patients with AMI in China. The main findings were as follows: (1) Ten independent predictors were found in the final logistic regression model that include age, sex, history of PCI treatment, history of stroke, presentation with STEMI, heart rate, SBP, initial serum creatinine level, initial NT-proBNP level and PCI treatment during hospitalization; (2) The novel HAMIOT risk score was established to predict in-hospital mortality and showed excellent discrimination and calibration ability; (3) Similar discrimination capacity was found in the validation cohorts (internal and external), and in various important clinical subgroups, such as age, sex, BMI, presentation with STEMI, current smoking, history of stroke, Killip class, cardiac arrest, and PCI treatment during hospitalization; (4) The new simplified risk score model improved discrimination ability compared with the GRACE score and provided a clinically convenient risk stratification tool for future patients with AMI.

Several risk score models have been developed to predict in-hospital mortality and have presented excellent performance of risk stratification in patients with ACS/AMI. Among them, the GRACE risk score (2) has been extensively recommended and used in clinical practice. The GRACE risk score was derived from an international registry of non-consecutive patients with ACS from 1999 to 2001, and the in-hospital mortality was 4.6%, which was higher than the mortality of 1.6% in the HAMIOT cohort. There were several reasons for the low mortality rates in this study. First, the GRACE registry was performed nearly 20 years earlier, and the treatment strategy, such as PCI treatment, was relatively less frequently used (less than 30%) (23) than in the HAMIOT cohort (72.13%). Second, the risk factors of the population with AMI included in the HAMIOT cohort have changed over time. Compared with the GRACE cohort, patients in our study were younger, had fewer females and smokers, and had higher incidence of previous diseases (diabetes, hypertension, PCI, and coronary artery bypass graft). Third, the contributing hospitals participating in the HAMIOT cohort tended to be chest pain centers. Fan et al. (24) and Sun et al. (25) reported that chest pain center accreditation presented a higher PCI treatment rate and a low short term all-cause mortality in patients with AMI in China. Thus, with the low mortality rate and different risk factors, an updated risk score is necessary for the current clinical practice.

The HAMIOT risk score contained 10 independent predictors, including age, sex, history of PCI treatment, history of stroke, presentation with STEMI, heart rate, SBP, initial serum creatinine level, initial NT-proBNP level and PCI treatment). Among the variables, age, heart rate, serum creatinine, and SBP were mainly confirmed in some risk scores (2, 4, 6, 8). There were initially six new predictors included in the HAMIOT risk score: sex, history of PCI treatment or stroke, presentation with STEMI,

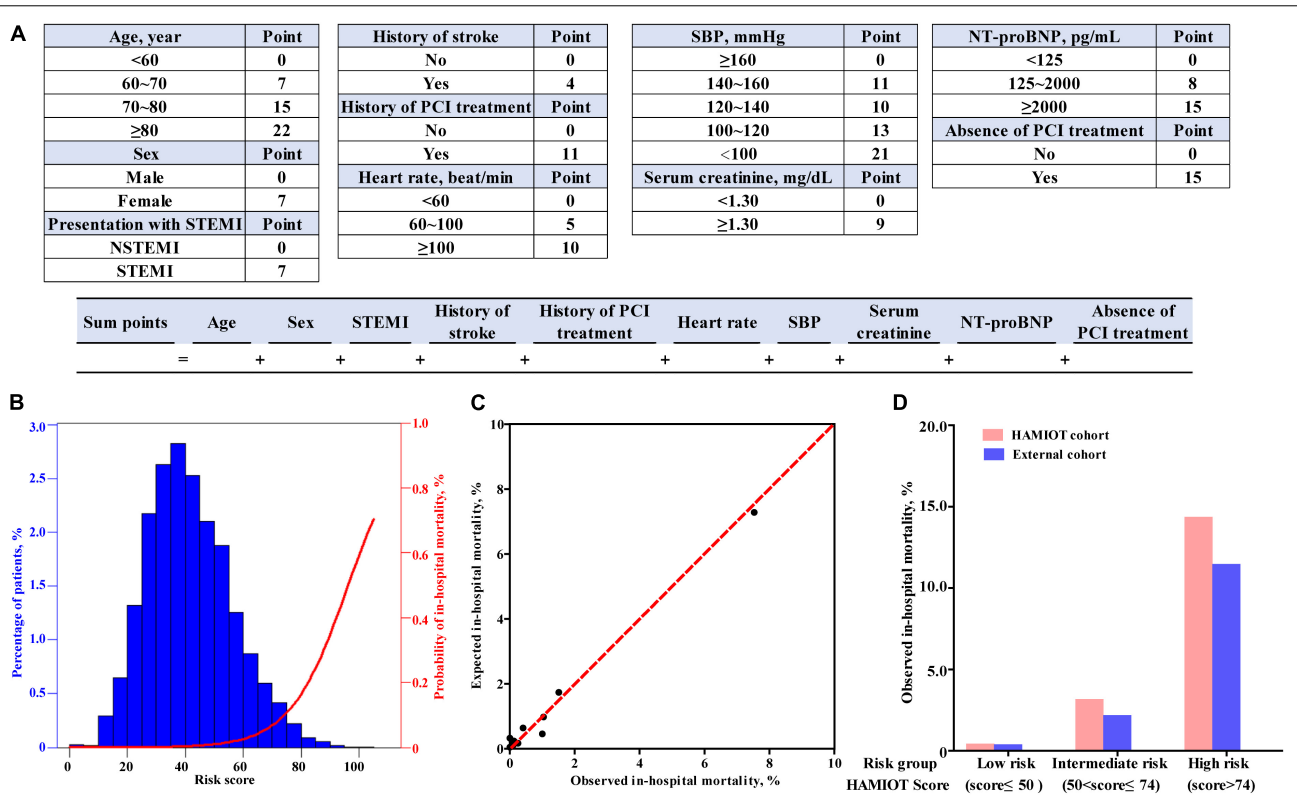

FIGURE 3 | (A) Risk score calculator of in-hospital mortality for patients with AMI. **(B)** Distribution of HAMIOT risk score and the probability of in-hospital mortality. **(C)** Relationship between the observed and expected in-hospital mortality across deciles of risk. **(D)** Observed in-hospital mortality of HAMIOT cohort and external cohort stratified by three risk groups (low risk, intermediate risk, and high risk groups). The observed in-hospital mortality rates were 0.35, 3.09, and 14.29% in the HAMIOT cohort, and 0.31, 2.21, and 11.39% in the external cohort, respectively. HAMIOT, the Heart failure after Acute Myocardial Infarction with Optimal Treatment, STEMI, ST-segment elevation myocardial infarction; NSTEMI, non-ST-segment elevation myocardial infarction; SBP, systolic blood pressure; NT-proBNP, N-terminal pro-B-type natriuretic peptide; PCI, percutaneous coronary intervention.

initial NT-proBNP level and absence of PCI treatment during hospitalization.

For sex, female patients with AMI had been demonstrated to have a higher risk of short-term and long-term mortality than male patients in previous studies (26–30); however, the adjusted risk between sex and mortality was not clear. In our study, females had a higher in-hospital mortality risk than males (2.52 vs. 0.97%), and the OR was 1.63(1.10, 2.42) after adjustment for other predictors. This means that the risk of death was increased by 63% in female patients compared to male patients. In our study, we found that patients with previous diseases (diabetes, hypertension, coronary artery bypass graft, PCI or stroke), presented with high in-hospital mortality. Among them, patients with previous PCI treatment or stroke had an increased risk of death by 81 and 56%, respectively. For patients with STEMI, risk was not found for the presence of ST-segment elevation at the time of presentation in the GRACE risk score (2). However, the ACTION Registry–GWTG mortality risk model (6) reported that patients with STEMI had an approximately 80% higher risk than patients with NSTEMI. Considering the inconsistency of risks, patients with ST-segment elevation were considered in our study. In the univariate analysis, in-hospital mortality rates of patients with STEMI and NSTEMI were similar (1.51 and 1.11%, respectively). However, the association between STEMI and mortality was 2.08 (1.31, 3.32) in the multivariate analysis, presenting a 2.08-fold increased risk. The increased initial NT-proBNP level had proven to be an important predictor of early and late mortality (31), and has been recommended as a prognostic indication of death and heart failure (14, 32). The association between $\log_{10}$(NT-proBNP) and in-hospital mortality in our study was presented as 2.16 (1.87, 2.49) in the univariate analysis and 2.29 (1.58, 3.33) in the multivariate analysis. PCI has been widely proven and recommended for patients with AMI (13, 14), and some risk models of long-term mortality have been established and validated for patients with ACS undergoing PCI treatment (33, 34). While PCI treatment has an obvious benefit for patient with AMI, risk models rarely considered it a predictor of in-hospital mortality. Moreover, the proportion of PCI treatment was relatively low (50%) for patients with AMI in China (25), which could lead to serious outcomes, such as cardiac arrest or even death in hospital. In our study, the absence of PCI treatment was included, and the in-hospital mortality between the absence and presence of the PCI treatment were 3.34 and 0.64%, respectively. The adjusted OR was 4.30 (2.86, 6.47), showing a 4.3-fold increased risk of death. Other factors known

TABLE 4 | The performance of discrimination ability in the subgroups between the HAMIOT risk score and GRACE risk score.

Subgroups	Training cohort			Validation cohort			All patients		
	n	GRACE	HAMIOT	n	GRACE	HAMIOT	n	GRACE	HAMIOT
Age, years									
~60	3600	0.88	0.84	1485	0.57	0.81	5085	0.8	0.84
60~	4831	0.72	0.85*	2127	0.65	0.77*	6958	0.7	0.83*
Sex									
Male	2259	0.7	0.83*	1026	0.68	0.75	3285	0.7	0.81*
Female	6172	0.86	0.89	2586	0.72	0.85*	8758	0.81	0.88*
Presentation with STEMI									
STEMI	5913	0.8	0.88*	2521	0.73	0.81*	8434	0.78	0.86*
NSTEMI	2518	0.83	0.87	1091	0.72	0.81	3609	0.81	0.85
BMI, kg/m^2									
<25	4554	0.76	0.86*	2024	0.72	0.83*	6578	0.75	0.85*
≥25	3877	0.86	0.89	1588	0.71	0.79	5465	0.82	0.86
Current smoking									
No	4949	0.77	0.85*	2142	0.72	0.78	7091	0.75	0.83*
Yes	3482	0.86	0.92	1470	0.66	0.89*	4952	0.82	0.91*
History of stroke									
No	7322	0.81	0.88*	3087	0.72	0.82*	10409	0.79	0.87*
Yes	1109	0.76	0.81	525	0.7	0.76	1634	0.74	0.8
Killip class									
I	5950	0.79	0.88*	2518	0.65	0.77*	8468	0.75	0.85*
II–IV	439	0.75	0.79	206	0.82	0.79	645	0.78	0.79
Cardiac arrest									
No	8355	0.81	0.87*	3583	0.72	0.82*	11938	0.78	0.86*
Yes	76	0.97	0.98	29	0.84	0.89	105	0.94	0.96
PCI treatment during hospitalization									
No	2337	0.8	0.84	1019	0.72	0.78	3356	0.78	0.82*
Yes	6094	0.78	0.83	2593	0.71	0.79	8687	0.76	0.82*

*Abbreviations are in **Tables 1**, **2**. *P < 0.05 between the HAMIOT risk score vs the GRACE risk score.*

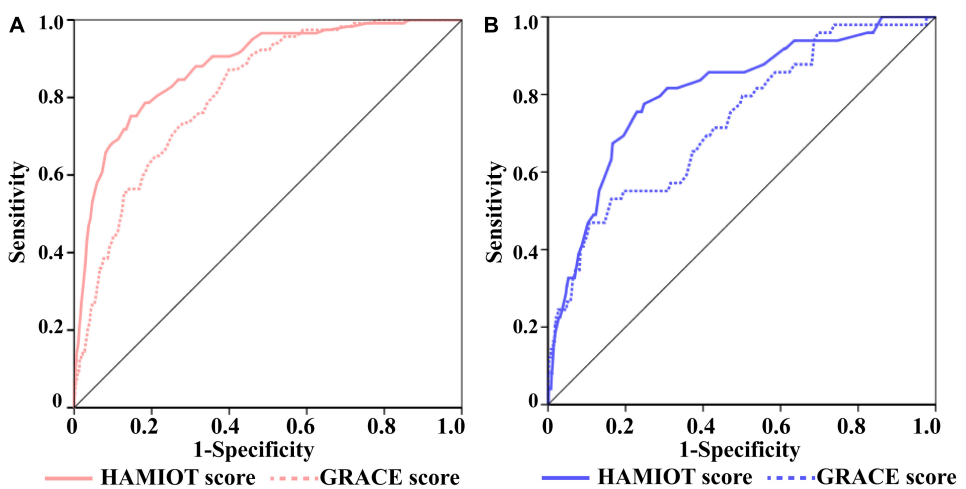

FIGURE 4 | The ROC Curves of the HAMIOT and the GRACE risk score. **(A)** In the training cohort, the c-statistic in the HAMIOT score 0.88(0.84,0.91) was higher than the GRACE score 0.81(0.77,0.84). **(B)** In the validation cohort, the c-statistic in the HAMIOT score 0.82(0.76,0.88) was higher than the GRACE 0.72(0.65,0.8). HAMIOT, the Heart failure after Acute Myocardial Infarction with Optimal Treatment; GRACE, the Global Registry of Acute Coronary Events; ROC, receiver operating characteristic.

to be associated with in-hospital mortality, including Killip class and cardiac arrest (2–4, 8, 11), were considered in the logistic regression model, but hardly contributed to in-hospital mortality.

The simplified HAMIOT risk score presented excellent discrimination and calibration, and it was better than the GRACE risk score in the training and validation (internal and external) cohorts. The c-statistic was comparable to other risk scores in patients with AMI (2, 4, 6, 10). In our study, the HAMIOT risk score had higher c-statistic values compared with the Simplified CAMI-NSTEMI and CCC-ACS scores which were built based on Chinese patients with AMI in the HAMIOT cohort (training cohort: 0.88 vs. 0.72, 0.88 vs. 0.82; validation cohort: 0.82 vs. 0.74, 0.82 vs. 0.78). Moreover, the simplified risk score performed well in several subgroups, especially in patients with smoking or cardiac arrest (the Harrel's c-statistics were higher than 0.90). Besides, the c-statistic in the novel risk score was better than the GRACE risk score, especially in some subgroups (older, presentation with STEMI, normal BMI index, absence of previous stroke, I level of Killip class and presentation without cardiac arrest). Thus, the novel HAMIOT risk score may be more useful to predict in-hospital mortality.

Study Limitations

Although the HAMIOT risk score is a novel and practical tool that can stratify the risk of in-hospital mortality in patients with AMI, it has several limitations. First, the HAMIOT score was based on Chinese population, whether it can be applied to other ethnicities needs further validation. Second, although we validated our risk score model in the validation and an independent prospective external cohort, the HAMIOT risk score needs to be verified in large cohorts. Third, patients with a history of chronic heart failure were excluded from our study, clinicians should take special caution when applying these results to these patients. Fourth, since the HAMIOT risk score only assessed in-hospital mortality, long-term mortality risk predictors should be further studied.

CONCLUSION

In conclusion, the HAMIOT risk score demonstrated that the risk of in-hospital mortality in patients with AMI could be reliably predicted using 10 highly predictive variables. All of these variables could be easily obtained during hospitalization. Since the novel risk score tool is simple and easy to calculate, clinicians can rapidly apply to predict the risk of mortality and to provide the correct therapies or management strategies.

DATA AVAILABILITY STATEMENT

The original contributions presented in the study are included in the article/**Supplementary Material**, further inquiries can be directed to the corresponding authors.

ETHICS STATEMENT

The studies involving human participants were reviewed and approved by the Ethics Committee of the Second Affiliated Hospital of Harbin Medical University. The patients/participants provided their written informed consent to participate in this study.

AUTHOR CONTRIBUTIONS

LlL contributed to the conception, design and statistical analyses of the study. XZ, YW, XY, CL, WZ, WY, BL, LxL, and NT screened for eligible patients and conducted the data acquisition of the cohort. HJ and JH contributed to the critical manuscript revision. BY and KL were substantial contribution to the design of research and critical manuscript revision. All authors contributed to manuscript revision, and they have read and approved the submitted version.

FUNDING

This work was supported by National Key Research and Development Program of China (2016YFC1301100).

ACKNOWLEDGMENTS

We sincerely thank all colleagues and patients who participated in this study.

SUPPLEMENTARY MATERIAL

The Supplementary Material for this article can be found online at: https://www.frontiersin.org/articles/10.3389/fcvm.2022.840485/full#supplementary-material

REFERENCES

1. Ma L, Chen W, Gao R, Liu L, Zhu M, Wang Y, et al. China cardiovascular diseases report 2018: an updated summary. *J Geriatr Cardiol.* (2020) 17:1–8. doi: 10.11909/j.issn.1671-5411.2020.01.001
2. Granger CB, Goldberg RJ, Dabbous O, Pieper KS, Eagle KA, Cannon CP, et al. Predictors of hospital mortality in the global registry of acute coronary events. *Arch Intern Med.* (2003) 163:2345–53. doi: 10.1001/archinte.163.19.2345
3. Kurz DJ, Bernstein A, Hunt K, Radovanovic D, Erne P, Siudak Z, et al. Simple point-of-care risk stratification in acute coronary syndromes: the amis model. *Heart.* (2008) 95:662–8. doi: 10.1136/hrt.2008.145904
4. Chin CT, Chen AY, Wang TY, Alexander KP, Mathews R, Rumsfeld JS, et al. Risk adjustment for in-hospital mortality of contemporary patients with acute myocardial infarction: the acute coronary treatment and intervention outcomes network (action) registry® –get with the guidelines (gwtg)™ acute

myocardial infarction mortality model and risk score. *Am Heart J.* (2011) 161:113–22. doi: 10.1016/j.ahj.2010.10.004
5. AlFaleh HF, Alsheikh-Ali AA, Ullah A, AlHabib KF, Hersi A, Suwaidi JA, et al. Validation of the canada acute coronary syndrome risk score for hospital mortality in the gulf registry of acute coronary events-2. *Clin Cardiol.* (2015) 38:542–7. doi: 10.1002/clc.22446
6. McNamara RL, Kennedy KF, Cohen DJ, Diercks DB, Moscucci M, Ramee S, et al. Predicting in-hospital mortality in patients with acute myocardial infarction. *J Am Coll Cardiol.* (2016) 68:626–35. doi: 10.1016/j.jacc.2016.05.049
7. Qi Y, Wang W, Zhang K, An S, Wang S, Zheng J, et al. Development and validation of women acute myocardial infarction in-hospital mortality score (wami score). *Int J Cardiol.* (2018) 259:31–9. doi: 10.1016/j.ijcard.2017.12.010
8. Song C, Fu R, Dou K, Yang J, Xu H, Gao X, et al. The cami-score: a novel tool derived from cami registry to predict in-hospital death among acute myocardial infarction patients. *Sci Rep.* (2018) 8:9082. doi: 10.1038/s41598-018-26861-z
9. Song C, Fu R, Li S, Yang J, Wang Y, Xu H, et al. Simple risk score based on the china acute myocardial infarction registry for predicting in-hospital mortality among patients with non-st-segment elevation myocardial infarction: results of a prospective observational cohort study. *Bmj Open.* (2019) 9:e30772. doi: 10.1136/bmjopen-2019-030772
10. Ran P, Yang J, Li J, Li G, Wang Y, Qiu J, et al. A risk score to predict in-hospital mortality in patients with acute coronary syndrome at early medical contact: results from the improving care for cardiovascular disease in china-acute coronary syndrome (ccc-acs) project. *Ann Transl Med.* (2021) 9:167. doi: 10.21037/atm-21-31
11. Huynh T, Kouz S, Yan A, Danchin N, Loughlin JO, Schampaert E, et al. Canada acute coronary syndrome risk score: a new risk score for early prognostication in acute coronary syndromes. *Am Heart J.* (2013) 166:58–63. doi: 10.1016/j.ahj.2013.03.023
12. Morrow DA, Antman EM, Charlesworth A, Cairns R, Murphy SA, de Lemos JA, et al. Timi risk score for st-elevation myocardial infarction: a convenient, bedside, clinical score for risk assessment at presentation: an intravenous npa for treatment of infarcting myocardium early ii trial substudy. *Circulation.* (2000) 102:2031–7. doi: 10.1161/01.cir.102.17.2031
13. Ibanez B, James S, Agewall S, Antunes MJ, Bucciarelli-Ducci C, Bueno H, et al. 2017 esc guidelines for the management of acute myocardial infarction in patients presenting with st-segment elevation. *Eur Heart J.* (2018) 39:119–77. doi: 10.1093/eurheartj/ehx393
14. Collet J, Thiele H, Barbato E, Barthélémy O, Bauersachs J, Bhatt DL, et al. 2020 esc guidelines for the management of acute coronary syndromes in patients presenting without persistent st-segment elevation. *Eur Heart J.* (2021) 42:1289–367. doi: 10.1093/eurheartj/ehaa575
15. Jneid H, Addison D, Bhatt DL, Fonarow GC, Gokak S, Grady KL, et al. 2017 aha/acc clinical performance and quality measures for adults with st-elevation and non-st-elevation myocardial infarction. *J Am Coll Cardiol.* (2017) 70:2048–90. doi: 10.1016/j.jacc.2017.06.032
16. Bueno H, Fernández-Avilés F. Use of risk scores in acute coronary syndromes. *Heart.* (2011) 98:162–8. doi: 10.1136/heartjnl-2011-300129
17. D'Ascenzo F, Biondi-Zoccai G, Moretti C, Bollati M, Omedè P, Sciuto F, et al. Timi, grace and alternative risk scores in acute coronary syndromes: a meta-analysis of 40 derivation studies on 216,552 patients and of 42 validation studies on 31,625 patients. *Contemp Clin Trials.* (2012) 33:507–14. doi: 10.1016/j.cct.2012.01.001
18. Bawamia B, Mehran R, Qiu W, Kunadian V. Risk scores in acute coronary syndrome and percutaneous coronary intervention: a review. *Am Heart J.* (2013) 165:441–50. doi: 10.1016/j.ahj.2012.12.020
19. Kolovou GD, Katsiki N, Mavrogeni S. Risk scores after acute coronary syndrome. *Angiology.* (2017) 68:185–8. doi: 10.1177/0003319716661069
20. Sullivan LM, Massaro JM, D'Agostino RB. Presentation of multivariate data for clinical use: the framingham study risk score functions. *Stat Med.* (2004) 23:1631–60. doi: 10.1002/sim.1742
21. Núñez E, Steyerberg EW, Núñez J. Regression modeling strategies. *Rev Esp Cardiol.* (2011) 64:501–7.
22. Pencina MJ, D' Agostino RB, D' Agostino RB, Vasan RS. Evaluating the added predictive ability of a new marker: from area under the roc curve to reclassification and beyond. *Stat Med.* (2008) 27:157–72. doi: 10.1002/sim.2929
23. Steg PG, Goldberg RJ, Gore JM, Fox KA, Eagle KA, Flather MD, et al. Baseline characteristics, management practices, and in-hospital outcomes of patients hospitalized with acute coronary syndromes in the global registry of acute coronary events (grace). *Am J Cardiol.* (2002) 90:358–63. doi: 10.1016/s0002-9149(02)02489-x
24. Fan F, Li Y, Zhang Y, Li J, Liu J, Hao Y, et al. Chest pain center accreditation is associated with improved in-hospital outcomes of acute myocardial infarction patients in china: findings from the ccc-acs project. *J Am Heart Assoc.* (2019) 8:e13384. doi: 10.1161/JAHA.119.013384
25. Sun P, Li J, Fang W, Su X, Yu B, Wang Y, et al. Effectiveness of chest pain centre accreditation on the management of acute coronary syndrome: a retrospective study using a national database. *BMJ Qual Saf.* (2021) 30:867–75. doi: 10.1136/bmjqs-2020-011491
26. Lv J, Ni L, Liu K, Gao X, Yang J, Zhang X, et al. Clinical characteristics, prognosis, and gender disparities in young patients with acute myocardial infarction. *Front Cardiovasc Med.* (2021) 8:720378. doi: 10.3389/fcvm.2021.720378
27. Zheng X, Dreyer RP, Hu S, Spatz ES, Masoudi FA, Spertus JA, et al. Age-specific gender differences in early mortality following st-segment elevation myocardial infarction in china. *Heart.* (2015) 101:349–55. doi: 10.1136/heartjnl-2014-306456
28. Bucholz EM, Butala NM, Rathore SS, Dreyer RP, Lansky AJ, Krumholz HM. Sex differences in long-term mortality after myocardial infarction. *Circulation.* (2014) 130:757–67. doi: 10.1161/CIRCULATIONAHA.114.009480
29. Chung SC, Gedeborg R, Nicholas O, James S, Jeppsson A, Wolfe C, et al. Acute myocardial infarction: a comparison of short-term survival in national outcome registries in Sweden and the UK. *Lancet.* (2014) 383:1305–12. doi: 10.1016/S0140-6736(13)62070-X
30. Simon T, Mary-Krause M, Cambou J, Hanania G, Guéret P, Lablanche J, et al. Impact of age and gender on in-hospital and late mortality after acute myocardial infarction: increased early risk in younger women. *Eur Heart J.* (2006) 27:1282–8. doi: 10.1093/eurheartj/ehi719
31. Khan SQ, Narayan H, Ng KH, Dhillon OS, Kelly D, Quinn P, et al. N-terminal pro-b-type natriuretic peptide complements the grace risk score in predicting early and late mortality following acute coronary syndrome. *Clin Sci.* (2009) 117:31–9. doi: 10.1042/CS20080419
32. Thygesen K, Mair J, Mueller C, Huber K, Weber M, Plebani M, et al. Recommendations for the use of natriuretic peptides in acute cardiac care: a position statement from the study group on biomarkers in cardiology of the esc working group on acute cardiac care. *Eur Heart J.* (2012) 33:2001–6. doi: 10.1093/eurheartj/ehq509
33. Palmerini T, Genereux P, Caixeta A, Cristea E, Lansky A, Mehran R, et al. A new score for risk stratification of patients with acute coronary syndromes undergoing percutaneous coronary intervention. *JACC Cardiovasc Interv.* (2012) 5:1108–16. doi: 10.1016/j.jcin.2012.07.011
34. Palmerini T, Genereux P, Caixeta A, Cristea E, Lansky A, Mehran R, et al. Prognostic value of the syntax score in patients with acute coronary syndromes undergoing percutaneous coronary intervention. *J Am Coll Cardiol.* (2011) 57:2389–97. doi: 10.1016/j.jacc.2011.02.032

Conflict of Interest: The authors declare that the research was conducted in the absence of any commercial or financial relationships that could be construed as a potential conflict of interest.

frontiers | Frontiers in Cardiovascular Medicine

ORIGINAL RESEARCH
published: 28 April 2022
doi: 10.3389/fcvm.2022.832014

Renal Denervation Attenuates Adverse Remodeling and Intramyocardial Inflammation in Acute Myocardial Infarction With Ischemia–Reperfusion Injury

Kun Wang[1†], Yu Qi[1†], Rong Gu[1†], Qing Dai[1], Anqi Shan[2], Zhu Li[1], Chenyi Gong[1], Lei Chang[3], Han Hao[1], Junfeng Duan[1], Jiamin Xu[1], Jiaxin Hu[1], Dan Mu[4], Ning Zhang[5], Jianrong Lu[1], Lian Wang[1], Han Wu[1], Lixin Li[6], Lina Kang[1] and Biao Xu[1,7]**

[1] Department of Cardiology, Nanjing Drum Tower Hospital, The Affiliated Hospital of Nanjing University Medical School, Nanjing, China, [2] Department of Emergency, Nanjing Drum Tower Hospital, The Affiliated Hospital of Nanjing University Medical School, Nanjing, China, [3] Department of Cardiology, Nanjing Drum Tower Hospital, Clinical College of Nanjing Medical University, Nanjing, China, [4] Department of Radiology, Nanjing Drum Tower Hospital, The Affiliated Hospital of Nanjing University Medical School, Nanjing, China, [5] Department of Ultrasound, Nanjing Drum Tower Hospital, The Affiliated Hospital of Nanjing University Medical School, Nanjing, China, [6] Physician Assistant Program, The Herbert H. and Grace A. Dow College of Health Professions, Central Michigan University, Mount Pleasant, MI, United States, [7] State Key Laboratory of Pharmaceutical Biotechnology, Nanjing University, Nanjing, China

Background: Inhibition of sympathetic activity and renin–angiotensin system with renal denervation (RDN) was proved to be effective in managing refractory hypertension, and improving left ventricular (LV) performance in chronic heart failure. The inhibition of sustained sympathetic activation prevents or delays the development of cardiac fibrosis and dysfunction that occurs after myocardial infarction and ischemia–reperfusion (I/R) injury. The translational efficiency of RDN remains to be defined in preclinical animal studies.

Objectives: This study investigated the therapeutic role of RDN in adverse remodeling and intramyocardial inflammation in myocardial ischemia–reperfusion (MI/R) injury.

Methods: Herein, 15 minipigs were subjected to 90-min percutaneous occlusion of the left anterior descending artery followed by reperfusion. Eight animals received simultaneous RDN using catheter-based radiofrequency ablation (MI/R-RDN). Cardiac function and infarct volume were measured *in vivo*, followed by histological and biochemical analyses.

Results: The infarct volume in I/R-RDN pigs reduced at 30 days postreperfusion, compared to I/R-Sham animals. The levels of catecholamine and cytokines in the serum, kidney cortex, the border, and infarcted regions of the heart were significantly reduced in I/R-RDN group. Moreover, the gene expression of collagen and the protein expression of

OPEN ACCESS

Edited by:
Pier Leopoldo Capecchi, University of Siena, Italy

Reviewed by:
Jie Yuan, Fudan University, China
Jing Shi, Nanjing Medical University, China

***Correspondence:**
Lina Kang
kanglina@njglyy.com
Biao Xu
xubiao62@nju.edu.cn

[†] These authors have contributed equally to this work and share first authorship

Specialty section:
This article was submitted to General Cardiovascular Medicine, a section of the journal Frontiers in Cardiovascular Medicine

Received: *26 January 2022*
Accepted: *22 March 2022*
Published: *28 April 2022*

Citation:
Wang K, Qi Y, Gu R, Dai Q, Shan A, Li Z, Gong C, Chang L, Hao H, Duan J, Xu J, Hu J, Mu D, Zhang N, Lu J, Wang L, Wu H, Li L, Kang L and Xu B (2022) Renal Denervation Attenuates Adverse Remodeling and Intramyocardial Inflammation in Acute Myocardial Infarction With Ischemia–Reperfusion Injury. Front. Cardiovasc. Med. 9:832014. doi: 10.3389/fcvm.2022.832014

adrenergic receptor beta 1 in heart were also decreased in I/R-RDN mice. Additionally, RDN therapy alleviated myocardial oxidative stress.

Conclusion: RDN is an effective therapeutic strategy for counteracting postreperfusion myocardial injury and dysfunction, and the application of RDN holds promising prospects in clinical practice.

Keywords: acute myocardial infarction, sympathetic nervous system, renal denervation, cardiac remodeling, inflammation

INTRODUCTION

Acute myocardial infarction (AMI), the most severe manifestation of coronary artery disease, is one of the leading causes of morbidity and mortality worldwide (1). The early mortality of AMI has decreased dramatically due to timely successful reperfusion therapy with percutaneous coronary intervention (PCI) that protects the heart from permanent damage. However, restoration of blood flow and reoxygenation in the heart is frequently associated with an exacerbation of tissue injury and a profound inflammatory response that is known as ischemia–reperfusion (I/R) injury (2). Myocardial injury induces significant changes in left ventricular (LV) structure which contributes to 75% of AMI survivors who develop heart failure within 5 years (3). The therapeutic approaches focusing on the prognosis of AMI with I/R injury remain to be developed.

It is well established that neurohormonal activation, the overactivation of both sympathetic nervous system (SNS) and renin–angiotensin–aldosterone system (RAAS), as well as an intense sterile inflammatory response are major contributors to reperfusion injury and cardiac remodeling (4). Pharmacotherapies that target the autonomic nervous system improve the prognosis of patients with I/R injury. However, high non-adherence rates limit the optimal use of these drugs due to many adverse effects (5). Novel adjunct cardioprotective maneuvers post-I/R are therefore crucial. Recently, alternative interventional therapeutic treatment, a catheter-based radiofrequency renal denervation (RF-RDN), is already used clinically to reduce SNS and RAAS activation, and seems to be a potential treatment for resistant hypertension (6–9). Furthermore, renal denervation (RDN) treatment exerted a beneficial effect by reducing cardiac remodeling in a porcine model of chronic heart failure (10, 11). Herein, we hypothesize that the function of RDN therapy postreperfusion could limit infarct size and prevent HF development.

Here, a catheter-based bilateral renal sympathetic nerve ablation followed by reperfusion was applied to an established porcine model of AMI with extensive ST-segment elevation myocardial infarction (STEMI). Involvement of both neuronal and humoral pathways allow us to study the signal transfer between renal and heart. We observed that RDN therapy has cardioprotective effects in AMI with I/R injury through improvement in cardiac function and structure. We also found that the protective effect of RDN acts through multiple pathways, including reversing adverse remodeling, decreasing infarct area, reducing neurohumoral changes, and decreasing of inflammation levels.

Abbreviations: Adrb1, adrenergic receptor beta 1; BZs, border zones; ECG, electrocardiogram; IVS, interventricular septal thickness; IZs, infarct zones; LAD, left atrial diameter; LC/MS, liquid chromatography–mass spectrometry; LGE, late gadolinium enhancement; LVEF, left ventricular ejection fraction; MDA, malondialdehyde; MI/R, myocardial ischemia–reperfusion; CMR, cardiac magnetic resonance imaging; NE, norepinephrine; PCI, percutaneous coronary intervention; RAAS, renin–angiotensin–aldosterone system; RF-RDN, radiofrequency renal denervation; RZs, remote zones; SNS, sympathetic nervous system; SOD, superoxide dismutase; STEMI, ST-segment elevation myocardial infarction; TH, tyrosine hydroxylase; TNF-α, tumor necrosis factor-alpha; TTE, transthoracic echocardiography.

MATERIALS AND METHODS

Ethics Statement and Animal Preparation

All animal experimental procedures were approved by the Ethics Committee of Nanjing Drum Tower Hospital, The Affiliated Hospital of Nanjing University Medical School (ethics code: 20200508) and conformed to the Guide for the Care and Use of Laboratory Animals according to Chinese National Regulations.

Eighteen 3-month-old Bama miniature pigs, weighing 15 ± 2 kg each, purchased from Taizhou Taihe Biotechnology Co., Ltd., were housed in animal care facilities. Prior to surgery, pigs were fasted for 12 h but with free water. Zoletil® 50 (Virbac) and atropine sulfate were injected intramuscularly for anesthesia, and peripheral venous access was established. Propofol (5 mg/kg/h) was slowly injected intravenously during the operation for general anesthesia. After tracheal intubation to assist breathing, pigs were mechanically ventilated using a non-invasive ventilator (tidal volume limited to 0.4–0.6 L/min, 18 breaths/min, oxygen concentration of 60%). An IntelliVue MP30 electrophysiological recorder was connected to the subjects for continuously dynamically monitoring heart rate, respiration, oxygen saturation, and blood pressure. Randomization was set preoperatively which was blinded to the operator, and when the animals established the acute myocardial I/R, they were grouped with renal denervation **(MI/R-RDN)** or sham **(MI/R-Sham)** procedures accordingly.

Acute Myocardial Infarction With Ischemia–Reperfusion Injury Minipig Model

All interventional procedures were performed under general anesthesia and electrocardiographic monitoring. A percutaneous sheath was placed in the femoral artery with a standard sterile technique. An 8F Fast-Cath (St. Jude, United States)

was used for LV angiography and heparin (2000 U/h, I.V.) injections, and a 6F EBU3.5 (Medtronic, United States) was placed at the ostia of the left coronary artery descending (LAD). Myocardial ischemia was induced by angioplasty balloon occlusion (2.0 × 15 mm, Maverick, Boston Scientific) with 10 atm. Preconditioned minipigs were successively subjected to triple episodes of 30 s, 1 and 5 min occlusion and 1 min occlusion followed by 5 and 15 min reperfusion, respectively, before the prolonged ischemia. Then LAD was occluded for 90 min followed by reperfusion before they were immediately treated with sham- or RF-RDN (the procedure is shown in **Figure 1**), and a cine angiogram was performed to confirm total occlusion (shown in **Figure 2A**). The STEMI model was successfully established when an elevated T wave was observed in the electrocardiogram (ECG) (shown in **Figure 2C**), and heart rate was recorded (**Supplementary Table 1**). An external defibrillator was always available after balloon inflation, and it was used appropriately when a pig developed fatal arrhythmias. Eight pigs experienced ventricular fibrillation during blood flow occlusion, seven pigs were rescued successfully, and one pig died without establishment of the model.

Radiofrequency Renal Artery Denervation

Via percutaneous femoral artery access, an 8F renal artery Mach 1 RDC (Boston, Scientific, United States) was placed at the ostia of the renal artery, and then a 12 mm radiofrequency ablation catheter (GL-6W, Shanghai Golden Leaf Medtech Co., Ltd., China) was introduced into the main renal artery. The catheter had six electrodes to sequentially deliver radiofrequency energy, which were mounted on a basket that could be opened to achieve solid contact with the vessel wall. We performed a 120-s ablation with each electrode and two sets of ablations in the renal artery from the ostia to the bifurcation (10–12 total ablations per renal artery), and then repeated the procedure on the other side. The temperature was 60°C. Renal angiography was performed before, during, and after RF-RDN to confirm patency of the arteries (shown in **Figure 2B**). The MI/R-Sham group procedure involved the same guide catheter and ablation catheter placement without activation of the RF generator.

Benzylpenicillin was administered intramuscularly for two consecutive days to prevent postoperative infection. Two pigs died after the operation: one in the MI/R-Sham group died within 24 h after the surgery, and the other in the MI/R-RDN group died during the first magnetic resonance imaging scanning due to the anesthetic overdose.

Transthoracic Echocardiography

Two-dimensional transthoracic echocardiography (TTE) was performed with a CX-50 ultrasound system (Phillips, Amsterdam, Netherlands) equipped with an S5-1 array sector transducer probe at a frequency range of 3.5–5.5 MHz. To assess cardiac function, echocardiographic examinations of each minipig were performed under anesthesia to produce quality images at 1, 7, and 30 days post-myocardial ischemia–reperfusion (MI/R). Left ventricular diameter at end-systole or end-diastole (LVESD, LVEDD), interventricular septal thickness (IVS), and left ventricular posterior wall thickness (LVPW) were measured from M-mode in parasternal short-axis or long-axis view at a level close to the papillary muscles. Three to six representative contraction cycles were used for analyses, and the left ventricular ejection fraction (LVEF) was calculated using the biplane Simpson method with the accompanying software. LV mass was calculated according to the recommendations of the American Society of Echocardiography and the European Association of Cardiovascular Imaging. LV diastolic function was evaluated using the ratio of early transmitral flow velocity (E) to late transmitral flow velocity (A) and the mean of transmitral E to early diastolic medial LV tissue velocity of the lateral wall (e′ lateral). The velocity-time integral (VTI) of the left ventricular outflow tract (LVOT) was obtained from pulsed Doppler imaging by positioning the sample volume at the LVOT approximately 0.5 cm below the aortic valve. Two blinded examiners performed all measurements.

Cardiac Magnetic Resonance Imaging

Cardiac magnetic resonance imaging (CMR) was performed to assess the infarct area and cardiac function 5 and 30 days after the MI/R-Sham or MI/R-RDN operation using an Ingenia CX 3.0T system (Philips Healthcare, Best, Netherlands). Steady-state free-precession cine imaging was performed using a 32-element phased-array body coil with ECG gating in cardiac vertical and horizontal short-axis and long-axis orientations.

The following scanning parameters were used: time of repetition (TR), 3.5 ms; time of echo (TE), 1.72 ms; field of view (FOV), 320 mm × 320 mm; layer thickness, 8 mm; the number of layers in the LV short axis, 8; the number of layers in the rest of the image, 3; flip angle (FA), 45°; and the number of excitations, 30 cardiac cycles. Ten to 15 min after the contrast agent injection (gadodiamide, 0.1 mmol/kg), a T1-weighted segmented phase-sensitive inversion recovery gradient-echo sequence was acquired for cine images to detect late gadolinium enhancement (LGE). The following scanning parameters were used: TR, 5.1 ms; TE, 2.5 ms; FOV, 255 mm × 255 mm; layer thickness, 8 mm; the number of layers in the LV short axis, 8; the number of layers in the rest of the image, 3; FA, 45°; and the number of excitations, 30 cardiac cycles. The infarct area was assessed as the area of hyperenhancement on the LGE images, which was measured as absolute mass or as a percentage of the entire LV myocardial mass. The images were analyzed by two independent investigators with software (QMass MR 7.5, Medis, Netherlands) according to the manufacturer's instructions.

Catecholamine Measurements

Peripheral blood samples were collected at baseline, post-MI, and 1, 7, and 30 days post-RDN. Renal cortex tissue and myocardial tissue were harvested at 30 days post-RDN, immediately frozen in liquid nitrogen, and stored at −80°C until catecholamine assays were performed. Portions of tissue from the necrotic, border zone (BZ), and remote zone (RZ) of the heart and right and left kidney cortex were mechanically homogenized in 10 volumes of ice-cold NaCl using a homogenizer. Plasma and tissue homogenates were assayed using high-performance liquid chromatography

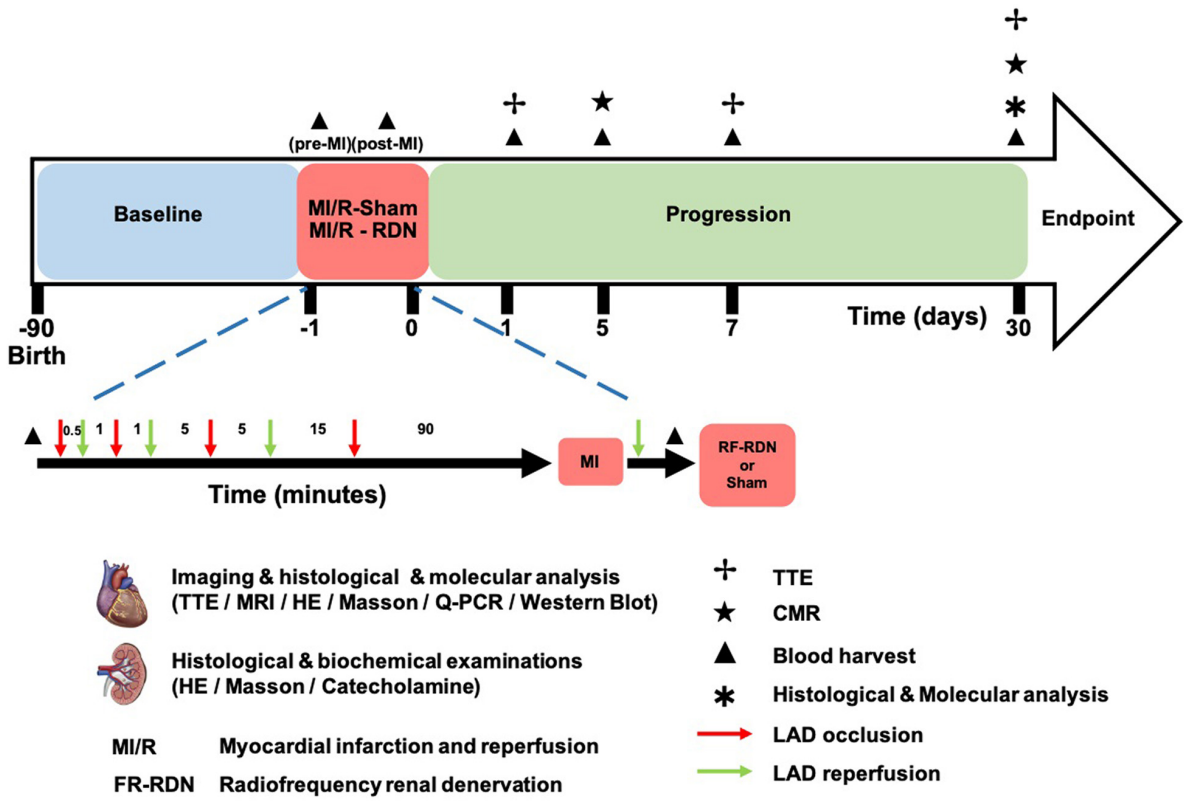

FIGURE 1 | MI/R-RDN experimental protocols. Preconditioned minipigs were subjected to triple episodes of 30 s, 1 and 5 min occlusion followed by 1, 5, and 15 min reperfusion, respectively, before the prolonged ischemia. Then LAD was occluded for 90 min followed by reperfusion before they were immediately treated with sham- or RF-RDN. TTE was performed at 1, 7, and 30 days after RDN therapy. CMR was performed at 5 and 30 days after RDN therapy. Peripheral blood was collected pre-MI/R, post-MI/R, and 1, 5, and 30 days post-MI/R. HE, hematoxylin and eosin; LAD, left coronary artery descending; TH, tyrosine hydroxylase.

(HPLC, Thermo Scientific UltiMate 3000). Analytical run times of norepinephrine, adrenaline, and dopamine were 3.5, 3.95, and 8.10 min, respectively. The data are graphed as nanograms of analyte per gram (ng/g) of total tissue.

ELISA and Cardiac Troponin T Detection

Blood samples were collected and centrifuged at 3000 rpm for 20 min. Serum was collected to measure the plasma levels of tumor necrosis factor-alpha (TNF-α) (R&D, PTA00) using ELISA kits according to the manufacturer's protocol. High-sensitivity cardiac troponin T (cTnT) (Roche Diagnostics) was measured on Cobas e411 and i1000SR analyzers using the manufacturer's calibrators and quality controls (12). The detection limit of the cTnT assay was set to 3 ng/L by the manufacturer.

Oxidative Stress Measurements

Malondialdehyde (MDA) and superoxide dismutase (SOD) levels in LV BZ tissues were measured using kits (Jiancheng Bio, China) according to the manufacturer's instructions.

Histological Staining

Thirty days after reperfusion, pigs were euthanized with potassium chloride (40 mEq/kg, I.V.). Tissues, including renal arteries and hearts, were collected for histological, biochemical, and molecular analyses. The renal arteries and surrounding tissues were subjected to immunohistochemical staining for hematoxylin and eosin (HE) and tyrosine hydroxylase (TH, Abcam, ab41528, 1:1000). Briefly, renal artery segments were harvested and fixed in 4% paraformaldehyde for 24 h, washed and placed in 70% ethyl alcohol until tissue processing for paraffin embedding. Renal artery samples were embedded and sliced into 2 μm thick serial cross-cryosections. LV tissue isolated from the infarct zones (IZs), BZs, and RZs was cut into 1 cm sections and 5 μm cross-sections were mounted onto glass slides and stained with HE and Masson's trichrome staining for analysis of the infarct area and fibrosis. CD163 (Proteintech, 16646-1-AP, 1:200) were stain for inflammatory cells under established protocol.

RNA Extraction and Quantitative Real-Time Polymerase Chain Reaction

The LV IZ, BZ, and RZ were lysed with RNAiso plus Reagent (Takara, 9109) according to the manufacturer's instructions, and total RNA was extracted. Purified RNA was quantified, and cDNA was synthesized using SuperMix (Vazyme, R223) and amplified with SYBR Green Master Mix (Vazyme, Q711) in a Quant Studio 6 Flex Real-Time PCR System (Applied Biosystems). GAPDH

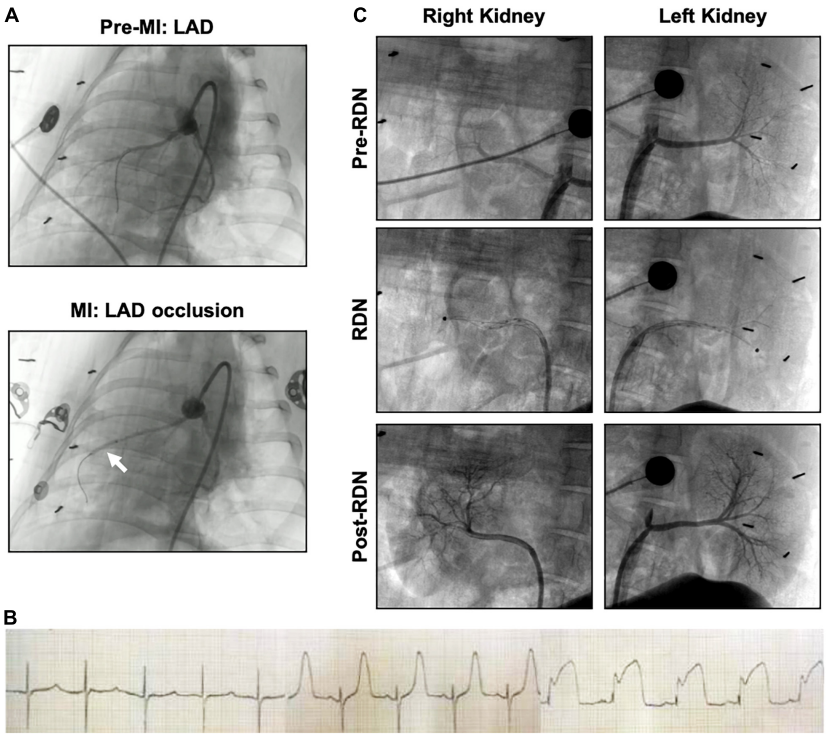

FIGURE 2 | Angiography of acute myocardial infarction and reperfusion (MI/R) and the RDN procedure in the porcine model. **(A)** Coronary artery angiography was performed before and during occlusion. The white arrow indicates the balloon position. **(B)** Representative ECG of the interventional procedure of MI/R. ST segment elevation of the anterior wall lead was observed. **(C)** Renal angiography was performed before, during, and after RDN in a bilateral manner. During the RDN procedure, the ablation catheter (black dot) can be observed in both renal arteries. Lack of stenosis was confirmed post-RDN.

was used as a housekeeping gene, and the $2^{-\Delta\Delta CT}$ formula was used for data analysis. The primers sequences are shown in **Supplementary Table 2**.

Western Blot

Heart tissue was quickly removed and immediately homogenized in EDTA-free RIPA buffer (Cat No. P0013B, Beyotime) at 4°C. After protein concentration measurement, the lysate was stored at −80°C for Western blot analysis. The lysate protein (20 μg) was electrophoresed and transferred to polyvinylidene difluoride (PVDF) membranes. After blocking with 5% non-fat dry milk, the membrane was incubated with primary antibodies at 4°C overnight. The following antibodies were used: beta 1 adrenergic receptor (Invitrogen, PA5-28808, 1:2000), and GAPDH (Proteintech, 10494-1-AP, 1:5000). The next day, membranes were incubated with secondary antibodies at RT for 1 h, followed by protein detection with SuperSignal West Femto Maximum Sensitivity Substrate (Thermo Fisher, 34096). Total protein expression was normalized to GAPDH.

Statistical Analysis

Data were statistically analyzed using GraphPad Prism 8.4.0 software with Student's unpaired *t*-test for two-tailed comparisons at a single time point and two-way analysis of variance with Bonferroni correction to account for multiple comparisons. All data are presented as the mean ± standard error of the mean (SEM), and a (corrected) *p*-value less than 0.05 was indicative of statistically significance.

RESULTS

Validation of Acute Myocardial Infarction and Reperfusion Porcine Model

Representative angiographic heart images before and during the induction of MI with balloon occlusion are showed in **Figure 2A**. The white arrow indicates the balloon position. The STEMI in the ECG indicated that the AMI model was successfully established (**Figure 2B**). The time and the extent of ischemic injury were similar in both groups, as demonstrated by ECG. Eight minipigs experienced ventricular fibrillation after balloon occlusion, seven minipigs were rescued successfully, and one pig died. Besides, two pigs died after the operation: one died within 24 h of AMI model establishment, and the other died during CMR scanning due to anesthetic overdose.

Validation of Catheter-Based Renal Sympathetic Denervation Effectiveness

Representative pre-, during-, and post-RDN angiographic renal images confirmed patency of the arteries (**Figure 2C**). The locations of ablation delivery are indicated by small black points in the vessels. Thirty days after RDN therapy, renal

arteries were collected and sectioned for HE and TH staining to assess nerve viability and the catecholamine production. TH is the rate-limiting enzyme in catecholamine biosynthesis, and is expressed primarily in the perivascular area. Representative photomicrographs illustrated the reduced TH staining in the MI/R-RDN group compared to the MI/R-Sham group (**Figures 3A,B**). Furthermore, to assess kidney structure, HE and Masson's trichrome staining were also performed and showed no changes (**Figures 3C,D**). These data clearly demonstrated that the RDN procedure reduced catecholamine production from the renal sympathetic nerves without impairing renal artery or kidney structure.

Renal Denervation Therapy Affects Catecholamine Levels

Peripheral blood samples were obtained at baseline, post-MI, and 1, 7, and 30 days post-RDN. The renal cortex was obtained at 30 days post-RDN. Serum samples and kidney cortex tissues from the MI/R-RDN and MI/R-Sham groups were analyzed using liquid chromatography–mass spectrometry (LC/MS). Serum dopamine (DA), adrenaline (E), and norepinephrine (NE) levels were significantly reduced at 7 days post-RDN but not at 30 days post-RDN (**Figure 3E**). Kidney NE, E, and DA levels were significantly reduced in the MI/R-RDN group (**Figure 3F**). The catecholamine concentrations in the heart were evaluated and revealed that NE, E, and DA levels from the IZs were significantly reduced. While heart NE levels also decreased in the RZ, other indicators remained unchanged in the BZs and the RZ (**Figure 3G**).

Cardiac Magnetic Resonance Imaging Indicated That Renal Denervation Inhibits Left Ventricular Remodeling

To assess cardiac contractile function, we measured LV dimensions and volumes using TTE. There were no changes in LVEF, LVESD, LVEDD, LV mass, or IVS between the groups at 1, 7, and 30 days post-RND. However, diastolic function was improved at 7 days in the MI/R-RDN group compared to the MI/R-Sham group (**Figure 4A**). In addition, serum cTnT levels, which evaluate myocardial injury after MI/R injury, were increased in all pigs. Interestingly, the cTnT level did not reach a significant threshold 24 h post-RDN between the two groups, but showed a lower level at 5 days in the MI/R-RDN group (**Figure 4B**). Furthermore, to verify whether RDN effectively treated cardiac remodeling in MI/R, we performed experiments with CMR using LGE at 5 and 30 days post-RND. The infarct area (percentage of the enhanced volume) was similar between the two groups at 5 days. However, it was significantly decreased in the MI/R-RDN group at 30 days compared to the MI/R-Sham group (**Figures 4C,D**).

Renal Denervation Therapy Attenuates Oxidative Stress and Fibrosis

Ventricular morphology was assessed with HE staining, and collagen content was quantified using Masson's trichrome staining (**Figures 5A–C**). LV homogenates from the BZ were analyzed to quantify the levels of oxidative stress at 30 days post-RDN. As depicted in **Figure 5D**, myocardial oxidative stress (MDA levels) was reduced in the MI/R-RDN group compared to the MI/R-Sham group. Furthermore, the protein expression of antioxidant enzyme (SOD) was upregulated after RDN therapy (**Figure 5D**). Gene expressions of collagen 1 and 3, as fibrotic proteins comprising approximately 90% of all cardiac collagens, were significantly reduced in the IZ and BZ but not in the RZ (**Figure 5E**). Taken together, these results indicated that immediate RDN therapy after reperfusion attenuated cardiac oxidative stress levels and significantly decreased fibrosis at the infarcted and border sites.

Sympathetic Activity and Myocardial Inflammation Outcome

Sustained sympathetic signaling results in overactivation of beta-adrenergic receptor (Adrbs) and triggers deranged neural-inflammation circuits that lead to exacerbation of myocardial injury (13). We next examined whether RDN attenuates adrenergic activation in the heart. Notably, the protein expression of adrenergic receptor beta 1 (Adrb1) was significantly decreased in the IZ and BZ but not in the RZ with RDN therapy compared to sham treatment (**Figure 6A**). The highly prevalent nature of systemic and cardiac inflammation, as a common pathobiological feature, was linked to the development, progression, and complication of poor outcomes of AMI-reperfusion injury. To address the possibility that RDN attenuates inflammation, we performed ELISA assay on serum samples collected on days 5 and 30 after MI/-RDN and quantitative real-time polymerase chain reaction (Q-PCR) on heart tissue samples derived from the IZ, BZ, and RZ collected on day 30 after MI/-RDN. The circulating TNF-α level was significantly decreased in the MI/R-RDN group at day 30 (**Figure 6B**). Cytokines, including proinflammatory signaling IL-1β, IL-6, TNF-α, and myocardial fibrosis signaling TGF-β, were significantly reduced in the BZ. However, only IL-1β was decreased in the IZ and no significant difference in INF-γ level or proinflammatory resolving lipid mediator IL-10 mRNA levels were detected in the IZ and BZ (**Figure 6C**). These results suggested that RDN treatment had a beneficial effect of on heart inflammation.

DISCUSSION

The main findings of our preclinical work are that RF-RDN therapy reduces catecholamine levels, improves adverse cardiac remodeling, decreases infarct volumes and inhibits inflammation in an AMI/reperfusion minipig model. Taken together, our results indicate that RF-RDN is a simple, fast, and effective intervention therapy that allows us to address the crosstalk between the renal sympathetic system and the heart adrenergic system. Therefore, RDN is a potential supplementary therapy for AMI after revascularization.

In the current study, the STEMI model was established by performing increasing episodes before reaching the index 90 min occlusion. Ischemic preconditioning could protect heart from a subsequent prolonged period of ischemia and offer

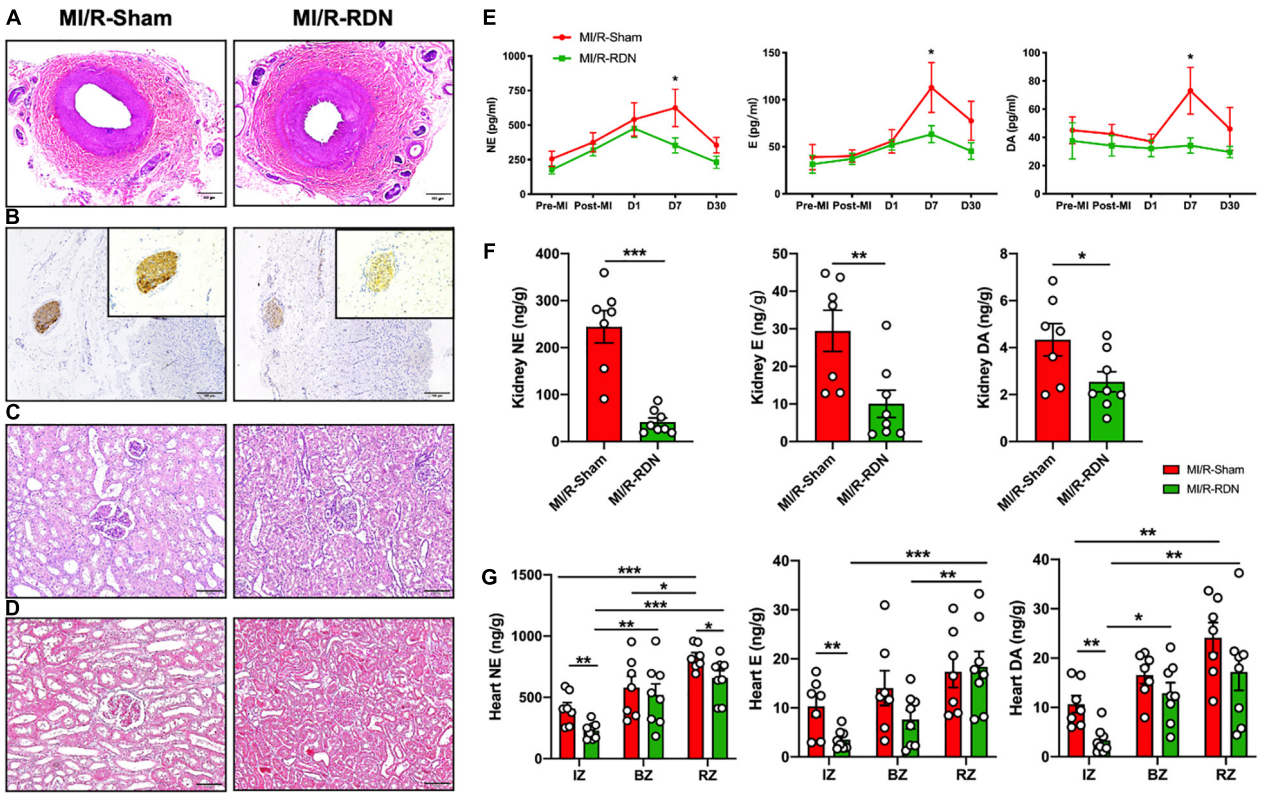

FIGURE 3 | Histological staining of the kidneys and renal arteries and catecholamine levels in the circulation, renal cortex, and heart. **(A)** Representative images of hematoxylin and eosin (HE) staining of the renal arteries at the 30-day endpoint following sham or RDN therapy. **(B)** Representative images of tyrosine hydroxylase (TH) staining on the nerves in the adventitial layer of the renal arteries at the 30-day endpoint following sham or RDN therapy. Inserts indicate renal artery nerves and magnified photomicrographs (20×) of TH staining. The scale bar is 100 mm. **(C)** Representative images of HE staining of the kidney at the 30-day endpoint following sham or RDN therapy. The scale bar is 100 mm. **(D)** Representative images of Masson's trichrome staining of the kidney at the 30-day endpoint following sham or RDN therapy. The scale bar is 100 mm. **(E)** Norepinephrine (NE), epinephrine (E), and dopamine (DA) concentrations in the circulation pre-AMI, post-AMI, and 1, 7, and 30 days post-RDN. **(F)** NE, E, and DA concentrations per gram of kidney cortex tissue. **(G)** NE, E, and DA concentrations per gram of heart IZ, BZ, and RZ tissue. $n = 7$ in the IM/R-Sham group, $n = 8$ in the IM/R-RDN group. IZs, infarct zones; BZs, border zones; and RZs, remote zones. Data are shown as the mean ± SEM **(E–G)**. p-Values were obtained by two-way ANOVA with Bonferroni test **(E)**, unpaired, two-tailed t-test **(F)**, and two-tailed t-test and one-way ANOVA with Bonferroni test **(G)**. $^{*}p < 0.05$, $^{**}p < 0.01$, and $^{***}p < 0.001$ (compared with the MI/R-Sham or MI/R-RDN group).

one of the most powerful mechanisms for reducing the speed and extent of myocardial cell damage and the occurrence of malignant arrhythmia in an acute or sustained ischemic insult (14, 15). Hence, it is highly possible that the rapid adaptation to ischemia protects the ischemic heart against a following prolonged ischemic periods and eventually improves pig survival.

The beneficial role of RDN in attenuating ventricular remodeling was confirmed in current study through assessing cardiac function and structure using cardiac TTE and CMR techniques. Clinical guidelines recommend TTE as the first-line diagnostic modality for the evaluation of cardiac diseases. Interesting results showed that at post-RDN day 7, there was an improvement in the E/A. Nevertheless, neither LVEF nor LV mass showed differences at post-RDN day 30 between the I/R-RDN group and the I/R-Sham group. This may due to the low value of LVEF at baseline resulting in no significant difference after the MI operation. CMR is well accepted as the gold standard for the quantification of infarct area (16–18). Our results showed that at 30 days post-RDN, the percentage of infarct size was significantly decreased in the MI/R-RDN group compared with the MI/R-Sham group, indicating that RDN therapy promotes faster repair of the myocardium.

Acute myocardial infarction results in a severe imbalance of metabolic supply and demand of oxygen and nutrients, and leading to tissue hypoxia, which initiates a primary pathophysiological process that is compensated by SNS and RAAS activation (19). Longstanding high levels of NE released from SNS induce changes in cardiomyocyte phenotype by reducing the oxygen supply and increasing the oxygen demand, which contribute to the progression of LV remodeling and myocardial stunning. Recently, Polhemus et al. observed that RDN exhibited cardioprotective actions in the chronic hypertensive SHRs (20). Sharp et al. investigated that RDN prevented heart failure progression via inhibition of renal NE and circulating angiotensin I and II expression in Yucatan minipigs (11), indicating that RDN reduces catecholamine levels in the kidney instead of heart tissue. However, the underlying mechanism of how RDN protects against heart failure

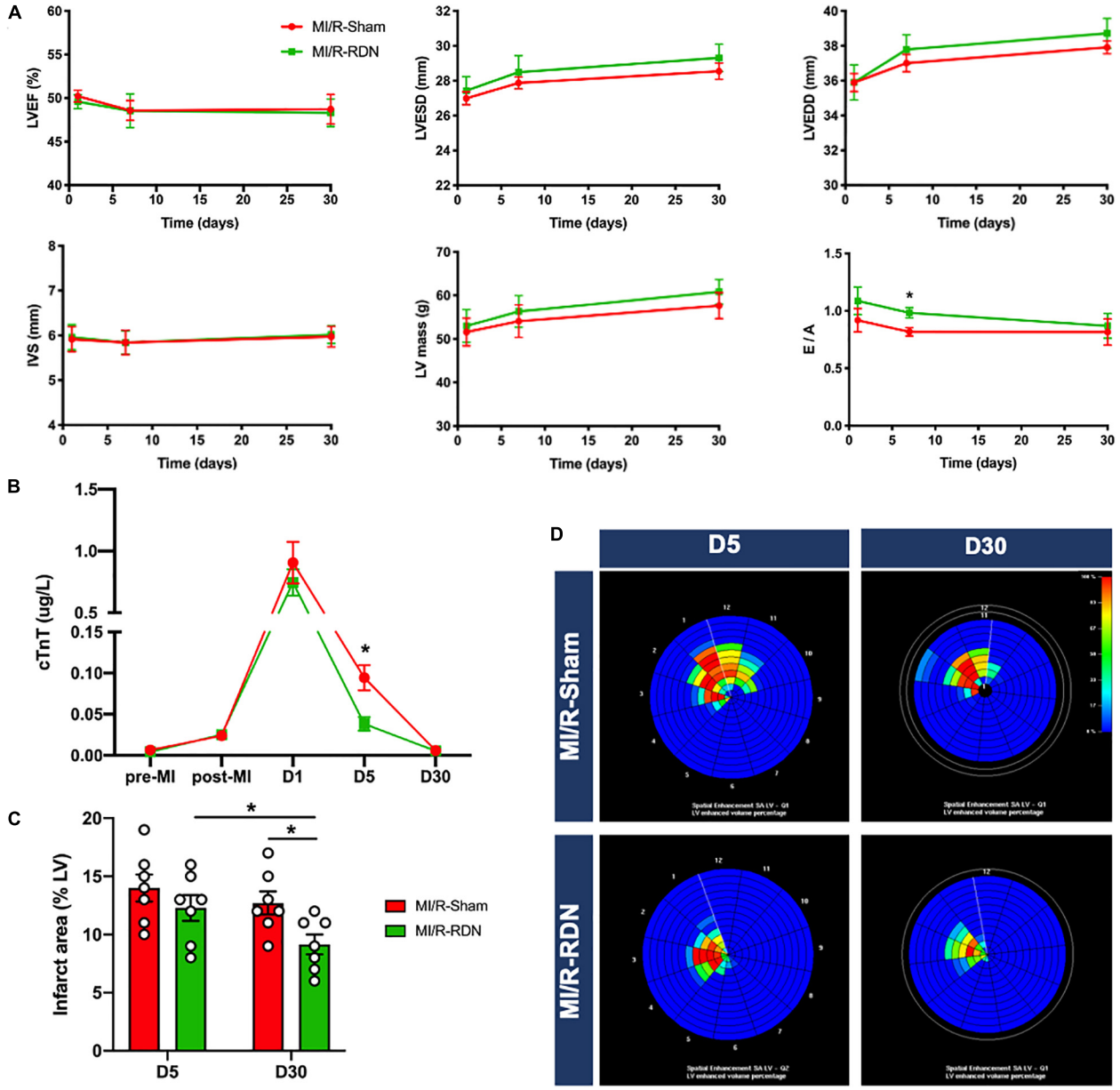

FIGURE 4 | Echocardiography and CMR outcomes. **(A)** The parameters of echocardiography, left ventricular ejection fraction (LVEF), interventricular septal thickness (IVS), LV mass, and the ratio of early transmittal flow velocity to late transmittal flow velocity (E/A) were measured with TTE ($n = 7$ each group). **(B)** Serum cardiac troponin T (cTnT) was measured pre-AMI, post-AMI, and 1, 5, and 30 days post-RDN ($n = 7$ each group). **(C)** Analysis of the percentage of the enhanced volume ($n = 7$ each group). **(D)** Representative graphs of the percentage of the enhanced volume assessed using CMR. Data are shown as the mean ± SEM **(A–C)**. *p*-Values were shown and assessed by two-way ANOVA with Bonferroni test **(A–C)**. *$p < 0.05$ (compared with the MI/R-Sham group).

progression has not been identified (16). Furthermore, the signal transduction of RDN in cardiac remodeling after AMI, especially reperfusion, was not reported in detail in previous studies. In this study, we founded that serum DA, E, and NE levels were significantly reduced at 7 days with RND therapy, while catecholamine levels downregulation in both kidney cortex and heart tissues at 30 days post-RDN (**Figure 3**). These results showed that RDN therapy had the potential to attenuate cardiac catecholamine levels.

Catecholamines enhance the mechanical performance of the heart by activating cardiac Adrb. Although cardiomyocytes coexpress β1 and β2, β1 is the predominant subtype and principal driver of catecholamine-driven sympathetic responses in the healthy heart. We examined the protein expression of Adrb1 and observed a significantly reduction in the IZ and BZ of the hearts with RDN therapy but not in the RZ. These results indicated that RDN attenuated only overactivated SNS, but had no obvious inhibitory effect on the normal SNS.

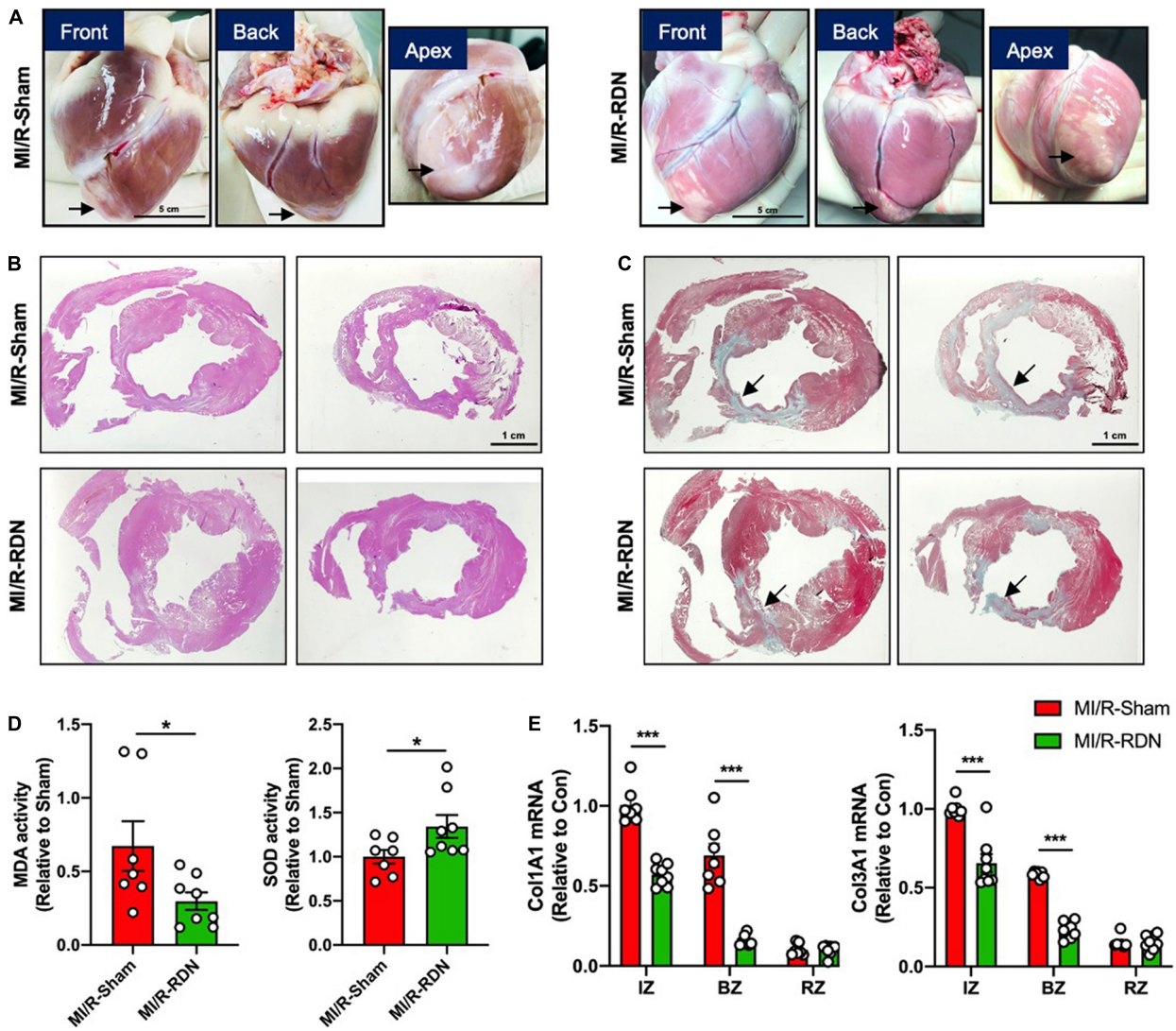

FIGURE 5 | Histological analysis and collagens expression levels. **(A)** Minipig heart tissue was taken from the front, back, and apex. **(B)** Representative photomicrographs of HE-stained heart sections from the MI/R-sham- and MI/R-RDN-treated animals. **(C)** Representative photomicrographs of Masson's trichrome-stained heart sections from the MI/R-sham- and MI/R-RDN-treated animals. **(D)** Activity of the malondialdehyde (MDA) and the antioxidant enzyme superoxide dismutase (SOD) in the border zone of LV were detected. The data are shown as the fold change relative to the MI/R-Sham group. **(E)** Fibrotic gene profile consisting of the mRNA expression of collagen 1 (Col1A1) and collagen 3 (Col3A1). The expression of these genes was normalized to GAPDH expression and is shown as the fold change relative to the IZ in the MI/R-Sham group. $n = 7$ in the IM/R-Sham group, $n = 8$ in the IM/R-RDN group. Data are shown as the mean ± SEM **(D,E)**. p-Values were shown and assessed by unpaired, two-tailed t-test **(D)** and two-way ANOVA with Bonferroni test **(E)**. $^{*}p < 0.05$, $^{***}p < 0.001$ (compared with the MI/R-Sham group).

Besides, immune cells also express Adrbs. So, we performed the histological staining of CD168 for inflammatory cells staining (**Supplementary Figure 1**), which showed less numbers of CD168 positive cells in the BZ in the MI/R-RDN group compared with the MI/R-Sham group (data not show). Thus, the lower Adrb1 expression detected in heart tissue cannot be ruled out as a result of reduced inflammatory cell recruitment and infiltration. Considering the heterogeneity and plasticity of immune cells, we will further explore immune cell dynamic balance and molecular mechanisms in myocardial injury and repair in the future. In addition, we observed that RDN reduced heart rate slightly, although there was no difference between I/R-RDN group and I/R-Sham group (**Supplementary Table 1**). Notably, RDN did not introduce hypotension, which indicated that RF-RDN was safe for the acute hemodynamic changes during the myocardial infarction/reperfusion period.

The proinflammatory cytokines TNF, TL-1β, and IL-6 are markedly and consistently increased in experimental models of AMI or I/R injury and have provided important insights into the mechanisms of inflammation-induced adverse LV remodeling, which may be mediated by uncoupling of Adrb and impaired calcium cycling (17, 18, 21). Our data suggested

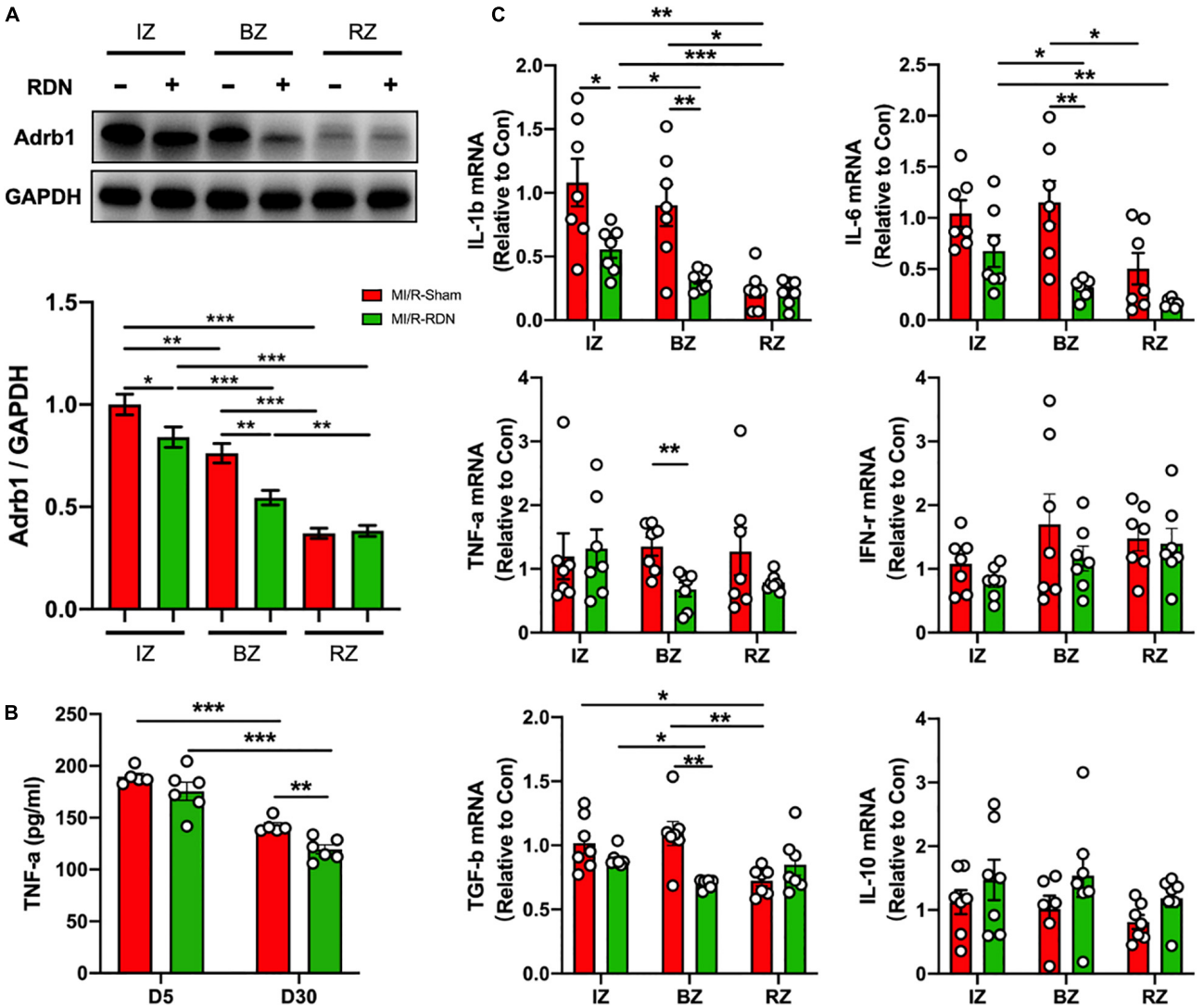

FIGURE 6 | Sympathetic activity and inflammation level in the LV IZ/BZ/RZ in MI/R following with sham or RDN treatment. **(A)** Western blots and statistics of the expression of adrenergic receptor beta 1 (Adrb1) in the infarct zones (IZs), border zones (BZs), and remote zones (RZs) of heart tissues ($n = 7$ each group). **(B)** TNF-α levels in the circulation at 5 and 30 days post-RDN therapy were measured using ELISA ($n = 5$ in the IM/R-Sham group, $n = 6$ in the IM/R-RDN group). **(C)** mRNA levels of inflammatory mediators in heart tissues. The expression of these genes was normalized to GAPDH expression and is shown as the fold change relative to the IZ in the MI/R-Sham group ($n = 6$–7 each group). Data are shown as the means ± SEM. p-Values were shown and assessed by two-way ANOVA with Bonferroni test **(A–C)**. $^{*}p < 0.05$, $^{**}p < 0.01$, and $^{***}p < 0.001$ (compared with the MI/R-Sham group).

that RDN treatment leads to a significant reduction on cardiac inflammatory cytokines, including TNF-α, IL-1β, IL-6, and TGF-β. Furthermore, circulating TNF-α levels were also decreased in the MI/R-RDN group. The TNF-α concentration is an independent predictor of mortality and has emerged as a potential therapeutic strategy in AMI and HF. As a highly pleiotropic mediator, TNF-α also protects cardiomyocytes from apoptosis. Excessive TNF-α expression and subsequent activation of cardiomyocyte TNF receptor type 1 induces cardiac contractile dysfunction, hypertrophy, and fibrosis, while a lower TNF-α concentration and subsequent activation of cardiomyocyte TNF receptor type 2 induces a cardiac protective effect (21). However, based on the results from two large clinical trials, high-intensity TNF-α blockade therapy did not improve outcomes in chronic HF patients (22, 23), suggesting that TNF-α may function as a biomarker for anti-inflammatory effects rather than an appropriate therapeutic target. Treatment with an anti-IL-6 receptor antibody not only attenuated adverse remodeling in an infarct mouse model (24) but also increased myocardial salvage in patients with acute STEMI (25). Therefore, timely downregulation of IL-6 levels might be crucial for infarct healing. The TGF-β signaling cascade is a key molecular link between the inflammatory and reparative pathways and regulates the fibrogenic response in the remodeling myocardium (26). Neurohumoral mediators, such as aldosterone, are important for fibroblast activation (27), thus

their effects might be mediated in part through activation of TGF-β signaling. Therefore, anti-inflammatory and anti-fibrosis are important therapeutic strategies for improving outcomes following I/R injury.

Infarction and necrosis trigger a strong inflammatory response that induces endothelial cell adhesion molecule synthesis and leads to the recruitment of inflammatory cells to clear the wound of dead cells or matrix debris (28). The spleen as a reservoir for inflammatory cells, plays a central role in the systemic immune response (26). Adrenoceptors are involved in the mobilization of leukocytes from the spleen (29). Splenic activation regulated by SNS, boosts extramedullary hematopoiesis and contributes to a sustained increase in monocyte/macrophage infiltration following I/R injury. The role of the spleen in I/R injury was also demonstrated by positron emission tomography imaging of splenic fluor-deoxyglucose uptake in patients with acute syndrome and at postmortem autopsy (30, 31). Recent evidence suggests the cardioprotection effect of the spleen in remote ischemic preconditioning in pigs and rats model after the denervation experiments, but fail to distinguish between parasympathetic and sympathetic innervation in that study (32). Thus, there is a crosstalk between the splenic immune cells mobilization and cardiac inflammation, and whether RDN can regulate this interplay remains to be further explored.

CONCLUSION

Taken together, our data demonstrate that RDN ameliorates oxidative stress, neurohormonal activation, adverse LV remodeling, and inflammation in a large animal model of AMI with I/R injury. These results provide strong evidence of the feasibility and therapeutic efficacy of RDN and suggest the necessity for further development of this therapeutic modality.

STUDY LIMITATIONS

There are some limitations of our study. First, hemodynamic evaluations of parameters, such as the mean aortic pressure, were not recorded but no intraoperative hypotension was observed during the study. Second, circulating IL-1 and IL-6 levels after MI were below detection range in our model. Therefore, we were unable to assess the direct effect of RDN on systemic cytokines level. In addition, the long-term effects of RDN and its ability to treat complex models in clinical practice should be evaluated. Although, the severity and mortality of MI are higher in female patients regardless of age, our study did not evaluate gender differences and only female animals were used in the present study. Besides, this mice strain is sexually mature at 3 months of age. In order to compare with other miniature pig strains, the weight somewhat limits the age range. Last but not least, the lower Adrb1 expression detected in heart tissue cannot be ruled out as a result of reduced inflammatory cell recruitment and infiltration. Considering the heterogeneity and plasticity of immune cells, we will further explore their dynamic balance and molecular mechanism in myocardial injury and repair in the future.

PERSPECTIVES

Clinical Competencies

Renal denervation treatment attenuated cardiac remodeling and intramyocardial inflammation by inhibiting sympathetic activity in a porcine AMI with I/R injury model, which is similar to pharmacotherapies that target the autonomic nervous system to improve the prognosis.

Translational Outlook

Understanding the cardioprotective effects of RDN therapy in AMI with I/R injury is essential in developing clinical management strategies that is in conjunction with primary PCI for STEMI patients to prevent late-onset heart failure.

DATA AVAILABILITY STATEMENT

The raw data supporting the conclusions of this article will be made available by the authors, without undue reservation.

ETHICS STATEMENT

The animal study was reviewed and approved by the Ethics Committee of Nanjing Drum Tower Hospital, The Affiliated Hospital of Nanjing University Medical School (20200508).

AUTHOR CONTRIBUTIONS

LK and BX conceived and designed the work. KW, LK, YQ, and QD performed the PCI and RDN surgeries. All co-authors participated in the material preparation, molecular experiments, and data collection. YQ, KW, and RG performed the data analyses. DM assisted the interpretation of CMR measurement data. NZ blindly performed the echocardiogram examination and statistically analyzed the data. YQ and KW wrote the first draft of the manuscript. BX, LK, LL, and RG revised the manuscript critically for important intellectual content. All authors read and approved the final manuscript.

FUNDING

This research was supported by the National Natural Science Foundation of China (Nos. 82070366 to BX, 81870291 to RG, and 81970296 to HW) and the Nanjing Medical Science and Technical Development Foundation (No. ZKX20018 to LK).

SUPPLEMENTARY MATERIAL

The Supplementary Material for this article can be found online at: https://www.frontiersin.org/articles/10.3389/fcvm.2022.832014/full#supplementary-material

REFERENCES

1. Reed GW, Rossi JE, Cannon CP. Acute myocardial infarction. *Lancet.* (2017) 389:197–210. doi: 10.1016/s0140-6736(16)30677-8
2. Eltzschig HK, Eckle T. Ischemia and reperfusion–from mechanism to translation. *Nat Med.* (2011) 17:1391–401. doi: 10.1038/nm.2507
3. Uriel N, Sayer G, Annamalai S, Kapur NK, Burkhoff D. Mechanical unloading in heart failure. *J Am Coll Cardiol.* (2018) 72:569–80. doi: 10.1016/j.jacc.2018.05.038
4. Hartupee J, Mann DL. Neurohormonal activation in heart failure with reduced ejection fraction. *Nat Rev Cardiol.* (2017) 14:30–8. doi: 10.1038/nrcardio.2016.163
5. Ivers NM, Schwalm JD, Bouck Z, McCready T, Taljaard M, Grace SL, et al. Interventions supporting long term adherence and decreasing cardiovascular events after myocardial infarction (ISLAND): pragmatic randomised controlled trial. *BMJ.* (2020) 369:m1731. doi: 10.1136/bmj.m1731
6. Kandzari DE. Renal denervation for hypertension: what is needed, and what is next. *Eur Heart J.* (2019) 40:3483–5. doi: 10.1093/eurheartj/ehz369
7. Kiuchi MG, Esler MD, Fink GD, Osborn JW, Banek CT, Bohm M, et al. Renal denervation update from the international sympathetic nervous system summit: JACC state-of-the-art review. *J Am Coll Cardiol.* (2019) 73:3006–17. doi: 10.1016/j.jacc.2019.04.015
8. Ram CVS. Status of renal denervation therapy for hypertension. *Circulation.* (2019) 139:601–3. doi: 10.1161/CIRCULATIONAHA.118.037937
9. Fengler K, Rommel KP, Blazek S, Besler C, Hartung P, von Roeder M, et al. A three-arm randomized trial of different renal denervation devices and techniques in patients with resistant hypertension (RADIOSOUND-HTN). *Circulation.* (2019) 139:590–600. doi: 10.1161/CIRCULATIONAHA.118.037654
10. Bohm M, Ewen S, Wolf M. Renal denervation halts left ventricular remodeling and dysfunction in heart failure: new shores ahead. *J Am Coll Cardiol.* (2018) 72:2622–4. doi: 10.1016/j.jacc.2018.09.027
11. Sharp TE III, Polhemus DJ, Li Z, Spaletra P, Jenkins JS, Reilly JP, et al. Renal denervation prevents heart failure progression via inhibition of the renin-angiotensin system. *J Am Coll Cardiol.* (2018) 72:2609–21. doi: 10.1016/j.jacc.2018.08.2186
12. Welsh P, Preiss D, Shah ASV, McAllister D, Briggs A, Boachie C, et al. Comparison between high-sensitivity cardiac troponin T and cardiac troponin I in a large general population cohort. *Clin Chem.* (2018) 64:1607–16. doi: 10.1373/clinchem.2018.292086
13. Jakob MO, Murugan S, Klose CSN. Neuro-immune circuits regulate immune responses in tissues and organ homeostasis. *Front Immunol.* (2020) 11:308. doi: 10.3389/fimmu.2020.00308
14. Taggart P, Yellon DM. Preconditioning and arrhythmias. *Circulation.* (2002) 106:2999–3001. doi: 10.1161/01.cir.0000041803.03687.7a
15. Heusch G. Cardioprotection: chances and challenges of its translation to the clinic. *Lancet.* (2013) 381:166–75. doi: 10.1016/s0140-6736(12)60916-7
16. Sharp Iii TE, Lefer DJ. Renal denervation to treat heart failure. *Annu Rev Physiol.* (2020) 83:39–58. doi: 10.1146/annurev-physiol-031620-093431
17. Liberale L, Ministrini S, Carbone F, Camici GG, Montecucco F. Cytokines as therapeutic targets for cardio- and cerebrovascular diseases. *Basic Res Cardiol.* (2021) 116:23. doi: 10.1007/s00395-021-00863-x
18. Yokoyama T, Vaca L, Rossen RD, Durante W, Hazarika P, Mann DL. Cellular basis for the negative inotropic effects of tumor necrosis factor-alpha in the adult mammalian heart. *J Clin Invest.* (1993) 92:2303–12. doi: 10.1172/jci116834
19. Levy B, Clere-Jehl R, Legras A, Morichau-Beauchant T, Leone M, Frederique G, et al. Epinephrine versus norepinephrine for cardiogenic shock after acute myocardial infarction. *J Am Coll Cardiol.* (2018) 72:173–82. doi: 10.1016/j.jacc.2018.04.051
20. Polhemus DJ, Trivedi RK, Gao J, Li Z, Scarborough AL, Goodchild TT, et al. Renal Sympathetic denervation protects the failing heart via inhibition of neprilysin activity in the kidney. *J Am Coll Cardiol.* (2017) 70:2139–53. doi: 10.1016/j.jacc.2017.08.056
21. Kleinbongard P, Schulz R, Heusch G. TNFalpha in myocardial ischemia/reperfusion, remodeling and heart failure. *Heart Fail Rev.* (2011) 16:49–69. doi: 10.1007/s10741-010-9180-8
22. Mann DL, McMurray JJ, Packer M, Swedberg K, Borer JS, Colucci WS, et al. Targeted anticytokine therapy in patients with chronic heart failure: results of the randomized etanercept worldwide evaluation (RENEWAL). *Circulation.* (2004) 109:1594–602. doi: 10.1161/01.Cir.0000124490.27666.B2
23. Chung ES, Packer M, Lo KH, Fasanmade AA, Willerson JT. Randomized, double-blind, placebo-controlled, pilot trial of infliximab, a chimeric monoclonal antibody to tumor necrosis factor-alpha, in patients with moderate-to-severe heart failure: results of the anti-TNF therapy against congestive heart failure (ATTACH) trial. *Circulation.* (2003) 107:3133–40. doi: 10.1161/01.Cir.0000077913.60364.D2
24. Kobara M, Noda K, Kitamura M, Okamoto A, Shiraishi T, Toba H, et al. Antibody against interleukin-6 receptor attenuates left ventricular remodelling after myocardial infarction in mice. *Cardiovasc Res.* (2010) 87:424–30. doi: 10.1093/cvr/cvq078
25. Broch K, Anstensrud AK, Woxholt S, Sharma K, Tollefsen IM, Bendz B, et al. Randomized trial of interleukin-6 receptor inhibition in patients with acute ST-segment elevation myocardial infarction. *J Am Coll Cardiol.* (2021) 77:1845–55. doi: 10.1016/j.jacc.2021.02.049
26. Frangogiannis NG. The inflammatory response in myocardial injury, repair, and remodelling. *Nat Rev Cardiol.* (2014) 11:255–65. doi: 10.1038/nrcardio.2014.28
27. Rossignol P, Cleland JG, Bhandari S, Tala S, Gustafsson F, Fay R, et al. Determinants and consequences of renal function variations with aldosterone blocker therapy in heart failure patients after myocardial infarction: insights from the eplerenone post-acute myocardial infarction heart failure efficacy and survival study. *Circulation.* (2012) 125:271–9. doi: 10.1161/circulationaha.111.028282
28. Frangogiannis NG. Regulation of the inflammatory response in cardiac repair. *Circ Res.* (2012) 110:159–73. doi: 10.1161/CIRCRESAHA.111.243162
29. Dutta P, Courties G, Wei Y, Leuschner F, Gorbatov R, Robbins CS, et al. Myocardial infarction accelerates atherosclerosis. *Nature.* (2012) 487:325–9. doi: 10.1038/nature11260
30. Emami H, Singh P, MacNabb M, Vucic E, Lavender Z, Rudd JH, et al. Splenic metabolic activity predicts risk of future cardiovascular events: demonstration of a cardiosplenic axis in humans. *JACC Cardiovasc Imaging.* (2015) 8:121–30. doi: 10.1016/j.jcmg.2014.10.009
31. van der Laan AM, Ter Horst EN, Delewi R, Begieneman MP, Krijnen PA, Hirsch A, et al. Monocyte subset accumulation in the human heart following acute myocardial infarction and the role of the spleen as monocyte reservoir. *Eur Heart J.* (2014) 35:376–85. doi: 10.1093/eurheartj/eht331
32. Lieder HR, Kleinbongard P, Skyschally A, Hagelschuer H, Chilian WM, Heusch G. Vago-splenic axis in signal transduction of remote ischemic preconditioning in pigs and rats. *Circ Res.* (2018) 123:1152–63. doi: 10.1161/CIRCRESAHA.118.313859

Conflict of Interest: The authors declare that the research was conducted in the absence of any commercial or financial relationships that could be construed as a potential conflict of interest.

Advantages of publishing in Frontiers

OPEN ACCESS
Articles are free to read for greatest visibility and readership

FAST PUBLICATION
Around 90 days from submission to decision

HIGH QUALITY PEER-REVIEW
Rigorous, collaborative, and constructive peer-review

TRANSPARENT PEER-REVIEW
Editors and reviewers acknowledged by name on published articles

Frontiers
Avenue du Tribunal-Fédéral 34
1005 Lausanne | Switzerland

Visit us: www.frontiersin.org
Contact us: frontiersin.org/about/contact

REPRODUCIBILITY OF RESEARCH
Support open data and methods to enhance research reproducibility

DIGITAL PUBLISHING
Articles designed for optimal readership across devices

FOLLOW US
@frontiersin

IMPACT METRICS
Advanced article metrics track visibility across digital media

EXTENSIVE PROMOTION
Marketing and promotion of impactful research

LOOP RESEARCH NETWORK
Our network increases your article's readership